National Research Council Canada

Conseil national de recherches Canada

NRC · CNRC

Canadian Journal of Fisheries and Aquatic Sciences

Journal canadien des sciences halieutiques et aquatiques

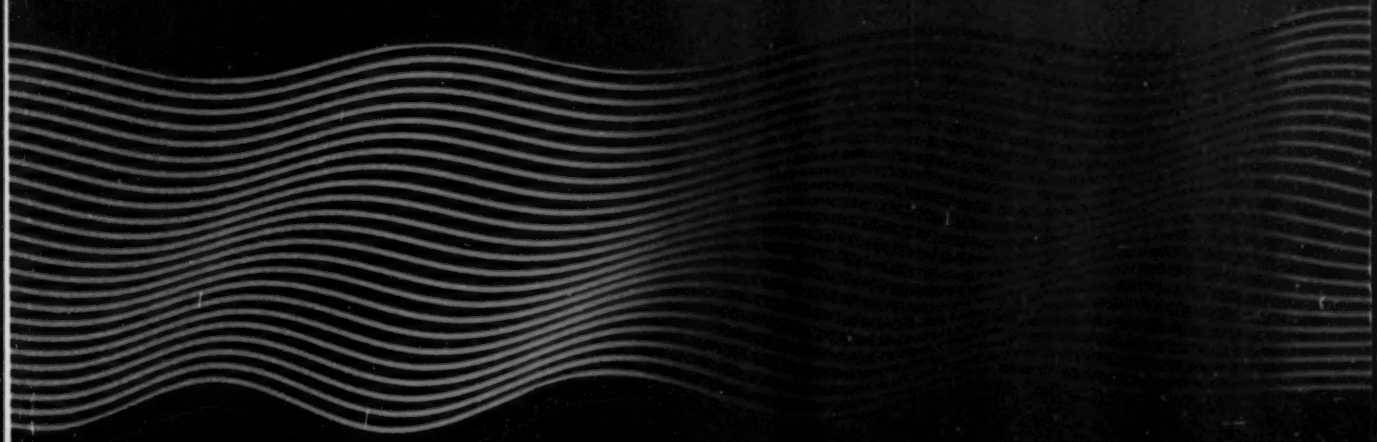

http://cjfas.nrc.ca

http://jcsha.cnrc.ca

ISSN 0706-652X / CJFSDX 61(6) 857–1059 (2004)

The *Canadian Journal of Fisheries and Aquatic Sciences*, previously published as *Contributions to Canadian Biology* 1901–1925, *Contributions to Canadian Biology and Fisheries* 1926–1934, *Journal of the Biological Board of Canada* 1934–1937, and *Journal of the Fisheries Research Board of Canada* 1938–1979, is issued monthly to form annual volumes of 12 numbers plus supplements.

Editorial policy. The Journal publishes original research articles, perspectives (syntheses, critiques, re-evaluations), discussions (comment and reply), and rapid communications. Manuscripts may concern cells, organisms, populations, communities, ecosystems, or processes that affect aquatic systems. They may cover a range of disciplines including biology and ecology of marine and freshwater organisms, limnology, oceanography, physiology, toxicology, genetics, economics, disease, and management. Preference will be given to manuscripts that emphasize understanding of observed phenomena and interpretation of experimental results. The Journal encourages papers that lead from clearly stated purpose or rationale and from testable hypotheses, concepts, or questions to identifiable conclusions or syntheses. Such papers may amplify, modify, question, or redirect accumulated knowledge embodied in contemporary perceptions of a particular state of aquatic sciences. The Journal discourages papers that are essentially descriptive, except in emerging disciplines; have only site-specific or local applications (a certain year, place, taxon, chemical compound, etc.); only confirm previously established principles; or apply standard techniques without breaking new methodological ground.

Manuscripts for publication should be submitted to the Senior Editor, *Canadian Journal of Fisheries and Aquatic Sciences*, Department of Zoology, University of Guelph, Guelph, ON N1G 2W1, Canada (519-824-4120 ext. 52646; fax: 519-767-9798; e-mail: cjfas@uoguelph.ca).

Submissions in either English or French are acceptable. The information must be original, that is, not copyrighted, published, or submitted elsewhere except in abstract form or unless by written consent of the Editor.

Correspondence concerning accepted manuscripts and corrected proofs should be sent to NRC Research Press, National Research Council of Canada, Ottawa, ON K1A 0R6, Canada (fax: 613-952-7656; e-mail: pubs@nrc-cnrc.gc.ca).

Instructions to Authors are published once a year in the first issue of each volume. Copies are available from NRC Research Press or at http://cjfas.nrc.ca. The **Publication Policy** of NRC Research Press is available at http://pubs.nrc-cnrc.gc.ca.

Microfilm. Issues from 1934 through the current volume can be purchased on 16- or 35-mm microfilm. Photocopies of individual articles or issues can be purchased from University Microfilms International, 330 North Zeeb Road, Ann Arbor, MI 48106, U.S.A.

U.S. periodical postage paid at Champlain, N.Y., and at additional mailing offices. Attention U.S. POSTMASTER: Send address changes to **Canadian Journal of Fisheries and Aquatic Sciences**, c/o USACAN Media Distribution Center, P.O. Box 2888, Plattsburg, NY 12901, U.S.A.

Publié sans interruption depuis 1901, le *Journal canadien des sciences halieutiques et aquatiques* a paru sous plusieurs titres : *Contributions to Canadian Biology* 1901–1925, *Contributions to Canadian Biology and Fisheries* 1926–1934, *Journal of the Biological Board of Canada* 1934–1937, et *Journal of the Fisheries Research Board of Canada* 1938–1979. Le Journal paraît tous les mois, formant ainsi un volume de 12 numéros, et offre en plus jusqu'à deux suppléments par année.

Politique éditoriale. On publie, dans le Journal, des articles rendant compte de recherche originale, des perspectives (synthèses, critiques et réévaluations), des discussions (commentaires et réponses) et des communications rapides. Les documents peuvent porter sur les cellules, organismes, populations, communautés, écosystèmes ou processus qui affectent les systèmes aquatiques. Ils peuvent relever de divers domaines y compris la biologie et l'écologie des organismes marins et d'eau douce, la limnologie, l'océanographie, la physiologie, la toxicologie, la génétique, l'économie, la pathologie et la gestion. On accorde la préséance aux articles qui contribuent à la compréhension de phénomènes observés et à l'interprétation de résultats expérimentaux. On invite les auteurs à soumettre des articles ayant des objectifs précis ou relevant d'hypothèses, de concepts ou de questions vérifiables et se terminant par de solides conclusions ou d'utiles synthèses. Ces articles enrichissent, changent, mettent en question ou réorientent les connaissances acquises sur divers aspects des sciences aquatiques. On décourage toutefois la soumission d'articles simplement descriptifs (à moins qu'il ne s'agisse de nouvelles disciplines), d'application très limitée (applicables à une seule année, une seule région ou un seul taxon, portant sur un unique composé chimique, etc.); d'articles qui ne font que reprendre les principes énoncés dans des articles précédents; et d'articles rendant compte de l'application de normes sans gain de méthodologie.

Les auteurs voudront adresser leurs **manuscrits** à la directrice scientifique principale, *Journal canadien des sciences halieutiques et aquatiques*, Department of Zoology, University of Guelph, Guelph, ON N1G 2W1, Canada (519-824-4120 poste 52646; télécopieur : 519-767-9798; courriel : cjfas@uoguelph.ca).

Les contributions peuvent être en anglais ou en français. Elles doivent être originales, c.-à.-d. qu'elles ne doivent pas avoir fait l'objet d'un copyright, avoir été publiées ou soumises ailleurs, sauf sous forme abrégée ou avec le consentement du rédacteur. Le CNRC ne se tient en aucune façon responsable des opinions exprimées par un collaborateur ou des déclarations qui pourrait faire ce dernier.

La correspondance ayant trait aux manuscrits acceptés et les **épreuves corrigés** doivent être envoyées aux Presses scientifiques du CNRC, Conseil national de recherches du Canada, Ottawa, ON K1A 0R6, Canada (télécopieur : 613-952-7656; courriel : pubs@nrc-cnrc.gc.ca).

Les Recommandations aux auteurs sont publiées une fois par année dans le premier numéro de chaque volume. Des copies sont disponibles auprès du Bureau de la rédaction aux Presses scientifiques du CNRC ou au http://jcsha.cnrc.ca. **La Politique de publication** est disponible auprès des Presses scientifiques du CNRC ou au http://pubs.nrc-cnrc.gc.ca.

Microfilms. On peut acheter sur microfilms de 16 ou 35 mm tous les numéros depuis 1934. Des photocopies d'articles ou de numéros individuels sont aussi en vente auprès de University Microfilms International, 330 North Zeeb Road, Ann Arbor, MI 48106, É.-U.

This Journal is indexed or abstracted in / Cette revue est signalée ou résumée dans

ABSEARCH, Applied Science and Technology Index and Abstracts, Aquatic Sciences and Fisheries Abstracts, Biological Abstracts, Biological and Agricultural Abstracts, CAB Abstracts, Chemical Abstracts, Current Contents, Elsevier BIOBASE, Environmental Abstracts, ETDE Energy Database, General Science Index and Abstracts, GEOBASE, GeoRef, Life Sciences Collection, Meteorological and Geoastrophysical Abstracts, Oceanic Abstracts, PASCAL Database, and Science Citation Index.

Volume 61, Number 6, June 2004

Canadian Journal of Fisheries and Aquatic Sciences

Published by the National Research Council of Canada

Volume 61, numéro 6, juin 2004

Journal canadien des sciences halieutiques et aquatiques

Publié par le Conseil national de recherches du Canada

Senior Editor / Directrice scientifique principale **Moira M. Ferguson**

Editors / Directeurs

Jeffrey A. Hutchings, *Dalhousie University, Halifax*
Pierre Pepin, *Northwest Atlantic Fisheries Centre, DFO/MPO, St. John's, Newfoundland*
W. Gary Sprules, *University of Toronto at Mississauga*
Assistant to the Editors / Adjointe aux directeurs scientifiques **Holly Foster**

Associate Editors / Directeurs scientifiques associés

D. Boisclair, *Université de Montréal*
U. Borgmann, *Environment Canada, Burlington*
M.J. Bradford, *DFO/MPO and Simon Fraser University*
S.E. Campana, *DFO/MPO, Dartmouth*
R. Carignan, *Université de Montréal*
J.J. Dodson, *Université Laval*
G.T. Evans, *DFO/MPO, St. John's, Newfoundland*
K.T. Frank, *DFO/MPO, Dartmouth*
J.W.A. Grant, *Concordia University*
M.M. Hansen, *Danish Institute for Fisheries Research, Silkeborg, Denmark*
R. Hilborn, *University of Washington*
A. Hontela, *Université du Québec à Montréal*
D.F. Houlihan, *University of Aberdeen*
F.A. Huntingford, *University of Glasgow*
G.S. Jamieson, *DFO/MPO, Nanaimo*
J.M. Jech, *NFSC/NOAA, Woods Hole, Mass.*
B. Jonsson, *Norwegian Institute for Nature Research, Oslo, Norway*
D.L. MacLatchy, *University of New Brunswick, St. John*
P. Magnan, *Université du Québec à Trois Rivières*
C.T. Marshall, *University of Aberdeen*
R.B. Millar, *University of Auckland, New Zealand*
W.P. Patterson, *University of Saskatchewan*
Y.T. Prairie, *Université du Québec à Montréal*
T.J. Quinn II, *University of Alaska–Fairbanks, Juneau, Alaska*
T.P. Quinn, *University of Washington*
C.W. Ramcharan, *Laurentian University*
R.D. Robarts, *Environment Canada, Saskatoon*
B. Sainte-Marie, *DFO/MPO, Mont-Joli*
D.W. Schindler, *University of Alberta*
R.E.H. Smith, *University of Waterloo*
S.J. Smith, *DFO/MPO, Dartmouth*
W.F. Vincent, *Université Laval*
R.D. Vinebrooke, *University of Alberta*
C.J. Walters, *University of British Columbia*
R.D. Ward, *CSIRO Marine Research, Australia*
B. de Young, *Memorial University of Newfoundland*

NRC Research Press / Presses scientifiques du CNRC

Editor-in-Chief / Directeur général **Bruce P. Dancik**
Assistant Editor-in-Chief / Directeur général adjoint **Iain E.P. Taylor**

Journals Program / Programme des revues

Fax / Télécopieur : 613-952-7656; e-mail / courriel : pubs@nrc-cnrc.gc.ca; URL / URL : pubs.nrc-cnrc.gc.ca
Director / Directeur **Cameron D. Macdonald**
Acting Business Manager / Gestionnaire des affaires par intérim **Mike Boroczki**
Manager, Journals Program / Gestionnaire, Programme des revues **Carolyn Brown**
Managing Editor / Rédactrice administrative **Cecily M. Pearson** (613-993-9099)
Publication Officer / Agente de publication **Jennifer McColl**
Advertising / Annonces publicitaires **Judy Gorman** (613-993-0151)
Reprints / Tirés à part **Roxanne Landriault** (613-990-2254)
Subscriptions / Abonnements **Eileen Evans-Nantais** (613-990-7873)

The National Research Council of Canada accepts no responsibility for statements or opinions expressed by a contributor. Acceptance of an advertisement, announcement, or other material does not imply endorsement by either the Journal's Senior Editor or the National Research Council.

© National Research Council of Canada 2004. All rights reserved.

No part of this publication may be reproduced, stored, or transmitted in any form or by any means, without the written permission of the publisher, except as stated below.

The National Research Council of Canada grants **permission*** to individuals to make single copies of articles for personal use. Any person may reproduce short excerpts from articles in the journal for any purpose that respects the moral rights of authors, provided that the source is fully acknowledged. As a courtesy, the consent of authors of such material should be obtained directly from the author.

Authorization to reproduce items for other than personal use, as stated above, is granted by the National Research Council of Canada provided that the copyright fee of $7.00 per copy is paid directly to CANCOPY, One Yonge Street, Suite 1900, Toronto, ON M5E 1E5, Canada.

*The above permission does not extend to other kinds of copying, such as copying for general distribution, for advertising, or promotional purposes, for creating new collective works, or for resale. For such copying, arrangements must be made with the publisher, National Research Council of Canada, Ottawa, ON K1A 0R6, Canada.

Subscription information

The *Canadian Journal of Fisheries and Aquatic Sciences* (ISSN 0706-652X) is published monthly by the National Research Council of Canada. The 2004 annual subscription rates (second class postage) for Canada are $830CAN institutional and $257CAN personal, for US & foreign $830US institutional and $257US personal. For air mail add $175US to foreign rate. Canadian customers please include 7% GST (business no. 12149 1807 RT 0275). Subscriptions are entered for the calendar year. Remittances should be made payable to the Receiver General for Canada, credit NRC. Price for regular single issues: institutional, $105.00; personal, $35.00. Supplements will be priced separately. Special rates apply to members of Canadian scientific and engineering societies if they subscribe through their respective societies.

There are no refunds on cancelled subscriptions once delivery has begun. Claims for missing issues should be made within four months (N. America) or six months (outside N. America) following the date of publication. The publisher expects to supply missing issues only when losses have occurred in transit and when the reserve stock will permit. For change of address and subscription enquiries: Subscription Office, NRC Research Press, National Research Council of Canada, Ottawa, ON K1A 0R6, Canada; tel.: 613-993-9084; fax: 613-952-7656; e-mail: pubs@nrc-cnrc.gc.ca.

Microform backfiles are available from UMI, P.O. Box 1346, Ann Arbor, MI 48106-1346, U.S.A., and Micromedia Ltd., 20 Victoria St., Toronto, ON M5C 2N8, Canada.

All issues of the *Canadian Journal of Fisheries and Aquatic Sciences* since 1996 are available on the Web. Pricing information can be found at http://pubs.nrc-cnrc.gc.ca.

Le Conseil national de recherches du Canada ne se tient en aucune façon responsable des opinions exprimées par un collaborateur ou des déclarations que pourrait faire ce dernier. La publication d'annonces publicitaires, d'avis et autres n'implique pas l'endossement de leur contenu par la directrice principale de la Revue ou le CNRC.

© Conseil national de recherches du Canada 2004. Tous droits réservés.

Il est interdit de reproduire, de sauvegarder ou de transmettre quelque partie de la présente publication dans quelque format ou de quelque façon sans le consentement écrit de l'éditeur, à l'exception des conditions suivantes.

Le Conseil national de recherches du Canada accorde aux particuliers le droit de faire des copies individuelles pour leur usage personnel. Toute personne peut reproduire de courts extraits des articles de la Revue pour autant que les droits moraux de l'auteur soient respectés et que la mention de provenance soit clairement indiquée. Il est de convenance de demander le consentement de l'auteur avant de faire mention de son travail.

On obtiendra l'autorisation de reproduire des articles à d'autres fins que l'usage personnel (tel qu'on l'a décrit ci-dessus) auprès du Conseil national de recherches du Canada pour autant que des redevances de droits d'auteurs de 7,00 $/copie soient versées au CANCOPY, 1, rue Yonge, bureau 1900, Toronto, ON M5E 1E5, Canada.

*La permission ci-dessus ne s'applique pas à la reproduction à grande échelle, telle que la reproduction aux fins de distribution générale, publicitaire ou promotionnelle, de compilation de nouveaux ouvrages collectifs ou de revente. Dans de tels cas, il faudra ratifier une entente particulière avec l'éditeur, le Conseil national de recherches du Canada, Ottawa, ON K1A 0R6, Canada.

Renseignements sur l'abonnement

Journal canadien des sciences halieutiques et aquatiques (ISSN 0706-652X) est une publication mensuelle du Conseil national de recherches du Canada. Le prix de l'abonnement annuel en 2004 au Canada (courrier de deuxième classe) est de 830 $CAN pour les organismes et de 257 $CAN pour les particuliers. À l'étranger (y compris les É.-U.), le prix de l'abonnement est de 830 $US pour les organismes et de 257 $US pour les particuliers. L'expédition par avion exige des frais de 175 $US en sus du prix d'abonnement à l'étranger. Les clients du Canada doivent ajouter la TPS de 7% (numéro d'entreprise 12149 1807 RT 0275). Les abonnements sont pour l'année civile. Tout paiement doit être adressé au Receveur général du Canada, crédit du CNRC. Le prix par numéro est de 105 $ pour les organismes et de 35 $ pour les particuliers. Le prix des hors-série varie. Les membres des sociétés canadiennes de sciences et de génie bénéficient de taux préférentiels en s'abonnant via leurs sociétés respectives.

Aucun remboursement ne sera accordé ni aucune annulation acceptée une fois que les livraisons auront commencé. Les réclamations de numéros manquants devront être soumises dans les quatre mois (Amérique du Nord) ou dans les six mois (à l'extérieur de l'Amérique du Nord) suivant la date de publication. L'éditeur ne fournira de numéros manquants que si le document a été perdu pendant l'expédition et que si le stock le permet. Adressez tout changement d'adresse ou toute question quant à l'abonnement au : Bureau des abonnements, Presses scientifiques du CNRC, Conseil national de recherches Canada, Ottawa, ON K1A 0R6, Canada; téléphone : 613-993-9084; télécopieur : 613-952-7656; courriel : pubs@nrc-cnrc.gc.ca.

On peut obtenir les fichiers rétrospectifs sur **microforme** auprès de UMI, P.O. Box 1346, Ann Arbor, MI 48106-1346, É.-U., et auprès de Micromedia Ltée, 20, rue Victoria, Toronto, ON M5C 2N8, Canada.

À partir de 1996, tous les numéros de *Journal canadien des sciences halieutiques et aquatiques* sont accessibles sur le Web. On trouvera des renseignements sur les tarifs à http://pubs.nrc-cnrc.gc.ca.

Ecological correlates of fish movement in a network of Virginia streams

Brett Albanese, Paul L. Angermeier, and Sundar Dorai-Raj

Abstract: Identifying factors that influence fish movement is a key step in predicting how populations respond to environmental change. Using mark–recapture (four species) and trap capture (eight species) data, we examined relationships between three attributes of movement and 15 ecological variables. The probability of emigrating from a reach was positively related to intermittency (one species) and body size (one species) and negatively related to distance from the mainstem creek (two species) and habitat complexity (one species). The number of fish moving upstream through traps was positively related to increases in flow (five species), day length (three species), and water temperature (two species); the number moving through downstream traps was positively associated with increases in flow (three species). Distance moved was greater for fish moving through unsuitable reaches (one species). Floods have a pervasive effect on fish movement, and human activities that affect flows will have widespread implications. The importance of other factors varies interspecifically, which may translate into variation in persistence and colonization rates. For example, species that exhibit reach fidelity in complex habitats may increase movement if habitats are homogenized. These species may suffer population declines because of the cost of increased movement and may ultimately be replaced by ecological generalists.

Résumé : L'identification des facteurs qui affectent les déplacements des poissons est une étape essentielle dans la prédiction des réactions des populations aux changements environnementaux. Des données de marquage–recapture (quatre espèces) et de capture au piège (huit espèces) nous ont servi à examiner les relations entre trois caractéristiques du déplacement et 15 variables écologiques. La probabilité d'émigration d'une section donnée est reliée positivement à l'intermittence du milieu (1 espèce) et à la taille du corps (1 espèce) et négativement à la distance du cours d'eau principal (2 espèces) et à la complexité de l'habitat (1 espèce). Le nombre de poissons qui se déplacent vers l'amont dans les pièges est relié positivement à l'augmentation du débit (5 espèces), à la longueur du jour (3 espèces) et à la température de l'eau (2 espèces); le nombre de poissons se déplaçant vers l'aval dans les pièges est en relation positive avec l'augmentation du débit (3 espèces). Les distances parcourues sont plus grandes chez les poissons qui traversent des sections inadéquates (1 espèce). Les crues ont des effets multiples sur les déplacements des poissons et les activités humaines qui affectent le débit auront aussi des effets étendus. L'importance des autres facteurs varie d'une espèce à l'autre, ce qui peut s'expliquer en fonction des variations de la permanence du milieu et des taux de colonisation. Par exemple, les espèces qui ont une haute fidélité à une section donnée dans des habitats complexes peuvent accroître leurs déplacements si les habitats sont uniformisés. Ces espèces peuvent alors subir des déclins de population à cause du coût accru des déplacements et elles peuvent éventuellement être remplacées par des espèces à valence écologique plus étendue.

[Traduit par la Rédaction]

Introduction

Over scales ranging from an individual habitat unit to entire basins, movement is a critical process that allows fishes to meet their resource needs in spatially and temporally variable stream environments (Schlosser and Angermeier 1995; Fausch et al. 2002). At smaller scales, movement allows individual fish to occupy the most suitable habitats for survival and growth (Gowan and Fausch 2002). At larger scales, movement also permits migrations between habitats used by different life-history stages, exploitation of refugia from large-scale disturbances, gene flow and demographic

Received 17 April 2003. Accepted 16 April 2004. Published on the NRC Research Press Web site at http://cjfas.nrc.ca on 23 July 2004.
J17478

B. Albanese.[1] Georgia Natural Heritage Program, 2117 U.S. Highway 278 S.E., Social Circle, GA 30025-4714, USA.
P.L. Angermeier. United States Geological Survey, Virginia Cooperative Fish and Wildlife Research Unit,[2] Virginia Polytechnic Institute and State University, Blacksburg, VA 24061-0321, USA.
S. Dorai-Raj.[3] Department of Statistics, Virginia Polytechnic Institute and State University, Blacksburg, VA 24061-0439, USA.

[1]Corresponding author (e-mail: brett_albanese@dnr.state.ga.us).
[2]The Unit is sponsored by US Geological Survey, Virginia Polytechnic Institute and State University, and Virginia Department of Game and Inland Fisheries.
[3]Present address: PDF Solutions, 101 W. Renner Road, Suite 325, Richardson, TX 75082, USA.

 doi: 10.1139/F04-096 © 2004 NRC Canada

rescue for small populations, and colonization or recolonization of unoccupied habitats (Brown and Kodric-Brown 1977; Peterson and Bayley 1993; Northcote 1997). These larger-scale movements are essential for persistence of individual populations and metapopulations (Meffe and Sheldon 1990; Schlosser and Angermeier 1995). Thus, solid conceptual and empirical knowledge of movement is necessary to improve our understanding of stream fish ecology and also to inform conservation efforts for fishes occurring in systems that are increasingly modified by humans (Warren et al. 1997; Wiens 2001).

Dams and other barriers to movement have an obvious impact on fish populations by preventing migrations, gene flow, and colonization (Warren and Pardew 1998; Pringle et al. 2000). Less recognized are impacts to the environmental factors that influence movement. Fishes that readily move under certain ecological conditions may fail to do so in other situations (Gowan et al. 1994). Identifying ecological factors that drive dispersal-mediated life-history events (e.g., spawning migrations) is a key step in predicting how fishes will respond to natural and anthropogenic changes in environmental conditions (Railsback et al. 1999). In addition, successful colonization may depend directly on factors influencing movement from source habitats, as well as factors that influence the decision to stop moving.

Managing fish populations is far more complicated when factors influencing movement vary among species, and there is considerable evidence for such variation among birds and mammals (Macdonald and Johnson 2001). Diverse life histories and habitat requirements suggest that factors may also be species specific in fishes. However, despite the multiplicity of factors that have been associated with dispersal in terrestrial animals, some environmental conditions seem to be more pervasive than others (Ims and Hjermann 2001). For instance, movement has been associated with physical structure (i.e., presence of cover) for many stream-fish species (e.g., Aparicio and Sostoa 1999; Harvey et al. 1999; Gilliam and Fraser 2001). Identifying common factors that influence movement across species may facilitate management efforts that benefit entire assemblages.

Despite the importance of movement to theory and management, few studies have linked movement of stream fish to ecological factors (Gowan et al. 1994; Gilliam and Fraser 2001). Most studies that have examined ecological correlates of movement have been limited in the number of factors and (or) number of attributes of movement examined, which leads to an incomplete understanding of movement (Ims and Hjermann 2001). Furthermore, we are aware of no studies that have explicitly examined how ecological correlates of movement vary within an assemblage of fishes.

The primary objective of this study was to identify factors associated with the movement of fishes in a network of streams. This objective was addressed by examining three attributes of movement: the probability of an individual leaving a reach within a 3-month period, the number of fish moving through a trap per day, and the distance moved by an individual over a 3-month period. In our study, these attributes primarily reflected seasonal movements associated with changing habitat conditions between spring and summer. In addition to seasonal variation in movement, the trap data also integrate short-term movements associated with more rapidly changing physical conditions. Although the specific functions (e.g., movements to spawning habitats, drought refugia, or flood refuge.) underlying these short-term and seasonal movements vary with the life histories of the study species, both types may transfer fishes to different habitats and have important implications for colonization and persistence of stream-fish populations (Matthews 1998).

We examined relationships between each attribute of movement and a suite of predictor variables related to reach-specific habitat characteristics and attributes of individual fish. Based on existing theory, relationships documented for other fishes, and our knowledge of the study area, we predicted that the following factors would have a pervasive influence on fish movement (i.e., influence movement for multiple fish species). (1) Cover: we predicted that fish would be less likely to emigrate from reaches with more cover because of the refugia provided from predators and fast currents (Fausch et al. 1995; Harvey et al. 1999; Aparicio and Sostoa 1999). (2) Drought: because the quality and quantity of stream habitat typically declines during droughts, we predicted that the probability of emigrating from a reach would be negatively related to stream depth (Heggenes et al. 1991; Aparicio and Sostoa 1999; Magoulick 2000). We also predicted that fishes would be more likely to emigrate from intermittent vs. perennially flowing reaches. (3) Habitat complexity: because fishes can presumably meet more of their resource needs when a variety of habitat types is present, we predicted that fish would be less likely to emigrate from reaches with high habitat complexity (Gorman 1986; Harvey et al. 1999). (4) Increases in stream flow: we predicted that the number of fish moving would increase during floods. Such movements may permit fishes to exploit previously inaccessible habitats or find refuge from high current velocities (Hall 1972; Ross and Baker 1983; Schlosser 1995). (5) Body size: we predicted that larger fish would move longer distances and would be more likely to emigrate from reaches because energetic requirements increase with body size (Gatz and Adams 1994; Minns 1995; Aparicio and Sostoa 1999).

Materials and methods

Study area and focal species

The study area consisted of a network of streams tributary to Johns Creek (James River drainage) in Craig County, Virginia, and comprised over 4 km of contiguous streams (Fig. 1). Habitat characteristics ranged widely across the study area. Little Oregon Creek and lower Dicks Creek were wider and of lower gradient than the tributaries. The occurrence of several beaver dams and their associated pools within these mainstem creeks also contrasted with the riffle–pool and cascade (Middle Creek and White Branch only) habitats that dominated the smaller tributary streams. Middle Creek and White Branch were spring-fed and exhibited continuous flow throughout the study. In contrast, reaches of Little Oregon Creek (above Middle Creek confluence only), Mudlick Creek, and upper Dicks Creek were chronically affected by drought during the summers of 1998 and 1999. Reaches in the intermittent sections consisted of stagnant pools separated by long dry stretches.

© 2004 NRC Canada

Fig. 1. Network of streams in the James River drainage, Craig County, Virginia, USA, that was sampled (solid lines) during the mark–recapture study in 1999. The unsampled section (unfilled line) of stream that was not contiguous with Johns Creek coincided with a series of beaver ponds that were too deep to sample effectively. Two bidirectional fish traps (×) were operated daily between 26 May and 19 August. With the exception of White Branch, the upstream boundaries of the study streams were bounded by impoundments and a small farm pond (shaded polygons). Abbreviations: U., upper; L., lower; Cr., Creek; Br., Branch. Mark reaches are not shown but were distributed throughout the study area upstream of the beaver dams.

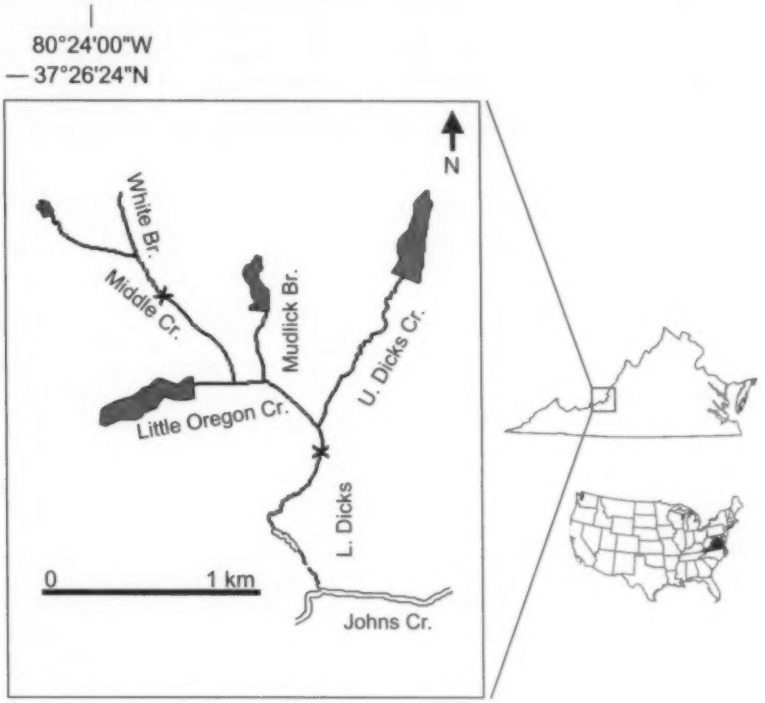

Over 20 native fish species have been recorded from the study area (Albanese 2001). We selected focal species based on their suitability for marking (see Albanese (2001) for mark–retention data), the likelihood that they would provide sufficient sample sizes for analyses, and their ability to represent the ecological diversity of fish assemblages in eastern North America. Collectively, our focal species represented considerable variation in taxonomic and ecological characteristics (Table 1). In general, species were associated either with habitats in the upstream reaches of smaller tributary streams (mountain redbelly dace (*Phoxinus oreas*) and blacknose dace (*Rhinichthys atratulus*)) or with habitats in the mainstem creek and downstream reaches of tributary streams (fallfish (*Semotilus corporalis*), common shiner (*Luxilus cornutus*), margined madtom (*Noturus insignis*), and Blue Ridge sculpin (*Cottus caeruleomentum*)). There were two notable exceptions to this pattern. *Nocomis leptocephalus* (bluehead chub) is a habitat generalist that was abundant throughout the entire study area, and *Thoburnia rhothoeca* (torrent sucker) was only abundant in high-gradient, bedrock-dominated reaches that occurred in limited portions of Middle Creek and the two mainstem creeks.

Mark–recapture study

The study area was divided into 88 reaches averaging 49 m (standard deviation (SD) = 14) in length. Reach boundaries coincided with prominent hydraulic features (e.g., pool–riffle boundary, tributary confluence), and each reach contained riffle, run, and pool habitats. This design allowed us to compare movements among reaches of similar length and ensure that small-scale movements within a single habitat unit did not influence analyses.

To ensure that mark reaches were distributed across the full range of habitat diversity within the stream network, the study area was divided into 12 contiguous sections, and one to two mark reaches were randomly selected from each. Focal species were marked in 15 mark reaches that were sampled by electrofishing (three passes per reach) during a 3-week period in May–June 1999. To maximize sampling efficiency across reaches, sampling was restricted to baseflow conditions, and 6.4-mm-mesh block nets were set at upstream and downstream boundaries of each reach. All *S. corporalis*, *N. leptocephalus*, and *T. rhothoeca* ≥60 mm total length (TL) and all *R. atratulus* ≥45 mm TL were given reach-specific batch marks (photonic tags; New West Technologies, Inc., Santa Rosa, Calif.); *N. leptocephalus* and *T. rhothoeca* ≥80 mm TL and *S. corporalis* ≥100 mm TL were also individually marked with passive integrated transponder (PIT) tags (Biomark, Inc., Boise, Idaho). Marking of additional species and selection of additional mark reaches was constrained by the availability of marking techniques and field-processing time. The entire network of streams

© 2004 NRC Canada

Table 1. Taxonomic and ecological characteristics of focal species.

Species	Body size (mm SL)	Family	Rep. season	Rep. behavior	Vertical position
Phoxinus oreas	40–55	Cyprinidae	April–July	Broadcaster[a]	Water column
Rhinichthys atratulus	40–70	Cyprinidae	April–July	Broadcaster[b]	Benthic
Semotilus corporalis	150–300	Cyprinidae	April–May	Pit-ridge nest builder	Water column
Nocomis leptocephalus	70–160	Cyprinidae	May–July	Mound nest builder	Water column
Luxilus cornutus	65–100	Cyprinidae	May–June	Pit nest builder[c]	Water column
Thoburnia rhothoeca	85–150	Catostomidae	March–May	Broadcaster[d]	Benthic
Noturus insignis	90–120	Ictaluridae	May–June	Cavity nester[e]	Benthic
Cottus caeruleomentum	50–80	Cottidae	March–April	Cavity nester[e]	Benthic

Note: Information is from Jenkins and Burkhead (1993), Johnston and Page (1992), and our own observations. Body size is the typical size range of adults. Rep., reproductive; SL, standard length.

[a]Eggs are broadcasted over gravel nests built by other cyprinids.
[b]May spawn as a simple lithophil or over nests built by other species.
[c]Pits may be located on top of nests built by other cyprinids.
[d]Little is known about the reproductive behavior of this species.
[e]Exhibits postspawning parental care.

(i.e., all 88 reaches) was electrofished (two passes per reach) for recaptures during a 3-week period in August 1999. To minimize variation in the time available for fish to move from different mark reaches, we sampled reaches in approximately the same order during mark and recapture sampling.

A similar, but less extensive, study was conducted over the same period in 1998. Fishes were marked in 11 reaches, but lower and upper Dicks Creek, White Branch, and the section of Middle Creek upstream of the White Branch confluence were not sampled for recaptures. Mark reaches were distributed in Little Oregon Creek, Middle Creek, and Mudlick Branch during both years; additional reaches in lower and upper Dicks Creek were selected for marking during 1999. More information about study design can be found in Albanese et al. (2003) and Albanese (2001).

Reach-specific correlates of movement

Factors associated with an individual fish leaving its mark reach were identified using logistic regression, which models a binary response variable (e.g., staying or leaving) as a function of independent variables. Each fish recaptured during August was classified according to the response variable. Fishes captured in their original mark reach or an adjacent reach were categorized as non-movers and were represented by a zero in the data set. Fishes that moved beyond adjacent reaches (a movement of at least 50 m) were considered movers and were represented by a one in the data set. This conservative definition of movement allowed us to emphasize longer-distance movements between reaches rather than shorter, possibly temporary movements.

Six predictor variables representing a broad range of habitat characteristics were evaluated in models. Raw data for habitat variables were collected in each mark reach during transect-based surveys in June 1998 and June 1999. Within each year, all reaches were sampled within a 7-day period under baseflow conditions. Transects were spaced three mean-stream-widths apart and depth, current velocity, and dominant substrata were measured every 0.5 m along each transect (Simonson et al. 1994). Mean depth and mean current velocity were calculated over all sample points within the reach. Dominant substrata were visually classified into one of 10 categories: silt, sand, gravel, pebble, cobble, boulder, bedrock, vegetation, wood, and detritus. Depth, current velocity, and dominant substrata data were used to construct an index of habitat complexity (Angermeier and Schlosser 1989). This index was computed by dividing data for each variable into discrete categories (Table 2) and then calculating the Shannon diversity of three-dimensional category combinations for the entire reach (Brower et al. 1990).

Cross-sectional area was calculated for each transect by multiplying stream width by mean depth; cross-sectional area was then averaged across all transects within the reach to represent stream size. Cover included all submerged and overhanging logs that measured at least 10 cm in diameter and 1 m in length, along with debris dams and submerged root wads that measured at least 1 m in any dimension. To adjust for differences in cover related to variation in mark-reach length, the number of pieces of cover per metre of stream length was used in analyses. Finally, repeated surveys during the summers of 1998 and 1999 were used to classify the intermittency of each mark reach. Reaches that exhibited considerable or complete reductions in stream flow were coded as ones in the data set; reaches with perennial flow were coded as zeros.

Data were also available for three biotic variables and two variables that indicated the location of the mark reach within the stream network. Total length (hereafter body size) was measured at recapture because TL at marking was unknown for smaller individuals that were batch-marked. However, among PIT-tagged fishes, TL at recapture was strongly correlated with TL during marking (all Spearman's $r > 0.92$, all P values < 0.0001 for *S. corporalis*, *N. leptocephalus*, and *T. rhothoeca*). Focal species density (hereafter density) was measured as the number of fish/m^2 within the reach during marking. Distance from each reach to the nearest downstream confluence (distance to confluence) and distance from each reach to Little Oregon Creek (distance to mainstem) represented the position of each reach within the stream network. Reaches within Little Oregon Creek or lower Dicks Creek were 0 m from the mainstem.

Small sample size prevented us from conducting a simultaneous analysis on all 10 predictor variables, so we carried out best-subsets regression for each species. Because of the large number of recaptures of *N. leptocephalus* collected in

© 2004 NRC Canada

Table 2. Discrete categories for current velocity, depth, and substrata used to create the index of habitat complexity.

Categories	Current velocity ($cm \cdot s^{-1}$)	Depth (cm)	Dominant substrata
1	0–1	1–5	Silt, sand, or gravel
2	2–15	6–30	Pebble or cobble
3	>15	>30	Boulder or bedrock
4	NA	NA	Vegetation, wood, or detritus

Note: NA, not applicable.

1999 (n = 104), it was not necessary to utilize the 1998 data set for this species. Small sample sizes for *R. atratulus*, *S. corporalis*, and *T. rhothoeca* made it necessary to combine data from the 1998 and 1999 mark–recapture studies. Combined sample sizes were still relatively small (n = 48, 33, and 37, respectively) compared with the *N. leptocephalus* data set, and only a small number of predictor variables could be included in each model. We attempted to equalize the number of observations per predictor variable across all analyses to ensure comparable power. Thus, two-variable models were fit for *S. corporalis* and *T. rhothoeca*, a three-variable model was fit for *R. atratulus*, and a six-variable model was fit for *N. leptocephalus*.

All logistic regression analyses were carried out in SAS version 8.0 using Proc Logistic (SAS Institute Inc., Cary, N.C.). Model fit was assessed using the generalized coefficient of determination (R^2, rescaled to have a maximum value of one) and the proportion of accurately classified observations. We also examined Hosmer-Lemeshow goodness-of-fit tests, which never indicated a significant lack of fit (Wright 1995). If likelihood-ratio tests indicated that the overall model was significant at $\alpha = 0.05$, significance of the individual regression coefficients was evaluated at the same significance level. We also tested for year effects to ensure that it was appropriate to combine data across years for *R. atratulus*, *S. corporalis*, and *T. rhothoeca*. Because no year effects were detected, this variable was dropped from the analyses. The effect of multicollinearity on analyses was estimated by examining variance inflation factors and correlations among predictor variables. Correlations among predictor variables never exceeded 0.66, and variance inflation factors never exceeded 3.0.

Correlates of movement rates through weirs

Movement rates, the number of fish moving past a point in the stream per day, were measured in bidirectional fish traps (hereafter weirs). Weirs consisted of an upstream and downstream trap and v-shaped wings that led fishes into these traps. Traps and wings were covered with 6.4-mm-mesh plastic, and fishes entered traps through a clear plastic cylinder (diameter = 6.4 cm). Additional design specifications are given in Albanese (2001).

Weirs were set in lower Dicks Creek and Middle Creek between 26 May and 19 August 1999 (Fig. 1). These locations (a headwater and mainstem creek) were selected to broaden the range of physical conditions under which movement was measured; specific locations within these creeks were determined by their suitability for weir placement (i.e., gradually sloping banks and a bedrock-free substrate were required). Traps were checked each morning; captured fishes were identified, measured, and released in their direction of travel. Traps captured fishes from 20 to 360 mm TL, but fishes <45 mm TL were excluded from counts because most could easily pass through the weir mesh. Twenty-four-hour escapement trials for five species indicated that upstream traps retained a high percentage of captured fish (89% of 72 fishes tested), but downstream traps retained fewer fishes (61% of 67 fishes tested; Albanese 2001). Thus, we expected that our ability to detect relationships was better for the upstream movement data.

We collected data on four abiotic variables associated with captures in weirs: day length, increases in discharge (hereafter flow event), mean temperature, and stage. Crest gauges (Gordon et al. 1992) were checked each morning to measure water level to the nearest 0.5 cm (stage) and to determine if water levels had risen by 1 cm or more during the preceding 24 h (i.e., a flow event). Although crest gauges can be used to record the maximum water height during a sampling interval, flow event was recorded as a categorical variable (i.e., 0 = no flow event, 1 = flow event) because cork particles rarely formed discrete rings within gauges. Water temperatures were measured every 15 min in each trap using tidbit temperature loggers (Onset Computer Corporation, Bourne, Mass.); daily means were calculated over the same 24-h period that traps collected fishes (approximately 0900 to 0900). Day lengths were measured to the nearest one-hundredth of an hour and were obtained from sunrise–sunset times published for Newcastle, Craig County, Virginia (US Naval Observatory 2000).

Poisson regression models were used to explore relationships between the number of fish caught each day (a count) and the abiotic variables. Because observations were not temporally independent, an autoregressive parameter was used to adjust standard errors for regression coefficients (Littell et al. 1999). Autoregressive models correct for temporal autocorrelation and avoid the biases encountered when ordinary statistical techniques are applied to observations that are not independent (Carroll and Pearson 2000).

Models were built using the Proc Glimmix macro in SAS version 8.0 (Littell et al. 1999). Model fit was assessed by examining Akaike's information criterion, standardized residuals, and observed vs. predicted values (Burnham and Anderson 1998; Littell et al. 1999). Significance of the individual regression coefficients was evaluated at $\alpha = 0.05$. Significant relationships were often driven by 1 or 2 days with unusually high movement; we report only relationships that were still significant after these observations were removed. The effect of multicollinearity on analyses was estimated by examining variance inflation factors and correlations among predictor variables. None of the predictor variables was highly correlated ($r > 0.70$), and variance inflation factors never exceeded 1.9 at either trap.

Models were built for *R. atratulus*, *S. corporalis*, *N. leptocephalus*, and *T. rhothoeca* to complement information obtained from the mark–recapture study. *Phoxinus oreas* and *Luxilus cornutus* were also modeled because they exhibited wide variation in movement rates within Middle Creek and lower Dicks Creek, respectively. Models were built for

© 2004 NRC Canada

Table 3. Number of observations, coefficient of determination (R^2), proportion of accurately classified observations, and standardized regression coefficients for models predicting the probability that an individual fish emigrated from its mark reach between May and August.

Overall model or predictors	*Rhinichthys atratulus*	*Semotilus corporalis*	*Nocomis leptocephalus*	*Thoburnia rhothoeca*
Number of observations	48	33	104	37
Fit (R^2)	0.75	0.34	0.77	0.40
Classification (%)	88	73	85	78
Body size	0.82	0.48	1.02[a]	—
Cover	—	—	0.99[a]	–0.48
Density	0.44	—	—	—
Distance to confluence	—	—	—	—
Distance to mainstem	–6.16[a]	—	—	–1.10[b]
Habitat complexity	—	–1.29[a]	–1.37	—
Intermittency	—	—	6.05[c]	—
Mean current velocity	—	—	—	—
Mean depth	—	—	–0.72	—
Stream size	—	—	1.33[a]	—

Note: Models were fit for each species using best-subsets logistic regression. Predictor variables were measured in mark reaches (except body size) and are defined in the text; each predictor variable subjected to the best-subset procedure is listed in the table. To ensure comparable power across species, models for species with more observations included more variables. Relationships with cover and stream size did not appear meaningful when plotted. Blank entries indicate variables that were not selected in the best-subset model.

[a] $P < 0.05$.
[b] $P < 0.01$.
[c] $P < 0.0001$.

Noturus insignis and *Cottus caeruleomentum* to expand the taxonomic breadth of the analyses.

Correlates of distance moved

Relationships between distance moved and initial length and growth of individual fish were assessed using data from the 1999 mark–recapture study. Distance moved was calculated as the distance between mark-reach and recapture-reach midpoints. Relationships between distance moved and TL were assessed for *R. atratulus*, *S. corporalis*, *N. leptocephalus*, and *T. rhothoeca*.

We also examined relationships between distance moved and absolute growth in length for PIT-tagged fishes. Absolute growth in length was calculated using the formula from Busacker et al. (1990):

$$(1) \qquad \text{Absolute growth} = Y_2 - Y_1$$

where Y_1 and Y_2 refer to length measurements at marking and recapture, respectively. Distance moved, TL, and absolute growth in length were not Gaussian before or after transformation, so we calculated Spearman's coefficient of rank correlation (Sokal and Rohlf 1995). Because two hypotheses were examined for each species, significance was evaluated at a Bonferroni-adjusted critical value of 0.025 (0.05/2; Rice 1989).

Results

Reach-specific correlates of movement

In contrast to our predictions, cover, drought, habitat complexity, and body size did not appear to have a pervasive effect on movement. However, with the exception of cover, each of these factors did influence movement for a single species, and relationships were in the direction that we predicted. Cover was positively associated with movement for *N. leptocephalus* (Table 3), but this relationship did not appear meaningful when plotted. *Nocomis leptocephalus* was more likely to emigrate from intermittent reaches than perennial reaches (Table 3; Fig. 2), but depth was not a significant predictor of movement for any species. The probability of movement decreased with increasing habitat complexity for *S. corporalis* (Table 3; Fig. 2). Finally, larger *N. leptocephalus* were more likely to move than smaller *N. leptocephalus* (Table 3; Fig. 2).

Distance to mainstem was the only variable that was significant for more than one species. The probability of movement was negatively associated with distance to mainstem for *R. atratulus* and *T. rhothoeca* (Table 3; Fig. 2). The probability of movement was also positively associated with stream size for *N. leptocephalus* (Table 3), but this relationship did not appear meaningful when plotted.

Correlates of movement through weirs

In agreement with our prediction, floods had a pervasive effect on fish movement. The number of fish moving through upstream traps was positively associated with flow events for *P. oreas* in Middle Creek and *S. corporalis*, *N. leptocephalus*, *L. cornutus*, and *T. rhothoeca* in lower Dicks Creek (Table 4). A large number of *N. leptocephalus* ($n = 33$) also moved upstream through the Middle Creek trap during a flow event, but this relationship was not significant. The number of fish moving through the downstream trap in lower Dicks Creek was positively associated with flow events for *S. corporalis*, *N. leptocephalus*, and *L. cornutus*. For each species, relatively large numbers of fish were captured in traps during flow events (Table 5).

© 2004 NRC Canada

Fig. 2. Number of (*a*) *Rhinichthys atratulus*, (*b*) *Semotilus corporalis*, and (*c* and *d*) *Nocomis leptocephalus* that either stayed within (open bars) or moved from (solid bars) original mark reaches. All variables shown were significant in the logistic regression analyses. A significant negative relationship between the probability of movement and distance to mainstem was also detected for *Thoburnia rhothoeca* (not shown).

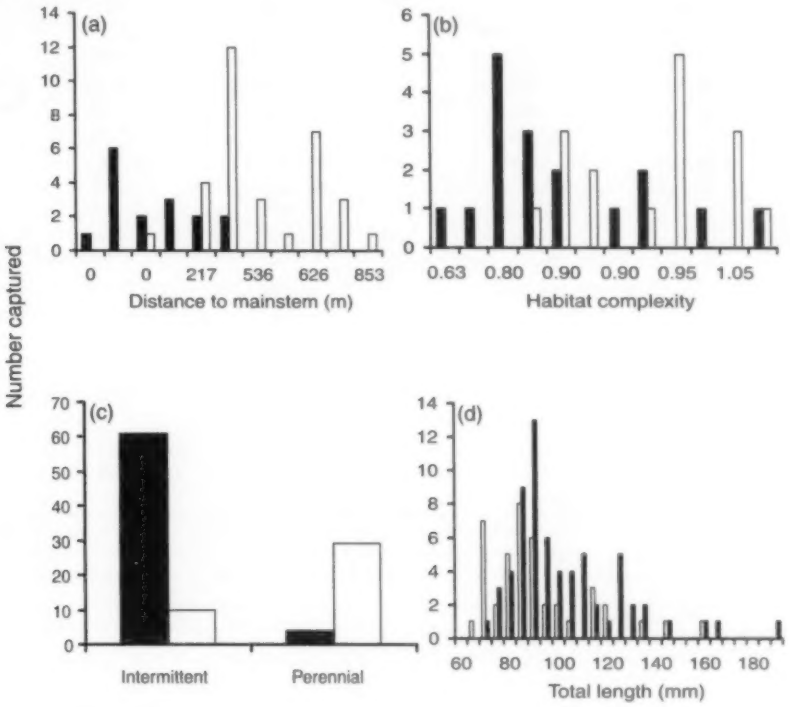

Two other variables were associated with movement through traps but did not affect as many species as flow events. The number of fish moving through upstream traps was positively associated with day length for *P. oreas* in Middle Creek and *S. corporalis* and *L. cornutus* in lower Dicks Creek (Table 4; Fig. 3). The number of *P. oreas* and *N. leptocephalus* moving through the upstream trap in Middle Creek was positively associated with temperature (Table 4; Fig. 3). Movement rates were never significantly associated with stage. The upstream model for *T. rhothoeca* in Middle Creek would converge only after removing stage from the data set. Convergence failure suggests that none of the variables measured (including stage) was related to movement rate in *T. rhothoeca*, and this interpretation was supported in scatterplots.

Correlates of distance moved

Distance moved was largely unrelated to measured variables. In contrast to our prediction, it was not correlated with body size in *R. atratulus* ($n = 39$, $r = 0.04$, $P = 0.803$), *S. corporalis* ($n = 37$, $r = -0.02$, $P = 0.917$), or *T. rhothoeca* ($n = 32$, $r = -0.05$, $P = 0.795$). Distance moved was weakly correlated with body size in *N. leptocephalus* ($n = 120$, $r = 0.19$, $P = 0.034$), but this relationship was not significant after Bonferroni adjustment of α. Distance moved was not correlated with absolute growth in length for *N. leptocephalus* ($n = 68$, $r = 0.05$, $P = 0.704$) or *T. rhothoeca* ($n = 29$, $r = 0.26$, $P = 0.167$). There was marginal evidence for a relationship between growth and distance moved for *S. corporalis* ($n = 26$, $r = 0.39$, $P = 0.049$), but this relationship was not significant after Bonferroni adjustment of α.

Overall, the number of factors influencing movement varied across species. The probability of emigrating from a reach was associated with more than a single factor only for *N. leptocephalus*, despite our efforts to ensure comparable power across analyses. The number of fish moving through weirs was associated with multiple factors for *P. oreas*, *S. corporalis*, *N. leptocephalus*, and *L. cornutus*. In contrast, the number of fish moving through weirs was only associated with a single factor for *T. rhothoeca* and with none of the factors measured for *R. atratulus*, *N. insignis*, and *C. caeruleomentum*.

Discussion

Reach-specific correlates of movement

The probability of leaving a reach presumably depends on relationships between fitness and reach-specific characteristics; characteristics that tend to decrease fitness relative to other reaches should promote emigration (Railsback et al. 1999; Gowan and Fausch 2002; Croft et al. 2003). Other studies have found that emigration from reaches increases when predators are present (Gilliam and Fraser 2001; Schaefer 2001), decreases (Aparicio and Sostoa 1999;

© 2004 NRC Canada

Table 4. Model fit (Akaike information criterion (AIC), smaller is better) and regression coefficients from autoregressive Poisson-regression models relating the number of fish moving through traps each day to four predictor variables.

Species	Stream	Direction	AIC	Day length	Flow	Stage	Temperature
Phoxinus oreas	Middle	Upstream	350	2.46[b]	0.94[b]	–0.09	0.29[b]
Phoxinus oreas	Middle	Downstream	376	0.03	–0.12	–0.27	–0.06
Rhinichthys atratulus	Middle	Upstream	376	–0.44	–0.38	0.23	0.05
Rhinichthys atratulus	Middle	Downstream	437	–2.40	0.72	–0.03	0.04
Nocomis leptocephalus	Middle	Upstream	349	1.67	1.29	–0.42	0.35[c]
Nocomis leptocephalus	Middle	Downstream	395	0.17	–1.14	–0.04	–0.11
Thoburnia rhothoeca	Middle	Upstream	366	0.41	0.40	—	0.05
Thoburnia rhothoeca	Middle	Downstream	542	0.03	0.43	0.28	0.05
Semotilus corporalis	Dicks	Upstream	383	2.55[a]	1.85[d]	0.22	0.22
Semotilus corporalis	Dicks	Downstream	429	–0.85	1.99[c]	0.14	–0.11
Nocomis leptocephalus	Dicks	Upstream	285	–0.65	1.33[d]	0.12	0.08
Nocomis leptocephalus	Dicks	Downstream	299	–0.58	0.88[b]	–0.00	–0.01
Luxilus cornutus	Dicks	Upstream	338	2.47[a]	0.79[b]	0.15	–0.16
Luxilus cornutus	Dicks	Downstream	369	1.66	0.97[b]	0.05	–0.21
Thoburnia rhothoeca	Dicks	Upstream	363	2.38	0.95[a]	0.04	0.00
Thoburnia rhothoeca	Dicks	Downstream	373	1.17	0.72	–0.08	–0.12
Noturus insignis	Dicks	Upstream	316	–0.88	–0.22	0.12	0.13
Noturus insignis	Dicks	Downstream	346	0.98	–0.10	0.13	0.07
Cottus caeruleomentum	Dicks	Upstream	323	–0.20	–0.00	0.11	0.15
Cottus caeruleomentum	Dicks	Downstream	594	–0.85	1.53	–0.48	0.59

Note: The autoregressive model allows estimation of regression coefficients when observations are not temporally independent. Upstream and downstream traps were operated between 26 May and 19 August 1999 in Middle Creek and Dicks Creek; separate models were built for each species × trap combination. The upstream model for *Thoburnia rhothoeca* in Middle Creek would not converge without removing the stage variable.

[a] $P < 0.05$.
[b] $P < 0.01$.
[c] $P < 0.001$.
[d] $P < 0.0001$.

Table 5. Mean and maximum (Max.) number of fish moving through traps during periods of elevated stream flow (flow event) and normal discharge (no flow event).

			Flow event		No flow event	
Species	Stream	Direction	Mean	Max.	Mean	Max.
Phoxinus oreas	Middle	Upstream	4.1	18	1.4	16
Semotilus corporalis	Dicks	Upstream	9.1	59	1.0	10
Nocomis leptocephalus	Dicks	Upstream	8.4	24	1.9	13
Luxilus cornutus	Dicks	Upstream	8.6	28	2.3	30
Thoburnia rhothoeca	Dicks	Upstream	1.8	6	0.4	5
Semotilus corporalis	Dicks	Downstream	1.8	14	0.2	2
Nocomis leptocephalus	Dicks	Downstream	4.4	21	1.6	13
Luxilus cornutus	Dicks	Downstream	10.2	34	2.4	45

Note: Poisson-regression analyses documented a positive relationship between flow events and the number of fish moving for each species listed in the table.

Harvey et al. 1999) or increases (Gilliam and Fraser 2001) when cover is present, and decreases with increasing current velocity (Schaefer 2001), depth (Aparicio and Sostoa 1999), and the length of riffle habitat adjacent to the reach (Lonzarich et al. 2000; Schaefer 2001). In this study, the probability of emigrating from a reach was related to the position of the reach within the drainage network, habitat complexity, reach intermittency, and body size.

The probability of movement for *R. atratulus* and *T. rhothoeca* decreased with increasing distance from the mainstem creek. Both species exhibit their highest densities in tributary reaches remote from the mainstem, which contained high-quality habitats for both of these species (Jenkins and Burkhead 1993). These results are thus consistent with habitat-use models that predict lower emigration rates from high-quality habitats (Winker et al. 1995).

Higher emigration rates from the mainstem may reflect its role as a movement corridor that transfers fishes to high-density reaches in tributaries (sensu Fraser et al. 1999). One *T. rhothoeca* that was originally marked in the mainstem during spring 1998 was recaptured in August 1999 over 1000 m away in the upper reaches of Middle Creek. Another *T. rhothoeca* made a 759-m movement from the mainstem creek into the upper reaches of Middle Creek during 1999. Similarly, one *R. atratulus* moved over 1000 m from the mainstem into Middle Creek during 1999.

© 2004 NRC Canada

Fig. 3. Number of (*a*) *Phoxinus oreas* and (*b*) *Luxilus cornutus* captured in the Middle Creek and lower Dicks Creek upstream traps, respectively. Both plots illustrate variables that were significant in the Poisson regression analyses. The number of fish moving through upstream traps was also positively related to temperature for *Nocomis leptocephalus* (Middle Creek, not shown) and to day length for *Phoxinus oreas* (Middle Creek, not shown) and *Semotilus corporalis* (Dicks Creek, not shown).

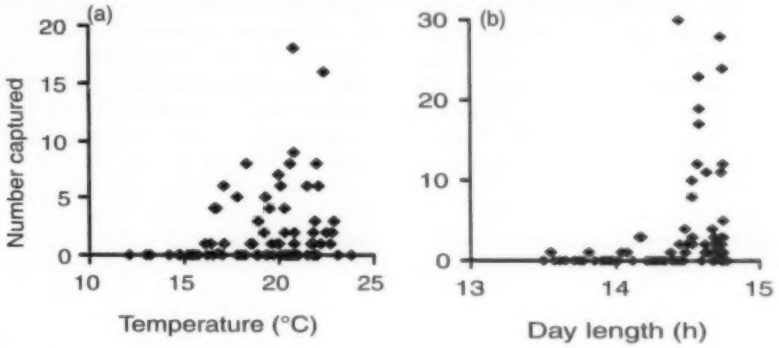

Small sample size (four species) and the lack of information on this variable from other studies preclude us from concluding that distance to mainstem has a pervasive effect on fish movement across species. Given longitudinal variation in habitat characteristics, however, this variable may influence the movement behavior of many species. We predict that longitudinal position within a stream ecosystem will be especially important for species that occupy spatially restricted habitats or in systems with a high degree of longitudinal heterogeneity in habitat characteristics.

The probability of movement decreased with increasing habitat complexity for *S. corporalis*. Gorman (1986) suggested that fishes in rivers with low habitat complexity are more mobile. At the reach scale, fishes living in complex habitats should be able to meet multiple resource needs within a small area. In this study, reaches with high habitat complexity contained runs, deep pools, and an abundance of cover. These sites likely provided *Semotilus corporalis* with foraging habitat and a refuge from drought and predators (Jenkins and Burkhead 1993). Although this variable clearly did not have a pervasive effect on fish movement in this study, we expect it to be important in systems with high between-reach variation in habitat complexity. For example, habitat complexity is likely to influence movement in systems where channelized reaches are contiguous with nonchannelized reaches.

Nocomis leptocephalus was more likely to emigrate from intermittent than perennial sections. Intermittency was a major component of habitat change during both summers and should exert strong selection pressures on movement behavior (Poff and Ward 1989). Many studies have shown high mortality rates for fishes that become isolated in stagnant pools (Larimore et al. 1959; Chapman and Kramer 1991; Matthews 1998), and we also found hundreds of dead fishes (including *N. leptocephalus*) within intermittent reaches. Thus, the relationship between intermittency and emigration seems important for increasing survival during drought conditions.

Notably, the relationship between intermittency and movement was based only on the movement patterns of surviving marked fish that were recaptured. The importance of this relationship may be overstated if nonemigrating *N. leptocephalus* die at higher rates than emigrants, which was clearly possible given the harsh physical conditions encountered within the intermittent reaches. However, we believe that differences in survival had a weak impact on the analysis for two reasons. First, the proportion of *N. leptocephalus* recaptured was slightly higher for fish marked in intermittent reaches than in perennial reaches (38.0% vs. 33.6%). If high emigration rates from intermittent reaches only reflected higher death rates among nonemigrants, then the overall proportion of fish recaptured from intermittent reaches should have been relatively low. Second, patterns for the other species indicate that it was possible to recapture a large proportion of nonemigrating fish within the intermittent reaches. For example, of 12 recaptured *R. atratulus* originally marked in an intermittent reach in Mudlick Creek, 10 were captured alive in that same reach during August. All five of the recaptured *S. corporalis* that were originally marked in an upper Dicks Creek reach were recaptured in that same reach during August. Although we do not believe that differential survival of movers and non-movers biased our analyses, it is an important assumption that should be addressed in future movement studies. This assumption will be especially important when factors affecting survival (i.e., predators, refugia, abiotic harshness) differ substantially between mark and recapture sites.

Drought did not appear to have a pervasive effect on fish movement in this study. Nonetheless, we expect that drought has an important but varied influence on fish movement patterns. For example, in contrast to *N. leptocephalus*, high site fidelity in intermittent reaches may be adaptive for species like *S. corporalis* that exploit deep refuge pools within intermittent reaches (Chapman and Kramer 1991; Fausch and Bramblett 1991). Other species may respond to drought by not immigrating into intermittent reaches. In accordance with this latter idea, *T. rhothoeca* was rarely collected in intermittent reaches before or after the drought (mean number per linear distance of stream = 0.015 fish·m^{-1} vs. 0.229 fish·m^{-1} in intermittent and perennial reaches during spring 1999, respectively; mean density per linear distance of stream = 0.001 fish·m^{-1} vs. 0.162 fish·m^{-1} in intermittent and perennial reaches during August 1999, respectively). Drought may thus interact with movement behavior to explain the absence

© 2004 NRC Canada

of regional species from local sites (Angermeier and Winston 1998).

Nocomis leptocephalus was the only species that exhibited a relationship between body size and the probability of emigrating from reaches. Skalski and Gilliam (2000) also found that the probability of movement increased with body size in *N. leptocephalus*, but only for slow-growing individuals. Among temperate freshwater fishes, larger species typically require larger home ranges to meet their resource needs (Minns 1995; Gowan and Fausch 1996). In addition, fishes may have to migrate to new habitats as they grow through different phases of their life cycle. Although body size did not have a pervasive effect on fish movement in this study, expanding the size range of fish marked in future studies will likely result in the detection of more patterns with body size. However, these relationships may not always be positive, as Hughes (2000) found for *Thymallus arcticus* (Arctic char).

Correlates of movement rates through weirs

Movement rates, measured as the number of fish moving upstream through weirs per day, also reflect factors that promote emigration from reaches. However, daily sampling permits analysis of factors that affect movement over finer temporal scales than are typically considered in mark–recapture studies. In addition, relationships are integrated over the entire population rather than in marked fishes alone. In this study, movement rates were associated with flow events, day length, and water temperature.

Five (*P. oreas*, *S. corporalis*, *N. leptocephalus*, *L. cornutus*, and *T. rhothoeca*) of the eight species studied increased their movement rates in association with flow events. Increases in stream flow clearly had a pervasive effect on fish movement in this study. Movement during high flow events may permit access to spawning and foraging habitats or may simply be a mechanism to locate refuge from the flood itself (Ross and Baker 1983; Matheny and Rabeni 1995; Schlosser 1995). In this study, fishes moving during high flow events could also access newly inundated reaches within the intermittent sections, escape from intermittent sections that became reconnected by flow, or circumvent natural barriers (e.g., steeply inclined bedrock slabs) to invade the upper reaches of Middle Creek (see Adams et al. 2000).

The positive relationship between day length and movement rates reflects a seasonal effect on movement for *P. oreas*, *S. corporalis*, and *L. cornutus*. Movement rates for these species were relatively high during June and early July. Dodson and Young (1977) also documented a relationship between day length and movement behaviors in laboratory-held *L. cornutus*. *Phoxinus oreas* and *L. cornutus* spawn over *N. leptocephalus* mound-nests in May and June, and movements by these species may allow them to access spawning habitats (Jenkins and Burkhead 1993). Weir captures by *S. corporalis* were dominated by a narrow size range of juvenile fish and likely reflected movements to rearing habitats. Many other studies have documented seasonal movements to spawning, rearing, and overwintering habitats (Hall 1972; Gatz and Adams 1994; Simpkins et al. 2000). As a surrogate for seasonality, day length may affect the movement patterns of many species. However, because fishes may respond to other seasonal cues (e.g., temperature, seasonal flows), we do not expect day length to be as pervasive as other factors that influence movement.

Stream temperature affected movement rates over a narrow range of temperatures and was a significant predictor of movement for only two species. Upstream movement rates in *N. leptocephalus* and *P. oreas* were positively associated with temperature in Middle Creek. Examination of scatterplots suggests a threshold effect where few or no fishes move at low temperatures but the number moving at higher temperatures is highly variable. Large numbers of *P. oreas* and *N. leptocephalus* did not begin moving until temperatures surpassed 15 °C in Middle Creek. After setting an additional weir in lower Dicks Creek during spring 2000, Albanese (2001) observed that *S. corporalis*, *N. insignis*, and *C. caeruleomentum* did not begin moving until water temperatures surpassed 13 °C. Similarly, Hall (1972) indicated that few fishes moved when water temperatures dropped below 7 °C in a North Carolina piedmont stream. Thus, temperature may be an important trigger of movement to spawning habitats during the spring or later in the year in spring-fed streams with relatively cool temperatures (e.g., Middle Creek). Because temperature has a strong effect on metabolism, increased movement during warming periods may also reflect increased foraging to meet higher energy demands (Gowan and Fausch 1996). Stream temperature did not have a pervasive effect on fish movement in this study. Although it may affect movement for many species, these effects are probably limited to transitional periods between cold and warm seasons.

Correlates of distance moved

After emigrating from a reach, the distance moved by an individual fish should depend on the distance to a suitable habitat. Longer distances presumably occur when suitable habitats are widely spaced (Wiens 2001). Suitability is determined in part by the physical habitat requirements of the species but may also be affected by factors such as competitor density, food availability, predation, and attributes of the individual fish (Gowan and Fausch 1996; Railsback et al. 1999; Ims and Hjermann 2001). In this study, no relationships were detected between distance moved and body size or growth. Skalski and Gilliam (2000) also did not find a relationship between distance moved and body size or growth for *N. leptocephalus*, *Semotilus atromaculatus* (creek chub), or *Clinostomus funduloides* (rosyside dace). Similarly, Smithson and Johnston (1999) did not find a relationship between body size and distance moved among four Ouachita highland stream fishes. Although the relationship between body size and distance moved may be strong for some species (e.g., Gatz and Adams 1994; Aparicio and Sostoa 1999), it is clearly not pervasive.

Given the multiplicity of factors that may determine when a fish immigrates to a reach, it is not surprising that distance moved is not a simple function of body size or growth. A major shortcoming of our and other studies is the inability to characterize the habitat suitability of potential immigration reaches — it is much easier to measure body size or growth than to measure attributes of all of the reaches that fishes could occupy. An a posteriori examination of the data for *N. leptocephalus* suggests that such an approach would nonetheless be fruitful. Most (61 of 74 = 82.4%) of the fish

© 2004 NRC Canada

marked in intermittent reaches were later captured in perennial reaches. These fish moved significantly longer distances than fish marked in perennial reaches (median = 240 vs. 0 m; $P < 0.0001$; Mann–Whitney test), presumably because they had to move through longer reaches of unsuitable habitat. Gilliam and Fraser (2001) also found that distance moved depends on attributes of reaches outside of marking locations: *Rivulus harti* (Hart's Rivulus) moved longer distances within a reach inhabited by a predator than within a reach where the predator was absent.

Implications for colonization and persistence

Movement has been associated with increases in stream flow for cyprinid, catostomid, ictalurid, gasterosteid, poeciliid, and centrarchid fishes (Chapman and Kramer 1991; Schlosser 1995; this study). Indeed, this factor has a pervasive influence on stream fish movement. In this study, maximum movement rates were documented for *P. oreas*, *S. corporalis*, *N. leptocephalus*, and *T. rhothoeca* during elevated flow. To put this in perspective, 64.2% of the *S. corporalis* captured during the 87-day trapping period moved during the 15 days with elevated flow; 30% were captured on a single day when flow was elevated.

The relationship between flow and movement has important implications for colonization and persistence. Given the large number of fishes moving during floods, this relationship may facilitate colonization or demographic rescue of isolated habitats. This may be especially important in systems affected by drought, and flow-mediated dispersers may be resilient to extirpation in regions subjected to increased intermittency associated with climate change or overappropriation of water for human uses (Poff et al. 2001). Flow-mediated dispersers may also be pre-adapted to escape erosive flooding conditions in channelized reaches, provided that refugia are still accessible. We caution, however, that flow-mediated dispersal may not always be adaptive in human-altered environments (Macdonald and Johnson 2001). Flow-mediated dispersers may be more vulnerable to extirpation in systems where dams block movement pathways or alter the natural flow regime. Because effects of hydrological alterations on the movement behavior of fishes are largely unknown, protecting and restoring natural flow regimes is the most prudent strategy for promoting colonization and persistence of fish populations (Poff et al. 1997).

Although flow was an important predictor of movement for the majority of species, other factors were clearly less pervasive and had a varied effect on fish movement. Interspecific variation in ecological correlates of movement also has important implications for colonization and persistence. For example, habitat homogenization should increase movement for species that exhibit high reach fidelity in complex habitats. These species may suffer population declines because of the cost of increased movement between suitable habitats that are widely spaced (Wiens 2001). Ultimately, they may be replaced by generalist invaders that find the homogeneous habitat suitable (Scott and Helfman 2001).

Another prediction is that species that move in association with a large number of correlates (presumed triggers) will be better colonists than species that do not. In this study, movement rates for *P. oreas* in Middle Creek were positively related to flow events, temperature, and day length. In contrast, movement rates for *T. rhothoeca* and *R. atratulus* in Middle Creek were not related to any of the factors measured. If a disturbance event extirpated populations of all three species in this stream, *P. oreas* would be a superior colonist because large numbers of individuals would immigrate during the next flow event or rise in temperature. Some disturbances may be accompanied by ecological changes in source areas, which should also accelerate colonization for species that move in association with multiple factors.

We identified seven ecological correlates of movement for an assemblage of stream fishes in Virginia. Our focus on three different attributes of movement permitted us to detect more relationships and provided a more complete understanding of movement than studies that examine only a single attribute of movement. Some factors (e.g., flow) clearly have a pervasive influence on fish movement, facilitating efforts to predict how fishes respond to environmental change. The importance of other factors varies among species, and such variation may translate into differences in persistence and colonization rates. Given the importance of movement to conservation and management, the relationship between ecological factors and different attributes of fish movement is an important area for future experimental and field research.

Acknowledgments

This project was supported in part by the Virginia Department of Game and Inland Fisheries and the US Army Corps of Engineers. The Raney Award from the American Society of Ichthyologists and Herpetologists provided funds to build the weirs. G. Galbreath, D. Harpole, K. MacQuarrie, D. Nuckols, M. Rogers, C. Roghair, and many volunteers assisted with fieldwork. A. Dolloff, C. Gowan, C. Haas, and D. Orth provided valuable comments on the manuscript. The use of trade names in this manuscript does not imply endorsement by the US government.

References

Albanese, B. 2001. Movement of fishes in a network of streams and implications for persistence. Ph.D. dissertation, Virginia Polytechnic and State University, Blacksburg, Va. [available online at http://etd.vt.edu].

Albanese, B., Angermeier, P.L., and Gowan, C. 2003. Designing mark–recapture studies to reduce effects of distance-weighting on movement distance distributions of stream fishes. Trans. Am. Fish. Soc. **132**: 925–939.

Adams, S.B., Frissel, C.A., and Reiman, B.E. 2000. Movements of nonnative brook trout in relation to stream channel slope. Trans. Am. Fish. Soc. **129**: 623–638.

Angermeier, P.L., and Schlosser, I.J. 1989. Species–area relationships for stream fishes. Ecology, **70**: 1450–1462.

Angermeier, P.L., and Winston, M.R. 1998. Local vs. regional influences on local diversity in stream fish communities of Virginia. Ecology, **79**: 911–927.

Aparicio, E., and de Sostoa, A. 1999. Pattern of movements of adult *Barbus haasi* in a small Mediterranean stream. J. Fish Biol. **55**: 1086–1095.

Brown, J.H., and Kodric-Brown, A. 1977. Turnover rates in insular biogeography: effect of immigration on extinction. Ecology, **58**: 445–449.

© 2004 NRC Canada

Brower, J.E., Zar, J.H., and von Ende, C.N. 1990. Field and laboratory methods for general ecology. 3rd ed. Wm. C. Brown Publishers, Dubuque, Ind.

Burnham, K.P., and Anderson, D.R. 1998. Model selection and inference: a practical information-theoretic approach. Springer-Verlag, New York.

Busacker, G.P., Adelman, I.R., and Goolish, E.M. 1990. Growth. *In* Methods for fish biology. *Edited by* C.B. Schreck and P.B. Moyle. American Fisheries Society, Bethesda, Md. pp. 363–382.

Carroll, S.S., and Pearson, D.L. 2000. Detecting and modeling spatial and temporal dependence in conservation biology. Conserv. Biol. **14**: 1893–1897.

Chapman, L.J., and Kramer, D.L. 1991. The consequences of flooding for the dispersal and fate of a poeciliid fish in an intermittent tropical stream. Oecologia, **87**: 299–306.

Croft, D.P., Albanese, B., Arrowsmith, B.J., Botham, M., Webster, M., and Krause, J. 2003. Sex-biased movement in the guppy (*Poecilia reticulata*). Oecologia, **137**: 62–68.

Dodson, J.J., and Young, J.C. 1977. Temperature and photoperiod regulation of rheotropic behavior in prespawning common shiners, *Notropis cornutus*. J. Fish. Res. Board Can. **34**: 341–346.

Fausch, K.D., and Bramblett, R.G. 1991. Disturbance and fish communities in intermittent tributaries of a western Great Plains river. Copeia, 1991: 659–674.

Fausch, K.D., Gowan, C., Richmond, D., and Riley, S.C. 1995. The role of dispersal in trout population response to habitat formed by large woody debris. Bull. Fr. Peche Piscis. **338**: 179–190.

Fausch, K.D., Torgersen, C.E., Baxter, C.V., and Li, H.W. 2002. Landscapes to riverscapes: bridging the gap between research and conservation of stream fishes. BioScience, **52**: 483–498.

Fraser, D.F., Gilliam, J.F., MacGowan, M.P., Arcaro, C.M., and Guillozet, P.H. 1999. Habitat quality in a hostile river corridor. Ecology, **80**: 597–607.

Gatz, A.J., Jr., and Adams, S.M. 1994. Patterns of movement of centrarchids in two warmwater streams in eastern Tennessee. Ecol. Freshw. Fish, **3**: 35–48.

Gilliam, J.F., and Fraser, D.F. 2001. Movement in corridors: enhancement by predation threat, disturbance, and habitat structure. Ecology, **82**: 258–273.

Gordon, N.D., McMahon, T.A., and Finlayson, B.L. 1992. Stream hydrology: an introduction for ecologists. John Wiley & Sons, Chichester, England.

Gorman, O.T. 1986. Assemblage organization of stream fishes: the effect of rivers on adventitious streams. Am. Nat. **128**: 611–616.

Gowan, C., and Fausch, K.D. 1996. Mobile brook trout in two high-elevation Colorado streams: re-evaluating the concept of restricted movement. Can. J. Fish. Aquat. Sci. **53**: 1370–1381.

Gowan, C., and Fausch, K.D. 2002. Why do foraging stream salmonids move during summer? Environ. Biol. Fishes, **64**: 139–153.

Gowan, C., Young, M.K., Fausch, K.D., and Riley, S.C. 1994. Restricted movement in resident stream salmonids: a paradigm lost? Can. J. Fish. Aquat. Sci. **51**: 2626–2637.

Hall, C.A.S. 1972. Migration and metabolism in a temperate stream ecosystem. Ecology, **53**: 585–604.

Harvey, B.C., Nakamoto, R.J., and White, J.L. 1999. Influence of large woody debris and a bankfull flood on movement of adult resident coastal cutthroat trout (*Oncorhynchus clarki*) during fall and winter. Can. J. Fish. Aquat. Sci. **56**: 2161–2166.

Heggenes, J., Northcote, T.G., and Peter, A. 1991. Spatial stability of cutthroat trout (*Oncorhynchus clarki*) in a small, coastal stream. Can. J. Fish. Aquat. Sci. **48**: 757–762.

Hughes, N.F. 2000. Testing the ability of habitat selection theory to predict interannual movement patterns of a drift-feeding salmonid. Ecol. Freshw. Fish, **9**: 4–8.

Ims, R.A., and Hjermann, D.O. 2001. Condition-dependent dispersal. *In* Dispersal. *Edited by* J. Clobert, E. Danchin, A.A. Dhondt, and J.D. Nichols. Oxford University Press, New York. pp. 203–216.

Jenkins, R.E., and Burkhead, N.M. 1993. Freshwater fishes of Virginia. American Fisheries Society, Bethesda, Md.

Johnston, C.E., and Page, L.M. 1992. The evolution of complex reproductive strategies in North American minnows. *In* Systematics, historical ecology and North American freshwater fishes. *Edited by* R.L. Mayden. Stanford University Press, Stanford, Calif. pp. 600–621.

Larimore, R.W., Childers, W.F., and Heckrotte, C. 1959. Destruction and re-establishment of stream fish and invertebrates affected by drought. Trans. Am. Fish. Soc. **88**: 261–285.

Littell, R.C., Milliken, G.A., Stroup, W.W., and Wolfinger, R.D. 1999. SAS system for mixed models. SAS Institute Inc., Cary, N.C.

Lonzarich, D.G., Lonzarich, M.R., and Warren, M.L., Jr. 2000. Effects of riffle length on the short-term movement of fishes among stream pools. Can. J. Fish. Aquat. Sci. **57**: 1508–1514.

Macdonald, D.W., and Johnson, D.D.P. 2001. Dispersal in theory and practice: consequences for conservation biology. *In* Dispersal. *Edited by* J. Clobert, E. Danchin, A.A. Dhondt, and J.D. Nichols. Oxford University Press, New York. pp. 358–372.

Magoulick, D.D. 2000. Spatial and temporal variation in fish assemblages of drying stream pools: the role of abiotic and biotic factors. Aquat. Ecol. **34**: 29–41.

Matheny, M.P., IV, and Rabeni, C.F. 1995. Patterns of movement and habitat use by northern hogsuckers in an Ozark stream. Trans. Am. Fish. Soc. **124**: 886–897.

Matthews, W.J. 1998. Patterns in freshwater fish ecology. Kluwer Academic Press, Norwell, Mass.

Meffe, G.K., and Sheldon, A.L. 1990. Post-defaunation recovery of fish assemblages in southeastern blackwater streams. Ecology, **71**: 657–667.

Minns, C.K. 1995. Allometry of home range size in lake and river fishes. Can. J. Fish. Aquat. Sci. **52**: 1499–1508.

Northcote, T.G. 1997. Potamodromy in Salmonidae — living and moving in the fast lane. N. Am. J. Fish. Manag. **17**: 1029–1045.

Peterson, J.T., and Bayley, P.B. 1993. Colonization rates of fishes in experimentally defaunated warmwater streams. Trans. Am. Fish. Soc. **122**: 199–207.

Poff, N.L., and Ward, J.V. 1989. Implications of streamflow variability and predictability for lotic community structure: a regional analysis of streamflow patterns. Can. J. Fish. Aquat. Sci. **46**: 1805–1818.

Poff, N.L., Allen, J.D., Bain, M.B., Karr, J.R., Prestegaard, K.L., Richter, B.D., Sparks, R.E., and Stromberg, J.C. 1997. The natural flow regime. BioScience, **47**: 769–784.

Poff, N.L., Angermeier, P.L., Cooper, S.D., Lake, P.S., Fausch, K.D., Winemiller, K.O., Mertes, L.A.K., Oswood, M.W., Reynolds, J., and Rahel, F.J. 2001. Fish diversity in streams and rivers. *In* Global biodiversity in a changing environment: scenarios for the 21st century. *Edited by* F.S. Chapin III, O.E. Sala, and E. Huber-Sannwald. Springer-Verlag, New York. pp. 315–349.

Pringle, C.M., Freeman, M.C., and Freeman, B.J. 2000. Regional effects of hydrologic alterations on riverine macrobiota in the new world: tropical–temperate comparisons. BioScience, **50**: 807–823.

Railsback, S.F., Lamberson, R.H., Harvey, B.C., and Duffy, W.E. 1999. Movement rules for individual-based models of stream fish. Ecol. Model. **123**: 73–89.

© 2004 NRC Canada

Rice, W.R. 1989. Analyzing tables of statistical tests. Evolution, **43**: 223–225.

Ross, S.T., and Baker, J.A. 1983. The response of fishes to periodic spring floods in a southeastern stream. Am. Midl. Nat. **109**: 1–14.

Schaefer, J. 2001. Riffles as barriers to interpool movement by three cyprinids (*Notropis boops*, *Campostoma anomalum* and *Cyprinella venusta*). Freshw. Biol. **46**: 379–388.

Schlosser, I.J. 1995. Dispersal, boundary processes, and trophic-level interactions in streams adjacent to beaver ponds. Ecology, **76**: 908–925.

Schlosser, I.J., and Angermeier, P.L. 1995. Spatial variation in demographic processes of lotic fishes: conceptual models, empirical evidence, and implications for conservation. *In* Evolution and the aquatic ecosystem: defining unique units in population conservation. *Edited by* J.L. Nielsen. Am. Fish. Soc. Symp. **17**: 392–401.

Scott, M.C., and Helfman, G.S. 2001. Native invasions, homogenization, and the mismeasure of integrity of fish assemblages. Fisheries, **26**(11): 6–15.

Simonson, T.D., Lyons, J., and Kanehl, P.D. 1994. Quantifying fish habitat in streams: transect spacing, sample size, and a proposed framework. N. Am. J. Fish. Manag. **14**: 607–615.

Simpkins, D.G., Hubert, W.A., and Wesche, T.A. 2000. Effects of fall-to-winter changes in habitat and frazil ice on the movements and habitat use of juvenile rainbow trout in a Wyoming tailwater. Trans. Am. Fish. Soc. **129**: 101–118

Skalski, G.T., and Gilliam, J.F. 2000. Modeling diffusive spread in a heterogeneous population: a movement study with stream fish. Ecology, **81**: 1685–1700.

Smithson, E.B., and Johnston, C.E. 1999. Movement patterns of stream fishes in a Ouachita Highlands stream: an examination of the restricted movement paradigm. Trans. Am. Fish. Soc. **128**: 847–853.

Sokal, R.R., and Rohlf, F.J. 1995. Biometry. 3rd. ed. W.H. Freeman Co., New York.

US Naval Observatory. 2000. Sunrise and sunset times. Available online at http://www.usno.navy.mil/.

Warren, M.L., Jr., and Pardew, M.G. 1998. Road crossings as barriers to small-stream fish movement. Trans. Am. Fish. Soc. **127**: 637–644.

Warren, M.L., Jr., Angermeier, P.L., Burr, B.M., and Haag, W.R. 1997. Declines of a diverse fish fauna: patterns of imperilment and protection in the southeastern United States. *In* Aquatic fauna in peril: the southeastern perspective. *Edited by* G.W. Benz and D.E. Collins. Lenz Design and Communications, Decatur, Ga. pp. 105–164.

Wiens, J.A. 2001. The landscape context of dispersal. *In* Dispersal. *Edited by* J. Clobert, E. Danchin, A.A. Dhondt, and J.D. Nichols. Oxford University Press, New York. pp. 97–109.

Winker, K., Rappole, J.H., and Ramos, M.A. 1995. The use of movement data as an assay of habitat quality. Oecologia, **101**: 211–216.

Wright, R.E. 1995. Logistic regression. *In* Reading and understanding multivariate statistics. *Edited by* L.G. Grimm and P.R. Yarnold. American Psychological Association, Washington, D.C. pp. 217–244.

© 2004 NRC Canada

Abundance of minke whales (*Balaenoptera acutorostrata*) in the Northeast Atlantic: variability in time and space

Hans J. Skaug, Nils Øien, Tore Schweder, and Gjermund Bøthun

Abstract: Regional sighting surveys with two independent observers on each vessel were conducted each year from 1996 to 2001. Northern minke whales (*Balaenoptera acutorostrata*) are mostly solitary animals and are only available for observation at moments when they surface to breath. Thus, a stochastic point process model is developed for how the data are generated. The hazard probability of initially sighting a whale that surfaces depends on relative spatial coordinates and on other covariates. The parameters of the model are estimated by maximum likelihood. To account for interannual variation in spatial distribution of minke whales, a random effects model is developed and estimated by comparing current and past (1989 and 1995) survey data. A simulation approach is taken to remove bias from parameter estimates and to assess the uncertainty in the results. For total abundance, the result is a log-normal confidence distribution with quantiles $107\,205 \cdot \exp(0.137z)$, i.e., an abundance estimate of 107 205 with a coefficient of variation of ≈0.14. Together with these and earlier survey data, past data on catch, mark–recapture, and satellite tracking are reviewed to elucidate distribution and migration patterns in Northeastern Atlantic minke whales.

Résumé : Chaque année, de 1996 à 2001, il y a eu des inventaires visuels régionaux avec deux observateurs indépendants à bord de chaque navire. Les petits rorquals (*Balaenoptera acutorostrata*) sont généralement des animaux solitaires et ils ne sont visibles que lorsqu'ils remontent à la surface pour respirer. C'est pourquoi nous avons mis au point un modèle de processus ponctuel stochastique pour étudier comment les données sont générées. La probabilité de hasard de percevoir initialement un rorqual quand il refait surface dépend de coordonnées spatiales relatives et d'autres covariables. Les paramètres du modèle sont estimés par une méthode de vraisemblance maximale. Un modèle à effets aléatoires estimé par la comparaison des données d'inventaire actuelles et passées (1989 et 1995) permet de tenir compte de la variation d'une année à l'autre de la répartition des rorquals. L'abondance totale obtenue est une distribution de confiance log-normale avec les quantiles $107\,205 \cdot \exp(0{,}137z)$, soit une estimation d'abondance de 107 205 avec un coefficient de variation de ≈0,14. Un revue de ces données d'inventaire et de celles du passé, des données du passé sur les pêches et des données de surveillance par satellite nous a servi à élucider les patterns de répartition et de migration des petits rorquals du nord-est de l'Atlantique.

[Traduit par la Rédaction]

Introduction

Minke whales (*Balaenoptera acutorostrata*) are found throughout the North Atlantic, although their main distribution is thought to be over continental shelf areas, particularly at its edge. They undertake feeding migrations northwards in the spring and then enter areas of the Northeast Atlantic (Fig. 1). Their winter distribution in the North Atlantic is poorly known as there are few sighting records from that time of the year. Wintering minke whales in the North Atlantic have been reported from the northern coasts, from the Gulf of Mexico, and from south of Bermuda (Horwood 1990).

Exploitation of minke whales in the Northeast Atlantic by Norwegian fishermen escalated in the 1920s and reached its peak in the 1950s with a yearly catch of some 3500 animals (International Whaling Commission 1992). From 1959, the exploitation declined because of harvest regulations and came to a halt in 1987. In 1993, commercial minke whaling was started up again under Norwegian regulation based on the Revised Management Procedure developed by the IWC (International Whaling Commission). The yearly catch has been some 500 animals in the recent decennium. The abundance of minke whales feeding in the North Atlantic, and its temporal and spatial distribution, is of interest not only for whaling management, but also for fisheries management and ecological studies.

The first attempt to estimate the abundance of minke whales in the Northeast Atlantic was based on catch–effort data and yielded an estimate of about 30 000 minke whales (Ugland 1976). Based on two recaptures from 15 minke

Received 31 March 2003. Accepted 24 January 2004. Published on the NRC Research Press Web site at http://cjfas.nrc.ca on 23 July 2004.
J17437

H.J. Skaug, N. Øien, and G. Bøthun. Institute of Marine Research, Box 1870 Nordnes, 5817 Bergen, Norway.
T. Schweder. Department of Economics, University of Oslo, Box 1095 Blindern, 0317 Oslo, Norway.

[1]Corresponding author (e-mail: skaug@imr.no).

 doi: 10.1139/F04-020 © 2004 NRC Canada

Fig. 1. The Northeast Atlantic split into survey regions with synoptic coverage in single years. These regions coincide with the five small areas of the International Whaling Commission (delimited by blue, solid lines): CM, EB, EC, EN, and ES, except for EB which was covered during three different years (see blue, broken, thin line). The ice edge was read from ice charts (Norwegian Meteorological Institute) for mid-July for the year when the adjacent survey blocks were covered.

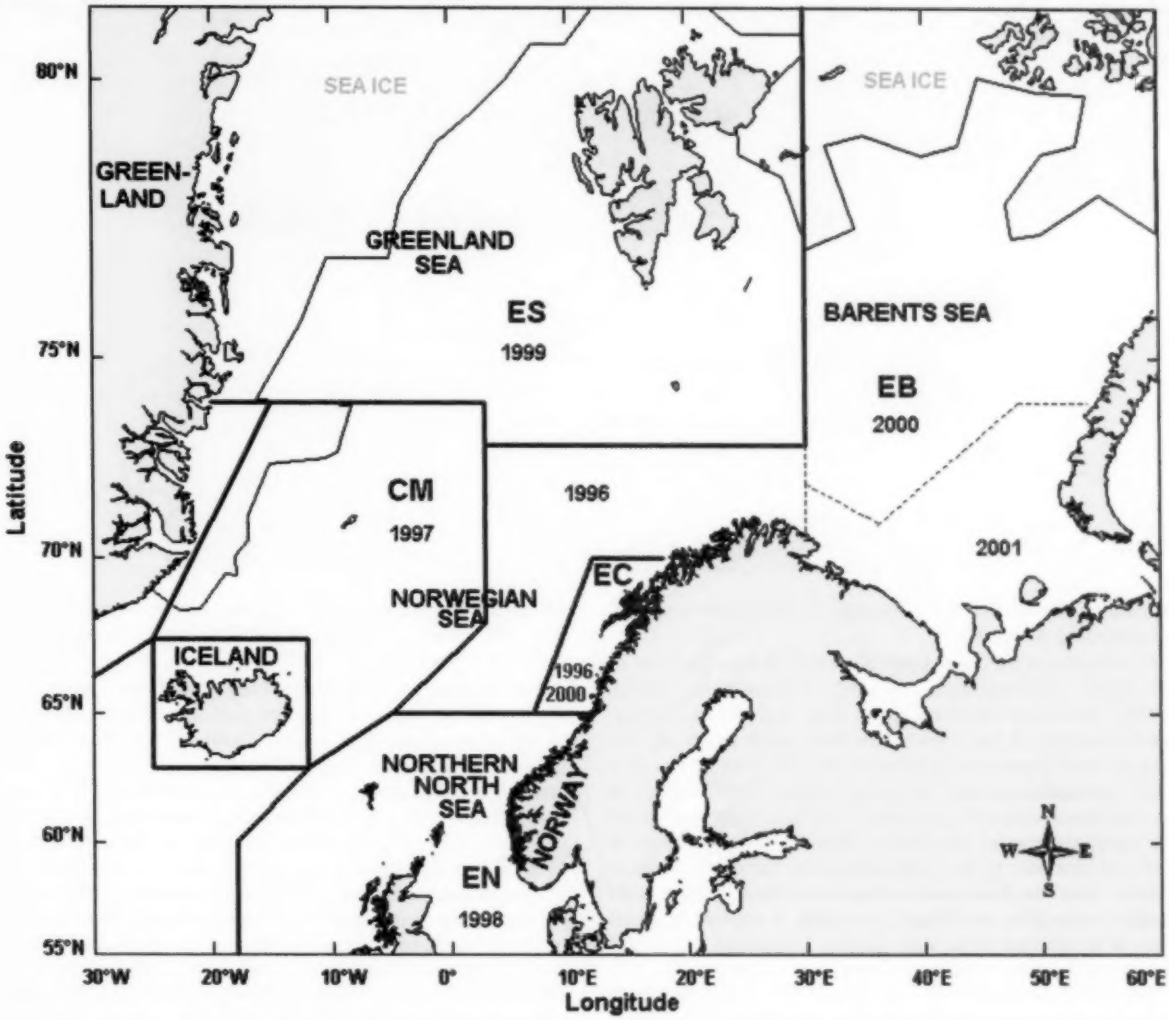

whales marked in 1964 and 1965, Ugland (1976) obtained an independent estimate of 40 700 animals. Over the period 1974–1978, a total of 333 minke whales were tagged in the Barents Sea, and from recaptures of these tags, Christensen and Rørvik (1981) obtained an estimate of 113 000 animals. Of these, the number of whales recruited to the areas north of 70°N was estimated to be 55 000. Based on the same marking experiment, but with more years of recaptures, Beddington et al. (1984) found point estimates of the Northeast Atlantic stock of minke whales from 81 500 to 121 000 animals based on multiyear recaptures and 66 000 based on next-year recaptures only. The IWC concluded in 1983 that the multiyear recapture estimates should be discarded and, therefore, that a best estimate for the total stock should be 60 000 animals.

Schweder et al. (1997) presented two independent abundance estimates of Northeast Atlantic minke whales: one based on a combination of data from shipborne sighting surveys (Fig. 2) conducted in 1988 and 1989 and the other based on a double-platform shipborne survey carried out in 1995. Here, we present an abundance estimate based on a series of regional sighting surveys conducted in the period from 1996 to 2001.

The abundance estimates presented in this paper came about in the context of regulating the harvest of minke whales in the North Atlantic. The Norwegian reservation against the moratorium on commercial whaling decided by IWC in 1982 makes the Norwegian minke whaling legal under international law. In 1982, IWC also requested its Scientific Committee to develop a management procedure for commercial harvesting of baleen whales. This work was basically completed in 1991 with a proposed Revised Management Procedure (RMP). The Commission has still not implemented any scheme for commercial whaling (http://www.iwcoffice.org), but its Scientific

© 2004 NRC Canada

Fig. 2. Double-platform shipborne sighting surveys. Observer platform A is placed in the barrel as shown, and observer platform B (not shown) is placed at the wheelhouse roof. The depicted scenario involves a single whale making three surfacings, which are all detected by platform A. Platform B sees only the last surfacing. Thus, A1 is the initial sighting of the whale, whereas A3 and B1 form a duplicate sighting, as indicated by the broken line. Because of measurement error in distance and sighting angle, the recorded relative positions of A3 and B1 differ. In the statistical analysis, the second and third surfacings form Bernoulli trials for platform B. (Artist: Åsa Gan Schweder.)

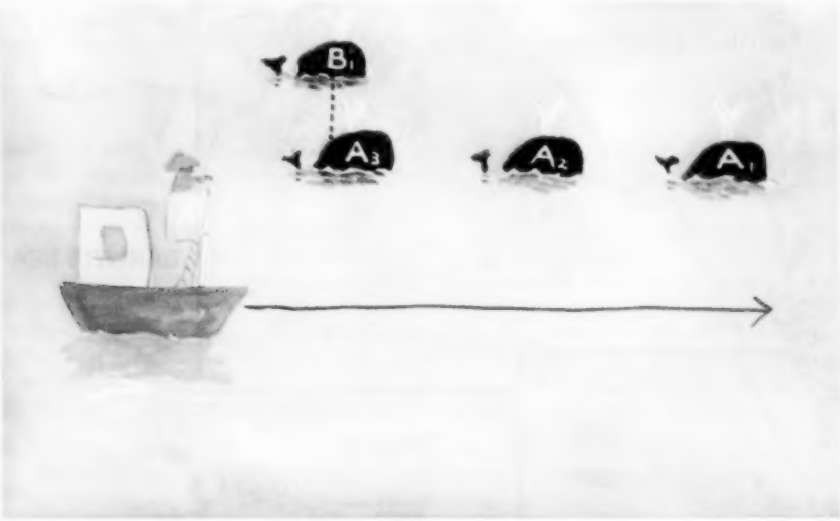

Committee assures that the Norwegian management is carried out according to the RMP.

A semi-Bayesian catch limit algorithm forms the core of the RMP (International Whaling Commission 1994*a*, 1994*b*). Based on historical catch data and absolute abundance estimates of the stock in question, catch limits are calculated via a posterior distribution for the parameters of a crude production model. To guard against uncertainties in the abundance estimates that might not have been accounted for, standard errors of abundance estimates are quadrupled in these calculations. In the implementation, the ocean basin is divided into medium-sized areas and then further into smaller areas. The catch limit algorithm is applied to small areas or to medium areas with catches distributed over small areas in proportion to current abundance estimates. The latter method is called catch cascading. The RMP is robust against a wide range of uncertainties concerning stock structure and status of the stock (Cooke 1999; Butterworth and Punt 1999).

In the current RMP implementation, the North Atlantic is split into three medium areas: west, central, and east. Whaling is carried out in the small area CM (Fig. 1) of the central medium area and in the four eastern small areas (Fig. 1). For the eastern small areas, catch cascading is applied. This implementation was put in place in 1996 and was thoroughly reviewed in 2003 by the Scientific Committee. The implementation review centred on stock structure and area divisions and on the abundance estimates presented here (International Whaling Commission 2004, Annex D). The implementation was essentially upheld.

The estimates presented here are slight modifications of those in Skaug et al. (2002). These modifications result from the inclusion of additional data on surfacing rates in northern minke whales and also from some minor changes in methodology. We present an abundance estimate for each of five IWC small areas (Fig. 1), in addition to an estimate for the total survey area.

The surveys in 1996 to 2001 are visual line transect surveys with independent observer platforms. Northeast Atlantic minke whales are mostly solitary on their feeding grounds in the north (Øien 1989; Sigurjonsson et al. 1989) and are only observed in the short moments (ca. 2 s) when they surface to breath between their dives (mean diving time ca. 80 s). They are therefore regarded as showing discrete availability in the visual survey, i.e., they are observed only at discrete points in time. Following Schweder (1974, 1977), we model the sighting process as a stochastic point process in space, representing the locations of the individual whales, and in time, representing the surfacings of the whale, and a sequence of Bernoulli experiments representing whether the animal was observed or not at the given surfacing. The success probability of these Bernoulli experiments is called the hazard probability as it is the conditional probability of sighting given that the observer previously was unaware of the animal. The hazard probability depends not only on the position of the whale relative to the observer, but also on other variables such as the sea state (Beaufort), visibility, glare, etc. Buckland et al. (2001) present "standard" line transect methodology and its history, with emphasis on the detection function $g(x)$, defined as the probability of detecting an animal located at perpendicular distance x from the transect line. A basic assumption for standard line transect methods is that $g(0) = 1$, i.e., all animals located on the transect line are detected.

As the result of discrete availability, $g(0) < 1$ in visual line transecting of Northeast Atlantic minke whales. To estimate $g(0)$ and the effective strip half-width, the surveys are conducted with independent observers. The observers are placed

© 2004 NRC Canada

Fig. 3. Survey block definitions (red lines), transect lines (black lines), and minke whale (*Balaenoptera acutorostrata*) sightings (black diamonds) made while on primary search effort.

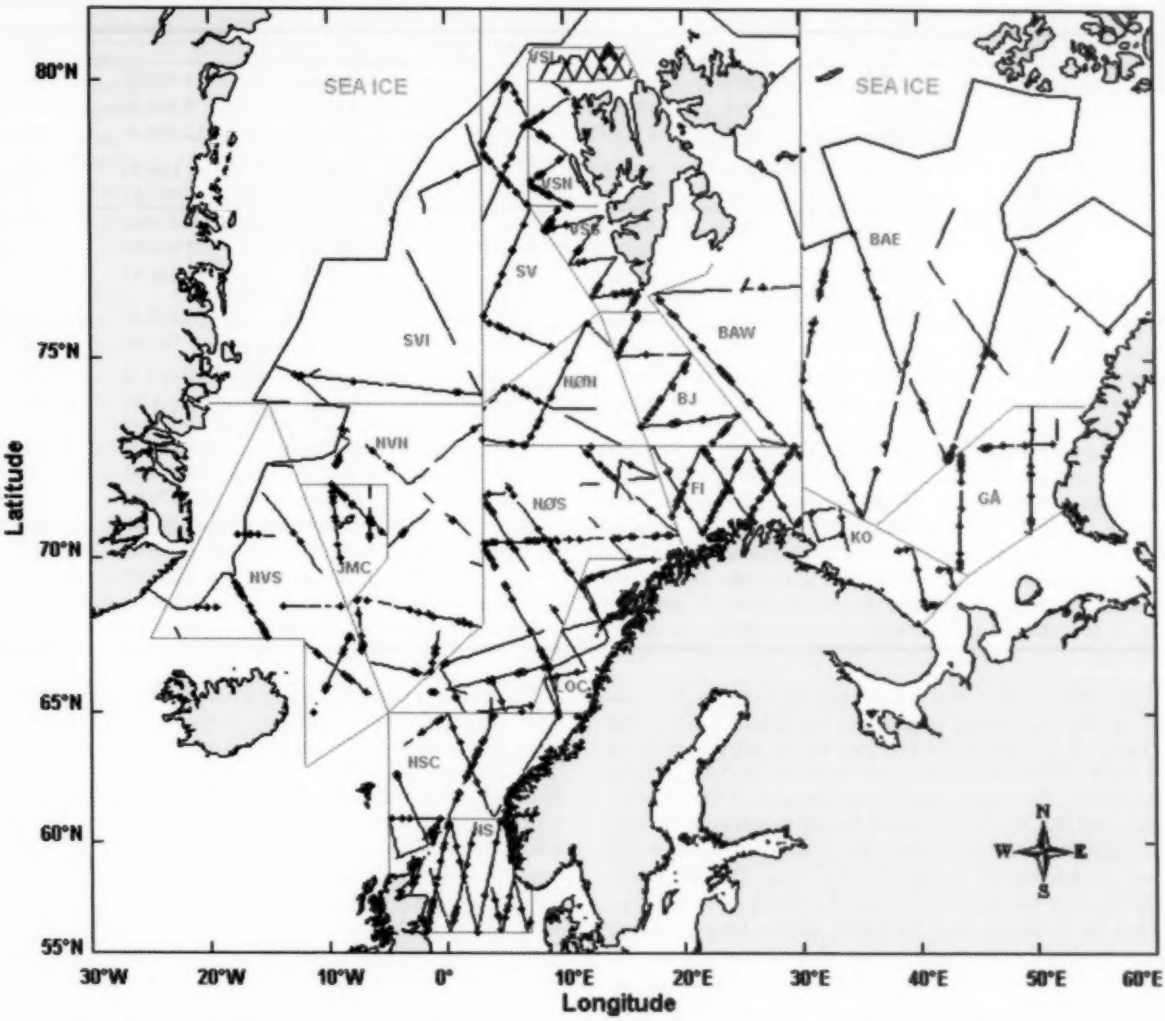

on separate platforms without audible or visual contact. Butterworth et al. (1982) were the first to realize that data from independent observers can be used to estimate effective strip half-width when $g(0) < 1$. Schweder and Høst (1992) were the first to apply hazard probability methods with independent observers in animal abundance estimation. Cooke (1997), Schweder et al. (1999), and Okamura et al. (2003), among others, have further developed the methodology.

Material and methods

Data collection 1996–2001

Surveys

During the period 1996–2001, the survey covered the Northeast Atlantic, i.e., the northern North Sea, the Norwegian Sea, the Greenland Sea, and the Barents Sea (Fig. 1). Although the North and Barents seas are shelf waters with typical average depths of about 100 m and 230 m, respectively, the Norwegian and Greenland seas are oceans with deep basins of several thousand metres. The eastern part of the Norwegian Sea was surveyed in 1996, the western Norwegian Sea in 1997, the North Sea in 1998, the Greenland Sea with adjacent shelf areas of Svalbard in 1999, and the Barents Sea in 2000 and 2001.

The total survey area was divided into blocks (see Fig. 3) based on feasibility surveys conducted in the 1980s and information extracted from catch data collected since 1938 when a licence system was introduced for Norwegian small-type whaling. Areas with assumed uniform densities were defined, also taking into consideration topographical and oceanographic features. The survey effort available within a specific block was divided between two transects to ensure at least one full coverage. Transects were constructed as zigzag tracks with a random starting point (Fig. 3). Realized track lengths in different survey blocks are provided (Table 1).

© 2004 NRC Canada

Table 1. Summary of survey results by survey block: survey region, survey block, area of survey block, survey year, transect length (L), total number of sightings ($n^{(A)} + n^{(B)}$), average total effective strip half-width ($w^{(A)} + w^{(B)}$), abundance estimate ($\hat{N}$) with associated estimate of standard deviation (SD).

Region	Block	Area (km^2)	Year	L (km)	$n^{(A)} + n^{(B)}$	$w^{(A)} + w^{(B)}$	$\hat{N}$	SD
CM	JMC	67 272	1997	615.77	38	468.35	4 432.05	921.23
	NVN	324 808	1997	1945.58	59	515.51	9 553.52	1789.07
	NVS	299 523	1997	1741.72	84	567.27	12 732.47	3426.41
EB	BAE	492 171	2000	3349.07	73	462.20	11 605.35	4887.62
	FI	94 145	1996	1658.91	120	503.59	6 761.67	1563.04
	GA	159 224	2001	1046.90	56	427.11	9 970.62	3730.05
	KO	94 034	2001	857.68	25	556.97	2 460.57	819.23
	NOS	394 260	1996	4167.66	125	453.52	13 036.93	2477.94
EC	LOC	93 839	1996	918.02	2	447.87	228.23	796.69
	LOC	93 839	2000	1074.67	10	492.18	887.06	860.98
EN	NS	259 502	1998	4032.07	146	401.10	11 713.39	3455.07
	NSC	308 918	1998	2560.35	43	419.65	6 181.51	1368.45
ES	BAW	123 082	1999	857.76	30	688.04	3 128.29	1516.23
	BJ	73 909	1999	907.22	43	917.53	1 908.97	403.40
	NON	88 141	1999	957.01	24	428.54	2 579.02	703.61
	SV	91 523	1999	967.74	59	593.68	4 699.40	1213.78
	SVI	189 072	1999	1130.84	10	432.69	1 932.07	1314.58
	VSI	8 665	1999	399.97	25	1193.38	226.93	140.33
	VSN	19 618	1999	466.39	43	587.25	1 540.04	304.38
	VSS	29 113	1999	710.94	63	597.52	2 158.87	859.82

The speed of the vessel was logged on a regular basis, as well as data on sighting conditions. The intended speed was 10 knots. In addition to the ordinary survey activity, distance and angle estimation experiments were conducted. In these experiments, the survey vessel was operated in the ordinary modus and the observers were instructed to estimate distance and angle to a stationary buoy, the exact position of which could be determined by the vessel's radar. Further details about the regional surveys are given by Skaug et al. (2002).

Data on surfacing rates for minke whales have been collected by VHF radio-tagging. The data used here are the same as those used in previous studies (Schweder et al. 1997). In addition, surfacing data from five minke whales were collected in 2001 and 2002. Most of the tagged whales were sampled in near-coastal waters within IWC small areas EC and ES. In addition, there is one whale from the North Sea (EN) and one whale from the Norwegian Sea (EB).

Observational routines

Observations of whales were made by naked eye from two platforms: platform A (a barrel placed 15 m above sea level; Fig. 2) and platform B (the wheelhouse roof), each manned by a team consisting of two observers. Each vessel had four such observer teams working 2-h shifts. With a few exceptions, the composition of teams did not change within a specific year. Most observers had experience from earlier surveys, and most had participated in all years (1996–2001). Within a team, one of the observers was instructed to scan the port 45° sector, while the other scanned the starboard 45° sector. Observers had side view, and sightings were also made outside the protocol sector. We retained sightings within the full 180° sector ahead.

The unit of observation was a track of observed surfacings, with estimated time and relative position (radial distance r and sighting angle θ (the angle between the sighting line and the track line)) recorded for every sighted surfacing. Radial distances were estimated visually, whereas sighting angles were measured using an angle board. Time was measured automatically when a button was pushed to allow the relative position to be recorded on a tape. A track represents the sighted surfacings judged by the observer to belong to the same whale. For a certain proportion of observations, the position was incompletely recorded, i.e., either r or θ was missing. This proportion was much lower for the initial sightings than for resightings. Because distance estimation is uncertain at long distances, only observations for which $r \leq 2000$ m were included in the analysis below. Further, because detection probabilities at short distances may vary substantially across platforms, observations for which $r \leq 100$ m were left out.

In addition to information directly related to sightings of whales, data on environmental conditions (weather conditions, visibility, glare, and Beaufort state; Table 2) were recorded. Certain levels of these covariates were combined to obtain a more parsimonious model (Table 2). Individual observers were grouped into three categories according to their ability to detect whales at long distances. This classification was based on the general impression that the cruise leaders had gained during the surveys and as little as possible on the actual data. On this basis, every combination of observers into teams that occurred in the survey was classified as either "long" or "short" according to their assumed ability to detect whales at long distance. In the analysis below, these two team categories were assigned a separate ρ_t parameter

© 2004 NRC Canada

Table 2. Covariates recorded on an hourly basis during the survey.

		Transformed covariate[a]		
Covariate	Description	Abbreviation	Levels	Definition
Platform	Platform indicator	P	A, B	
Weather	12 categories	W	W0, W1	W0, clear sky; W1, cloudy
Visibility	Numerical (metres)	V	High, low	High, larger than 3000 m
Glare	4 categories	G	G0, G1	G0, no glare; G1, glare
Beaufort	0–12 scale[b]	B	BI, BII, BIII	BI, 0–1; BII, 2; BIII, 3–4
Observer/team	Individual observer codes	T	Short, long	See Material and methods

[a]Transformed covariate indicates the aggregation of covariate levels used in the analysis.
[b]The survey effort used in the analysis only involves Beaufort states 0–4.

(see eq. 7 below). Our a priori belief was that $\rho_r^{long} > \rho_r^{short}$, although this constraint was not put on the model during parameter estimation. The proportion of realized effort time (sum over both platforms) with long teams was 60%.

Two teams were concurrently on watch. Neither team could be seen or heard by the other. Each team reported to the cruise leader but was not informed of sightings made by the other. The two teams were thus independent.

Statistical methodology 1996–2001

The first step in the analysis was to match tracks from the two platforms corresponding to the same whale. This matching was performed by an automatic routine mainly acting on recorded times. The parameters of the hazard probability function were then estimated by maximizing the likelihood of the observed data, disregarding matching errors and other complications. A bias-correction procedure was applied to the resulting parameter estimates to account for matching errors, measurement error in r and θ, etc. Finally, the effective search area was calculated from the estimated model, and abundance estimates were obtained by equating whale density in the whole survey stratum with observed whale density over the estimated effective search area.

The bias correction of parameter estimates was conducted by simulating the survey under realistic assumptions and for a sequence of parameter vectors. Simulations also provided standard errors on parameter estimates. Bias-corrected abundance estimates and coefficients of variation for each of the yearly surveys were also obtained from simulations, as were confidence distributions of abundance representing confidence intervals at arbitrary levels.

Finally, a combined abundance estimate for the Northeast Atlantic stock of minke whales was obtained from the sequence of yearly regional surveys. In addition to the sampling variability inherent in the regional surveys, there was a component of variation resulting from varying spatial minke whale distribution over the years 1996–2001, when the regional abundance estimates were combined to an abundance estimate for the entire stock. This additional variance was obtained by fitting a random effects model representing the changes in spatial distribution of the stock over the survey area and period.

Matching tracks

The likelihood function developed below was based on matched pairs of tracks supposedly representing the same whale seen from the two platforms and on single tracks without any match. Identification of matching tracks, and matching surfacings within tracks, was done by an automatic routine (Schweder et al. 1997), because it could be applied to numerous replicates of simulated survey data. Because it was based on a finite number of rules on observer behaviour, the automatic routine occasionally made mistakes that were easy for the human eye to spot. Because the same set of rules were used in the simulations, the problem did not occur for the simulated data. Thus, it was found necessary to augment the matching results for the real data with a small number of manually judged duplicates.

Each matched pair of tracks, such as that shown in Fig. 2, as well as each track without a match, was decomposed as follows. A combined initial sighting was the first observed surfacing of the whale. It was sighted by platform A, platform B, or both platforms simultaneously. For each combined initial sighting, there was an associated trinomial trial. The outcome of the trial was denoted by u, with different outcomes $u = A$ (seen from platform A only), $u = B$ (seen from platform B only), or $u = AB$ (seen from both platforms simultaneously).

Situations in which one platforms detected the whale before the other ($u = A$ or $u = B$) provided additional information on the conditional detection probability. Assume for simplicity that platform A detects the whale before platform B (Fig. 2), then each subsequent surfacing detected by A sets up a Bernoulli trial with outcomes seen or not seen by platform B. The initial sighting in the A track does not count as a Bernoulli trial as it is included as a trinomial trial. Trials were only registered until the first success for platform B occurs.

Hazard probability model

The starting point for the standard line transect theory (Buckland et al. 2001) is the detection function $g(x)$, defined as the probability that an animal located at perpendicular distance x from the transect line is detected. From an estimate of $g(x)$, one can obtain an estimate of the effective strip half-width:

$$(1) \qquad w = \int_0^\infty g(x)\,dx$$

which is the key parameter in the abundance estimation. For animals with discrete availability, it is possible to start the modelling at a more fundamental level, that is, we can model the probability of detecting individual surfacings.

Let the hazard probability function $Q(r, \theta)$ be defined as the probability of sighting a whale that makes a surfacing at position (r, θ), given that the observer is previously unaware

© 2004 NRC Canada

of the whale. The other component of the hazard probability model is the stochastic point process governing the availability of individual whales for detection, i.e., the surfacing process. As shown below, the surfacing process together with Q determine $g(x)$, and hence w, as well as the probability density for the position of the initial sighting of a whale.

Consider first a single observer platform with hazard probability function Q. The bivariate probability density of the position of an initial sighting is denoted by $f(r, \theta)$. It is simpler mathematically to work with Cartesian coordinates $(x, y) = (r\sin(\theta), r\cos(\theta))$ than with polar coordinates (r, θ). Here, y is the forward distance along the transect line. Under the assumption that dive times follow a Poisson point process with intensity α, it may be shown (Schweder et al. 1996) that

$$(2) \quad f(x,y) = w^{-1}\frac{\alpha}{v}Q(r_{x,y},\theta_{x,y})\exp\left\{-\frac{\alpha}{v}\int_y^\infty Q(r_{x,u},\theta_{x,u})\,du\right\}$$

where v is the vessel speed, $r_{x,y} = (x^2 + y^2)^{1/2}$, and $\theta_{x,y} = \arctan(x/y)$. Because

$$g(x) = w\int f(x,y)dy$$

(Buckland et al. 2001, p. 53), it follows that the detection function is given as

$$(3) \quad g(x) = 1 - \exp\left\{-\frac{\alpha}{v}\int_0^\infty Q(r_{x,y},\theta_{x,y})\,dy\right\}$$

When there are two independent observer platforms, A and B, with separate hazard probability functions Q^A and Q^B, then the hazard probability of the combined platform $A \cup B$ is

$$(4) \quad Q^{A\cup B}(r,\theta) = 1 - (1 - Q^A(r,\theta))(1 - Q^B(r,\theta))$$

Each whale sighted by $A \cup B$ sets up an experiment with trinomial outcome $u \in \{A, B, AB\}$, as explained above. Conditionally on the position (r, θ), the probability distribution of u is

$$(5) \quad q(u) = \{Q^{A\cup B}(r,\theta)\}^{-1}\cdot\begin{cases} Q^A(r,\theta)\{1 - Q^B(r,\theta)\}, & u = A \\ Q^B(r,\theta)\{1 - Q^A(r,\theta)\}, & u = B \\ Q^A(r,\theta)Q^B(r,\theta)\}, & u = AB \end{cases}$$

Assume that Q belongs to a parametric class of hazard probability functions. The contribution to the likelihood function coming from a matched pair of tracks (or a track without a match) may be decomposed as follows: the probability density (eq. 2) of the position of the initial sighting, the probability (eq. 5) in the trinomial experiment, and subsequent Bernoulli trials in situations where the initial sighting is made only by one platform ($u = A$ or $u = B$). These likelihood components are conditionally independent and hence are multiplied together. The likelihoods for different matched pairs or unmatched tracks are also independent.

A 15-point Gauss-Laguerre quadrature formula (Press et al. 1992, p. 151) is used to evaluate the integrals involved in eqs. 1, 2, and 3. The likelihood function is maximized using the optimization software AD Model Builder (Fournier 2001).

The following parametric class of hazard probability function is inherited from Schweder et al. (1997):

$$(6) \quad Q(r,\theta) = \mu Q_1(r)Q_2(\theta)$$

where $Q_1(r) = h(-\lambda_r(r - \rho_r))/h(\lambda_r\rho_r)$ and $Q_2(\theta) = h(-\lambda_\theta(\theta - \rho_\theta))/h(\lambda_\theta\rho_\theta)$ with $h(x) = \exp(x)/(\exp(x) + 1)$ being the logistic function. The basic parameters λ_r, ρ_r, λ_θ, ρ_θ, μ of the model have the following interpretations: μ is the hazard probability at the origin (where the observer is placed), ρ_r is the distance (in metres) at which the hazard probability has dropped to 50%, and λ_r is the steepness of the hazard probability curve at distance ρ_r. There parameters ρ_θ and λ_θ have the same interpretation as ρ_r and λ_r, respectively, but for sighting angle instead of distance.

The basic parameters are allowed to depend on covariates (see Table 2) through exponential and logistic link functions:

$$(7) \quad \rho_r = \exp(\eta_r)$$

$$\rho_\theta = \exp(\eta_\theta)$$

$$\mu = \exp(\eta_\mu)/\{1 + \exp(\eta_\mu)\}$$

where η_r, η_θ, and η_μ are linear predictors (linear combinations of covariate effects). To allow platforms A and B to have different hazard probability functions (Q^A and Q^B), the intercept term in the linear predictors may be platform-specific. The vector of all parameters in the model (λ_r, λ_θ, and the parameters associated with η_r, η_θ, and η_μ) is denoted by β.

Abundance estimation

For the purpose of abundance estimation, the subareas EN, EC, EN, EC, and CM are split into survey blocks (Fig. 3) believed to be homogeneous with whale density.

Changes in the values of covariates will cause w to vary along the transect line. Let the effective strip half-width at position l be denoted by $w(l)$ and the total survey length be denoted by L. The average effective strip half-width in the survey block is given as

$$(8) \quad \overline{w} = \frac{1}{L}\int_0^L w(l)\,dl$$

The abundance estimate $\hat{N}$ for the survey block is obtained by equating whale density in the survey block with observed whale density over the effective search area:

$$(9) \quad \hat{N} = \frac{n^{(A)} + n^{(B)}}{2L(\overline{w}^{(A)} + \overline{w}^{(B)})}\text{AREA}$$

where $n^{(A)}$ and $n^{(B)}$ are the total number of sighted whales for platform A and B, respectively, L is total transect length, $\overline{w}^{(A)}$ and $\overline{w}^{(B)}$ are platform-specific averages of w, and AREA is the area of the survey block. Note that a common hazard probability model is fitted for all survey blocks. This causes estimates of $\overline{w}$, and hence $\hat{N}$, from different survey blocks to be correlated.

Simulation model

The presence of measurement errors in the spatial and temporal data (related to observed surfacings), matching errors, spatial clustering of whales, and other difficulties have made it impossible for us to obtain unbiased estimates and valid standard errors without recourse to simulation. Models for these various components of the data-generating process have been estimated, as detailed below, and combine to a more realistic model for the surveys. An implementation of

© 2004 NRC Canada

this model as a computer program is used to simulate artificial data in the same format as collected in the surveys.

The program simulates a virtual sighting vessel with two independent observer platforms moving through an "ocean" of predistributed whales. The virtual whales are available for detection at discrete time points determined by dive time series obtained from radio-tagged minke whales. Each surfacing that an individual makes is detected by the observers according to the hazard probability $Q(r, \theta)$. The spatial distribution of whales is determined by a Neyman-Scott clustered-point process (Hagen and Schweder 1994). The Neyman-Scott process is characterized by the following three parameters: $\gamma^{N\text{-}S}$ (the intensity of clusters), $\mu^{N\text{-}S}$ (the average number of whales per cluster), and $\rho^{N\text{-}S}$ (the cluster radius, i.e., the standard deviation in the bivariate Gaussian distribution that governs the position of whales relative to the cluster center).

In addition, we simulate measurement errors in radial distance r, sighting angle θ, and time point of observation (see below), incomplete tracking (the observer fails to report information about subsequent surfacings), and missing values in r and θ.

A model for measurement error was developed by Schweder (1997). This model has been modified and fitted to data from the survey period 1996–2001, yielding

$$(10)\quad r = 0.898 r' \exp[N(0,1)\cdot 1.371\cdot (r')^{-0.2375}]$$

$$(11)\quad \theta = 1.057\theta' + N(0,1)\cdot 4.826\cdot \exp[0.0117\cdot \min(|\theta'|, 55)]$$

where r' and θ' are the true quantities, and the $N(0, 1)$ denote standard normal random variables. The following error model for time has been adopted from Schweder (1997):

$$(12)\quad t = t' + \max[0,\ 7 + 3.4\cdot N(0, 1)],$$

where t' denotes true time.

Simulation-based inference for separate surveys

Computer simulation of a parametric model for inferential purposes is often called parametric bootstrapping (Efron and Tibshirani 1993). We use simulation to remove bias from parameter estimates obtained under the hazard probability model, to estimate standard errors, and to establish a confidence distribution (Schweder and Hjort 2002) for the abundance of minke whales. The main source of bias in the maximum likelihood estimation is the measurement error added in the simulation model, but not accounted for in the pure hazard probability model. As noted earlier, measurement error in distance and angle estimates leads to errors in the track-matching procedure, which in turn affect the estimate of the hazard probability.

Schweder et al. (1999) used the simulation model of the previous section to remove bias from the Bernoulli part of the likelihood. Here, our aim is to obtain asymptotically unbiased inference under the assumptions of the simulation model. We thus apply bias correction to the full likelihood under the pure hazard probability model. This is done by correcting the maximum likelihood estimate $\tilde{\beta}$ by Δ to

$$(13)\quad \hat{\beta} = \tilde{\beta} - \Delta$$

The correction Δ is calculated iteratively. Start with $\beta_1 = \tilde{\beta}$. At the ith step, simulate a large data set D_i^* (we use 30 times the size of the real survey data) using $\beta = \beta_i$. This leads to a maximum likelihood estimate $\tilde{\beta}_i^*$ based on D_i^*. The bias estimate at this stage is $\Delta_i = \tilde{\beta}_i^* - \beta_i$. The next large data set to simulate is based on $\beta_{i+1} = \tilde{\beta} - \Delta_i$. We have found this process to converge fairly rapidly. The process leads to an asymptotic bias correction in the sense that $\hat{\beta}$ given by eq. 13 converges to the true value of β as the amount of data becomes large (Kuk 1995).

To study the sampling distribution of the abundance estimator, 1000 data sets of the same size as the observed data set are simulated at $\beta = \hat{\beta}$. The simulations are set up with effort at covariate levels as in the real survey. (The large data sets used to evaluate Δ do also have effort similarly distributed.) For each simulated data set, we first evaluate $\hat{\beta}$ through eq. 13, then calculate the effective strip half-width w, and finally calculate $\hat{N}$ from the abundance formula (eq. 9). The number of sightings $n^{(A)} + n^{(B)}$ in the abundance formula is also generated using the simulation model, but from a different (independent) simulation replica than that used to estimate $\hat{\beta}$. For the purpose of simulating the variance of $\hat{N}$, separate Neyman-Scott parameters are used for each survey block (see Table 3), whereas in evaluating the bias correction factor Δ, the same set of Neyman-Scott parameters is used for all survey blocks.

To obtain a confidence distribution for total abundance, a few additional bootstrap runs are carried out. A confidence distribution represents confidence intervals by its quantiles. The interval between the confidence quantiles at 2.5% and 97.5% is, for example, the 95% confidence interval. The confidence density provides a graphical representation of confidence intervals at all conceivable levels of confidence and might be regarded as the frequentist analogue to the Bayesian posterior density (Schweder and Hjort 2002). The bootstrap runs are carried out at various levels of abundance around $\hat{N}$. To simplify matters, we only vary the intensity of clusters in the Neyman-Scott process. The degree of clustering and the other parameters (β) are fixed at their estimated values. For each parametric bootstrap sample, a bootstrap estimate of abundance ($\hat{N}$), is obtained as the estimate (eq. 9). From the series of these, an approximate pivot $p(\hat{N}, N)$ with cumulative distribution function F is constructed. From Schweder and Hjort (2002), the approximate confidence distribution will then simply have cumulative distribution function $C(N) = F(p(\hat{N}, N))$.

Combination of yearly regional surveys

Because of interannual variations in spatial prey distribution, the proportion of whales present in the different survey regions (Fig. 1) will vary between years. For the purpose of estimating the total minke whale abundance in the Northeast Atlantic, this variation has no effect when the total area used by the stock is covered in a synoptic survey (such as is assumed for the years 1989 and 1995). The surveys in 1996–2001 all had partial coverage. The IWC small areas (Fig. 1) constitute areas with synoptic survey coverage in single years, except for EB which was covered during 3 years. Below, the index α refers to these small areas, together with the three parts of EB.

© 2004 NRC Canada

Table 3. Estimates of Neyman-Scott parameters based on Ripley's *K* function.

Region	Block	$\gamma^{N\text{-}S}$ (km^{-2})	$\mu^{N\text{-}S}$	$\rho^{N\text{-}S}$ (km)	κ	τ
CM	JMC		Poisson point process			2.36
	NVN	2.149×10^{-2}	1.57	1.154	2.6500	2.76
	NVS	7.093×10^{-4}	73.40	7.277	0.0812	4.41
EB	BAE	6.153×10^{-4}	41.40	1.213	1.1300	10.90
	FI	2.938×10^{-3}	23.30	1.677	0.3640	6.01
	GA	3.387×10^{-3}	22.90	0.848	1.3100	7.64
	KO	1.086×10^{-3}	26.50	7.029	0.0358	2.70
	NOS	3.484×10^{-4}	97.00	13.218	0.0390	3.44
EC	LOC96	4.133×10^{-5}	883.00	27.058	0.0662	9.86
	LOC00	4.133×10^{-5}	883.00	27.058	0.0662	11.30
EN	NS	4.252×10^{-6}	11 004.00	51.126	0.1910	57.40
	NSC	5.981×10^{-3}	3.48	1.549	0.0681	1.98
ES	BAW	9.425×10^{-4}	26.80	2.485	0.1850	5.99
	BJ		Poisson point process			2.85
	NON		Poisson point process			2.30
	SV	4.501×10^{-3}	12.00	2.130	0.1320	3.39
	SVI	4.631×10^{-4}	82.30	8.199	0.0678	4.29
	VSI	1.252×10^{-3}	25.90	2.484	0.1830	7.28
	VSN		Poisson point process			2.53
	VSS	4.631×10^{-4}	169.00	8.199	0.1390	8.79

Note: The parameter κ defined in eq. 18 is a measure of the average whale density within clusters. The overdispersion coefficient τ is defined as $\tau = \mathrm{Var}(n^{(A)} + n^{(B)})/E(n^{(A)} + n^{(B)})$, where both the variance and the expectation are calculated under the Neyman-Scott model.

To assess the level of additional variance in the combined estimate resulting from temporal–regional variability, we also use data from 1989 and 1995. Let N_y be the true abundance in year y in the total survey area (Fig. 1). We let N_{1989} and N_{1995} be free parameters in the model, but for the period $1996 \le y \le 2001$, it is assumed that the population grows exponentially, i.e.,

$$(14) \quad \log(N_y) = \log(N_{y-1}) + \omega$$

where ω is the unknown rate of growth (or decline). Denote by $p_{a,y}$ the proportion of whales present in the area a in year y, so that the number of whales present in the area is $p_{a,y}N_y$. The following random effects model for the ps is assumed:

$$(15) \quad p_{a,y} = \exp(\mu_a + \xi_{a,y})/c(y)$$

where $c(y) = \Sigma_a \exp(\mu_a + \xi_{a,y})$ is a normalizing factor ensuring that $\Sigma_a p_{a,y} = 1$ for all y. The fixed-effect parameter μ_a accounts for time-invariant differences in abundance between areas, and the random-effect parameter $\xi_{a,y}$ accounts for interannual changes in whale distribution. These random effects are assumed to be independent and normally distributed with zero mean and variance σ^2. The parameter σ will be referred to as the additional variance parameter.

Denote by $\hat{N}_{a,y}$ the abundance estimate for area a in year y. Assuming that $\hat{N}_{a,y}$ is conditionally log-normally distributed (given the true abundance that year), we have

$$(16) \quad \log(\hat{N}_{a,y}) = \log(N_y) + \log(p_{a,y}) + e_{a,y}$$

where the survey error terms $e_{a,y}$ are assumed to be zero mean normally distributed random variables. Equation 16 illustrates how the total error in $\hat{N}_{a,y}$ can be broken down into additional variance (variation in $p_{a,y}$) and survey error ($e_{a,y}$). There are three survey periods: 1989, 1995, and 1996–2001. The terms $e_{a,y}$ are correlated within survey period due to the use of a common estimated model for the effective strip half-width. The terms $p_{a,y}$ are correlated within year due to the normalization factor c in eq. 15 but are uncorrelated across years. Note that an estimate of the correlation structure of $\{e_{a,y}\}$ is available from the bootstrap method described earlier.

To obtain an estimate of σ, the method of restricted maximum likelihood (Punt et al. 1997) is used. Denote by $L(N, \omega, \sigma, \mu, \xi)$ the likelihood function based on the area estimates from 1989, 1995, 1996–2001, where μ and ξ are vectors and $N = (N_{1989}, N_{1995}, N_{1996})$. When evaluating L we use the assumption of conditional normality (eq. 16) together with the assumptions of eqs. 14 and 15. The restricted maximum likelihood estimate of σ is obtained by maximizing the marginal likelihood:

$$(17) \quad L(\sigma) = \int L(N, \omega, \sigma, \mu, \xi)\, dN\, d\omega\, d\mu\, d\xi$$

where the numerical integration is done by Laplace's method (Tierney and Kadane 1986). Because data are sparse with respect to information about σ, the resulting estimate can be expected to be biased (in addition to having a large variance). Thus, we use the simulation methodology described earlier to remove the bias in the estimate of σ. In the present setting, eqs. 14, 15, and 16 constitute the simulation model.

Results

Minke whales were found throughout the survey area, but with a spatially varying density (Fig. 3 and Table 1). A total number of 1078 sightings (totally for both platforms) was

© 2004 NRC Canada

Fig. 4. Normalized frequency distribution of observed perpendicular distances by observer platform, together with fitted probability densities (solid lines). Also shown are histograms for radial distances, forward distances, and sighting angles. The bottom two panels show estimated success probabilities by radial distance for the Bernoulli trials. The broken line is a nonparametric smoother applied to the data, and the solid line is the model predicted success probability. Vertical lines are 95% confidence intervals for the nonparametric estimate.

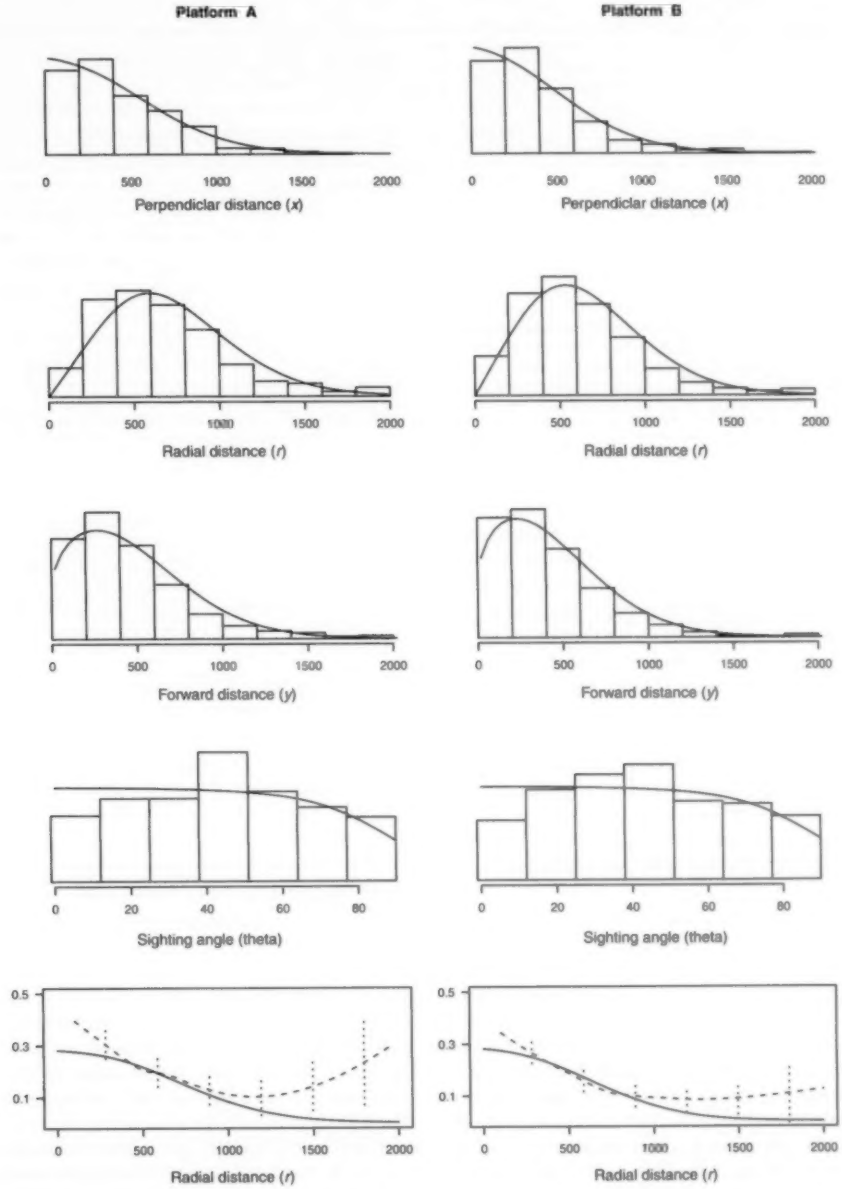

used in the estimation of whale density. Most of the observations (95%) were made within a strip 1000 m wide on each side of the transect line (Fig. 4). When fitting the hazard probability model, tracks with missing positional information (missing either r or θ) for all surfacings were left out. The proportion of tracks left out for this reason was approximately 1%. The track-matching routine identified 200 duplicate whales. Manual judgment identified two additional duplicate whales. The resulting number of initial sightings (for the combined platform A $\cup$ B), after applying the data-truncation rules, was 870, and the number of Bernoulli trials was 623.

Likelihood analysis

Initial attempts to fit the model showed that it was not possible to simultaneously estimate the two sighting-angle parameters ρ_θ and λ_θ. As a consequence, we fixed the slope at the rather arbitrary (but not unrealistic) value $\lambda_\theta = 0.1$, which was also used by Schweder et al. (1997), and we esti-

© 2004 NRC Canada

Table 4. Comparison of different covariate models (Table 2) for the linear predictor η_r.

η_r	Deviance	df	Abundance
B+W+V+G+P+T	0	0	111 000
W+V+G+P+T	–109.5	2	109 000
B+ V+G+P+T	**–3.4**	**1**	**110 000**
B+W+ G+P+T	–8.7	1	112 000
B+W+V+ P+T	–21.3	1	111 000
B+W+V+G+ T	–16.8	1	112 000
B+W+V+G+P	–36	1	109 000
B	–86.8	5	112 000
W	–215.1	6	109 000
V	–206.7	6	104 000
G	–201.9	6	104 000
P	–199.1	6	106 000
T	–181.4	6	107 000
	–220.3	7	107 000

Note: The selected model is printed with bold type. Deviance is two times the log-likelihood ratio relative to the full model (first row), and df is the degrees of freedom to use in a likelihood ratio test. Abundance estimates (last column) are given for the total survey area without bias correction.

mated ρ_θ as a free parameter. The deviances for a set of selected covariate models are shown in Table 4, ranging from the model without covariates (bottom line) to the full covariate model (first line). A backwards model selecting scheme was used to eliminate covariates from the full model. The likelihood ratio test was used to compare nested models. "Weather" was the only covariate that could be removed from the full model (p value 0.065), leaving a model with the linear predictor $\eta_r = B + V + G + P + T$ (see Table 2 for covariate abbreviations). This model selection was carried out within the pure hazard probability model (no bias correction). A similar analysis was attempted to identify covariates affecting the level parameter μ. Here, none of the covariates yielded a significant increase in the likelihood value, and hence only the intercept term was included in the linear predictor for μ.

For the chosen model, the maximum likelihood estimate $\hat{\beta}$ was bias-corrected using eq. 13. Parameter estimates (uncorrected and bias-corrected) are shown (Table 5), together with estimates of average effective strip half-width. Sum-to-zero constraints were imposed on the parameters associated with the different levels of categorical covariates, except for the platform covariate P. For instance, the table does not show the parameter estimate for level BIII of the Beaufort covariate as this parameter is determined by those of levels BI and BII. The platform effect was added only to the linear predictor of platform B. Thus, a negative estimated value of the parameter means that platform B looked at shorter range than platform A.

During the survey, 39 different combinations of covariate levels occurred. These covariate strata varied largely with respect to estimated effective strip half-width (Table 6).

Externally determined parameters

There are several parameters in the hazard probability model that were not estimated from the likelihood function. The mean surfacing rate α was estimated from 13 VHF-tagged whales to be $\alpha = 0.0129$ surfacings per second. The Neyman-Scott parameters (used in the simulation model) were estimated by matching the theoretical K function (Ripley 1977) to its empirical counterpart. A separate Neyman-Scott model was fitted to each survey block (Table 3). In four survey blocks (VSN, NON, BJ, JMC), the estimated Neyman-Scott model is consistent with a homogenous Poisson process (which is a special case of the Neyman-Scott model).

As seen from the table, the estimates for the survey block NS deviated strongly from those of the other survey blocks. A comparison of the empirical and theoretical K function indicated that the Neyman-Scott model did not fit data well for survey block NS. To resolve this problem, NS was split into two more homogenous subareas (the coast off Aberdeen and the rest of NS), and a separate estimate of τ (the coefficient of overdispersion) was obtained for each area (H.J. Skaug, unpublished data). From these estimates, an effort-weighted average $\tau = 8.96$ was calculated, and the Neyman-Scott parameters for NS were chosen to yield this level of overdispersion (under the constraint that $\gamma^{N\text{-}S}\mu^{N\text{-}S}$ was equal to the observed whale density in NS), yielding $\gamma^{N\text{-}S} = 4.34e-11$, $\mu^{N\text{-}S} = 1079$, and $\rho^{N\text{-}S} = 25\,563$. (Note that the superscript "N-S" refers to the term Neyman-Scott, and not to the survey block NS.) These estimates replace those in Table 3.

In the bias-correction procedure presented above, a common set of Neyman-Scott parameters was used for all survey blocks. This estimate was obtained by ranking the survey blocks according to their value of the quantity

$$(18) \quad \kappa = 0.5\mu^{N\text{-}S}(\gamma^{N\text{-}S} + (4\pi(\rho^{N\text{-}S})^2)^{-1})$$

which is proportional to the error rate in the track-matching algorithm (Schweder et al. 1997). It was found, by excluding blocks where the fitted Neyman-Scott process was consistent with a Poisson process and using the median value of κ as the criterion, that a representative set of Neyman-Scott parameters was that of the survey block SV ($\gamma^{N\text{-}S} = 4.50e-09$, $\mu^{N\text{-}S} = 12.0$, and $\rho^{N\text{-}S} = 2130$).

Abundance estimates 1996–2001

Abundance estimates were calculated for each survey block (Table 1) using eq. 9. Estimates for IWC small areas were obtained by summing the contribution from the constituting survey blocks (Table 7). In the variance calculations, intrablock correlation was automatically accounted for by the parametric bootstrap approach. The table also contains estimates for the total survey area (TOTAL) and a separate estimate for the IWC eastern medium area. The latter forms the "Eastern North Atlantic medium area" in the IWC terminology. In the estimation of the additional variance parameter σ, it was necessary to exclude the survey block NVS, which was not covered in 1989 and 1995. Based on data from 1989, 1995, and 1996–2001, we obtained the estimate $\hat{\sigma} = 0.28$ (SD = 0.15), but when the bias correction explained earlier was applied, the estimate became $\hat{\sigma} = 0.22$. When ignoring additional variance (putting $\sigma = 0$), the corresponding estimates of standard error for the total area (TOTAL) was 10 821.

Parametric bootstrapping was carried out at 90%, 100%, and 110% of the total abundance estimate $\hat{N} = 107\,205$ in order to study the sampling distribution of the estimator of

© 2004 NRC Canada

Table 5. Estimated regression coefficients for the chosen hazard probability model.

	β_r	W, BI	W, BII	V, High	G, G0	T, Long	P, B	β_θ	β_μ	λ_r	$w^{(A)}$	$w^{(B)}$
$\tilde{\beta}$	6.459	0.374	0.068	0.175	0.146	0.15	–0.141	4.532	–0.565	0.0052	263	224
$\hat{\beta}$	6.729	0.332	0.050	0.177	0.121	0.129	–0.133	4.489	–0.932	0.0058	273	227
SD($\hat{\beta}$)	0.089	0.042	0.039	0.046	0.038	0.029	0.036	0.039	0.147	0.00021	17	14

Note: The parameters β_r, β_θ, and β_μ are the intercept terms in the linear predictors η_r, η_θ, and η_μ, respectively. Following the β_r column, the coefficients associated with covariates (Table 2) are given. Parameter estimates are given both with ($\hat{\beta}$) and without ($\tilde{\beta}$) bias correction. Estimates of standard deviation (SD) are given for the bias-corrected estimate. Effort weighted mean effective strip half-widths ($w^{(A)}$ and $w^{(B)}$) are also given.

Table 6. Effective strip half-width w (in metres) and $g(0)$ for selected combinations of covariate levels (Table 2).

Covariates									
Beaufort	Visibility	Glare	Team A	Team B	$w^{(A)}$	$w^{(B)}$	$g^{(A)}(0)$	$g^{(B)}(0)$	Time (%)
BIII	Low	G1	Short	Short	118	104	0.264	0.2468	0.9
BIII	Low	G0	Short	Long	153	178	0.304	0.3295	12.5
BIII	Low	G0	Long	Short	212	132	0.360	0.2807	12.9
BIII	Low	G0	Long	Long	212	178	0.360	0.3295	14.0
BII	High	G1	Short	Long	320	388	0.440	0.4801	0.1
BII	High	G0	Short	Long	465	566	0.520	0.5640	0.4
BI	High	G0	Long	Long	1078	879	0.715	0.6669	0.5

Note: The last column gives the proportion of realized survey time. The first and last rows show the lowest and highest effective strip half-widths, respectively, that occurred during the survey. Also included are the covariate settings that were dominate in terms of realized survey time.

Table 7. Abundance estimates ($\hat{N}$) by survey region (small areas in the terminology of the International Whaling Commission) in comparison with estimates for 1989 and 1995, together with coefficient of variation (CV), taken from Schweder et al. (1997).

	1989		1995		1996–2001	
Area	$\hat{N}$	CV	$\hat{N}$	CV	$\hat{N}$	CV
EB	34 712	0.203	56 330	0.136	43 835	0.15
ES	13 370	0.192	25 969	0.112	18 174	0.25
EC	2 602	0.249	2 462	0.228	584	0.26
EN	14 046	0.276	27 364	0.206	17 895	0.25
CM	2 650[a]	0.484	6 174[a]	0.357	26 718	0.14
Total	67 380	0.190	118 299	0.103	107 205	0.13
Eastern	64 730	0.192	112 125	0.104	80 487	0.15

Note: The bottom row (eastern) shows estimates for the eastern medium area of the International Whaling Commission.

[a]In 1989 and 1995, the estimates for CM did not include survey block NVS.

total abundance and to obtain a confidence distribution for this parameter. The number of bootstrap replicates were 1000, 1000, and 636, respectively. It turns out that the abundance estimator was practically normally distributed on the log scale (Fig. 5), with standard deviations 0.134, 0.145, and 0.129, respectively, and a pooled standard deviation of 0.137. These standard deviations are significantly different (p value = 0.003, Bartlett test). Because of the lack of linear pattern in the standard deviations, we base our pivot on the assumption that the standard deviation is constant on the log scale in the neighbourhood of $\hat{N}$. On the log scale, there is no significant bias in $\hat{N}$ (Fig. 5). The pivot is $p(\hat{N}, N) = (\log(N) - \log(\hat{N}))/0.137$, and F is the cumulative normal distribution function. The confidence distribution (Fig. 6) for total abundance is thus log-normal with median $\hat{N}$ and a scale parameter of 0.137. The confidence intervals for N are thus $\hat{N}[\exp(-0.137z), \exp(0.137z)]$ for appropriate normal quantiles z.

Discussion

Variation in abundance

Our abundance estimate at the stock level is lower for the period 1996–2001 than it was for 1995, but higher than for 1989. The p value for a change in abundance since 1995 is 0.18 (excluding the survey block in CM that was not covered in the 1995 survey). Is this evidence for a decline in the Northeast Atlantic stock of minke whales? Just as Schweder et al. (1997) found it difficult to ascribe the more dramatic increase in the abundance estimate from 1989 to 1995 to population growth alone, we find it difficult to ascribe the decline in estimates to a decline in the stock. One possible explanation for a decline in the eastern IWC medium area stock is that the eastern and central stocks are less separated than previously believed, at least on the feeding grounds.

Alternatively, the migration patterns of minke whales may vary because of as yet unidentified factors. According to the

© 2004 NRC Canada

Fig. 5. Normal probability plots of bootstrapped logged total abundance estimates. The panel to the left refers to simulation at $N = 0.9\hat{N}$, etc.

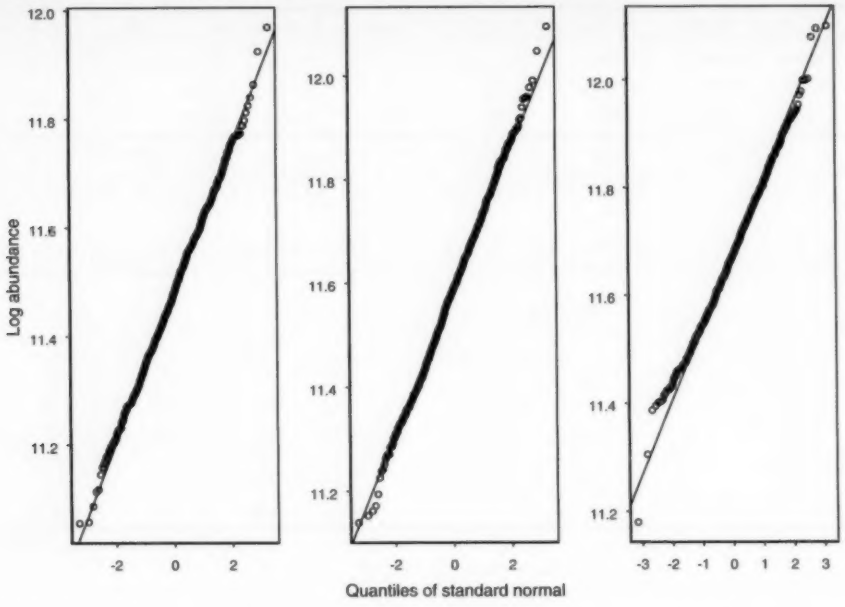

Fig. 6. Confidence density for total abundance. The median of the confidence distribution (vertical line) is nearly equal to $\hat{N} = 107\,205$.

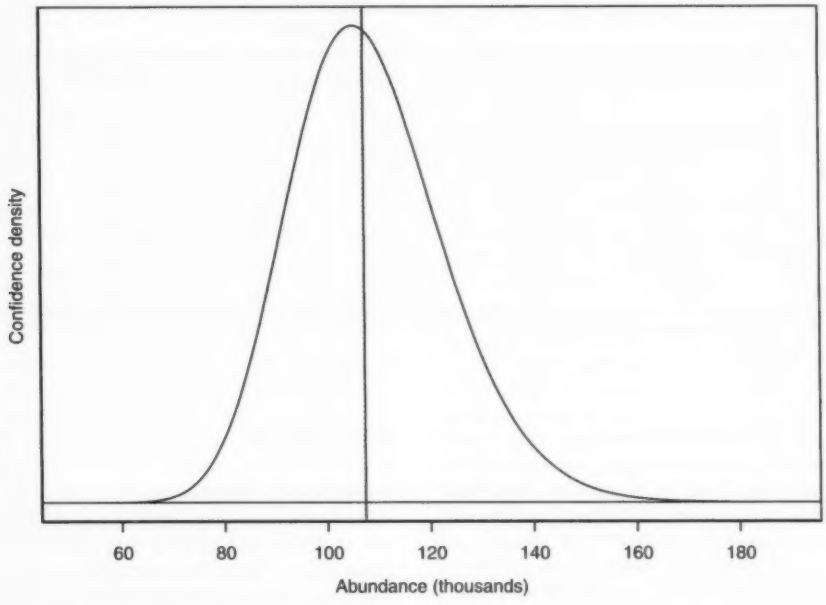

estimated random effects model described above, the proportion of the total stock (CM and eastern small areas) present in CM each year varies randomly between 18% and 33% (lower and upper 5% prediction intervals). The increase in the estimate for the CM area from 1996 to 2001 is quite marked and could be due to more whales from the eastern areas being present in CM when it was surveyed in 1997 than was the case in 1995. Although it is possible to find alternative explanations for an apparent decline in abundance estimates from 1995 to 1996–2001 not being real, the possibility of a decline should not be ruled out. Seen over the longer period 1989–2001, however, the impression is that there might have been some growth in the population.

In 1938, a compulsory logbook system was introduced in Norwegian small-type whaling (Christensen and Øien 1990) requiring detailed information on each whale caught and all participating vessels. It is reasonable to assume that the geographical distribution of catches reflects the distribution, and changes in distribution, of whales. The catch distributions indicate that within the Barents Sea, changes have taken

© 2004 NRC Canada

Fig. 7. Geographical positions of caught minke whales (*Balaenoptera acutorostrata*) for the selected years 1952 (green) and 1980 (red). The gradient in background blue color reflects the change from several thousand metres depth in the Norwegian Sea to the shallow Barents Sea proper.

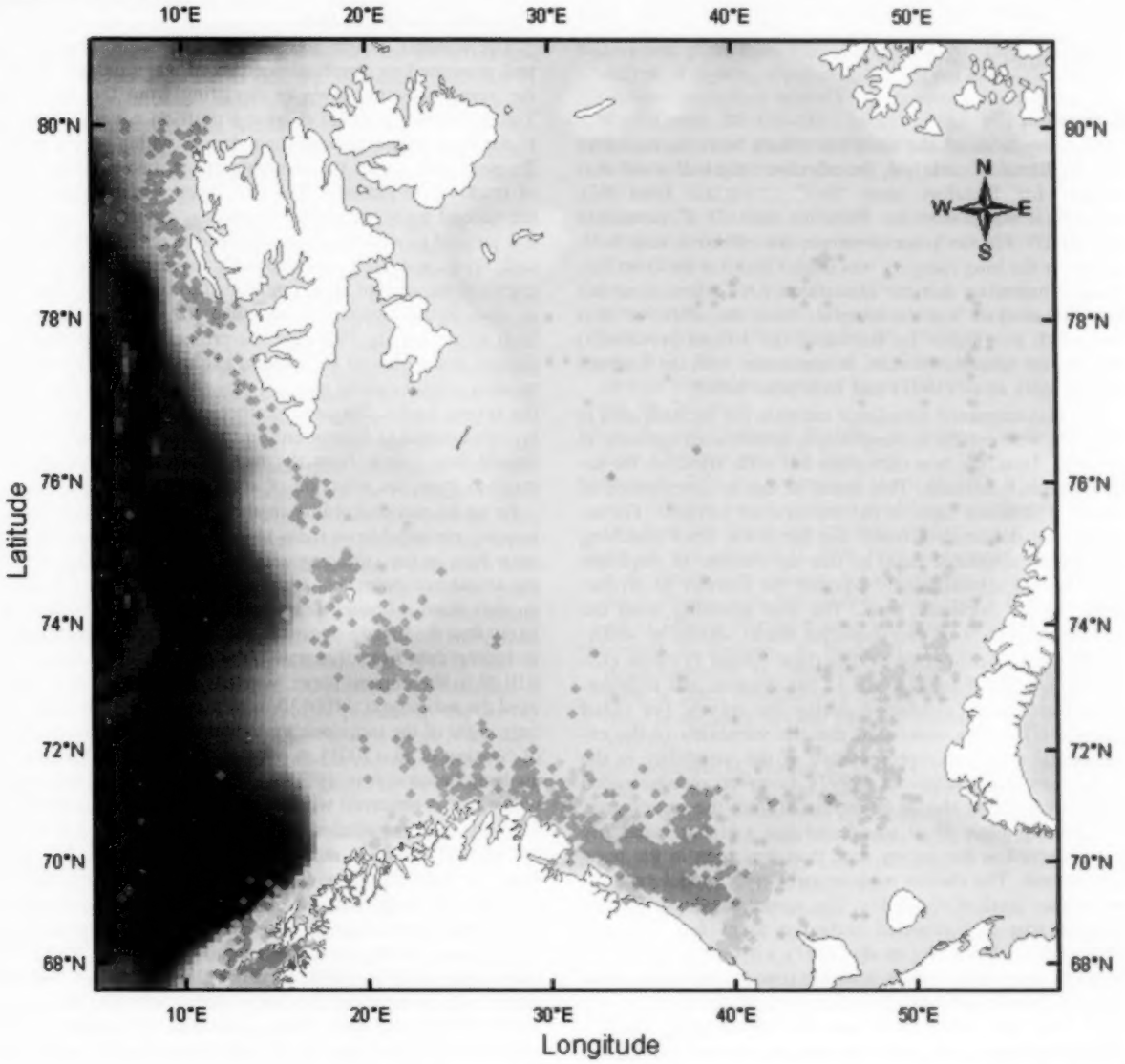

place over the years between eastern distributions (for example in 1952, see Fig. 7) and western distributions (for example in 1980, see Fig. 7).

Large temporal changes in abundance are also seen at smaller geographical scales. For instance, the survey block Kola in the Barents Sea has shown large variations in abundance during the period since 1989 (Schweder et al. 1997). The same applies to the survey block NS (North Sea), which in our survey in 1995 had a very high abundance estimate. A survey conducted in 1994 with a somewhat different methodology (Hammond et al. 2002) resulted in a much lower estimate.

Migration of minke whales into Norwegian and Arctic waters in the spring is segregated with respect to both length and sex (Jonsgård 1951; Øien 1988). From markings of minke whales, mainly in the period 1974–1978 within the Barents Sea, there is at least some indication that a regional fidelity exists (International Whaling Commission 1991). So far, instrumentation with radio and satellite tags has not given answers to questions regarding large-scale movements of minke whales in the Northeast Atlantic, but tracking over about 1-month-long periods indicates regional fidelities in Norwegian waters (Heide-Jørgensen et al. 2001), as well as Icelandic waters (Heide-Jørgensen, Greenland Institute of Natural Resources, Box 570, DK-3900 Nuuk, Greenland, unpublished data).

All of this indicates that there are large year-to-year variations in regional minke whale abundance, as is reflected in the high estimate of the additional variance parameter (σ^2).

© 2004 NRC Canada

Presumably, these variations are related to changes in abundance and distribution of possible prey species, although this has not yet been satisfactorily demonstrated. Finally, it is of course possible that a component of the minke whale stock stays outside the surveyed area and that the size of this component varies from year to year.

Estimation

The directions of the covariate effects were as expected. For the Beaufort covariate, the effective strip half-width was highest for Beaufort state "0–1" (covariate level BI), whereas it was lowest for Beaufort state "3–4" (covariate level BIII). For the team covariate, the effective strip half-width for the long category was higher than for the short category, illustrating that the classification of teams done before the analysis was meaningful. Also, the effective strip half-width was higher for the barrel (as defined previously) than for the wheelhouse roof, in agreement with the findings in Schweder et al. (1997) and with prior belief.

The bias-corrected abundance estimate for the total area is 107 205, whereas the corresponding uncorrected estimate is 110 000. Thus, the bias correction has little effect on the total abundance estimate. This could be due to cancellation of biases of different signs in the uncorrected estimate. For instance, we deliberately tuned the automatic track-matching routine (on simulated data) so that the number of duplicate pairs missed approximately equaled the number of erroneously judged duplicate pairs. The bias resulting from the manual judgement of two duplicate tracks should be small.

The measurement error models (eqs. 10 and 11) were estimated from the data collected in the distance and sighting-angle experiments conducted during the survey. For radial distance (r), it was concluded that the variability in the experimental data was representative of the variability in the real survey data. Schweder (1997), however, recommended that the variability should be estimated from the survey data. For sighting angle (θ), it was found that a higher variability was observed in the survey data than was seen in the buoy experiments. The chosen measurement error model captures this higher level of variability. The model for the difference between true and reported surfacing times (eq. 12) was adopted from Schweder et al. (1997) without modification. A priori, one expects more accurate time points in the present data than in the 1995 data, because the observers on average were more experienced than those participating in 1995.

Diagnostic plots illustrate that the distribution of distances to initial sightings are reasonably well predicted by the model, whereas the angular distribution is less well fitted. In these plots, the probability density is a weighted average (according to the number of observations) of the probability densities for the different covariate strata. We do not understand the large number of observations around 45° and the low number of sightings close to the track line. For large values of θ, the fit is reasonably good, so there is no indication that the choice $\lambda_\theta = 0.1$ made earlier is inconsistent with data. The bottom row represents diagnostic plots based on the Bernoulli trials. There are surprisingly many successes at large radial distance, especially for platform A, and more than predicted by the model. This might be explained by unmodelled heterogeneity in cue strength, partially resulting from the angle at which the whale shows its back when surfacing.

Potential sources of bias

The transect design was nonadaptive. Each detected animal generated an observational record when passed, without the vessel slowing down or deviating from the track line. Transects were planned to give a uniform coverage and not to correlate with expected whale density within survey blocks. To make full use of the available effort, two uniform layers of tracks were planned. The first layer was mandatory, and the second layer was to be covered as extensively as possible, subject to weather conditions and practicalities. The second layer was only incompletely covered. Selectivity of tracks in the second layer could lead to bias in the coverage, as also would temptation to move to regions of expected high whale density. However, the protocol specified that secondary tracks should be selected exclusively on logistic and weather considerations and that they should be discussed with the survey leader. Because weather and Beaufort Sea state is accommodated as a covariate in the analysis model, no bias should thus follow from the lack of uniform coverage that resulted from the selection of secondary tracks.

In the hazard probability method, an estimate of surfacing rate (α), obtained from radio-tagged animals, is used. A negative bias in the surfacing rate will yield a positive bias in the abundance estimates. Although our estimate of α is based on data from a limited number of individuals (13), it is not likely that the bias in our estimate of α is large. The effect of including data from five new individuals was not large (α = 0.0129 in the current paper, whereas Schweder et al. (1997) used the estimate $\alpha = 0.0130$, which was based on data from only eight of the individuals). Visual dive time data, as those of Stockin et al. (2001), have not been used in the present analysis because it is difficult to ascertain that it is a single whale that is observed without radio-marking the individual.

In the analysis, whales are assumed to be immobile except for diving. Random motion between surfacings has been found to bias abundance estimates positively when not accounted for (Schweder et al. 1996). Responsive behavior could bias abundance estimates even more. From an analysis of recorded swim directions in the 1995 data, Palka and Hammond (2001) found evidence for Northeast Atlantic minke whales avoiding the vessel when the radial distance is less than approximately 700 m. Based on the evidence available in 1995, Schweder et al. (1997) concluded that the direction and size of a potential bias resulting from random or responsive whale behavior is unknown, but if the bias is positive, its size is likely to be small in the abundance estimates.

Tracking of whales is assumed to be unbiased in the sense that the number of tracks recorded from one platform is an unbiased estimate of the number of whales actually seen. Because it is possible to break up tracks (count a whale twice) or to merge different tracks into one recorded track (count two whales as one), unbiased tracking is not self-evident. Incorrect tracking can be detected in cases where the whale has been seen by both platforms, although it is usually difficult to determine in retrospect which platform made the mistake. However, during the manual validation of the duplicate pairs, only a few such instances were discovered.

© 2004 NRC Canada

No attempt has been made to incorporate the inherent uncertainty in model selection into the estimates of variance for abundance. The variance estimates are calculated conditionally on the selected covariate model being the true model and do not reflect the fact that other covariate models might have been chosen. However, as long as the Beaufort covariate is included in the model, the abundance estimate is relatively insensitive to model choice. Further, the additional variance parameter σ was weakly determined (CV approximately 0.5 for uncorrected estimate). If σ has been underestimated, the variance estimate for the total abundance estimate will be too low.

In conclusion, the abundance estimate for the survey period 1996–2001 is practically unbiased or possibly negatively biased. In 1995 and 1988–1989, the surveys were synoptic with nearly complete coverage. In 1996–2001, the survey design could be characterized as a sequence of partial designs. Except for this difference, the survey methodology and the method of data analysis were similar for the three surveys. Differences between abundance estimates for 1989, 1995, and 1996–2001 should thus be approximately unbiased. These differences seem to indicate that the stock has increased from 1989 to 1995 and then decreased. The estimated decline since 1995 is larger than the cumulated catch (approximately 3000 minke whales) over the period. This picture of stock abundance over time prevails even when taking the standard errors in the abundance estimates into account, at least for the increase in the first period. Such variability in true stock abundance is, however, inconsistent with conventional population dynamics models for minke whales (International Whaling Commission 1991) and is likely to be less than estimated. A potential explanation is that the fraction of the stock that is present in the survey area varies from year to year, either because there is substantial contact between the central and the eastern stocks or because a variable stock component keeps to more southern latitudes at a varying degree.

Acknowledgments

This work has been generously funded by the Norwegian Government and the Norwegian Research Council (grant No. 111043/120). We are grateful to Kjell Arne Fagerheim and Siri Hartvedt at the Institute of Marine Research for preparing the data. We are also grateful to Magne Aldrin, Marit Holden, Ingunn Friede Tvete, and Gro Hagen at the Norwegian Computing Center for performing the data analysis leading to the models of eqs. 10 and 11 and to Table 3 (see Skaug et al. (2002) for further details). We also thank all of the team leaders and observers who participated in the surveys during the 6-year period. Finally, our active discussion colleagues in the Scientific Committee of the IWC are gratefully acknowledged, as well as two anonymous referees.

References

Beddington, J.R., Cooke, J.G., Christensen, I., Øritsland, T., Øien, N., and Rørvik, C.J. 1984. Assessments of the Northeast Atlantic stock of minke whales. Rep. Int. Whal. Comm. **34**: 285–91.

Buckland, S.T., Anderson, D.R., Burnham, K.P., Laake, J.L., Borchers, D.L., and Thomas, L. 2001. Introduction to distance sampling: estimating abundance of biological populations. Oxford University Press, Oxford, UK.

Butterworth, D.S., and Punt, A.E. 1999. Experiences in the evaluation and implementation of management procedures. ICES J. Mar. Sci. **56**: 985–998.

Butterworth, D.S., Best, P.B., and Basson, M. 1982. Results of analysis of sighting experiments carried out during the 1980/81 southern hemisphere minke whale assessment cruise. Rep. Int. Whal. Comm. **32**: 819–834.

Christensen, I., and Øien, N. 1990. Operational patterns of the Norwegian minke whale fishery. Rep. Int. Whal. Comm. **40**: 343–347.

Christensen, I., and Rørvik, C. 1981. Analysis of markings and recaptures of minke whales in the Barents Sea 1974–79. Rep. Int. Whal. Comm. **31**: 255–257.

Cooke, J.G. 1997. An implementation of a surfacing-based approach to abundance estimation of minke whale from shipborne surveys. Rep. Int. Whal. Comm. **47**: 513–528.

Cooke, J.G. 1999. Improvement of fishery-management advice through simulation testing of harvest algorithms. ICES J. Mar. Sci. **56**: 797–810.

Efron, B., and Tibshirani, R. 1993. An introduction to the bootstrap. Chapman and Hall, New York.

Fournier, D. 2001. An introduction to AD MODEL BUILDER version 6.0.2 for use in nonlinear modeling and statistics. (Available from http://otter-rsch.com/admodel.htm.)

Hagen, G., and Schweder, T. 1994. Point clustering of minke whales in the Northeastern Atlantic. *In* Developments in marine biology. Vol. 4. Whales, seals, fish and man. *Edited by* A.S. Blix, L. Walløe, and Ø. Ulltang. Elsevier Science BV, Amsterdam. pp. 27–34.

Hammond, P., Berggren, P., Benke, H., Borchers, D., Collet, A., Heide-Jørgensen, M., Heimlich, S., Hiby, A., Leopold, M., and Øien, N. 2002. Abundance of harbour porpoise and other cetaceans in the north sea and adjacent waters. J. Appl. Ecol. **39**: 361–376.

Heide-Jørgensen, M., Nordøy, E., Øien, N., Folkow, L., Kleivane, L., Blix, A., Jensen, M., and Laidre, K. 2001. Satellite tracking of minke whales (*Balaenoptera acutorostrata*) off the coast of northern Norway. J. Cetacean Res. Manag. **3**(2): 175–178.

Horwood, J. 1990. Biology and exploitation of the minke whale. CRC Press, Inc., Boca Raton, Fla.

International Whaling Commission (1991). Appendix 3. Annex F. Report of the sub-committee on North Atlantic minke whales. Rep. Int. Whal. Comm. **41**: 132–171.

International Whaling Commission. 1992. Annex K. Report of the working group on North Atlantic minke trials. Rep. Int. Whal. Comm. **42**: 246–251.

International Whaling Commission 1994*a*. Report of the Scientific Committee. Annex H. The Revised Management Procedure (RMP) for baleen whales. Rep. Int. Whal. Comm. **44**: 145–167.

International Whaling Commission. 1994*b*. Report of the Scientific Committee. Annex J. Guidelines for conducting surveys and analysing data within the Revised Management Scheme. Rep. Int. Whal. Comm. **44**: 168–173.

International Whaling Commission. 2004. Report of the Scientific Committee. J. Cetacean Res. Manag. **6**(Suppl.): 107–154.

Jonsgård, Å. 1951. Studies on the little piked whale or minke whale (*Balaenoptera acutorostrata* Lacépède). Norsk Hvalfangsttidende, **40**: 80–95. [In Norwegian.]

Kuk, A.Y.C. 1995. Asymptotically unbiased estimation in generalized linear-models with random effects. J. R. Stat. Soc. Ser. B Methodological, **57**: 395–407.

© 2004 NRC Canada

Øien, N. 1988. Length distributions in catches from the Northeastern Atlantic stock of minke whales. Rep. Int. Whal. Comm. **38**: 289–295.

Øien, N. 1989. Sighting estimates of Northeast Atlantic minke whale abundance from the Norwegian shipboard survey in July 1987. Rep. Int. Whal. Comm. **39**: 417–421.

Okamura, H., Kitakado, T., Hiramatsu, K., and Mori, M. 2003. Abundance estimation of diving animals by the double-platform line transect method. Biometrics, **59**: 512–520.

Palka, D., and Hammond, P. 2001. Accounting for responsive movement in line transect estimates of abundance. Can. J. Fish. Aquat. Sci. **58**: 777–787.

Press, W.H., Teukolsky, S.A., Vetterling, W.T., and Flannery, B.P. 1992. Numerical recipes in C. The Art of Scientific Computing. Cambridge University Press, Cambridge, UK.

Punt, A.E., Cooke, J.G., Borchers, D.L., and Strindberg, S. 1997. Estimating the extent of additional variance for southern hemisphere minke whales from the results of the IWC/IDCR cruises. Rep. Int. Whal. Comm. **47**: 431–434.

Ripley, B.D. 1977. Modelling spatial patterns (with discussion). J. R. Stat. Soc. Ser. B, **47**: 172–212.

Schweder, T. 1974. Transformation of point processes: application to animal sighting and catch problems, with special emphasis on whales. Ph.D. thesis, University of California, Berkeley, Calif.

Schweder, T. 1977. Point process models for line transect experiments. *In* Recent developments in statistics. *Edited by* J. Barra. North Holland Publishing Co., Amsterdam. pp. 221–242.

Schweder, T. 1997. Measurement error models for the Norwegian minke whale survey in 1995. Rep. Int. Whal. Comm. **47**: 485–488.

Schweder, T., and Hjort, N.L. 2002. Confidence and likelihood. Scand. J. Stat. **29**: 309–332.

Schweder, T., and Høst, G. 1992. Integrating experimental data and survey data to estimate $g(0)$: a first approach. Rep. Int. Whal. Comm. **42**: 575–582.

Schweder, T., Hagen, G., Helgeland, J., and Koppervik, I. 1996. Abundance estimation of Northeastern Atlantic minke whales. Rep. Int. Whal. Comm. **46**: 391–405.

Schweder, T., Skaug, H.J., Dimakos, X., Langaas, M., and Øien, N. 1997. Abundance estimates for Northeastern Atlantic minke whales. Estimates for 1989 and 1995. Rep. Int. Whal. Comm. **47**: 453–484.

Schweder, T., Skaug, H.J., Langaas, M., and Dimakos, X. 1999. Simulated likelihood methods for complex double-platform line transect surveys. Biometrics, **55**: 678–687.

Sigurjonsson, J., Gunnlaugsson, T., Ensor, P., Newcomer, M., and Vikingsson, G. 1989. North Atlantic sightings survey 1989 (NASS-89): shipboard surveys in Icelandic and adjacent waters July–August 1989. Rep. Int. Whal. Comm. **41**: 559–572.

Skaug, H.J., Øien, N., Bøthun, G., and Schweder, T. 2002. Abundance of Northeastern Atlantic minke whales for the survey period 1996–2001. Paper SC/54/RMP5, the Scientific Committee of the International Whaling Commission. Available from bemata.imr.no/whales.

Stockin, K., Fairbairns, R., Parsons, E., and Sims, D. 2001. Effects of diel and seasonal cycles on the dive duration of the minke whale (*Balaenoptera acutorostrata*). J. Mar. Biol. Assoc. U.K. **81**: 189–190.

Tierney, L., and Kadane, J.B. 1986. Accurate approximations for posterior moments and marginal distributions. J. Am. Stat. Assoc. **81**: 82–86.

Ugland, K. 1976. Population studies on eastern North Atlantic minke whales, *Balaenoptera acutorostrata* Lacepede. Rep. Int. Whal. Comm. (Sci. Rep.), **26**: 366–381.

© 2004 NRC Canada

Grazer–collector facilitation hypothesis supported by laboratory but not field experiments

Stephen B. Heard and Corinne K. Buchanan

Abstract: Grazing invertebrates in streams feed by harvesting algal cells from surfaces, and in doing so release fine particulate organic matter (FPOM). The "grazer–collector facilitation hypothesis" holds that FPOM production by grazers facilitates growth and (or) survival of FPOM-collecting invertebrates. We tested for grazer–collector facilitation in laboratory and field experiments. In recirculating flumes in the laboratory, we tested for facilitation of the collector *Hydropsyche slossonae* by the grazers *Physa gyrina*, *Glossosoma intermedium*, and *Baetis tricaudatus*. All three grazers increased FPOM levels in flume water, but only *Physa* facilitated *Hydropsyche* growth. In the field, we manipulated *Physa* and *Glossosoma* densities to test for facilitation (at a local scale) of natural collector assemblages in an eastern Iowa stream. We did not detect facilitation of any collector by either grazer in the field, despite high power to detect such interactions. We suspect that grazer–collector facilitation was not observed in the field because (unlike in our laboratory flumes) field FPOM levels are often high and extremely variable in time and space and because organic particles can arise from sources other than grazer activity (= grazer-independent processing). Therefore, at local scales, collectors may not be significantly limited by the supply of grazer-derived FPOM.

Résumé : Les invertébrés brouteurs dans les cours d'eau se nourrissent en récoltant les cellules d'algues sur diverses surfaces et, ce faisant, ils libèrent de fines particules de matière organique (FPOM). L'hypothèse de « la facilitation brouteurs–collecteurs » veut que la production de FPOM par les brouteurs facilite la croissance et (ou) la survie des invertébrés collecteurs de FPOM. Nous avons vérifié l'existence des cette facilitation brouteurs–collecteurs dans des expériences en laboratoire et sur le terrain. Dans des canalisations de laboratoire avec recirculation de l'eau, nous avons vérifié la présence de facilitation chez le collecteur *Hydropsyche slossonae* par les brouteurs *Physa gyrina*, *Glossosoma intermedium* et *Baetis tricaudatus*. Les trois brouteurs augmentent les concentrations de FPOM dans l'eau des canalisations, mais seul *Physa* favorise la croissance d'*Hydropsyche*. Sur le terrain, dans un cours d'eau de l'est de l'Iowa, nous avons fait varier les densités de *Physa* et de *Glossosoma* afin de vérifier s'il y a de la facilitation (à l'échelle locale) dans la communauté naturelle de collecteurs. En nature, nous n'avons observé aucune facilitation chez les divers collecteurs par ni l'un ni l'autre des brouteurs, malgré notre capacité élevée de détecter de telles interactions. Nous soupçonnons que la facilitation brouteurs–collecteurs n'a pas été observée en nature car, contrairement à ce qui se passe dans les canalisations de laboratoire, les concentrations de FPOM y sont fortes et extrêmement variables dans le temps et dans l'espace et parce qu'il y a des sources de particules organiques autres que les brouteurs (= décomposition indépendante des brouteurs). Ainsi, aux échelles locales, les collecteurs ne sont peut-être pas limités significativement par l'apport de FPOM en provenance des brouteurs.

[Traduit par la Rédaction]

Introduction

Food webs in temperate streams are generally based on organic matter from two sources: detritus, largely in the form of coarse particulate organic matter (CPOM) of terrestrial origin; and primary production by periphyton (and to a lesser extent aquatic macrophytes). The processing of detrital material and periphyton to fine particulate organic matter (FPOM) has long been thought to play an important ecological role in stream communities. FPOM production has been an important element of conceptual models for stream ecosystem function (e.g., Minshall et al. 1985; Wallace and Webster 1996) and underlies hypothesized interactions among three functional groups of benthic stream invertebrates: shredders (that feed on CPOM), grazers (or "scrapers" that scrape or shear algal cells from periphyton), and collectors (that feed on FPOM filtered from the water column or collected from the substrate). Shredders process CPOM to FPOM as a byproduct of their feeding activity and therefore are widely assumed to facilitate growth and (or) survival of collectors (Heard and Richardson 1995). Similarly, grazers release FPOM as they feed, and as a result, they have been suggested to facilitate collectors (e.g., McCullough et al. 1979; Lamberti et al. 1987; Power et al. 1988). However, field experiments testing for either hypothesized interaction have been entirely lacking, with the shredder–collector and grazer–collector facilitation hypothe-

Received 20 May 2003. Accepted 26 January 2004. Published on the NRC Research Press Web site at http://cjfas.nrc.ca on 23 July 2004.
J17534

S.B. Heard.[1] Department of Biology and Canadian Rivers Institute, University of New Brunswick, Fredericton, NB E3B 6E1, Canada.
C.K. Buchanan.[2] Department of Biological Sciences, University of Iowa, Iowa City, IA 52242, USA.

[1]Corresponding author (e-mail: sheard@unb.edu).
[2]Present address: 8947 Terrace Road NE, Blaine, MN 55434, USA.

 doi: 10.1139/F04-022 © 2004 NRC Canada

ses supported instead by laboratory experiments and by correlative data (Heard and Richardson 1995). In this paper, we report laboratory- and field-based experimental tests of the grazer–collector facilitation hypothesis (in a future paper, we will report parallel tests of the shredder–collector facilitation hypothesis).

Grazing invertebrates are ubiquitous and often abundant members of benthic stream faunas. They are especially important in unshaded to moderately shaded streams in which primary productivity is relatively high: for instance, streams typical of grasslands, agricultural areas, aridlands, tundra, and other areas lacking continuous forest canopy. Effects of grazers on periphyton standing crop and productivity (review: Hillebrand 2002) and on stream nutrient transport and cycling (Lamberti et al. 1987, 1989; Sallenave et al. 1994) have been studied at length, but much less is known about how grazers interact with invertebrates in other feeding groups. Our focus is on the hypothesis that grazers, by processing algal cells and associated organic material to FPOM, facilitate growth and (or) survival of collectors downstream.

A grazer–collector interaction is plausible because grazers produce FPOM by several mechanisms: by dislodging particles as they move across the periphyton layer (Lamberti et al. 1987; Scrimgeour et al. 1991), by releasing harvested but uningested particles into the water column (Hart 1985), and by releasing fecal particles (Shepard and Minshall 1984; Lamberti et al. 1987, 1989). Particles of each origin enter the FPOM pool available to collectors (McCullough et al. 1979; Benke and Wallace 1980, 1997). Grazer-derived FPOM can be of high nutritional quality: dislodged but uningested algal particles can be three- to five-fold higher in quality compared with the overall detrital pool (Benke and Wallace 1980; Fuller and Mackay 1981), and even fecal particles can be superior to nonfecal detritus (Shepard and Minshall 1981) and can contribute significantly to collector production (Shepard and Minshall 1984; Wotton et al. 1998).

Grazer–collector interactions are not inevitable, however, because grazer activity is not the only route by which periphyton can be processed to particles. Other routes for periphyton processing, collectively referred to as "grazer-independent processing", include sloughing of dead and dying cells (Lamberti et al. 1987) and scouring of periphyton by inorganic particles in suspension (Chauvet et al. 1993). The nature of the interaction between grazers and collectors is likely to depend on the relative rates of grazer-dependent and grazer-independent processing of periphyton to FPOM: grazer–collector interactions should be facilitative when grazer-independent processing is slow but could be neutral or even amensal (negative) when grazer-independent processing is substantial (Heard 1994; Heard and Richardson 1995). Furthermore, periphyton is not the only source of particles in streams: FPOM also enters streams in runoff (Roeding and Smock 1989; Yule 1996; Wallace et al. 1999) and is produced by shredders feeding on CPOM (Heard and Richardson 1995), by mechanical abrasion of CPOM (Heard et al. 1999), and by flocculation of dissolved organic matter (Lush and Hynes 1973; Petersen 1986). In light of the variety of FPOM sources and agents of periphyton processing in streams, it is by no means inevitable that FPOM produced by grazer activity will limit collector growth or survival.

We tested for effects of grazers on collectors in both laboratory and field settings. For laboratory experiments, we chose one focal collector (the caddisfly *Hydropsyche slossonae*) and three grazers with distinct feeding ecologies: the snail *Physa gyrina*, the caddisfly *Glossosoma intermedium*, and the mayfly *Baetis tricaudatus*. Our laboratory experiments were intended to test for grazer–collector facilitation under ideal conditions: highly controlled experimental flumes with little spatial or temporal variation in FPOM except that associated with the presence or absence of grazers. In addition, we chose stocking densities of grazers and collectors to maximize the probability of detecting facilitation if it could exist. In the field, we manipulated two of the grazers that we studied in the laboratory (*Physa* and *Glossosoma*) in caging experiments to determine whether grazers facilitate collectors under natural conditions (which include higher and more variable amounts of FPOM). Our experiments were designed to test for interactions at a local scale, that is, effects of a local aggregation of grazers (≈50 individuals in ≈100 cm^2) on collector populations immediately downstream. Although grazer–collector interactions are also possible at the reach scale (integrating the effects of thousands to millions of collectors over hundreds to thousands of metres), such a hypothesis will require separate, quite different experimental tests and is not pursued here.

Methods

Laboratory flume experiments

Study species

In flume experiments, we tested for facilitation of a focal collector (the caddisfly *Hydropsyche slossonae* Banks (Trichoptera: Hydropsychidae)) by each of three grazers: the snail *Physa gyrina* Say (Gastropoda: Physidae), the caddisfly *Glossosoma intermedium* (Klapalek) (Trichoptera: Glossosomatidae), and the mayfly *Baetis tricaudatus* Dodds (Ephemeroptera: Baetidae). These species are among the dominant members of their guilds at our field site (Big Mill Creek, eastern Iowa; see below). We chose grazers differing in feeding behavior and mouthpart morphology because we suspected that they might differ in the quantity and quality of FPOM that they produced.

Hydropsyche larvae inhabit hard substrates where they spin nets to capture drifting organic particles including detritus, algal cells, and small invertebrates. They also collect and graze periphyton cells, and the relative importance of these items to the diet depends on availability and varies among species and instars (Fuller and Mackay 1980, 1981). *Hydropsyche slossonae* is widespread in cool and unpolluted streams across northeastern and central North America. In its later instars (used in our experiments), it makes nets with mesh sizes between 60 μm × 90 μm (third instar) and 180 μm × 300 μm (fifth instar) (Fuller and Mackay 1980). Its diet can include both algal and detrital particles (Fuller and Mackay 1981), with use of algal cells increasing in later instars (Fuller and Mackay 1980).

Physa snails (including *P. gyrina*) use their toothed radulae to scrape periphyton and other organics from hard substrates or to feed on plant tissues or occasionally carrion, with periphyton generally preferred (Brown 1991). *Physa*

© 2004 NRC Canada

gyrina ranges from the Arctic to the Gulf of Mexico and is abundant in both riffles and pools in Big Mill Creek.

Glossosoma larvae have cutting mandibles that shear and scrape periphyton at the substrate surface (McAuliffe 1984) and are important grazers in many cold-water streams (Kohler 1992). *Glossosoma intermedium* has a Holarctic distribution and is common and locally abundant in cool, fast streams in the midwestern United States.

Baetis larvae have brush-like mouthparts that sweep through the upper layers of periphyton to remove loosely attached diatoms and other algal, bacterial, and detrital particles (Dudley 1992). *Baetis tricaudatus* ranges across much of North America, prefers cold-water, rapid streams with hard substrate, and can be a dominant grazer in the Midwest (Kohler 1992). Both periphyton and detrital particles are important elements of baetid diets (Shapas and Hilsenhoff 1976).

Flume setup

Recirculating flumes (Fig. 1) were constructed of 64-mm (inside diameter) polyvinyl chloride pipe cut lengthwise to give a semicircular cross section. Each flume was oval in layout, with a watercourse falling 3 cm over its 90-cm run, and held about 1.7 L of water recirculated at 0.1 $L \cdot s^{-1}$ by an aquarium pump (Aqua-Tech 5-15; Regent Pet Products, Moorpark, Calif.). Two experimental compartments were demarcated with screens of 2-mm mesh (fiberglass window screen): one upstream for grazers and one downstream for collectors. Each compartment was 15 cm long and 6 cm in wetted width and had water 15–20 mm deep. We kept the flumes in environmental chambers (Percival I36-LL; Percival Scientific, Boone, Iowa) set at 8 °C and a 12 h light – 12 h dark photoperiod.

We set up experiments with invertebrates, periphyton-covered gravel, and water collected from Big Mill Creek. We hand-picked invertebrates in the field, holding undamaged animals in stream water kept on ice and aerated by aquarium bubblers for return to the laboratory. We held all invertebrates in the environmental chambers for 7–10 days before use in flumes. Gravel was also kept on ice for transport to the laboratory and held (without invertebrates) in the environmental chambers until use. Water was filtered through 2-mm mesh to remove large debris and stored in the chambers until needed.

We compared FPOM production and *Hydropsyche* (collector) growth in flumes with and without each grazer. Each experimental run used 10 replicate flumes (five "control" and five "grazer"). We performed four runs with *Physa* (November–December 1998), four with *Baetis* (April–June 1999), and five with *Glossosoma* (October 1998 and February–March 1999). Each flume received, in its upstream compartment, 10 pieces (20–40 mm in diameter) of periphyton-covered gravel. In grazer flumes, but not in controls, this compartment also received 10 grazer individuals (*Physa*, *Glossosoma*, or *Baetis*). For all three grazers, this is toward the high end of the range of natural densities at Big Mill Creek. In the downstream compartment of each flume, we placed one third- or fourth-instar *Hydropsyche* larva along with several pieces of fine gravel (2–4 mm in diameter) and broken ceramic tile (10–40 mm × 10 mm × 6 mm) to which the *Hydropsyche* could anchor nets. *Hydropsyche* larvae were randomly assigned to grazer or control treatments. The grazer to collector ratio was held higher than typical for our field site deliberately to increase the potential impact of grazers on collectors and therefore maximize the probability of detecting facilitation if it could exist. Each experimental run lasted 2 weeks, during which time we replaced stream water lost by evaporation and cleaned screens with a toothbrush as necessary to maintain water flow. To the extent that cleaning of screens produces new FPOM (as opposed to resuspending FPOM filtered by the screens), it should make the detection of grazer–collector facilitation less likely, and therefore make our tests conservative.

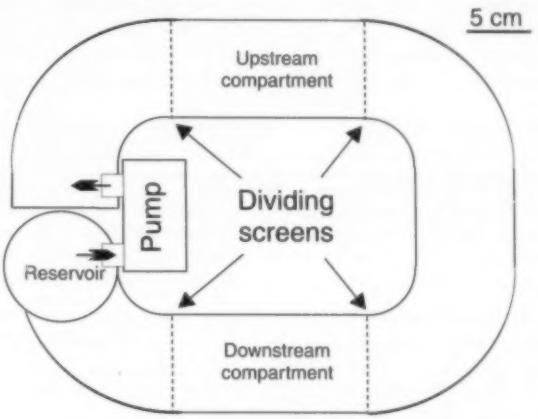

Fig. 1. Design of recirculating laboratory flumes (top view). Water flow is clockwise. The compartment above is for grazers and periphyton-covered gravel; the compartment below is for *Hydropsyche* (the collector).

Some grazer individuals died during our experiments. There was little mortality among *Physa* or *Glossosoma* (never more than three per flume); to minimize disturbance to flumes, dead *Physa* or *Glossosoma* were not replaced. More *Baetis* died in our flumes, however, and we replaced dead *Baetis* as needed (average of seven replacements per flume). Disturbances to grazer flumes during *Baetis* replacement were replicated in controls. We found *Baetis* generally difficult to maintain in the laboratory, with substantial mortality in collection and maintenance. However, most dead *Baetis* had been feeding actively (they had algal cells in their guts).

Chlorophyll a

We measured chlorophyll *a* to test for effects of grazers on periphyton standing crops. We collected each flume's gravel after each run, extracted pigments in 90% acetone, and assayed chlorophyll *a* spectrophotometrically (LKB Ultraspec 2-D model 4050; UKB Biochrom Ltd., Cambridge, England) using standard methods (Steinman and Lamberti 1996). We used total chlorophyll *a* (micrograms) from the gravel in each flume as our index of periphyton standing crop. Periphyton on flume surfaces was not measured.

© 2004 NRC Canada

Table 1. Design summaries for field experiments.

Experiment	Start date	Duration (days)	Grazer species	Treatment	Replicates per treatment	Substrate sampling method	FPOM data?
Fall 1997	7 August	56	*Physa gyrina*	Grazers vs. no grazers Cobble vs. no cobble 2- vs. 12-mm-mesh cage[a]	5		Yes
Fall 1998	18 September	21	*Physa gyrina*	Grazers vs. no grazers	19	Hess samples and substrate trays	Yes
Spring 1999	17 April	28	*Glossosoma intermedium*	Grazers vs. no grazers	20	Hess samples	No

Note: FPOM, fine particulate organic matter.

[a]Incomplete factorial design: for 12-mm-mesh cages, grazers cannot be manipulated because the mesh size allows free entry and egress to benthic invertebrates. All other possible combinations were used for a total of six treatments.

FPOM

We measured FPOM production as ash-free dry mass per flume. After each run, we collected the entire water volume from each flume, after gentle brushing with a soft toothbrush to resuspend sedimented particles. We determined ash-free dry mass from a 300-mL subsample (and then corrected to total flume volume) by filtration through a preweighed 0.7-μm glass-fiber filter (Advantec MFS GF7547), drying at 60 °C for 48 h, and weighing before and after ashing for 1 h at 500 °C. Analyses based instead on dry mass after filtration through 0.22-μm polycarbonate membrane filters (to include grazer effects on small particles) were very similar, so we report only the ash-free dry mass data.

We also measured size distributions of organic particles (both uningested periphyton particles and grazer fecal particles) produced by each grazer. Size distribution data came from one control flume for each grazer species and were based on a 1-mL subsample from the flume's collected (as above) total water volume. From each subsample, we sized (longest axis) 100 fecal particles and 100 periphyton particles using an ocular micrometer at 400× magnification.

Collector performance

We measured fresh mass gain or loss of each *Hydropsyche* larva as an index of collector performance. Before and after the 2-week experiment, each larva was gently blotted with a paper towel, weighed to the nearest 1 μg on a microbalance (Mettler MT-5; Mettler-Toledo Inc., Switzerland), and immediately returned to water. Blotting and weighing took about 20 s and caused no apparent harm to the larvae.

Statistical analysis

For each grazer, we compared chlorophyll *a*, FPOM production, and collector performance between grazer and control flumes (fixed effect) and among runs (random effect) using mixed-model two-way analyses of variance (ANOVAs). Nonsignificant interactions ($P > 0.05$) were dropped and their sums of squares pooled with the error. We compared FPOM size distributions among grazers using one-way ANOVAs, evaluating significance of F values by randomization (10 000 randomizations) because size distributions were strongly nonnormal. Otherwise, all statistical analyses were conducted in SAS version 7.0 (SAS Institute Inc., Cary, N.C.) using Type III sums of squares.

Field caging experiments

Study site

We conducted experiments in Big Mill Creek (Jackson County, Iowa; 42°17′N, 90°33′W), a spring-fed second-order stream with approximately 50 $L \cdot s^{-1}$ baseflow, incomplete shading, and a limestone cobble–gravel substrate. Riffle sections are approximately 3–5 m wide and 10–20 cm deep at baseflow, and spring inputs occur within the study reach and along a ≈2 km upstream run. Upstream sections also drain some low-intensity pasture and a small pond. The dominant grazers are *P. gyrina*, *G. intermedium*, and *Baetis* spp., mostly *B. tricaudatus* and *B. brunneicolor* (Ephemeroptera: Baetidae). The dominant collectors are *Hydropsyche* spp. (mostly *H. slossonae*) and *Cheumatopsyche* spp. (Trichoptera: Hydropsychidae), and black flies (Diptera: Simuliidae).

General design

We conducted three caging experiments, which were similar in overall design but differed in some details (Table 1). Our strategy was to target local-scale interactions by comparing FPOM concentration and collector abundance immediately downstream of cages with or without high densities of grazing invertebrates. We used cages without grazers as controls, rather than no cage at all, to ensure that differences in local flow patterns could not drive apparent treatment effects. We ran experiments with two of the three dominant grazers at Big Mill Creek: *P. gyrina* and *G. intermedium*. We were unable to manipulate *Baetis* densities in the field, since they easily escaped through any mesh open enough to allow water flow through cages.

In most experiments, we used cages (13.5 cm × 8.5 cm × 4 cm) of 2-mm plastic mesh (Plastic Canvas; Darice, Strongsville, Ohio) sewn shut with fishing line. In one experiment (fall 1997), some treatments used cages of 12-mm-mesh metal hardware cloth fastened with florists' wire. Large-mesh cages tested for effects of flow restriction and shading by the smaller mesh material but did not allow grazer manipulation. Cages were stocked immediately before placement in the stream with the desired combinations of grazers and periphyton-covered cobbles. Grazers were hand-picked in Big Mill Creek the same day they were used. Periphyton-covered cobbles (20–50 mm in diameter) were collected from Big Mill Creek, cleaned of invertebrates, and allowed to stand 1 week in stream water in an environmental

© 2004 NRC Canada

chamber (at 8 °C and a 12 h light – 12 h dark photoperiod) to increase periphyton density. We used four to six cobbles per cage (enough to loosely fill the cage). We did not measure periphyton biomass at the end of the experiments, but a visible periphyton layer remained on the cobbles (so grazers still had access to food).

To deploy cages, we attached them crosswise to the tops of standard clay bricks with plastic cable ties. Each brick was then dug into the stream bottom (parallel to the current) so the cage sat slightly above the surrounding substrate. We anchored bricks with steel reinforcing rods driven into the stream bottom. We placed cages in riffles at spots where water depth at baseflow was 12–20 cm. Cage exteriors were cleaned weekly of sediments and periphyton with a nylon brush to maintain water flow.

FPOM

In two experiments (Table 1), we used a direct count technique to measure FPOM levels in the field. At each sampling date, we took simultaneous 20-mL water samples immediately upstream and downstream of each cage (using syringes placed to sample water from the flow through the cage). Samples were returned to the laboratory on ice and then preserved in 4% formalin and stored at 4 °C. We stained (25 min at 0 °C) 500-µL subsamples with 5 nM 4′,6-diamidino-2-phenylindole, a DNA-binding fluorescent stain that allows discrimination of bacteria, protozoa, algae, and organic debris particles under epifluorescence microscopy (400×, excitation 365 nm). We filtered the subsamples onto 0.2-µm black polycarbonate membrane filters (Poretics K02CP02500), mounted the filters in immersion oil, and counted bacteria and organic particles in 10 haphazardly chosen microscope fields. The difference between upstream- and downstream-of-cage counts is an estimate of net particle production across the cage (possibly negative if cages tend to filter or sediment particles). We included bacterial counts because a variety of collectors have been shown either to consume bacterial cells directly or to strip bacteria from surfaces of more refractory detrital particles (e.g., Edwards and Meyer 1990).

Collector abundance

In two experiments (Table 1), we sampled invertebrates from artificial and (or) natural substrates downstream of our cages. Artificial substrates allowed control for fine-scale spatial heterogeneity in the streambed, whereas sampling natural substrate relaxed this control but provided a more realistic sample of the invertebrate community. Artificial substrates were made of 5-cm crushed limestone ballast (≈20 pieces, ≈800 g total) held in 12-mm-mesh hardware cloth trays 15 cm square and 2 cm deep. We positioned a tray 1 m downstream of each cage in the plume of water that passed through the cage (determined using food dye tracers). We set trays flush with the stream bottom, anchoring them with steel reinforcing rods. At the end of the experiment, each tray was gently lifted free and its contents (ballast and associated invertebrates) preserved in 70% ethanol. To sample invertebrates from natural substrate, we took a single sample with a 15-cm-diameter Hess sampler 50 cm downstream of each cage, preserving collected invertebrates in 70% ethanol. We identified collectors using standard references (Merritt and Cummins 1996; Wiggins 1996; black flies and chironomids to family and other taxa usually to genus). We counted individuals of each taxon and determined dry masses after drying for 48 h at 60 °C. Because our design allows migration of individuals to and from substrates during the course of the experiment, our collector abundance data will reflect differences between treatments in immigration or emigration, as well as growth and survival.

Fall 1997 experiment

In fall 1997, we caged *P. gyrina*. We used both 2- and 12-mm-mesh cages in six treatments with five replicates each (total 30 cages). The 2-mm-mesh cages were deployed in a two-way factorial design, with and without periphyton-covered cobble and with 0 or 50 *Physa* (four treatments). The 12-mm-mesh cages were set up with and without cobble (two treatments; local grazer populations had free access to these cages). Fifty *Physa* per cage (4400·m^{-2}) is a very high density for Big Mill Creek (and about fivefold higher than we used in our laboratory flumes). We chose such a dramatic treatment to achieve high grazer exploitation of available periphyton and therefore to maximize our likelihood of detecting grazer–collector interactions, if they existed. Treatments were interspersed randomly along the study reach with at least 5 m between cages. We took water samples for FPOM analysis weekly for 8 weeks but did not measure collector abundance.

Fall 1998 experiment

In fall 1998, we caged *Physa* again. Because there had been no significant treatment effects in our fall 1997 experiment, we simplified our design, using only the 2-mm-mesh cages and 19 replicates each of two treatments: (*i*) periphyton-covered cobble and (*ii*) periphyton-covered cobble plus 50 *Physa*. To further increase our power, we adopted a paired design, with control cages placed beside *Physa* cages across the breadth of the stream. Cages in a pair were separated by at least 1 m to ensure that downstream substrate samples were exposed to water flow passing through only one of the cages in a pair. Pairs of cages were at least 5 m apart, and *Physa* cages were alternated from left to right of their pairs every two cage sites. We ran this experiment later in the fall than the 1997 experiment (Table 1) and halted it after 3 weeks to avoid overlap with autumn leaf-fall (with its high organic matter availability). We took water samples for FPOM weekly and sampled invertebrates via both artificial substrate and Hess samples.

Spring 1999 experiment

In spring 1999, we caged *G. intermedium*. We used two treatments with 20 replicates of each: (*i*) periphyton-covered cobble and (*ii*) periphyton-covered cobble plus 38 *Glossosoma* (3400·m^{-2}, much higher than typical in the field). The design was again paired, but this time, we kept all *Glossosoma* cages on the same side of the stream. At these scales, mixing of particles across the width of the stream will be incomplete between pairs of cages (Heard et al. 2001); therefore, this design will tend to amplify differences between treatments as particles from one experimental cage are transported across the next. Randomized (fall 1997) or alternating designs (fall 1998) are more conservative for detecting local

© 2004 NRC Canada

Table 2. Chlorophyll *a*, fine particulate organic matter (FPOM, dry mass), and collector performance analyses for laboratory flume experiments.

		Physa flumes				*Glossosoma* flumes				*Baetis* flumes			
Measure	Source	df	MS[a]	*F*	*P*	df	MS[a]	*F*	*P*	df	MS[a]	*F*	*P*
Chlorophyll *a*	Grazer	1	94.9	5.47	0.026	1	245	6.97	0.012	1	7.0	0.59	0.45
	Run	3	826	47.6	<0.0001	4	167	4.76	0.0030	3	23	11.3	<0.0001
	Error	31	17.3			41	35.2			3	1	28.5	
FPOM	Grazer	1	0.507	13.22	0.0083	1	1.52	96.9	<0.0001	1	0.648	14.03	0.0007
	Run[b]	—	—	—	—	3[c]	0.097	6.19	0.0018	3	0.200	4.34	0.012
	Error	7	0.038			34	0.016			31	0.046		
Collector performance	Grazer	1	0.086	19.8	<0.0001	1	0.17	0.02	0.90	1	0.015	0.82	0.37
	Run	3	0.007	1.69	0.19	4	14.2	1.40	0.25	3	0.002	0.12	0.95
	Error	32	0.004			42	10.2			30	0.019		

Note: All *F* and *P* values are calculated after pooling nonsignificant grazer × run interactions with the error.

[a]Except for *Glossosoma* flume collector performance, MS = entry × 10^3.

[b]The analysis for *Physa* flume FPOM has no "run" effect because we determined ash-free dry mass for only one run of flumes. An analysis based on dry mass has similar results.

[c]We had five *Glossosoma* runs, but only four had associated ash-free dry mass measurements.

effects of grazers, but the same-side design includes some reach-level effects of high grazer densities and is therefore potentially more powerful. This experiment lasted 4 weeks, after which we sampled invertebrates using the Hess sampler (artificial substrates were lost in a spring freshet).

Statistical analysis

FPOM data (particle differences across cages) were analyzed with repeated-measures ANOVA. With one exception, we pooled nonsignificant ($P > 0.05$) interactions with the error. The exception was the time × grazer interaction, which we retained throughout because it was of strong a priori interest (an effect of grazers accumulating over time would produce such an interaction). In fall 1997, the main effect of mesh (2 versus 12 mm) was nonsignificant and was also pooled with the error (results would not differ if we simply omitted 12-mm-mesh cages). We report univariate tests of the time effect, but multivariate tests gave similar results. For the fall 1998 experiment, an alternative approach would take advantage of the paired design by summing particle differences across sampling dates and analyzing the totals using paired *t* tests; results of such tests did not differ from the repeated measures ANOVAs and are not reported. Collector abundance and mass data were analyzed using paired *t* tests contrasting control and experimental cages in a pair (our unpaired fall 1997 experiment did not include collector data). We analyzed abundance and mass of the most common collector taxa (*Hydropsyche* and black flies) individually and also analyzed total abundance and mass of all collectors. We calculated statistical power for effects on collector abundance and mass data using tables in Cohen (1988). We performed all analyses with SAS version 7.0 (SAS Institute Inc., Cary, N.C.) using Type III sums of squares.

Results

Laboratory flume experiments

Chlorophyll a

For *Physa* and *Glossosoma*, periphyton standing crop, measured as chlorophyll *a*, was significantly reduced (17% and 35%, respectively) in grazer flumes (Table 2; Fig. 2*a*). *Baetis* may also have reduced periphyton standing crop, but its effect (8%) was far from significant. Not surprisingly, there were often significant differences in periphyton growth among runs, but the effect of each grazer was consistent among runs (no grazer × run interactions).

FPOM

FPOM levels (ash-free dry mass) were significantly greater in flumes containing any of our three grazer species (Table 2; Fig. 2*b*). *Physa* and *Glossosoma* produced the most FPOM (100% and 86% more FPOM, respectively, than control flumes), whereas *Baetis* produced somewhat less (45% increase over controls). As for the chlorophyll analysis, there were significant run effects but no grazer × run interactions.

FPOM size distributions also differed among grazers for both uningested algal particles and fecal particles (algal particles: $F_{[2,297]} = 4.05$, $P = 0.018$; fecal particles: $F_{[2,297]} = 63.1$, $P < 0.0001$) (Fig. 3). For both particle types, *Physa* produced the largest particles, *Glossosoma* intermediate-sized particles, and *Baetis* the smallest particles. For all grazers, particles of uningested periphyton were much larger (three- to four-fold) than fecal particles.

Collector performance

Hydropsyche larvae lost mass in the control flumes of all runs (Fig. 2*c*). In contrast, *Hydropsyche* gained mass in flumes with *Physa*, and *Physa*'s facilitation of *Hydropsyche* was highly significant (Table 2). In *Glossosoma* and *Baetis* flumes, *Hydropsyche* larvae lost less mass than in corresponding controls (Fig. 2*c*), but neither difference was significant. Once again, there were significant run effects but no significant grazer × run interactions.

Field experiments

FPOM

We measured particles in our first two experiments (fall 1997 and fall 1998). Particle densities and differences across cages were extremely variable (Fig. 4), a result consistent with other measurements in the system (S.B. Heard, unpub-

© 2004 NRC Canada

Fig. 2. Results from laboratory flume experiments for grazer (solid bars) and control (open bars) flumes. Error bars show ±2 SEs after removing run effects. (*a*) Periphyton standing crop measured as micrograms of chlorophyll *a* extracted from the gravel in the upstream compartment; (*b*) fine particulate organic matter (FPOM) production measured as milligrams ash-free dry mass (AFDM) filtered from the total water volume of each flume; (*c*) fresh mass gain or loss of the *Hydropsyche* larvae (collector) in each flume.

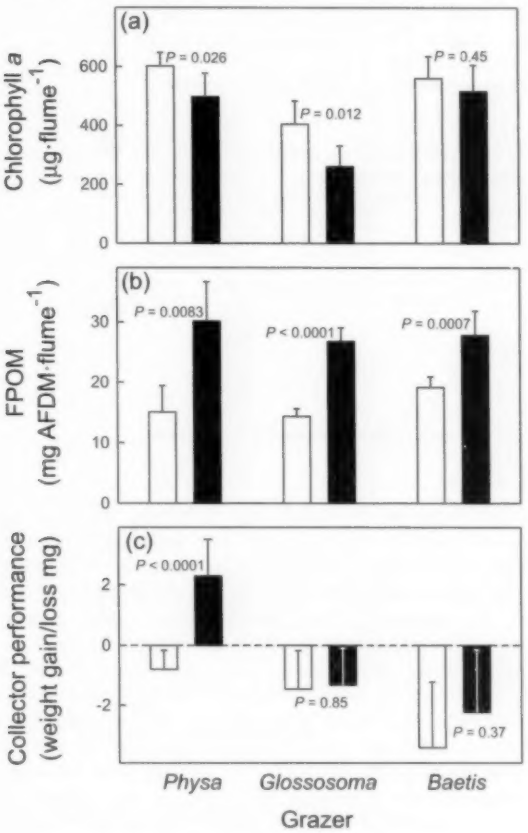

Fig. 3. Particle sizes for fine particulate organic matter from grazer flumes (shaded bars, periphyton particles; open bars, fecal particles). For both particle types, differences among grazers are significant (periphyton, $P = 0.018$; fecal particles, $P < 0.0001$). Dots are means, center lines are medians, box boundaries are 25th and 75th percentiles, whiskers are 5th and 95th percentiles, and plus symbols represent extreme observations.

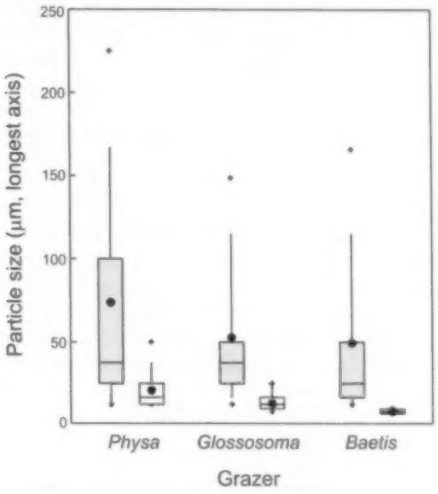

Fig. 4. Effects of control and grazer cages on particle densities (4′,6-diamidino-2-phenylindole counts) in water samples (expressed as downstream count minus upstream count, as a percentage of upstream count). Solid bars, grazer cages; open bars, control cages. Counts are pooled across the nonsignificant effect of date. For 1997, differences are also pooled across nonsignificant mesh and rock treatments. No bars are significantly different from zero height (no effect of treatment, all $P > 0.6$). Error bars show ±2 SEs.

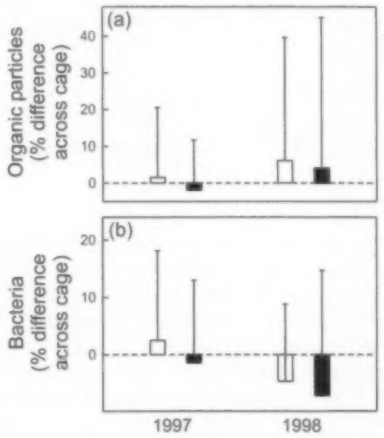

lished data). In neither experiment did particle differences across cages (for either particle type) differ significantly among treatments (Tables 3 and 4). (In 1998, we deleted from our analysis three cages with particle differences that were extreme outliers; however, none of our conclusions would be affected had we retained all of the cages.) None of the treatment (or treatment × time) effects were close to significance (all $F < 1$, all $P > 0.6$). In fact, there was never any significant change in particle densities across any set of cages (Fig. 4). Furthermore, changes in particle densities were never more positive (or less negative) across grazer cages, in contrast with the prediction from the grazer–collector facilitation hypothesis.

Collectors

We sampled collectors in our fall 1998 and spring 1999 experiments; in 1998, we used two parallel sampling techniques. In neither experiment (and for neither sampling technique) did collector abundance or dry mass differ between samples taken downstream of control and grazer cages. This held true for collectors as a guild and also for the two dominant collectors (*Hydropsyche* spp. and black flies) considered separately (Fig. 5). Two grazer effects were nearly significant (black fly abundance in 1998 Hess samples and

© 2004 NRC Canada

Table 3. Repeated-measures ANOVAs for particle counts (fall 1997 field experiment).

	Bacteria				Organic particles			
Source	df	MS[a]	*F*	*P*	df	MS[a]	*F*	*P*
Between-subjects effects								
Time	5	213	1.65	0.15	5	4.88	0.63	0.68
Time × grazers	5	80.8	0.62	0.68	5	5.2	0.66	0.65
Error	110	129			110	7.8		
Within-subjects effects								
Cobble	1	74.9	0.32	0.58	1	9.25	0.99	0.33
Grazers	1	0.466	0.00	0.96	1	0.32	0.03	0.85
Error	22	233			22	9.32		

[a]MS = entry × 10^3.

Table 4. Repeated-measures ANOVAs for particle counts (fall 1998 field experiment).

	Bacteria				Organic particles			
Source	df	MS[a]	*F*	*P*	df	MS[a]	*F*	*P*
Between-subjects effects								
Time	1	147	1.51	0.23	1	30.4	1.93	0.17
Time × grazers	1	9.02	0.09	0.76	1	3.05	0.19	0.66
Error	32	97			32	15.7		
Within-subjects effects								
Grazers	1	9.82	0.21	0.65	1	0.287	0.03	0.87
Error	32	46			32	11		

[a]MS = entry × 10^3.

Hydropsyche weight in 1999 Hess samples), but both effects were negative and therefore inconsistent with the grazer–collector facilitation hypothesis.

Our designs had substantial power to detect grazer–collector facilitation, had it been present. All individual comparisons (i.e., one taxon's abundance or mass measured in one experiment by one sampling method) had >98% power for effects giving $r^2 > 0.2$ (20% of total variance in mass or abundance explained by treatment; Cohen 1988). The aggregate power of our combined experiments was very high: probabilities of our detecting facilitation for at least one collector in at least one experiment were >99% and >94% for effects giving $r^2 = 0.06$ and $r^2 = 0.04$, respectively (treatment explaining only 6% and 4% of total variance).

Discussion

Although the grazer–collector facilitation hypothesis is certainly plausible, few studies have focused on grazer–collector interactions and none have directly tested the facilitation hypothesis in natural streams. Our results suggest that grazer–collector facilitation can be detected in highly controlled laboratory experiments but that local-scale facilitation does not play an important role in natural populations at our field site. Of course, we cannot rule out interactions over larger spatial scales or at other sites.

Grazer–collector facilitation in laboratory flumes

Grazers in our laboratory flumes processed periphyton to FPOM and thereby depressed periphyton standing crop (significantly so for two of three grazers). Flumes with grazers experienced substantial increases in FPOM levels (45–100% depending on grazer species and including both dislodged but uningested periphyton cells and fecal particles). These results are consistent with previous experiments documenting periphyton removal and FPOM production by grazers, with effects varying among grazer species (e.g., Lamberti et al. 1987; Scrimgeour et al. 1991; Hillebrand 2002).

Although all three grazers generated substantial FPOM, only one had a detectable effect on collector growth: *Physa* significantly facilitated *Hydropsyche*, whereas *Baetis* and *Glossosoma* did not. We believe that ours is the first experiment to connect FPOM production by grazers to increases in collector growth (although Sallenave et al. (1994) documented collector ingestion of grazer-released FPOM). Two important points follow: first, it is indeed possible for collectors to profit from FPOM production by grazers, but second, there may be differences in the occurrence or strength of these interactions among species. Our three grazers may have differed in their effects for several reasons. Although *Physa* produced the most FPOM, this cannot entirely explain our results because *Physa* and *Glossosoma* differed only by about 20% in FPOM production but differed dramatically in their effects on collector growth. FPOM particle size may also be important: *Physa* produced the largest particles of the three grazers and, in particular, by far the most particles >50 µm, a size range important in our experiments because nets spun by late-instar *H. slossonae* have relatively large openings (between 60 µm × 90 µm and 180 µm × 300 µm; Fuller and Mackay 1980). Finally (although we did not attempt to measure this), the nutrient content and (or) digestibility of particles produced could have differed among grazer species (e.g., Shepard and Minshall 1984; Wotton 1994).

© 2004 NRC Canada

Fig. 5. Collector abundance (solid bars) and dry mass (open bars) contrasts between (paired) substrate samples downstream of grazer control and grazer cages. (*a*) 1998 experiment, data from artificial substrates; (*b*) 1998 experiment, data from Hess samples; (*c*) 1999 experiment, data from Hess samples. All contrasts are expressed as a percentage of control; error bars show ±2 SEs. *P* values (from paired *t* tests) not shown were >0.20.

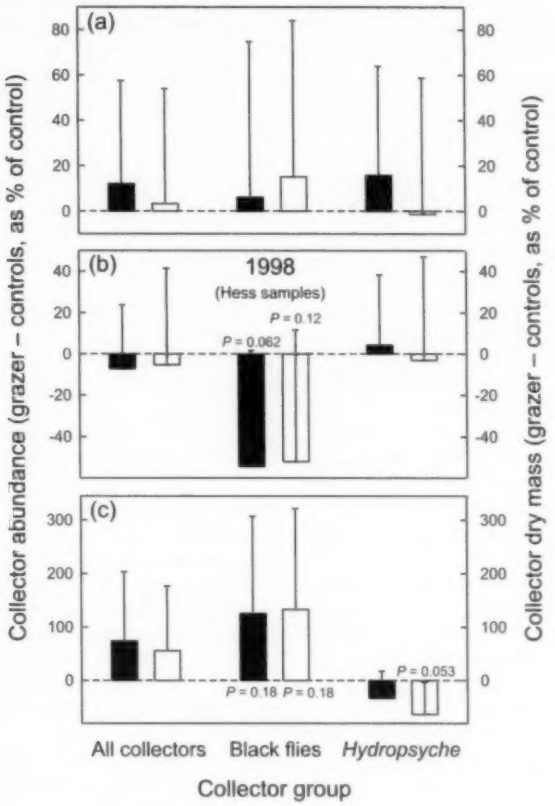

No grazer–collector facilitation in the field

We could detect neither particle production nor local-scale collector facilitation by grazers in any of our field experiments. This was true even though our experiments were designed to maximize the probability of detecting such effects: we used very high local grazer densities, we used grazers known to produce large amounts of FPOM in laboratory flumes, and we used increasingly powerful experimental designs in our later experiments. In particular, in our third experiment, we kept all grazer cages on one side of the stream so that treatment effects would be amplified by incomplete mixing of suspended particles (Heard et al. 2001) along the study reach. Our failure to detect local grazer–collector facilitation is not an artifact of low statistical power: combined, the two experiments yielding data on collectors had over 94% power to detect effects so small as to account for only 4% of the variance in collector mass or abundance. Although we cannot rule out even smaller effects of grazers on collectors, we expect that most ecologists would consider such weak effects to be of limited interest.

Our negative field results must be interpreted in light of the spatial scale at which our investigations were directed. We cannot rule out the possibility that, even though grazer–collector interactions appear negligible at a local scale, taken together, all of the grazers in a stream reach produce enough FPOM to significantly facilitate collectors downstream. Patterns observed in stream (and other) communities can depend strongly on spatial scale, with small-scale patterns either intensified (e.g., Cooper et al. 1998) or dissipated (e.g., McAuliffe 1984) at larger spatial scales. No reach-scale experimental tests of the grazer–collector facilitation hypothesis have been performed. Such tests will be very difficult in natural streams, as selective removal of grazers from whole reaches is probably impossible, while grazer addition at that scale would require logistically fearsome numbers of individuals. Whole-stream manipulations using chemical insecticides have reduced FPOM export (Cuffney et al. 1990), but these treatments cannot isolate effects of one functional group because they remove all insects. A more promising approach would be to manipulate grazer densities in artificial stream channels large enough for the operation of reach-level effects but small enough for stocking to produce significant differences in grazer densities.

Reconciling laboratory and field results

Whether or not grazer–collector facilitation might be detectable at larger scales, we are left with an apparent conflict between our local-scale laboratory and field results. In the laboratory, we detected FPOM production by all three grazers and facilitation of *Hydropsyche* by *Physa*, but in the field, neither *Physa* nor *Glossosoma* had detectable effects on FPOM or on collectors. We believe that these contrasting results have important implications for our understanding of benthic stream communities.

The grazer–collector facilitation hypothesis focuses on the role of grazers in converting periphyton to FPOM, which is then available to collectors. Our laboratory experiments confirm that grazers in Big Mill Creek produce FPOM and that this FPOM can increase collector growth. However, laboratory experiments cannot test a critical component of the grazer–collector facilitation hypothesis: that the rate of FPOM production by grazers can limit collector performance (growth or survival) in the field. Our field data strongly suggest that, at the local scale at which we worked, collectors in Big Mill Creek are not limited by grazer-derived FPOM. It may be that collectors are not limited by FPOM supply at all; or perhaps collectors are limited by FPOM but local grazer populations do not contribute significantly to local-scale variation in FPOM levels.

Surprisingly, it remains an open question whether (or how often) collectors are limited by FPOM in natural streams (Heard and Richardson 1995). Even if collectors are limited by particles, however, grazer–collector facilitation is not assured. In the field, there are many sources of FPOM other than grazer activity (Heard and Richardson 1995), including runoff, mechanical abrasion of CPOM and periphyton, CPOM processing by shredders, and flocculation of dissolved organic matter. No study (including ours) has ever quantified the proportional contribution of grazers to total FPOM production, but if it is small, detection of grazer–

© 2004 NRC Canada

collector facilitation will be difficult. Perhaps more important, given the local scale of our study, is the contribution of grazers to spatial variance in FPOM levels: if variation ascribable to other factors swamps the contribution of local grazer populations, then grazers will not explain a significant proportion of variance in collector performance even if collectors are particle limited. Studies of benthic FPOM generally find high fine-scale spatial heterogeneity (e.g., Hill et al. 1992; Martinez et al. 1998), and in Big Mill Creek, suspended FPOM is highly heterogeneous even on small (submetre and subminute) spatial and temporal scales (S.B. Heard, unpublished data). In this light, perhaps it should not be surprising that (according to our power analyses) local-scale patterns in grazer abundance are unlikely to account for more than a tiny fraction of variance in collector performance.

In summary, we suspect that the different outcomes of our laboratory and field experiments can be explained by differences between laboratory and field in quantity and heterogeneity of suspended FPOM. In our flumes, conditions were highly controlled (suppressing FPOM heterogeneity) and FPOM levels were relatively low (because we prevented or minimized gains through runoff, mechanical abrasion, and flocculation). Therefore, our flume experiments magnified the relative contribution of grazer-derived particles to overall FPOM abundance. This was a deliberate feature of our design: our flume experiments were not intended to mimic field conditions but rather to maximize our likelihood of detecting grazer–collector interactions if they could ever exist. Our laboratory experiments show that collectors can profit from FPOM produced by grazers, but our field experiments strongly suggest that, at least at a very local scale, they do not. Further experimental effort will be necessary to test the hypothesis that grazer–collector interactions might exist at reach or larger spatial scales.

Acknowledgements

We are grateful to Steve and Peggy Roling for access to their property on Big Mill Creek and to Kristie Heard for technical assistance. Dan Buchanan built a nifty water sampler. Many people helped with field and laboratory work, including Dan Buchanan, Branda Breaden, Chris Gienapp, Tamara Griesel, Kristie Heard, Cassie Kasun-Lewis, Jim Lemire, Matt St. Pierre, Mark Schneebeck, and Fred Williams; Jessica Ferrie and Ross Wilming made particularly important contributions. We thank Joseph Culp, Kristie Heard, Steve Hendrix, and John Nason for comments on the manuscript and John Richardson for extensive help with conceptual development. This research was funded by the National Science Foundation (DEB-9628969) and by the Avis Cone Foundation.

References

Benke, A.C., and Wallace, J.B. 1980. Trophic basis of production among net-spinning caddisflies in a southern Appalachian stream. Ecology, **61**: 108–118.

Benke, A.C., and Wallace, J.B. 1997. Trophic basis of production among riverine caddisflies: implications for food web analysis. Ecology, **78**: 1132–1145.

Brown, K.M. 1991. Mollusca: Gastropoda. *In* Ecology and classification of North American freshwater invertebrates. *Edited by* J.H. Thorp and A.P. Covich. Academic Press, New York. pp. 285–314.

Chauvet, E., Giani, N., and Gessner, M.O. 1993. Breakdown and invertebrate colonization of leaf litter in two contrasting streams: significance of oligochaetes in a large river. Can. J. Fish. Aquat. Sci. **50**: 488–495.

Cohen, J. 1988. Statistical power analysis for the behavioral sciences. Lawrence Erlbaum Associates, Hillsdale, N.J.

Cooper, S.D., Diehl, S., Kratz, K., and Sarnelle, O. 1998. Implications of scale for patterns and processes in stream ecology. Aust. J. Ecol. **23**: 27–40.

Cuffney, T.F., Wallace, J.B., and Lugthart, G.J. 1990. Experimental evidence quantifying the role of benthic invertebrates in organic matter dynamics of headwater streams. Freshw. Biol. **23**: 281–299.

Dudley, T.L. 1992. Beneficial effects of herbivores on stream macroalgae via epiphyte removal. Oikos, **65**: 121–127.

Edwards, R.T., and Meyer, J.L. 1990. Bacterivory by deposit-feeding mayfly larvae (*Stenonema* spp.). Freshw. Biol. **24**: 453–462.

Fuller, R.L., and Mackay, R.J. 1980. Feeding ecology of three species of *Hydropsyche* (Trichoptera: Hydropsychidae) in southern Ontario. Can. J. Zool. **58**: 2239–2251.

Fuller, R.L., and Mackay, R.J. 1981. Effects of food quality on the growth of three *Hydropsyce* species (Trichoptera: Hydropsychidae). Can. J. Zool. **59**: 1133–1140.

Hart, D.D. 1985. Grazing insects mediate algal interactions in a stream benthic community. Oikos, **44**: 40–46.

Heard, S.B. 1994. Processing chain ecology: resource condition and interspecific interactions. J. Anim. Ecol. **63**: 451–464.

Heard, S.B., and Richardson, J.S. 1995. Shredder–collector facilitation in stream detrital food webs: is there enough evidence? Oikos, **72**: 359–366.

Heard, S.B., Schultz, G.A., Ogden, C.B., and Griesel, T.C. 1999. Mechanical abrasion and organic matter processing in an Iowa stream. Hydrobiologia, **400**: 179–196.

Heard, S.B., Gienapp, C.B., Lemire, J.F., and Heard, K.S. 2001. Transverse mixing of transported material in simple and complex stream reaches. Hydrobiologia, **464**: 207–218.

Hill, B.H., Gardner, T.J., and Ekisola, O.F. 1992. Benthic organic matter dynamics in Texas prairie streams. Hydrobiologia, **242**: 1–5.

Hillebrand, H. 2002. Top-down versus bottom-up control of autotrophic biomass — a meta-analysis on experiments with periphyton. J. North Am. Benthol. Soc. **21**: 349–369.

Kohler, S.L. 1992. Competition and the structure of a benthic stream community. Ecol. Monogr. **62**: 165–188.

Lamberti, G.A., Ashkenas, L.R., Gregory, S.V., and Steinman, A.D. 1987. Effects of three herbivores on periphyton communities in laboratory streams. J. North Am. Benthol. Soc. **6**: 92–104.

Lamberti, G.A., Gregory, S.V., Ashkenas, L.R., Steinman, A.D., and McIntire, C.D. 1989. Productive capacity of periphyton as a determinant of plant–herbivore interactions in streams. Ecology, **70**: 1840–1856.

Lush, D.L., and Hynes, H.B.N. 1973. The formation of particles in freshwater leachates of dead leaves. Limnol. Oceanogr. **18**: 968–977.

Martinez, B., Velasco, J., Suarez, M.L., and Vidal-Abarca, M.R. 1998. Benthic organic matter dynamics in an intermittent stream in south-east Spain. Arch. Hydrobiol. **141**: 303–320.

© 2004 NRC Canada

McAuliffe, J.R. 1984. Resource depression by a stream herbivore: effects on distributions and abundances of other grazers. Oikos, **42**: 327–333.

McCullough, D.A., Minshall, G.W., and Cushing, C.E. 1979. Bioenergetics of lotic filter-feeding insects *Simulium* spp. (Diptera) and *Hydropsyche occidentalis* (Trichoptera) and their function in controlling organic transport in streams. Ecology, **60**: 585–596.

Merritt, R.W., and Cummins, K.W. (*Editors*). 1996. An introduction to the aquatic insects of North America. 3rd ed. Kendall-Hunt, Dubuque, Iowa.

Minshall, G.W., Cummins, K.W., Petersen, R.C., Cushing, C.E., Bruns, D.A., Sedell, J.R., and Vannote, R.L. 1985. Developments in stream ecosystem theory. Can. J. Fish. Aquat. Sci. **42**: 1045–1055.

Petersen, R.C., Jr. 1986. In situ particle generation in a southern Swedish stream. Limnol. Oceanogr. **31**: 432–437.

Power, M.E., Stewart, A.J., and Matthews, W.J. 1988. Grazer control of algae in an Ozark mountain stream: effects of short-term exclusion. Ecology, **69**: 1894–1898.

Roeding, C.E., and Smock, L.A. 1989. Ecology of macroinvertebrate shredders in a low-gradient sandy-bottomed stream. J. North Am. Benthol. Soc. **8**: 149–161.

Sallenave, R.M., Day, K.E., and Kreutzweiser, D.P. 1994. The role of grazers and shredders in the retention and downstream transport of a PCB in lotic environments. Environ. Toxicol. Chem. **13**: 1843–1847.

Scrimgeour, G.J., Culp, J.M., Bothwell, M.L., Wrona, F.J., and McKee, M.H. 1991. Mechanisms of algal patch depletion: importance of consumptive and non-consumptive losses in mayfly–diatom streams. Oecologia, **85**: 343–348.

Shapas, T.J., and Hilsenhoff, W.L. 1976. Feeding habits of Wisconsin's predominant lotic Plecoptera, Ephemeroptera, and Trichoptera. Gt. Lakes Entomol. **9**: 175–188.

Shepard, R.B., and Minshall, G.W. 1981. Nutritional value of lotic insect feces compared with allochthonous materials. Arch. Hydrobiol. **90**: 467–488.

Shepard, R.B., and Minshall, G.W. 1984. Role of benthic insect feces in a Rocky Mountain stream: fecal production and support of consumer growth. Holarct. Ecol. **7**: 119–127.

Steinman, A.D., and Lamberti, G.A. 1996. Biomass and pigments of benthic algae. *In* Methods in stream ecology. *Edited by* F.R. Hauer and G.A. Lamberti. Academic Press, New York. pp. 295–313.

Wallace, J.B., and Webster, J.R. 1996. The role of macroinvertebrates in stream ecosystem function. Annu. Rev. Entomol. **41**: 115–139.

Wallace, J.B., Eggert, S.L., Meyer, J.L., and Webster, J.R. 1999. Effects of resource limitation on a detrital-based ecosystem. Ecol. Monogr. **69**: 409–442.

Wiggins, G.B. 1996. Larvae of the North American caddisfly genera (Trichoptera). 2nd ed. University of Toronto Press, Toronto, Ont.

Wotton, R.S. 1994. Particulate and dissolved organic matter as food. *In* The biology of particles in aquatic systems. 2nd ed. *Edited by* R.S. Wotton. Lewis Publishers, Boca Raton, Fla. pp. 235–288.

Wotton, R.S., Malmqvist, B., Muotka, T., and Larsson, K. 1998. Fecal pellets from a dense aggregation of suspension-feeders in a stream: an example of ecosystem engineering. Limnol. Oceanogr. **43**: 719–725.

Yule, C.M. 1996. Trophic relationships and food webs of the benthic invertebrate fauna of two aseasonal tropical streams on Bougainville Island, Papua New Guinea. J. Trop. Ecol. **12**: 517–534.

© 2004 NRC Canada

The influence of oceanic and lagoonal plume waters on otolith chemistry

Heather M. Patterson, Michael J. Kingsford, and Malcolm T. McCulloch

Abstract: To determine how ocean and lagoonal plume waters from within the same reef were reflected in the chemical composition of otoliths, we conducted an experiment over three consecutive summers where conditions of temperature and food were held constant. Presettlement *Pomacentrus coelestis* were held in replicate tanks of the two water masses for 9 days. The sagittae were then analyzed at high spatial resolution (5 μm × 50 μm × 4 μm) using laser ablation inductively coupled plasma mass spectrometry. Ba/Ca and Sr/Ca varied between water masses and the rank of these elemental ratios changed among years. Although the reason for this change in rank is not known, likely mechanisms include upwelling and (or) the episodic appearance of phytoplankton blooms inside the lagoon. This is the first demonstration that the elemental signatures of otoliths can vary significantly over small spatial scales in reef systems in the absence of confounding factors, thus complicating studies attempting to discriminate reef-based stocks or elucidate natal origins using otolith chemistry.

Résumé : Afin de déterminer comment les eaux des panaches de l'océan et de la lagune dans un même récif se reflètent dans les composition des otolithes, nous avons procédé à une expérience dans des conditions constantes de température et d'alimentation au cours de trois étés consécutifs. Nous avons gardé des *Pomacentrus coelestis* dans un double jeu d'aquariums contenant chacun de l'eau de l'une des deux masses d'eau pendant 9 jours. Nous avons ensuite analysé les sagittas avec une forte résolution spatiale (5 μm × 50 μm × 4 μm) par ablation laser et un couplage de la spectrométrie de masse et de la spectrométrie d'émission à plasma par induction (spectrométrie LA–ICP–MS). Les rapports Ba/Ca et Sr/Ca diffèrent entre les masses d'eau et le rang de ces rapports d'éléments change d'une année à l'autre. Bien que la cause de ce changement de rang reste inconnue, les mécanismes possibles incluent la présence de résurgences et (ou) d'effloresences de phytoplancton à l'intérieur de la lagune. C'est la première fois qu'on démontre que la signature des éléments dans les otolithes peut varier sur de petites échelles spatiales dans un système lagunaire en l'absence de facteurs confondants, ce qui complique les études qui cherchent, à l'aide de la chimie des otolithes, à distinguer les stocks associés aux divers récifs et à retrouver les origines de ces stocks.

[Traduit par la Rédaction]

Introduction

Over the past 10 years, otolith chemistry has emerged as an alternative or complimentary method to tagging and genetic studies for examining the population structure as well as the movement patterns of marine fishes. The geochemical signature encoded within the aragonite matrix of the otolith can act as a natural tag. Otolith chemistry has been used to address issues such as determining nursery habitats (Gillanders and Kingsford 1996, 2000), examining stock structure (Campana et al. 1994; Patterson et al. 1999), estimating natal homing rates in a population (Thorrold et al. 2001), and estimating larval retention near reefs (Swearer et al. 1999). Like other biogenic carbonates, such as corals and foraminifera, otoliths may provide useful proxies for the reconstruction of temperature and environmental histories (Patterson et al. 1993; Bath et al. 2000). Such research relies on the assumption that the chemical signature of the otolith to some degree reflects the chemical signature of the water in which the organism resides. This assumption appears to be valid for marine fish, especially as otolith chemistry has proven to be useful in distinguishing geographically separated groups (see Campana (1999) for a review).

However, otolith deposition is a poorly understood process, and the synergies of ambient and physiological processes by which elements are deposited in the otolith matrix are complex. One of the most pressing issues yet to be fully addressed is the importance of microscale differences to interpreting otolith chemistry results. Several studies have demonstrated variation in otolith chemistry over small spatial scales, which could make attempts to discriminate fish on larger spatial scales more difficult. For example, Wells et

Received 7 August 2003. Accepted 14 February 2004. Published on the NRC Research Press Web site at http://cjfas.nrc.ca on 23 July 2004.
J17687

H.M. Patterson[1,2] **and M.J. Kingsford.** School of Marine Biology and Aquaculture, James Cook University, Townsville, Queensland 4811, Australia.
M.T. McCulloch. Research School of Earth Sciences, The Australian National University, Canberra, Australian Capital Territory 0200, Australia.

[1]Corresponding author (e-mail: hmpatt@unimelb.edu.au).
[2]Present address: Department of Zoology, University of Melbourne, Victoria 3010, Australia.

 doi: 10.1139/F04-036 © 2004 NRC Canada

al. (2003) noted that attempts to examine large-scale patterns of fish movement in a freshwater system might be confounded by fine-scale variation in water chemistry (i.e., at the individual stream level). Similarly, Thorrold et al. (1998) found elemental differences in the otoliths of fish collected from different sites within the same river, whereas Kingsford and Gillanders (2000) found significant differences in both the otoliths and eye lenses of fish collected from different depths within the same site. In addition, several studies have documented temporal variation in otolith signatures both within (Thorrold et al. 1998; Thorrold and Shuttleworth 2000) and among years (Patterson et al. 1999; Campana et al. 2000; Gillanders 2002), which could potentially confound the interpretation of spatial variability in otolith signatures. Thus, if otolith signatures are to be used for management purposes, these signatures will likely need to be recalibrated periodically (Campana et al. 2000; Gillanders 2002).

Studies examining otolith chemistry in general, and small-scale differences in particular, have been largely restricted to coastal areas (but see Patterson et al. 1999; Swearer et al. 1999), where differences in water chemistry, and therefore otolith chemistry, are more likely to be detectable due to terrestrial inputs and mixing processes (Thorrold et al. 2002). However, as coral reefs have become increasingly threatened (Knowlton 2001), it has become important to understand the population dynamics of reef species to provide adequate protection. Otolith chemistry may prove to be a useful tool in elucidating issues of connectivity and natal origins of reef fish, but no study to our knowledge has examined differences in otolith chemistry at small spatial scales (i.e., hundreds of metres) in these systems, despite the potential importance of such differences in interpreting larger scale results.

Our novel approach was to use manipulative experiments conducted in the field to determine if the chemistry of reef fish otoliths varied between plume and inter-reef waters (hereafter referred to as ocean waters) at a single reef in the Great Barrier Reef. We experimentally exposed presettlement reef fish to these two water masses (ocean versus plume) in the absence of confounding exogenous factors (i.e., temperature and food differences) to determine if differences in otolith chemistry at small spatial scales existed and if these differences were consistent over time. We used *Pomacentrus coelestis* as the study species because they were abundant in the waters around the study site, were easily captured in light traps, and are known to be robust to experimentation. The otoliths from these fish were analyzed using laser ablation inductively coupled plasma mass spectrometry (LA–ICP–MS) at high spatial resolution.

Materials and methods

Study site

This study was conducted on One Tree Island (OTI) in the southern Great Barrier Reef (23°30′S, 152°06′E) (Fig. 1). This type of platform reef is rare on the Great Barrier Reef; at low tide, the reef crest emerges and the lagoon water is isolated for 3–5 h until the next high tide (Maxwell 1968; Ludington 1979). This ponding behavior, in conjunction with the shallow nature of the lagoon, allows temperature differences of several degrees between the lagoon and surrounding ocean waters to develop (Atema et al. 2002). Thus, the geochemical properties of the lagoon water may develop in a distinct manner from ocean water. Transient, visible ebb tide plumes form on the leeward side of the reef (Atema et al. 2002), potentially exposing nearby organisms to lagoonal waters. Thus, OTI presented a unique opportunity to conduct a natural experiment examining the effects of the splitting and isolation of a single water mass on otolith chemistry at small spatial scales.

Fig. 1. Map of OTI (23°30′S, 152°06′E) off the eastern coast of Australia (inset) with the locations of the light traps depicted by squares. Solid squares indicate light traps that were fished in 2000 only and shaded squares indicate light traps that were fished during all years of the experiment. Water for the experimental plume treatments was taken just south of the light traps (shaded squares only) in the plume waters at the entrance of the lagoon, while ocean water was taken just north of the light traps (shaded squares only) outside the plume waters.

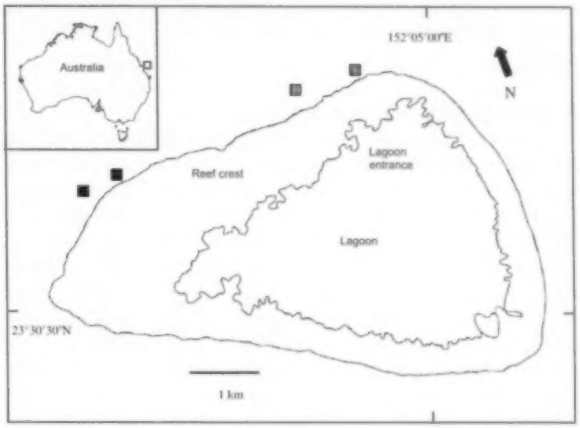

Fish collections

Presettlement *P. coelestis* were collected using two to four moored light traps at several sites within 100 m of the reef slope (Fig. 1) during three consecutive austral summer field seasons (2000–2002). Traps were illuminated for 3 h a night (2100–2200, 2400–0100, and 0300–0400) and were checked at the first morning high tide. Catches from the traps were sorted on the boat and nontarget species that were readily identifiable were recorded and returned to the ocean. Unknown and target species were taken to the laboratory to be counted and identified.

Experimental design

The experimental design for each year was nearly identical and differed only in the number of replicate fish placed in each tank at the beginning of the experiment (6 in 2000, 10 in 2001, and 3 in 2002). Experimental fish were allowed a minimum of 24 h to acclimate to experimental conditions before the start of the experiment. Three replicates of each treatment (plume water versus ocean water) were set up in 20-L tanks and replicate fish were randomly placed in each tank. Tanks were kept under shade cloth in a wet laboratory and aerated. Water was collected and changed daily (~90%). Fish were fed twice a day (morning and afternoon) with

© 2004 NRC Canada

Artemia and wild zooplankton and the water temperature was recorded at each feeding (mean for all years and treatments ± SE; morning feeding: 26.5 °C ± 0.09; afternoon feeding: 28.22 °C ± 0.09). For all years of the experiment, there were no significant differences in water temperature by tank nested in treatment (analysis of variance (ANOVA); morning: $F_{[1,4]} = 0.09$, $p > 0.05$; afternoon: $F_{[1,4]} = 0.06$, $p > 0.05$) or by treatment (ANOVA; morning: $F_{[1,4]} = 2.61$, $p > 0.05$; afternoon: $F_{[1,4]} = 5.13$, $p > 0.05$). Fish were maintained in this manner for a total of 9 days. At the end of the 9 days, three fish from each tank were frozen for elemental analysis.

Sample preparation and analysis

In the laboratory, standard length was measured and the sagittae were dissected in a laminar flow hood using only acid-washed plastic and glass instruments. The standard length of the *P. coelestis* used in the experiment (mean ± SE = 15.23 mm ± 0.07) did not differ between treatment groups for any year of the experiment (ANOVA; 2000: $F_{[1,16]} = 3.31$, $p > 0.05$; 2001: $F_{[1,16]} = 1.43$, $p > 0.05$; 2002: $F_{[1,16]} = 2.4$, $p > 0.05$) or among years ($F_{[2,51]} = 0.24$, $p > 0.05$). The otoliths were triple rinsed in Milli-Q water and were allowed to dry. Sagittae were embedded in Epofix resin and polished with grit size 800 lapping paper on a grinding machine and by hand until the primordium was visible and rings could be counted. Multiple otoliths (10 per slide) were then affixed in random order to a single slide with Crystalbond 509 adhesive in preparation for LA–ICP–MS.

Otoliths were analyzed using a Resonetics ArF excimer laser system coupled with a 7500 series Agilent ICP-MS (Table 1) (for a more extensive description of the system, see Eggins et al. (1998) or Sinclair (1999)). The calibration of the ICP–MS was achieved using NIST glass standard 612 (National Institute of Standards and Technology, Gaithersburg, Maryland). Relative standard deviation values were used as a measure of precision and were <5% for the standard. Each otolith was pre-ablated to remove surface contamination using a mask in the shape of a square slit ~530 µm × 530 µm. The pre-ablation procedure consisted of 10 individual laser pulses at ~90 mJ energy, with each pulse estimated to remove 0.10 µm (Eggins et al. 1998). The mask was then changed to a rectangular slit, producing a rastering (hereafter referred to as a laser footprint) 5 µm × 50 µm running perpendicular to the increments with an average depth of ~4 µm. The laser was pulsed at 10 Hz using ~90 mJ energy across the shortest axis of the otoliths from one edge to the other passing through the sulcus and the primordium. This allowed approximately seven data points to be collected per laser footprint. Data points on the edge of footprints were not used for any analyses to ensure that there was no overlap between footprints. Background levels and standards were collected before each series began and after each series, with each series comprising a maximum of five otoliths.

Otoliths were analyzed for ^{26}Mg, ^{43}Ca, ^{55}Mn, ^{88}Sr, and ^{138}Ba based on a preliminary analysis of three otoliths. Calcium was used as an internal standard, as it did not vary in concentration across the laser trajectory. Limits of detection (3σ of mean blank values in parts per million) were calculated as follows: ^{26}Mg, 1.47; ^{43}Ca, 0.11; ^{55}Mn, 0.11; ^{88}Sr, 0.027; ^{138}Ba, 0.014. The Epofix resin was analyzed as well and was determined not to contribute any contamination to the otoliths, as the resin was several orders of magnitude lower in elemental concentration than the otoliths. The surface of the otoliths was also kept free of resin and Crystalbond, and the otoliths were pre-ablated before analysis to err on the side of caution.

Table 1. Operating parameters of the LA–ICP–MS used in this study.

LA–ICP–MS	Agilent 7500s
Acquisition mode	Time resolved
Coolant gas flow rate	14 L·min^{-1}
Auxiliary gas flow rate	1 L·min^{-1}
Carrier gas flow rate (Ar)	1.15 L·min^{-1}
Carrier gas flow rate (He)	0.3 L·min^{-1}
RF power	1250 W
Dwell time	20 ms (per mass)
Detector mode	Dual simultaneous
Time slice	112.2 ms
Laser	Resonetics LPX120i
Laser type	ArF Excimer
Energy output	100 mJ
Wavelength	193 nm
Repetition rate	10 Hz
Spot size	150 µm × 1 mm
Crater size	5 µm × 50 µm × 4 µm

Image analysis

After the otoliths were sampled with the LA–ICP–MS, the daily increments were counted and measured using an image analysis system to determine the position of the pre-experimental and experimental portions of the otoliths. A drop of immersion oil was placed on each otolith to enhance its appearance and an image of each otolith was captured and saved at a magnification of 400× using a Leica DC300 digital video camera. Using the software package Leica IM50, the distance between each increment on the nonsulcal side of each otolith was measured; the sulcus of the otolith was not used in any analyses, as the increments in the sulcus were compressed and often difficult to discern and measure. Footprints, and the daily increments to which they corresponded, were also assigned a code based on the life history stage to which they were linked. The first three footprints from the dorsolateral margin of the primordium towards the ventrolateral margin of the otolith were designated the "natal region", while the fourth footprint through the start of the experiment was designated the "pre-experimental region". The last nine daily increments, corresponding to the 9 days of the experiment, were assigned to the "experimental region". It has previously been established with tetracycline marking that *P. coelestis* increments are deposited daily (Flood 2000). The footprints bordering a different life history region of the otolith were not used for any analyses.

Data analysis

Elemental data were normalized to Ca and expressed as molar ratios. Intensities were blank corrected, standardized to Ca, and interpolated to NIST values to correct for possible instrument drift using an Excel macro. Data were tested

© 2004 NRC Canada

Table 2. ANOVA results of $\ln(x + 1)$-transformed elemental ratios before the start of the experiment.

		Mg/Ca		Mn/Ca		Sr/Ca		Ba/Ca	
Source	df	MS	*F*	MS	*F*	MS	*F*	MS	*F*
Year	2	1.74	6.12*	0.08	1.66 ns	0.008	1.99 ns	0.06	0.50 ns
Treatment	1	0.83	0.77 ns	0.05	0.60 ns	0.004	0.57 ns	0.01	0.04 ns
Year × treatment	2	1.07	3.75 ns	0.08	1.61 ns	0.008	2.02 ns	0.27	2.17 ns
Tank (year × treatment)	12	0.29	1.19 ns	0.05	1.26 ns	0.004	0.99 ns	0.12	2.77**
Residual	36	0.24		0.04		0.004		0.04	

Note: $*p < 0.05$; $**p < 0.01$; ns, not significant.

for homogeneity of variances using a Cochran's *C* test and all elemental ratios were $\ln(x + 1)$ transformed; data were found to be homogeneous after transformation. To analyze increments corresponding to both the pre-experimental and experimental phases, mixed-model ANOVAs for each elemental ratio (Mg/Ca, Mn/Ca, Sr/Ca, and Ba/Ca) were used. In this design, there were three factors (year, treatment, and tank nested within the year × treatment interaction term). Treatment was a fixed factor and year and tank were random factors.

We used discriminant function analyses to determine how accurately we could classify fish to experimental water mass treatment. It was determined with a Box's *M* test that variance–covariance matrices were unequal. A quadratic discriminant function analysis was used, therefore, to determine how accurately otolith chemistry could distinguish fish from the different treatments by calculating a jackknife cross-validation. We acknowledge that this method produces classification accuracies higher than if a training data set were used. However, an independent data set was unavailable and using a subset of the experimental data was not practical given the small sample size per treatment and year. As there were two treatment groups per year that produced single canonical variates, we plotted those variates using jittered dot density plots to illustrate separation in multivariate space.

Fig. 2. Elemental ratios (+SE) for the pre-experimental region of the otoliths ($n = 9$ fish). Solid bars denote ocean treatment and shaded bars denote plume treatment for each ratio. (*a*) Sr/Ca; (*b*) Mg/Ca; (*c*) Ba/Ca; (*d*) Mn/Ca.

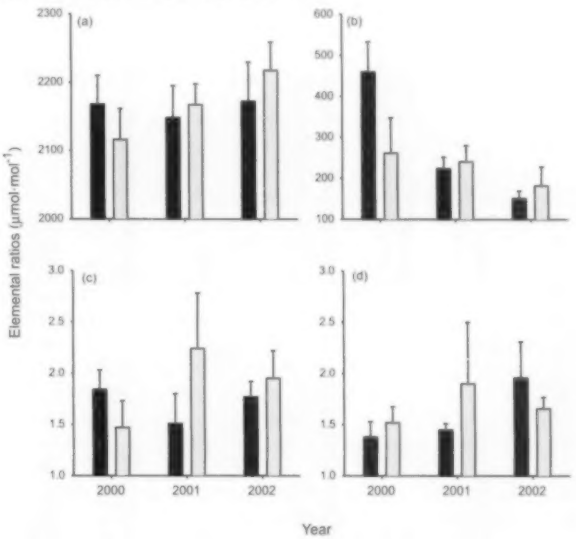

Results

Pre-experiment

No differences in otolith chemistry existed between the treatment groups and no interactions were detected prior to the start of the experiment (Table 2; Fig. 2). However, a significant year difference was found for Mg/Ca. In addition, there were differences among tanks nested in the year × treatment interaction term for Ba/Ca. This was not unexpected, as the fish collected for the experiment could have encountered different water masses during the pelagic phase of their life history, thus accounting for differences in their otolith microchemistry. This difference was not present during the experimental phase.

Experiment

Elemental ratios of Ba/Ca and Sr/Ca varied between otoliths exposed to different water masses during the experiment. The ranking of these ratios, however, varied among years, as indicated by a significant interaction between year and treatment (Table 3). For example, Ba/Ca was higher in ocean waters in 2000, similar to that in plume water in 2001, and was much higher than in plume water in 2002 (Fig. 3). No interaction was found for Mn/Ca and Mg/Ca. The Mg/Ca ratios for both treatment groups were greater in 2001 than in other years of the experiment.

We were able to obtain good accuracy in classifying fish to water mass treatment using a multivariate (discriminant function analysis) approach. Correct classification rates ranged from 67% to 100% for individual years, with 2000 displaying the best separation (Table 4; Fig. 4). The elements driving the separation between treatment groups varied among years, with Ba/Ca and Sr/Ca contributing in 2000, Sr/Ca being the major discriminator in 2001, and Ba/Ca being the major discriminator in 2002.

Discussion

This study has demonstrated that the otolith chemistry of reef fish can vary over small spatial scales (hundreds of metres). Although we were not able to directly attribute these differences to water chemistry, it seems likely that variation between plume and oceanic waters at OTI was the source of the noted differences. The separation and isolation of lagoon water may have modified the chemical composition

© 2004 NRC Canada

Table 3. ANOVA results for $\ln(x + 1)$-transformed elemental ratios measured in otoliths during the experimental period.

		Mg/Ca		Mn/Ca		Sr/Ca		Ba/Ca	
Source	df	MS	*F*	MS	*F*	MS	*F*	MS	*F*
Year	2	5.64	12.24**	0.33	2.38 ns	0.27	26.68***	1.61	46.95***
Treatment	1	0.01	0.54 ns	0.02	0.59 ns	0.13	1.71 ns	1.08	0.22 ns
Year × treatment	2	0.02	0.04 ns	0.02	0.17 ns	0.08	7.62**	0.34	9.94**
Tank (year × treatment)	12	0.46	1.19 ns	0.14	1.57 ns	0.01	0.57 ns	0.03	0.49 ns
Residual	36	0.39		0.39		0.12		0.45	

Note: $^{**}p < 0.01$; $^{***}p < 0.001$; ns, not significant.

Fig. 3. Elemental ratios (+SE) for the experimental region of the otoliths by year of the experiment and treatment (n = 9 fish). Solid bars denote ocean treatment and shaded bars denote plume treatment for each ratio. (*a*) Sr/Ca; (*b*) Mg/Ca; (*c*) Ba/Ca; (*d*) Mn/Ca.

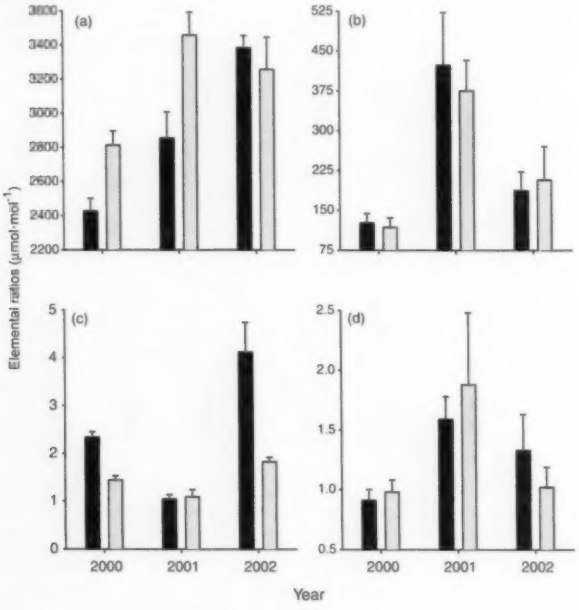

Table 4. Results of the jackknife cross-validation procedures to classify fish from the two experimental treatments by year and with all years combined.

Year	*n*	df	Ocean	Plume	*F*
2000	9	4,13	89	100	13.37*
2001	9	4,13	89	67	2.34 ns
2002	9	4,13	89	67	5.79*
All years	54	4,49	78	74	5.34*

Note: Correct classifications are noted as percentages for each experimental treatment group (ocean or plume), and the Pillai trace F statistic resulting from the discriminant function analysis is also noted. n, the number of individuals; *, $p < 0.01$; ns, not significant.

relative to the surrounding ocean water. Indeed, previous studies have demonstrated that not only can presettlement fish at OTI distinguish between plume and ocean waters (Atema et al. 2002) but also that *P. coelestis* appear to actively avoid settling within plume/lagoon waters (Doherty et al. 1996). Thus, the two water masses were likely influenced by different mechanisms, which would vary temporally. On a large scale, such mechanisms could include freshwater input (Secor et al. 1995), which is unlikely, since OTI is well offshore (>80 km), natural biogeochemical cycling of elements (Bruland 1983), and changes in horizontal circulation that may result in the delivery of different packets of water to the area (Doherty et al. 1996; Haskew 2002).

Fig. 4. Jittered dot density plots using the canonical variates derived from the quadratic discriminant function analyses for (*a*) 2000, (*b*) 2001, and (*c*) 2002 (n = 9 fish). Circles indicate ocean treatment and triangles indicate plume treatment.

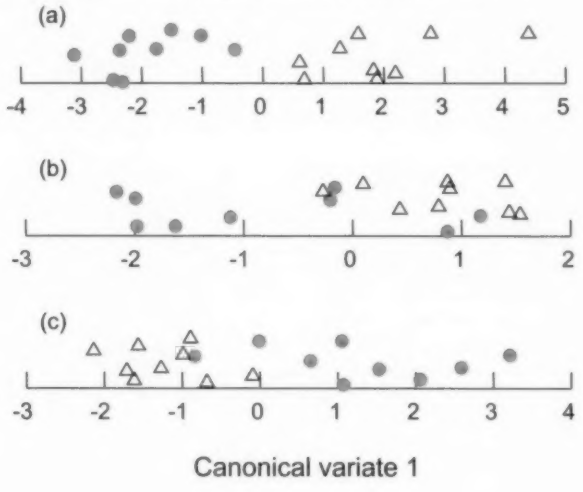

On a more local scale, upwelling and phytoplankton blooms may play a role. Upwelling, which has been documented at OTI (Haskew 2002), has been shown to influence the chemistry of corals (Shen et al. 1987; Lea et al. 1989) and has been suggested as a mechanism for variation in otolith chemistry (Patterson et al. 1999). Settled *P. coelestis* collected in 2002 from the reef slope (~20 m) around OTI and several other reefs in the region revealed very high Ba/Ca levels in the postsettlement portions of their otoliths (~30 μmol·mol^{-1}), suggesting that these fish were in upwelled waters enriched in Ba (Patterson et al. 2004). Although the Ba/Ca levels of the experimental fish were not nearly as high (~4 μmol·mol^{-1}) in 2002, they were much higher than Ba/Ca levels measured in the plume treatment fish from 2002, as well as fish from the other years of the experiment.

© 2004 NRC Canada

A less studied mechanism that may influence plume water is phytoplankton blooms within the OTI lagoon. It has been documented that the precipitation of barite ($BaSO_4$), the primary natural source of Ba, is elevated in areas of high productivity and may be facilitated by the decay of phytoplankton blooms (Dehairs et al. 1980; Bishop 1988; Stecher and Kogut 1999). Phytoplankton blooms do occur in the OTI lagoon, particularly during neap tides when oceanic waters do not adequately flush the lagoon for several days (H.M. Patterson and M.J. Kingsford, personal observations). It is possible that these blooms, facilitated by isolation from oceanic waters due to the ponding lagoon and neap tides, reduce the dissolved Ba in the water column and in fish otoliths. Conversely, cyclones and storms in the areas may facilitate more exchange with ocean waters through storm surge over the reef crest, thus reducing any accumulated differences from blooms or other mechanisms in the lagoon water.

Irrespective of the basis of this difference in otolith chemistry, the consequences are quite clear. Future studies attempting to discriminate reef fish using otolith chemistry or attempting to assign fish to a reef of origin could potentially be confounded by small-scale variation within a reef. Such variation has been documented in several other studies in temperate systems (Thorrold et al. 1998; Kingsford and Gillanders 2000; Wells et al. 2003). Thus, large effect sizes will be required to distinguish reefs or populations given the high variability within a reef. Such effect sizes have been attainable in temperate systems (Thorrold et al. 1998) and may be possible to attain in reef systems (Patterson et al. 2004), although distinct water masses such as those present at OTI due to the ponding lagoon may be less distinct elsewhere. However, low flushing or semienclosed areas may be able to develop chemistries distinct from those of the surrounding water masses, as may areas with seasonal upwelling. Additionally, elemental signatures of reef fish are not temporally stable, compounding the problem. This temporal instability in signatures has also been demonstrated in temperate fish (Campana et al. 2000; Rooker et al. 2001; Gillanders 2002), and thus, signatures being used as stock or nursery markers will need to be recharacterized, likely on annual scales at least, to prevent significant drift between marker characterization and application (Campana et al. 2000; Gillanders 2002). Our results suggest that studies of tropical species will have to recharacterize relevant elemental signatures periodically as well.

In conclusion, this is the first demonstration that reef fish in natural water masses separated by small spatial scales (hundreds of metres) can have distinct otolith chemistries, independent of differences in temperature and food. The variation between fish in the experimental treatments likely represented a complex coupling of multiple factors that remains to be fully explained, although upwelling and phytoplankton blooms within those water masses probably played a role. Our findings have major implications for the use of otolith chemistry in connectivity and stock discrimination applications and suggest small-scale variation and temporal fluctuations should be considered in future studies. Although more research is required to fully understand the complex oceanographic and biological processes that may contribute to water and otolith chemistry, the high resolution possible with LA–ICP–MS is promising for the continued use of otolith chemistry as a tool for examining complex ecological issues.

Acknowledgements

We thank M. Flood, J. Browne, J. Eagle, J. Hughes, and S. Burgess for assistance in the field. M. Shelley, D. Sinclair, S. Fallon, T. Wyndham, and L. Kinsley provided assistance with the LA–ICP–MS and technical advice. The manuscript was improved by the comments of B. Gillanders and several anonymous reviewers. A Doctoral Merit Research Scholarship from James Cook University, CRC Reef Research Centre Grant, and GBRMPA Augmentative Grant to H.M.P. and an ARC grant to M.J.K. supported this project.

References

Atema, J., Kingsford, M.J., and Gerlach, G. 2002. Larval reef fish could use odour for detection, retention and orientation to reefs. Mar. Ecol. Prog. Ser. **241**: 151–160.

Bath, G.E., Thorrold, S.R., Jones, C.M., Campana, S.E., McLaren, J.W., and Lam, J.W.H. 2000. Strontium and barium uptake in aragonite otoliths of marine fish. Geochim. Cosmochim. Acta, **64**: 1705–1714.

Bishop, J.K. 1988. The barite – opal – organic carbon association in oceanic particulate matter. Nature (Lond.), **332**: 341–343.

Bruland, K.W. 1983. Trace elements in sea-water. *In* Chemical oceanography. Vol. 8. *Edited by* J.P. Riley and R. Chester. Academic Press, London, UK. pp. 157–215.

Campana, S.E. 1999. Chemistry and composition of fish otoliths: pathways, mechanisms and applications. Mar. Ecol. Prog. Ser. **188**: 263–297.

Campana, S.E., Fowler, A.J., and Jones, C.M. 1994. Otolith elemental fingerprinting for stock discrimination of Atlantic cod (*Gadus morhua*) using laser ablation ICPMS. Can. J. Fish. Aquat. Sci. **51**: 1942–1950.

Campana, S.E., Chouinard, G.A., Hanson, J.M., Frechet, A., and Brattey, J. 2000. Otolith elemental fingerprints as biological tracers of fish stocks. Fish. Res. **46**: 343–357.

Dehairs, F., Chesselet, R., and Jedwab, J. 1980. Discrete suspended particles of barite and the barium cycle in the open ocean. Earth Planet. Sci. Lett. **49**: 528–550.

Doherty, P.J., Kingsford, M.J., Booth, D.J., and Carleton, J. 1996. Habitat selection before settlement by *Pomacentrus coelestis*. Mar. Freshw. Res. **47**: 391–399.

Eggins, S.M., Kinsley, L.P.J., and Shelley, J.M. 1998. Deposition and fractionation processes during atmospheric pressure laser sampling for analysis by ICP–MS. Appl. Surf. Sci. **127–129**: 278–286.

Flood, M.J. 2000. Otolith microstructure in pre- and post-settlement *Pomacentrus coelestis* (Pisces: Pomacentridae). Honours thesis, University of Sydney, Sydney, Australia.

Gillanders, B.M. 2002. Temporal and spatial variability in elemental composition of otoliths: implications for determining stock identity and connectivity of populations. Can. J. Fish. Aquat. Sci. **59**: 669–679.

Gillanders, B.M., and Kingsford, M.J. 1996. Elements in otoliths may elucidate the contribution of estuarine recruitment to sustaining coastal reef populations of a temperate reef fish. Mar. Ecol. Prog. Ser. **141**:13–20.

© 2004 NRC Canada

Gillanders, B.M., and Kingsford, M.J. 2000. Elemental fingerprints of otoliths may distinguish estuarine "nursery" habitats. Mar. Ecol. Prog. Ser. **201**: 273–286.

Haskew, R. 2002. Circulation around One Tree Reef, Great Barrier Reef, Australia. M.Sc. thesis, University of Waikato, Hamilton, New Zealand.

Lea, D.W., Shen, G.T., and Boyle, E.A. 1989. Coralline barium records temporal variability in equatorial Pacific upwelling. Nature (Lond.), **340**: 373–376.

Ludington, C.A. 1979. Tidal modifications and associated circulation in a platform reef lagoon. Aust. J. Mar. Freshw. Res. **30**: 425–430.

Kingsford, M.J., and Gillanders, B.M. 2000. Variation in concentrations of trace elements in the otoliths and eye lenses of a temperate reef fish, *Parma microlepis* as a function of depth, spatial scale and age. Mar. Biol. **137**: 403–414.

Knowlton, N. 2001. The future of coral reefs. Proc. Nat. Acad. Sci. U.S.A. **98**: 5419–5425.

Maxwell, W.G.H. 1968. Atlas of the Great Barrier Reef. Elselvier, Amsterdam, Netherlands.

Patterson, H.M., Thorrold, S.R., and Shenker, J.M. 1999. Analysis of otolith chemistry in Nassau grouper (*Epinephelus striatus*) from the Bahamas and Belize using solution-based ICP–MS. Coral Reefs, **18**: 171–178.

Patterson, H.M., Kingsford, M.J., and McCulloch, M.T. 2004. Elemental signatures of *Pomacentrus coelestis* at multiple spatial scales on the Great Barrier. Mar. Ecol. Prog. Ser. **270**: 229–239.

Patterson, W.P., Smith, G.R., and Lohmann, K.C. 1993. Continental paleothermometry and seasonality using the isotopic composition of aragonite otoliths of freshwater fishes. Geophys. Monogr. **78**: 191–202.

Rooker, J.R., Secor, D.H., Zdanowicz, V.S., and Itoh, T. 2001. Discrimination of northern bluefin tuna from nursery areas in the Pacific Ocean using otolith chemistry. Mar. Ecol. Prog. Ser. **218**: 275–282.

Secor, D.H., Henderson-Arzapalo, A., and Piccoli, P.M. 1995. Can otolith microchemistry chart patterns of migration and habitat utilization in anadromous fishes? J. Exp. Mar. Biol. Ecol. **192**: 15–33.

Shen, G.T., Boyle, E.A., and Lea, D.W. 1987. Cadmium in corals as a tracer of historical upwelling and industrial fallout. Nature (Lond.), **328**: 794–796.

Sinclair, D.J. 1999. High spatial-resolution analysis of trace elements in corals using laser ablation ICP-MS. Ph.D. thesis, The Australian National University, Canberra, Australia.

Stecher, H.A., and Kogut, M.B. 1999. Rapid barium removal in the Delaware estuary. Geochim. Cosmochim. Acta, **63**: 1003–1012.

Swearer, S.E., Caselle, J.E., Lea, D.W., and Warner, R.R. 1999. Larval retention and recruitment in an island population of a coral-reef fish. Nature (Lond.), **402**: 799–802.

Thorrold, S.R., and Shuttleworth, S. 2000. In situ analysis of trace elements and isotope ratios in fish otoliths using laser ablation sector field inductively coupled plasma mass spectrometry. Can. J. Fish. Aquat. Sci. **57**: 1232–1242.

Thorrold, S.R., Jones, C.M., Campana, S.E., McLaren, J.W., and Lam, J.H.W. 1998. Trace element signatures in otoliths record natal river of juvenile American shad (*Alosa sapidissima*). Limnol. Oceanogr. **43**: 1826–1835.

Thorrold, S.R., Latkoczy, C., Swart, P.K., and Jones, C.M. 2001. Natal homing in a marine fish metapopulation. Science (Wash., D.C.), **291**: 297–299.

Thorrold, S.R., Jones, G.P., Hellberg, M.E., Burton, R.S., Swearer, S.E., Neigel, J.E., Morgan, S.G., and Warner, R.R. 2002. Quantifying larval retention and connectivity in marine populations with artificial and natural markers. Bull. Mar. Sci. **70**(Suppl.): 291–308.

Wells, B.K., Rieman, B.E., Clayton, J.L., Horan, D.L., and Jones, C.M. 2003. Relationships between water, otolith, and scale chemistries of westslope cutthroat trout from the Coeur d'Alene River, Idaho: the potential application of hard-part chemistry to describe movements in freshwater. Trans. Am. Fish Soc. **132**: 409–424.

© 2004 NRC Canada

Influence of river speed on path selection by migrating adult sockeye salmon (*Oncorhynchus nerka*)

Emily M. Standen, Scott G. Hinch, and Peter S. Rand

Abstract: We applied stereovideographic techniques to investigate path selection, ground speed, and swimming speed in adult sockeye salmon (*Oncorhynchus nerka*) ascending the Seton River, British Columbia. We tracked three-dimensional trajectories of salmon through 10 reaches and characterized the current profile at each site. At sites with relatively slow currents, the encountered river current speeds along the fish's trajectory were significantly lower than the mean current speed of the site. However, at higher current speed sites, fish experienced current speeds at or above the average current speed of the site and increased their ground speed through these sites. Observed in situ swimming speeds were 1.4–76.0 times greater than swimming speeds expected based on tailbeat frequency – swimming speed predictive relationships established in flume studies. We conclude that (*i*) at sites with relatively slow or moderate current speeds, fish minimize exposure to high-speed currents to minimize energy expenditure, (*ii*) at sites with high-speed currents, fish may change their migration strategy, minimizing time spent searching for low current speed pathways and increasing their ground speed to expedite passage, and (*iii*) laboratory-derived predictive equations may only be appropriate for predicting in situ swimming costs at sites with moderate and linearly flowing currents.

Résumé : Nous avons utilisé des techniques de vidéographie stéréo pour étudier le choix des voies de passage, la vitesse au sol et la vitesse de nage chez des saumons rouges (*Oncorhynchus nerka*) adultes qui remontent la rivière Seton, en Colombie-Britannique. Nous avons suivi les trajectoires tridimensionnelles des saumons à travers 10 sections du cours d'eau et avons décrit les profils des courants à chaque site. Aux sites de courants relativement lents, la trajectoire des poissons traverse des vitesses de courant significativement plus faibles que la vitesse de courant moyenne de la rivière à ce site. Cependant, aux sites de courants plus forts, les poissons rencontrent des vitesses de courant égales ou supérieures à la vitesse de courant moyenne du site et augmentent leur vitesse au sol en traversant ces sites. Les vitesses de nage observées dans le milieu sont 1,4–76,0 fois plus élevées que celles qui sont attendues d'après les relations prédictives entre la fréquence de battement de la queue et la vitesse de nage établies en canal expérimental. Nous concluons que (*i*) aux sites de vitesses de courant relativement lentes ou moyennes, les poissons minimisent leur exposition aux courants rapides afin de réduire leurs dépenses énergétiques au minimum, (*ii*) aux sites de forts courants, les poissons changent probablement de stratégie de migration en réduisant le temps consacré à la recherche de voies à faibles courants et en accélérant leur vitesse au sol de manière à réduire leur temps de traversée et (*iii*) les équations prédictives obtenues en laboratoire ne semblent pouvoir servir à évaluer les coûts de la nage in situ qu'aux sites de courants modérés à flux linéaire.

[Traduit par la Rédaction]

Introduction

Most anadromous adult fish cease feeding upon starting spawning migrations and must complete the upriver journey and spawn using reserve energy. Body constituent analyses of fish sampled at the start and at the end of the migration have revealed that these migrations can be energetically demanding (e.g., 50–70% of initial energy may be used; Brett 1995; Jonsson et al. 1997; Leonard and McCormick 1999). Migrants may use several different behavioural tactics to conserve energy including selecting low-speed current paths, burst-and-coast swimming, or swimming steadily at metabolic optimal speeds, defined as the speed that minimizes energy expenditure per metre traveled (reviewed in Webb 1995).

In addition, migrants may choose areas of reduced flow. This hypothesis to minimize energy consumption during migration was first postulated decades ago (Osborne 1961).

Received 22 September 2003. Accepted 13 January 2004. Published on the NRC Research Press Web site at http://cjfas.nrc.ca on 23 July 2004.
J17752

E.M. Standen[1,2] **and S.G. Hinch.** Department of Forest Science, University of British Columbia, Vancouver, BC V6T 1Z4, Canada.
P.S. Rand. The Wild Salmon Center, 721 NW 9th Avenue, Suite 280, Portland, OR 97209-3451, USA.

[1]Corresponding author (e-mail: standen@fas.harvard.edu).
[2]Present address: Department of Organismic and Evolutionary Biology, Harvard University, 26 Oxford Street, Cambridge, MA 02139, USA.

 doi: 10.1139/F04-035 © 2004 NRC Canada

Past studies of salmon migration behaviour based on visual observations and split-beam echosounders have shown that salmon swim linearly along the banks and bottom of river systems (Ellis 1966*a*; Xie et al. 1997). In a report on the migration behaviour of salmon, Ellis (1966*a*) showed salmon to migrate preferentially in nearshore and deeper water with marked lower current speeds. Fretwell (1981) has also shown adult fish to migrate near shore in current speeds below that of the average river flow. These observations suggest that salmon are able to distinguish between high- and low-speed flow fields on a large (entire river) scale. Salmon have also been shown to initiate upriver migration on incoming tides presumably taking advantage of the decrease in downstream river flow when possible (reviewed in Groot and Margolis 1991). As a result, salmon appear to preferentially migrate in lower speed flow areas within large river systems.

More recent studies using physiological telemetry on upriver-migrating adult Pacific salmon (*Oncorhynchus* spp.) have demonstrated that current speed and flow turbulence are important environmental features affecting energy use (Hinch and Rand 1998; Standen 2001; Standen et al. 2002). These studies have suggested that differences among species, sexes, or reaches in relative energy use are largely attributed to differences in behaviour (e.g., swim speeds, migratory paths). Within these studies, fish were also found to migrate close to shore and to the bottom, suggesting that fish are avoiding high current speed, energetically expensive areas within the river. These telemetry studies provide measures of behaviour at relatively coarse scales over reaches of 50–1000 m in length. The objective of the present study was to determine if migrants can take advantage of finer scale speed current variations within a reach towards improving our understanding of how swimming behaviours may affect energy utilization or conservation during migration.

Underwater stereovideography was recently employed to explore the behavioural tactics used by upriver-migrating adult sockeye salmon (*Oncorhynchus nerka*) to conserve energy on a fine scale (Hinch and Rand 2000). This study concluded that salmon minimized energy costs per metre traveled when encountered currents were slow (i.e., <0.25 m·s^{-1}). It also suggested that at this fine scale, salmon might actively select low-speed or reverse-flow current pathways as additional means of conserving energy (Osborne 1961). However, there were significant limitations to the methodological approach of Hinch and Rand (2000). Their camera calibration technique limited data collection only to those individuals that swam along a plane within the field of view. Therefore, it was not possible to fully explore the hypotheses that salmon were choosing certain pathways (e.g., low current speed or reverse-flow areas) over others. Consequently, energy cost estimations that were based on laboratory-derived metabolic rates for rectilinear swimming ignore fish taking more circuitous paths. While Pacific salmon do exhibit "line swimming" behaviour, with relatively straight trajectories within nearshore areas of reduced flow in large, fast flowing rivers (Ellis 1966*a*), migrations are less directed and they display higher levels of meandering in small rivers and streams. Thus, the "planar" observational approach that Hinch and Rand (2000) relied on in their video methodology may not be appropriate for studying migration behaviours of many stocks and locations of anadromous fish.

The present study examines behaviours of fish exhibiting both linear and nonlinear migration pathways within chosen reduced flow areas by employing a three-dimensional stereovideographic approach (Hughes and Kelly 1996). We follow actual trajectories through the water to determine swimming speed and speed over the ground of adult sockeye salmon during segments of their upriver migration. Using bioenergetic equations found in the literature, we also compare observed swimming speeds (U_{obs}) with theoretical optimal swimming speeds (U_{opt}) in an attempt to describe fish migration behaviour in situ and improve upon previously published description techniques.

Methods

Study site and animals

We focused our study on Gates Creek sockeye salmon, a relatively abundant Fraser River stock. In July and August of each year, mature adults migrate nearly 600 km, gaining 300 m in elevation, from the Fraser River mouth to spawning grounds. In 2000, we selected 10 sites in the upper and lower Seton River for video observations. The Seton River is a relatively small river with a maximum width of 20 m, a depth between 0.5 and 3 m, and a gradient ranging from 0.1% to 0.8%. Sites were selected to include the full range of average current speeds. All were easily accessible and had excellent water clarity. We videotaped migrating fish (average length = 64.4 cm, SD = 13.5 cm) from 27 July to 8 August.

Video system

We used four black and white charged couple device cameras. Two were Panasonic WV-BP312 with 570 lines of horizontal resolution and two were Cohu model 2100 with 570 lines of horizontal resolution and were fitted with a spherical high-speed aperture lens (Panasonic WV-LA408C3 with 4.5-mm focal length and Cosmicar/Pentax with 3.7-mm focal length, respectively). Each pair of cameras was oriented in parallel (optical axis separation of 11.3 and 8.2 cm, respectively) and fixed to a stand located 1–5 m away from the subject. Each camera was enclosed in a cylindrical anodized aluminum housing fitted with flat Plexiglas ports. Video signals were sent to a multiplexer-quad unit (Panasonic WJ-420) and then to a VHS time-lapse recorder (Panasonic AG-6124) where images from all cameras were recorded simultaneously on the same video frame at 60 frames·s^{-1}. Thus, the recorded video image was a composite of four independent, time-synched images, one for each camera. A black and white LCD monitor (1024 × 768 pixels) (OmniVision Inc., Sunnyvale, Calif.) was used to assist with focus, calibration, camera orientation, and determination of water and fish speeds. All components of the system were powered by two 12-V deep-cycle batteries. At all sites, cameras were positioned underwater facing the centre of the river, with their optical axis parallel to the surface of the water. Cameras were able to clearly record images of fish at up to 10 m into the river within which most of the migrating fish were located.

© 2004 NRC Canada

Fig. 1. Diagram of the underwater video setup. Cameras situated underwater sent video signals through cables to a multiplexer-quad unit (A) and then to a VHS time-lapse recorder (B) where all signals were recorded simultaneously on the same video frame. Images were viewed on a television monitor (C). All components were powered by two 12-V deep-cycle batteries (D). Inset: the video image was calibrated using an aluminum cube placed momentarily in the field of view of the cameras and digitized to provide a scaled grid from which to measure all other distances. River velocity was also measured in a 27-point grid within the field of view of the cameras.

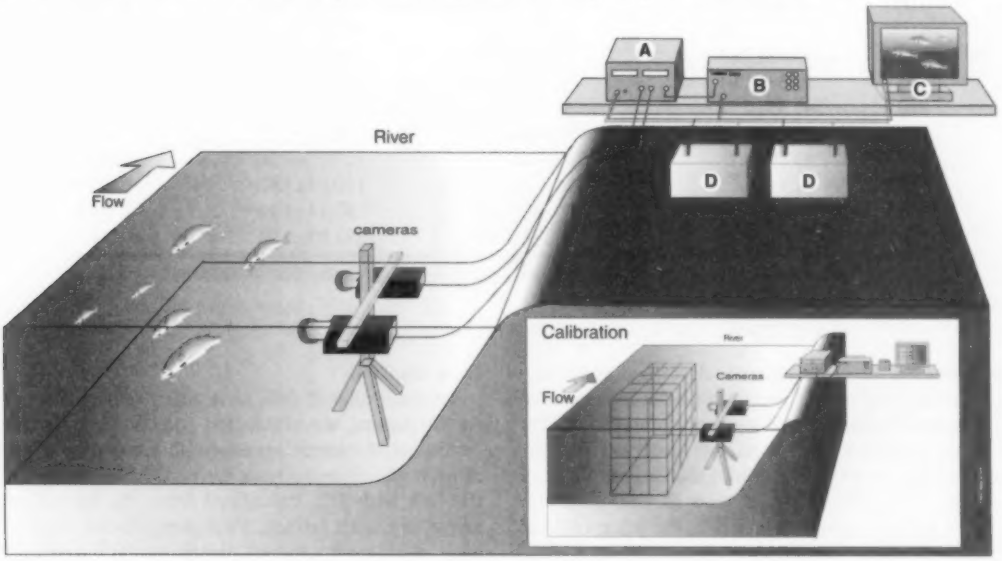

Camera calibration and data collection

Camera calibration was conducted according to methods developed by Hughes and Kelly (1996) and is described below. Cameras were calibrated using a 0.3 m × 0.5 m × 0.5 m aluminum quadrat. The quadrat resembled a cage with horizontal and vertical aluminum bars (each 1 cm in diameter) at 10-cm intervals (hereafter referred to as nodes). Each pair of cameras was set up and secured so that they were immobile during the observations. The quadrat was placed in the field of view of each pair of cameras (see example in Fig. 1 inset) to ensure that at least nine nodes from both the near and far face of the quadrat were visible in both cameras. To reduce calibration error, the quadrat was placed within the path of the majority of fish as seen from shore (Fig. 1 inset). After the quadrat's image was recorded, it was removed from the water. In the laboratory, video images were replayed and a single frame video image of the quadrat was captured and digitized. The nodes of the near and far face were digitized for each camera to get two sets of x,y coordinates of the quadrat. The x,y coordinates were then analyzed using algorithms in Hughes and Kelly (1996), which allowed us to take two-dimensional stereo images and calculate three-dimensional x,y,z real-world coordinates. We found error (estimated by determining error of locating corner nodes on the quadrat) in determining positional fixes to be low (≤2 cm).

Current speed within the field of view was measured using a CMC-2 current meter with a number 3 propeller of size 50 mm × 0.025 m (Hydrological Services Ltd., Sydney, Australia). Current speeds were assessed in a three-dimensional grid pattern within the field of view of the camera. Each site location consisted of about 2.5 m^3 of water (1.3 m × 1.3 m × 1.5 m) within which 27 current speed measurements were taken; the average distance between adjacent measurements was 25.7 cm (SD = 17.4). Average site velocity is calculated as the average of the 27 current speed measurements. Current speed measurements were made at the end of each site recording session and water heights were measured multiple times daily to ensure that water discharge was constant throughout the data collection process. The net direction of flow at each site was always in the downriver direction. Depth was also recorded at each position where speeds were measured. These depth measurements were used to compute mean water depth at each of our sites. The propeller of the current meter was videotaped and digitized to determine the three-dimensional location of the measured current points. These current values, as well as their location, were then interpolated (Matlab, version 5.3.0.14912a(R11)) (The Mathworks, Inc., Natick, Mass.) based on distance averaging with a linear smoothing factor to predict current speeds between measured points. In this manner, current speed at any point within 50 cm of the measured calibration points in the camera field of view could be calculated.

Cameras recorded fish migrations for 2–8 h, during daylight, at each site. The range in recording times depended on the frequency of fish passage at a particular site. Fish were selected from video images based on their visual clarity. Generally, fish positioned within 3 m of the cameras produced the clearest images and were thus used. To decrease error, fish that were greater than 50 cm from the nearest quadrat or current measurement point were not used. At least 30 fish were recorded swimming by the cameras at each site, 20 of which were randomly selected and digitized

© 2004 NRC Canada

Table 1. Theoretical optimal swimming speed (U_{opt}) and observed swimming speed (U_{obs}) for each video site.

Site	Encountered velocity ($cm \cdot s^{-1} \pm SE$)	U_{opt} ($cm \cdot s^{-1} \pm SE$)	U_{obs} ($cm \cdot s^{-1} \pm SE$)	P
SD12	4.46±0.08	54.46±0.08	125.24±8.16	<0.001*
SD34	9.61±0.83	59.61±0.83	92.53±3.26	<0.001*
B12	10.73±2.03	60.73±2.03	77.42±13.59	0.301
E34	34.54±1.91	84.53±1.91	71.40±3.83	<0.001*
E12	41.55±0.58	91.55±0.58	86.25±3.38	0.160
J34	43.76±0.75	93.76±0.75	95.91±4.77	0.635
J12	57.19±0.78	107.19±0.78	123.71±3.56	<0.001*
O12	61.11±1.01	111.11±1.01	120.43±3.67	0.025*
D212	70.60±1.31	120.60±1.31	142.13±4.41	<0.001*
V34	140.56±1.12	190.56±1.12	291.95±6.52	<0.001*

Note: P values from paired t tests are listed with an asterisk denoting significant differences between U_{opt} and U_{obs} for given sites.

for analysis following the same methods described above for the quadrat. If the digitized fish were within the minimal error range of the calibration cube, they were included in the analysis. Migration pathway was digitized based on rostrum tip location at the point of first entry into the camera field of view and first exit out of the field of view as well as every one quarter of a second in between. Using the interpolation program described above, the current speed that each fish encountered (hereafter referred to as encountered current speed) was estimated at each digitized location along the fish pathway as well as at all midpoints between digitized locations. Speed over the ground for each fish was determined by measuring the distance that the fish traveled over 15 video frames (frame rate was 1/60th of a second). Fish not only make headway through the water, but as the water flows downstream, they must also make headway over the ground. Therefore, U_{obs} for each fish was calculated as the sum of the encountered current speed and the speed over the ground.

We also calculated U_{opt} at each site using the sockeye salmon bioenergetics model used in Hinch and Rand (1998) to define the cost of transport curve from which U_{opt} is calculated (Table 1) (see Videler (1993) for a theoretical explanation of the calculation of U_{opt}). We then compared U_{obs} at each site with the U_{opt} calculated from the bioenergetics equation to facilitate discussion of observed migration behaviour.

We viewed the tapes in slow motion and determined the tailbeat frequency (TBF) (one complete oscillation of the caudal peduncle was considered one tailbeat) of each fish as it passed through a site. We then estimated the speed expected at the measured TBF, which we defined as tailbeat swimming speed, from a previously published laboratory-derived relationship between TBF and rectilinear swimming speed (Brett 1995). This approach for estimating swimming speed had been used in recent field examinations of salmon migrations (Hinch and Rand 1998; Standen et al. 2002). However, this approach may underestimate costs of migration because of this rectilinear assumption. We will compare this previous approach with our more realistic three-dimensional one.

Data analysis

To determine if fish were using low-speed current fields for migration, we conducted paired t tests to compare fish encountered current speeds with average site current speed at each site. Paired t tests were also used to compare U_{obs} of the fish with U_{opt} calculated from the bioenergetics model and again with tailbeat swimming speed. Analysis of variance, with least squared means as the a posteriori method, was used to compare speed over the ground, U_{obs} and tailbeat swimming speed among sites. All statistical tests were based on $P \leq 0.05$, and Bonferroni's correction was made to control for Type I errors when making multiple comparisons. If error variance heteroscedasticity was present in the raw data, variables were log transformed prior to analysis.

Results

Average site current velocities calculated from flow velocity measurements ranged from 6.2 to 119.9 $cm \cdot s^{-1}$ among sites (grand mean = 52.7 $cm \cdot s^{-1}$, SE = 9.9, total n = 10) (Fig. 2). Among sites, the mean encountered current speeds ranged from 4.5 to 140.6 $cm \cdot s^{-1}$ (grand mean = 47.4 $cm \cdot s^{-1}$, SE = 12.6, total n = 10) (Fig. 2). Encountered current speeds were lower than average site current speeds at sites E34 (P = 0.0213), J12 (P = 0.0427), J34 (P = 0.0004), SD12 (P = 0.0025), and SD34 (P = 0.0010) (Fig. 2). There were no differences between encountered current speed and average site current speed at sites B12 (P = 0.0530), D212 (P = 0.0572), E12 (P = 0.1302), and O12 (P = 0.7270) (Fig. 2). Encountered current speed was greater than average site current speed at site V34 (P = 0.0069) (Fig. 2). It may be prudent to note that site B12 and site D212 both have near significant P values, suggesting a trend in the data that is evident in Fig. 2. Specifically, average encountered speeds appear to be lower than average site speeds at low and moderate current sites but equal to or potentially higher at high current speed sites.

Speeds over the ground were normalized by log transformation. Speeds over the ground varied among some sites ($F_{[9,138]}$ = 60.30, P = 0.0001) (Fig. 3). Comparisons of least square means revealed that fish exhibited fastest speeds over

© 2004 NRC Canada

Fig. 2. Mean (+1 SE) encountered current speed (open bars) and site current speed (solid bars) for each site. Sites are arranged in increasing mean encountered current speed along the horizontal axis. Stars represent significant differences ($P \leq 0.05$) between mean encountered current speed and mean site current speed. The first row along the horizontal axis gives site name codes, the second row gives mean site depths, and the third row gives average river gradients for each site. Sample size is noted by numbers above each bar.

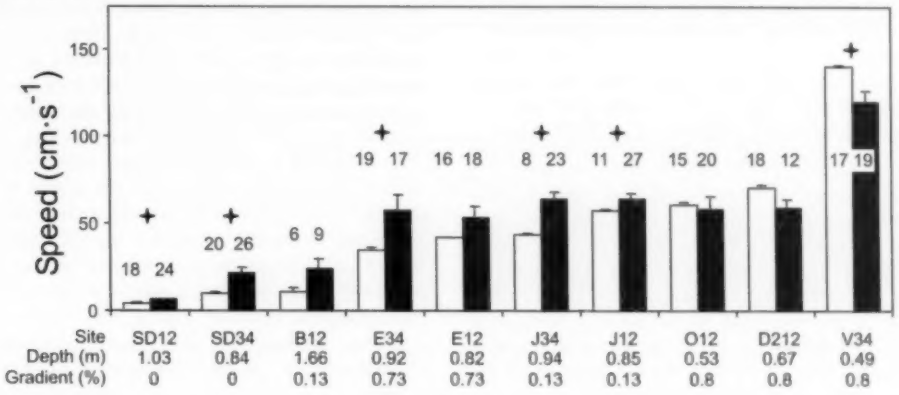

Fig. 3. Mean tailbeat swimming speed (TBFss ± SE; shaded bars), mean observed swimming speed (U_{obs} ± 95% CI; open bars), and mean speed over the ground (GS ± 95% CI; solid bars) for each site. Significant differences between sites for tailbeat swimming speed, mean observed swimming speed, and mean speed over the ground are listed along the *x* axis; within each variable, corresponding letters represent no significant differences between sites. Sites are arranged in increasing mean encountered current speed along the *x* axis.

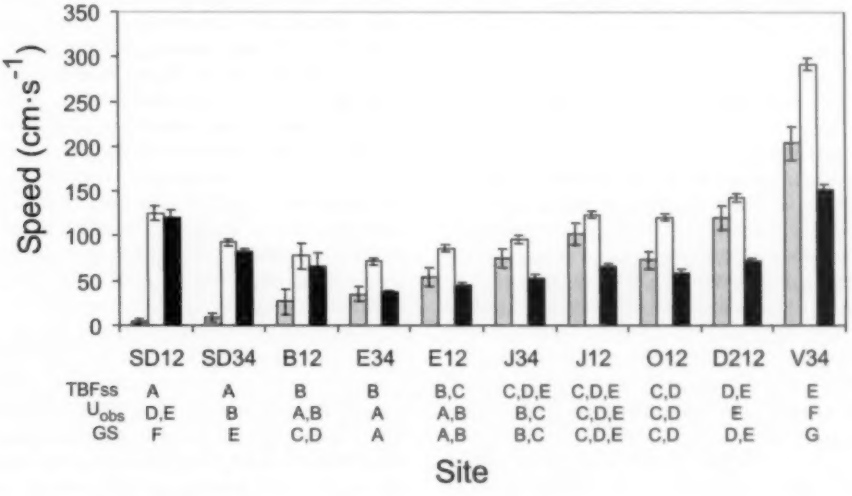

the ground at sites SD12 and V34 compared with all other sites ($P \leq 0.0001$ for all contrasts) and the slowest speeds in site E34 compared with the other sites ($P \leq 0.0003$ for all contrasts), although site E12 did not differ from site E34. Significant differences ($P \leq 0.005$) in speeds over the ground among the remainder of the sites can be found in Fig. 3. The U_{obs} also varied among some sites ($F_{[9,138]} = 151.29$, $P = 0.0001$) (Fig. 3). Least square means comparisons revealed that U_{obs} values were fastest at site V34 relative to all other sites ($P = 0.0001$ for all contrasts) and slowest at site E34 relative to all other sites. Significant differences ($P \leq 0.005$) in U_{obs} among the remaining sites can be found in Fig. 3. When compared using a simple *t* test, U_{obs} values were higher than U_{opt} for sites SD12, SD34, J12, O12, D212, and V34 ($P \leq 0.0001$ for all contrasts). The U_{obs} was lower than U_{opt} at site E34 ($P \leq 0.025$) and did not differ significantly from that at all other sites (Table 1).

TBF swimming speeds also were normalized using a log transformation. Tailbeat swimming speed varied between some sites ($F_{[9,138]} = 42.7$, $P = 0.0001$) (Fig. 3). Least square means comparisons revealed that tailbeat swimming speeds were slowest at sites SD12 and SD34 compared with all other sites ($P \leq 0.0013$ for all contrasts). Tailbeat swimming speed did not differ among sites B12, E34, and E12 ($P \geq 0.0474$ for all contrasts), sites E12, O12, J34, and J12 ($P \geq 0.0154$ for all contrasts), or sites O12, J34, J12, and D212 ($P \geq 0.1509$ for all contrasts). Tailbeat swimming speed was higher at site V34 than at all other sites ($P \leq 0.0029$) with

© 2004 NRC Canada

the exception of sites J34 ($P = 0.0191$), J12 ($P = 0.0756$), and D212 ($P = 0.0937$). When compared using a simple t test, tailbeat swimming speed was lower than U_{obs} at all sites ($P \leq 0.0289$ for all contrasts) with the exception of sites J34 ($P = 0.0897$), J12 ($P = 0.1256$), and D212 ($P = 0.1372$).

Discussion

Active selection of low-flow pathways during migration to reduce exposure to higher speed river currents has been hypothesized by a number of researchers who have studied adult salmon migration over coarse spatial scales (Osborne 1961; Brett 1995; Hinch and Rand 1998). Hydroacoustic surveys (Xie et al. 1997) and visual observations and telemetry (Ellis 1966*b*; Fretwell 1981; Hinch et al. 2002) show that swimming paths of salmon tend to be closely associated with river banks and bottom features in fast rivers where current speeds are usually lower than the mean speed of the river (Henderson 1966). In addition, the hydraulic complexity (turbulence and vorticity) of a river is associated with river topography creating complex flow features around obstacles associated with the banks and bottom of the river. This study selected sites on the general migratory paths of salmon, close to the banks and bottom of the river. Within these lower current speed areas, fish preferentially swam in even lower speed current pathways. However, we found that at higher current speed sites, fish did not use lower speed pathways, instead encountering current speeds at or above the average speed for the immediate vicinity. This behaviour is counterintuitive. High-speed sites represent the most expensive areas for upriver migration where one might assume that fish seeking low current speed would achieve the greatest benefit. In addition, we found that in sites with high current speeds, fish actually increase their speed over the ground.

We propose that fish change their migratory strategy from one of energy conservation to that of time conservation, increasing ground speed above the energetic optimal when encountering high-speed currents to minimize the amount of time spent in these high-speed areas. To test this idea, we have taken a general cost of swimming model presented by Videler (1993) and commonly used to produce species specific bioenergetic models and calculated minimal energy costs to traverse a given ground distance against currents of different speeds. We have taken parameters from Beauchamp et al. (1989) to make the general model specific to sockeye salmon. Within this sockeye specific cost of transport curve, U_{opt} for still water is the tangent to the curve that passes through the origin (see Videler 1993). Following the same mathematical principles, one can change the x-intercept of the tangent to the curve, which in turn changes the point at which the tangent meets the curve. As in the still water example, the x-intercept of the tangent represents the speed of the current in which the fish is swimming and the point of the tangent line represents the U_{opt} at that specific encountered velocity. For example, the tangent of the line passing through point (10,0) represents the U_{opt} for a fish swimming against a velocity of 10 $cm \cdot s^{-1}$. This exercise shows us that in order for a fish to minimize the cost of transport as it encounters faster current speeds, it must increase its swimming speed to maintain its speed over the ground.

The fact that our data show that fish increase their ground speed to above the predicted optimal through both very low and high velocity current speeds supports the idea that fish may change their migratory strategies from energy conservation to time conservation when encountering river currents that permit them to gain large distances over the ground quickly (very low speed current areas) as well as river currents that would cause them long delays in time if they were to swim at an optimal speed (very high speed current areas). In both cases, fish are deviating from U_{opt} and decreasing time in transit to navigate a given area. From our data, this decrease in time appears to be the result of both increasing ground speed and decreasing effort in choosing low current speed pathways. These results are supported by Hinch and Rand (2000), who came to similar conclusions using more primitive video methodologies and algorithms for calculating optimality.

A recent study using free-swimming smallmouth bass (*Micropterus dolomieu*) may help explain why fish are increasing ground speed and, in turn, not spending time looking for low-speed pathways. Similar to the results of this study, Peake (2002) found that bass increased their ground speed when encountering high-speed current velocities as well as increasing swimming speed by using unsteady swimming (anaerobic metabolism). These fish when tested for muscle lactate, plasma lactate, and oxygen consumption had only marginally different mean metabolite concentrations from animals that swam at more moderate speeds for twice as long (Peake 2002). These findings suggest that fish may have physiological mechanisms that allow them to increase exercise intensity for a decrease in duration of exercise with no significant rise in energetic costs compared with longer duration steady swimming. It may be that the disadvantage of experiencing higher velocities for a shorter period is less than the disadvantage of spending extra time to seek out moderately lower velocity pathways at a given site. The fish in our study may then be gaining an energetic advantage by swimming faster for a shorter period of time.

In addition to defining path choices of fish, we compared U_{obs} with swimming speed estimated from TBF. We found that tailbeat swimming speeds were significantly lower than U_{obs} at the majority of sites. Clearly, this shows that swimming speed – TBF relationships determined in flumes and swimming tunnels should be used with caution when extrapolating to field settings. Under natural conditions, flow is more turbulent than in experimental water tunnels and flumes. It might be expected that this would require additional forces to stabilize posture and swimming trajectories, resulting in higher TBF speeds than U_{obs}.

Recent laboratory experiments have shown that fish placed in a trail of staggered, counter-rotating vortices (a von Karman trail) are capable of changing their body movement to match the encountered vortices, minimizing muscle activity while maintaining position in a net downstream current (Liao et al. 2001). In addition, vortices shed from a fish's own fins or body (Muller et al. 2000; Drucker and Lauder 2001; Muller et al. 2001) or from neighbouring members of a school (Abrahams and Colgan 1985, 1987; Herskin and Steffensen 1998) may interact with caudal fin vortices potentially increasing thrust for a given tailbeat. Such interactions with fine-scale flow features would result

© 2004 NRC Canada

in tailbeat swimming speeds lower than U_{obs}, as demonstrated by our results and postulated by Hinch and Rand (2000). Therefore, our results suggest that fish can sense and respond to local fine-scale flow variation in such a way that they achieve higher actual speeds than expected based on the TBF.

Our results underscore the need to conduct research into two areas. First, we feel that it is important to develop alternative means to characterize the complex, small-scale turbulent features through which these fish commonly swim. New methods may allow us to better characterize the flow complexity and allow us to place the observed swimming path choice in better context to flow features common in natural channels. There has been some important advancement in recent years in three-dimensional flow visualization and measurement. Particle imaging velocimetry methods involving suspended neutrally buoyant glass beads and sheets of laser light have enabled investigators to visualize flow structure around swimming fish in laboratory situations (e.g., Nauen and Lauder 2001). An application of this method to a more natural stream channel could help in understanding how fish may be taking advantage of hydraulic conditions during their migration. Others have applied acoustic Doppler current profilers to map three-dimensional current patterns in rivers (Nikora and Goring 1998, 2000) that could be used to better link environmental conditions to animal behaviour in situ.

Second, we need to work toward developing better methods of estimating true transport costs through complex river flow features. This may be achieved by conducting a comprehensive study of muscle recruitment involving electromyograms to more accurately estimate power requirements of different gaits adopted by adult migrating salmon through complex hydraulic conditions encountered in situ. This approach has been used with success at a coarse spatial scale (Hinch and Rand 1998; Standen et al. 2002), but we are not aware of any studies done at the fine time and space scales examined in the present study.

Acknowledgements

We thank the following for field assistance: Shannon MacLaughlin, Yuho Okada, and Andrew Lotto. Particular thanks to Yuho Okada for hours of data digitizing, Nigel Phillips and Keith Head for mathematical consultation, and Noboru Yonemitsu for hydrotechnical support. Thanks as well to Paul Webb for providing a thorough and valuable review of several earlier drafts. Logistic support was provided by BC Hydro and the Seton Lake First Nations. Funding was provided by a Natural Sciences and Engineering Research Council of Canada strategic grant to M.C. Healey, A.P. Farrell, and S.G. Hinch and a Natural Sciences and Engineering Research Council of Canada discovery grant to S.G. Hinch.

References

Abrahams, M.V., and Colgan, P.W. 1985. Risk of predation, hydrodynamic efficiency and their influence on school structure. Environ. Biol. Fishes, **13**: 195–202.

Abrahams, M.V., and Colgan, P.W. 1987. Fish schools and their hydrodynamic function: a reanalysis. Environ. Biol. Fishes, **20**: 79–80.

Beauchamp, D.A., Stewart, D.J., and Thomas, G.L. 1989. Corroboration of a bioenergetics model for sockeye salmon. Trans. Am. Fish. Soc. **118**: 597–607.

Brett, R.J. 1995. Energetics. *In* Physiological ecology of Pacific salmon. Series. *Edited by* C. Groot, L. Margolis, and W.C. Clarke. University of British Columbia Press, Vancouver, B.C. pp. 1–68.

Drucker, E.G., and Lauder, G.V. 2001. Locomotor function of the dorsal fin in teleost fishes: experimental analysis of wake forces in sunfish. J. Exp. Biol. **204**: 2943–2958.

Ellis, D.V. 1966*a*. A survey of the behaviour of salmon on spawning migration through a large river system. Bull. Fish. Res. Board Can. No. 876.

Ellis, D.V. 1966*b*. Swimming speeds of sockeye and coho salmon on spawning migration. J. Fish. Res. Board Can. **23**: 181–187.

Fretwell, M.R. 1981. Migration of adult sockeye salmon in the Nechako River system in 1980. International Pacific Salmon Commission. (Available from Pacific Salmon Commission Library, 1155 Robson Street No. 600, Vancouver, BC V6E 1B5, Canada)

Groot, C., and Margolis, L. (*Editors*). 1991. Pacific salmon life histories. University of British Columbia Press, Vancouver, B.C.

Henderson, F.M. 1966. Open channel flow. Collier Macmillan Canada Ltd., New York.

Herskin, J., and Steffensen, J.F. 1998. Energy savings in sea bass swimming in a school: measurements of tail beat frequency and oxygen consumption at different swimming speeds. J. Fish Biol. **53**: 366–376.

Hinch, S.G., and Rand, P.S. 1998. Swim speeds and energy use of upriver-migrating sockeye salmon (*Oncorhynchus nerka*): role of local environment and fish characteristics. Can. J. Fish. Aquat. Sci. **55**: 1821–1831.

Hinch, S.G., and Rand, P.S. 2000. Optimal swimming speeds and forward-assisted propulsion: energy-conserving behaviours of upriver-migrating adult salmon. Can. J. Fish. Aquat. Sci. **57**: 2470–2478.

Hinch, S.G., Standen, E.M., Healey, M.C., and Farrell, A.P. 2002. Swimming patterns and behaviour of upriver migrating adult pink (*Oncorhynchus gorbuscha*) and sockeye (*O. nerka*) salmon as assessed by EMG telemetry in the Fraser River, British Columbia, Canada. Hydrobiologia, **483**: 147–160.

Hughes, N.F., and Kelly, L.H. 1996. New techniques for 3-D video tracking of fish swimming movements in still or flowing water. Can. J. Fish. Aquat. Sci. **53**: 2473–2483.

Jonsson, N., Jonsson, B., and Hansen, L.P. 1997. Changes in proximate composition and estimates of energetic costs during upstream migration and spawning in Atlantic salmon *Salmo salar*. J. Anim. Ecol. **66**: 425–436.

Leonard, J.B.K., and McCormick, S.D. 1999. Effects of migration distance on whole-body and tissue-specific energy use in American shad (*Alosa sapidissima*). Can. J. Fish. Aquat. Sci. **56**: 1159–1171.

Liao, J., Beal, D.N., Lauder, G.V., and Triantafyllou, M. 2001. Novel body kinematics of trout swimming in a von Karman trail; can fish tune to vortices? Am. Zool. **41**: 1505–1506.

Muller, U.K., Stamhuis, E.J., and Videler, J.J. 2000. Hydrodynamics of unsteady fish swimming and the effects of body size: comparing the flow fields of fish larvae and adults. J. Exp. Biol. **203**: 193–206.

Muller, U.K., Smit, J., Stamhuis, E.J., and Videler, J.J. 2001. How the body contributes to the wake in undulatory fish swimming: flow fields of a swimming eel (*Anguilla anguilla*). J. Exp. Biol. **204**: 2751–2762.

© 2004 NRC Canada

Nauen, J.C., and Lauder, G.V. 2001. Locomotion in scombrid fishes: visualization of flow around the caudal peduncle and finlets of the chub mackerel *Scomber japonicus*. J. Exp. Biol. **204**: 2251–2263.

Nikora, V.I., and Goring, D.G. 1998. ADV turbulence measurements: can we improve their interpretation. J. Hydraul. Eng. **124**: 630–634.

Nikora, V.I., and Goring, D.G. 2000. Flow turbulence over fixed and weakly mobile gravel beds. J. Hydraul. Eng. **126**: 679–690.

Osborne, M.F.M. 1961. The hydrodynamical performance of migratory salmon. J. Exp. Biol. **38**: 365–390.

Peake, S. 2002. A comparison of locomotory behaviour and physiology of confined and free-swimming smallmouth bass (*Micropterus dolomieu*). Ph.D. thesis, Simon Fraser University, Burnaby, B.C. Microfiche AS 0446614, National Library of Canada, Ottawa, Ont.

Standen, E.M. 2001. Effects of hydraulic characteristics on energy use and behaviour of adult upriver migrating sockeye (*Oncorhynchus nerka*) and pink (*O. gorbuscha*) salmon. M.Sc. thesis, University of British Columbia, Vancouver, B.C.

Standen, E.M., Hinch, S.G., Healey, M.C., and Farrell, A.P. 2002. Energetic costs of migrating upriver through the Fraser River canyon, British Columbia, in adult pink (*Oncorhynchus gorbuscha*) and sockeye (*O. nerka*) salmon as assessed by EMG telemetry. Can. J. Fish. Aquat. Sci. **59**: 1809–1818.

Videler, J.J. 1993. Fish swimming. Chapman and Hall, London, UK.

Webb, P. 1995. Locomotion. *In* Physiological ecology of Pacific salmon. Series. *Edited by* M.M.C. Groot and C. Clarke. University of British Columbia Press, Vancouver, B.C. pp. 69–100.

Xie, Y., Cronkite, G., and Mulligan, T.J. 1997. A split beam echosounder perspective on migratory salmon in the Fraser River: a progress report on the split-beam experiment at Mission, B.C., in 1995. Rep. No. 8. Pacific Salmon Commission, Vancouver, B.C.

© 2004 NRC Canada

Factors influencing stream temperatures in small streams: substrate effects and a shading experiment

Sherri L. Johnson

Abstract: The temperature of stream water is an important control of many in-stream processes. To better understand the processes and consequences of solar energy inputs to streams, stream temperature dynamics were examined before, during, and after experimental shading of a 150-m reach of a second-order stream in the Oregon Cascade Range. Maximum water temperatures declined significantly in the shaded reach, but minimum and mean temperatures were not modified. Heat budget calculations before shading show the dominance of solar energy as an influence of stream temperature. The influence of substrate type on stream temperature was examined separately where the water flowed first over bedrock and then through alluvial substrates. Maximum temperatures in the upstream bedrock reach were up to 8.6 °C higher and 3.4 °C lower than downstream in the alluvial reach. Better understanding of factors that influence not only maximum but minimum temperatures as well as diurnal temperature variation will highlight types of reaches in which stream temperature would be most responsive to changes in shading. Many apparent discrepancies in stream temperature literature can be explained by considering variation in the relative importance of different stream temperature drivers within and among streams and over time.

Résumé : Dans les cours d'eau, la température de l'eau est un important facteur de contrôle de plusieurs processus internes. Afin de mieux comprendre les processus reliés à l'apport d'énergie solaire dans les cours d'eau et d'en évaluer les conséquences, nous avons examiné la dynamique thermique avant, pendant et après une expérience dans laquelle nous avons ombragé expérimentalement une section de 150 m d'un ruisseau d'ordre deux dans la chaîne des monts Cascades en Oregon. Les températures maximales de l'eau ont décru significativement dans la section ombragée, mais les températures minimales et moyennes sont restées inchangées. Les calculs de bilans thermiques avant l'expérience ont montré que l'énergie solaire a une influence dominante sur la température du cours d'eau. L'effet du type de substrat sur la température du cours d'eau a pu être examiné séparément là où l'eau coule d'abord sur la roche-mère pour ensuite traverser des substrats alluviaux. Les températures maximales dans la section de roche-mère d'amont sont jusqu'à 8,6 °C supérieures et 3,4 °C inférieures à celles de la section alluviale d'aval. Une meilleure compréhension des facteurs qui influencent non seulement les températures maximales et minimales, mais aussi la variation journalière de la température, permettra d'identifier les sections dans lesquelles la température du cours d'eau est plus susceptible d'être affectée par les changements d'ombrage. Plusieurs contradictions apparentes dans la littérature scientifique concernant la température des cours d'eau peuvent s'expliquer en considérant les variations dans le temps, ainsi que dans un même cours d'eau et d'un cours d'eau à un autre, de l'importance relative des différents facteurs qui régissent la température des cours d'eau.

[Traduit par la Rédaction]

Introduction

The temperature of stream water has been a focus of study for many years because of the importance of temperature in governing in-stream processes such as metabolism, organic matter decomposition, and solubility of gases as well as the effects of temperature on stream biota. Stream temperature in many regions has increased as a result of land use practices (Beschta and Taylor 1988; Sugimoto et al. 1997), resulting in undesirable impacts on cold-water species such as salmonids (Beschta et al. 1987; Bisson et al. 1992; Li et al. 1994). Stream temperature is controlled by multiple factors (Sinokrot and Stefan 1993; Poole and Berman 2001) whose influences and magnitude can be difficult to examine independently.

There is conflicting information in the peer-reviewed literature about the relative ranking of contributing factors of stream temperature. Although incoming solar radiation is generally recognized to be the major source of thermal energy for streams (Brown and Krygier 1970; Sinokrot and Stefan 1993; Webb and Zhang 1999), some have suggested that air temperature is a major influence of stream tempera-

Received 29 March 2003. Accepted 24 January 2004. Published on the NRC Research Press Web site at http://cjfas.nrc.ca on 24 July 2004.
J17433

S.L. Johnson. US Forest Service, Pacific Northwest Research Station, 3200 SW Jefferson Way, Corvallis, OR 97331, USA (e-mail: sherrijohnson@fs.fed.us).

 doi: 10.1139/F04-040 © 2004 NRC Canada

ture (Smith and Lavis 1975; Sullivan and Adams 1990). The role of shade as an influence of stream temperature has been questioned (Larson and Larson 1996), and decreases in stream temperature under shade have been primarily attributed to convective heat exchanges (Larson et al. 2002) rather than to reduced incoming radiation. Strong correlations between stream temperature fluctuations and other environmental factors (Sullivan and Adams 1990; Brosofske et al. 1997) can also result in potential misidentification of causative factors (Johnson 2003).

A factor that has historically been disregarded or misinterpreted as an influence of stream temperature is the type of substrate through which and over which the water flows (Brown 1969; Beschta and Weatherred 1984; Sugimoto et al. 1997). Brown (1969), for example, suggested that bedrock reaches dampened diurnal fluctuations and that gravel alluvial-type substrates had little influence on temperature dynamics. Although hyporheic or subsurface flows have been shown to exhibit dampened diurnal fluctuations compared with in-stream water (Ringler and Hall 1975; White et al. 1987; Evans and Petts 1997), hyporheic flows have been considered to be a very minor influence on in-stream temperature dynamics. However, recent studies of dynamic thermal regimes in the hyporheic zone (Malard et al. 2001), along with an improved understanding of the hyporheic zone as an important flow path of surface water (Haggerty et al. 2002; Kasahara and Wondzell 2003), now suggest that the hyporheic zone may play an important role in influencing stream temperature in alluvial reaches.

Questions also exist concerning longitudinal patterns of stream temperature and whether temperatures, once they have increased, will decrease downstream as a stream enters a shaded reach. Based on energy balance considerations, Beschta et al. (1987) suggested that streams do not "cool" when they flow through shaded reaches; others, however, have observed decreases in stream temperature within shaded reaches downstream of clearcuts (Zwieniecki and Newton 1999) or other openings (Torgerson et al. 1999).

Changes in vegetation near streams can have major impacts on stream temperature (Brown and Krygier 1970; Beschta and Taylor 1988; Johnson and Jones 2000). Streams and their riparian areas have been greatly modified across most ecosystems (Bisson et al. 1992; Sugimoto et al. 1997). Small forested streams historically have not been protected under riparian management guidelines or forest harvest best management practices; agricultural or urban streams of all sizes have had even less protection. The response of stream temperature to changes in near-stream vegetation has been shown to vary, with water temperature in some small streams dramatically increasing following disturbance and removal of riparian vegetation (Brown and Krygier 1970; Johnson and Jones 2000), while other streams show much less response (Ziewienski and Newton 1999). Understanding the mechanisms of stream temperature responses to shade and to various substrates would be valuable, especially for management or restoration activities.

To evaluate some of the competing views of influences and controls of stream temperature, I examined the influence of type of substrate, using comparison of adjacent reaches within a study stream, and the role of shade in one of these reaches, using experimental methods. Experimental manipulations are well suited to examining shading separately from the other functions of riparian vegetation that can also influence stream temperatures. Questions addressed in this paper include: Do different types of substrates influence summer stream temperatures? Do stream temperatures decrease as the water flows through a shaded reach? What is the relative magnitude of influence of air temperature versus shade on stream temperature?

Fig. 1. Location of the study reach in Watershed 3, H.J. Andrews Experimental Forest, Oregon, USA, showing upstream bedrock (open areas) and downstream alluvial (stippled areas) sections, the portion of the bedrock reach that was shaded (shaded area), and locations of sites A–C temperature sensors (●), photosynthetically active radiation sensors (*), and stream gauge and temperature sensor (⊙).

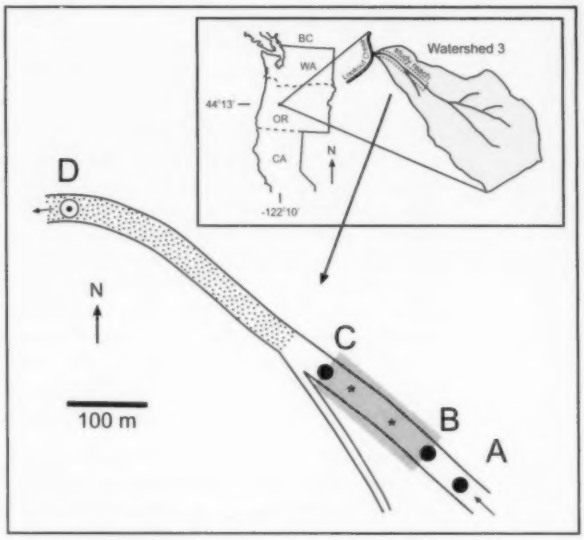

Methods

The study stream in Watershed 3 (WS 3) in the H.J. Andrews Experimental Forest, western Cascades Range, Oregon (Fig. 1), had over 1 km of its length scoured to bedrock by debris flows in 1964 and again in 1996. Downstream of the exposed bedrock, alluvial and colluvial materials scoured from upstream have been deposited, creating a 300-m-long reach with an extensive hyporheic zone (Haggerty et al. 2002; Kasahara and Wondzell 2003). All riparian vegetation along both the bedrock and alluvial reaches of the stream was removed during the debris flows and the stream is exposed to full incoming solar radiation midday during summer. Steep valley walls with coniferous trees provide topographic and vegetative shading in early morning and late afternoon. A stream gauging station is located at the downstream end of the alluvial reach and approximately 100 m upstream of the confluence of WS 3 with Lookout Creek.

To examine the effects of substrates and shading on stream temperature dynamics, water and air temperature sensors (Onset Stowaway, ±0.1 °C resolution) were deployed at multiple sites in WS 3 (Fig. 1). Before being deployed, sensors were cross-validated to account for potential differences in

© 2004 NRC Canada

Fig. 2. Photograph during shading of the bedrock reach. Shade was suspended approximately 2 m above the water surface. For scale, note the person standing at the water level on the edge of stream.

accuracy and programmed to record instantaneous temperatures at half-hour intervals. Each water temperature sensor was placed into the stream in a protective, open-ended, 5-cm-diameter white plastic tube to prevent incoming solar radiation from directly striking the sensor. Air temperature sensors were placed 1.5–2.0 m above the water surface in a half-circle white protective housing, again to block direct radiation of the sensor.

Shading experiment

Two hundred metres of the bedrock portion of WS 3 was selected for the stream shading experiment. Air and water temperatures were recorded for 3 weeks before shading, 3 weeks during shading, and 3 weeks after shading. Temperature sensors were placed at the upstream (site A) and downstream extent (site C) of the bedrock reach to be shaded (Fig. 1) and stream and air temperatures were recorded from 25 June to 26 August 1997. From 15 July through 5 August, the entire wetted channel through this study reach was shaded. Black plastic sheeting (2-mil (50.8-μm) thickness), supported by a rope suspension system, was located approximately 2 m above the water surface to block incoming solar radiation and yet to allow natural air movement beneath the plastic (Fig. 2). To quantify the influence of shade on air temperature, additional air temperature sensors were placed under the shade 1 m above the water surface at site B (upstream end of shade) and site C (downstream end of shade). Photosynthetically active radiation (PAR) sensors (CR 10 data loggers, Campbell Scientific, Inc.) measured and recorded incoming solar radiation at 15-min intervals at two locations in the center of the stream in the shaded reach from 27 July to 25 August. At each location, PAR sensors were set vertically, with one sensor located above the shade and a second sensor located below the shade and 0.2 m above the water surface.

Substrate differences

To examine the influences of substrates on stream temperature dynamics in WS 3, a temperature sensor was also deployed at the downstream end of a 300-m-long unshaded alluvial reach (Fig. 1, site D) to compare with the upstream bedrock reach. The following physical variables were measured in both the bedrock and alluvial study reaches during August 1997 and averages for each reach calculated: wetted width of the channel and water depth at three points across the channel were measured every 5 m along the length of each study reach, channel slope for each reach was measured using a laser level, potential open sky for July was calculated for each reach from Solar Pathfinder® traces made every 20 m along the channel (Solar Pathways Inc., Glenwood Springs, CO 81601, USA), percent cover provided by vegetation and topography was measured every 20 m using a spherical densiometer (Platts et al. 1987), and aspect was also noted every 20 m using a compass. Water velocity was measured in the bedrock and alluvial reaches using several methods: point measurements (Marsh-McBirney flowmeter) of cross-sectional velocities in three transects within each reach and travel time of the visible leading edge of fluorescein dye releases over three 10 m sections. These were compared with median water velocity rates calculated

© 2004 NRC Canada

from multiple day solute releases in each reach (S. Wondzell, US Forest Service, Pacific Northwest Research Station, Olympia, Wash., unpublished data). Discharge was calculated from depth and flow measurements taken at the downstream end of the bedrock reach and at the gauge.

Analyses

Regression relationships of daily maximum stream temperature at sites C and A, where stream temperature at site A is the independent variable and at site C is the dependent variable, were compared for three time periods: before, during, and after shading. Sums of squares for the full model were calculated and compared with sums of squares and mean square error of partial models ("dummy variables in regressions"; Kleinbaum et al. 1998). Regression relationships were evaluated to see if lines were parallel and (or) coincident. Daily minimum and mean stream temperatures at sites A and C were similarly analyzed.

Heat budgets for the bedrock reach were calculated for the hour nearest maximum incoming solar inputs on 20 July 1997, with and without shading (Appendix A) (Monteith and Unsworth 1990; Sinokrot and Stefan 1993; Webb and Zhang 1999). Incoming solar radiation with and without shading was measured in the reach. Reflected radiation was measured with a downward facing pyranometer. Long-wave radiation without shade was calculated using published values of net flux between incoming and reflected long wave (Monteith and Unsworth 1990). During shading, the black plastic would have blocked direct incoming long-wave radiation (Oke 1987), but net long-wave fluxes during shading were assumed to continue owing to reflection and reradiation from surfaces that were not shaded (M. Unsworth, Department of Forest Science, Oregon State University, Corvallis, OR 97331, USA, personal communication). Evaporation and convection were calculated using onsite measures of wind speed, relative humidity, and air and water temperatures. Conduction was calculated using estimates of subsurface temperatures within the bedrock.

Results

Substrate influences on stream temperature

Throughout the summer, diurnal fluctuations of stream temperature in the bedrock reach were much greater than downstream in the alluvial reach (Fig. 3). Daily maximum temperatures were higher and minimum temperatures lower in the bedrock reach than downstream in the alluvial reach. Mean daily temperatures, however, were similar. Short intervals of rainy and (or) cloudy days resulted in higher maximum temperatures at site D than at site A. Stream temperatures increased through the summer, with the seasonal maximum temperature occurring on 20 July at site A in the bedrock reach and on 7 August at site D in the alluvial reach (Fig. 3).

Within each reach, temperatures changed over very short distances. As the stream flowed through the bedrock reach from site A to site C (200 m), daily maximum stream temperatures increased several degrees (Figs. 4*a* and 4*c*). In the alluvial reach, between sites C and D (350 m), daily maximum temperatures decreased by as much as 8.7 °C and minimum temperatures increased by 3.9 °C.

Fig. 3. Daily maximum and minimum stream temperatures during the summer 1997 in adjacent bedrock and alluvial reaches. Site A, in the bedrock reach (grey line), is 550 m upstream of site D at the downstream portion of the alluvial reach (black line).

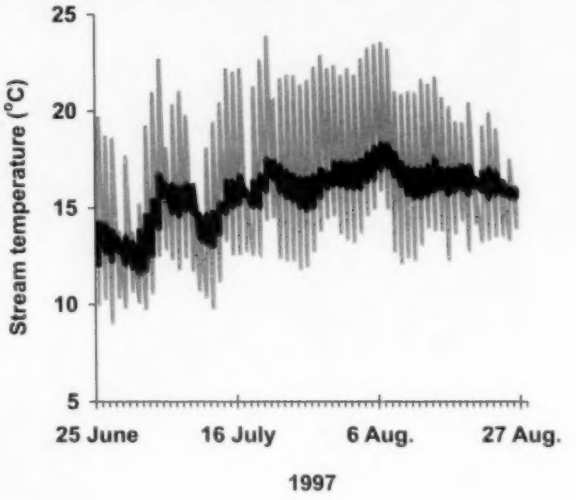

Although physical characteristics in the two reaches were generally similar (Table 1), estimates of water velocity differed dramatically, depending on the measurement method (Table 2). Average water velocity from point measurements in the two reaches were similar, but velocity calculated from dye releases or from median travel time from solute releases was very different between reaches (Table 2). Using leading edge of dye, average water velocity in the alluvial reach was two-fifths that in the bedrock reach. However, using conservative solute releases, median water velocity in the alluvial reach was 1/100th of the rate in the bedrock reach. Median retention time of water in the 200-m section of bedrock was 1.1 h but was 18 h in the 300-m alluvial reach (Table 2) (S. Wondzell, US Forest Service, Pacific Northwest Research Station, Olympia, Wash., unpublished data).

No groundwater inputs were visible in the bedrock reach. There was an increase in discharge between site C and the gauge at site D (Table 1), most of which can be accounted for by a small tributary that entered 50 m below site C. Stream temperatures just downstream of the bedrock reach and this confluence of the small tributary with WS 3 stream were within 0.1 °C of those at site C for 22 h each day and were up to 1.0–1.5 °C higher during full summer sun (noon to 1300) (S.L. Johnson, unpublished data). These increases likely occurred as the water traveled through an additional section of 50 m of bedrock and were similar to temperature increases upstream between sites A and B.

Effects of shading on stream temperatures

The experimental shading resulted in decreases in maximum water temperature at the downstream end of the shaded reach. Before and after shading, maximum water temperature was up to 3–4 °C higher at site C than at site A 200 m upstream (Fig. 4). During the shading experiment, maximum water temperature at site C was up to 1 °C lower than at site A (Fig. 5). However, the mean and minimum temperatures at

© 2004 NRC Canada

Fig. 4. Maximum (◆), minimum (▲), and mean (○) stream temperatures at sites A–D in WS 3 for 3 days representative of (*a*) before shading on 14 July, (*b*) during shading on 23 July, and (*c*) after shading on 8 August. Site A is the most upstream site and shading occurred from site B downstream to site C.

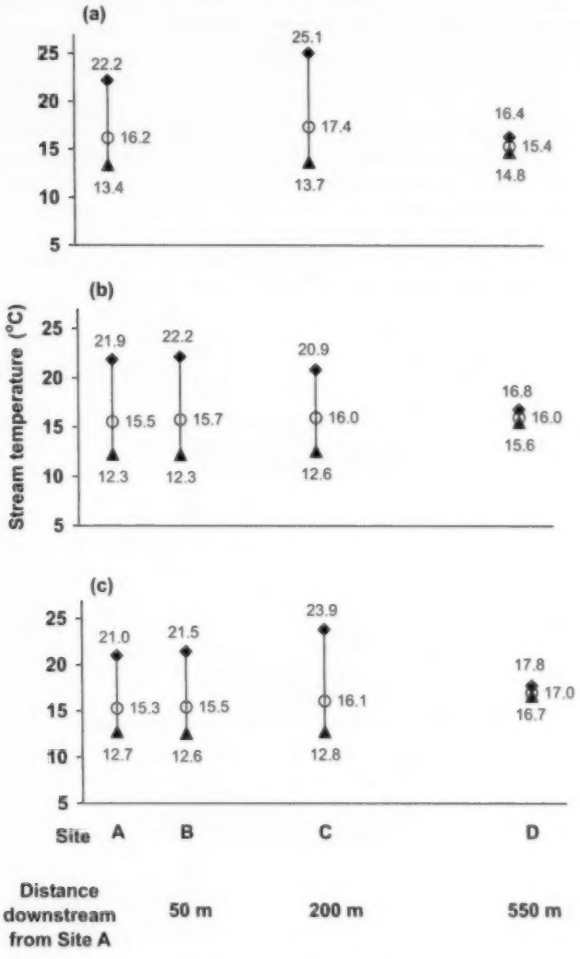

site C continued to be greater than at sites A and B (Figs. 4 and 5).

Additional temperature sensors were added at site B because the plastic shading could not be suspended over the upper 50 m of the bedrock study reach. Maximum temperatures increased in the 50 m between sites A and B (Fig. 4) and the decrease from shading would have been greater if sites B and C were compared. However, sites A and C were used for statistical analysis because of the existence of pretreatment data.

The slope of the regression of maximum daily temperatures at sites A and C during shading was significantly different from that before or after shading ($f = 9.36$, $p < 0.01$). Shading did not significantly change the slopes of the regression relationship of temperature at sites A and C for daily mean or minimum temperatures (mean: $f = 1.42$, $p > 0.05$; minimum: $f = 0.96$, $p > 0.05$). Owing to seasonal trends in stream temperature, the intercepts of regression relationships before and after shading were significantly different for maximum and minimum daily stream temperatures ($f = 20.67$, $p < 0.001$; $f = 3.73$, $p < 0.05$) but not for means ($f = 3.16$, $p > 0.05$).

Table 1. Physical characteristics of study reaches in WS 3.

Parameter	Bedrock reach	Alluvial reach
Wetted width, average (m)	2.13	2.11
Water depth, average (m)	0.07	0.08
Water depth, maximum (m)	0.36	0.49
Discharge ($L \cdot s^{-1}$)	3.4	4.0
Channel gradient ($m \cdot m^{-1}$)	0.14	0.13
Percent open sky (Solar Pathfinder®)	40	28
Percent canopy density (densiometer)	28	38
Aspect (upstream)	70°	62°

Note: Percent open sky is the mean for July from Solar Pathfinder® data. Discharge was measured at the most downstream point in each reach on 31 July 1997. A small tributary (0.40 $L \cdot s^{-1}$) entered downstream of the bedrock reach and at the top of the alluvial reach.

Shading reduced incoming solar radiation as well as air temperature. Daily maxima of PAR under the shade were less than 1/200th of that in the sun (10 versus 2100 $\mu mol \cdot m^{-2} \cdot s^{-1}$). Maximum air temperatures under the shade were lower than in sun by approximately 3–4 °C (Fig. 6). Air temperatures under the shade were slightly lower at the upstream site, site B, than at site C downstream, possibly because of upstream winds during the heat of the day. Minimum air temperatures under the shade were slightly warmer than upstream or downstream (Fig. 6).

Heat budget using microclimatic data

An energy heat budget was constructed for midday summer conditions in the bedrock reach to quantify factors influencing stream temperature and to model the effects of the shading experiment on stream temperature. Incoming radiation and stream and air temperatures were measured on site during the shading experiment and relative humidity, wind speed, and soil temperature data were available from the H.J. Andrews Primary Meteorological Station 2 km away. However, because microclimatic conditions near streams differ from those at even nearby upland climatic stations (Brosofske et al. 1997; S.L. Johnson, unpublished data), these same variables were remeasured on site during the summer of 2001 using a portable climatic station (Campbell Scientific, Inc.) in the bedrock reach of WS 3. Comparisons of climatic data between 19–20 July 1997 and 19–20 July 2001 for the Primary Meteorological Station show that conditions between years were similar (incoming solar, $R^2 = 0.91$; wind speed, $R^2 = 0.86$; air temperature, $R^2 = 0.82$; relative humidity, $R^2 = 0.87$; $p < 0.001$ for all); therefore, incoming radiation, wind speed, relative humidity, and soil temperatures from the WS 3 microclimatic station on 20 July 2001 were used for the heat budget calculations of the shading experiment to have modeled conditions represented by the budget as close as possible to those occurring on site during the shading experiment (Appendix A).

Midday stream temperature heat budgets with and without shading differed dramatically in the amount of radiative

© 2004 NRC Canada

Table 2. Average velocity of stream water in bedrock and alluvial reaches in WS 3.

Measurement method	Bedrock reach ($m \cdot s^{-1}$) (SE)	Alluvial reach ($m \cdot s^{-1}$) (SE)
Flowmeter	0.20 (0.06)	0.15 (0.05)
Dye release, leading edge	0.10 (0.05)	0.04 (0.03)
Solute release, median velocity	0.050*	0.005*

Note: Median velocity using solute releases was calculated as reach length·(median retention time)$^{-1}$. An asterisk denotes unpublished data from S. Wondzell, US Forest Service, Pacific Northwest Research Station, Olympia, Wash.

Fig. 5. Differences in daily maximum (black line), minimum (grey line), and mean (broken line) stream temperatures between sites C and A during the summer of 1997. The shading experiment occurred 16 July through 5 August.

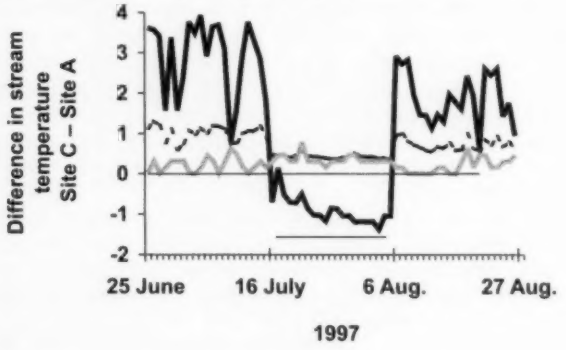

Fig. 6. Maximum (◆), minimum (▲), and mean (○) air temperatures on 23 July during the shading experiment in WS 3. Air temperature sensors were paired at sites B and C, with a sensor (Shade) located under the shade midway between the stream surface and the shade and a second sensor (Sun) located at a similar height above the stream but 1.5 m upstream or downstream of the shade.

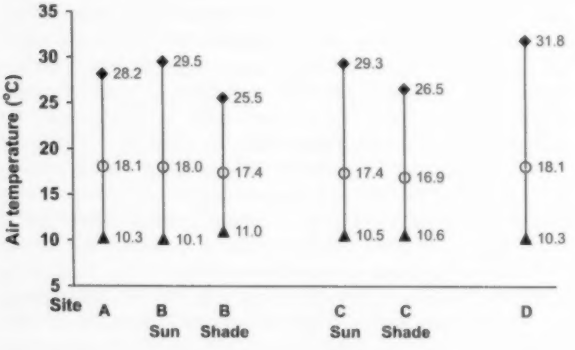

inputs (Fig. 7). Net energy fluxes without shading were dominated by solar inputs (Fig. 7*a*); the sum of these positive and negative fluxes (580 $W \cdot m^{-2}$) slightly overestimated temperature increases for the calculated volume of stream in this 150-m reach. During shading, net energy fluxes were dramatically reduced (Fig. 7*b*); the sum of fluxes under shade (–149 $W \cdot m^{-2}$) corresponds to approximately a 1 °C decrease of maximum temperature through this reach. These calculations assume that the conditions measured at the microclimatic station were representative of those throughout the reach and that one-half volume of water calculated for the reach moved through the reach during the hour.

Fig. 7. Heat energy budgets for 1200, 20 July 1997, in the bedrock reach: (*a*) full sun, the sum of fluxes is 580 $W \cdot m^{-2}$ towards the stream; (*b*) under shade, the sum of fluxes is 149 $W \cdot m^{-2}$ away from the stream.

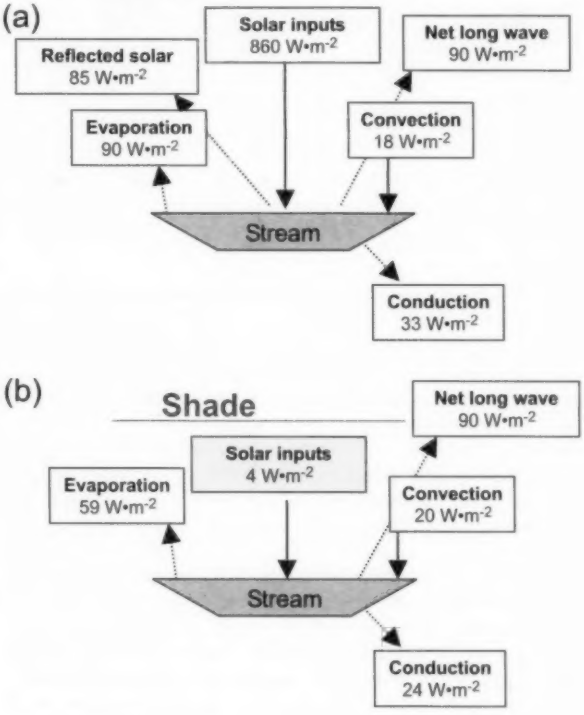

Although solar inputs were decreased by the shading experiment, the magnitude of other fluxes showed little change during shading. However, with reduced solar inputs, the relative proportion of the total energy budget from these other fluxes greatly increased. Under shade, the largest energy fluxes were evaporation and net long-wave radiation. Evaporative fluxes result in movement of heat energy away from the stream and are greatly influenced by wind speed and relative humidity of the overlying air mass. Convective fluxes are determined by temperature differences between the water and air and, on a warm summer day when the air is warmer than the stream, result in energy moving toward the stream. Convective exchanges increased only slightly under shade as a result of slight changes in vapor pressure with decreases in air temperature. Excess heat accumulated in the immediate vicinity of the plastic but because of the movement of the air

© 2004 NRC Canada

beneath the plastic, air temperatures under the shade were less than in full sun (Fig. 6). Shading did not interfere with wind above the stream; with the plastic 2 m above the channel, much air circulation was observed under the shade.

Conduction is a function of temperature differences between water and the substrates or within the substrates. Rates of exchange depend on the thermal conductivity of the bed material as well as the gradients of temperature within the substrate. Conduction was calculated using a one-dimensional heat equation, which underestimates energy fluxes (Hondzo and Stefan 1994; Evans et al. 1998), but other methods of calculating conduction require more data on subsurface temperatures (Hondzo and Stefan 1994; Evans et al. 1998). Using these standard steady-state methods and estimated temperatures of bedrock, fluxes between the water and bedrock or within the bedrock to the cooler bedrock interior accounted for a very small portion of the heat budget with or without shading.

Discussion

Effects of shading on stream temperatures

Maximum stream temperatures significantly decreased during shading of the water surface of a 150-m bedrock reach, but minimum and mean temperatures were not substantially affected. Reduced maximum temperatures in a shaded reach without a corresponding decrease in mean or minimum temperatures could occur because the distribution of daily stream temperature in the bedrock reach was unsymmetrical; mean temperatures are lower than what would be calculated by simple averages of daily maximum and minimum. Thus, short sections of shade can decrease instantaneous energy fluxes at midday, while the daily energy balance for stream temperature remains essentially unchanged.

Dissipation of a portion of the water's heat energy as the water moves downstream has been suggested to not be common (Beschta et al. 1987), but this experiment shows that it is possible to have longitudinal maximum temperatures influenced by shade. Maximum stream temperature immediately responded to the placement and the removal of shade, showing the importance of incoming radiation in controlling daily maximum stream temperatures. Using the median travel time of water in the bedrock reach of approximately 1 h allows examination of the temperature of the water entering the reach and temperature dynamics as it moves through the reach. Early in the day, water temperature, lagged by the median travel time, increased between sites B and C, while at midday under shade, temperature declined in the shaded reach (Appendix B). Although the heat budget analysis of the shaded reach during midday highlights evaporation as a possible mechanism for energy transfer away from the stream, conduction may also have contributed but was likely underestimated because of unavailability of temperature data from within the bedrock.

Minimum temperatures were not influenced by the shade. Theoretically, minimum water temperature could have been expected to either increase or decrease as the stream flowed through the shaded reach. Streams under vegetative cover can exhibit higher minimum temperature in response to reduced radiative losses of long-wave energy (Oke 1987; Monteith and Unsworth 1990); if this was a dominant mechanism during this experiment, minimum stream temperatures would have increased as a result of the shading. Alternatively, shading could have the opposite effect if results were extrapolated from studies of natural reestablishment of riparian vegetation over time, where minimum temperature decreased under shade (Brown and Krygier 1970; Johnson and Jones 2000). These potential opposing hypotheses of response of minimum stream temperature to cover over a stream suggest that more examination of the controls of minimum stream temperature is warranted.

Several factors in this experiment, such as the type of material used for shading or that shading only covered the wetted portion of the stream channel, may have not functioned in a similar manner to the influence of riparian vegetation on stream temperatures; however, these same factors allowed examination of the role of shade independent of the myriad other functions of riparian vegetation. Riparian vegetation influences streams and stream temperature through multiple pathways in addition to providing shade. Riparian vegetation influences microclimatic conditions through biological functions such as evapotranspiration and release of water vapor as well as through physical means such as decreasing wind speeds. Vegetation also provides bank stability, which can impact width to depth ratios and the exposed surface area of the stream. Accumulations of large organic matter inputs have an effect on hydraulic retention times. Although incoming radiation levels in dense natural forests can be as low as those under the experimental shade, riparian forests would have more variability of incoming light levels because of the shape and structure of the vegetation.

The lack of influence of this shading experiment on minimum and mean stream temperatures suggests that because not all stream metrics are equally responsive, each metric should be considered individually when evaluating stream temperature responses to mitigation or restoration activities. Biologically, maximum as well as minimum stream temperatures are important. Maximum temperatures have become the foci of many water quality standards because high water temperature can increase stress and metabolic rates for cold-water salmonids, increase viability of disease vectors, and potentially serve as barriers for migrating fishes (Beschta et al. 1987; Li et al. 1994). Less is known about the influences of minimum temperature or how organisms respond to diurnal fluctuations of temperature (Cox and Rutherford 2000). Concluding that downstream shading ameliorates upstream temperature increases (Zwieniecki and Newton 1999) is premature without examination of minimum and mean temperatures.

Substrate influences on stream temperatures

Substrate type can be an important influence on maximum and minimum stream temperatures, as demonstrated by the dramatic differences in maximum, minimum, and diel fluctuations between the bedrock reach and the reach with alluvial substrates and hyporheic flows. The juxtaposition of substrate types, as found in WS 3, provided a natural experiment, where the stream flows through a bedrock reach and then through an alluvial reach with extensive hyporheic exchange. The influence of substrate type on diel temperature fluctuations is very dramatic in WS 3 because of the homogeneity of each reach type and the volume of water exposed

© 2004 NRC Canada

to each substrate type. Most streams have high heterogeneity of substrate conditions, which may explain why the influence of specific substrates on in-stream temperature dynamics is not broadly recognized (i.e., Clark et al. 1999).

In this study, the bedrock reach showed high maximum temperatures, low minimum temperatures, and wide diurnal fluctuations. Although Brown (1969) and Beschta and Weatherred (1984) suggested that bedrock reduces maximum temperature and dampens diurnal fluctuations by absorbing energy in the heat of the day and releasing the stored energy later, this was not observed in the bedrock reach of WS 3. The high daytime water temperatures in the bedrock reach were likely influenced by reflection of solar energy from the smooth bedrock surfaces into the shallow stream. The bedrock under the shallow stream may have been absorbing some incoming solar energy and serving as a minor heat sink but not to the extent predicted by Brown (1969). Minimum stream temperatures in the bedrock reach were much cooler than those in nearby streams (Johnson and Jones 2000); therefore, the nighttime rerelease of stored energy from daytime was not apparent in the thermograph of temperature from this reach.

As the water from the bedrock reach flowed into the alluvial reach, stream temperatures were dramatically dampened, with lower maxima and higher minima. The influence of hyporheic flow on in-stream temperature has been previously thought to be fairly localized (White et al. 1987). Dampening of subsurface diurnal water temperatures has been documented as a function of depth into subsurface gravels (Ringler and Hall 1975; Evans et al. 1998; Malcolm et al. 2002). Influences of hyporheic exchange flows on surface stream temperatures have generally been observed only at microscales, such as upwelling locations or within small side channels (White et al. 1987; Evans et al. 1998; Clark et al. 1999), creating important thermal refugia for biota.

Hyporheic flow could influence downstream temperature maxima and minima by several possible mechanisms. Reach residence time is lengthened by hyporheic flow paths (Poole and Berman 2001; Haggerty et al. 2002). Increased hydraulic retention and the large volume of subsurface storage could lead to simple mixing of warm daytime water and cooler nighttime water, thereby moderating downstream temperatures. However, while the water is in contact with the subsurface substrates, conduction would also occur, transferring heat energy from warmer to cooler surfaces. Water warmed during the daytime and flowing over cooler rocks in the subsurface would transfer heat to the substrates. During the night, cooler stream water entering the subsurface and passing over warmer rocks would absorb heat. These processes also occur on a small scale, in-stream (Brown 1969), but the magnitude of surface area of substrates within a porous hyporheic zone can greatly dwarf the exposed surface area of a stream channel. The potential influence of alluvial substrates on surface stream temperature is related to the proportion of total stream flow passing through the hyporheic zone, which, in the lower 100 m of WS 3, is the majority of stream flow (Kasahara and Wondzell 2003).

Many factors influence fluxes of energy and determine the magnitude of heat transfer between a stream and its surroundings (Brown 1969; Clark et al. 1999; Poole and Berman 2001). Ultimately, heat fluxes are influenced by the duration of time over which exchanges can occur as well as the rates controlling potential energy exchanges. In the bedrock reach, where median water velocities were high and the hydraulic retention time of water was short, dominant energy exchange processes must have been those with very high rates to result in rapid temperature increases and decreases over a short reach. Alternatively, in the alluvial reach, complex flow paths resulted in slow median water velocities and therefore long hydraulic retention times. These slow velocities led to mixing of daytime and nighttime water between and within the channel and hyporheic zone, allowing processes with lower rates of energy exchange to have a potentially significant impact on stream temperature. The duration of contact between water and its surroundings influences stream temperature energy exchanges and highlights the need for information on reach-scale hydraulic retention to understand the extent to which energy flux dynamics vary from habitat to habitat.

Addressing conflicts within the literature

Stream temperature dynamics, especially heat budgets, are complicated and the relative magnitude of different components can shift among sites with differing biotic and geophysical properties. This has led to apparently contradictory findings within the scientific literature (Beschta 1997; Beschta et al. 2003; Johnson 2003). Although some authors have suggested that shade is not an important factor for stream temperature (Larson and Larson 1996; Larson et al. 2002), maximum temperatures in this study were strongly influenced by the reduction of incoming solar radiation over even a short reach. Heat budget calculations for the bedrock reach demonstrate the importance of incoming solar radiation as a dominant factor influencing stream temperature.

The heat budgets also showed that convective or sensible heat exchanges between warm air and cooler streams comprise a relatively small portion of the total heat flux. Therefore, air temperature is apt to be a relatively weak determinant of stream temperature. While other published accounts suggest that air temperature is a dominant driver (Smith and Lavis 1975; Sullivan and Adams 1990; Larson and Larson 1996), this conclusion is based on an observed strong correlation between air and stream temperature. Rather than indicating a causal relationship, however, the correlation exists because both air and water temperature are responding to the same temporal fluctuations in solar heat inputs.

Although substrate type was recognized by Brown (1969) and more recently by others (Evans et al. 1998; Clark et al. 1999; Webb and Zhang 1999) to be a factor in heat budgets, it has not been generally envisioned as important to stream temperature dynamics (Beschta et al. 1987; Sugimoto et al. 1997). Observations of stream temperature in bedrock and alluvial reaches in WS 3, as well as other emerging research (R.D. Moore, Department of Geography and Forest Resources Management, University of British Columbia, Vancouver, BC V6T 1Z2, Canada, personal communication), show that the type of substrate can have important influences on in-stream temperatures.

Longitudinal temperature dynamics are also complex and many questions remain to be answered. Historically, stream

© 2004 NRC Canada

temperature was not thought to decrease downstream once it had warmed (Beschta et al. 1987). However, recent technological advances (Hobo®, Stowaway®, Ibutton®, FLIR®) have provided methods to easily measure instantaneous temperature at many more points than previously possible. Studies with high densities of measurements sites along a stream have revealed increased complexity of longitudinal and lateral stream temperature dynamics (Clark et al. 1999; Torgerson et al. 1999; Arscott et al. 2001). Although longitudinal trends in stream temperature exist in most stream networks, local deviation from those trends can be substantial. Use of average longitudinal temperature trends (Zwieniecki and Newton 1999) is therefore inappropriate for determining whether stream temperature has "recovered" from an upstream perturbation as well as for other applications where precise, accurate estimates of predisturbance conditions are required. A better knowledge of the mechanisms of energy exchanges will help us understand interactions among the controlling factors of stream temperature and the multiple functions of shade over streams.

In conclusion, the type of substrate over which a stream flows may have implications for stream management activities and may explain some of the variability in temperature responses to riparian removal or forest harvest. Streams flowing over bedrock may be more responsive to slight changes of incoming solar radiation, while those on alluvial substrates may be buffered by longer hydraulic retention times, resulting in dampened diurnal fluctuations in stream temperatures. Although the reduction of incoming shortwave solar radiation was greater in this shading experiment than what would generally occur with patchy riparian vegetation, decreases in maximum stream temperatures were observed in a short (150 m) shaded reach. However, downstream shading of a stream does not appear to totally remediate the effects of upstream disturbances or riparian removal on stream temperatures because mean and minimum temperatures were only minimally affected.

Acknowledgments

Funding for this research was provided by a Postdoctoral Fellowship from the National Science Foundation and through the USDA Forest Service Pacific Northwest Research Station Ecosystem Processes Team. Additional support was provided by the H.J. Andrews Long Term Ecological Research (DEB 9632921) program. Many individuals helped with field work, construction of experimental shading, and calibration and setup of the portable climate station and their contributions to this project are greatly appreciated. I particularly thank Cedar Fowler, who collaborated in planning and provided much logistical assistance, and Steve Wondzell, whose research quantifying hyporheic flows co-occurred at these sites in WS 3. John Moreau provided technical expertise in selection, construction, and programming of the portable climate station. Dave Plaehn consulted on statistical methodology. Tim Warren assisted with the heat budget calculations. Ryan Ulrich, Kristin May, Nicole Walters, and the students in the 1997 Research Experience for Undergraduates at H.J. Andrews Experimental Forest also assisted with field work. Geoff Poole, Bob Beschta, Fred Swanson, Linda Ashkenas, and anonymous reviewers greatly improved this manuscript through their helpful comments.

References

Arscott, D.B., Tockner, K., and Ward, J.V. 2001. Thermal heterogeneity along a braided floodplain river (Tagliamento River, northeastern Italy). Can. J. Fish. Aquat. Sci. **58**: 2359–2373.

Beschta, R.L. 1997. Riparian shade and stream temperature: an alternative perspective. Rangelands, **19**: 25–28.

Beschta, R.L., and Taylor, R.L. 1988. Stream temperature increases and land use in a forested Oregon watershed. Water Res. Bull. **24**: 19–25.

Beschta, R.L., and Weatherred, J. 1984. A computer model for predicting stream temperatures resulting from the management of streamside vegetation. WSDG-AD-00009. US Department of Agriculture, Forest Service, Fort Collins, Colorado.

Beschta, R.L., Bilby, R.E., Brown, G.W., Holtby, L.B., and Hofstra, T.D. 1987. Stream temperature and aquatic habitat: fisheries and forestry interactions. *In* Streamside management: forestry and fishery interactions. *Edited by* E.O. Salo and T.W. Cundy. Institute of Forest Resources, University of Washington, Seattle, Wash. pp. 191–232.

Beschta, R.L., McIntosh, B.A., and Torgerson, C.E. 2003. Comment: perspectives on water flow and the interpretation of FLIR images. [J. Range Manag. **55**: 106–111, 2002.] J. Range Manag. **56**: 97–99.

Bisson, P.A., Quinn, T.P., Reeves, G.H., and Gregory, S.V. 1992. Best management practices, cumulative effects, and long-term trends in fish abundance in Pacific Northwest river systems. *In* Watershed management: balancing sustainability and environmental change. *Edited by* R.J. Naiman. Springer-Verlag, New York. pp. 189–232.

Brosofske, K.D., Chen, J., Naiman, R.J., and Franklin, J.F. 1997. Harvesting effects on microclimatic gradients from small streams to uplands in western Washington. Ecol. Appl. **7**: 1188–1200.

Brown, G.W. 1969. Predicting temperatures of small streams. Water Resour. Res. **5**: 68–75.

Brown, G.W., and Krygier, J.T. 1970. Effects of clear-cutting on stream temperature. Water Resour. Res. **6**: 1133–1139.

Clark, E., Webb, B.W., and Ladle, M. 1999. Microthermal gradients and ecological implications in Dorset rivers. Hydrol. Processes, **13**: 423–438.

Cox, T.J., and Rutherford, J.C. 2000. Thermal tolerances of two stream invertebrates exposed to diurnally varying temperature. N.Z. J. Mar. Freshw. Res. **34**: 203–208.

Evans, E.C., and Petts, G.E. 1997. Hyporheic temperature patterns within riffles. Hydrol. Sci. J. **42**: 199–213.

Evans, E.C., McGregor, G.R., and Petts, G.E. 1998. River energy budgets with special reference to river bed processes. Hydrol. Processes, **12**: 575–595.

Haggerty, R., Wondzell, S.M., and Johnson, M.A. 2002. Power-law residence time distribution in the hyporheic zone of a 2nd-order mountain stream. Geophys. Res. Lett. **29**: 13 (doi: 10.1029/2002GL014743).

Hondzo, M., and Stefan, H.G. 1994. Riverbed heat conduction prediction. Water Resour. Res. **30**: 1503–1513.

Johnson, S.L. 2003. Stream temperature: scaling of observations and issues for modelling. Hydrol. Processes, **17**: 497–499.

Johnson, S.L., and Jones, J.A. 2000. Stream temperature responses to forest harvest and debris flows in western Cascades, Oregon. Can. J. Fish. Aquat. Sci. **57**: 30–39.

© 2004 NRC Canada

Kasahara, T., and Wondzell, S.M. 2003. Geomorphic controls on hyporheic exchange flow in mountain streams. Water Resour. Res. **39**: 1005 (doi: 10.1029/2002WR001386).

Kleinbaum, D.G., Kupper, L.L., and Muller, K.E. 1998. Applied regression analysis and other multivariable methods. 3rd ed. Duxbury Press, Boston, Mass.

Larson, L.L., and Larson, S.L. 1996. Riparian shade and stream temperature: a perspective. Rangelands, **18**: 149–152.

Larson, S.L., Larson, L.L., and Larson, P.A. 2002. Perspectives on water flow and the interpretation of FLIR images. J. Range Manag. **55**: 106–111.

Li, H.W., Lamberti, G.A., Pearsons, T.N., Tait, C.K., and Buckhouse, J.C. 1994. Cumulative effects of riparian disturbances along high desert trout streams of the John Day Basin, Oregon. Trans. Am. Fish. Soc. **123**: 627–640.

Malard, F., Alain, M., Uehleinger, A.M., and Ward, J.V. 2001. Thermal heterogeneity in the hyporheic zone of a glacial floodplain. Can. J. Fish. Aquat. Sci. **58**: 1319–1335.

Malcolm, I.A., Soulsby, C., and Youngson, A.F. 2002. Thermal regime in the hyporheic zone of two contrasting salmonid spawning streams: ecological and hydrological implications. Fish. Manag. Ecol. **9**: 1–10.

Monteith, J.L., and Unsworth, M. 1990. Principles of environmental physics. 2nd ed. Arnold Press, London, UK.

Oke, T.R. 1987. Boundary layer climates. 2nd ed. Routledge Press, London, U.K.

Poole, G.C., and Berman, C.H. 2001. An ecological perspective on in-stream temperature: natural heat dynamics and mechanisms of human-caused thermal degradation. Environ. Manag. **27**: 787–802.

Platts, W.S., Armour, C., Booth, G.D., Bryant, M., Bufford, J.L., Culpin, P., Jensen, S., Lienkaemper, G.W., Minshall, G.W., Monsen, S.B., Nelson, R.L., Sedell, J.R., and Tuhy, J.S. 1987. Methods for evaluating riparian habitats with applications to management. Gen. Tech. Rep. INT-221. US Department of Agriculture, Forest Service, Intermountain Research Station, Ogden, Utah.

Ringler, N.H., and Hall, J.D. 1975. Effects of logging on water temperature and dissolved oxygen in spawning beds. Trans. Am. Fish. Soc. **104**: 111–121.

Sinokrot, B.A., and Stefan, H.G. 1993. Stream temperature dynamics: measurements and modeling. Water Resour. Res. **29**: 2299–2312.

Smith, K., and Lavis, M.E. 1975. Environmental influences on the temperature of a small upland stream. Oikos, **26**: 228–236.

Sugimoto, S., Nakamura, F., and Ito, A. 1997. Heat budget and statistical analysis of the relationship between stream temperature and riparian forest in the Toikanbetsu River Basin, northern Japan. J. For. Res. **2**: 103–107.

Sullivan, K., and Adams, T.A. 1990. The physics of forest stream heating: 2. An analysis of temperature patterns in stream environments based on physical principles and field data. Weyerheauser Tech. Rep. 004-5002.90/2. Technology Center, Tacoma, Wash.

Torgerson, C.E., Price, D.M., Li, H.W., and McIntosh, B.A. 1999. Multiscale thermal refugia and stream habitat associations of chinook salmon in northeastern Oregon. Ecol. Appl. **9**: 301–319.

Webb, B.W., and Zhang, Y. 1999. Water temperatures and heat budgets in Dorset chalk water courses. Hydrol. Processes, **13**: 309–321.

White, D.S., Elzinga, C.H., and Hendricks, S.P. 1987. Temperature patterns within the hyporheic zone of a northern Michigan river. J. North Am. Benthol. Soc. **6**: 85–91.

Zwieniecki, M., and Newton, M. 1999. Influence of streamside cover and stream features on temperature trends in forested streams of western Oregon. West. J. Appl. For. **14**: 106–112.

Appendix A. Heat budget parameters

Abbreviations, units, and sources of equations are indicated.

Incoming solar radiation ($W \cdot m^{-2}$): measured with a pyranometer on 20 July 2001; average calculated for noon to 1300. Radiation under shade calculated from average of two PAR (photosynthetically active radiation) sensors under shade for noon to 1300, 28 July 1997. Conversion: 2.35 $W \cdot m^{-2}$ = 1.0 $\mu mol \cdot m^{-2} \cdot s^{-1}$ (Oke 1987).

Reflected radiation ($W \cdot m^{-2}$): measured with downfacing pyranometer in full sun at noon, 20 July 2001.

Net long-wave radiation ($W \cdot m^{-2}$): calculated difference between incoming and reflected long-wave radiation (Monteith and Unsworth 1990).

Evaporative energy flux (H_{evap}, $W \cdot m^{-2}$): $E_v L_v \rho$ (Webb and Zhang 1999).

- E_v evaporation rate ($mm \cdot day^{-1}$) = $0.165(0.8 + U/100)(E_w - E_a)$ where U = wind speed ($km \cdot day^{-1}$) measured at noon, 20 July 2001, as 0.81 $m \cdot s^{-1}$ (E_v units converted to $m \cdot s^{-1}$ before further calculations)
- E_w saturated vapor pressure (mbar, 1 bar = 100 kPa) at T_w (Oke 1987) calculated from T_w to be 31.7 mbar in sun and 25 mbar under shade
- E_a vapor pressure (mbar) at T_a (Oke 1987) calculated from T_a to be 18.5 mbar in sun and 16 mbar under shade
- L_v latent heat of vaporization ($°C \cdot J \cdot g^{-1}$) = $2454.9 - 2.366T_a$ (Webb and Zhang 1999)
- ρ density of water ($g \cdot m^{-3}$) at 25 °C.
- T_a air temperature, 29.5 °C in sun and 26.0 °C under shade on 20 July 1997
- T_w water temperature, 25.0 °C in sun and 20.9 °C under shade on 20 July 1997

Convective energy flux (H_{conv}, $W \cdot m^{-2}$): $[(0.61P(T_w - T_a)/(E_w - E_a))/1000]H_{evap}$ (Webb and Zhang 1999).

- P atmospheric pressure, assumed to be 970 mbar

Conduction (H_{cond}, $W \cdot m^{-2}$): $K(dt/dz)$ (Brown 1969; Sinokrot and Stefan 1993).

- K thermal conductivity of substrate ($J \cdot m^{-1} \cdot s^{-1} \cdot °K^{-1}$), estimated to be 2.19 for stone (Oke 1987), and dt/dz = temperature gradient between surface of substrate, where the surface was assumed to be water temperature and substrate at 1 m depth assumed to be 10 °C

References

Brown, G.W. 1969. Predicting temperatures of small streams. Water Resour. Res. **5**: 68–75.

Monteith, J.L., and Unsworth, M. 1990. Principles of environmental physics. 2nd ed. Arnold Press, London, UK.

Oke, T.R. 1987. Boundary layer climates. 2nd ed. Routledge Press, London, UK.

Sinokrot, B.A., and Stefan, H.G. 1993. Stream temperature dynamics: measurements and modeling. Water Resour. Res. **29**: 2299–2312.

Webb, B.W., and Zhang, Y. 1999. Water temperatures and heat budgets in Dorset chalk water courses. Hydrol. Processes, **13**: 309–321.

© 2004 NRC Canada

Appendix B

Table B1. Synchronous stream temperatures at sites in WS 3 on 23 July 1997.

	Temperature (°C)			
Time (PST)	Site A	Site B	Site C	Site D
0007	14.8	14.9	15.7	16.2
0037	14.6	14.6	15.4	16.2
0107	14.3	14.4	15.2	16.0
0137	14.1	14.3	14.9	16.0
0207	14.0	14.0	14.8	16.0
0237	13.8	13.8	14.5	16.0
0307	13.7	13.6	14.3	15.9
0337	13.4	13.5	14.1	15.9
0407	13.4	13.3	14.0	15.9
0437	13.1	13.0	13.8	15.9
0507	12.9	12.9	13.5	15.7
0537	12.9	12.7	13.4	15.7
0607	12.7	12.7	13.4	15.7
0637	12.6	12.6	13.1	15.7
0707	12.4	12.4	13.1	15.6
0737	12.4	12.3	12.9	15.6
0807	12.3	12.3	12.8	15.6
0837	12.3	12.3	12.6	15.6
0907	12.4	12.3	12.6	15.6
0937	12.4	12.4	12.8	15.6
1007	12.6	12.6	12.8	15.6
1037	12.7	13.0	12.9	15.6
1107	13.1	14.1	13.2	15.7
1137	15.2	15.1	13.8	15.9
1207	17.2	17.1	14.9	16.2
1237	19.7	18.9	16.2	16.0
1307	21.9	21.0	17.6	16.0
1337	21.9	22.2	18.9	16.0
1407	21.5	22.0	20.0	16.2
1437	20.4	21.3	20.9	16.2
1507	19.4	20.5	20.9	16.2
1537	18.4	19.7	20.5	16.2
1607	18.0	19.0	20.0	16.4
1637	17.8	18.6	19.6	16.7
1707	17.6	18.4	19.2	16.8
1737	17.5	18.2	18.9	16.8
1807	17.5	18.2	18.7	16.8
1837	17.3	17.8	18.4	16.5
1907	17.2	17.8	18.3	16.5
1937	17.0	17.4	18.1	16.4
2007	16.8	17.1	17.8	16.2
2037	16.5	16.8	17.6	16.2
2107	16.4	16.5	17.5	16.2
2137	16.0	16.3	17.1	16.2
2207	15.7	16.0	16.8	16.0
2237	15.6	15.7	16.7	16.0
2307	15.2	15.4	16.3	16.0
2337	15.1	15.2	16.0	16.0

Note: Experimental shading occurs between sites B and C and flow of water is from site A to site D (Fig. 1).

© 2004 NRC Canada

Effects of an invasive bivalve (*Dreissena polymorpha*) on fish in the Hudson River estuary

David L. Strayer, Kathryn A. Hattala, and Andrew W. Kahnle

Abstract: Despite predictions that the zebra mussel (*Dreissena polymorpha*) invasion of North America would damage fisheries, analyses of actual effects on fish have been few and equivocal. We analyze 26 years of data on fish populations in the Hudson River to quantify changes associated with the zebra mussel invasion. Based on our measurements of changes in the lower food web, we predicted that populations of open-water fish species (e.g., *Alosa* spp.) would suffer and populations of littoral fish species (e.g., Centrarchidae) would prosper from the zebra mussel invasion. We found that the median decrease in abundance of open-water species was 28%, whereas the median increase in abundance of littoral species was 97%. Populations of open-water species shifted downriver away from the zebra mussel population, whereas those of littoral species shifted upriver. Median apparent growth rates fell by 17% among open-water species and rose by 12% in the single littoral species studied. Many of the observed changes were large and involved species of commercial or recreational importance (e.g., American shad (*Alosa sapidissima*), black basses (*Micropterus* spp.)). The influence of zebra mussels on fish should vary widely across ecosystems as a function of system morphology, factors that limit primary production, and diets of the fish species.

Résumé : Malgré les prédictions voulant que l'invasion des moules zébrées (*Dreissena polymorpha*) en Amérique du Nord soit néfaste pour les pêches, les analyses d'effets réels sont rares et équivoques. Nos analysons 26 années de données sur les populations de poissons du fleuve Hudson pour quantifier les changements associés à l'invasion des moules zébrées. D'après notre évaluation des modifications de la partie inférieure du réseau alimentaire, nous avions prédit que les populations de poissons d'eau libre (e.g., *Alosa* spp.) seraient défavorisées et que les populations littorales (e.g., les Centrarchidae) seraient avantagées par l'invasion des moules zébrées. Le déclin médian de l'abondance des espèces d'eau libre est de 28 %, alors que l'accroissement médian de l'abondance des espèces littorales est de 97 %. Les populations d'espèces d'eau libre se sont déplacées vers l'aval loin de la population de moules zébrées, alors que celles des espèces littorales ont remonté vers l'amont. Les taux médians apparents de croissance ont chuté de 17 % chez les espèces d'eau libre et augmenté de 12 % chez la seule espèce littorale étudiée. Plusieurs des changements observés sont considérables et impliquent des espèces d'importance commerciale ou sportive (e.g., l'alose savoureuse (*Alosa sapidissima*), les achigans (*Micropterus* spp.)). Les effets des moules zébrées sur les poissons devraient varier beaucoup dans les écosystèmes en fonction de la morphologie des systèmes, des facteurs limitants de la production primaire et du régime alimentaire des espèces de poissons.

[Traduit par la Rédaction]

Introduction

Species introductions are now one of the most important of human impacts on the world's ecosystems (e.g., Office of Technology Assessment 1993; Mack et al. 2000). Ecosystems near centers of human activity often contain dozens to hundreds of introduced species, with more arriving each year. These invasions may have large, diverse ecological and economic effects that are difficult to mitigate or reverse. The effects of species invasions can be difficult to quantify, requiring good measurements of the ecosystem before and after the invasion. Indirect effects of an invader that are propagated through the ecosystem can be especially difficult to measure or predict because the initial effect of the invader can be damped, amplified, or even reversed by the ecosystem.

The impact of zebra mussels (*Dreissena polymorpha*) on fish populations is an example of an important indirect effect that has been difficult to measure. When zebra mussels appeared in North America in 1988, experts predicted economic damages of US$ 4 billion in the first 10 years in the Great Lakes alone (Roberts 1990), largely from losses of sport fisheries. However, no evidence of damage to sport fisheries has yet appeared.

Received 23 April 2003. Accepted 24 January 2004. Published on the NRC Research Prss Web site at http://cjfas.nrc.ca on 24 July 2004.
J17482

D.L. Strayer.[1] Institute of Ecosystem Studies, P.O. Box AB, Millbrook, NY 12545, USA.
K.A. Hattala and A.W. Kahnle. New York State Department of Environmental Conservation, 21 South Putt Corners Road, New Paltz, NY 12561, USA.

[1]Corresponding author (e-mail: strayerd@ecostudies.org).

 doi: 10.1139/F04-043 © 2004 NRC Canada

In fact, while zebra mussels have been shown to have strong effects on phytoplankton (e.g., Caraco et al. 1997; Smith et al. 1998), zooplankton (MacIsaac et al. 1995; Pace et al. 1998), vegetation (Skubinna et al. 1995; Stuckey and Moore 1995), water chemistry (Fahnenstiel et al. 1995*b*; Effler et al. 1996), and zoobenthos (Nalepa et al. 1998; Strayer and Smith 2001), the few studies on fish have had inconsistent results. Experimental studies in which fish were exposed to different densities of zebra mussels showed that fish growth can increase (Thayer et al. 1997), decrease (Jennings 1996), or be unaffected (Richardson and Bartsch 1997) by the mussels. In any case, it is difficult to apply the results of these studies to nature because they were conducted on such short scales of time and space that they excluded many potentially important mechanisms.

Detecting zebra mussel impacts from field data requires long runs of high-quality data, preferably including the parts of the food web that link zebra mussels to fish, and is often complicated by changes in other external variables during the invasion period. Consequently, such analyses are few and have given equivocal results. Scientists detected little or no effect of the zebra mussel invasion on abundance or growth of young-of-the-year (YOY) fish in the open waters of Lake Erie (Gopalan et al. 1998; Dermott et al. 1999; Trometer and Busch 1999), but these analyses are complicated by the invasion of an important alien fish species (white perch (*Morone americana*)) and large reductions in nutrient loading in Lake Erie during the period of analysis. Likewise, the zebra mussel invasion did not seem to reduce phytoplankton or zoobenthos biomass in Rice Lake, Ontario, and did not affect the diets or growth rates of two of three fish species studied (Mercer et al. 1999). Growth rates of the third species (pumpkinseed (*Lepomis gibbosus*)) increased. In Oneida Lake, New York, Mayer et al. (2000) found that apparent growth rates of YOY yellow perch (*Perca flavescens*) rose following the zebra mussel invasion but that the abundance of YOY and the abundance and apparent growth rates of adult perch were unchanged. In contrast, Ryan et al. (1999) reported that the catch rates of many species of fish in Long Point Bay (Lake Erie) fell significantly when zebra mussels invaded. In southeastern Lake Michigan, the diet of lake whitefish (*Coregonus clupeaformis*) changed and body condition and growth declined after the zebra mussel invasion caused the abundance of a favored food item (the amphipod *Diporeia*) to decline (Pothoven et al. 2001). Karataev and Burlakova (1995) reported very large increases in the biomass and production of fish in Lukomskoe Lake, Belarus, following the arrival of zebra mussels and linked this increase to increases in zoobenthic prey. Unfortunately, a large powerplant began operations on this lake at almost the same time as the zebra mussel invasion, so it is difficult to separate powerplant effects (e.g., entrainment, temperature) from zebra mussel effects. No clear picture emerges from these analyses of field data, except that zebra mussels might have strong effects in some cases and no effects in others and that analyses have been hampered by inadequate data.

Here, we analyze extensive long-term (up to 26 years) data sets on YOY fish in the Hudson River estuary, New York, to quantify zebra mussel effects on fish. Unlike most other ecosystems that have been studied, we also have access to long-term records of most other parts of the Hudson's food web over the invasion period, and there is no evidence of major confounding changes in external driving variables to the Hudson River ecosystem during the invasion period.

Materials and methods

Study area

The study area is the Hudson River estuary, which extends 248 km from New York City to Troy in eastern New York. Over most of its length, the Hudson estuary is 1–4 km wide and 5–20 m deep, although the morphology is varied and there are extensive shallows and areas as deep as 66 m (Cooper et al. 1988). Above about river kilometre (rkm) 100 (kilometres upriver from The Battery in New York City), the river usually is fresh, but below rkm 100, sea salt may be present in various concentrations, depending on freshwater flow and tides. The entire area is subject to tides of ~1 m; tidal flows are much larger than the average freshwater flow of 577 $m^3 \cdot s^{-1}$ (Cooper et al. 1988). The water in the Hudson is alkaline (pH ~ 7–8), warm (annual mean 12 °C), turbid (Secchi transparency ~ 1 m), and nutrient rich (PO_4-P > 10 $\mu g \cdot L^{-1}$, NO_3-N ~ 0.4 $mg \cdot L^{-1}$) (Limburg et al. 1986; Caraco et al. 1997).

Allochthonous matter dominates organic carbon inputs to the Hudson (69% of total), but primary production by phytoplankton and submersed macrophytes is important (Howarth et al. 1996; Caraco et al. 2000). Primary production by phytoplankton (and presumably submersed macrophytes) is light limited (Cole et al. 1992; Harley and Findlay 1994). The Hudson's zooplankton is dominated by rotifers and the cladoceran *Bosmina freyi* (Pace et al. 1998), and its diverse zoobenthos is dominated by tubificid oligochaetes, amphipods, and chironomid midges (Strayer and Smith 2001). The estuary supports warmwater fishes, including several abundant diadromous species.

Zebra mussels first appeared in the Hudson in 1991 and have been a dominant part of the Hudson's biota since September 1992 (Strayer et al. 1996). Since that time, combined suspension-feeding by all species increased 30-fold, biomass of phytoplankton fell 80%, biomass of microzooplankton fell 76%, biomass of macrozooplankton fell 52%, biomass of deepwater zoobenthos fell 40%, and biomass of shallow-water zoobenthos rose 10% in the freshwater tidal parts of the Hudson (Strayer et al. 1999; Strayer and Smith 2001). The 45% increase in water clarity may have led to increases in the coverage and productivity of submersed macrophytes (Strayer et al. 1999; Caraco et al. 2000), although this process has not been well studied in the Hudson. Zebra mussels are quantitatively important only in freshwater parts of the Hudson, and their effects extend from the head of the estuary (rkm 248) down to approximately rkm 100 (Strayer et al. 1996; Caraco et al. 1997; Pace et al. 1998). Most relevant to the fish, we found that the biomass of forage invertebrates (i.e., zooplankton and macrozoobenthos excluding the large bivalves that are eaten by few species of fish in the Hudson (Schmidt et al. 1995; Strayer 2004)) fell by 70% in the pelagic zone, fell by 40% in the deepwater benthos, and rose by 10% in the shallow-water benthos (Pace et al. 1998;

© 2004 NRC Canada

Strayer and Smith 2001). We suspect that our estimate of the increase in shallow-water benthos in the Hudson is too low, as it is based on the areal density of macroinvertebrates per square metre of macrophyte bed and excludes any increases that may have occurred in the extent of macrophyte beds. Such increases in macrophyte coverage have been seen in other ecosystems invaded by bivalves (e.g., Phelps 1994; Skubinna et al. 1995) but have not been quantified in the Hudson.

Hypotheses

We hypothesized that these changes in the food web might have affected the Hudson's fish community. Larvae and juveniles of several abundant fish species in the Hudson (i.e., American shad (*Alosa sapidissima*), blueback herring (*Alosa aestivalis*), alewife (*Alosa pseudoharengus*), gizzard shad (*Dorosoma cepedianum*), white perch, and striped bass (*Morone saxatilis*)) feed heavily on plankton and drifting benthic invertebrates in the water column (summarized by Strayer and Smith 2001) and so might be negatively affected by the zebra mussel invasion. We hypothesized that the abundance or growth rates of these species would decline following the zebra mussel invasion or that their distributions within the river would shift downriver away from the zone of greatest zebra mussel impacts. In contrast, many fish species (common carp (*Cyprinus carpio*), spottail shiner (*Notropis hudsonius*), fourspine stickleback (*Apeltes quadracus*), banded killifish (*Fundulus diaphanus*), redbreast sunfish (*Lepomis auritus*), bluegill (*Lepomis macrochirus*), pumpkinseed, smallmouth bass (*Micropterus dolomieu*), largemouth bass (*Micropterus salmoides*), and tessellated darter (*Etheostoma olmstedi*)) are associated with vegetated shallows in the Hudson, where they feed chiefly on benthic invertebrates (summarized by Strayer and Smith 2001). We hypothesized that the abundance or growth rates of these species would increase following the zebra mussel invasion or that their distributions within the river would shift upriver into the zone of greatest zebra mussel impacts.

Sources of data

Our analysis was based on three data sets: the utilities' long-river ichthyoplankton survey (LRS), the utilities' beach seine survey (UBSS), and the Department of Environmental Conservation's beach seine survey (DECBSS) (the "utilities'" surveys are conducted by contractors of the electric utilities, which are required to monitor fish populations in the river as a condition for withdrawing cooling water from the Hudson). The utility companies collected ichthyoplankton samples annually from 1974 to 1999. This program was described by Klauda et al. (1988), Heimbuch et al. (1992), and Young et al. (1992). Samples were taken biweekly beginning in March, weekly from April through June, and then biweekly until late September. The river between The Battery (rkm 0) and Troy (rkm 248) was divided into 13 sections and several habitat strata (channel, bottom, shoal, and shore) from which samples were taken in a stratified random design. At least two samples were taken from each stratum in each sampling period resulting in ~2400 samples·year^{-1}. Samples were taken with a Tucker trawl or an epibenthic sled having an aperture of 1 m^2 and mesh of 505 μm resulting in a typical sample volume of ~300 m^3. Species and life stages (egg, yolk-sac larva, post-yolk-sac larva, or 0+ juvenile) were identified and enumerated, and lengths of selected species (alewife, American shad, blueback herring, white perch, striped bass, and spottail shiner) were measured. We analyzed the abundance of post-yolk-sac larvae from this data set. We excluded data from "region 0" (rkm 0–21), which was not sampled before 1988. Post-yolk-sac larvae of blueback herring and alewife were combined into a single taxon called "river herring" for our analysis because the early life stages of these two species cannot be readily distinguished; presumably, most river herring are bluebacks.

The UBSS began in 1974. This survey was riverwide, with the goal of measuring the distribution and abundance of selected species. Samples were taken biweekly from mid-June until October. Approximately 1000 samples were taken each year, in a stratified random design based on the river sections described above, using a 30.5-m beach seine. Fish were identified to species and life stage (YOY or older) and counted, and lengths of selected species (as for the ichthyoplankton survey) were measured. We analyzed data from this survey for YOY (i.e., 0+ juveniles) only.

We analyzed data from the DECBSS from 1985 to 1999. The goal of this survey was to estimate relative abundance of juvenile *Alosa* spp., primarily American shad and blueback herring. Samples were taken biweekly (alternating with the UBSS) from late June to October at 28 fixed sites near Newburgh Bay, Poughkeepsie, Coxsackie, and Albany. Samples were taken with a 0.64-cm-mesh beach seine with 12.2 m × 3.05 m wings and a 6.1 m × 3.7 m bag. Fish were identified and counted, and lengths of selected species (alewife, American shad, blueback herring, striped bass, largemouth bass, smallmouth bass, and other sport fish) were measured. We analyzed data from this survey for YOY (i.e., 0+ juveniles) only.

Statistical analyses

Abundance

We tested for effects of the zebra mussel invasion on the estimated riverwide population of fish ("riverwide standing crop") using two data sets, the LRS of post-yolk-sac larvae and the UBSS of 0+ juveniles. In the LRS, we calculated the mean number of post-yolk-sac larvae in the river over the weeks in which each species usually was present and samples were taken throughout the river (samples were not always taken above rkm 124 after week 27). This time period differed among species as follows: American shad, weeks 19–27; river herrings, weeks 18–27; white perch, weeks 18–27; striped bass, weeks 20–27; common carp, weeks 21–27; tessellated darter, weeks 19–27.

We modeled log-transformed abundance using multiple regression with the following independent variables: year (which allows for temporal trends in the data), mean water temperature and mean freshwater flow during the period of analysis, and the presence or absence of zebra mussel effects (coded as 0 for 1974–1992 and 1 for 1993–1999). If the data set contained zeroes, we substituted a $\log(X + c)$ transformation, where c was the minimum nonzero value observed for that species. Because we could not exclude the single or combined influence of any of these variables, we ran all pos-

© 2004 NRC Canada

Table 1. Statistical models to predict log-transformed abundance of selected age-classes of fish in the Hudson River.

Species	Year	Flow ($m^3 \cdot s^{-1}$, $\times 10^{-5}$)	Temperature (°C)	Zebra
Post-yolk-sac larvae				
Blueback herring + alewife	0.34	0.31	0.71	0.34
	0.015 (0.022)	33 (99)	–0.21 (0.12)	–0.24 (0.37)
American shad	0.82	0.23	0.41	0.99
	0.022 (0.010)	–1.9 (39)	–0.055 (0.044)	–0.58 (0.19)
Striped bass	1.00	0.23	0.27	0.24
	0.064 (0.008)	–1.9 (41)	0.031 (0.047)	0.065 (0.19)
White perch	0.82	0.27	0.27	0.65
	0.018 (0.010)	–12 (32)	–0.018 (0.046)	–0.25 (0.17)
Common carp	1.00	0.29	0.27	0.27
	0.16 (0.026)	–125 (60)	0.096 (0.15)	0.37 (0.60)
Tessellated darter	0.87	0.24	0.26	0.31
	0.013 (0.006)	–0.70 (30)	0.016 (0.035)	0.014 (0.15)
0+ juveniles				
Alewife	0.99	0.26	0.86	0.41
	–0.048 (0.015)	–34 (89)	0.19 (0.076)	0.30 (0.25)
American shad	0.41	0.46	0.37	0.72
	–0.010 (0.008)	120 (122)	–0.045 (0.040)	–0.22 (0.097)
Blueback herring	0.68	0.24	0.50	0.29
	–0.027 (0.014)	8.7 (97)	–0.14 (0.091)	–0.073 (0.31)
Gizzard shad	0.47	0.31	0.44	0.36
	0.028 (0.023)	88 (162)	0.17 (0.15)	0.29 (0.41)
Striped bass	0.36	0.51	0.33	0.33
	–0.005 (0.009)	–67 (50)	–0.017 (0.057)	0.028 (0.16)
White perch	0.80	0.47	0.24	0.48
	–0.030 (0.011)	–98 (35)	–0.020 (0.072)	–0.36 (0.23)
Spottail shiner	0.44	0.37	0.34	0.35
	–0.007 (0.008)	–111 (103)	0.004 (0.054)	–0.032 (0.14)
Banded killifish	0.99	0.98	0.30	0.48
	–0.048 (0.014)	–239 (67)	–0.066 (0.076)	0.34 (0.24)
Fourspine stickleback	0.91	0.30	0.49	0.56
	–0.073 (0.024)	–149 (106)	–0.15 (0.12)	–0.72 (0.42)
Bluegill	0.56	0.33	0.48	0.49
	–0.021 (0.019)	–44 (88)	0.095 (0.089)	0.30 (0.31)
Redbreast sunfish	0.39	0.97	0.28	0.55
	0.023 (0.020)	–385 (109)	–0.078 (0.12)	0.48 (0.29)
Pumpkinseed	0.33	0.82	0.28	0.28
	–0.009 (0.015)	–180 (74)	–0.027 (0.089)	0.038(0.24)
Smallmouth bass	0.44	0.25	0.51	0.73
	0.021 (0.015)	–26 (76)	0.10 (0.07)	0.47 (0.19)
Largemouth bass	0.33	0.33	0.54	0.36
	0.00 (0.015)	–30 (96)	–0.10 (0.086)	0.12 (0.24)
Tessellated darter	1.00	0.35	0.21	0.91
	–0.041 (0.012)	–56 (121)	–0.006 (0.055)	0.44 (0.17)

Note: The table shows the summed Akaike weight for each variable (upper number) along with the model-averaged slope and standard error (lower numbers) for each variable. Year is number of years since 1974.

sible subsets of regression models and presented model-averaged estimates of parameters (Burnham and Anderson 2002). We present two measures of the importance of the independent variables in predicting fish abundance. First, we present the sum of Akaike weights (w_i) for all models containing a given variable, which is the likelihood that the most appropriate model to describe the data includes that variable. Second, we present the model-averaged estimates of the slopes ($\bar{\beta}_i$) for each variable, along with their standard errors. There are two ways in which to calculate these model-averaged slopes: averaging over only models in which the variable actually appears and averaging over all possible models, including those in which the variable does not appear (see Burnham and Anderson (2002) for a discussion of this point). We present the former estimate, which is interpreted as an estimate of the slope given that the variable is assumed to be included in the model. The slope estimates based on all models can be calculated as the product of the Akaike weight and the slope estimates that we present. Inspection of autocorrelation and partial autocorrelation func-

© 2004 NRC Canada

Fig. 1. Abundance of post-yolk-sac larvae of several species of fish in the Hudson River before (solid circles) and after (open circles) the zebra mussel invasion based on data from the utilities' long-river survey. The regression lines are fit to preinvasion data. Open circles falling below the line indicate that a species decreased after the zebra mussel invasion, whereas open circles falling above the line indicate that a species increased after the zebra mussel invasion. Note that the *y* axes are logarithmic.

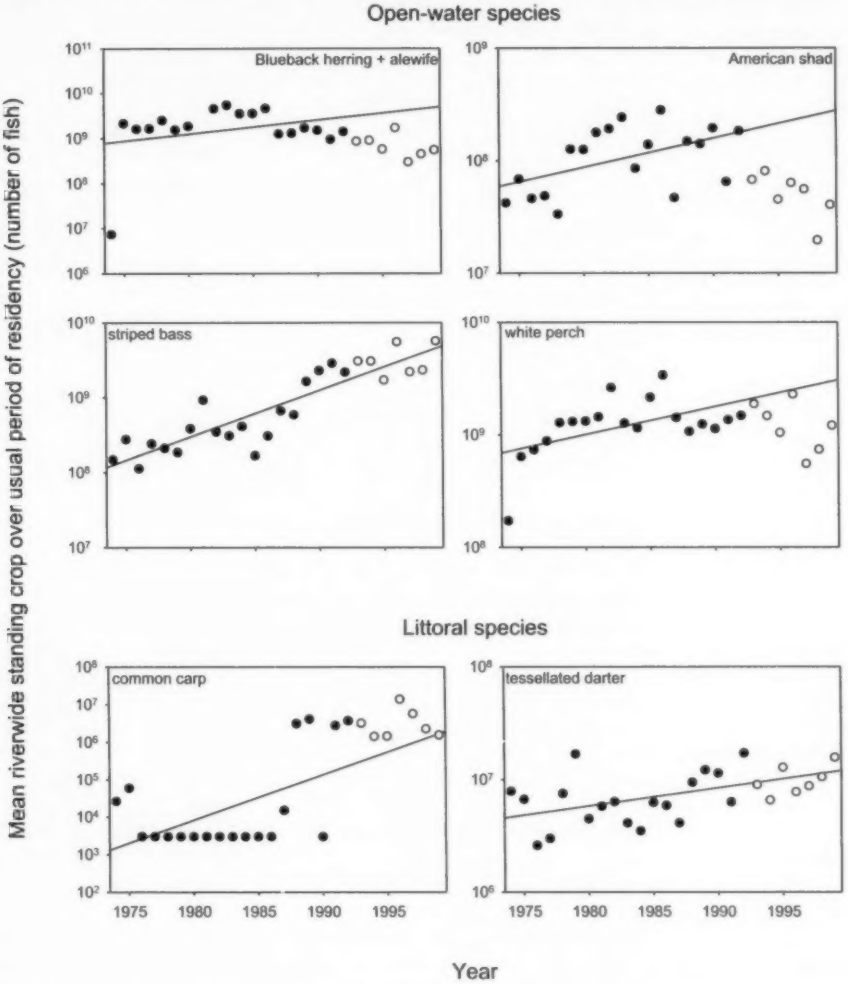

tions of the residuals from a selection of the best models (those with the lowest values of the Akaike information criterion) suggested that the residuals were not significantly temporally autocorrelated.

UBSS data were consistently available only for weeks 32–40 each year, so we restricted our analysis to this period. The dependent variable was the mean riverwide standing crop over weeks 32–40, and the analysis proceeded as for the LRS.

Distribution

To assess the distribution of fish within the Hudson, we compared the number of fish of each species in the freshwater estuary, which has been heavily affected by the zebra mussel invasion, with that in the brackish estuary, which presumably has been affected little or not at all by zebra mussels. We chose rkm 100 as a breakpoint because zebra mussel impacts on plankton appear to disappear near this point (Caraco et al. 1997, 2000; Pace et al. 1998). We calculated the mean standing crop of each species above and below rkm 100 for the same time periods used for the analysis of abundance (above). Then, we calculated an index of distribution (D)

$$D = \log\left(\frac{\text{standing crop above rkm 100}}{\text{standing crop below rkm 100}}\right)$$

where positive values of D indicate that most of the population was upriver of rkm 100 and negative values indicate that most of the population was downriver of rkm 100. If the data set contained zeroes, we substituted a $\log(X + c)$ transformation, where c was the minimum nonzero value observed in that data set. We modeled D using the same procedures as described for modeling abundance. Inspection of auto-

© 2004 NRC Canada

Fig. 2. Abundance of YOY of several species of fish in the Hudson River before (solid circles) and after (open circles) the zebra mussel invasion based on data from the utilities' beach seine survey. The regression lines are fit to preinvasion data. Open circles falling below the line indicate that a species decreased after the zebra mussel invasion, whereas open circles falling above the line indicate that a species increased after the zebra mussel invasion. Note that the *y* axes are logarithmic.

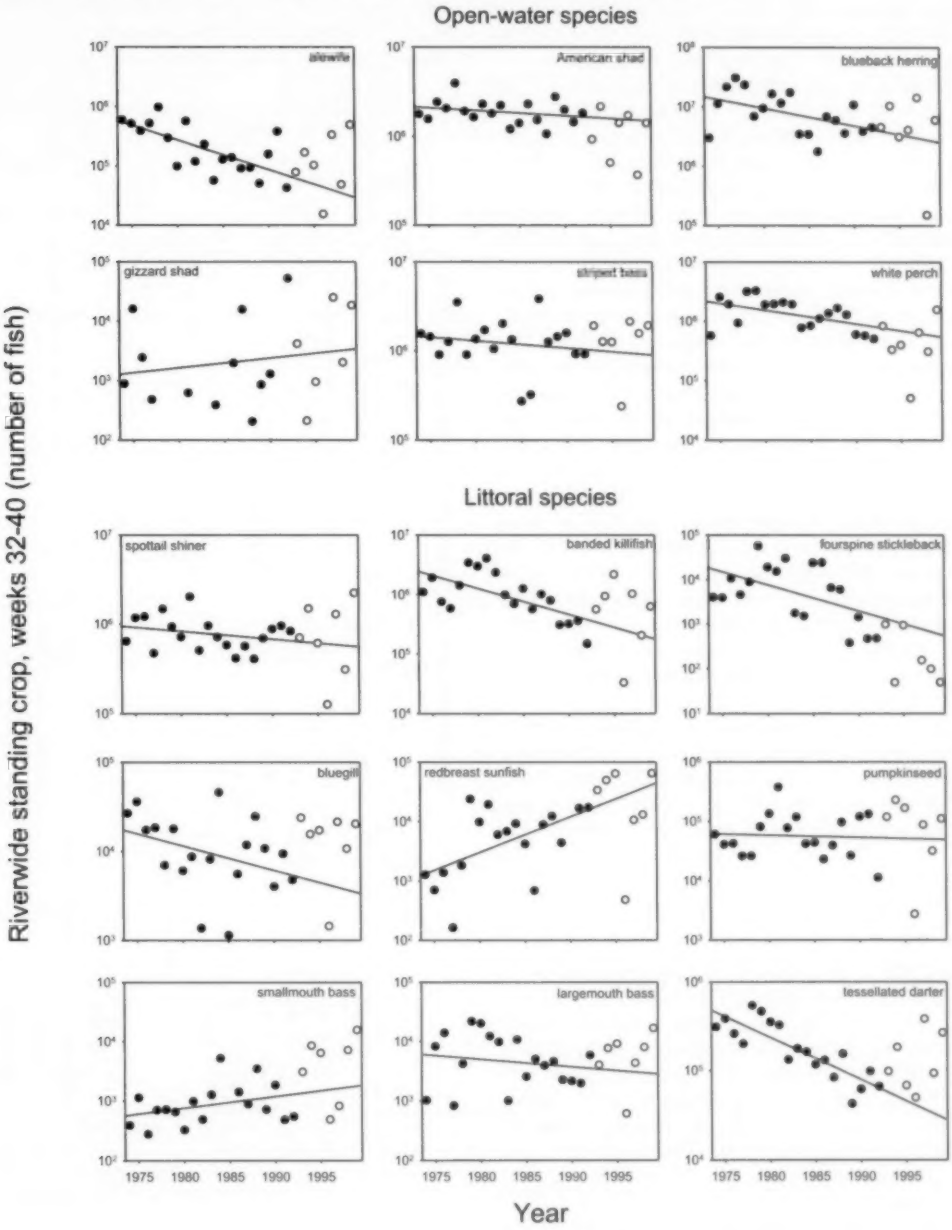

correlation and partial autocorrelation functions of residuals from a selection of the best models showed that temporal autocorrelations were small and insignificant.

Apparent growth

We analyzed trends in apparent growth rates of YOY fish in three data sets: LRS, UBSS, and DECBSS. We define apparent growth rate (g) as the rate of change in mean fish size between two successive sampling dates. Thus,

$$g = \ln(L_{t+1}/L_t)/t$$

where L_{t+1} and L_t are mean total lengths at two successive sampling times separated by t weeks of time. Mean total lengths were calculated for each week and river region sepa-

© 2004 NRC Canada

rately (see below). We estimated apparent growth rates only if $n \geq 30$ fish were measured in a given week (we relaxed this standard to $n \geq 10$ fish for alewife in the DECBSS data to allow us to analyze the apparent growth of this less frequently caught species). We modeled growth by multiple regression. Models contained the following independent variables: mean freshwater discharge and water temperature (during the 2 weeks in which growth was estimated), mean body length of fish, and a term to represent zebra mussel effects. This term was 0 in 1974–1992 and below rkm 100 and was 1 only for estimates made above rkm 100 in 1993–1999. Body length was included in all models. Preliminary models showed that population size (i.e., density dependence) was ineffective at predicting growth rates, so this factor was not included in our final models. Growth data from the LRS of post-yolk-sac larvae were not available before 1979 (striped bass) or 1982 (white perch and American shad).

Most of the littoral zone species whose growth rates that we hypothesized would increase were not caught in sufficient numbers to support a complete statistical analysis. We supplemented our formal analysis with a simpler, less formal procedure to try to include information on some of the less abundant littoral species. Using the DECBSS data set, we calculated the mean length of each species of fish in the upper river (rkm 195–226) for each week (regardless of year) before and after the zebra mussel invasion. That is, we pooled the data for 1985–1992 and for 1993–1999 for each species. We required only five fish to be measured to estimate mean length for a given week over these two time periods. We then simply compared whether mean length was larger for each week before or after the zebra mussel invasion.

For all analyses, we use two levels of statistical significance: the traditional $\alpha = 0.05$ as well as $\alpha = 0.2$. We believe that Type II errors have serious consequences in our study and have followed recent advice to adopt more lenient α values to more nearly balance Type I and Type II errors.

Results

Abundance

Many of the fish in the Hudson had temporal trends in abundance prior to or unrelated to the zebra mussel invasion: post-yolk-sac larvae of American shad, common carp, striped bass, white perch, and tessellated darter all have been increasing, whereas 0+ juveniles of alewife, blueback herring, banded killifish, fourspine stickleback, white perch, and tessellated darter all have been decreasing (Table 1; Figs. 1 and 2). Neither temperature nor freshwater flow was significantly correlated with abundance of most fish species in the Hudson (Table 1).

Changes in the estimated riverwide abundance of several species of fish (over what would have been expected given temporal trends, flow, and temperature) coincided with the zebra mussel invasion (Table 1; Figs. 1 and 2). Significant ($p < 0.2$) declines in post-yolk-sac larvae of American shad and white perch and 0+ juveniles of American shad and white perch were associated with the zebra mussel invasion (Fig. 3). In contrast, the zebra mussel invasion was associated with significant increases in 0+ juveniles of banded killifish, bluegill, redbreast sunfish, smallmouth bass, and tessellated darter (Fig. 3). Abundance of 0+ juveniles of alewife and fourspine stickleback changed in a direction opposite to our hypotheses. The median change in log-transformed abundance of open-water species was 0.15, corresponding to a decline of 28%, whereas the median log-transformed abundance of littoral species rose by 0.295, corresponding to an

Fig. 3. Summary of the effects of the zebra mussel invasion on abundance of fish in the Hudson River: (*a*) post-yolk-sac larvae; (*b*) 0+ juveniles. The circle represents the mean effect, and the thick and thin vertical bars represent the 60% and 90% confidence intervals on the mean (i.e., the 20% and 5% significance levels in one-tailed tests). The horizontal lines indicate no change owing to the zebra mussel invasion.

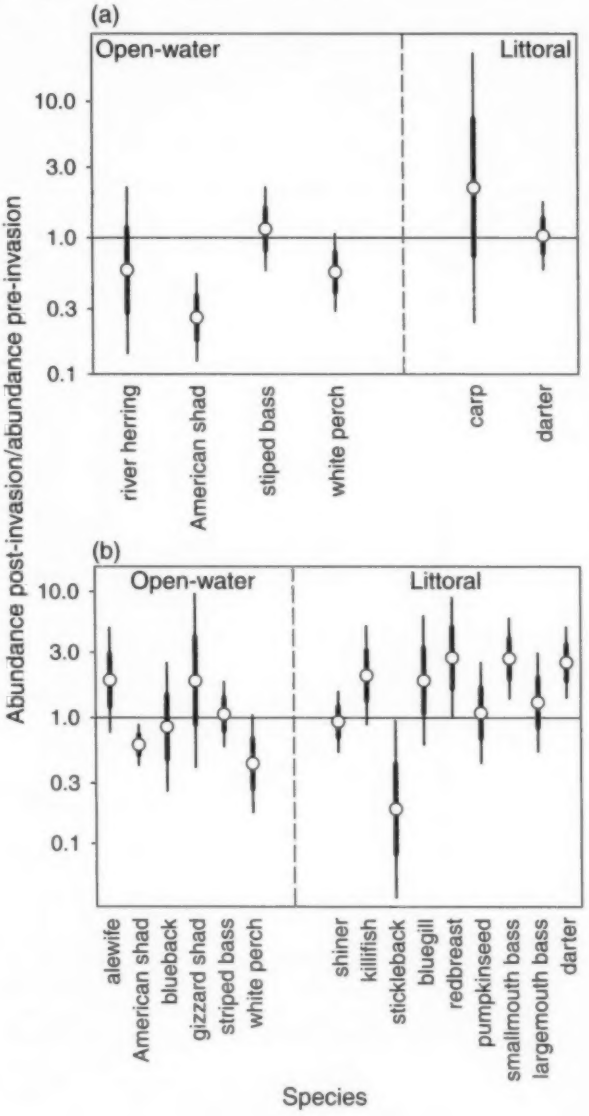

© 2004 NRC Canada

Table 2. Statistical models to predict distribution of fish within the Hudson River.

Species	Year	Flow ($m^3 \cdot s^{-1}$, $\times 10^{-4}$)	Temperature (°C)	Zebra
Post-yolk-sac larvae				
Blueback herring and alewife	0.26	0.86	0.29	0.31
	0.004 (0.014)	−15 (5.3)	0.062 (0.10)	0.17 (0.22)
American shad	0.56	0.93	0.27	0.35
	0.026 (0.016)	−22 (7.1)	0.077 (0.12)	0.27 (0.30)
Striped bass	0.31	0.38	0.48	0.38
	<0.001 (0.007)	−2.7 (3.6)	0.045 (0.039)	−0.09 (0.11)
White perch	0.57	0.34	0.29	0.45
	0.009 (0.006)	4.0 (3.6)	0.020 (0.044)	0.13 (0.11)
Common carp	0.38	0.25	0.66	0.74
	−0.023 (0.084)	1.5 (12)	0.21 (0.12)	−0.69 (0.36)
Tessellated darter	0.51	0.27	0.81	0.30
	0.015 (0.011)	7.2 (9.6)	0.15 (0.073)	0.08 (0.24)
0+ juveniles				
Alewife	0.58	0.51	0.29	0.38
	0.033 (0.022)	−19 (16)	0.055 (0.12)	−0.29 (0.44)
American shad	0.96	0.61	0.23	0.56
	0.030 (0.012)	−10 (5.4)	0.023 (0.062)	−0.30 (0.19)
Blueback herring	0.32	0.61	0.36	0.39
	0.007 (0.019)	−16 (8.7)	0.16 (0.15)	−0.24 (0.29)
Gizzard shad	0.70	0.68	0.25	0.33
	−0.033 (0.016)	21 (10)	0.027 (0.12)	−0.25 (0.34)
Striped bass	0.96	0.23	0.28	0.25
	0.026 (0.008)	−1.2 (5.8)	0.041 (0.057)	−0.008 (0.20)
White perch	0.38	0.34	0.46	0.39
	0.008 (0.009)	−4.8 (6.1)	0.068 (0.055)	0.14 (0.15)
Spottail shiner	0.57	0.75	0.60	0.29
	0.021 (0.013)	−16 (7.2)	0.13 (0.073)	−0.11 (0.26)
Banded killifish	0.94	0.29	0.25	0.97
	0.040 (0.014)	−6.0 (2.7)	−0.039 (0.074)	0.74 (0.25)
Fourspine stickleback	0.60	0.31	0.45	0.74
	−0.047 (0.033)	11 (15)	−0.18 (0.14)	0.86 (0.52)
Bluegill	0.30	0.89	0.25	0.76
	0.012 (0.022)	−26 (9.0)	0.053 (0.11)	0.53 (0.24)
Redbreast sunfish	0.89	0.84	0.26	0.31
	0.073 (0.025)	−39 (14)	−0.086 (0.17)	0.51 (0.59)
Pumpkinseed	0.99	0.47	0.28	0.27
	0.051 (0.016)	−13 (7.8)	0.063 (0.089)	−0.006 (0.38)
Smallmouth bass	0.53	0.49	0.25	0.95
	−0.029 (0.021)	−14 (9.5)	−0.041 (0.10)	0.76 (0.33)
Largemouth bass	0.68	0.66	0.25	0.43
	0.025 (0.035)	−14.5 (7.0)	0.038 (0.082)	0.29 (0.22)
Tessellated darter	0.76	0.40	0.26	0.31
	0.018 (0.011)	−7.1 (3.8)	−0.007 (0.065)	0.08 (0.20)

Note: The dependent variable is the log(number of fish upriver of rkm 100/number of fish downriver of rkm 100); thus, positive values indicate a predominance of fish in the freshwater part of the estuary and negative values indicate a predominance of fish in the brackish part of the estuary. The table shows the summed Akaike weight for each variable (upper number) along with the model-averaged slope and standard error (lower numbers) for each variable. Year is number of years since 1974.

increase of 97%. Fish abundance changed consistent with our hypotheses; some of these changes were large (>50%).

Distribution

The distribution of several fish species shifted significantly upriver over time (Table 2; Figs. 4 and 5). In addition, freshwater flow was significantly correlated with distribution of many species in the Hudson. Generally, populations were centered further downriver in years of high flow (Table 2). The gizzard shad showed the opposite pattern, with populations centered further upriver in high-flow years.

The zebra mussel invasion was associated with changes in the distributions of several fish species (Table 2; Fig. 4). Post-yolk-sac larvae of common carp showed a significant distributional change associated with the zebra mussel invasion in a direction opposite to that we postulated (Fig. 4).

© 2004 NRC Canada

Fig. 4. Distribution of post-yolk-sac larvae of several species of fish in the Hudson River before (solid circles) and after (open circles) the zebra mussel invasion based on data from the utilities' long-river survey. The regression lines are fit to preinvasion data. Open circles falling below the line indicate that an increased proportion of the population was found downriver after the zebra mussel invasion, whereas open circles falling above the line indicate that an increased proportion of the population was found upriver after the zebra mussel invasion.

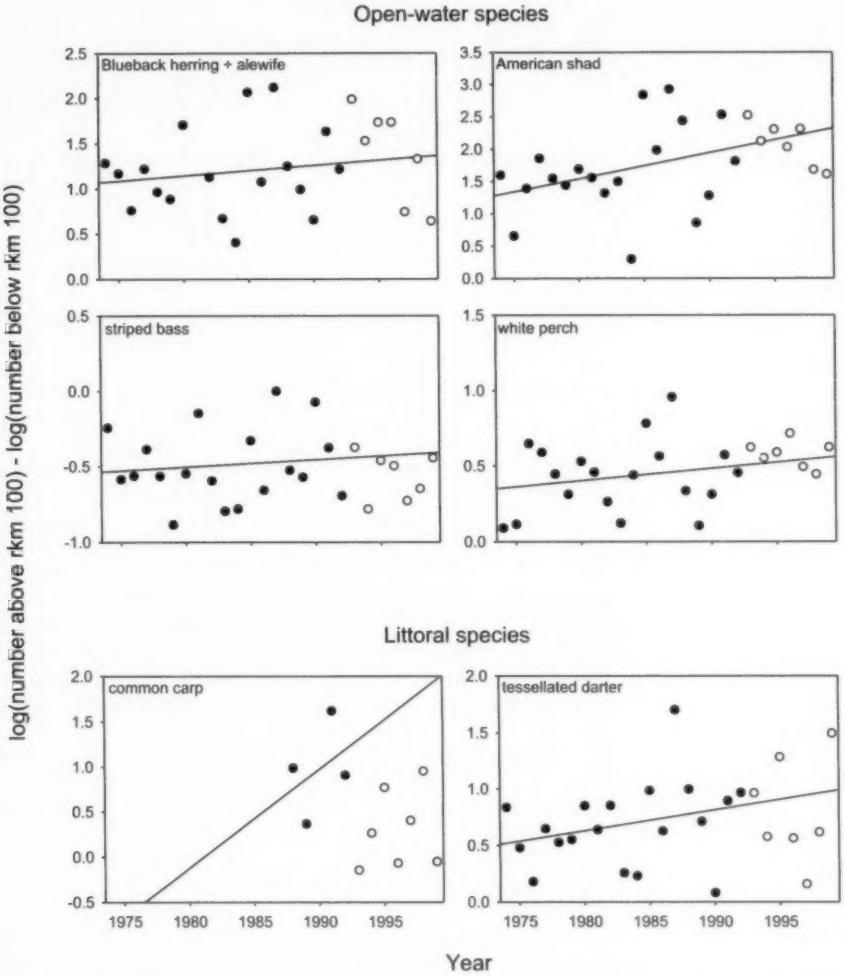

Among 0+ juveniles, populations of almost all littoral species were centered further upriver after the zebra mussel invasion; this change was significant ($p < 0.2$) for banded killifish, fourspine stickleback, bluegill, redbreast sunfish, smallmouth bass, and largemouth bass (Fig. 5). Although populations of post-yolk-sac larvae of clupeids were centered slightly further upriver after the zebra mussel invasion, clupeid 0+ juveniles tended to occur further downriver after the invasion. Both post-yolk-sac larvae and 0+ juveniles of white perch tended to occur further upriver after the zebra mussel invasion, contrary to our hypothesis. While distributional changes among post-yolk-sac larvae were not consistent, the median distributional index for 0+ juveniles of open-water species dropped by 0.24, indicating that the ratio (freshwater population/brackish water population) fell by 43%, while the median distributional index for littoral species rose by 0.51, indicating that the ratio of freshwater population to brackish water population rose by 224%. Thus, we observed shifts in the distribution of 0+ juveniles within the river that were large and consistent with the hypothesized zebra mussel effect (Fig. 6).

Apparent growth

We were able to test for effects of the zebra mussel invasion on apparent growth of fish in 14 cases (Table 3). In nearly all cases, apparent growth changed in the direction that we postulated; the change was significant ($p < 0.2$) in nine of these cases. We observed no significant changes in apparent growth that contradicted our hypotheses (Fig. 7). In many cases, the changes in apparent growth rates were large (Table 4; Fig. 7). Median apparent growth of open-water species, averaged over all life stages and species, fell by 17%, while apparent growth of the single littoral species rose by 12%. Other important determinants of apparent

© 2004 NRC Canada

Fig. 5. Distribution of YOY of several species of fish in the Hudson River before (solid circles) and after (open circles) the zebra mussel invasion based on data from the utilites' beach seine survey. The regression lines are fit to preinvasion data. Open circles falling below the line indicate that an increased proportion of the population was found downriver after the zebra mussel invasion, whereas open circles falling above the line indicate that an increased proportion of the population was found upriver after the zebra mussel invasion.

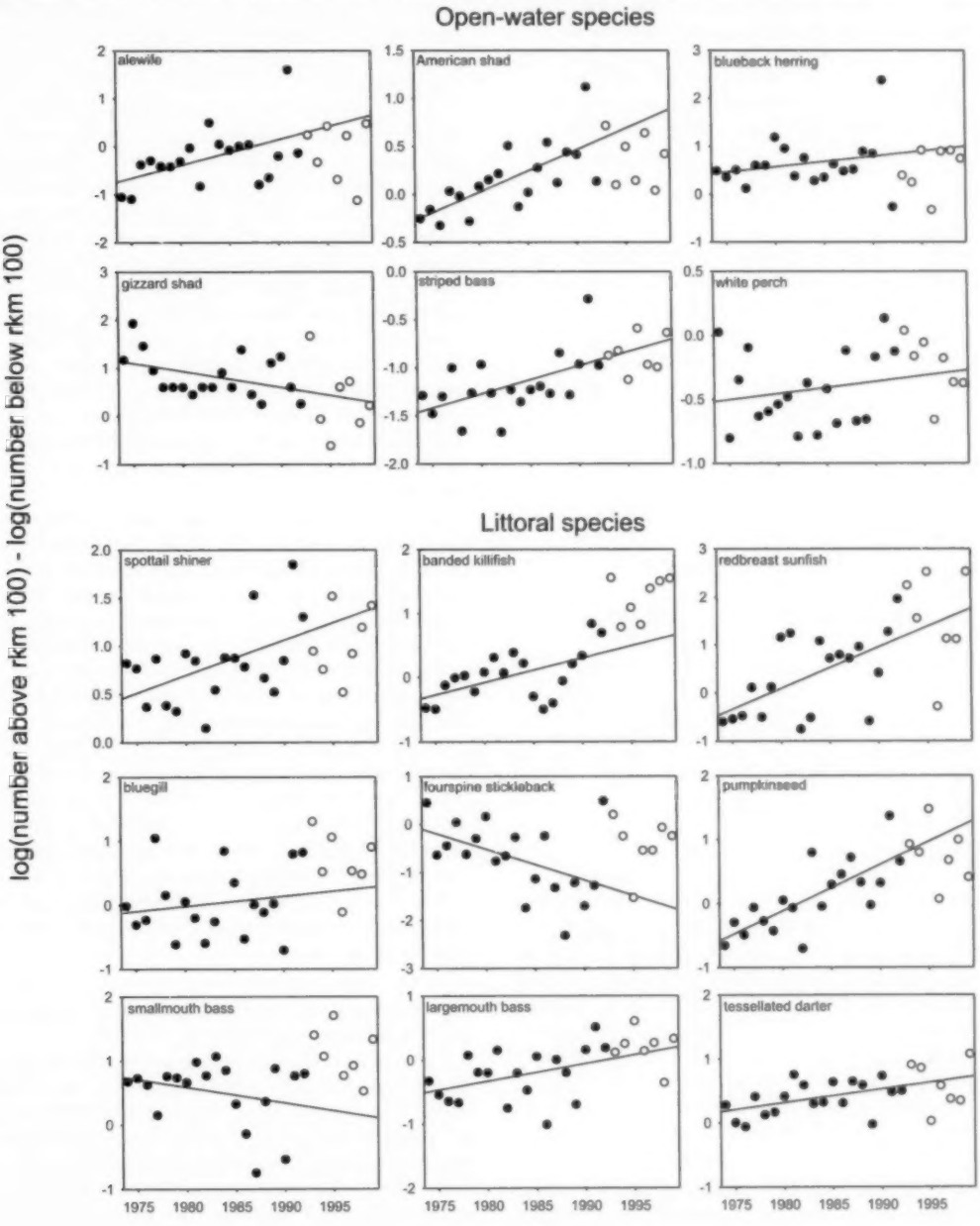

growth rates were fish size (strongly negative) and freshwater flow (negative); temperature and region occasionally were important.

The less formal analysis of changes in fish lengths also supported the hypothesis of differential impacts on apparent growth in different groups of fish species. For *Alosa* spp. (shad and herrings) and *Morone* spp. (white perch and striped bass), we found that preinvasion lengths were greater than post-invasion lengths in 68 of 86 cases, while for the very few littoral species other than spottail shiner for which we had data (yellow bullhead (*Ameiurus natalis*), largemouth and smallmouth bass, and yellow perch), we found that post-invasion lengths were greater in five of nine cases. A χ^2 analysis of these data gives a value of 11.97 (p = 0.0005),

© 2004 NRC Canada

Fig. 6. Summary of the effects of the zebra mussel invasion on distribution of fish in the Hudson River: (*a*) post-yolk-sac larvae; (*b*) 0+ juveniles. The circle represents the mean effect, and the thick and thin vertical bars represent the 60% and 90% confidence intervals on the mean (i.e., the 20% and 5% significance levels in a one-tailed test). The horizontal lines indicate no change owing to the zebra mussel invasion.

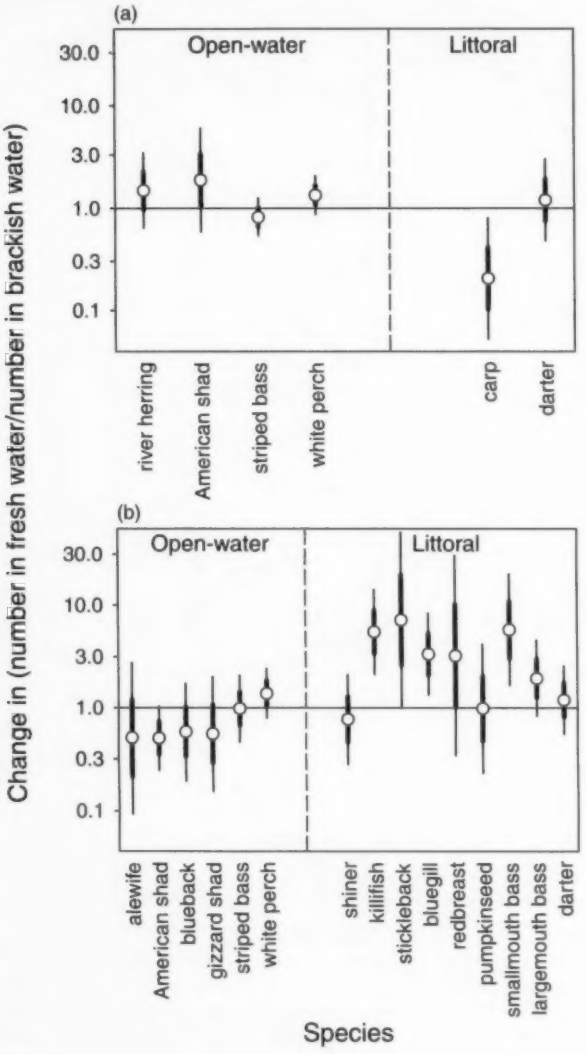

supporting our hypothesis that the apparent growth of littoral zone fishes increased after the zebra mussel invasion at the same time that apparent growth of open-water fishes decreased.

Discussion

Overview of effects in the Hudson

The zebra mussel invasion was associated with large, pervasive changes in YOY fish in the Hudson River. Open-water fishes such as *Alosa* spp. and *Morone* spp. declined in abundance, had their populations shift downriver away from the infested part of the Hudson, and suffered declines in apparent growth rates. At the same time, littoral zone species (centrarchids and several others) showed exactly the opposite effects. These changes are highly consistent with our hypotheses about the effects of a changed forage base on the fish community.

To the extent that we can discern differential effects among species, it appears that *Alosa* spp. and centrarchids responded most strongly to the zebra mussel invasion (although in opposite directions), while the response of *Morone* spp. and littoral species other than centrarchids was more muted. Although our estimates of effect sizes are imprecise, many of the changes associated with the zebra mussel invasion were large. Many of the changes in fish abundance and distribution were >50% and many of the changes in growth rates were >20% of preinvasion growth rates. We do not have the information needed to calculate changes in the overall biomass or production of the Hudson River fish community. Because open-water species are much more abundant than the littoral species, overall biomass and production of YOY fish in the Hudson probably fell after the zebra mussel invasion.

Two other changes could have affected fish populations in the Hudson during 1974–1999. Improving environmental quality around Albany (rkm 228) and New York City (~rkm 10) made these areas more suitable for fish. Changes in harvest of two major anadromous species outside the Hudson itself (increased protection of immature striped bass in ocean waters in 1984–1995 (Kahnle and Hattala 2001) and rising offshore catches of American shad starting in the mid-1980s (Hattala and Kahnle 1998)) would be expected to affect populations in the Hudson. While we saw evidence that these changes affected fish populations in the Hudson, it is difficult to see how these changes could have caused the complex pattern of change that we attributed to the zebra mussel invasion. The timing, direction of changes, geographical pattern of changes, multiple variables involved, and differential effects on open-water versus littoral species are highly consistent with a zebra mussel effect but not with these other causes.

How strong is the connection between suspension-feeding bivalves and fish?

Changes in bivalve populations can cause large changes in phytoplankton in lakes, rivers, estuaries, and shallow coastal waters (e.g., Cohen et al. 1984; Dame 1996; Makarewicz et al. 1999). In some cases, these effects have been shown to reach primary consumers such as zooplankton (e.g., Kimmerer et al. 1994; Pace et al. 1998) and zoobenthos (e.g., Stewart and Haynes 1994; Nalepa et al. 1998), but most studies of the zebra mussel invasion have reported small or no effects on the fish community. The two studies that did find effects on fish were contradictory, with Karataev and Burlakova (1995) reporting increases in fish populations but Ryan et al. (1999) reporting decreases in fish populations.

Why do bivalve effects on fish vary so much among studies? Some of the differences between our findings of large effects and prior studies that reported little or no effect may

© 2004 NRC Canada

Table 3. Statistical models to predict apparent growth rates of fish in the Hudson River.

Species	Body length	Flow ($m^3 \cdot s^{-1}$, $\times 10^{-5}$)	Temperature (°C)	Region	Zebra
Post-yolk-sac larvae					
American shad	—	0.41	1.00	0.38	0.28
	–0.025 (0.003)	–4.1 (3.5)	0.024 (0.005)	–0.018 (0.018)	–0.006 (0.018)
Striped bass	—	0.85	1.00	0.30	0.27
	–0.021 (0.003)	–7.1 (3.1)	0.023 (0.003)	0.007 (0.013)	0.000 (0.017)
White perch	—	0.42	1.00	0.35	0.37
	–0.038 (0.004)	–2.7 (2.4)	0.026 (0.003)	–0.010 (0.012)	–0.014 (0.015)
0+ juveniles					
Alewife (UBSS)	—	0.51	0.31	0.63	0.36
	–0.021 (0.0007)	–12 (8.1)	0.003 (0.006)	–0.028 (0.017)	–0.011 (0.019)
Alewife (DECBSS)	—	0.81	0.33	0.32	0.62
	–0.001 (0.0005)	–13 (5.9)	–0.0018 (0.0032)	–0.0037 (0.0083	–0.020 (0.012)
American shad (UBSS)	—	0.32	0.80	0.30	0.60
	–0.0020 (0.0006)	–12 (8.9)	0.0040 (0.0056)	–0.0028 (0.018)	–0.016 (0.018)
American shad (DECBSS)	—	0.99	0.47	0.42	0.35
	–0.0018 (0.0002)	–6.7 (2.1)	–0.0012 (0.0009)	–0.0028 (0.0025)	–0.0038 (0.0046)
Blueback herring (UBSS)	—	0.70	0.28	0.33	0.84
	–0.0021 (0.0005)	–7.4 (3.9)	0.00018 (0.0014)	–0.0054 (0.0097)	–0.018 (0.008)
Blueback herring (DECBSS)	—	0.40	0.30	0.28	0.49
	–0.0017 (0.0003)	–3.1 (2.9)	0.00059 (0.0012)	–0.00028 (0.0038)	–0.0093 (0.0068)
Striped bass (UBSS)	—	0.93	0.84	0.31	0.69
	–0.0033 (0.0002)	–7.7 (2.9)	–0.0027 (0.0011)	0.0008 (0.008)	–0.014 (0.0077)
Striped bass (DECBSS)	—	0.28	0.62	0.99	0.96
	–0.0034 (0.0003)	–0.9 (4.3)	–0.0028 (0.0016)	0.015 (0.0043)	–0.025 (0.0086)
White perch (UBSS)	—	0.46	0.51	0.30	0.29
	–0.0033 (0.0002)	–2.9 (2.3)	0.0012 (0.0009)	0.0028 (0.0050)	0.0028 (0.0062)
White perch (DECBSS)	—	0.93	0.35	0.44	0.70
	–0.0027 (0.0002)	–9.8 (3.7)	0.00098 (0.0012)	0.0039 (0.0034)	–0.010 (0.0055)
Spottail shiner (UBSS)	—	0.31	0.51	0.28	0.47
	–0.0034 (0.0003)	–2.8 (4.7)	–0.0026 (0.0018)	–0.0016 (0.0095)	0.0096 (0.0074)

Note: The table shows the summed Akaike weight for each variable (upper number) along with the model-averaged slope and standard error (lower numbers) for each variable. UBSS, utilities' beach seine survey of 0+ juveniles; DECBSS, Department of Environmental Conservation's beach seine survey of 0+ juveniles.

be due to differences in statistical power among the analyses. However, there is every reason to expect that the effects of bivalves truly differ across ecosystems.

The impact of bivalves is propagated through the ecosystem, where it may be damped or amplified. Several pathways link suspension-feeding bivalves to fish, and the strength of each of these pathways varies across ecosystems. Neglecting direct effects, in which bivalves serve as food (e.g., French 1993; French and Bur 1996) or spawning sites (e.g., Chatelain and Chabot 1983; Reynolds et al. 1997) for fish, there are three indirect pathways leading from suspension-feeding bivalves to fish (Fig. 8). For simplicity, we describe the changes expected from an increase in bivalve populations, but the opposite changes may be induced by a decline in bivalve populations (e.g., the decline of oysters in Chesapeake Bay (Newell 1988; Ulanowicz and Tuttle 1992)).

Links to fish via phytoplankton and edible consumers

Bivalve grazing may reduce phytoplankton, leading to losses of edible consumers and then fish (arrows 1, 3, and 6 in Fig. 8). This presumably is the pathway responsible for the large declines in abundance and apparent growth rates of open-water fishes in the Hudson. To affect fish populations by this pathway, bivalve grazing must be large enough to reduce biomass or production of phytoplankton. Specifically, grazing rates must be large compared with phytoplankton growth and other loss terms (i.e., advection, sinking, grazing by other suspension-feeders (Dame 1996; Strayer et al. 1999)). Further, the bivalve population must coincide in space and time with areas and periods of phytoplankton growth. Finally, if the increase in light and nutrients resulting from bivalve grazing stimulates the growth of remaining phytoplankton or increases the depth of the photic zone (Idrisi et al. 2001), there may be little change in phytoplankton biomass, and phytoplankton production may even increase (Caraco et al. 1997).

All three of these conditions favored large losses of phytoplankton in the Hudson. Zebra mussel grazing is much larger than advective losses or grazing by other suspension-feeders (Strayer et al. 1999), and it is focused precisely on those areas of the river that formerly supported the greatest phytoplankton growth (Caraco et al. 1997). The increases in dissolved nutrients that accompanied the zebra mussel invasion in the Hudson (Caraco et al. 1997) did not stimulate growth of the light-limited phytoplankton (Cole et al. 1992), and light penetration increased only modestly because trans-

© 2004 NRC Canada

Fig. 7. Summary of the effects of the zebra mussel invasion on apparent growth of fish in the Hudson River. The circle represents the mean effect, and the wide and thin vertical bars represent the 60% and 90% confidence intervals on the mean (i.e., the 20% and 5% significance levels in a one-tailed test). The horizontal lines indicate no change owing to the zebra mussel invasion. For comparison, mean apparent growth rates before the zebra mussel invasion were 0.11·week^{-1} for post-yolk-sac larvae and 0.06·week^{-1} for 0+ juveniles. LRS, long-river survey; DECBSS, Department of Environmental Conservation's beach seine survey; UBSS, utilities' beach seine survey.

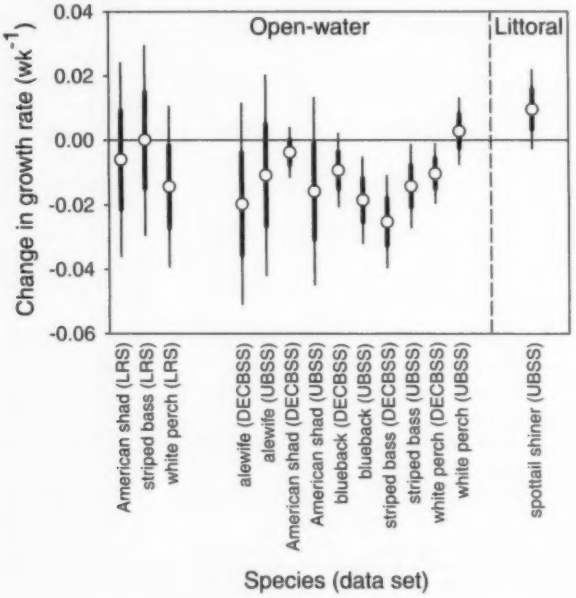

parency of the Hudson is controlled chiefly by inedible silt particles. Consequently, the feedback loop from the grazer to the phytoplankton was weak, and phytoplankton biomass fell steeply (80%) (Caraco et al. 1997).

Conditions in other lakes and rivers invaded by zebra mussels often lead to smaller impacts on phytoplankton (Table 5). Populations of zebra mussels often are too small to control phytoplankton (>50% of European lakes invaded by zebra mussels had lakewide mean densities of <300·m^{-2} and estimated filtration rates of <15% of the mixed zone/day (from Strayer 1991)). In stratified or large lakes, spatial separation between zebra mussels and phytoplankton provides a refuge for phytoplankton. This spatial separation probably is responsible for the modest losses of phytoplankton in the offshore waters of the Great Lakes (Makarewicz et al. 1999). Finally, increased light and nutrients from grazing substantially increase growth rates of remaining phytoplankton or the depth of the photic zone in many lakes (e.g., Fahnenstiel et al. 1995*a*; Idrisi et al. 2001).

To the extent that bivalve populations reduce phytoplankton, zooplankton and zoobenthos that depend on phytoplankton should decrease. Declines in zooplankton (e.g., Beeton and Hageman 2001) and zoobenthos (e.g., Dermott and Kerec 1997; Nalepa et al. 1998; Strayer and Smith 2001) following the zebra mussel invasion have been attributed to this mechanism. Thus, the size and spatial distribution of the zebra mussel population and the nature of factors that limit plankton determine whether bivalves and fish are strongly or weakly linked by this pathway.

Links via biodeposits and shelter in zebra mussel beds

The food (feces and pseudofeces) and shelter provided by zebra mussel beds may lead to large increases in populations of forage invertebrates (e.g., amphipods and chironomid midges) living among those beds (e.g., Ricciardi et al. 1997; Stewart et al. 1998). These increases in forage invertebrates may benefit fish, although the structural complexity provided by bivalve beds may make fish foraging inefficient (Stewart et al. 1999; Mayer et al. 2001), so fish may not receive the full benefit of this increased forage. This pathway (arrows 5 and 6 in Fig. 8) does not require that the bivalve population be large enough to deplete phytoplankton but merely that either biodeposition or shelter provided by the bivalves be large enough locally to benefit invertebrates. Presumably, the larger the area of sediment covered by bivalves, the larger the effect on fish. This pathway should benefit fish that feed on benthic invertebrates. It is not clear if this pathway is important in nature; we know of no examples of changes in fish that can be clearly attributed to this mechanism.

Links via enhanced littoral production

The loss of phytoplankton may clear the water enough to benefit submersed macrophytes and attached algae, the invertebrates that feed on or live among these plants, and ultimately fish (arrows 1, 2, 4, and 6 in Fig. 8). For this pathway to be important, it is first necessary for the bivalve population to significantly reduce phytoplankton (see discussion above). Further, this pathway will be important only if macrophytes and attached algae are light limited and the ecosystem contains substantial areas of sediment lying in the photic zone. This pathway should benefit fish that live among macrophytes and feed on benthic and epiphytic invertebrates and presumably is behind the observed increases in abundance and growth of littoral fishes (e.g., centrarchids) in the Hudson.

The strength of this pathway should vary widely across ecosystems. We expect to see large changes in littoral fish following the zebra mussel invasion in shallow, clear lakes and rivers and much smaller effects in deep lakes and rivers in which light penetration is controlled by inedible particles (e.g., silt). Although the increase in light penetration that accompanied the zebra mussel invasion of the Hudson was modest (~45%; Caraco et al. 1997) and only ~15% of the Hudson is shallow enough to support littoral production (Findlay et al. 2004), littoral primary production may have doubled (Caraco et al. 2000). In lakes or rivers where large areas of the bottom are at or near the limit of the photic zone, the increase in benthic primary production following bivalve invasion may be even larger (e.g., Fahnenstiel et al. 1995*a*; Skubinna et al. 1995).

Net effects of bivalves on fish

The net effect of suspension-feeding bivalves on fish populations depends on the strength and balance among all of the interaction pathways. In general, planktivorous fish should

© 2004 NRC Canada

Table 4. Summary of analyses of effects of the zebra mussel invasion on apparent growth rates of fish in the Hudson River.

Species	Mean growth rate ($week^{-1}$) before invasion	Change ($week^{-1}$)	Change (%)
Post-yolk-sac larvae			
American shad	0.105	–0.006	–6
Striped bass	0.119	0.00006	0
White perch	0.118	–0.014	–12
0+ juveniles			
Alewife (UBSS)	0.056	–0.011	–19
Alewife (DECBSS)	0.051	–0.020	–39
American shad (UBSS)	0.071	–0.016	–22
American shad (DECBSS)	0.054	–0.004	–7
Blueback herring (UBSS)	0.037	–0.018	–50
Blueback herring (DECBSS)	0.037	–0.009	–25
Striped bass (UBSS)	0.084	–0.014	–17
Striped bass (DECBSS)	0.070	–0.025	–36
White perch (UBSS)	0.086	0.003	+3
White perch (DECBSS)	0.069	–0.010	–15
Spottail shiner (UBSS)	0.079	0.010	+12

Note: The mean growth rates are simple unweighted means from the preinvasion period and are given to indicate the size of the changes attributed to the zebra mussel invasion by the regression models. UBSS, utilities' beach seine survey of 0+ juveniles; DECBSS, Department of Environmental Conservation's beach seine survey of 0+ juveniles.

Fig. 8. Schematic diagram of indirect interactions that link bivalve populations to fish.

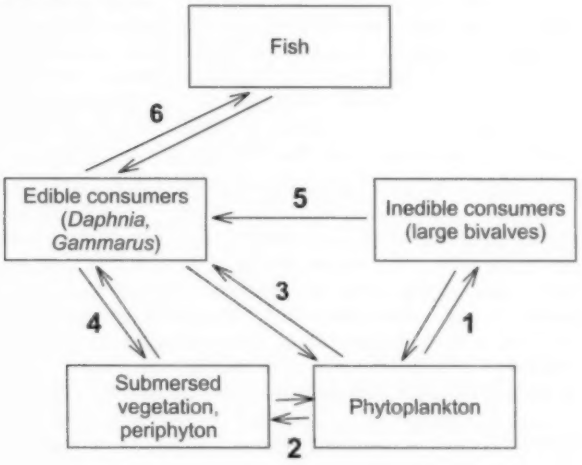

suffer and littoral zone fish should benefit, as was seen in the Hudson, but the size of these changes may vary widely. It will be difficult to predict the responses of fish that feed on open-water benthos (which may rise or fall with rising bivalve populations), fish that are flexible enough to exploit various kinds of food, and the overall production or biomass of all fish species combined. Increasing populations of suspension-feeding bivalves could have net positive or negative effects on fish populations, shift the composition but not biomass of the fish community, or have no effect. Consequently, instead of simply extrapolating from our study to predict the response of fish to changes in suspension-feeders in other ecosystems, it is necessary to consider the interaction pathways that link suspension-feeding bivalves to fish.

Table 5 suggests that the effects of zebra mussels on fish and zoobenthos are more variable across ecosystems than the effects on phytoplankton. The indirect effects of alien species (or any species) probably are usually more variable and less predictable than their direct effects because of the variable modulation of effects through different ecosystems.

Analytical issues

Analyzing the response of fish to the zebra mussel invasion (or any perturbation) in a large ecosystem presents analytical problems. Because of natural variability in fish population size, distribution, and somatic growth and the difficulty in estimating these variables accurately, analyses of temporal or spatial changes in fish populations are plagued with large errors. Consequently, the statistical power to detect zebra mussel effects may be low, and estimates of effect sizes usually are imprecise. In our analyses, changes in abundance of <1.5-fold usually were too small to attain statistical significance even at $p = 0.2$. Likewise, the thresholds for statistical detection of effects (at $p = 0.2$) in fish distribution and apparent growth were ~1.7-fold and ~0.011·$week^{-1}$, respectively. Changes below these thresholds certainly could be of interest, but our analysis was simply not powerful enough to detect them statistically.

Two strategies to improve the detection of impacts on fish communities are to use variables with high signal to noise ratios and to use long runs of data. Apparent growth rates were a more sensitive indicator of zebra mussel impacts than fish distribution or population size (64% of tests of growth rates were significant at $p = 0.2$ compared with 33% and 43% for abundance and distribution, respectively). Growth rates may be a good indicator because average fish size is

© 2004 NRC Canada

Table 5. Effects of the zebra mussel invasion on food webs in several lakes and rivers where fish populations have been studied.

Site	Phytoplankton biomass	Zooplankton biomass	Zoobenthic biomass	Fish response
Rice Lake, Ontario	No change	No data	No change?	Increase in pumpkinseed growth; no changes in growth of bluegill or yellow perch
Lake Erie (offshore)	–43% to no change	–20% to no change	+4–82%	Few changes in growth or abundance of any fish species
Oneida Lake, New York	–25%	No change	Increase in shallow bays only	Modest changes in growth and diet of yellow perch
Long Point Bay, Lake Erie	No data	No data	No data	Declines in abundance of five species
Lukomskoe Lake, Belarus	–72%	–60%	+1200%	Very large increase (>200%) in fish biomass; increase in benthic species
Hudson River, New York	–80%	–70%	–40%	Widespread decreases in growth and abundance of open-water species; corresponding increases in littoral species; changes in fish distribution

Note: Zoobenthic biomass excludes large bivalves (Unionidae and Dreissenidae); data on Lake Erie zooplankton are based on deviation from expected biomass as predicted from total phosphorus (Johannsson et al. 1999). From Karataev and Burlakova (1995), Caraco et al. (1997), Mayer (1998), Pace et al. (1998), Johannsson et al. (1999, 2000), Makarewicz et al. (1999), Mercer et al. (1999), Idrisi et al. (2001), Strayer and Smith (2001), and Mayer et al. (2002).

easier to estimate precisely than are fish numbers or distribution and because covariates (fish length, freshwater flow, and temperature) can account for some of the variation in apparent growth rates. An alternative explanation, that apparent growth rates were affected more severely than population size or distribution, seems not to be true: the median absolute change in apparent growth rates was 16%, whereas the median absolute change in abundance was 57%.

The second strategy to increase statistical power is to increase the length of the data record. Most published analyses of zebra mussel effects on fish used fewer than 5 years each of pre- and post-invasion data, which reduced statistical power to undesirable levels. Unfortunately, long runs of data are expensive to collect and often do not exist. Further, as the length of the data record increases, so does the possibility that the study system was subject to important changes other than the zebra mussel invasion, which may confound the analysis. Thus, practical problems limit the extent to which statistical power may be increased by lengthening data runs.

Implications for understanding and managing fish populations in the Hudson

Our analyses shed light on processes other than the zebra mussel invasion that may affect fish populations in the Hudson. Years of high freshwater flow were associated with slow apparent growth and downriver movement of fish populations. Wet years are years of poor development of plankton in the Hudson because of light limitation and high advective losses (Caraco et al. 1997; Pace and Lonsdale 2004). Presumably, this low plankton production, possibly along with lower light levels, translates to poor feeding conditions for young fish in the freshwater part of the river.

In addition to the large distributional shifts associated with the zebra mussel invasion, the distribution of most species of fish shifted upriver before the zebra mussel invasion. This upriver movement of fish populations may have been a response to the improvement of upriver habitats associated with the control of pollution from the Albany metropolitan area in the mid- and late 1970s.

Finally, our results have important implications for the management of fish populations in the Hudson. The changes that we observed in abundance, distribution, and growth of young fishes may well translate into changes in adults, the life stage of interest to the multimillion dollar recreational and commercial fisheries. The changes that we observed may lead to fewer adults of species such as American shad and striped bass and more adults of species such as redbreast sunfish and black basses in the Hudson. The magnitude and persistence of any such changes are unclear at this point.

The zebra mussel invasion has imposed an additional important constraint on fish populations in the Hudson that limits the scope of possible management activities. For instance, the sharply reduced recruitment of American shad limits the range of possible combinations of recreational harvest, commercial harvest, and habitat management that will result in a sustainable fishery for this species. Management of the affected fish species will become more difficult.

Further, changes in the dynamics of fish populations in the Hudson will make it more difficult to predict the impacts of management actions. Management of anadromous fish in the Hudson relies on monitoring abundance or relative abundance of different life stages or ages, monitoring of survival between life stage or age, and modeling the interactions among these parameters. Where possible, information on interactions between fish and characteristics of the environment such as flow or water temperature is added. Such models allow us to identify optimum characteristics of fish populations and harvest and to predict the implications of various harvest options on these characteristics. These population models are based on a long time series of data and assume some sort of average steady state in intra- and inter-specific interactions. When the ability of a system to support young fish changes, the steady state changes. This introduces added uncertainty to fish population models and models become

© 2004 NRC Canada

less able to predict future conditions. This in turn complicates the crafting and evaluation of management measures.

Acknowledgments

We are greatly indebted to the many people who collected and processed the samples and managed the databases upon which our analyses were based. We thank the Hudson River Foundation for their support of this work, Nina Caraco, Jon Cole, Kurt Fausch, Stuart Findlay, Cliff Kraft, Karin Limburg, Paul Lukacs, Mike Pace, Quentin Ross, Bob Schmidt, and three anonymous reviewers for helpful discussions and advice, and especially John Young, Nancy Decker, and Bill Dey for providing access to the utilities' data sets. This is a contribution to the program of the Institute of Ecosystem Studies.

References

Beeton, A.M., and Hageman, J. 2001. Changes in zooplankton populations in western Lake Erie after establishment of *Dreissena polymorpha*. Verh. Int. Ver. Theor. Angew. Limnol. **27**: 3798–3804.

Burnham, K.P., and Anderson, D.R. 2002. Model selection and multimodel inference: a practical information-theoretic approach. 2nd ed. Springer-Verlag, New York.

Caraco, N.F., Cole, J.J., Raymond, P.A., Strayer, D.L., Pace, M.L., Findlay, S.E.G., and Fischer, D.T. 1997. Zebra mussel invasion in a large, turbid river: phytoplankton response to increased grazing. Ecology, **78**: 588–602.

Caraco, N.F., Cole, J.J., Findlay, S.E.G., Fischer, D.T., Lampman, G.G., Pace, M.L., and Strayer, D.L. 2000. Dissolved oxygen declines associated with the invasion of the zebra mussel (*Dreissena polymorpha*). Environ. Sci. Technol. **34**: 1204–1210.

Chatelain, R., and Chabot, J. 1983. Utilization d'accumulation de coquilles d'Unionidae comme frayeres par le touladi. Nat. Can. **110**: 363–365.

Cohen, R.R.H., Dresler, P.V., Phillips, E.J.P., and Cory, R.L. 1984. The effect of the Asiatic clam, *Corbicula fluminea*, on phytoplankton of the Potomac River. Limnol. Oceanogr. **29**: 170–180.

Cole, J.J., Caraco, N.F., and Peierls, B. 1992. Can phytoplankton maintain a positive carbon balance in a turbid, freshwater, tidal estuary? Limnol. Oceanogr. **37**: 1608–1617.

Cooper, J.C., Cantelmo, F.R., and Newton, C.E. 1988. Overview of the Hudson River estuary. Am. Fish. Soc. Monogr. **4**: 11–24.

Dame, R.F. 1996. Ecology of marine bivalves: an ecosystem approach. CRC Press, Boca Raton, Fla.

Dermott, R., and Kerec, D. 1997. Changes in the deepwater benthos of eastern Lake Erie since the invasion of *Dreissena*: 1979–1993. Can. J. Fish. Aquat. Sci. **54**: 922–930.

Dermott, R., Munawar, M., Witzel, L., and Ryan, P.A. 1999. An assessment of food-web changes in eastern Lake Erie: impact of *Dreissena* spp., and phosphorus management on rainbow smelt *Osmerus mordax*. *In* State of Lake Erie: past, present, and future. *Edited by* M. Munawar, T. Edsall, and I.F. Munawar. Backhuys Publishers, Leiden, the Netherlands. pp. 367–385.

Effler, S.W., Brooks, C.M., Whitehead, K., Wagner, B., Doerr, S.M., Perkins, M.G., Siegfried, C.A., Walrath, L., and Canale, R.P. 1996. Impact of zebra mussel invasion on river water quality. Water Environ. Res. **68**: 205–214.

Fahnenstiel, G.L., Bridgeman, T.B., Lang, G.A., McCormick, M.J., and Nalepa, T.F. 1995*a*. Phytoplankton productivity in Saginaw Bay, Lake Huron: effects of zebra mussel (*Dreissena polymorpha*) colonization. J. Gt. Lakes Res. **21**: 465–475.

Fahnenstiel, G.L., Lang, G.A., Nalepa, T.F., and Johengen, T.H. 1995*b*. Effects of zebra mussel (*Dreissena polymorpha*) colonization on water quality parameters in Saginaw Bay, Lake Huron. J. Gt. Lakes Res. **21**: 435–448.

Findlay, S.E.G., Wigand, C., and Nieder, W.C. 2004. Submersed macrophyte distribution and function in the tidal freshwater Hudson River. *In* The Hudson River estuary. *Edited by* J.S. Levinton. Cambridge University Press, New York. In press.

French, J.R.P. 1993. How well can fishes prey on zebra mussels in eastern North America? Fisheries (Bethesda), **18**: 13–19.

French, J.R.P., and Bur, M.T. 1996. The effect of zebra mussel consumption on the growth of freshwater drum in Lake Erie. J. Freshw. Ecol. **11**: 283–289.

Gopalan, G., Culver, D.A., Wu, L., and Trauben, B.K. 1998. Effects of recent ecosystem changes on the recruitment of young-of-the-year fish in western Lake Erie. Can. J. Fish. Aquat. Sci. **55**: 2572–2579.

Harley, M.T., and Findlay, S.E.G. 1994. Photosynthesis–irradiance relationships for three species of submersed macrophytes in the tidal freshwater Hudson River. Estuaries, **17**: 200–205.

Hattala, K., and Kahnle, A.W. 1998. Stock status and definition of over-fishing rate for American shad of the Hudson River Estuary. *In* American shad stock assessment. Peer-review report of the Atlantic States Marine Fisheries Commission, Washington, D.C. pp. 178–217.

Heimbuch, D.G., Dunning, D.J., and Young, J.R. 1992. Post-yolk-sac larvae abundance as an index of year class strength of striped bass in the Hudson River. *In* Estuarine research in the 1980s. *Edited by* C.L. Smith. SUNY Press, Albany, N.Y. pp. 376–391.

Howarth, R.W., Schneider, R., and Swaney, D. 1996. Metabolism and organic carbon fluxes in the tidal freshwater Hudson River. Estuaries, **19**: 848–865.

Idrisi, N., Mills, E.L., Rudstam, L.G., and Stewart, D.J. 2001. Impact of zebra mussels (*Dreissena polymorpha*) on the pelagic lower trophic levels of Oneida Lake, New York. Can. J. Fish. Aquat. Sci. **58**: 1430–1441.

Jennings, C.A. 1996. Effects of zebra mussel (*Dreissena polymorpha*) density on the survival and growth of juvenile fathead minnows (*Pimephales promelas*): implications for North American river fishes. Hydrobiologia, **324**: 157–161.

Johannsson, O.E., Graham, D.M., Einhouse, D.W.E., and Mills, E.L. 1999. Historical and recent changes in the Lake Erie zooplankton community and their relationship to ecosystem function. *In* State of Lake Erie: past, present, and future. *Edited by* M. Munawar, T. Edsall, and I.F. Munawar. Backhuys Publishers, Leiden, the Netherlands. pp. 169–196.

Johannsson, O.E., Dermott, R., Graham, D.M., Dahl, J.A., Millard, E.S., Myles, D.D., and LeBlanc, J. 2000. Benthic and pelagic secondary production in Lake Erie after the invasion of *Dreissena* spp. with implications for fish predation. J. Gt. Lakes Res. **26**: 31–54.

Kahnle, A.W., and Hattala, K.A. 2001. Hudson River striped bass fishery fact sheet. New York State Department of Environmental Conservation, New Paltz, N.Y.

Karataev, A.Y., and Burlakova, L.E. 1995. The role of *Dreissena* in lake ecosystems. Russ. J. Ecol. **26**: 207–211.

Kimmerer, W.J., Gartside, E., and Orsi, J.J. 1994. Predation by an introduced clam as the likely cause of substantial declines in zooplankton of San Francisco Bay. Mar. Ecol. Prog. Ser. **113**: 81–93.

Klauda, R.J., Muessig, P.H., and Matousek, J.A. 1988. Fisheries data sets compiled by utility-sponsored research in the Hudson River estuary. *In* Fisheries research in the Hudson River. *Edited by* C.L. Smith. SUNY Press, Albany, N.Y. pp. 7–88.

© 2004 NRC Canada

Limburg, K.E., Moran, M.A., and McDowell, W.H. 1986. The Hudson River ecosystem. Springer-Verlag, New York.

MacIsaac, H.J., Lonnee, C.J., and Leach, J.H. 1995. Suppression of microzooplankton by zebra mussels: importance of mussel size. Freshw. Biol. **34**: 379–387.

Mack, R.N., Simberloff, D., Lonsdale, W.M., Evans, H., Clout, M., and Bazzaz, F.A. 2000. Biotic invasions: causes, epidemiology, global consequences, and control. Ecol. Appl. **10**: 689–710.

Makarewicz, J.C., Lewis, T.W., and Bertram, P. 1999. Phytoplankton composition and biomass in the offshore waters of Lake Erie: pre- and post-*Dreissena* introduction (1983–1993). J. Gt. Lakes Res. **25**: 135–148.

Mayer, C.M. 1998. The effects of zebra mussel (*Dreissena polymorpha*) introduction on the benthos and yellow perch (*Perca flavescens*) of Oneida Lake. Ph.D. thesis, Cornell University, Ithaca, N.Y.

Mayer, C.M., VanDeValk, A.J., Forney, J.L., Rudstam, L.G., and Mills, E.L. 2000. Response of yellow perch (*Perca flavescens*) in Oneida Lake, New York, to the establishment of zebra mussels (*Dreissena polymorpha*). Can. J. Fish. Aquat. Sci. **57**: 742–754.

Mayer, C.M., Rudstam, L.G., Mills, E.L., Cardiff, S.G., and Bloom, C.A. 2001. Zebra mussels (*Dreissena polymorpha*), habitat alteration, and yellow perch (*Perca flavescens*) foraging: system-wide effects and behavioural mechanisms. Can. J. Fish. Aquat. Sci. **58**: 2459–2467.

Mayer, C.M., Keats, R.A., Rudstam, L.G., and Mills, E.L. 2002. Scale-dependent effects of zebra mussels on benthic invertebrates in a large eutrophic lake. J. North Am. Benthol. Soc. **21**: 616–633.

Mercer, J.L., Fox, M.G., and Metcalfe, C.D. 1999. Changes in benthos and three littoral zone fishes in a shallow, eutrophic Ontario lake following the invasion of the zebra mussel (*Dreissena polymorpha*). J. Lake Reservoir Manage. **15**: 310–323.

Nalepa, T.F., Hartson, D.J., Fanslow, D.L., Lang, G.A., and Lozano, S.J. 1998. Declines in benthic macroinvertebrate populations in southern Lake Michigan, 1980–1993. Can. J. Fish. Aquat. Sci. **55**: 2402–2413.

Newell, R.I.E. 1988. Ecological changes in Chesapeake Bay: are they the result of overharvesting the Eastern oyster (*Crassostrea virginica*)? *In* Understanding the estuary: advances in Chesapeake Bay research. *Edited by* M. Lynch. Publ. 129. Chesapeake Research Consortium Gloucester, Point, Va. pp. 536–546.

Office of Technology Assessment. 1993. Harmful nonindigenous species in the United States. Office of Technology Assessment, U.S. Congress, Washington, D.C.

Pace, M.L., and Lonsdale, D.J. 2004. Ecology of the Hudson zooplankton community. *In* The Hudson River estuary. *Edited by* J.S. Levinton. Cambridge University Press, New York. In press.

Pace, M.L., Findlay, S.E.G., and Fischer, D.T. 1998. Effects of an invasive bivalve on the zooplankton community of the Hudson River. Freshw. Biol. **39**: 103–116.

Phelps, H.L. 1994. The Asiatic clam (*Corbicula fluminea*) invasion and system-level ecological change in the Potomac River estuary near Washington, D.C. Estuaries, **17**: 614–621.

Pothoven, S.A., Nalepa, T.F., Schneeberger, P.J., and Brandt, S.B. 2001. Changes in diet and body condition of lake whitefish in southern Lake Michigan associated with changes in benthos. N. Am. J. Fish. Manag. **21**: 876–883.

Reynolds, J.D., Debuse, V.J., and Aldridge, D.C. 1997. Host specialization in an unusual symbiosis: European bitterlings spawning in freshwater mussels. Oikos, **78**: 539–545.

Ricciardi, A., Whoriskey, F.G., and Rasmussen, J.B. 1997. The role of the zebra mussel (*Dreissena polymorpha*) in structuring macroinvertebrate communities on hard substrata. Can. J. Fish. Aquat. Sci. **54**: 2596–2608.

Richardson, W.B., and Bartsch, L.A. 1997. Effects of zebra mussels on food webs: interactions with juvenile bluegill and water residence time. Hydrobiologia, **354**: 141–150.

Roberts, L. 1990. Zebra mussel invasion threatens U.S. waters. Science (Wash., D.C.), **249**: 1370–1372.

Ryan, P.A., Witzel, L.D., Paine, J., Freeman, M., Hardy, M., Scholten, S., Sztramko, L., and MacGregor, R. 1999. Recent trends in fish populations in eastern Lake Erie in relation to changing lake trophic state and food web. *In* State of Lake Erie: past, present, and future. *Edited by* M. Munawar, T. Edsall, and I.F. Munawar. Backhuys Publishers, Leiden, the Netherlands. pp. 241–289.

Schmidt, R.E., Chandler, W.E., and Strayer, D. 1995. Fishes consuming zebra mussels in the tidal Hudson River. *In* Final reports of the Tibor T. Polgar Fellowship Program for 1994. *Edited by* W.C. Nieder, J.R. Waldman, and E.A. Blair. Hudson River Foundation, New York. pp. IV-1–IV-20.

Skubinna, J.P., Coon, T.G., and Batterson, T.R. 1995. Increased abundance and depth of submersed macrophytes in response to decreased turbidity in Saginaw Bay, Lake Huron. J. Gt. Lakes Res. **21**: 476–488.

Smith, T.E., Stevenson, R.J., Caraco, N.F., and Cole, J.J. 1998. Changes in phytoplankton community structure during the zebra mussel (*Dreissena polymorpha*) invasion of the Hudson River, New York. J. Plankton Res. **20**: 1567–1579.

Stewart, T.W., and Haynes, J.M. 1994. Benthic macroinvertebrate communities of southwestern Lake Ontario following invasion of *Dreissena*. J. Gt. Lakes Res. **20**: 479–493.

Stewart, T.W., Miner, J.G., and Lowe, R.L. 1998. Quantifying mechanisms for zebra mussel effects on benthic macroinvertebrates: organic matter production and shell-generated habitat. J. North Am. Benthol. Soc. **17**: 81–94.

Stewart, T.W., Gafford, J.C., Miner, J.G., and Lowe, R.L. 1999. *Dreissena*-shell habitat and antipredator behavior: combined effects on survivorship of snails co-occurring with molluskivorous fish. J. North Am. Benthol. Soc. **18**: 274–283.

Strayer, D.L. 1991. Projected distribution of the zebra mussel, *Dreissena polymorpha*, in North America. Can. J. Fish. Aquat. Sci. **48**: 1389–1395.

Strayer, D.L. 2004. The benthic animal communities of the riverine Hudson River estuary. *In* The Hudson River estuary. *Edited by* J.S. Levinton. Cambridge University Press, New York. In press.

Strayer, D.L., and Smith, L.C. 2001. The zoobenthos of the freshwater tidal Hudson River and its response to the zebra mussel (*Dreissena polymorpha*) invasion. Arch. Hydrobiol. (Suppl.), **139**: 1–52.

Strayer, D.L., Powell, J., Ambrose, P., Smith, L.C., Pace, M.L., and Fischer, D.T. 1996. Arrival, spread, and early dynamics of a zebra mussel (*Dreissena polymorpha*) population in the Hudson River estuary. Can. J. Fish. Aquat. Sci. **53**: 1143–1149.

Strayer, D.L., Caraco, N.F., Cole, J.J., Findlay, S., and Pace, M.L. 1999. Transformation of freshwater ecosystems by bivalves: a case study of zebra mussels in the Hudson River. BioScience, **49**: 19–27.

Stuckey, R.L., and Moore, D.L. 1995. Return and increase in abundance of aquatic flowering plants in Put-in-Bay Harbor, Lake Erie, Ohio. Ohio J. Sci. **95**: 261–266.

Thayer, S.A., Haas, R.C., Hunter, R.D., and Kushler, R.K. 1997. Zebra mussel (*Dreissena polymorpha*) effects on sediment, other zoobenthos, and the diet and growth of adult yellow perch (*Perca flavescens*) in pond enclosures. Can. J. Fish. Aquat. Sci. **54**: 1903–1915.

© 2004 NRC Canada

Trometer, E.S., and Busch, W.-D.N. 1999. Changes in age-0 fish growth and abundance following the introduction of zebra mussels *Dreissena polymorpha* in the western basin of Lake Erie. N. Am. J. Fish. Manag. **19**: 604–609.

Ulanowicz, R.E., and Tuttle, J.H. 1992. The trophic consequences of oyster stock rehabilitation in Chesapeake Bay. Estuaries, **15**: 298–306.

Young, J.R., Keppel, R.G., and Klauda, R.J. 1992. Quality assurance and quality control aspects of the Hudson River utilities environmental studies. *In* Estuarine research in the 1980s. *Edited by* C.L. Smith. SUNY Press, Albany, N.Y. pp. 303–322.

© 2004 NRC Canada

Acute cadmium biotic ligand model characteristics of laboratory-reared and wild yellow perch (*Perca flavescens*) relative to rainbow trout (*Oncorhynchus mykiss*)

S. Niyogi, P. Couture, G. Pyle, D.G. McDonald, and C.M. Wood

Abstract: This study evaluated the >400-fold tolerance to acute waterborne Cd of a metal-tolerant fish, yellow perch (YP, *Perca flavescens*), relative to a sensitive model fish, rainbow trout (RBT, *Oncorhynchus mykiss*), from the perspective of the acute Cd biotic ligand model (BLM). Three-hour gill binding characteristics for Cd and its competitor, Ca, in both species exhibited only small quantitative differences, but gill Cd accumulations at 3 h and 24 h, which were associated with 50% lethality at 96 h (3- and 24-h LA50s), were 52- to 60-fold higher in YP relative to RBT. However, the acute Cd BLM cannot be extended from RBT to YP by simple adjustments of LA50 values because unlike RBT, in YP, LA50s (3 and 24 h) were 26- to 47-fold greater than the capacity of the characterized set of Cd-binding sites. Moreover, 3-h gill Ca and Cd binding characteristics in wild YP, collected from one clean (Geneva) and two metal-contaminated softwater lakes (Hannah and Whitson) around Sudbury region, northern Ontario, revealed that chronic waterborne factors like hardness and Cd preexposure can influence both Cd and Ca binding in fish gills and could have major implications for the future refinement of the acute Cd BLM approach.

Résumé : Notre étude examine la tolérance à une exposition aiguë au cadmium (Cd) dans l'eau chez la perchaude (YP, *Perca flavescens*), un poisson tolérant aux métaux, tolérance plus de 400 fois plus élevée que celle de la truite arc-en-ciel (RBT, *Oncorhynchus mykiss*), un poisson modèle sensible, d'après le modèle du ligand biotique (BLM) de la toxicité aiguë du Cd. Les caractéristiques de liaison du cadmium et de son compétiteur, le calcium, au niveau de la branchie après 3 h n'affichent que de faibles différences quantitatives chez les deux espèces, mais les accumulations de cadmium après 3 h et 24 h, qui sont associées à une mortalité de 50 % après 96 h (LA50, 3 h et 24 h), sont de 52–60 fois plus élevées chez la perchaude que chez la truite. Cependant, le modèle BLM pour une exposition aiguë au cadmium ne peut être adapté de la truite à la perchaude par simple ajustement des valeurs de LA50 parce que, contrairement à la truite, la perchaude affiche des valeurs de LA50 (3 h et 24 h) 26–47 fois plus élevées que la capacité de la série caractérisée de sites de liaison du cadmium. De plus, les caractéristiques de liaison du calcium et du cadmium après 3 h dans la branchie de perchaudes sauvages, provenant d'un lac propre (Geneva) et de deux lacs contaminés (Hannah et Whitson), tous trois de faible dureté, de la région de Sudbury dans le nord de l'Ontario, démontrent que des facteurs aqueux chroniques, comme la dureté et l'exposition préalable au cadmium, peuvent affecter la liaison tant du cadmium que du calcium dans les branchies de poissons et peuvent avoir des conséquences majeures pour l'amélioration de la méthode BLM pour l'étude de l'exposition aiguë au Cd.

[Traduit par la Rédaction]

Introduction

The family Percidae is believed to be highly tolerant to many metals compared with the family Salmonidae, which is quite sensitive. For example, Percidae are reported to be 2–4 orders of magnitude more tolerant than Salmonidae to waterborne Cu (Taylor et al. 2003). However, virtually no information is available regarding differences in tolerance to waterborne Cd, a nonessential metal. Toxicity of Cd is generally attributed to the free divalent cation Cd^{2+} (Pagenkopf 1983). Waterborne Cd appears to enter mainly through chloride cells in the gills (Wicklund-Glynn et al. 1994) and accu-

Received 5 June 2003. Accepted 21 January 2004. Published on the NRC Research Press Web site at http://cjfas.nrc.ca on 24 July 2004.
J17565

S. Niyogi[1] and C.M. Wood. Department of Biology, McMaster University, 1280 Main Street West, Hamilton, ON L8S 4K1, Canada.
P. Couture.[2] Department of Biology, Laurentian University, Ramsey Lake Road, Sudbury, ON P3E 2C6, Canada.
G. Pyle. Department of Biology, Nipissing University, 100 College Drive, North Bay, ON P1B 8L7, Canada.
D.G. McDonald. Department of Zoology, University of Guelph, Guelph, ON N1G 2W1, Canada.

[1]Corresponding author (e-mail: niyogis@mcmaster.ca).
[2]Present address: Institut national de la recherche scientifique, Centre eau, terre, et environnement, Université du Québec, Sainte-Foy, QC G1V 4C7, Canada.

 doi: 10.1139/F04-044 © 2004 NRC Canada

mulates primarily in kidney, liver, and gills of fish (Hollis et al. 1999, 2000*a*, 2000*b*). At acute waterborne concentrations, Cd severely disrupts Ca homeostasis, which ultimately leads to death (Verbost et al. 1987; Reid and McDonald 1988). At the gill surface, Cd competes with Ca for high-affinity Ca-binding sites (Playle et al. 1993*a*, 1993*b*; Playle 1998) and once it enters inside the chloride cell blocks Ca uptake at the basolateral membrane through the inhibition of Ca^{2+}-ATPase (Verbost et al. 1987, 1989). The cumulative effect of these two processes causes acute hypocalcaemia in fish (Roch and Maly 1979; Verbost et al. 1987, 1989).

Among various water quality parameters (hardness, pH, alkalinity, and dissolved organic matter (DOM))that could potentially influence the Cd uptake, hardness is often reported to be the major factor influencing Cd toxicity (Calamari et al. 1980; Hollis et al. 1997, 2000*b*). As water hardness (defined as the sum of Ca and Mg concentrations, expressed as $CaCO_3$ equivalents) increases, acute Cd toxicity decreases (Carrol et al. 1979; Pascoe et al. 1986). This is thought to be due to the fact that the major hardness cation, Ca, outcompetes Cd for binding sites on the gills and thereby reduces toxicity (Spry and Wiener 1991). Moreover, the bioavailability and toxicity of Cd are less affected by DOM than are the bioavailability and toxicity of Cu (Giesy et al. 1977; Winner 1984; Block and Pärt 1986) because Cd binds about 10-fold less well to DOM than does Cu (Alberts and Giesy 1983; Morel and Herring 1993), but Cd binds about 16-fold more strongly at fish gills than Cu (Playle et al. 1993*b*). Calcium is, therefore, the most important modifier of Cd toxicity in fish rather than water pH or DOM, both of which play important roles in modifying the toxicity of other metals like Cu (Playle et al. 1993*a*; Erickson et al. 1996; MacRae et al. 1999).

The development of the "biotic ligand model" (BLM) in recent years has attempted to better account for the bioavailability and toxicity of metals to aquatic life (DiToro et al. 2001; De Schamphelaere and Janssen 2002; Paquin et al. 2002). The BLM, which quantifies the affinity and capacity of the gills (biotic ligand) of fish to bind metals and relates this binding to acute toxicity, has been proposed as a method for modeling metal toxicity in the aquatic environment based on site-specific water quality parameters. The acute Cu BLM (Santore et al. 2001) has already been approved by the US Environmental Protection Agency in 2000, provisional acute BLMs for Ag (Paquin et al. 1999; McGeer et al. 2000) and Zn (Santore et al. 2002) have been published recently, and an acute Cd BLM is now under active development through industrial – US Environmental Protection Agency consortia. However, only a few fish species (mainly rainbow trout (RBT) (*Oncorhynchus mykiss*) and fathead minnow (*Pimephales promelas*)) have been given emphasis so far for the development of BLM. There is a need to incorporate more species from different fish families, especially those present in metal-impacted environments, to widen the potential for its application.

Our study is mainly focussed on elucidating mechanistic differences in tolerance between yellow perch (YP) (*Perca flavescens*) (a resistant percid endemic to metal-impacted lakes of northern Ontario and Quebec) and a sensitive model species, RBT (a salmonid) from the perspective of the BLM. We compared the following aspects between the two species: (*i*) acute Cd toxicity (96-h LC50s (the concentrations of Cd lethal to 50% of the fish at 96 h)) in moderately hard water (120 mg $CaCO_3 \cdot L^{-1}$) to elucidate Cd sensitivity, (*ii*) the critical gill Cd burden at 3 and 24 h, which is associated with 50% lethality at 96 h (3- and 24-h LA50s), and (*iii*) short-term (3-h) gill Cd and gill Ca binding characteristics (binding affinity (log *K*) and binding capacity (B_{max})). YP were selected for this study because of their abundance and endemic nature to metal-contaminated areas like Sudbury, northern Ontario, and Rouyn-Noranda, northern Quebec (two major mining and smelting locations in Canada) (Sherwood et al. 2000; Couture and Kumar 2003). In addition, we also evaluated the gill Cd and gill Ca binding characteristics in wild YP populations collected from one clean (Geneva) and two metal-contaminated lakes (Hannah and Whitson) around the Sudbury region to test in the natural environments the applicability of the gill binding constants (log *K* and B_{max}) developed in YP populations reared in moderately hard water at our laboratory.

Materials and methods

Studies with laboratory-reared fish

Juvenile RBT (8–12 g) and YP (8–12 g) were obtained from Humber Springs Fish Hatchery (Orangeville, Ont.) and Kinmount Fish Farm (Kinmount, Ont.), respectively. Fish were maintained at least for 1 month in 500-L polyethylene tanks supplied at 2 $L \cdot min^{-1}$ with dechlorinated Hamilton tap water of moderate hardness (12–14 °C, pH 8.0, 0.6 mmol $Na^+ \cdot L^{-1}$, 0.7 mmol $Cl^- \cdot L^{-1}$, 1.0 mmol $Ca^{2+} \cdot L^{-1}$, 0.15 mmol $Mg^{2+} \cdot L^{-1}$, 120 mg hardness$\cdot L^{-1}$ as $CaCO_3$, 95 mg alkalinity$\cdot L^{-1}$ as $CaCO_3$, 3 mg DOM$\cdot L^{-1}$) before the experiments. Fish were fed once a day at 2% of their body weight with commercial trout food (granulated hatchery feed; Corey Feed Mills Ltd., Fredericton, N.B.) and organic debris was siphoned out daily. No fish mortality was observed during this period.

Acute toxicity and 24-h gill LA50 of Cd

The 96-h LC50s of Cd together with 24-h gill Cd burdens were determined in moderately hard water for both species. Fish (n = 10 per concentration) were exposed in duplicate (two sets per concentrations) in a flow-through system to five different Cd concentrations (YP: 16 548 ± 1067, 26 868 ± 801, 41 814 ± 887, 72 953 ± 2135, and 113 879 ± 3203 nmol$\cdot L^{-1}$, respectively; RBT: 51 ± 1, 136 ± 3, 237 ± 10, 394 ± 11, and 531 ± 7 nmol$\cdot L^{-1}$, respectively; n = 9 for all values) in addition to control conditions (background Cd concentration 0.98 ± 0.2 nmol$\cdot L^{-1}$, n = 9) at a temperature of 14 °C. Cadmium stocks ($Cd(NO_3)_2 \cdot 4H_2O$; Fisher Scientific, Canada) were supplied from Marriott bottles into diluent water in mixing head tanks. These tanks then fed 20-L polythene tanks at a rate of approximately 200 mL$\cdot min^{-1}$ each. The duplicate tanks (one for 96-h LC50 and the other for 24-h gill Cd burdens) for each concentration were interconnected so as to have the same water qualities. All tanks were allowed to equilibrate for 12 h before adding fish, individually covered, aerated, and checked for fish mortality every 6 h. No mortality was observed in the first 24 h for both fish species, and all 10 live fish were sampled from one of the tanks in each set of duplicate exposures.

© 2004 NRC Canada

The fish were killed individually by a blow to the head and entire branchial baskets were dissected out. Each branchial basket was rinsed separately for 20 s in "Nanopure" deionized water (Sybron Barnstead, Boston, Mass.) to remove excess blood and loosely adhered metal and blotted dry. Then, each basket was digested in five volumes of 1 mol·l^{-1} HNO_3 (trace metal grade; Fisher Scientific, Canada) for 48 h at 60 °C and analyzed for Cd after appropriate dilution (e.g., 10×, 50×, 100×, etc.) with 1% HNO_3 using a graphite furnace atomic absorption spectrophotometer (GFAAS) (model GTA 110; Varian Australia) and a certified Cd standard for GFAAS (Fisher Scientific, Canada). The other set of exposures was continued for 96 h and dead fish, whenever found, were removed immediately and the total number of dead fish at the end of 96 h in each tank was recorded. Water samples (5 mL) were taken after every 12 h, acidified with 50 µL of concentrated trace metal grade HNO_3, and analyzed for total Cd by GFAAS as described above. The 96-h LC50 values (±95% confidence intervals) were determined by log probit analysis using mean measured waterborne Cd concentrations. Lethal gill Cd accumulation at 24 h associated with 50% mortality at 96 h (24-h LA50) was determined by a regression analysis of 96-h mortality logit versus the 24-h log gill Cd concentrations (MacRae et al. 1999) where logit = $\log[M(1 - M)^{-1}]$ and M is mortality proportion.

Three-hour lethal gill Cd accumulation (3-h LA50)

Once the 96-h LC50 values were known for the two species, a simpler approach was used to determine the 3-h LA50 values. Ten individuals each of YP and RBT were exposed statically for 3 h in 20-L polyethylene tanks containing 10 L of aerated dechlorinated Hamilton tap water at 14 °C to 72 420 and 169 nmol waterborne Cd·L^{-1} (as $Cd(NO_3)_2{\cdot}4H_2O$ (Fisher Scientific, Canada)), respectively (i.e., at the corresponding 96-h LC50 concentrations for each species), radiolabeled with 3 µCi ^{109}Cd·L^{-1} (as $CdCl_2$, specific activity = 3.45 mCi·mg^{-1}, 1 Ci = 37 GBq) (Perkin-Elmer, USA)). After 3 h, fish were sacrificed with a blow to the head. Gill arches were dissected out, rinsed for 20 s in Nanopure deionized water, blotted dry, and placed in 20-mL polyethylene vials. Water samples (5 mL) were taken in duplicate at the beginning and end of the 3-h static exposure and acidified with 50 µL of concentrated trace metal grade HNO_3. Both water and gills were counted for radioactivity using a gamma counter (Packard Minaxi Auto-Gamma 5000 series). The appearance of radioactivity in the gills allowed for the calculation of "new Cd" in the gills (i.e., with no background). Water samples were analyzed for total Cd as described earlier. Gill ^{109}Cd concentrations were converted to absolute values (new Cd) using the measured specific activity (bc^{-1}) of the water:

$$a(bc^{-1})^{-1}$$

where a is ^{109}Cd counts in the gills (counts per minute per gram wet tissue weight), b is ^{109}Cd counts in water (counts per minute per litre), and c is the total Cd concentration in the water (micrograms per litre).

Short-term (3-h) gill Cd binding characteristics

To determine interspecific differences in the short-term nature of Cd binding in gills, we characterized the high-affinity gill Cd-binding sites using the 3-h radiolabeled ^{109}Cd technique (Hollis et al. 1999). Twenty-eight fish (of each species) were transferred into four clear plastic bags (seven per bag) containing 3 L of aerated synthetic water of moderate hardness (1 mmol $Ca^{2+}{\cdot}L^{-1}$ added as $Ca(NO_3)_2{\cdot}4H_2O$, 0.6 mmol $Na^+{\cdot}L^{-1}$, and 0.6 mmol $Cl^-{\cdot}L^{-1}$ added as NaCl plus 1.9 mmol $KHCO_3{\cdot}L^{-1}$ (all from Fisher Scientific, Canada) to achieve a pH of 8.0) and placed in a water bath to maintain stable temperature (14 °C). The concentrations of major ions (Ca^{2+}, Na^+, and Cl^-), alkalinity, and pH in the synthetic water were kept similar to dechlorinated Hamilton tap water in which fish were held before experiments. Each experimental polyethylene bag was spiked with $Cd(NO_3)_2{\cdot}4H_2O$ (Fisher Scientific, Canada) and then with 3 µC ^{109}Cd·L^{-1} (as $CdCl_2$, specific activity = 3.45 mCi·mg^{-1} (Perkin-Elmer, USA)) before fish were transferred to achieve approximate total Cd concentrations of 45, 89, 223, and 446 nmol·L^{-1} respectively.

Water samples (5 mL) were taken in duplicate at the beginning and end of the 3-h static exposure and acidified with 50 µL of concentrated trace metal grade HNO_3. At the end of the exposure, fish were sampled and killed by a blow to the head. Gills were dissected out, rinsed in Nanopure water for 20 s, blotted dry, and placed in 20-mL polyethylene vials. Both water and gills were counted for radioactivity using a gamma counter (Packard Minaxi Auto-Gamma 5000 series). Water samples were further analyzed for total Cd by GFAAS as described before and for total Ca and Na by flame atomic absorption spectrophotometer (FAAS, Varian Australia, Model 220FS). Gill ^{109}Cd concentrations were converted to absolute values (new Cd) following the method described earlier.

The affinity (log K_{Cd}) and capacity (B_{max}) of Cd-binding sites in the gills of both species were determined by the construction of Langmuir plots of Cd adsorption isotherms (Richards and Playle 1998). Free Cd (Cd^{2+}) concentrations were divided by new Cd concentrations in the gills and plotted against free Cd^{2+}. Free Cd^{2+} concentrations were estimated using the known water chemistry and the MINEQL+ aquatic chemistry program (Schecher and McAvoy 2001). The inverse of the slopes and log of the inverse of the intercepts of the respective regression lines provided the B_{max} and log K_{Cd}, respectively, for each species.

Short-term (3-h) gill Ca binding characteristics

Interspecific differences in the nature of short-term Ca binding in gills were also characterized using the same methodology as described above. Four polyethylene bags, each equipped with an airline, were filled with 3 L of synthetic Ca-free water (0.6 mmol $Na^+{\cdot}L^{-1}$ and 0.6 mmol $Cl^-{\cdot}L^{-1}$ added as NaCl, $KHCO_3$ = 1.9 mmol·L^{-1}, pH 8.0) and placed in a water bath (14 °C). Five minutes before the introduction of fish (28 of each species, seven per bag), each bag was spiked first with $Ca(NO_3)_2{\cdot}4H_2O$ (Fisher Scientific, Canada) and then with 7 µCi ^{45}Ca·L^{-1} (as $CaCl_2$, specific activity = 12.26 mCi·mg^{-1} (Perkin-Elmer, USA) to achieve approximate total Ca concentrations of 100, 250, 500, and 1000 µmol·L^{-1}, respectively. After 3 h of exposure, the fish were sacrificed as described before and gills were dissected and rinsed in Nanopure water for 20 s, blotted dry, and stored at –20 °C. Water samples (5 mL) were taken in duplicate at the beginning as well as at the end of the exposure. One of each duplicate water sample was diluted in 10 mL of

© 2004 NRC Canada

scintillation fluor (ACS, Amersham) and counted for ^{45}Ca in a beta counter (LKB Wallac 1217 Rackbeta liquid scintillation counter). The remaining water samples were analyzed for total Ca and Na, respectively, as described earlier.

Frozen gills were later transferred to liquid nitrogen and ground to fine powder with a mortar and pestle. Powdered gills (0.2 g) were placed in glass scintillation vials and were digested in 2 mL of liquid tissue solubilizer (NCS, Amersham) for 48 h at 50 °C. Samples were then neutralized with 20 µL of glacial acetic acid, diluted in 10 mL of scintillation fluor (OCS, Amersham), and counted for ^{45}Ca on the scintillation counter. Counting efficiencies were determined by internal standardization, i.e., by addition/recovery tests of known amounts of ^{45}Ca to individual samples. New Ca in the gill and the affinity (log K_{Ca}) and capacity (B_{max}) of gill Ca binding in both species were determined as described earlier in the case of gill Cd binding. Free Ca^{2+} concentrations were estimated using the known water chemistry and the MINEQL+ aquatic chemistry program (Schecher and McAvoy 2001).

Studies with field-collected YP

Fish were sampled during July 2002 in three lakes around the Sudbury region of northern Ontario, Geneva, Hannah, and Whitson lakes. Geneva Lake (46°45′N, 81°33′W), situated at a distance of more than 100 km from Sudbury's smelters, has not been affected by mining and smelting activities in Sudbury and is a clean or uncontaminated lake. In contrast, both Hannah Lake (46°26′N, 81°02′W) and Whitson Lake (46°28′N, 80°58′W) are located within 20 km of Sudbury's smelters and represent highly metal-contaminated lakes (Couture and Kumar 2003).

Fish and water sampling

Wild YP were captured live using seine net and minnow traps baited with styrofoam beads and placed in littoral zones in study lakes. Approximately 70–80 YP were sampled from each lake and returned to the laboratory live at Laurentian University in Sudbury in 40-L Rubbermaid containers with a portable aerator unit. On arrival, fish were allowed to settle down at a stable temperature of 14–15 °C in their respective lake water for 2 h before being used for experiments.

Water samples (150 mL) were collected with 2-L Van Dorn bottles from each study lake at three depths, 1, 3, and 5 m, from wherever the most fish were captured in the lake. Water pH levels were recorded immediately on site with a portable pH meter (Thermo Orion; Fisher Scientific, Canada). The pH meter was calibrated in the laboratory on each sampling day and calibration was verified using pH 4, 7, and 10 buffers (Fisher Scientific, Canada) in the field. Finally, labeled sampling containers were rinsed with lake water three times, filled to capacity (i.e., no head space), and placed on ice for transport back to the laboratory at Laurentian University. Immediately after reaching the laboratory, the water samples were acidified to pH 2 with trace metal grade HNO_3 for metal determination and then stored at 4 °C until analysis.

Short-term (3-h) gill Cd and Ca binding

Short-term (3-h in vivo) gill Cd- and gill Ca-binding properties were evaluated in wild YP collected from three different lakes following the same methodology as described earlier for laboratory-reared YP. Synthetic water of identical water chemistry and similar range of waterborne Cd and Ca exposure concentrations, used for laboratory-reared YP, was used. The binding affinity (log K) and binding capacity (B_{max}) of both Cd and Ca binding in the gill were also determined by the construction of Langmuir plots as described earlier. Free Cd^{2+} and Ca^{2+} concentrations were estimated with the MINEQL+ aquatic chemistry program (Schecher and McAvoy 2001).

Determination of Cd burden in the gills of wild YP by inductively coupled plasma (ICP) analysis

Approximately 10 YP from each lake were sacrificed by a blow to the head. The gills were dissected out and rinsed for 20 s in double-distilled water and blotted dry. The gills were weighed and dried at 60 °C to a constant weight (>24 h) and then microwave-digested in 3 mL of analytical-grade HNO_3 (Fisher Scientific, Canada) using Teflon vials. The efficacy of the digestion method for Cd recovery was monitored using National Research Council certified standards TORT-2, DORM-2, and DOLT-2 as well as method blanks of only HNO_3. Samples were allowed to cool overnight and then transferred to labeled, precleaned, acid-washed 50-mL Fisher brand specimen containers with 12 mL of double-distilled water. Cadmium concentrations in fish gills were determined by ICP analysis using Cd standards of known concentrations at Elliot Lake Research Field Station (Elliot Lake, Ont.).

Determination of metal concentrations in water via ICP analysis

Acidified water samples stored at 4 °C were vacuum-filtered through a prebaked Whatman 934-AH glass microfibre filter to remove suspended solids and analyzed for total dissolved Cd, Ca, and Mg by ICP analysis at Testmark Laboratories Ltd. (Sudbury, Ont.). Quality assurance samples were run at the beginning of each run that included blanks and 10 and 100 µg·L^{-1} of Canadian Association of Environmental Analytical Laboratories (CAEAL) certified standards of each metal measured. All samples passed the Canadian Association of Environmental Analytical Laboratories accredited quality control standards of Testmark Laboratories Ltd.

Statistical analyses

All data are presented as means ± SE of the mean except 96-h LC50 and 3- and 24-h LA50 data, which are expressed as means and 95% confidence intervals. Nonlinear regressions were performed using Sigma Plot 2000. The assumptions in the regression analyses, i.e., normality of residuals and homogeneity of variances, were tested using Shapiro–Wilk's test for normality and Levene's test for homogeneity of variance (both at $\alpha = 0.05$), respectively. All of the data met these assumptions. Significance of regressions and values were evaluated using a standard Student's t test. Significance of 96-h LC50 and 3- and 24-h LA50 values between YP and RBT was also tested using a Student's t test. Cadmium levels in YP gills and in water between clean and two contaminated lakes were analyzed for statistical significance by using a one-way analysis of variance followed by Bonferroni multiple comparisons tests. In the last two analyses, the data were again checked for normality and homogeneity of variances using Shapiro–Wilk's test and Levene's

© 2004 NRC Canada

test, respectively (both at $\alpha = 0.05$). Data not meeting the assumptions were adjusted with log transformation before proceeding with significance tests. The level of significance was set to $p < 0.05$ in all comparisons.

Results

Acute toxicity and lethal gill accumulation of Cd

When the 96-h LC50 values were compared between the two fish species, Cd was approximately 420 times more toxic to juvenile RBT than to YP in moderately hard water (Table 1). The Cd accumulation in the gill at 24 h increased with increasing waterborne Cd concentrations in both YP and RBT and approached saturation within the different ranges of waterborne concentrations used (Figs. 1*a* and 2*a*). The different scales between Figs. 1*a* and 2*a* reflect the very different sensitivities of the two species to Cd. Regression analyses of 96-h mortality logit versus the 24-h log gill concentrations yielded straight lines from which 24-h LA50 values, which are predictive of 96-h mortality, were calculated (Figs. 1*b* and 2*b*). The 24-h LA50 value of YP was almost 60 times higher than that of RBT (Table 1). Similarly, the 3-h LA50 value, measured by exposure of the two species to their respective 96-h LC50 levels of Cd, was more than 52 times greater in YP relative to RBT (Table 1).

Short-term (3-h) gill Cd binding characteristics

In both species, the short term (3-h) binding of Cd to the gills increased with increasing waterborne Cd concentrations and reached an apparent "plateau" at waterborne Cd concentrations between 223 and 446 nmol·L^{-1} (Fig. 3*a*). Approximately 91–96% of the total Cd was calculated to be present as free Cd^{2+} by the MINEQL+ aquatic chemistry program. The Langmuir plots of Cd adsorption isotherms (Fig. 3*b*) provided the affinity (log K_{Cd}) and capacity (B_{max}) of Cd binding in the gills of the respective species. The log K_{Cd} values were 7.34 and 7.20 and the B_{max} values were 0.85 and 0.67 nmol·g wet gill tissue^{-1} in RBT and YP, respectively. No significant differences were observed in either affinity or capacity of Cd binding in the gills between the two species. Interestingly, 3-h LA50 values corresponded to about 40% saturation of the short-term (3-h) gill Cd-binding sites in RBT yet more than 2600% saturation of the sites in YP (i.e., 26 times higher than B_{max}).

Short-term (3-h) gill Ca binding characteristics

Like Cd, the short term (3-h) binding of Ca to the gills also increased with increasing waterborne Ca concentrations and reached an apparent "plateau" at waterborne Ca concentrations between 500 and 1000 µmol·L^{-1} (Fig. 4*a*). Approximately 99% of the total Ca was calculated to be present as free Ca^{2+} by the MINEQL+ aquatic chemistry program. The Langmuir plots of Ca adsorption isotherms (Fig. 4*b*) provided the affinity (log K_{Ca}) and capacity (B_{max}) of Ca binding in the gills of the respective species. The log K_{Ca} values were 3.69 and 3.71 and the B_{max} values were 0.53 and 0.38 µmol·g wet gill tissue^{-1} in RBT and YP, respectively. Once again, no significant differences were observed in either affinity or capacity of Ca binding in the gills between the two species.

Water quality and Cd burden in the gills of wild YP

Among the three lakes, Hannah Lake had the highest Ca and Mg concentrations and pH levels in water followed by Whitson and Geneva lakes (Table 2). However, the Cd concentration in the water of Hannah and Whitson lakes was significantly higher (>2.5-fold) relative to the water of Geneva Lake (clean) (Table 2). Similarly, the Cd burdens in the gills of YP collected from metal-contaminated Hannah and Whitson lakes were also significantly higher (more than 10-fold) than that in the gills of YP from uncontaminated Geneva Lake (Table 2). Average fish weight was highest in uncontaminated Geneva Lake followed by contaminated Hannah Lake and then Whitson Lake (Table 2).

Short-term (3-h) gill Cd binding in wild YP

Short-term (3-h) in vivo gill Cd binding exhibited concentration-dependent increases against waterborne Cd in YP from all three lakes (Fig. 5*a*). At the lower waterborne Cd concentrations, values were similar in YP from the three lakes. However, the saturation in binding was observed only in YP collected from uncontaminated Geneva Lake, whereas the YP collected from contaminated Hannah and Whitson lakes exhibited linear increases and no saturation in binding within the concentration range of 44.6–446.0 nmol waterborne Cd·L^{-1}. The lack of saturation in binding did not allow the determination of Cd binding affinity (log K_{Cd}) and capacity (B_{max}) in YP from Hannah and Whitson lakes. The Langmuir plots of Cd adsorption isotherms (Fig. 5*b*) in YP from uncontaminated Geneva Lake yielded log K_{Cd} and B_{max} values of 7.19 and 2.01 nmol·g wet gill tissue^{-1}, respectively. Interestingly, the log K_{Cd} values in laboratory-reared YP and Geneva Lake populations of YP were very similar, although the B_{max} value was threefold higher (significant, $p < 0.05$) in the latter.

Short-term (3-h) gill Ca binding in wild YP

In contrast with Cd binding, the short-term (3-h) in vivo gill Ca binding exhibited saturation binding within the range of 100–1000 µmol waterborne Ca·L^{-1} in YP collected from all three lakes (Fig. 6*a*). The Langmuir plots of Ca adsorption isotherms (Fig. 6*b*) provided affinity (log K_{Ca}) values of 3.39, 3.63, and 3.28 and capacity (B_{max}) values of 1.59, 1.64, and 1.69 µmol·g wet tissue^{-1} for Geneva, Hannah, and Whitson lakes, respectively. No significant difference was observed in either affinity or capacity among YP collected from any of the lakes. Interestingly, Ca binding in gills of YP collected from all three natural lakes exhibited reduced affinity, i.e., lower log K (although not statistically significant) relative to that of laboratory-reared YP. However, the B_{max} of Ca binding was more than four times greater (significant, $p < 0.05$) in all three wild populations of YP compared with that in laboratory-reared YP.

Discussion

We addressed three questions through this study. First, did the difference in short-term Cd and Ca binding in the gills between YP and RBT reflect the difference in tolerance to acute Cd challenge? Second, were there any qualitative and (or) quantitative differences in short-term gill binding characteristics for Cd and Ca among wild YP collected from

© 2004 NRC Canada

Table 1. Acute toxicity (96-h LC50) and lethal gill accumulations (24- and 3-h LA50s) of Cd in YP and RBT in moderately hard dechlorinated Hamilton tap water.

Species	96-h LC50 (nmol·L^{-1}) (n = 60)	24-h LA50 (nmol·g wet tissue^{-1}) (n = 60)	3-h LA50 (nmol·g wet tissue^{-1}) (n = 10)
YP	72 420 (55 427 – 100 445)	31.67 (24.46–42.26)	17.81 (22.96–12.66)
RBT	169 (130–2 29)*	0.55 (0.45–0.64)*	0.34 (0.39–0.29)*

Note: Fish were acclimated to moderately hard water for a minimum of 4 weeks before experiments. Data are expressed as means (95% confidence interval in parentheses). Significant differences ($p < 0.05$) in values between two species are indicated by an asterisk.

Fig. 1. (*a*) Cadmium accumulation in the gills of YP after 24 h of exposure to a waterborne Cd concentration range of 0.98 (control) to 113 879 nmol·L^{-1} in moderately hard water (120 mg·L^{-1} as $CaCO_3$) at 14 °C. Data are presented as means ± SE of the mean (n = 10) and corrected for background Cd concentration (1.51 ± 0.43 nmol·g wet tissue^{-1}). (*b*) Determination of lethal accumulation at 24 h (24-h LA50) yielding 50% mortality in YP at 96 h. The YP 96-h mortality logit is plotted as a function of log gill Cd concentration from Fig. 1*a* determined on live fish at 24 h. The regression equation was log[M/(1 – M)] = log gill Cd × 1.88 – 2.79 (r^2 = 0.83). LA50 = 31.67 nmol·g wet tissue^{-1} (95% confidence interval: 24.46–42.26).

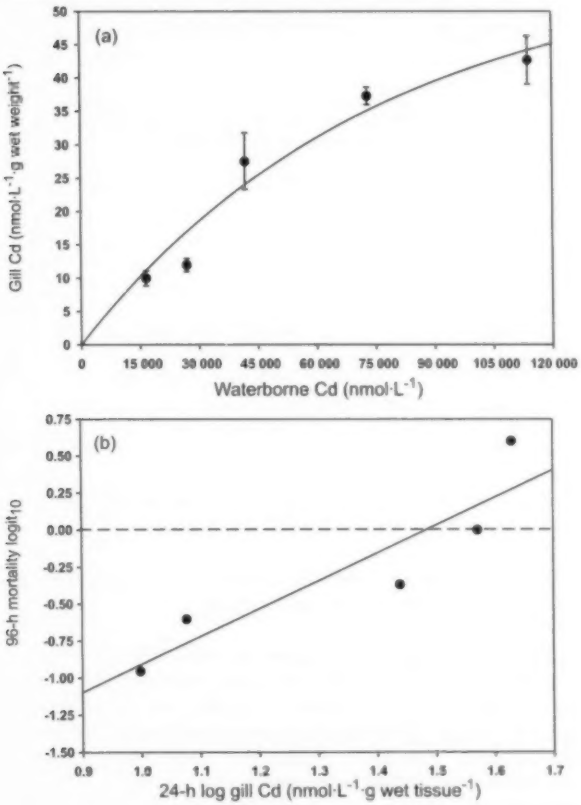

Fig. 2. (*a*) Cadmium accumulation in the gills of RBT after 24 h of exposure to a waterborne Cd concentration range of 0.98 (control) to 531 nmol·L^{-1} in moderately hard water (120 mg·L^{-1} as $caCO_3$) at 14 °C. Data are presented as means ± SE of the mean (n = 10) and corrected for background Cd concentration (1.07 ± 0.34 nmol·g wet tissue^{-1}). (*b*) Determination of lethal accumulation at 24 h (24-h LA50) yielding 50% mortality in RBT at 96 h. The RBT 96-h mortality logit is plotted as a function of log gill Cd concentration from Fig. 2*a* determined on live fish at 24 h. The regression equation was log[M/(1 – M)] = log gill Cd × 3.67 + 1.09 (r^2 = 0.92). LA50 = 0.55 nmol·g wet tissue^{-1} (95% confidence interval: 0.45–0.64).

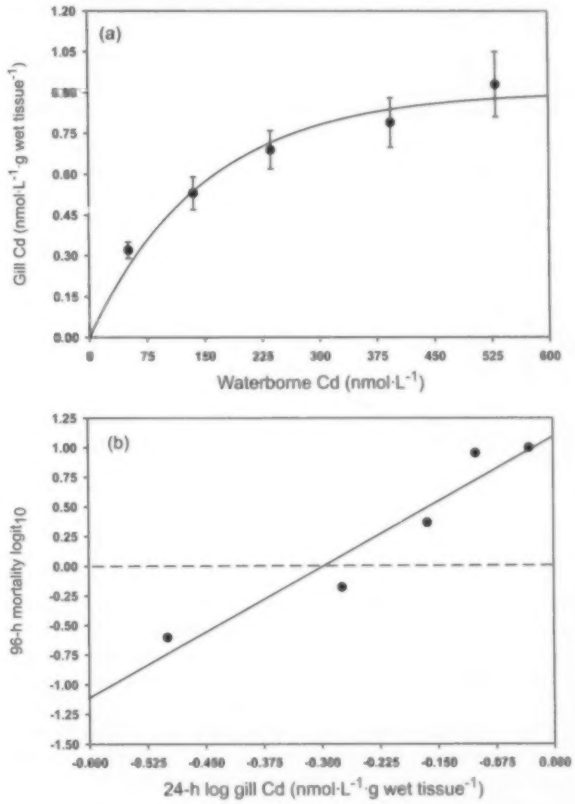

metal-contaminated as well as uncontaminated natural soft-water lakes and YP reared in moderately hard water in the laboratory? Third, what are the implications of these factors for the acute Cd BLM?

The short-term 3-h in vivo Cd and Ca binding characteristics in gills of the two fish species were qualitatively similar. The quantitative differences in Cd binding in the gill between YP and RBT were small and nonsignificant and did not reflect the actual magnitude of difference in toxicity.

© 2004 NRC Canada

Fig. 3. (*a*) New Cd (bound Cd) in the gills of YP and RBT after 3 h of exposure to radioactive ^{109}Cd in synthetic water at 14 °C plotted against free Cd^{2+} in the water as calculated by MINEQL+ (Schecher and McAvoy 2001). Data are expressed as means ± SE of the mean (n = 7). (*b*) Langmuir plots of gill Cd binding results from Fig. 3*a* for both YP and RBT. The regression equation for YP was $y = 1.49x + 93.67$ ($r^2 = 0.98$) (log $K_{Cd} = 7.20$, B_{max} = 0.67 nmol·g wet tissue^{-1}) and the equation for RBT was $y = 1.18x + 53.37$ ($r^2 = 0.99$) (log $K_{Cd} = 7.34$, $B_{max} = 0.85$ nmol·g wet tissue^{-1}). Regressions are not significantly different from one another. Solid and open circles represent YP and RBT, respectively, in both panels.

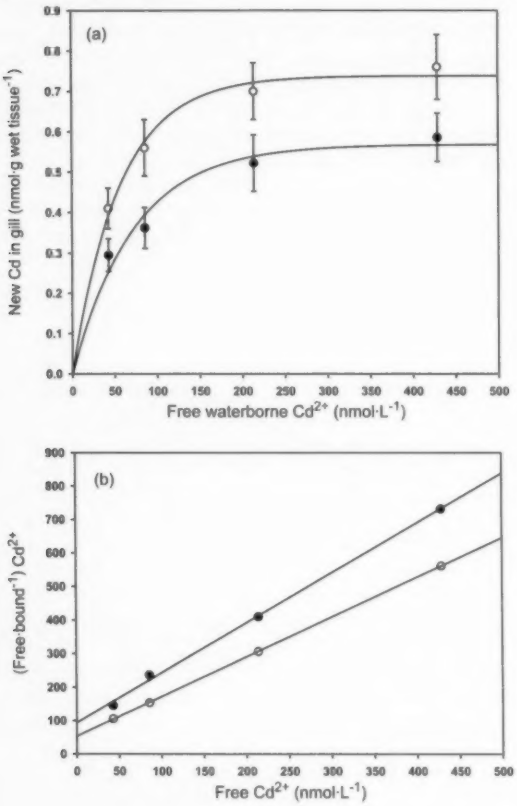

Fig. 4. (*a*) New Ca (bound Ca) in the gills of RBT after 3 h of exposure to radioactive ^{45}Ca in synthetic water at 14 °C plotted against free Ca^{2+} in the water as calculated by MINEQL+ (Schecher and McAvoy 2001). Data are expressed as means ± SE of the mean (n = 7). (*b*) Langmuir plots of gill Ca binding results from Fig. 4*a* for both YP and RBT. The regression equation for YP was $y = 2.59x + 503.74$ ($r^2 = 0.99$) (log $K_{Ca} = 3.71$, $B_{max} = 0.38$ µmol·g wet tissue^{-1}) and the equation for RBT was $y = 1.89x + 380.06$ ($r^2 = 0.98$) (log $K_{Ca} = 3.69$, $B_{max} = 0.53$ µmol·g wet tissue^{-1}). Regressions are not significantly different from one another. Solid and open circles represent YP and RBT, respectively, in both panels.

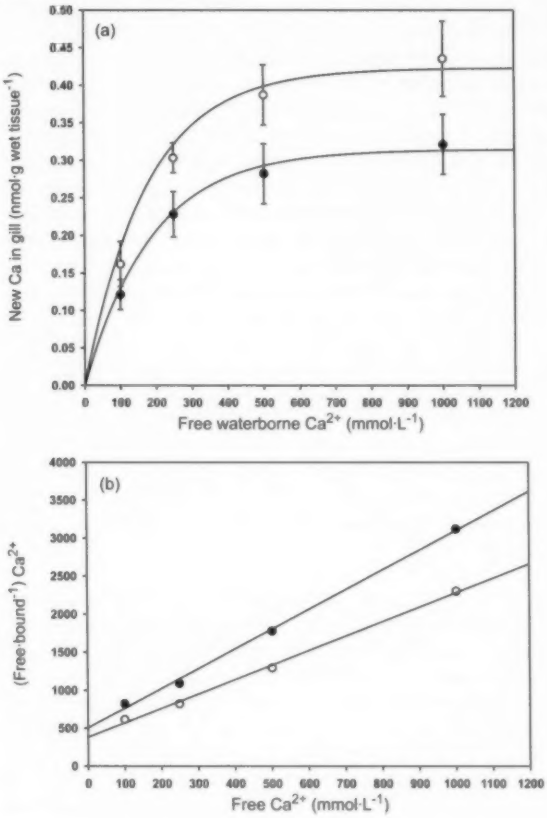

However, the large difference in Cd tolerance corresponded to the large differences in lethal accumulation of Cd in the gills (24-h or 3-h LA50) between the two species. The gill binding characteristics for both Cd and Ca were also qualitatively similar in nature between laboratory-reared and wild YP from the uncontaminated lake (Geneva), although there were quantitative differences in B_{max} (higher capacity in wild fish). However, the gill binding characteristics for Cd, but not for Ca, in wild YP collected from the metal-contaminated lakes (Hannah and Whitson) were both qualitatively and quantitatively different relative to those in YP of Geneva Lake. Overall, these findings indicate that the present acute Cd BLM approach developed in RBT has to be modified to make it applicable to the metal-tolerant species, YP. Furthermore, these findings also demonstrate that the chronic history of fish must be taken into consideration for future refinement of the present acute Cd BLM.

Acute toxicity and lethal accumulation (LA50)

Acute toxicity (2–7 days) or LC50 values for Cd in RBT vary considerably from study to study, but a majority of them are in the 150–850 nmol·L^{-1} range (Pascoe and Beattie 1979; Davies et al. 1993; Hollis et al. 1999), with occasionally further higher values in waters with very high alkalinity and hardness (Calamari et al. 1980; Pascoe et al. 1986). The 96-h LC50 value in RBT determined in the present study (169 nmol·L^{-1}) was similar to the value (196 nmol·L^{-1}) reported earlier from our laboratory (Hollis et al. 1999) in similar water chemistry. However, the extremely high tolerance to acute Cd challenge in YP relative to RBT (96-h LC50: 72 420 (YP) and 169 nmol·L^{-1} (RBT)) observed in the cur-

© 2004 NRC Canada

Table 2. Water quality, average fish weight, and gill Cd concentrations of YP populations from clean and metal-contaminated lakes of the Sudbury region, northern Ontario.

Lake	Water pH (n = 3)	Water Ca (mmol·L^{-1}) (n = 3)	Water Mg (mmol·L^{-1}) (n = 3)	Water Cd (nmol·L^{-1}) (n = 3)	Fish weight (g) (n = 70)	Gill Cd (nmol·g wet tissue^{-1}) (n = 8)
Geneva	6.61±0.05	0.07±0.003	0.03±0.001	ND	6.42±1.78	1.96±0.59
Hannah	7.39±0.14	0.25±0.002	0.14±0.003	2.67±0.18*	4.08±0.82	20.04±3.03*
Whitson	6.90±0.07	0.15±0.003	0.07±0.001	2.76±0.19*	2.96±2.19	21.10±1.79*

Note: Data are expressed as means ± SE of the mean. Significant differences ($p < 0.05$) in water Cd levels and gill Cd burden of YP between the clean lake (Geneva) and metal-contaminated lakes (Whitson and Hannah) are indicated by an asterisk. ND, not detectable; the detection limit for Cd was 0.45 nmol·L^{-1}.

Fig. 5. (*a*) New Cd (bound Cd) in the gills of YP collected from Geneva (clean) and Hannah and Whitson lakes (metal contaminated) after 3 h of exposure to radioactive ^{109}Cd in synthetic water at 14 °C plotted against free Cd^{2+} in the water as calculated by MINEQL+ (Schecher and McAvoy 2001). Data are expressed as means ± SE of the mean (n = 7). Geneva, Hannah, and Whitson lakes are represented by solid circles and solid line, solid circles and thin broken line, and triangles and thick broken line, respectively. (*b*) Langmuir plots of gill Cd binding results from Fig. 5*a* for YP from Geneva Lake. The regression equation was $y = 0.50x + 32.09$ ($r^2 = 0.98$) (log $K_{Cd} = 7.19$, $B_{max} = 2.01$ nmol·g wet tissue^{-1}). Langmuir plots could not be constructed for YP from Hannah and Whitson lakes because of the lack of saturation.

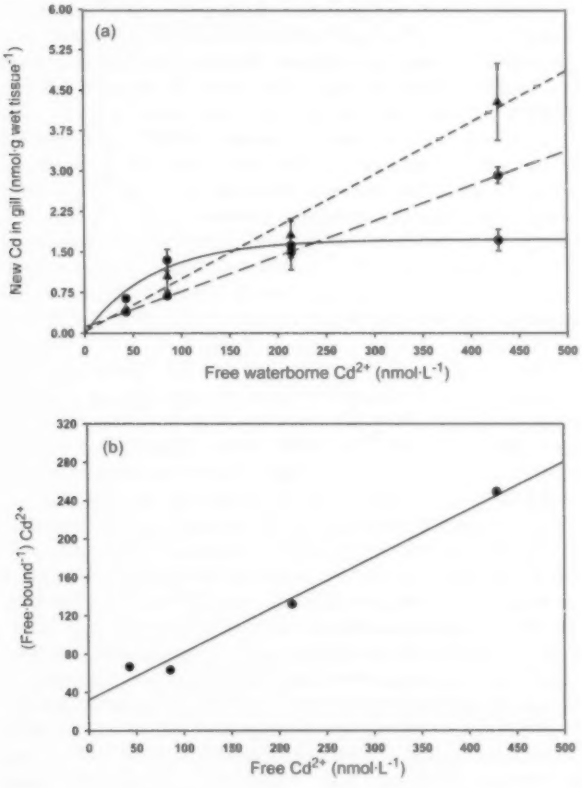

Fig. 6. (*a*) New Ca (bound Ca) in the gills of YP from Geneva (clean) and Hannah and Whitson lakes (metal contaminated) after 3 h of exposure to radioactive ^{45}Ca in synthetic water at 14 °C plotted against free Ca^{2+} in the water as calculated by MINEQL+ (Schecher and McAvoy 2001). Data are expressed as means ± SE of the mean (n = 7). (*b*) Langmuir plots of gill Ca binding results from Fig. 6*a* for YP from three lakes. The regression equations for YP from Geneva, Hannah, and Whitson lakes were $y = 0.63x + 251.96$ ($r^2 = 0.86$) (log $K_{Ca} = 3.39$, $B_{max} = 1.59$ µmol·g wet tissue^{-1}), $y = 0.61x + 143.41$ ($r^2 = 0.96$) (log $K_{Ca} = 3.63$, $B_{max} = 1.64$ µmol·g wet tissue^{-1}, and $y = 0.59x + 307.51$ ($r^2 = 0.97$) (log $K_{Ca} = 3.28$, $B_{max} = 1.69$ µmol·g wet tissue^{-1}), respectively. Regressions are not significantly different from one another. Geneva, Hannah, and Whitson lakes are represented by solid circles and solid line, open circles and thin broken line, and triangles and thick broken line, respectively, in both panels.

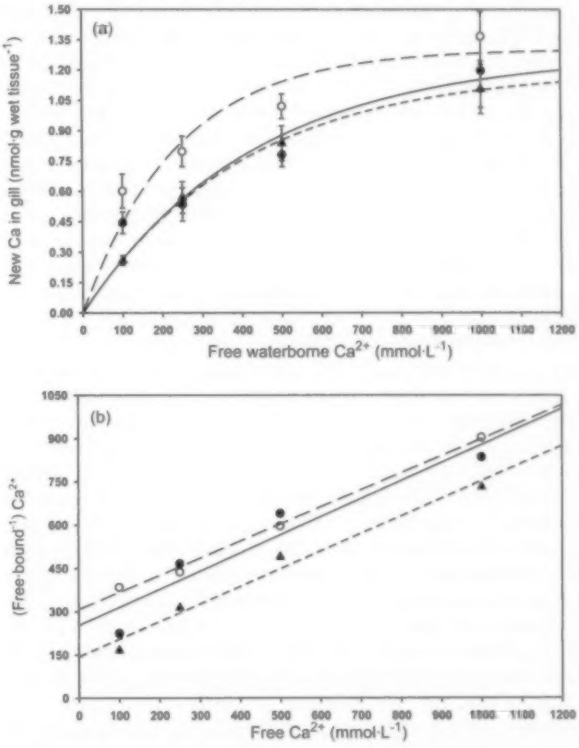

rent study could not be compared with any other published reports, since we evaluated this fish species for the first time.

The principal objective of the BLM is the prediction of toxicity of any metal at any given water chemistry. To predict toxicity, it is necessary to determine the amount of

© 2004 NRC Canada

short-term accumulation (3 or 24 h) of metal in the gill (the biotic ligand) that is associated with 50% mortality at 96 h (3- or 24-h LA50). The reason for considering short-term gill metal accumulation for this aspect is that the short-term rapid increase of gill metal accumulation is believed to play the main role in the toxic actions of metals, as it reflects binding to physiologically active receptor sites at the gill surface that control ion homeostasis in fish (DiToro et al. 2001; Paquin et al. 2002; Niyogi and Wood 2003). The 24-h Cd LA50 values, the amount of "newly accumulated Cd" in the gill at 24 h that could be predictive of 50% mortality at 96 h, were markedly different between the two species (YP: 31.67 nmol·g wet gill tissue^{-1}; RBT: 0.55 nmol·g wet gill tissue^{-1}). The 3-h LA50 values, or the "newly accumulated Cd" in the gill at 3-h, were also significantly higher in YP than in RBT (YP: 17.80 nmol·g wet gill tissue^{-1}; RBT: 0.34 nmol·g wet tissue^{-1}) and reflected a similar magnitude of difference as at 24 h. It should be noted that both 24- and 3-h Cd LA50s for RBT occurred well within the characterized set of saturable sites at the gill (B_{max} = 0.85 nmol·g wet gill tissue^{-1}). In contrast, both 24- and 3-h Cd LA50s in YP occurred far beyond the characterized saturable sites (B_{max} = 0.67 nmol·g wet gill tissue^{-1}), which indicated in addition to 100% filling of high-affinity, low-capacity sites that an unknown percentage of the low-affinity, high-capacity sites were filled by Cd, thereby suggesting their role in the toxic actions of Cd in YP.

Similar but less extreme differences have been reported by Taylor et al. (2003) in relation to differences in acute Cu toxicity between the two fish species. They evaluated the 3-h Cu LA50 values for both YP and RBT by exposing the fish at their respective 96-h LC50 concentrations of Cu in hard water and reported a ninefold greater LA50 value for YP relative to RBT. This higher value correlated with a fourfold higher 96-h LC50 value for Cu in YP than in RBT in the same water chemistry. Moreover, the 3-h Cu LA50 (3.1 nmol·g wet tissue^{-1}) was lower than the B_{max} (3.6 nmol·g wet tissue^{-1}) in RBT, whereas in YP, the 3-h Cu LA50 (27.8 nmol·g wet tissue^{-1}) was about threefold greater than the B_{max} (9.0 nmol·g wet tissue^{-1}).

MacRae et al. (1999) and later DiToro et al. (2001) compared the 24-h Cu LA50 for brook trout (*Salvelinus fontinalis*) and RBT acclimated to artificial soft water (0.125 mmol Ca·L^{-1}) and proposed that one critical gill accumulation value (~10 nmol·g wet gill tissue^{-1} (background corrected)) could be used to predict acute Cu toxicity irrespective of fish species and water chemistry. However, this concept appears to be ineffective in comparing Cd toxicity between YP and RBT in moderately hard water, as observed also by Taylor et al. (2003) in the case of Cu toxicity. Certainly from the perspective of developing an acute Cd BLM for YP, short-term gill binding for Cd has to be characterized at a much higher range of waterborne Cd concentrations relative to RBT to incorporate low-affinity, high-capacity Cd binding sites in the gills, which are presumably involved in acute Cd toxicity, in addition to high-affinity, low-capacity binding sites.

Short-term (3-h) gill Cd and Ca binding in laboratory-reared YP and RBT

The affinity (log K_{Cd}) and capacity (B_{max}) of high-affinity, low-capacity Cd binding sites in the gills determined by Langmuir plots were similar in YP and RBT. Taylor et al. (2003) also reported no significant differences in log K_{Cu} in hard water as well as in soft water between the same two species, although they observed significantly greater binding capacity for Cu in YP relative to RBT in both hard and soft water. The log K_{Cd} value in RBT of the present study (7.34) was in reasonable agreement with those (7.60 and 7.05) reported earlier by Hollis et al. (1999) and Szebedinszky et al. (2001), respectively, in RBT in moderately hard water. However, the value in this study is much less than the value (8.60) reported by Playle et al. (1993*a*, 1993*b*) in fathead minnow, which translates to a more than 20-fold greater affinity of fathead minnow gills for Cd compared with RBT. The use of synthetic, moderately hard water (without any synthetic or natural organic ligands) in the present study produced a very high yield of free Cd^{2+} (calculated by MINEQL+) and created a very simplified condition where the presence of other free ions like Ca^{2+}, Na^{+}, H^{+}, etc. likely exerted competitive effects, thereby reducing the apparent affinity or log K_{Cd}. In contrast, Playle et al. (1993*a*, 1993*b*) used synthetic soft water containing very low levels of cations as competitors to Cd^{2+} for the sites at fish gills; reduced Ca^{2+} competition would yield greater Cd accumulation and therefore greater log K_{Cd}. Moreover, the use of radioactive ^{109}Cd in comparison with cold Cd enabled us to calculate the newly accumulated Cd in fish gills with greater resolution, separate from the background levels.

The B_{max} value in RBT observed in our study (0.85 nmol·g wet gill tissue^{-1}) was lower than the value of 2.27 nmol·g wet gill tissue^{-1} reported in fathead minnow acclimated to synthetic soft water (0.05 mmol Ca·L^{-1}) by Playle et al. (1993*a*, 1993*b*). It was also lower than the values of 1.61 and 3.12 nmol·g wet gill tissue^{-1} reported in RBT, acclimated to the same water chemistry as that used in the present study, by Hollis et al. (1999) and Szebedinszky et al. (2001), respectively. This discrepancy in the number of gill binding sites (B_{max}) among studies was probably due to the size or batch differences in fish and also differences in feeding regime (Hollis et al. 2000*b*) and is certainly an issue that has to be given greater attention for further development of the present acute Cd BLM.

Short-term Ca binding properties of the gills were also qualitatively quite similar between the two species. The Ca binding affinities in gills (log K_{Ca}) in both species were almost identical (YP: 3.69; RBT: 3.71), while the maximum number of Ca binding sites (B_{max}) was lower, although not statistically significant, in YP (0.38 μmol·g wet gill tissue^{-1}) compared with that in RBT (0.53 μmol·g wet gill tissue^{-1}). The log K_{Ca} values of the present study were also lower than that (5.0) proposed by Playle et al. (1993*a*, 1993*b*). They calculated the log K_{Ca} value, following an indirect approach, from the competitive effect of two waterborne Ca concentrations (95 and 1050 μmol·L^{-1}) on the accumulation of Cd in the gill at 3 h using cold Cd and Ca. However, in the present study, the log K_{Ca} value was evaluated directly from the 3-h in vivo gill Ca binding assay using radioactive ^{45}Ca. This is certainly a method more sensitive than that used by Playle et al. (1993*a*, 1993*b*) and additionally may measure a different population of sites (i.e., not necessarily just those associated with Cd binding).

Overall, these findings suggest that similar affinity for short-term Cd and Ca binding regardless of the species is a

© 2004 NRC Canada

reflection of fundamental gill membrane characteristics when the fish are acclimated to the same water chemistry. This is not surprising, since the binding properties of the gill are probably modulated by basic physiological requirements for binding and uptake of essential osmoregulatory ions such as Ca^{2+} and Na^{+}.

Short-term (3-h) gill Cd and Ca binding in wild YP

The log K_{Cd} of the high-affinity, low-capacity Cd-binding sites in the gills of YP from uncontaminated Geneva Lake was 7.19, similar to that (7.20) found in our laboratory YP population acclimated to moderately hard water. However, it is also important to note here that the affinity for Cd binding in the gills of YP from Geneva Lake might be greater in the ambient water of Geneva Lake because we used synthetic water of approximately 14-fold greater waterborne Ca level for the binding assay, thus producing a greater competitive effect of Ca on Cd binding. In contrast, a threefold greater B_{max} was observed in YP of Geneva Lake compared to laboratory-reared YP, which was most likely due to the extremely soft nature (low waterborne Ca) of the water in Geneva Lake. A similar increase in B_{max} values from hardwater acclimation to softwater acclimation was also reported by Hollis et al. (1999, 2000*a*, 2000*b*) in RBT. They also reported a decrease in affinity (log K_{Cd}) in RBT acclimated to soft water; however, we did not observe any decrease in affinity in the YP population of Geneva Lake.

In contrast, the properties of the high-affinity, low-capacity Cd-binding sites of wild YP from Hannah and Whitson lakes showed large differences compared with those in laboratory-reared as well as Geneva Lake YP populations. The binding pattern changed from saturable to almost linear in fish from Hannah and Whitson lakes, preventing the determination of log K_{Cd} and B_{max} in those YP populations. The greater Cd concentration in the water as well as in the gills of YP from Hannah and Whitson lakes compared with those of Geneva Lake indicated that the former two YP populations are chronically preexposed to waterborne Cd. This chronic Cd exposure was likely the factor responsible for the observed changes in gill Cd binding pattern. Hollis et al. (1999, 2000*a*) also reported a similar loss of saturation in gill Cd binding in RBT upon laboratory acclimation to chronic waterborne Cd in both hard water (89 nmol $Cd{\cdot}L^{-1}$) and soft water (0.62 and 0.98 nmol $Cd{\cdot}L^{-1}$). Therefore, our findings in chronically Cd-preexposed wild YP validated the phenomenon previously observed in our laboratory with RBT. Likely, the phenomenon relates to a large loss of affinity (i.e., decreased log K_{Cd}), which tends to linearize the relationship, a phenomenon also seen by Szebedinszky et al. (2001) in RBT subjected to chronic dietary Cd exposure.

The Cd accumulation levels in laboratory-reared YP exposed to a waterborne Cd concentration range of 16 548 – 113 879 nmol·L^{-1} (i.e., concentration range for 96-h LC50 determination of YP) in moderately hard water for 24 h varied between 10 and 40 nmol·g wet $tissue^{-1}$ and were associated with 10–80% lethality at 96 h. Interestingly, the background gill Cd concentrations in YP from contaminated Hannah and Whitson lakes were 20.04 and 21.15 nmol·g wet $tissue^{-1}$, respectively (about 10-fold higher relative to that in YP from clean Geneva Lake). Hollis et al. (2000*a*) reported an approximately sixfold increase in background gill Cd concentration in RBT following 30 days of exposure to waterborne Cd concentrations of 0.62 and 0.98 nmol·L^{-1}, which were two- to four-fold lower than the waterborne Cd concentrations of Hannah and Whitson lakes (2.67 and 2.76 nmol·L^{-1}, respectively) in water of similar hardness (0.13 mmol $Ca{\cdot}L^{-1}$) to that of Hannah and Whitson lakes (0.25 and 0.15 mmol $Ca{\cdot}L^{-1}$, respectively). Therefore, it appears that chronic waterborne Cd exposure results in an increased Cd storage pool in the gills of fish, which probably leads to the alteration of gill Cd binding properties.

Contrary to Cd binding, there were no significant differences in the binding affinity (log K_{Ca}) of Ca in the gills of Cd-preexposed YP (Hannah Lake: 3.63; Whitson Lake: 3.28) as well as nonexposed YP populations (Geneva Lake: 3.39; laboratory reared: 3.71). However, about fourfold greater Ca binding capacity B_{max} was observed in all of the wild YP populations (Geneva Lake: 1.60 µmol·g wet gill $tissue^{-1}$; Hannah Lake: 1.69 µmol·g wet gill $tissue^{-1}$; Whitson Lake: 1.64 µmol·g wet gill $tissue^{-1}$) relative to that (0.39 µmol·g wet gill $tissue^{-1}$) of the moderately hardwater acclimated YP population of the laboratory. This phenomenon in wild YP is likely due to the upregulation of branchial Ca uptake processes as a mechanism to survive in ion-poor soft water of the lakes. Cadmium shares the same uptake pathway with Ca^{2+} in fish gills (Verbost et al. 1987) and Cd-binding sites in gills are probably part of the branchial Ca^{2+} transport system (Wood 2001). Thus, the higher B_{max} value for Cd in the gills of YP from Geneva Lake relative to that of laboratory-reared YP, as discussed before, was also probably indicative of an upregulation of the branchial Ca^{2+} transport process. Reid et al. (1991) reported a twofold greater value of the Ca binding capacity (B_{max}: 0.95 µmol·g wet tissue) in softwater (hardness: 20 mg·L^{-1} as $CaCO_3$) acclimated RBT relative to that (B_{max}: 0.53 µmol·g wet $tissue^{-1}$) found in RBT acclimated to moderately hard water in this study. Therefore, it appeared that the significantly higher B_{max} values in wild YP collected from extremely softwater lakes compared with hardwater-acclimated YP of our laboratory are in reasonable agreement with previous findings.

Overall, these findings suggest that acclimation to different water hardnesses has considerable effects on Cd as well as Ca binding characteristics in the gills of freshwater fish, manifested as alterations of the binding capacity (B_{max}) for both Cd and Ca. Furthermore, chronic preexposure to waterborne Cd may also have a major influence on the Cd binding properties of the gills and thus could have an effect on gill binding constants for Cd (log K_{Cd} and B_{max}) as well as the acute toxicity of waterborne Cd. Hollis et al. (1999) reported an 11- to 13-fold increase in acute Cd tolerance (increased 96-h LC_{50}) in RBT acclimated to chronic sublethal Cd (26.7 and 88.9 nmol·L^{-1}) in moderately hard water (1 mmol $Ca{\cdot}L^{-1}$).

Finally, although the majority of the work related to the acute BLM was carried out in soft water, our findings were in reasonable agreement with previous observations. The species difference in acute waterborne Cd toxicity was not reflected in the differences in short-term Cd and Ca gill binding characteristics (log K and B_{max}) but rather in the differences of lethal accumulation of Cd in the gills (LA50). However, it appeared that the acute Cd BLM approach developed in RBT (involving high-affinity, low-capacity binding sites) cannot be extended to YP by simple adjustments

© 2004 NRC Canada

of LA50 values because of the probable involvement of a different set of binding sites (low-affinity, high-capacity binding sites) in the gills for the toxic actions of Cd in YP.

In the present versions of BLMs (DiToro et al. 2001; De Schamphelaere and Janssen 2002; Santore et al. 2002), the binding affinity (log K) and binding capacity (B_{max}) values used for a certain metal are fixed for a particular aquatic organism, regardless of its background or chronic history. However, the present findings demonstrated that gill Cd binding characteristics can change under the influence of chronic waterborne factors like hardness and Cd preexposure, which vary greatly from place to place in the real environment, and thus can potentially influence the acute toxicity of waterborne Cd, since metal binding to the gill has a direct bearing on toxicity. Therefore, a more integrative approach, taking these factors into account, is needed for future refinement of the acute Cd BLM for fish to make it applicable in the real environment.

Acknowledgments

We thank D.W. Baker and C. Kamunde for their contribution to this study at McMaster University. Special thanks go to J.W. Rajotte for his great assistance in laboratory work at Laurentian University. This research was supported by the Metals in the Environment Research Network, International Copper Association Inc., Copper Development Association, Falconbridge Ltd., Cominco Ltd., International Lead Zinc Research Organization, Noranda Inc., Nickel Producers Environmental Research Association, and a strategic research grant from the Natural Sciences and Engineering Research Council of Canada. C.M. Wood is supported by the Canada Research Chair program.

References

Alberts, J.J., and Giesy, J.P. 1983. Conditional stability constants of trace metals and naturally occurring humic materials: application in equilibrium models and verification with field data. *In* Aquatic and terrestrial humic materials. *Edited by* R.F. Christman and E.T. Gjessing. Ann Arbor Science Publishers, Ann Arbor, Mich. pp. 333–348.

Block, M., and Pärt, P. 1986. Increased availability of cadmium to perfused rainbow trout (*Salmo gairdneri* Rich.) gills in the presence of the complexing agents diethyl dithiocarbamate, ethyl xanthate and isopropyl xanthate. Aquat. Toxicol. **8**: 295–302.

Calamari, D., Marchetti, R., and Vailati, G. 1980. Influence of water hardness on cadmium toxicity to *Salmo gairdneri* Rich. Water Res. **14**: 1421–1426.

Carrol, J.J., Ellis, S.J., and Oliver, W.S. 1979. Influences of hardness constituents on the acute toxicity of cadmium to brook trout (*Salvelinus fontinalis*). Bull. Environ. Contam. Toxicol. **22**: 575–581.

Couture, P., and Kumar, P.R. 2003. Impairment of metabolic capacities in copper and cadmium contaminated wild yellow perch (*Perca flavescens*). Aquat. Toxicol. **64**: 107–120.

Davies, P.H., Gorman, W.C., Carlson, C.A., and Brinkman, S.F. 1993. Effects of hardness on bioavailability and toxicity of cadmium to rainbow trout. Chem. Speciation Bioavailability, **5**: 67–77.

De Schamphelaere, K.A.C., and Janssen, C.R. 2002. A biotic ligand model predicting acute copper toxicity for *Daphnia magna*: the effect of calcium, magnesium, sodium, potassium, and pH. Environ. Sci. Technol. **36**: 48–54.

DiToro, D.M., Allen, H.E., Bergman, H.L., Meyer, J.S., Paquin, P., and Santore, R.C. 2001. Biotic ligand model of the acute toxicity of metals. 1. Technical basis. Environ. Toxicol. Chem. **20**: 2383–2396.

Erickson, R.J., Benoit, D.A., Mattson, V.R., Nelson, H.P., Jr., and Leonard, E.N. 1996. The effects of water chemistry on the toxicity of copper to fathead minnows. Environ. Toxicol. Chem. **15**: 181–193.

Giesy, J.P., Jr., Leversee, G.J., and Williams, D.R. 1977. Effects of naturally occurring aquatic organic fractions on cadmium toxicity to *Simocephalus serrulatus* (Daphnidae) and *Gambusia affinis* (Poecillidae). Water Res. **11**: 1013–1020.

Hollis, L., Muench, L., and Playle, R.C. 1997. Influence of dissolved organic matter on copper binding, and calcium on cadmium binding, by gills of rainbow trout. J. Fish Biol. **50**: 703–720.

Hollis, L., McGeer, J.C., McDonald, D.G., and Wood, C.M. 1999. Cadmium accumulation, gill Cd binding, acclimation, and physiological effects during long term sublethal Cd exposure in rainbow trout. Aquat. Toxicol. **46**: 101–119.

Hollis, L., McGeer, J.C., McDonald, D.G., and Wood, C.M. 2000*a*. Effects of long term sublethal Cd exposure in rainbow trout during soft water exposure: implications for biotic ligand modelling. Aquat. Toxicol. **51**: 93–105.

Hollis, L., McGeer, J.C., McDonald, D.G., and Wood, C.M. 2000*b*. Protective effects of calcium against waterborne cadmium exposure to juvenile rainbow trout. Environ. Toxicol. Chem. **19**: 2725–2734.

MacRae, R.K., Smith, D.E., Swoboda-Colberg, N., Meyer, J.S., and Bergman, H.L. 1999. Copper binding affinity of rainbow trout (*Oncorhynchus mykiss*) and brook trout (*Salvelinus fontinalis*) gills: implications for assessing bioavailable metal. Environ. Toxicol. Chem. **18**: 1180–1189.

McGeer, J.C., Playle, R.C., Wood, C.M., and Galvez, F. 2000. A physiologically based biotic ligand model for predicting the acute toxicity of waterborne silver to rainbow trout in freshwater. Environ. Sci. Technol. **34**: 4199–4207.

Morel, F.M.M., and Herring, J.G. 1993. Principles and applications of aquatic chemistry. John Wiley, Toronto, Ont.

Niyogi, S., and Wood, C.M. 2003. Effects of chronic waterborne and dietary metal exposures on gill metal-binding: implications for the biotic ligand model. Hum. Ecol. Risk Assess. **9**: 813–846.

Pagenkopf, G.K. 1983. Gill surface interaction model for trace-metal toxicity to fishes: role of complexation, pH, and water hardness. Environ. Sci. Technol. **17**: 342–347.

Paquin, P.R., DiToro, D.M., Santore, R.C., Trivedi, D., and Wu, K.B. 1999. A biotic ligand model of the acute toxicity of metals. III. Application to fish and *Daphnia* exposure to silver. integrated approach to assessing the bioavailability and toxicity of metals in surface waters and sediments. Section 3. A submission to the EPA Science Advisory Board, Office of Water. USEPA-822-E-99-001. Office of Research and Development, Washington, D.C. pp. 3-59–3-102.

Paquin, P.R., Gorsuch, J.W., Apte, S., Batley, G.E., Bowles, K.C., Campbell, P.G.C., Delos, C.G., DiToro, D.M., Dwyer, R.L., Galvez, F., Gensemer, R.W., Goss, G.G., Hogstrand, C., Janssen, C.R., McGeer, J.C., Naddy, R.B., Playle, R.C., Santore, R.C., Schneider, U., Stubblefield, W.A., Wood, C.M., and Wu, K.B. 2002. The biotic ligand model: a historical overview. Comp. Biochem. Physiol. C Comp. Pharmacol. Toxicol. **133**: 3–35.

Pascoe, D., and Beattie, J.H. 1979. Resistance to cadmium by pretreated rainbow trout alevins. J. Fish Biol. **14**: 303–308.

© 2004 NRC Canada

Pascoe, D., Evans, S.A., and Woodworth, J. 1986. Heavy metal toxicity to fish and the influence of water hardness. Arch. Environ. Contam. Toxicol. **15**: 481–487.

Playle, R.C. 1998. Modelling metal interactions at fish gills. Sci. Total Environ. **219**: 147–163.

Playle, R.C., Dixon, D.G., and Burnison, K. 1993*a*. Copper and cadmium binding to fish gills: modifications by dissolved organic carbon and synthetic ligands. Can. J. Fish. Aquat. Sci. **50**: 2667–2677.

Playle, R.C., Dixon, D.G., and Burnison, K. 1993*b*. Copper and cadmium binding to fish gills: estimates of metal–gill stability constants and modelling of metal accumulation. Can. J. Fish. Aquat. Sci. **50**: 2678–2687.

Reid, S.D., and McDonald, D.G. 1988. Effects of cadmium, copper, and low pH on ion fluxes in the rainbow trout, *Salmo gairdneri*. Can. J. Fish. Aquat. Sci. **45**: 244–253.

Reid, S.D., McDonald, D.G., and Rhem, R.R. 1991. Acclimation to sublethal aluminium: modifications of metal – gill surface interactions of juvenile rainbow trout (*Oncorhynchus mykiss*). Can. J. Fish. Aquat. Sci. **48**: 1996–2005.

Richards, J.G., and Playle, R.C. 1998. Cobalt binding to gills of rainbow trout (*Oncorhynchus mykiss*): an equilibrium model. Comp. Biochem. Physiol. C Comp. Pharmacol. Toxicol. **119**: 185–197.

Roch, M., and Maly, E.J. 1979. Relationship of cadmium-induced hypocalcemia with mortality in rainbow trout (*Salmo gairdneri*) and the influence of temperature on toxicity. J. Fish. Res. Board Can. **36**: 1297–1303.

Santore, R.C., DiToro, D.M., Paquin, P., Allen, H.E., and Meyer, J.S. 2001. Biotic ligand model of the acute toxicity of metals. 2. Application to acute copper toxicity in freshwater fish and daphnia. Environ. Toxicol. Chem. **20**: 2397–2402.

Santore, R.C., Mathew, R., Paquin, P.R., and DiToro, D.M. 2002. Application of the biotic ligand model to predicting zinc toxicity to rainbow trout, fathead minnow, and *Daphnia magna*. Comp. Biochem. Physiol. C Comp. Pharmacol. Toxicol. **133**: 271–285.

Schecher, W.D., and McAvoy, D.C. 2001. MINEQL+, user's manual. Environmental Research Software, Edgewater, Md.

Sherwood, G.D., Rasmussen, J.B., Rowan, D.J., Brodeur, J., and Hontela, A. 2000. Bioenergetic costs of heavy metal exposure in yellow perch (*Perca flavescens*): in situ estimates with a radiotracer (^{137}Cs) technique. Can. J. Fish. Aquat. Sci. **57**: 441–450.

Spry, D.J., and Wiener, J.G. 1991. Metal bioavailability and toxicity to fish in low-alkalinity lakes: a critical review. Environ. Pollut. **71**: 243–304.

Szebedinszky, C., McGeer, J.C., McDonald, D.G., and Wood, C.M. 2001. Effects of chronic Cd exposure via the diet or water on internal organ-specific distribution and subsequent gill Cd uptake kinetics in juvenile rainbow trout (*Oncorhynchus mykiss*). Environ. Toxicol. Chem. **20**: 597–607.

Taylor, L.N., Wood, C.M., and McDonald, D.G. 2003. An evaluation of sodium loss and gill metal binding properties to explain species differences in copper tolerance. Environ. Toxicol. Chem. **22**: 2159–2166.

Verbost, P.M., Flik, G., Lock, R.A.C., and Wendelaar Bonga, S.E. 1987. Cadmium inhibition of Ca^{2+} uptake in rainbow trout gills. Am. J. Physiol. **253**: R216–R221.

Verbost, P.M., Van Rooij, J., Flik, G., Lock, R.A.C., and Wendelaar Bonga, S.E. 1989. The movement of cadmium through fresh water trout branchial epithelium and its interference with calcium transport. J. Exp. Biol. **145**: 185–197.

Wicklund-Glynn, A., Norrgren, L., and Müssener, Å. 1994. Differences in uptake or inorganic mercury and cadmium in the gills of zebrafish, *Brachydanio rerio*. Aquat. Toxicol. **30**: 13–26.

Winner, R.W. 1984. The toxicity and bioaccumulation of cadmium and copper as affected by humic acid. Aquat Toxicol. **5**: 267–274.

Wood, C.M. 2001. Toxic responses of the gill. *In* Target organ toxicity in marine and freshwater teleosts. Vol. 1. Organs. *Edited by* D. Schlenk and W.H. Benson. Taylor and Francis, London, U.K. pp. 1–89.

© 2004 NRC Canada

Fish-habitat modeling for gap analysis to conserve the endangered Topeka shiner (*Notropis topeka*)

Steven S. Wall, Charles R. Berry, Jr., Carmen M. Blausey, Jonathan A. Jenks, and Chad J. Kopplin

Abstract: Decision support tools that predict fish distribution over broad spatial scales are needed to assist in planning watershed management and endangered species recovery. We developed a geographical information system model with multivariate logistic regression to rank valley segments for probable occurrence of the endangered Topeka shiner (*Notropis topeka*) using stream condition variables (stream size, groundwater potential, channel slope, streamflow, network position) and land-cover variables (percent pasture, percent trees) in streams characteristic of the North American Great Plains. The stream condition and land-cover models correctly classified 89% and 68% of outcomes (i.e., presence or absence), respectively. Field tests of maps of predicted species distribution resulted in more species occurrences than expected in valley segments classified as high potential for presence and less than expected in low-potential valley segments. Gaps between high-priority segments and protected land parcels were found in all basins. In 37 basins with Topeka shiners, protected land coverage was <1% in 17 basins, 1–5% in 10 basins, and 5–21.8% in 10 basins. Conservation activities in gaps are long-term conservation measures, but maps of predicted species distribution have many immediate applications.

Résumé : La planification de la gestion des bassins versants et du rétablissement des espèces menacées requiert la mise au point d'outils d'aide à la décision afin de prédire la répartition des poissons sur de grandes échelles spatiales. Nous avons conçu un modèle basé sur le système d'information géographique et la régression logistique multidimensionnelle pour coder des sections de vallées quant la probabilité de la présence du méné de Topeka (*Notropis topeka*), une espèce menacée, à partir de variables des conditions hydrographiques (taille du cours d'eau, apport potentiel d'eau phréatique, pente du chenal, débit, position dans le réseau) et du couvert végétal (pourcentage de pâturages, pourcentage d'arbres) dans des cours d'eau typiques de la région des grandes plaines de l'Amérique du Nord. Les modèles basés sur les conditions hydrographiques et le couvert végétal prédisent correctement les répartitions (i.e., présence ou absence) dans respectivement 89 % et 68 % des cas. La vérification sur le terrain des cartes de la répartition prédite de l'espèce indique plus de présences que prévu dans les sections classifiées comme possédant un bon potentiel de présence et moins que prévu dans les sections à faible potentiel. Il existe dans tous les bassins des zones de discontinuité entre les sections de cours d'eau de priorité élevée et les parcelles de terres protégées. Dans 37 bassins qui abritent le méné de Topeka, la surface couverte par les terres protégées représente <1 % dans 17 bassins, 1–5 % dans dix bassins et 5–21,8 % dans dix bassins. Les activités de conservation dans les zones de discontinuité sont des mesures à long terme; néanmoins, les cartes de prédiction de la répartition des espèces possèdent de multiples usages immédiats.

[Traduit par la Rédaction]

Introduction

The declining number of freshwater fishes across the world indicates a decrease in biodiversity and health of freshwater ecosystems. In North America, 364 of an estimated 1061 freshwater fish species (34%) are in need of protection (Williams et al. 1989; Warren and Burr 1994). Anthropogenic activities that result in habitat degradation have been cited as the leading cause of decline in freshwater fishes (Richter et al. 1997). Aquatic resource managers need decision support tools that identify potential fish distributions, (e.g., fish-habitat models; Olden and Jackson 2001; Filipe et al. 2002) and locations for conservation activities (e.g., gap analysis; Scott et al. 1993; Groves et al. 2002). In general, gap analysis seeks to identify "gaps" between a "target" for conservation and lands managed for natural resource conservation, such as public lands managed primarily for native species and natural ecosystems. Three general classes of conservation targets are (*i*) communities or ecosystems, (*ii*) abiotic targets based on physical variables, and (*iii*) special rare, endemic, indicator, or keystone species (Jennings 2000).

Many fish-habitat models are based on local-scale habitat, but transferability of model application between streams and watersheds has proved difficult (Dunham and Vinyard 1997). However, watershed-scale models are needed (Labbe and Fausch 2000) because watershed management is becoming a

Received 28 October 2002. Accepted 30 November 2003. Published on the NRC Research Press Web site at http://cjfas.nrc.ca on 24 July 2004.
J17158

S.S. Wall,[1] C.M. Blausey, J.A. Jenks, and C.J. Kopplin. Department of Wildlife and Fisheries Sciences, South Dakota State University, Brookings, SD 57007, USA.
C.R. Berry, Jr. US Geological Survey (BRD), South Dakota Fish and Wildlife Cooperative Research Unit, South Dakota State University, Brookings, SD 57007, USA.

[1]Corresponding author (e-mail: steven_wall@sdstate.edu).

 doi: 10.1139/F04-017 © 2004 NRC Canada

Fig. 1. Study area showing five ecoregional drainage units in South Dakota, USA, where Topeka shiners (*Notropis topeka*) were found that differ in biotic and abiotic features. EDU1, Great Plains steppe – James River drainage; EDU2, prairie parkland (temperate) – Lower Big Sioux and Vermillion River drainage; EDU3, prairie parkland (temperate) – Upper Big Sioux River drainage; EDU4, prairie parkland (temperate) – James River drainage; EDU5, Great Plains Palouse dry steppe – James River drainage.

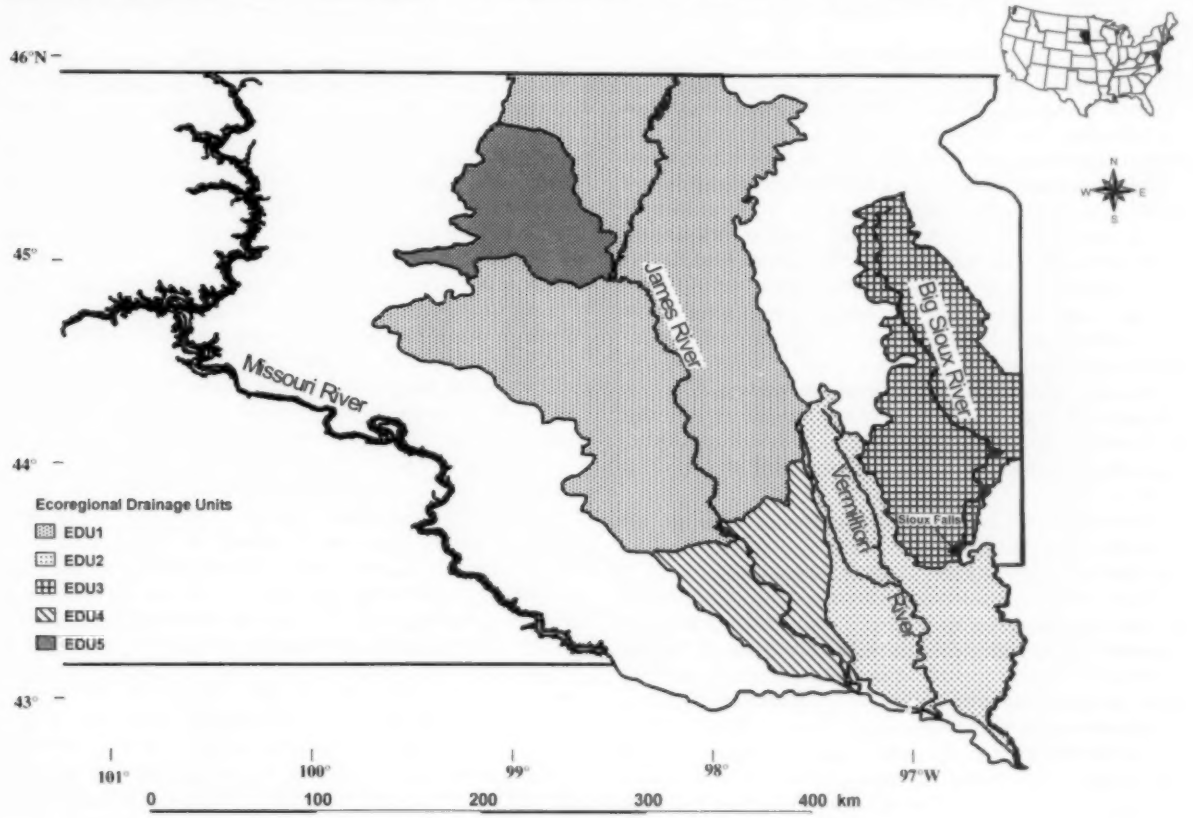

common fish conservation approach (Naiman 1992; Stroud 1992) and many species cover large geographic regions. Geographic information systems (GIS) meet this need for describing species distributions in a large spatial context. GIS can predict probable species occurrences based on habitat features at broad spatial scales and identify land areas needed to protect rare species of both terrestrial (e.g., Buehler 1995; Mladenoff et al. 1995; Sperduto and Congalton 1996) and aquatic organisms (e.g., Angermeier and Bailey 1992; Hoehn 1998; Gregr and Trites 2001). With this information, a portfolio of potential conservation lands can be assembled that includes sites for acquisition, easements, or other conservation practices potentially useful for conserving species. However, this approach has not been widely used and never for aquatic species of the dynamic rivers and streams of the Great Plains.

The Topeka shiner (*Notropis topeka*) is a small, stout minnow found in small streams in six Great Plains states (Iowa, Kansas, Minnesota, Missouri, Nebraska, South Dakota). Because of an estimated 80% reduction in occurrence of this species, the US Fish and Wildlife Service listed the species as endangered in January 1999 (Tabor 1998). Decline of this species has been attributed to habitat deterioration caused by siltation, channelization, and impoundments and predation by stocked fish (Tabor 1998; Schrank et al. 2001). Information on distribution and habitat requirements of the shiner was lacking (Tabor 1998). The Topeka shiner had been recorded in 24 streams in our study area before 1999. Our surveys (Blausey 2001) and unpublished data from other workers since 1999 confirmed its presence in 14 streams where it had been found and discovered the species in 21 new streams.

The goal of our study was to conduct a gap analysis to assist in Topeka shiner conservation planning. Specific objectives were (*i*) to identify habitat features associated with Topeka shiner presence at a large spatial scale, (*ii*) to predict the potential distribution of Topeka shiners based on habitat relationships, (*iii*) to test our model using independent data from field sampling, and (*iv*) to determine gaps between parcels of conservation land and segments of stream with some probability of Topeka shiner presence.

Methods

Study area

The study area included three major drainages where the Topeka shiner was historically found in eastern South Dakota (Fig. 1). Major drainages have been partitioned into

© 2004 NRC Canada

Table 1. List of modeled habitat variables, occurrence of each variable in five ecoregional drainage units (EDUs), and percent in valley segments with Topeka shiners and in all available valley segments.

Habitat variable and numeric code[a]	Number of EDUs with habitat (n = 5)	Valley segments with events (%) (n = 64)	Available valley segments (%) (n = 8693)
Stream size class			
1, headwater (link = 0 to 9)	5	29.3	79.5
2, creek (link = 10 to 75)	5	46.1	12.6
3, small river (link = 76 to 1500)	4	23.1	5.8
4, large river (link > 1500)	3	1.5	2.2
Channel slope class			
1, low (headwater <0.0043; creek <0.0009; small river <0.0004; large river <0.0004)	5	63.1	57.1
2, medium (headwater 0.0043 to 0.0087; creek 0.0009 to 0.0019; small river 0.0004 to 0.0022; large river 0.0004 to 0.0005)	5	33.8	21.8
3, high (headwater >0.0087; creek >0.0019; small river >0.0022; large river >0.0005)	5	3.1	21.1
Network position class			
0, none (no discrepancy, e.g., headwater to headwater)	5	80.0	81.8
1, headwater to creek (link = 0 to 9 and d-link = 10 to 75)	5	9.3	11.9
2, headwater to small river (link = 0 to 9 and d-link = 76 to 1500)	4	1.5	3.3
3, headwater to large river (link = 0 to 9 and d-link > 1500)	3	1.5	2.2
4, creek to small river (link = 10 to 75 and d-link = 76 to 1500)	4	4.6	0.7
5, creek to large river (link = 10 to 75 and d-link > 1500)	3	3.1	0.3
6, small river to large river (link = 76 to 1500 and d-link > 1500)	2	0.0	0.05
Parent material class			
1, alluvium	5	92.3	47.6
4, glacial till	5	3.1	25.9
9, outwash	5	3.1	17.0
8, loess	4	1.5	3.2
6, Sioux quartzite	2	0.0	1.1
14, shale	1	0.0	0.5
Other (i.e., eolian sands (3), silty glacial till (5), lacustrine (7), ponded soils (13))	5	0.0	4.7
Streamflow			
1, perennial (has surface water throughout the year in all years except during extreme drought, approximately once every 100 years)	5	12.3	8.3
2, intermittent (has surface water for most of the year)	5	69.2	19.0
3, seasonal (has surface water during growing season but is absent by the end of the season in most years)	5	18.5	50.3
4, temporary (has surface water for brief periods during the growing season)	5	0.0	22.6
Groundwater potential			
1, low	5	23	74.0
2, medium	5	29	15.5
3, high	5	48	10.5
Downstream connectivity			
0, no	5	98.5	96.4
1, yes	5	1.5	3.6
Upstream connectivity			
0, no	5	98.5	96.4
1, yes	5	1.5	3.6

© 2004 NRC Canada

Table 1 (*concluded*).

Habitat variable and numeric code[a]	Number of EDUs with habitat (n = 5)	Valley segments with events (%) (n = 64)	Available valley segments (%) (n = 8693)
Floodplain influence			
1, yes	4	4.6	3.3
2, no	5	95.4	96.7

[a]A hypothetical concatenated code for first three variables is 123123001, meaning headwater, medium slope, and network position of headwater to large river, alluvium, intermittent flow, high groundwater potential, no downstream connectivity, no upstream connectivity, floodplain influence.

subbasins termed hydrologic units that are given standardized codes (US Geological Survey 1974). Subbasins with an 11-digit hydrologic unit code (HUC) are from 16 000 ha to about 100 000 ha and are nested within an 8-digit HUC, which is from 100 000 ha to about 180 000 ha. Streams in these drainages are typically warm-water, low-gradient, moderately turbid streams that flow through pastures and farmed fields. Streamflows are usually quite variable and segments of some streams may become intermittent. Fish communities in such streams are largely affected by abiotic factors, which are predominantly systemic (e.g., climate, watershed features) but also local (e.g., riparian vegetation, substrate), rather than by biotic factors (Poff and Ward 1989).

We used historical data (South Dakota Game, Fish and Parks 2000) and data from field studies in 1999 and 2000 (Wall et al. 2001) to identify valley segments with Topeka shiners. A valley segment is a stream segment that can be as long as 60 km and is relatively homogeneous with respect to hydrology, topography, and geology. Valley segment delineation was based on a hierarchical classification system (Lammert et al. 1996) and procedures used by Sowa (1999*a*, 1999*b*). We used aquatic gap analysis protocols from Sowa (1998) with some modifications to identify systemic, stream condition, and land-cover variables for building GIS layers. We then associated systemic variables at the watershed and ecoregion scale and landscape variables at the valley segment scale with Topeka shiner presence. We used logistic regression to model stream conditions and land cover associated with Topeka shiner presence and combined these two models within a GIS to produce maps showing actual and predicted fish distribution.

GIS analysis was done using ArcView 3.2 (Environmental Systems Research Institute 1999), ARC/INFO version 8.2 (Environmental Systems Research Institute 2000), and ARC/INFO AMLs (Arc Macro Language) supplied by The Nature Conservancy (The Nature Conservancy Freshwater Initiative 2000).

Systemic variables

The study area was separated into five ecoregional drainage units (Fig. 1). An ecoregional drainage unit (EDU; Sowa 1999*a*) is part of a major drainage within an ecoregional province, which Bailey (1995) defines as a large landscape area that has uniform biotic and abiotic features. An EDU has a unique fish community because of geographic isolation by linear stream distance or natural barriers and also has unique stream features (Whittier et al. 1988; Lyons 1989).

The Upper Big Sioux River drainage is located above the Sioux Falls, which is a natural barrier to fish movement and fosters different fish communities above and below the falls (Kirby 2001; Milewski 2001). The Lower Big Sioux River drainage downstream from the falls was combined with the Vermillion River drainage to form the Lower Big Sioux – Vermillion River drainage based on similarities in fish community and geology and influence of the Missouri River. The James River drainage was the third major drainage based on the flat topography and fish-community similarities of the basin (Shearer 2001).

The EDU boundary was defined by the boundary of the major drainage if >90% of the drainage was located within one ecoregional province. Where a major drainage was divided by an ecoregional province, the EDU boundary was defined by the 11-digit hydrological unit boundaries closest to the provincial boundary to maintain hydroconnectivity.

Stream condition variables

River reach 3 files (RF3) at a scale of 1 : 100 000 formed the base hydrography layer (US Environmental Protection Agency 1999). Water bodies that were not part of the main watershed network (i.e., isolated streams and lacustrine and palustrine wetlands) were removed. Nine landscape-scale variables were used to classify valley segments according to a standard aquatic classification system (Lammert et al. 1996), literature (e.g., Lyons 1996), and expert opinion. In general, numeric values were assigned to stream-habitat features (Table 1), and the numeric values were concatenated to form a 9-digit code for each valley segment.

Stream size was determined by the Shreve link number. Shreve links were calculated for each RF3 stream segment using VISUAL BASIC (The Nature Conservancy Freshwater Initiative 2000). Stream size classes were headwaters, creeks, and small or large rivers (Table 1).

For streamflow, National Wetland Inventory (NWI) map layers were overlaid with the RF3 hydrography layer in ArcView. NWI flow regime classifications (Cowardin et al. 1979) were attributed to each segment in the RF3 data file. Line vectors representing a stream segment were attributed with the code of NWI wetland polygons that intersected the majority of the vector. System, subsystem, and water regime modifier codes (US Fish and Wildlife Service 1993) were used to classify each segment as perennial, intermittent, seasonal, or temporary (Table 1).

Dominant parent materials were identified using soil map units in the Soil Survey Geographic (SSURGO) database; the State Soil Geographic (STATSGO) database was used when SSURGO data were unavailable (US Department of Agriculture 1991, 1995). A parent material layer was created in ArcView by merging soil map units with similar dominant parent materials into polygons to create 10 parent material classes (Table 1).

Groundwater delivery was estimated using the MRI-DARCY groundwater model (Baker et al. 2000), a GIS application of

© 2004 NRC Canada

Darcy's Law, which states that groundwater velocity is proportional to hydraulic slope multiplied by hydraulic conductivity. Data sets needed for the MRI-DARCY model are a digital elevation model (DEM) of 30-m^2 grid cells and hydraulic conductivity values for each corresponding grid cell in the DEM. Hydraulic slope was estimated using changes in elevation from the DEM. The common ranges of texture, wetness, landscape position, salt content, permeability, and slope were used to assign hydraulic conductivity to parent materials. Hydraulic conductivity values were assigned to soil map units based on the median range of permeability (US Department of Agriculture 1996). Soil layers of contrasting permeability were assigned dual hydraulic conductivities. When the second soil series had slower hydraulic conductivity than did the dominant soil, we assigned the permeability ranges as minor and major, respectively. A hydraulic conductivity value in both permeability classes depended on the depth and composition of each soil layer (Wall et al. 2001). For parent materials from STATSGO, the hydraulic conductivity was the average value for the material. Grid cells with groundwater velocities less than the moderately slow class (US Department of Agriculture 1996) were assigned low groundwater delivery potential, cells with velocities in the moderate class were assigned medium potential, and cells in the rapid class were assigned high potential. RF3 stream segments were overlaid on MRI-DARCY output grids and attributed as high, medium, or low groundwater potential by the highest groundwater potential that intersected the segment (Table 1).

Channel slope for each segment was the average change in elevation from the DEM grid over segment length. Slope is associated with stream size (i.e., slope ranges decrease as stream size increases) and EDU physiogeographic characteristics (Sowa 1999*a*); thus slope classes were determined separately for each stream size class (e.g., headwater) by EDU. The upper and lower 10% of the slope ranges were excluded to eliminate outliers, and the middle 80% was divided into equal size classes termed high, medium, and low (Table 1).

Network position was determined using downstream link (d-link) of stream segments (Osborne and Wiley 1992). Downstream link refers to the Shreve link number of the next downstream segment and was calculated for each stream segment in the RF3 file. Six network position codes increased with increasing d-link number (Table 1).

A segment was judged in the floodplain of a larger river by using a GIS layer of slope created with the DEM for the major river basins. Major breaks in slope revealed the valley wall, and segments >250 m long in the floodplain were classified as floodplain segments. A stream segment was classified as connected upstream or downstream to a lake. Lakes were water bodies >1 ha in the RF3 database.

All streams within our study area were classified as warmwater streams. Blausey (2001) found Topeka shiners in streams with summer temperatures of 17–30.7 °C, which was similar to water temperatures found in streams throughout the study area.

Land-cover variables

The percent area of 11 cover types (Table 2) within the riparian zone was determined using a 30-m^2-grid map of land cover interpreted from 1992 Landsat imagery (Smith et al. 2002). We used ArcView to create 30-m buffer strips, which is a width recommended for stream conservation (US Department of Agriculture 1999). Because vectors representing streams in a GIS have no width, buffer width was 30 m plus one-half × average mean stream width measured by Blausey (2001) plus 1 standard deviation (SD). The 30-m^2-grid map was resampled to determine land cover in 5-m^2 cells. We calculated percent land cover, ratio of cultivated land to uncultivated land, and ratio of cultivated land to overall wetlands in each 30-m buffer.

Data analysis and modeling

Topeka shiner locations recorded before 2000 were used to attribute valley segments (n = 64; Fig. 2) as having the shiner present (termed "events"), whereas segments with no record of Topeka shiners were termed "nonevents". Valley segments classified as lakes or large rivers were not considered in analysis because Topeka shiners are associated with low-order streams (Tabor 1998).

Chi-square and analysis of variance (ANOVA) were used to determine if valley segments could be pooled for analysis (i.e., no differences among EDUs) or if they should be analyzed separately by EDU (i.e., differences among EDUs). Differences in habitat among EDUs may indicate differences in available habitat for Topeka shiners and thus different habitat associations.

To identify important stream-habitat variables, we randomly chose three times as many nonevents as events to account for differences in variance resulting from the difference in the number of nonevents to events as recommended for analysis (Pereira and Itami 1991; Sperduto and Congalton 1996). Chi-square analysis was used to identify stream-habitat variables significant in distinguishing events from nonevents for each EDU. Multivariate analysis was preformed using stepwise selection procedures to further identify significant variables in all EDUs combined. Identified variables were then assessed for biological meaning according to methods of Hosmer and Lemeshow (1989). Selected variables were analyzed using a logistic regression model.

We compared percent land cover within 30-m buffers of valley segments with and without events between 1982 and 2000. The random sample of nonevents had the same proportion of segments classified as headwaters, creeks, small rivers, and large rivers as did the sample of events to eliminate bias (Vannote et al. 1980; Wiley et al. 1990). A two-tailed t test was used to compare land cover surrounding events to land cover surrounding nonevents. Instances of unequal variances were accounted for using the Satterthwaite method (SAS Institute Inc. 1994). Variables significant (α = 0.05) to Topeka shiner presence were used in a logistic regression model.

A logistic regression model was used to determine habitat differences between events and nonevents for stream condition and land-cover variables. Land-cover variables were analyzed separately to determine land management practices influencing Topeka shiner populations. Logistic regression was an appropriate model because it allows for independent variables that are both quantitative and qualitative (Hosmer and Lemeshow 1989). Furthermore, logistic regression output describes two possible classes, which fit the binary nature of our data (i.e., events and nonevents). Variables that

© 2004 NRC Canada

Table 2. List of modeled land-cover variables and results of two-tailed *t* tests with 95% confidence intervals (CI) showing percent land-cover comparisons between 30-m riparian buffers surrounding valley segments where Topeka shiners had been found between 1982 and 1999 (events) with those where the shiner had not been found (nonevents) in eastern South Dakota.

Land-cover class	*n*	Topeka shiners found	Mean	CI	*p*
Cultivated land (row crop)	171	Nonevent	22.18	18.62–25.73	0.0591
	56	Event	17.04	13.00–21.08	
Hay land	171	Nonevent	4.84	3.69–6.00	0.7369
	56	Event	4.51	2.98–6.05	
Idle grass	171	Nonevent	6.61	5.33–7.88	0.6485
	56	Event	7.18	5.30–9.05	
Pasture	171	Nonevent	30.54	27.67–33.41	0.0011
	56	Event	38.63	34.75–42.51	
Trees	171	Nonevent	3.32	2.61–4.02	0.0387
	56	Event	4.77	3.64–5.91	
Semipermanent wetland	171	Nonevent	6.06	4.23–7.89	0.3060
	56	Event	4.47	1.97–6.96	
Seasonal wetland	171	Nonevent	5.73	4.36–7.11	0.4259
	56	Event	4.81	2.94–6.67	
Temporary wetland	171	Nonevent	2.24	1.55–2.94	0.1723
	56	Event	1.41	0.42–2.40	
Riverine wetland	171	Nonevent	17.92	14.87–20.98	0.3259
	56	Event	15.89	13.16–18.62	
Permanent wetland	171	Nonevent	0.27	–0.08–0.62	0.8191
	56	Event	0.35	–0.26–0.96	
Urban	171	Nonevent	0.29	0.01–0.57	0.3617
	56	Event	0.94	–0.45–2.33	
Wetlands (semipermanent + seasonal + temporary + riverine + permanent wetlands)	171	Nonevent	32.22	29.03–35.42	0.0157
	56	Event	26.92	24.01–29.83	
Grasses (hay land + idle grass + pasture)	171	Nonevent	41.99	38.77–45.20	0.0015
	56	Event	50.33	46.33–54.32	
(Cultivated land)·(wetlands)$^{-1}$	170	Nonevent	4.64	1.06–8.23	0.0330
	56	Event	0.74	0.53–0.94	
(Cultivated land)·(Uncultivated land (wetlands + grasses + trees))$^{-1}$	171	Nonevent	1.12	0.41–1.83	0.0215
	56	Event	0.27	0.17–0.37	

were associated with Topeka shiner presence by chi-square analysis (stream conditions), *t* tests (land-cover habitat), and a stepwise selection procedure (significance level entry of $\alpha = 0.5$ and a significance level stay of $\alpha = 0.05$) were used in the modeling process. An omnibus likelihood test, which is analogous to the omnibus *F* test in ANOVA or regression, was used to test the significance of modeled variables (SAS Institute Inc. 1994). The Hosmer–Lemeshow test was used to test model variables as "adequate" descriptors of the data, adequate meaning small error, small unexplained variability, and goodness-of-fit (Hosmer and Lemeshow 1989).

Categorical values of stream-condition variables and percent values for land cover were inserted into the logistic regression equation to calculate the probability of occurrence of Topeka shiners in each valley segment. A "cut point" was determined using the ROC (receiver operating characteristic) curve (SAS Institute Inc. 1994), which is a plot of sensitivity (the measure of accuracy for predicting events) vs. 1 – specificity (the measure of accuracy for predicting nonevents). The graph point at which specificity was equal to sensitivity was used to determine the cut point, which is often the probability at which the prediction of events and nonevents are both maximized. Valley segments with probability values equal to or greater than the probability at the cut point were classified as likely locations for Topeka shiners, whereas valley segments with probabilities below the cut-point value were classified as unlikely (Olden and Jackson 2001).

To classify valley segments into categories of high, high-to-moderate (Mod1), moderate-to-low (Mod2), and low potential for Topeka shiners (Table 3), we used model output for stream conditions and land cover, NWI data on stream modifications (e.g., excavation), fish presence (an event), and watershed geology. More importance was given to stream conditions indicative of Topeka shiner presence from modeling (89% accuracy) than to those from land cover (68% accuracy). Segments classified as high potential had both indicative stream conditions and land cover and were in watersheds with documented Topeka shiner presence. The Mod1 class included valley segments with both indicative stream conditions and land cover in watersheds without events and valley segments with only indicative stream conditions in watersheds with events. The Mod2 class included segments with indicative stream conditions but not land cover in watersheds without events, whereas in watersheds with events, Mod2 included valley segments with indicative land cover only. Segments with low probability had no indicative stream conditions, had modifications, or were within water-

© 2004 NRC Canada

Fig. 2. Geographic information system (GIS) model showing the probability of Topeka shiner (*Notropis topeka*) presence for each valley segment, location of sites used in model (before 2000), and location of field test sites where Topeka shiners were found and not found (after 1999).

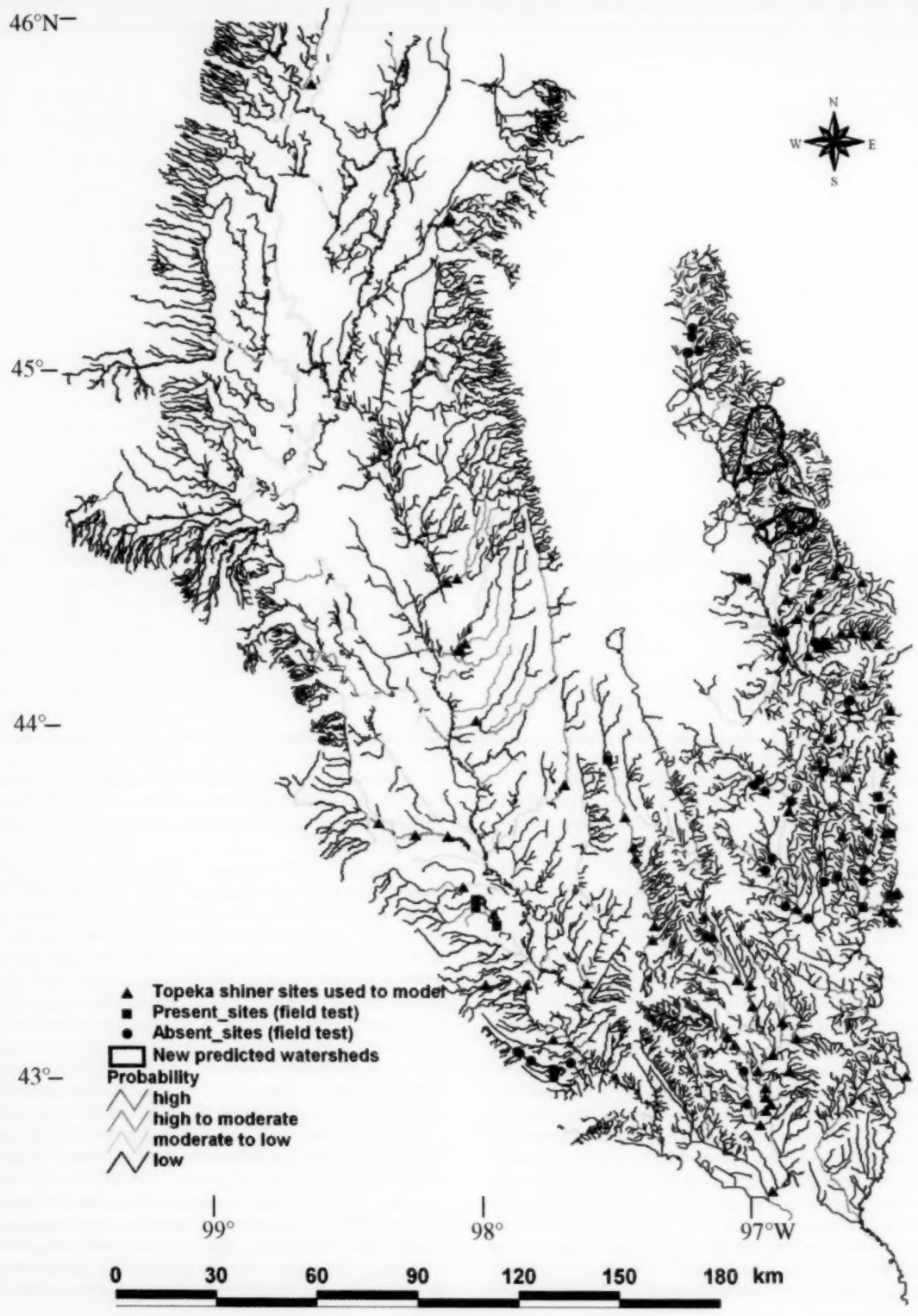

© 2004 NRC Canada

Table 3. Criteria for assigning four probability classes as high, high to moderate (Mod1), moderate to low (Mod2), and low to valley segments for presence of Topeka shiners, and total stream length (km) in each probability class by ecoregional drainage unit (EDU[a]) in eastern South Dakota.

Probability	Event (shiner found)	Suitable physical habitat	Suitable land cover	Stream length (km) EDU1	EDU2	EDU3	EDU4	EDU5
High	Yes	Yes	Yes	367	420	159	117	0
	No[b]	Yes	Yes					
Mod1	Yes	No	Yes	515	253	352	88	35
	Yes	Yes	No					
	Yes	No	No					
	No	Yes	Yes					
Mod2	No	Yes	No	695	278	346	137	142
	No	No	Yes[b]					
Low[c]	No	No	No	10 137	5068	5356	2389	1598
	No	No	Yes					

[a]EDU1, Great Plains steppe – James River drainage; EDU2, prairie parkland (temperate) – Lower Big Sioux and Vermillion River drainage; EDU3, prairie parkland (temperate) – Upper Big Sioux River drainage; EDU4, prairie parkland (temperate) – James River drainage; EDU5, Great Plains Palouse dry steppe – James River drainage.

[b]Segment is in a watershed where Topeka shiner was found.

[c]Modified valley segments (e.g., channelized, impounded, or drained) were classified as low for Topeka shiner presence, except when a Topeka shiner was found in a modified segment, then that segment was classified as Mod1.

sheds dominated by lacustrine parent materials, which contradict Topeka shiner presence (Wall et al. 2001).

We superimposed fish presence events on the modeling results to give valley segment classes more practical meaning because the presence of an endangered species is often the primary impetus for conservation activity. Consequently, our Mod1 class included streams with events regardless of habitat or the presence of stream modifications.

We field-tested the model because Topeka shiners were relatively abundant in South Dakota (Wall et al. 2001) and other surveys were underway to supply independent data. Other surveyors used one-pass seining at the reach scale (US Geological Survey 2001, 2002; Cunningham 2002; C. Milewski, Paul Smith College, Paul Smith, NY 12970, USA, personal communication), as did we (Blausey 2001). From other studies, we used presence–absence data from 53 sites distributed randomly throughout the James, Vermillion, and Big Sioux River basins but not in the same valley segments as those used in models. We compared observed and expected presence–absence data of Topeka shiners among valley segments classed as high, moderate, and low using chi-square analysis.

Gap analysis

We used standardized methods to map and classify conservation lands (Jennings 2000; Smith 2001) and developed a novel means of inventorying protected stream segments. In general, the first step was to obtain digital files of boundaries of public land and identify the land steward of 16-ha mapping units making up the study area. We obtained data from US agencies (e.g., US Fish and Wildlife Service, National Park Service, National Resources Conservation Service), state and local agencies (e.g., South Dakota Department of Game, Fish and Parks, municipalities), and nongovernmental conservation groups (e.g., The Nature Conservancy).

We next assigned one of four status codes for the degree of land protection in each conservation parcel. Status 1 denoted permanent protection from land-cover conversion, such as that found in most national parks. Status 2 denoted permanent protection but with uses that might degrade existing natural communities somewhat (e.g., wildlife food plots in a state park). Status 3 denoted permanent protection but with extractive uses that were low intensity (e.g., logging) or localized (e.g., mining). Status 3 group was larger than the others because of numerous permanent conservation easements in wetlands, grasslands, and riparian areas that the US Fish and Wildlife Service has on private land. We probably underestimated this group because the most recent data are for years before 1995. Status 4 was usually assigned to private lands that had no legal mandates to prevent natural habitat conversion or had short-term conservation easements (e.g., 10-year grassland reserve easements). Much private land is well managed, but the intent of the gap analysis program is long-term habitat conservation.

We summarized the amount of land in each conservation status in each stream basin and developed maps showing the spatial arrangement of conservation lands relative to stream segments that had been assigned probability values for Topeka shiner presence. High-priority valley segments that intersected or were adjacent to conservation land polygons were considered "protected". We used ArcView to summarize the number and length of protected valley segments.

Results

Systemic variables

Five EDUs were created (Fig. 1). The occurrence of eight habitat variables (frequency) and gradient (mean) were unequal among EDUs (chi-square and ANOVA, $p < 0.0001$, $\alpha = 0.05$; Table 1). However, Topeka shiners were associated with similar habitat in each EDU (Appendix A). For example, in each EDU, about 30% of the events were in headwater stream segments, but about 80% of the segments were classed as headwaters (Table 1). Stream size, streamflow, parent material, and groundwater potential were significantly

© 2004 NRC Canada

Table 4. Stream-condition variables and probability of association with Topeka shiner presence in each ecoregional drainage unit (EDU)[a] in eastern South Dakota.

	EDU1			EDU2			EDU3			EDU4		
Habitat variable[b]	χ^2	df	p	χ^2	df	p	χ^2	df	p	χ^2	df	p
Stream size	18.492	2	<0.0001	27.452	3	<0.0001	31.418	2	<0.0001	6.824	2	0.0330
Streamflow	31.429	2	<0.0001	30.508	2	<0.0001	19.781	3	0.0002	8.089	3	0.0442
Channel slope	1.968	2	0.3738	1.581	2	0.4537	10.030	2	0.0066	2.564	2	0.2775
Groundwater potential	26.531	2	<0.0001	23.250	2	<0.0001	8.087	2	0.0045	1.832	2	0.1760
Network position	5.081	3	0.1660	1.376	4	0.8484	6.529	3	0.0872	3.644	3	0.3025
Floodplain interaction[c]	***	0	***	0.070	1	0.7918	0.741	1	0.3894	0.351	1	0.5536
Parent material	9.600	3	0.0223	16.807	6	0.0100	13.388	5	0.0200	8.148	2	0.0170
Downstream connectivity	1.081	2	0.5820	2.109	2	0.3484	2.963	1	0.2273	0.351	1	0.5536
Upstream connectivity	1.467	2	0.4803	2.361	2	0.3071	2.963	1	0.2273	0.351	1	0.5536

[a]EDU1, Great Plains steppe – James River drainage; EDU2, prairie parkland (temperate) – Lower Big Sioux and Vermillion River drainage; EDU3, prairie parkland (temperate) – Upper Big Sioux River drainage; EDU4, prairie parkland (temperate) – James River drainage; no Topeka shiners were found in EDU5 (Great Plains Palouse dry steppe – James River drainage).

[b]Degrees of freedom for habitat variables varies among EDUs as number of variable classes differs among EDUs (e.g., in EDU1 stream size classes range from 1 (headwater) to 3 (small river) (df = 2), whereas in EDU2, stream size classes range from 1 (headwater) to 4 (large river) (df = 3).

[c]Floodplain interaction did not process for EDU1 as the data set used for analysis did not contain a valley segment with floodplain interaction (i.e., $n = 1$).

Table 5. Number of valley segments and types of valley segments with Topeka shiners (events), and total valley segment numbers for each ecoregional drainage unit in eastern South Dakota.

	Valley segments		Valley segment types	
Ecoregional drainage unit (EDU)	Total	With events	Total	With events
Prairie parkland (temperate) – Upper Big Sioux River drainage (3)	2104	19	555	12
Prairie parkland (temperate) – Lower Big Sioux and Vermillion River drainage (2)	1943	30	501	19
Prairie parkland (temperate) – James River drainage (4)	798	5	286	5
Great Plains steppe – James River drainage (1)	3259	11	669	8
Great Plains Palouse dry steppe – James River drainage (5)	589	0	206	0
Total	8693	65	2217	44

associated with events in at least three of four EDUs, whereas floodplain interaction, connectivity, network position, and channel slope were usually not associated with an event (Table 4). We also found redundant valley segment types among EDUs for the 64 segments with events, indicating that Topeka shiners were associated with similar habitat in each EDU. In EDU1, for example, 19 of the 555 valley segments with an event comprised 12 segment types (Table 5). There were 44 segments with events in all EDUs, but when redundant codes were removed, the 44 segments were composed of 31 segment types. Because of the similarities in event-associated habitat among EDUs, we combined valley segments from all EDUs into one model.

Stream-condition variables

Stream size, streamflow, and parent material were associated with Topeka shiner presence ($p < 0.05$) in all EDUs (Table 4), as was groundwater potential ($p < 0.05$) in three EDUs. Topeka shiners were found in valley segments with high groundwater three times more than were available, whereas they occurred less frequently in valley segments with low groundwater potential than were available (Table 1). Channel slope was associated ($p < 0.05$) with Topeka shiner presence in EDU3 (Table 4).

Descriptive statistics showed that percent of events in occupied habitat was unrelated to the percent of overall available habitat for all EDUs (Table 1). Topeka shiners were found most frequently in valley segments with stream sizes classified as creeks and small rivers, with alluvium parent material, with intermittent streamflow, and with medium to high groundwater potential when compared with frequency of available habitat. Frequency of occurrence of the shiner in valley segments with high channel slope was proportionally less (3.1%) than the 21.1% of valley segments with high channel slope available. Valley segments with a stream size classification of creek were associated most frequently with Topeka shiners in all EDUs except EDU2, where small rivers were associated most frequently with fish presence (Appendix A).

Stepwise regression indicated that stream size ($p = 0.0032$), groundwater potential ($p = 0.0001$), streamflow ($p = 0.0097$), channel slope ($p = 0.0300$), and network position ($p = 0.0152$) were significant to the logistic modeling process for all EDUs combined. Parent material was not significant in the stepwise regression, although it was in χ^2 tests for each individual EDU. When using multivariate analysis, some variables could be excluded from the model because of interactions with a closely related variable (i.e., parent material and groundwater potential), and others may be added (i.e., network position and channel slope) depending on how all variables interacted (SAS Institute Inc. 1994). An omnibus likelihood significance test for $H_0 = \beta_{\text{stream size}} =$

© 2004 NRC Canada

Table 6. Odds ratio estimates and confidence limits for each variable used in the logistic regression models to predict the presence or absence of Topeka shiners in eastern South Dakota.

	Point estimate	95% Wald	Confidence limits
Physical variable			
Stream size	2.813	1.414	5.594
Groundwater potential	2.465	1.556	3.904
Streamflow	0.402	0.201	0.802
Channel slope	0.506	0.273	0.0936
Network position	1.585	1.093	2.297
Land-use variable			
Percent pasture	1.028	1.009	1.046
Percent trees	1.075	1.009	1.146

$\beta_{\text{groundwater potential}} = \beta_{\text{streamflow}} = \beta_{\text{channel slope}} = \beta_{\text{network position}} = 0$, indicated that the variables entered into the model were significant ($\chi^2 = 102$, df = 5, $p < 0.0001$). The Hosmer–Lemeshow goodness-of-fit test (Hosmer and Lemeshow 1989) indicated that the model was statistically adequate ($\chi^2 = 9.4$, df = 7, $p = 0.2232$). The following equations were generated from the logistic regression model to calculate the probability of likely stream conditions for Topeka shiners.

$$(1) \quad Y = -1.2641 + 1.0342(\text{stream size}) + 0.9022(\text{groundwater potential}) - 0.9122(\text{streamflow}) - 0.6819(\text{channel slope}) + 0.4603(\text{network position})$$

$$(2) \quad p_{\text{likely habitat}} = e^{Y}(1 + e^{Y})^{-1}$$

where $p_{\text{likely habitat}}$ is the probability of likely habitat for Topeka shiners.

The odds ratios, which indicate the type and degree of association of variables with an event (SAS Institute Inc. 1994), indicated that increases in stream size, groundwater potential, and stream network position were associated with an increase in the probability of Topeka shiner presence (Table 6). As streamflow values increased from perennial to temporary, and as channel slope values increased, the odds for Topeka shiner presence decreased. The optimum cutoff point between likely and unlikely habitat estimated from the ROC curve was approximately 0.289. Values of variables making up each valley segment were entered into logistic regression eqs. 1 and 2 to determine which segment types had likely or unlikely habitat for Topeka shiners. Valley segments were classified in the GIS as having likely habitat with probability ≥0.289 according to the ROC curve (Olden and Jackson 2001) and unlikely habitat with probability <0.289. The model had a c value of 0.89 (i.e., ½(1 – Somers' D statistic) = 0), indicating a measure of predictive power of 89%.

Land-cover variables

The 30-m riparian buffers around segments with events had more pasture ($p = 0.0011$), trees ($p = 0.0387$), and grasses ($p = 0.0015$) and less wetlands ($p = 0.0157$) than did nonevent segments (Table 2). The ratios of cultivated land to uncultivated land ($p = 0.0215$) and cultivated land to wetlands ($p = 0.0330$) were less in 30-m buffers surrounding event segments than in buffers around nonevent segments. Stepwise regression using variables identified by the two-tailed t test showed that percentages of pasture ($p = 0.0031$) and trees ($p = 0.0255$) in 30-m buffers were significant to the logistic modeling process. An omnibus likelihood significance test for $H_0 = \beta_{\%\ \text{pasture}} = \beta_{\%\ \text{trees}} = 0$ showed that variables entered into the model were significant ($\chi^2 = 13.2$, df = 2, $p < 0.0013$). The Hosmer–Lemeshow goodness-of-fit test showed that the model was statistically adequate ($\chi^2 = 13.1$, df = 8, $p = 0.1073$).

Equations 3 and 4 were generated from the logistic regression model using percent pasture and percent trees to calculate the probability of suitable land cover within a 30-m buffer for Topeka shiners:

$$(3) \quad Y = -2.3516 + 0.0272(\%\ \text{pasture}) + 0.0727(\%\ \text{trees})$$

$$(4) \quad p_{\text{suitable land}} = e^{Y}(1 + e^{Y})^{-1}$$

where $p_{\text{suitable land}}$ is the probability of suitable land cover for Topeka shiner presence.

Odds ratios (Table 6) showed that for every unit of increase in percent pasture, the odds of finding Topeka shiners increased by about 1.028. For every unit increase in percent trees, the odds of finding Topeka shiners increased by about 1.075. The optimum cutoff point between likely and unlikely land cover within a 30-m buffer estimated from the ROC curve was about 0.365. The resulting model had a c value of 0.675, indicating a measure of predictive power of 67.5%. The logistic regression equation was applied to the 30-m buffer surrounding each valley segment. Each valley segment was classified as having likely ($p \geq 0.0365$) or unlikely ($p < 0.0365$) land cover within its 30-m buffer.

GIS model

GIS maps were produced showing the probability of Topeka shiner presence for valley segments (Fig. 2). EDU2 had the greatest length of valley segments classified as having high probability for Topeka shiner presence, followed by EDU1, EDU3, EDU4, and EDU5 (Table 3). The rank (highest to lowest) of EDUs by stream classified as having moderate to high probability for Topeka shiners was EDU1 > EDU3 > EDU2 > EDU4 > EDU5 (Table 3). The model predicted that 41 tributaries where the Topeka shiner has not been previously found had high potential for presence (Wall et al. 2001).

Topeka shiners were found at 16 of 53 test sites. Two new events occurred in predicted valley segments (Mod1, Mod2) in watersheds without previous record of Topeka shiners (Fig. 2), and one new event occurred in a stream with no recorded events but in a watershed that had events. Other new events occurred in watersheds with known events, and absences were usually recorded in watersheds without events. For example, in high-potential valley segments, one new event occurred adjacent to a known-event segment, and six new-event segments were separated from known-event segments by 2, 3, 5, 10, 12, and 21 km of stream with less predicted potential. Of 37 observed absences, 27 occurred in valley segments classified as Mod1, Mod2, and low potential in watersheds without events, and in six valley segments

© 2004 NRC Canada

classified as Mod1, Mod2, and low potential in watersheds with events. Four observed absences occurred in high-potential valley segments within watersheds with events.

There were differences ($\chi^2 = 10.11$, df = 3, $p < 0.05$) between observed and expected events and between observed and expected nonevents among high-probability, Mod1, Mod2, and low-probability classes (Table 7). The predictive ability was best demonstrated in the high- and low-probability classes. For example, in the high-probability class, four events were expected and eight were observed, whereas eight nonevents were expected but four were observed. In the low-probability class, 13 nonevents were expected and 15 were observed. Predictive ability was less for the Mod1 and Mod2 classes in that less events ($n = 4$) were observed than expected ($n = 6$).

Table 7. Observed and expected events and nonevents in classes of high, moderate-to-high (Mod1), moderate-to-low (Mod2), and low probability for Topeka shiner presence comparing observations from field tests with geographic information system (GIS) model predictions ($\chi^2 = 10.11$, df = 3, $p < 0.05$).

	Event		Nonevent	
Valley segment classification	Observed	Expected[a]	Observed	Expected[a]
High	8	4[b]	4	8
Mod1	2	4[b]	12	10
Mod2	2	2[b]	6	6
Low	4	6	15	13

[a]Value rounded to nearest whole number.
[b]When a value of 1 was added to each cell ($n = 16$) to account for cell values < 5, chi-square results remained significant ($\chi^2 = 8.33$, df = 3, $p < 0.05$).

Gap analysis

Lands in conservation statuses 1, 2, and 3 comprised 2.9% of the Big Sioux River basin area, 5.8% of the Vermillion River basin, and 14.8% of the James River basin (Table 8). In 17 of 37 subbasins with Topeka shiner records, the amount of land under conservation was <1%, and nine subbasins had no protected lands. In 10 subbasins, 1.0–5.0% was protected, and in 10 subbasins ≥5% of the land was in some conservation status (Fig. 3).

Topeka shiner presence had little relation to the amount of protected land in a basin (Table 8). Some watersheds where the fish had not been found since 1999 had 10% to 20% of the basin in some conservation status (e.g., Redstone Creek, 18.8%) and some had little or none in conservation (Flandreau Creek, 0%). Conversely, some streams with recent records had some protected land (e.g., Camp Creek, 6.8%) and some had little (e.g., Pipestone Creek, 0%).

About 1093 km in 221 valley segments were designated as high-priority, Topeka shiner habitat. When we overlaid the conservation lands map on the high-priority valley segment map, we found that only 22 valley segments (42 km) intersected a conservation land parcel (Table 9).

Three watershed maps represent three general patterns of conservation land distribution (Fig. 4). The first pattern suggests that existing conservation lands may protect nearby high-potential stream segments (Fig. 4*a*) and headwater areas in general (Fig. 4*b*). The second pattern indicates a gap between existing conservation lands and high-priority stream segments and headwater areas (Fig. 4*b*). Finally, conservations lands are absent in some subbasins with Topeka shiners and much stream distance designated high priority (Fig. 4*c*). About 3% of the Big Sioux Basin is protected, but 8 of 14 subbasins with Topeka shiners had no protected lands (Table 8).

Discussion

We used a multivariate approach (i.e., logistic regression) applied to a GIS to model habitat associated with the Topeka shiner. Many earlier GIS models of species–habitat relationships were based on literature review and univaritate statistics (e.g., Agee et al. 1989; Breininger et al. 1991; Buehler 1995). Logistic regression allows for the interactions of multiple independent variables (both quantitative and qualitative) and describes two possible classes (i.e., presence or absence). Several species–habitat models have used logistic regression (e.g., Mladenoff et al. 1995; Austin et al. 1996; Bian and West 1997) using a threshold for presence or absence equal to a probability of 0.5. However, a threshold of 0.5 does not necessarily account for model sensitivity (accuracy for predicting presence) and specificity (accuracy for predicting absence) (Olden and Jackson 2001). We chose a decision threshold (i.e., cut point) for presence or absence using a probability that maximized (i.e., sensitivity = specificity) prediction of both presence and absence from the ROC curve. Use of the ROC curve can result in a more powerful model by balancing errors of omission and commission (Olden and Jackson 2001) and was similar to methods used by Pereira and Itami (1991) to predict the occurrence of an endangered mammal. Because the Topeka shiner is endangered, we might have adjusted the model to include instances of omission by increasing the sensitivity, but such adjustments are subjective and problematic (Olden and Jackson 2001).

Valley segment habitat features and 30-m stream buffer conditions can be used to predict the presence of the Topeka shiner but may not necessarily indicate cause-and-effect relationships. Habitat variables significant in the model may be surrogates for other variables that influence Topeka shiner distribution. The logistic regression model using stream conditions showed agreement (89%) between predicted Topeka shiner distribution and occurrence in valley segments, and the model using land-cover features showed 68% agreement. Temporal changes in land cover (i.e., 15% land conversion to row crop since 1992 in the Big Sioux River Basin; unpublished data) probably contributed to lower accuracy of the land-cover model, whereas stream conditions at the valley segment scale are more stable (Frissell et al. 1986), lending to higher accuracy.

Systemic variables

Comparison of systemic variables at the catchment scale (e.g., land cover, geology) showed little difference between catchments with Topeka shiners and those without (Wall et al. 2001). Systemic controls important to the Topeka shiner at this scale appear to be somewhat intact and similar across the species range in South Dakota. We found Topeka shiners in 71% of the historic sites (Blausey 2001) compared with

© 2004 NRC Canada

Table 8. Watersheds with high priority habitat for the Topeka shiner, history of occurrence of Topeka shiner, and amount of land area protected in four categories of conservation status in eastern South Dakota.

Watershed and subbasin	Year that Topeka shiners found		Area (ha) in conservation status				Protected	
	Before 1999	1999–2000	1	2	3	4	ha	%
Big Sioux River basin			101	5 653	26 464	1 064 230	32 218	2.9
Brookfield Creek		▲	0	0	0	714	0	0.0
Flandreau Creek	■		0	0	0	5 627	0	0.0
Beaver Creek[a]		▲	0	0	63	11 883	63	0.5
Hidewood Creek		▲	0	0	0	24 391	0	0.0
Medary Creek	■	▲	19	0	45	27 503	64	0.2
N. Deer Creek	■	▲	0	0	25	32 194	25	0.1
Deer Creek		▲	0	0	0	18 212	0	0.0
Pipestone Creek[a]	■	▲	0	0	0	17 992	0	0.0
Six-Mile Creek	■	▲	0	0	387	18 837	387	2.0
Slip-up Creek		▲	0	0	0	8 421	0	0.0
Split Rock Creek[a]	■	▲	0	0	84	14 122	84	0.6
Spring Creek[a]		▲	0	0	0	12 399	0	0.0
W. Pipestone Creek	■	▲	0	0	0	22 478	0	0.0
Willow Creek	■		0	0	116	12 060	116	1.0
Vermillion River Basin			7	7 225	26 093	545 539	33 325	5.8
Blind Creek		▲	0	0	0	13 319	0	0.0
Camp Creek		▲	0	385	663	14 332	1 048	6.8
E. Fork Vermillion River	■		0	477	1 364	35 386	1 842	4.9
Long Creek		▲	0	26	144	19 232	170	1.0
Saddle Creek		▲	0	0	76	25 198	76	0.3
Turkey Ridge Creek	■	▲	0	11	153	45 743	164	0.4
Vermillion River 1	■	▲	0	68	4 119	46 717	4 187	8.2
Vermillion River 2	■	▲	0	266	2 715	56 704	2 981	5.0
W. Fork Vermillion River1	■	▲	0	9	98	27 051	107	0.4
W. Fork Vermillion River1	■	▲	0	1 494	141	36 172	1 635	4.3
James River Basin			8 913	11 580	465 439	2 801 611	485 932	14.8
Elm River[a]	■		0	0	28 369	101 903	28 369	21.8
Enemy Creek	■	▲	0	0	1 955	47 807	1 955	3.9
Firesteel Creek	■	▲	0	62	2 213	62 973	2 275	3.5
W. Firesteel Creek	■		0	150	3 276	35 570	3 426	8.8
Middle Pearl Creek	■	▲	0	0	1 435	12 645	1 435	10.2
Pearl Creek	■	▲	0	517	1 982	26 279	2 499	8.7
Shue Creek	■	▲	0	0	1 181	44 793	1 181	2.6
Dry Creek		▲	0	170	476	29 256	646	2.2
LoneTree Creek		▲	0	6	250	28 545	256	0.9
Twelve Mile Creek	■	▲	0	190	713	69 646	903	1.3
Rock Creek		▲	0	475	13 486	59 137	13 961	19.1
Redstone Creek	■		0	76	14 421	62 481	14 497	18.8
Wolf Creek	■		0	840	9 002	87 535	9 842	10.1

Note: Status 1, permanent protection from conversion of land cover; status 2, permanent protection but with uses that might degrade existing natural communities somewhat; status 3, permanent protection with extractive uses that were low intensity; status 4, private lands that have no legal mandates to prevent conversion of natural habitat types. Symbols indicating historical Topeka shiner presence match those used in each subbasin in Fig. 3.

[a]Percent conservation status calculated in South Dakota portion of the watershed, which has headwaters in Minnesota.

20% elsewhere in its range (Tabor 1998). Only 3% of the streams in our study basins have been altered by channelization (Johnson and Higgins 1997), and only about 30% of the wetlands drained compared with higher percentages in other parts of the range of this species (Dahl 1990). Additionally, conservation practices of individual landowners and short-term conservation easements have probably contributed to the persistence of the Topeka shiner and other native fishes. Stream conditions associated with Topeka shiners were similar across all EDUs even though distribution of stream conditions was significantly different among EDUs. Because systemic variables and stream conditions influencing the distribution of Topeka shiners were similar in all EDUs, the GIS model was based on stream conditions and land-cover variables at the valley segment scale.

Stream condition model

Stream conditions at the landscape scale significant to Topeka shiner presence were stream size, streamflow, groundwater delivery to streams, channel slope, and network

© 2004 NRC Canada

Fig. 3. Percent of conserved land in subbasins of the James, Vermillion, and Big Sioux watersheds where Topeka shiners (*Notropis topeka*) have been found in South Dakota and Minnesota.

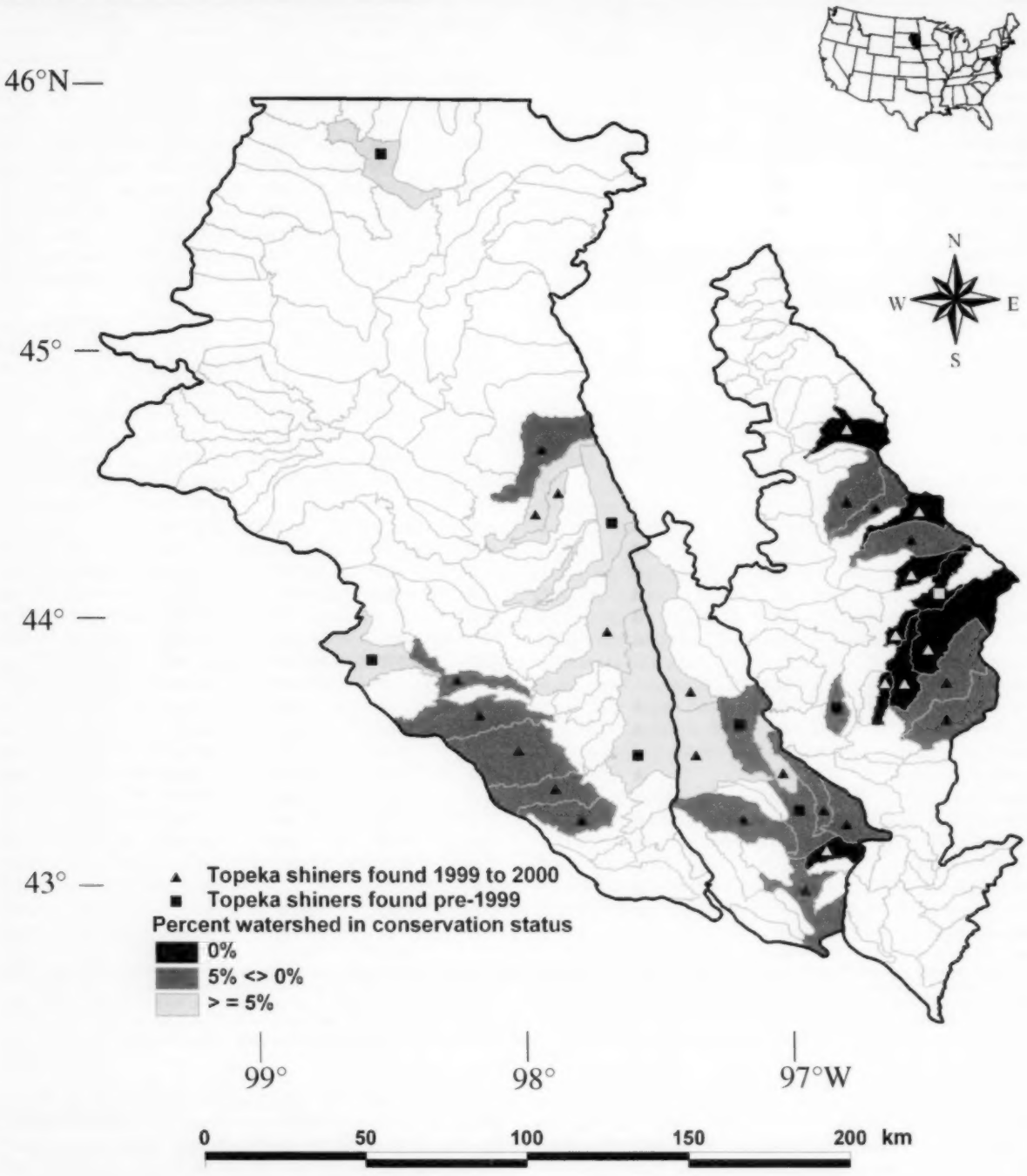

position. Others have associated Topeka shiners with similar factors (Clark 2000; Schrank et al. 2001). We associated Topeka shiners with streams classified as creeks and small rivers. Although Topeka shiners are considered a headwater fish (Cross and Collins 1995; Pflieger 1997; Tabor 1998), most of the segments classified as headwaters in our GIS model were temporary. Valley segments classified as creeks to small rivers were in lower-order streams that have some flow stability; however, these streams also are intermittent at times (Milewski 2001). The odds of finding a Topeka shiner

© 2004 NRC Canada

Table 9. Number of valley segments classified as high-potential, Topeka shiner habitat in the three South Dakota river basins and number and length of high-potential valley segments intersecting a conservation land parcel.

		Conserved segments	
River basin	No. of segments	Number	Length (km)
Big Sioux	78	4	5.9
James	68	14	25.6
Vermillion	75	4	10.8

increased as network position increased, so species presence is more likely upstream from a confluence than in the receiving stream.

The probability of Topeka shiner presence increased as streamflow changed from temporary to perennial. Our study area receives about 40% of the 400–610 mm of annual precipitation from May to June and is greatly influenced by spates and droughts. Topeka shiners often occurred in segments classed as intermittent with a high potential for groundwater delivery, which are conditions that seem contradictory. Such conditions exist in our study streams because seasonal flows vary greatly and shallow aquifers have localized groundwater inputs to streams. An intermittent midbasin stream section often separates flowing sections near headwaters and termini. The length of the intermittent section and the size of isolated pools are important to Topeka shiners (Tabor 1998) but vary with precipitation and depth of the water table. Greater streambed – water table intersection would occur in segments with low channel slope, and our data suggested that the probability of Topeka shiner presence increased as channel slope decreased. Low channel slopes foster low water velocities, which have also been associated with Topeka shiner presence (Kerns 1981; Barber 1986; Adams et al. 2000).

Topeka shiners seem to have higher reproductive success when streams become intermittent and form shallow, groundwater-fed pools than during periods of higher flow (Minckley and Cross 1959). One possible hypothesis is that the Topeka shiner has a spawning strategy that uses sunfish nests as clean spawning substrate (Pflieger 1997), unlike other nest-building species that depend on flow to scour silt from nests. Topeka shiners have been observed and recently filmed spawning over sunfish nests (Pflieger 1997; G. Sneegas, Kansas Biological Survey, University of Kansas, Lawrence, KS 66045, USA, personal communication).

Land-cover model

Conditions that conserve riverine habitat were more abundant in the 30-m riparian zone around valley segments with events than in segments without events. A 30-m buffer with a mix of trees, grass, and shrubs has been suggested as a minimum for protecting streams in Midwest agricultural settings (Schultz et al. 1996). Topeka shiner sites had more pasture, trees, grasses, uncultivated lands, and overall wetlands than nonevent sites. Association of Topeka shiners with less cultivated land and more pasture in 30-m buffers surrounding valley segments agrees with Blausey's (2001) findings at the reach scale, where riparian grasses and forbs were positively related to Topeka shiner presence. Results of our land-cover analysis of pastures suggest that livestock use can coincide with Topeka shiner presence. Blausey (2001) found that a high level of animal use was negatively associated with the shiner; however, well-managed grazing practices can protect streams with rare species (e.g., Topeka shiner, Niangua darter (*Etheostoma nianguae*)) and improve the economics of ranching operations (H. Kerns, Missouri Department of Conservation, St. Joseph, MO 64507, USA, personal communication).

Presence of trees is not commonly associated with Topeka shiners and was negatively associated with Topeka shiner presence at the reach scale (Clark 2000; Blausey 2001). Presence of trees in the 30-m buffer may be a surrogate for uncultivated land or low grazing (Smith and Flake 1983), which may be important to Topeka shiner presence (Minckley and Cross 1959; Pflieger 1997; Tabor 1998).

GIS model

Statistical accuracy of our model was relatively high (i.e., c values of 0.89 and 0.675); however, caution is warranted when models are verified using resubstitutional methods (Olden et al. 2002). Olden et al. (2002) suggest using a bootstrap approach to further scrutinize model accuracy. Instead, we employed a field test using fish collected at sites independent of our model predictions, which should provide a more robust test of model predictions (true classification) than by statistical means only. Topeka shiners are not excessively rare in South Dakota, reducing bias from low occurrence (Olden et al. 2002).

In our field tests, Topeka shiners were observed more than expected in valley segments classified as high potential for presence and were observed less than expected in low-potential valley segments. Because many valley segments with observations were located in subbasins (11-digit HUC) with historic records of Topeka shiners, spatial autocorrelation bias was possible. Spatial autocorrelation (i.e., similarity between sites correlated with distance between sites) is a natural phenomenon of ecological systems at all spatial scales (Legendre 1993). Our model was designed to account for this phenomenon by giving higher probability to valley segments in subbasins with events than to those outside. Certain findings at the valley segment scale indicate that spatial autocorrelation was minimized within subbasins. For example, new field observations were separated by many valley segment types from 2 to 21 km from historic observation sites, and one new field observation was made in a stream where the species was previously unknown. Two new field observations also were made in valley segments with potential habitat in subbasins without historic records. Ability of the model to identify disjunct valley segments as potential habitat demonstrates its usefulness at this scale.

Our model may be useful for designing future studies, as others with less (e.g., 18%) accuracy have been (Sperduto and Congalton 1996), by identifying high-priority segments within a stream. In a high-priority segment, Topeka shiner distribution is patchy because the species is associated with certain macrohabitat types and biotic factors at the reach scale (Blausey 2001). Surveyors should use adequate sampling effort to allow for discontinuity in fish distributions (Angermeier et al. 2002).

© 2004 NRC Canada

Fig. 4. Three subbasin maps showing three types of gaps between land parcels in three conservation classes and stream segments in four classes of habitat priority (red, high; green, moderate to high; orange, low to moderate; blue, low priority habitat) for the Topeka shiner (*Notropis topeka*). (*a*) Some headwaters and high-priority segments touch protected parcels; (*b*) gaps between protected land and high-priority habitat and headwaters; (*c*) little to no protected land. ●, Topeka shiner locations. Subbasins are not to scale. Conservation classes indicate protection of natural conditions that is complete (status 1), allows land-cover management that may cause minor degradation (status 2), or extractive uses that are localized or low intensity (status 3).

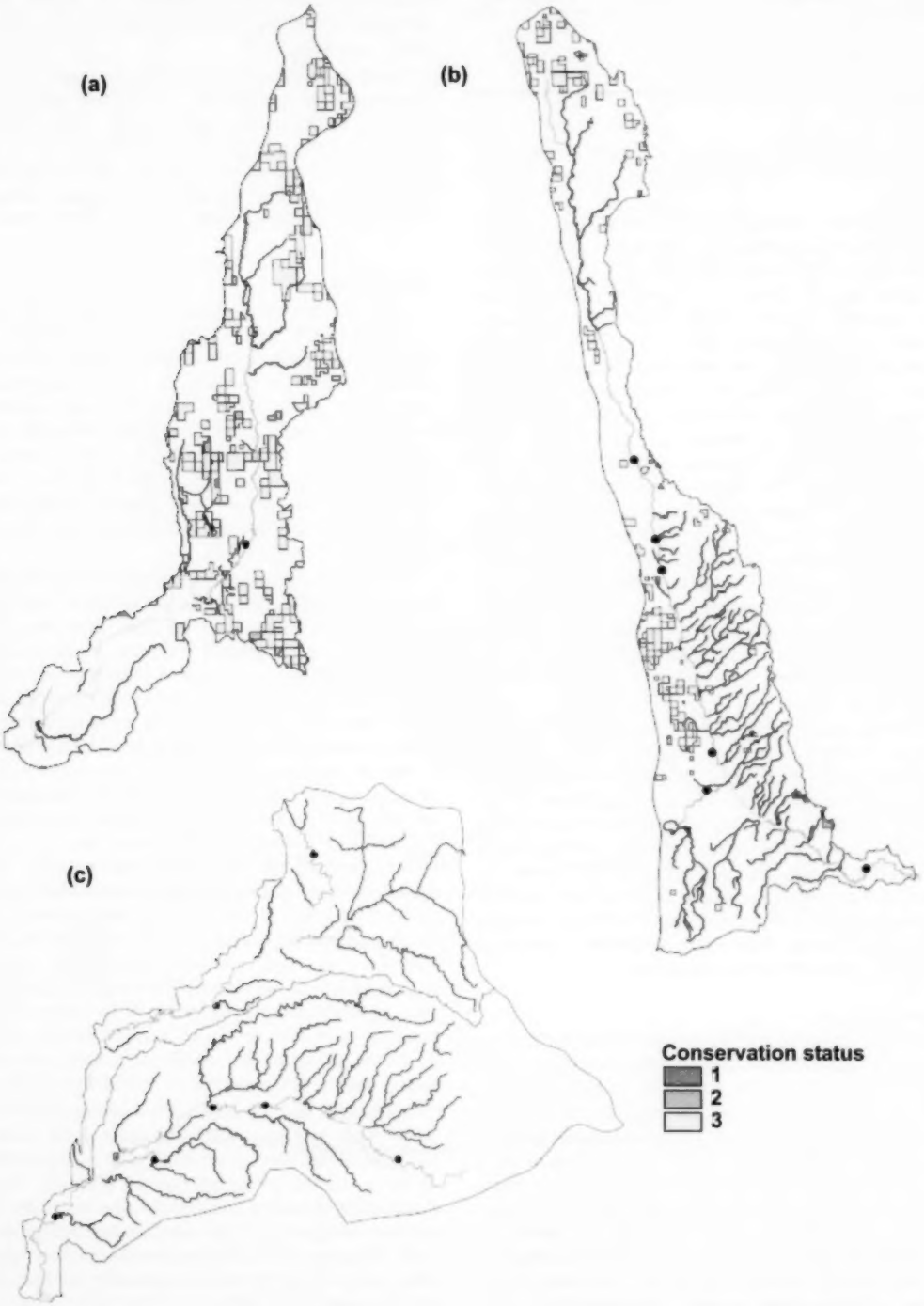

© 2004 NRC Canada

Model accuracy was affected by the inherent inaccuracies of GIS methods (Goodchild and Gopal 1989), by the pioneering nature of the species, by stream periodicity, and by inadequate representation of stream types sampled. More sampling has been done in stream segments classified as creeks to large rivers than in seasonal streams, thus perhaps biasing the model. Also, we sometimes found Topeka shiners in temporarily wet (i.e., classed as seasonal flow in this study), low-potential valley segments, thus indicating errors of omission (false nonevents). Topeka shiners may use the temporarily wetted segments as velocity refuges (Kerns 1981; Barber 1986; Adams et al. 2000) as they do off-channel habitats (Clark 2000; Dahle 2001). Errors of commission were indicated when Topeka shiners were not found in high-probability valley segments. For example, a high-probability valley segment may be dry but still be important to Topeka shiners, which is in a guild of pioneering species (Blausey 2001). We observed recolonization of previously dry stream segments, as have others (Minckley and Cross 1959; Barber 1986; Braaten 1993).

Low population size may have caused additional errors of omission and commission. Topeka shiners and most species usually comprise a small portion of the total fish community (e.g., Braaten 1993; Cunningham 1999; Wall et al. 2001), so it was difficult to identify true present sites. Conversely, it was impossible to identify true absence sites, so our random selection of nonevent sites used in the model possibly included some segments that actually had Topeka shiners. A model assumption was that habitat features associated with Topeka shiners would be less frequent in randomly chosen segments than in segments where presence was confirmed.

Gap analysis

A seven-step protocol for using gap analysis to conserve biodiversity has been suggested (Groves et al. 2002). We have provided information needed for most of the steps: step 1, identify conservation target; step 2, collect information; step 3, set conservation goals; step 4, assess existing areas; step 5, evaluate target persistence; step 6, assemble area portfolio; and step 7, identify priority areas. Our analysis suggests actions at several scales to protect the Topeka shiner.

At the regional scale, focus might be on ecological drainage units with the most high-priority habitat (e.g., EDU1, EDU2) or where fish reproduction is good, stressors few (e.g., landscape change, introduced species), and ecological processes intact (e.g., hydrograph). However, planning at the watershed scale is more practical because of the connection between watershed processes and health of riverine biota (Williams et al. 1997). How much of the landscape to reserve as conservation land is unknown, but levels of 10% to 20% have been mentioned for terrestrial species (Scott et al. 1993; Soule and Sanjayan 1998; Jennings 2000) or broader conservation objectives (Ontario Ministry of Natural Resources 1999). Five subbasins in the James River Basin have 10–20% of land area under conservation, but the spatial distribution of conservation lands leaves 95% of the high-priority stream segments unprotected.

We expected to find gaps because existing conservation lands were not intended for conservation of aquatic species. Some streams where Topeka shiners were frequently found had no conservation lands, whereas some streams where the species was rarely found had almost 20% of the watershed conserved. Placing conservation areas with the goal of conserving stream habitat should protect aquatic species better than ad hoc methods (Karr and Schlosser 1978; Whitworth and Martin 1990). However, where should gaps be filled? Most conservation land might be along headwater streams (watershed of <150 km^2) because of the strength of local controls on habitat in these streams (Roth et al. 1996; Milewski 2001). Furthermore, protecting headwater areas may temper large-scale factors (e.g., stream power, sediment load, flow regime) that can negate the benefits of restoration measures farther downstream (Frissell et al. 1986; Frissell and Nawa 1992). Conservation activities should be implemented to unite fragmented high-priority segments.

As originally intended for the gap analysis program, we can suggest where to place new reserves or conservation easements to fill gaps between high-priority Topeka shiner habitat and established conservation lands. However, establishing effective reserves is complex and scale-dependent (Schwartz 1999; Poiani et al. 2000). As an alternative to reserves, agencies might fill gaps by conservation activities on private lands, such as cost-sharing riparian fencing, providing livestock watering methods, implementing grazing programs, and establishing buffer strips. These methods might increase riparian habitat diversity and probably aquatic biodiversity (Whitworth and Martin 1990; Davie and Lant 1994; Cushing and Allen 2001). Riparian habitat factors associated with species presence are vegetated banks and managed livestock use, as well as other reach-scale factors (e.g., run macrohabitat and gravel or cobble substrate; Blausey 2001).

Maps of potential species distributions have uses other than identifying conservation gaps. Our maps have been used to identify sites where special permits might be needed to make land-use changes, to plan Topeka shiner recovery and critical habitat (defined in National Research Council 1995), and to assess the potential impact of agriculture and roadway construction. Furthermore, our maps indicate that future searches for Topeka shiner populations should focus on high-priority segments in several unsurveyed streams. Watersheds with much high-priority habitat might be sites for reintroduction, assuming that the landscape-scale variables that we associated with Topeka shiner presence are surrogates for conditions needed by the species.

In conclusion, the purpose of our research was to model landscape-scale variables derived from remote sensing and GIS to predict the possible distribution of Topeka shiners and use the models in an aquatic gap analysis. Our approach for modeling stream fish at large spatial scales uses variables that are relatively easy to create within a GIS from available data sets and may be useful for predicting species occurrences across watersheds and perhaps ecoregions. Distribution of the Topeka shiner was based on associations with certain landscape-scale variables (i.e., stream size, streamflow, groundwater potential, channel slope, network position, riparian zone conditions) that characterize small creeks to small rivers that may be intermittent. The utility of the model was validated by field tests. The gap analysis resulted in several recommendations for species conservation, but it is premature to assess effectiveness (Short and Hestbeck 1995; Jennings 2000; Shaffer et al. 2002). Nevertheless, other ben-

© 2004 NRC Canada

efits have accrued that might be used for triage while the long-term benefits are being evaluated.

Acknowledgements

We would like to thank the South Dakota Gap Analysis Project for providing many of the GIS layers needed for our model. We thank S. Sowa, M. Morey, and G. Annis, Missouri River Assessment Partnership (MoRAP), for aquatic gap methodology and tools used in GIS modeling. J. Higgins, M. Lammert, and T. FitzHugh, The Nature Conservancy, assisted with the use of GIS tools and the classification framework used in models. M. Baker, M. Wiley, and P. Seelbach allowed the use of the MRI-DARCY model to model groundwater. B. Kunze, Natural Resource Conservation Service, helped with interpreting the SSURGO soil database. M. Estey and M. Kjellsen, National Wetlands Inventory, supplied the GIS layer of wetlands. D. Backland, South Dakota Natural Heritage Program, provided the database of Topeka shiner locations. T. Wittig, South Dakota State University, advised on statistical methods. C. Pierce (Iowa State University, Ames, Iowa), I. Schlosser (University of North Dakota, Grand Forks, N.D.), J. Erickson (South Dakota Game, Fish and Parks, Rapid City, S.D.), E. Peters (University of Nebraska, Lincoln, Nebr.), and C. Milewski (Dakota State University, Madison, S.D.) advised on fish habitat and ecology. The US Fish and Wildlife Service, US Geological Survey – Biological Resources Division, US Army Corps of Engineers, and the US Environmental Protection Agency funded the project. We thank all those who reviewed and commented on this manuscript to improve its quality.

References

Adams, S.R., Hoover, J.J., and Killgore, K.J. 2000. Swimming performance of the Topeka shiner (*Notropis topeka*), an endangered midwestern minnow. Am. Midl. Nat. **144**: 178–186.

Agee, J.K., Stitt, S.C.F., Nyquist, M., and Root, R. 1989. A geographic analysis of historic grizzly bear sightings in the North Cascades. Photogr. ER, **55**(11): 1637–1642.

Angermeier, P.L., and Bailey, A. 1992. Use of geographic information systems in the conservation of rivers in Virginia, USA. *In* River conservation and management. *Edited by* P.J. Boon, P. Calow, and G.E. Petts. John Wiley and Sons. New York. pp. 151–160.

Angermeier, P.L., Krueger K.L., and Dolloff, C.A. 2002. Discontinuity in stream-fish distributions: implications for assessing and predicting species occurrence. *In* Predicting species occurrences: issues of accuracy and scale. *Edited by* J.M. Scott, P.J. Heglund, M.L. Morrison, J.B. Haufler, M.G. Raphael, W.A. Wall, and F.B. Samson. Island Press, Washington, D.C. pp. 519–528.

Austin, G.E., Thomas, C.J., Houston, D.C., and Thompson, D.B.A. 1996. Predicting the spatial distribution of buzzard *Buteo buteo* nesting areas using geographical information system and remote sensing. J. Appl. Ecol. **33**: 1541–1550.

Bailey, R.G. 1995. Description of the ecoregions of the United States. 2nd ed. (revised and expanded (1st ed. 1980). Misc. Publ. No. 1391 (rev.), US Department of Agriculture Forest Service, Washington, D.C.

Baker, M.E., Wiley, M.J., and Seelbach, P.W. 2000. Spatially explicit models of groundwater loading in glaciated landscapes: considerations and development in Lower Michigan. Michigan Department of Natural Resources, Fisheries Division, Box 30446, Lansing, Mich.

Barber, J.A. 1986. Ecology of Topeka shiners in Flint Hills streams. M.Sc. thesis, Emporia State University, Emporia, Kansas.

Bian, L., and, West, E. 1997. GIS modeling of elk calving habitat in a prairies environment with statistics. Photogr. ER, **63**(2): 161–167.

Blausey, C.M. 2001. The status and distribution of the Topeka shiner *Notropis topeka* in eastern South Dakota. M.Sc. thesis, South Dakota State University, Brookings, S.D.

Braaten, P.J. 1993. The influence of habitat structure and environmental variability on habitat use by fish in the Vermillion River, South Dakota. M.Sc. thesis, South Dakota State University, Brookings, S.D.

Breininger, D.R., Provancha, M.J., and Smith, R.B. 1991. Mapping Florida scrub jay habitat for purposes of land-use management. Photogr. ER, **57**(11): 1467–1474.

Buehler, D.A. 1995. A geographic information system to identify potential bald eagle breeding habitat for southeastern United States rivers and reservoirs. Proc. Annu. Conf. Southeast. Assoc. Fish Wildl. Agencies, **49**: 292–302.

Clark, S.J. 2000. Relationship of Topeka shiner distribution to geographical features of the Des Moines Lobe in Iowa. M.Sc. thesis, Iowa State University, Ames, Iowa.

Cowardin, L.M., Carter, V., Golet, F.C., and LaRoe, E.T. 1979. Classification of wetlands and deepwater habitats of the United States. US Department of the Interior, Fish and Wildlife Service, Office of Biological Services, Washington, D.C.

Cross, F.B., and Collins, J.T. 1995. Fishes in Kansas. 2nd ed. (revised). *Edited by* J.T Collins. Public Education Ser. No. 14, University Press of Kansas, Lawrence, Kansas.

Cunningham, G.R. 1999. A survey for the Topeka shiner (*Notropis topeka*) within the Big Sioux, Vermillion, and James river basins in South Dakota. Eco-Centrics, 2041 N. 66th St., Omaha, NE 68104.

Cunningham, G.R. 2002. Topeka shiner surveys and population estimates in eastern South Dakota survey year 1999. Eco-Centrics, 2041 N. 66th St., Omaha, NE 68104.

Cushing, C.E., and Allen, D. 2001 Streams: their ecology and life. Academic Press, New York.

Dahl, T. 1990. Wetlands losses in the United States 1780's to 1980's. US Department of the Interior, Fish and Wildlife Service, Washington, D.C.

Dahle, S.P. 2001. Studies of Topeka shiner (*Notropis topeka*) life history and distribution in Minnesota. M.Sc. thesis, University of Minnesota, Minneapolis, Minn.

Davie, D.K., and Lant, C.L. 1994. The effect of CRP enrollment on sediment loads in two southern Illinois streams. J. Soil Water Conserv. **49**: 407–412.

Dunham, J.B., and Vinyard, G.L. 1997. Incorporating stream level variability into analyses of site level fish habitat relationships: some cautionary examples. Trans. Am. Fish. Soc. **126**: 323–329.

Environmental Systems Research Institute. 1999. ArcView GIS. Version 3.2. Environmental Systems Research Institute, Redlands, Calif.

Environmental Systems Research Institute. 2000. ARC/INFO GIS. Version 8.0.2. Environmental Systems Research Institute, Redlands, Calif.

Filipe, A.F., Cowx, J.G., and Collares-Pereira, M.J. 2002. Spatial modeling of freshwater fish in semi-arid river systems: a tool for conservation. River Res. Appl. **18**: 123–136

Frissell, C.A., and Nawa, R.K. 1992. Incidence and causes of physical failure of artificial habitat structures in streams of western Oregon and Washington. N. Am. J. Fish. Manag. **12**: 182–197.

© 2004 NRC Canada

Frissell, C.A., William, J.L., Warren, C.E., and Hurley, M.D. 1986. A hierarchical framework for stream habitat classification: viewing streams in a watershed context. Environ. Manag. **10**(2): 199–214.

Goodchild, M.F., and Gopal, S. 1989. Accuracy of spatial databases. Tayler and Francis, London.

Gregr, E.J., and Trites, A.W. 2001. Predictions of critical habitat for five whale species in the waters of coastal British Columbia. Can. J. Fish. Aquat. Sci. **58**: 1265–1285.

Groves, C., Jensen, D., Valutis, L., Redford, K., Shaffer, M., Scott, J., Bargartner, J., Higgins, J., Beck, M., and Anderson, M. 2002. Planning for biodiversity conservation: putting conservation science into practice. BioScience, **52**: 499–512.

Hoehn, T. 1998. Rare and imperiled fish species of Florida: a watershed perspective. Office of Environmental Services, Florida Game and Fresh Water Fish Commission, Tallahassee, Fla.

Hosmer, D.W., Jr., and Lemeshow, S. 1989. Applied logistic regression. John Wiley and Sons, New York.

Jennings, M.D. 2000. Gap analysis: concepts, methods, and recent results. Landsc. Ecol. **15**: 5–20.

Johnson, R.R., and Higgins, K.F. 1997. Wetland resources of eastern South Dakota. South Dakota State University, Brookings, S.D.

Karr, J.R., and Schlosser, I.J. 1978. Water resources and the land–water interface. Science (Wash., D.C.), **201**: 229–234.

Kerns, H.A. 1981. *Notropis topeka* in Kansas: distribution, habitat, life history. M.Sc. thesis, University of Kansas, Lawrence, Kansas.

Kirby, D.J. 2001. An assessment of the channel catfish population in the Big Sioux River, South Dakota. M.Sc. thesis, South Dakota State University, Brookings, S.D.

Labbe, T.R., and Fausch, K.D. 2000. Dynamics of intermittent stream habitat regulate persistence of threatened fish at multiple scales. Ecol. Appl. **10**(6): 1774–1791.

Lammert, M., Higgins, J., Grossman, D., and Bryer, M. 1996. A classification framework for freshwater communities. *In* Proceedings of The Nature Conservancy's Aquatic Community Classification Workshop, 9–11 Apr. 1996, New Haven, Missouri. The Nature Conservancy, Arlington, Virginia.

Legendre, P. 1993. Spatial autocorrelation: trouble or new paridigm. Ecology, **74**(6): 1659–1673.

Lyons, J. 1989. Correspondence between the distribution of fish assemblages in Wisconsin streams and Omernik's ecoregions. Am. Midl. Nat. **122**: 163–182.

Lyons, J. 1996. Patterns in the species composition of fish assemblages among Wisconsin streams. Environ. Biol. Fishes, **45**: 329–341.

Milewski, C.L. 2001. Local and systemic controls on fish habitat in South Dakota rivers and streams: implications for management. Ph.D. dissertation, South Dakota State University, Brookings, S.D.

Minckley, W.L., and Cross, F.B. 1959. Distribution, habitat, and abundance of the Topeka shiner, *Notropis topeka* (Gilbert), in Kansas. Am. Midl. Nat. **61**: 210–217.

Mladenoff, D.J., Sickley, T.A., Haight, R.G., and Wydeven, A.P. 1995. A regional landscape analysis and prediction of favorable gray wolf habitat in the northern Great Lakes region. Conserv. Biol. **9**(2): 279–294.

Naiman, R.J. 1992. Watershed management, balancing sustainability and environmental change. Springer-Verlag, New York.

National Research Council. 1995. Science and the Endangered Species Act. National Academy Press, Washington, D.C.

Olden, J.D., and Jackson, D.A. 2001. Fish–habitat relationships in lakes: gaining predictive and explanatory insight by using artificial neural networks. Trans. Am. Fish. Soc. **130**: 878–897.

Olden, J.D., Jackson, D.A., and Peres-Neto, P.R. 2002. Predictive models of fish species distributions: a note on proper validation and chance predictions. Trans. Am. Fish. Soc. **131**: 329–336.

Ontario Ministry of Natural Resources 1999. Ontario's living legacy — land use strategy. Ontario Ministry of Natural Resources, Queen's Printer for Ontario, Toronto, Ont.

Osborne, L.L., and Wiley, M.J. 1992. Influence of tributary spatial position on the structure of warmwater fish communities. Can. J. Fish. Aquat. Sci. **49**: 671–681.

Pereira, J.M.C., and Itami, R.M. 1991. GIS-based habitat modeling using logistic multiple regression: a study of the Mt. Graham red squirrel. Photogr. ER, **57**(11): 1475–1486.

Pflieger, W.L. 1997. The fishes of Missouri. Missouri Department of Conservation, Columbia, Missouri.

Poff, N.L., and Ward, J.V. 1989. Implications of streamflow variability and predictability for lotic community structure: a regional analysis of streamflow patterns. Can. J. Fish. Aquat. Sci. **46**: 1805–1817.

Poiani, K.A., Richter, B., Anderson, M., and Richter, H. 2000. Biodiversity conservation at multiple scales: functional sites, landscapes, and networks. BioScience, **50**: 133–146.

Richter, B.D., Braun, D.P., Mendelson, M.A., and Master, L.L. 1997. Threats to imperiled freshwater fauna. Conserv. Biol. **11**(5): 1081–1093.

Roth, N.E., Allan, J., and Erickson, D. 1996. Landscape influences on stream biotic integrity assessed at multiple scales. Landsc. Ecol. **11**: 141–156.

SAS Institute Inc. 1994. SAS/STAT user's guide. Version 6. 4th ed. SAS Institute Inc., Cary, N.C.

Schrank, S.J., Guy, C.S., While, M.R., and Brock, B.L. 2001. Influence of instream and landscape-level factors on the distribution of Topeka shiners (*Notropis topeka*) in Kansas streams. Copeia, 2001(2): 413–421.

Schultz, R.C., Colletti, J.P., Isenhart, T.M., Rodrigues C.A., Wray, P.H., and Avant-Kuehl, A. 1996. Stewards of our streams: buffer strip design, establishment, and maintenance. Iowa State University Department of Forestry, Iowa State University, Ames, Iowa.

Schwartz, M. W. 1999. Choosing the appropriate scale of reserves for conservation. Annu. Rev. Ecol. Syst. **30**: 83–108.

Scott, J.M., Davis, F., Csuti, B., Noss, R., Butterfield, B., Groves, C., Anderson, H., Caicco, S., D'Erchia, F., Edwards, T.C, Ulliman, J., Jr., and Wright, R.G. 1993. Gap analysis: a geographic approach to protection of biological diversity. Wildl. Monogr. **123**: 1–41.

Shaffer, M.L., Scott, M., and Casey, F. 2002. Noah's options: initial cost estimates of a national system of habitat conservation areas in the United States. BioScience, **52**: 439–443.

Shearer, J.S. 2001. Temporal change in fish communities and modification of the index of biotic integrity for the James River of the Dakotas. M.Sc. thesis, South Dakota State University, Brookings, S.D.

Short, H.L., and Hestbeck, J.B. 1995. National biotic resource inventories and GAP analysis. BioScience, **45**: 535–539.

Smith, R.L., and Flake, L.D. 1983. The effects of grazing on forest regeneration along a prairie river. Prairie Nat. **15**(1): 41–44.

Smith, V.J. 2001. Mammal distributions and habitat models for South Dakota. M.S. thesis, South Dakota State University, Brookings, S.D.

Smith, V.J., Jenks, J.A., Berry, C.R., Jr., Kopplin, C.J., and Fecske, D.D. 2002. The South Dakota Gap Analysis Project, final report. US Department of the Interior, US Geological Survey, Reston, Virginia.

Soule, M.E., and Sanjayan, M.A. 1998. Conservation targets: do they help? Science (Wash., D.C.), **279**: 2060–2061.

© 2004 NRC Canada

South Dakota Game, Fish and Parks. 2000. South Dakota natural heritage database element occurrence records. South Dakota Game Fish and Parks, Wildlife Division, Pierre, S.D.

Sowa, S.P. 1998. Gap analysis in riverine environments. Gap Anal. Bull. **7**: 18–20.

Sowa, S.P. 1999*a*. Establishing initial conservation priorities. *In* Implementing the aquatic component of GAP analysis in riverine environments: a training workbook. Missouri Resource Assessment Partnership, Columbia, Mo. Section 4. pp. 1–14.

Sowa, S.P. 1999*b*. Revising initial conservation priorities and identifying specific sites for conservation. *In* Implementing the aquatic component of gap analysis in riverine environments: a training workbook. Missouri Resource Assessment Partnership, Columbia, Mo. Section 6. pp. 1–9.

Sperduto, M.B., and Congalton, R.G. 1996. Predicting rare orchid (small whorled pogonia) habitat using GIS. Photogr. ER, **62**(11): 1269–1279.

Stroud, R.H. 1992. Fisheries management and watershed development. Am. Fish. Soc. Symp. No. 13. American Fisheries Society, Bethesda, Md.

Tabor, V.M. 1998. Final rule to list the Topeka shiner as endangered. Federal Register 63 (240): 69 008 – 69 021. US Department of the Interior, US Fish and Wildlife Service, Manhattan, Kansas.

The Nature Conservancy Freshwater Initiative. 2000. GIS tools for aquatic macrohabitat classification. [www.freshwaters.org/ccwp/home.html, Feb. 14, 2000.]

US Department of Agriculture. 1991. State soil geographic (STATSGO) database — data use information. National Cartography and GIS Center, US Department of Agriculture, Natural Resources Conservation Service, Fort Worth, Texas. Misc. Publ. No. 1492.

US Department of Agriculture. 1995. Soil survey geographic (SSURGO) database — data use information. National Cartography and GIS Center, US Department of Agriculture, Natural Resources Conservation Service, Fort Worth, Texas. Misc. Publ. No. 1527.

US Department of Agriculture. 1996. National soil surveyor handbook (430-VI-NSSH, 1996). US Department of Agriculture, Natural Resources Conservation Service, US Government Printing Office, Washington, D.C.

US Department of Agriculture. 1999. South Dakota technical guide. Section IV. US Department of Agriculture, Natural Resources Conservation Service, US Government Printing Office, Washington, D.C.

US Environmental Protection Agency. 1999. Basins. Version 2.0. [www.epa.gov/ost/basins/download.htm, June 12, 1999.]

US Fish and Wildlife Service. 1993. NWI maps made easy: a users guide to National Wetlands Inventory maps of the mountain–prairie region. US Department of the Interior, Fish and Wildlife Service, National Wetlands Inventory, Denver, Co.

US Geological Survey. 1974. Hydrologic Unit Map — 1974 State of South Dakota. US Department of the Interior, Geological Survey, Denver, Co.

US Geological Survey. 2001. Environmental monitoring and assessment program activities in South Dakota. Annual progress report. US Geological Survey, Rapid City, S.D.

US Geological Survey. 2002. Environmental monitoring and assessment program activities in South Dakota. Annual progress report. US Geological Survey, Rapid City, S.D.

Vannote, R.L., Minshall, G.W., Cummins, K.W., Sedell, J.R., and Cushing, C.E. 1980. The river continuum concept. Can. J. Fish. Aquat. Sci. **37**: 130–137.

Wall, S.S., Blausey, C.M., Jenks, J.A., and Berry, C.R., Jr. 2001. Topeka shiner (*Notropis topeka*) population status and habitat conditions in South Dakota streams. South Dakota State University, Brookings, S.D.

Warren, M.L., Jr., and Burr, B.M. 1994. Status of freshwater fishes of the United States: overview of an imperiled fauna. Fisheries, **19**(1): 6–18.

Whittier, T.R., Hughes, R.M., and Larsen, D.P. 1988. Correspondence between ecoregions and spatial patterns in stream ecosystems in Oregon. Can. J. Fish. Aquat. Sci. **45**: 1264–1278.

Whitworth, M.R., and Martin, D.C. 1990. In-stream benefits of CRP filter strips. Trans. 55th N. Am. Wildl. Nat. Res. Conf. **55**: 41–45.

Wiley, M.J., Osborne, L.L., and Larimore, R.W. 1990. Longitudinal structure of an agricultural prairie river system and its relationship to current stream theory. Can. J. Fish. Aquat. Sci. **47**: 373–384.

Williams, J.E., Johnson, J.E., Hendrickson, D.A., Contreras-Balderas, S., Williams, J.D., Navarro-Mendoza, M., McAllister, D.E., and Deacon, J.E. 1989. Fishes of North America endangered, threatened, or of special concern: 1989. Fisheries, **14**(6): 2–20.

Williams, J.E., Wood, C., and Dombeck, M. 1997. Understanding watershed-scale restoration. *In* Watershed restoration principles and practices. *Edited by* J. Williams, C. Wood, and M. Dombeck. American Fisheries Society, Bethesda, Md. pp. 1–13.

© 2004 NRC Canada

Appendix A

Table A1. Frequency of physical habitat variables of valley segments with Topeka shiners (f_{TOS}) and frequency of physical habitat variables available in valley segments (f_{AVL}) for each ecoregional drainage unit (EDU[a]).

	EDU1		EDU2		EDU3		EDU4	
Habitat variable	f_{TOS} (n = 11)	f_{AVL} (n = 3284)	f_{TOS} (n = 30)	f_{AVL} (n = 2014)	f_{TOS} (n = 19)	f_{AVL} (n = 2126)	f_{TOS} (n = 5)	f_{AVL} (n = 286)
Stream size class								
Headwater	27.3	79.1	27.6	78.7	20.0	80.2	60.0	77.3
Creek	63.6	12.8	24.1	12.0	70.0	12.7	40.0	12.3
Small river	9.1	6.0	44.8	7.2	10.0	7.1	0.0	0.0
Large river	0.0	2.1	3.5	2.2	0.0	0.0	0.0	10.4
Channel slope class								
Low	54.5	64.9	65.5	50.1	60.0	46.7	80.0	56.0
Medium	45.4	17.7	27.6	25.1	40.0	26.9	20.0	20.9
High	0.0	17.4	6.9	24.4	0.0	26.4	0.0	23.1
Network position class								
None	91.0	83.9	86.2	78.7	80.0	80.3	60.0	78.5
Headwater to creek	0.0	11.1	10.3	12.5	10.0	13.1	20.0	12.5
Headwater to small river	0.0	3.1	0.0	2.8	0.0	5.6	0.0	0.0
Headwater to large river	0.0	1.1	3.5	4.9	0.0	0.0	0.0	7.6
Creek to small river	0.0	0.5	0.0	0.8	10.0	1.0	0.0	0.05
Creek to large river	9.0	0.2	0.0	0.2	0.0	0.0	20.0	1.4
Small river to large river	0.0	0.1	0.0	0.1	0.0	0.0	0.0	0.0
Parent material class								
Alluvium	81.8	40.1	93.1	52.2	95.0	64.4	100.0	30.7
Glacial till	0.0	35.1	3.5	20.2	5.0	8.5	0.0	38.2
Outwash	0.0	0.4	0.0	0.8	0.0	1.3	0.0	0.6
Loess	0.0	0.3	3.5	2.6	0.0	10.2	0.0	0.6
Sioux quartzite	0.0	0.0	0.0	1.0	0.0	0.1	0.0	0.0
Shale	0.0	0.5	0.0	0.0	0.0	0.0	0.0	0.0
Other	8.2	23.6	0.0	23.2	0.0	15.5	0.0	29.9
Streamflow								
Perennial	0.0	8.6	24.1	6.8	10.0	6.7	0.0	13.9
Intermittent	100.0	17.0	58.6	18.3	65.0	21.0	80.0	19.3
Seasonal	0.0	46.3	17.2	55.9	25.0	55.0	20.0	47.4
Temporary	0.0	28.1	0.0	19.0	0.0	17.3	0.0	19.4
Groundwater potential								
Low	9.0	84.4	27.6	77.0	20.0	51.0	40.0	65.5
Medium	18.2	9.4	27.6	11.7	40.0	30.8	20.0	20.3
High	72.7	6.2	44.8	11.3	40.0	18.3	40.0	14.2
Downstream connectivity								
No	91.0	95.0	100.0	98.0	100.0	97.0	100.0	96.7
Yes	9.0	5.0	0.0	2.0	0.0	3.0	0.0	3.3
Upstream connectivity								
No	100.0	95.0	96.6	98.0	100.0	97.0	100.0	96.7
Yes	0.0	5.0	3.4	2.0	0.0	3.0	0.0	3.3
Floodplain influence								
Yes	0.0	1.0	3.4	2.7	15.0	7.5	0.0	6.6
No	100.0	99.0	96.6	97.3	85.0	92.5	100.0	93.4

[a]EDU1, Great Plains steppe – James River drainage; EDU2, prairie parkland (temperate) – Lower Big Sioux and Vermillion River drainage; EDU3, prairie parkland (temperate) – Upper Big Sioux River drainage; EDU4, prairie parkland (temperate) – James River drainage; no Topeka shiners were found in EDU5 (Great Plains Palouse dry steppe – James River drainage.

© 2004 NRC Canada

An age-structured assessment model for chinook salmon (*Oncorhynchus tshawytscha*)

James W. Savereide and Terrance J. Quinn II

Abstract: Age-structured assessment models are rarely used for estimating the abundance of exploited salmon stocks. We developed such a model for a chinook salmon (*Oncorhynchus tshawytscha*) population in the Copper River, Alaska. Information consisted of catch-age data from three fisheries (commercial, recreational, and subsistence) and two sources of auxiliary data (escapement index and spawner–recruit relationship). Model parameters included brood-year returns, proportions of a brood year returning at age and year, annual exploitation rates, gear selectivity, spawner–recruit parameters, and a calibration parameter for the escapement index. Results suggested that population parameter estimates with high precision and low bias were produced by an approach that considered measurement error in the pooled catch-age data from all three fisheries and brood-year return proportions that varied over time. A sensitivity analysis revealed that brood-year return, catch, and escapement index estimates were insensitive to large changes in data weightings. The absence of strong deviations in the retrospective patterns of the brood-year returns suggested that there were no serious model misspecifications. The model integrated all sources of available information, accounted for uncertainty, and provided estimates of optimal escapement and its associated exploitation level. We believe that the model has broad application for use in assessments of chinook salmon systems.

Résumé : Les modèles d'évaluation avec structure d'âge servent rarement à l'estimation de l'abondance des stocks exploités de saumons. Nous avons mis au point un tel modèle pour les saumons quinnat (*Oncorhynchus tshawytscha*) de la rivière Copper, Alaska. Les informations de base comprennent des données de capture en fonction de l'âge de trois types de pêche (pêches commerciale et sportive et pêche de subsistance) et des données de sources complémentaires (indices d'échappement et relations reproducteurs–recrues). Les variables du modèle comprennent les retours par année de reproduction, les proportions de chaque cohorte reproductrice dans les retours en fonction de l'âge et de l'année, les taux annuels d'exploitation, la sélectivité des engins de pêche, les paramètres de la relation reproducteurs–recrues et un paramètre de calibration de l'indice d'échappement. Les résultats indiquent que les estimations des paramètres démographiques sont de haute précision et que l'erreur est faible par notre approche qui tient compte des erreurs de mesure des données combinées de capture en fonction de l'âge dans les trois types de pêche, ainsi que de la variation dans le temps des proportions des cohortes reproductrices dans les retours. Une analyse de sensibilité démontre que les estimations des retours des diverses cohortes reproductrices, des captures et des indices d'échappement ne sont pas affectées par de forts changements dans la pondération des données. L'absence de déviations importantes dans les patterns rétrospectifs des retours des différentes cohortes reproductrices indique que les spécifications du modèle ne comportent pas d'erreurs sérieuses. Le modèle intègre toutes les sources d'information disponibles, tient compte de l'incertitude et produit des estimations de l'échappement optimal et du niveau d'exploitation correspondant. Le modèle nous semble s'appliquer à de nombreux types d'évaluation dans le système du saumon quinnat.

[Traduit par la Rédaction]

Introduction

A hallmark of current assessment methodology is the construction of a complex model for a species or stock that integrates a variety of information sources through the development of biologically plausible equations and parameters (Quinn and Deriso 1999). Such models have found wide use for most age-structured species around the world. It is surprising, therefore, that more attention has not been placed on the construction of age-structured assessment models for those Pacific salmon (*Oncorhynchus* spp.) species with runs from multiple brood years over time. Only Kope (1987) developed a germane method to apply age-structured methodology to Pacific salmon.

A common assessment method for salmon populations is known as run reconstruction. This method utilizes spatial and temporal catch and escapement information to estimate salmon returns at various times throughout the run (Templin

Received 24 March 2003. Accepted 24 January 2004. Published on the NRC Research Press Web site at http://cjfas.nrc.ca on 24 July 2004.
J17418

J.W. Savereide.[1] Alaska Department of Fish and Game, Sport Fish Division, 1300 College Road, Fairbanks, AK 99701, USA.
T.J. Quinn II. Juneau Center, School of Fisheries and Ocean Sciences, University of Alaska Fairbanks, 11120 Glacier Highway, Juneau, AK 99801-8677, USA.

[1]Corresponding author (e-mail: james_savereide@fishgame.state.ak.us).

 doi: 10.1139/F04-039 © 2004 NRC Canada

Fig. 1. Schematic showing the temporal structure of an Alaskan chinook salmon population for a single brood. Events shown are spawning of eggs, emergence the following year, and the returns of maturing parts of the brood from ages 3 to 8. During the run, fish encounter commercial, recreational, and subsistence fisheries. Those that escape will spawn and die. N, total run at each age; R, the sum of N over brood or the sum of S and C over brood; C_c, commercial catch; C_r, recreational catch; C_s, subsistence catch. Escapement S equals $N - C_c - C_r - C_s$.

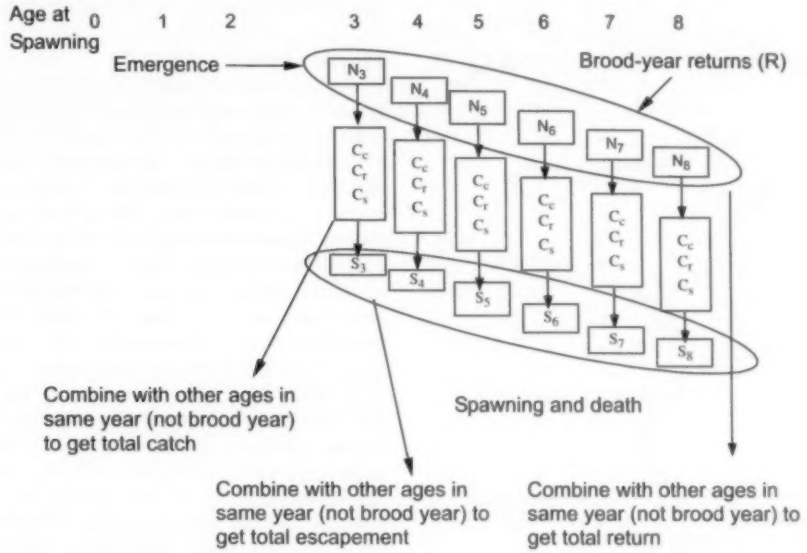

et al. 1996). One disadvantage to this approach is the inability to estimate complete brood-year returns until all ages in a brood year have returned (Fig. 1). Consequently, one cannot obtain estimates of total brood-year returns in the most recent years, often the main purpose of assessment, without ad hoc adjustments. Further, run reconstruction requires that abundance or escapement of returning salmon is known.

Catch-age analysis is an age-structured assessment method that provides estimates of population parameters based on processes like recruitment, catchability, the spawner–recruit relationship, and fishing and natural mortality. Deriso et al. (1985) showed that the addition of auxiliary information such as fishing effort or survey catches is typically required to constrain the catch-age analysis and obtain reliable population parameter estimates. But catch-age analysis is not strictly applicable to returning salmon populations because only the returning component of the brood year is observed (and caught), and that happens only once.

The Copper River in Alaska supports a chinook salmon (*Oncorhynchus tshawytscha*) population that is subject to commercial, subsistence, and recreational fisheries during migration to its spawning grounds. Currently, the chinook salmon run is managed under a fixed escapement policy. Imprecision of in-season management coupled with an inaccurate index of escapement places uncertainty on achieving the fixed escapement goal. To establish escapement goals and sustainable harvest guidelines in the absence of information about total run size or escapement, we developed a salmon catch-age analysis (SCAA) to provide a centerpiece for a dependable and cost-effective method for estimating the abundance of returning chinook salmon. The main purpose of this model was to provide a generic framework for multi-age returning salmon populations, which integrates age-structured information about the catch with an annual index of escapement. By modeling the process of salmon returning to spawn, the ability to estimate abundances associated with incomplete broods is possible.

Kope (1987) developed a catch-age model that separated fishing mortality rates into annual fishing effort and vulnerability at age. In our SCAA model, brood-year returns were modeled differently by estimating proportions of brood-year returns, thereby avoiding the necessity of incorporating estimates of natural mortality. We applied the model to data from the Copper River chinook salmon population, which consisted of brood years returning 3–8 years after spawning. We also developed an algorithm to use run reconstruction to provide starting values for brood-year return estimates for the SCAA model. Auxiliary information sources included an escapement index from aerial survey counts and a spawner–recruit relationship that constrained the model's recruitment estimates from deviating too far from a specified spawner–recruit relationship.

Quinn and Gates (1997) found that the maximum likelihood approach for parameter estimation is difficult to use when the data have different levels of precision and accuracy and contain autocorrelation. Because the commercial, subsistence, and recreational catch-age data are based on different levels of sampling, the population parameters in this study were determined by minimizing a least squares objective function containing elements of catch and escapement. Measurement errors in catch and escapement were known to occur and were provided for in the model.

Methods

Study area

The Copper River is a large glacial river that drains 61 440 km^2 and is the fifth largest watershed in Alaska

© 2004 NRC Canada

Fig. 2. Diagram showing the Copper River Valley and locations of the commercial, subsistence, and recreational fisheries.

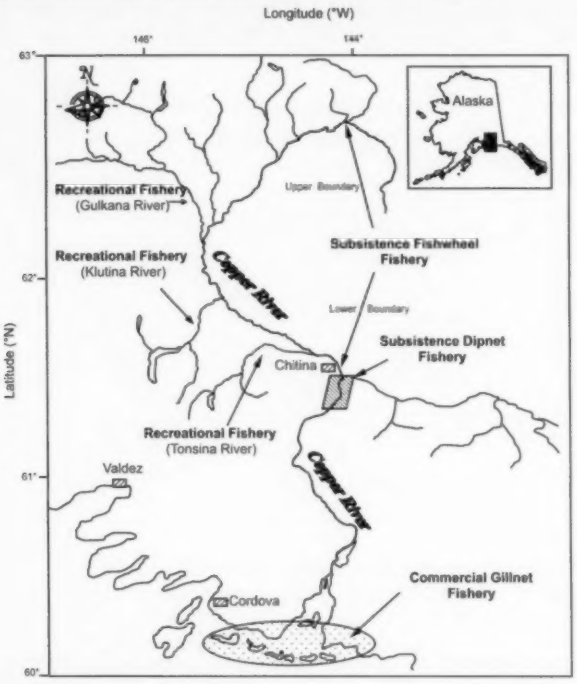

(Fig. 2). The river supports a significant population of chinook salmon that is harvested in commercial, subsistence, and recreational fisheries. The total annual harvest from 1995 to 1999 averaged 75 853 chinook salmon (Taube 2000). The commercial fishery is found at the mouth of the Copper River where drift gill nets are used to harvest chinook salmon. The subsistence fisheries occur in-river from just below Chitina upstream throughout the remainder of the Copper River and fishing is accomplished with either shore-positioned fishwheels or large dip nets. The recreational fisheries are found primarily on the Gulkana, Klutina, and Tonsina rivers where fishers utilize standard rod and reel fishing gear.

Catch-age data

Proportionate age composition of the harvest was estimated from random samples of scales from each fishery component (Savereide 2001). Estimates in numbers of the total catch at age in the commercial, subsistence, and recreational fisheries from 1980 to 1999 were obtained by multiplying the estimated proportion at each age in each fishery by the total harvest in each fishery. These estimates were then added together to form a pooled catch-age composition (Table 1). The commercial harvest was updated from fish ticket receipts at the end of each commercial opening and the total harvest was known at the end of the season. The subsistence dipnet and fishwheel harvests were determined from the return of fishery-specific harvest permits. The recreational fishery was estimated from the statewide annual harvest survey mailed to resident and nonresident sport fish license holders. Estimates are determined from the surveys returned. In years when no age compositions were available for the recreational or subsistence fisheries, the average proportion at each age across years with data was applied to the fishery-specific total harvest to determine the catch at age. In this study, ages are reported in years chronologically from the year of spawning, with the most common being ages 4–7.

SCAA model

The extent to which catch-age models can describe the random properties found in fish populations is based on the validity associated with the model's assumptions and parameters (Megrey 1989). The assumptions necessary to specify the SCAA model included the following: (*i*) returning salmon faced a commercial (c), subsistence (s), and recreational (r) fishery when migrating to their spawning grounds, (*ii*) the catch from each gear type is separable by age and year (as specified below), (*iii*) age composition estimates of the catch were from sampling and may have differed from the true composition, (*iv*) commercial catch comprised only Copper River stocks, (*v*) the expected value of an index of escapement obtained from aerial surveys was proportional to the true escapement, (*vi*) returning salmon not caught migrated to their spawning grounds, spawned, and died, and (*vii*) no natural mortality occurred before or during spawning.

The separability of each gear's (g) exploitation fraction into age (a) and year (t) factors is an important assumption in catch-age analysis (Doubleday 1976; Pope 1977). By letting gear selectivity be $s_{a,g}$ and exploitation rate be $\mu_{t,g}$, the exploitation fraction for age, year, and gear $\mu_{a,t,g}$ is simply the product of $s_{a,g}$ and $\mu_{t,g}$. In addition, $C_{a,t,g}$ is catch, $S_{a,t,g}$ is escapement, and γ is the proportion of the total escapement observed during aerial surveys.

The abundance or run of returning fish in a given year t is the total brood-year return R_y multiplied by the proportion returning from that year for each age $p_{a,y}$:

$$(1) \qquad N_{a,t} = R_y\, p_{a,y}$$

where brood-year $y = t - a$. Thus, the brood-year proportion pertains to return year $y + a$, and the sum of the proportions over age equals 1 for each brood-year. The catch in each fishery, which stems from extensions of the Baranov catch equation (Quinn and Deriso 1999), is the abundance multiplied by the exploitation fraction, or from the separability assumption:

$$(2) \qquad C_{a,t,g} = N_{a,t}\mu_{a,t,g} = N_{a,t}\, s_{a,g}\, \mu_{t,g}$$

The escapement (spawning abundance) is the number of fish left after fishing, or from assumptions *i*, *iv*, and *vi*:

$$(3) \qquad S_{a,t} = N_{a,t} - \sum_{g} C_{a,t,g} = N_{a,t} - C_{a,t,c} - C_{a,t,r} - C_{a,t,s}$$

Depending on the quality of the data for each gear type, various analyses can be made. The first approach (stratified) makes no common assumptions about gear selectivities and stratified the catch data among gear types. The second approach (commercial) allows for measurement error in the commercial catch data but treats the catch from the recreational and subsistence fisheries as being measured without error. The third approach (pooled) assumes that selectivities are constant among gear types and the data sources are

© 2004 NRC Canada

Table 1. Estimated pooled (commercial, subsistence, and recreational) catch-age composition and observed aerial escapement indices.

	Age (years)							
Year	3	4	5	6	7	8	Total	Escapement index
1980	98	650	6 101	6 101	596	39	13 586	718
1981	82	2306	11 708	9 260	1553	0	24 909	754
1982	252	4218	29 703	17 236	2319	0	53 728	1656
1983	232	2919	37 847	17 428	125	0	58 551	931
1984	79	1439	16 789	24 146	1315	0	43 769	2189
1985	116	3279	15 150	26 785	890	0	46 220	321
1986	134	3046	26 700	16 599	906	0	47 386	3182
1987	157	1206	10 455	17 948	1617	0	31 384	1228
1988	187	1540	10 880	19 117	2056	0	33 779	967
1989	146	1284	10 280	21 731	2678	0	36 118	1993
1990	241	2253	9 310	13 101	2315	67	27 287	1356
1991	349	2053	26 000	15 365	798	24	44 590	1303
1992	164	2640	10 511	32 909	2354	79	48 656	656
1993	152	3051	27 128	10 268	1028	0	41 626	1156
1994	62	4572	25 326	28 810	441	0	59 212	1682
1995	184	5171	44 916	27 971	741	0	78 983	720
1996	465	3912	36 442	26 578	323	23	67 743	2321
1997	129	5858	42 513	19 291	381	0	68 172	2250
1998	218	6505	56 298	22 648	656	0	86 325	1407
1999	31	7687	41 355	25 968	537	0	75 579	1047

pooled. This effectively treats the pooled data as being measured with error.

For Copper River chinook salmon, previous analyses used an analytical hierarchy process analysis (Saaty 1990; Merritt and Quinn 2000) to show that parameter estimability was enhanced by the third approach of pooling the data across gear types (Savereide 2001). In the Discussion, we briefly discuss stratification by gear type and its effect on the SCAA model. In further application of the model, we use the pooled approach, in which subscript "g" is dropped in all equations.

In our model, the separability assumption is extremely important because it simplified the parameter estimation by reducing the number of unknown exploitation rates and selectivity parameters from 120 (20 years × 6 ages) to 26 (20 years + 6 ages). To further reduce the number of parameters to be estimated, we assumed that selectivity was constant for salmon aged 5–8. Age-5 and age-6 salmon comprised the majority of the commercial catch, so it is likely that age-5 salmon and older were fully selected for in the commercial fishery. In the subsistence and recreational fisheries, the majority of the catch was 4–8 years of age. This implied that age-4 salmon and older may be fully selected in the noncommercial fisheries. Because the commercial catch-age composition comprised the majority of the pooled catch-age composition, the model was configured to estimate the selectivities for fish aged 3 and 4. Implicitly, we assume that the mix of commercial and noncommercial fisheries is sufficiently constant so that selectivity is considered constant over time.

To reduce the number of estimated parameters in the pooled approach, we constructed one configuration of the model, the constant-p approach, that assumed that proportions of a brood returning over time, $p_{a,y}$, were constant ($p_{a,y} = p_a$). However, we compiled catch proportions by brood and discovered that the proportions for age-5 and age-6 chinook salmon varied greatly over time but proportions for the other ages did not. The variation in catch proportions opened the possibility that the return proportions also varied in time. Therefore, we also examined a second configuration, called the time-varying approach. Proportions for salmon aged 3, 4, 7, and 8 years were assumed constant because there was relatively little variation in these age-classes. The model estimated annual proportions of age-5 fish and set age-6 proportions to 1 minus the sum of the remaining age-classes so that proportions for both ages varied over time.

Auxiliary information

Paloheimo (1980) and Dupont (1983) incorporated fishing effort into their catch-age models under the assumption that effort was proportional to full-recruitment fishing mortality. Deriso et al. (1985) believed that this assumption was limited because catchability often changes from year to year and full-recruitment fishing mortality is rarely known. Fournier and Archibald (1982) relaxed this assumption by modeling differences between fishing mortality and effort in a lognormal framework. Therefore, we did not include fishing effort information in the model.

Additionally, they developed methods to incorporate spawner–recruit relationships and aging error into the objective function. Following Fournier and Archibald (1982) and Deriso et al. (1985), we assumed that recruitment was dependent on the spawning abundance through a Ricker spawner–recruit relationship but subject to error:

$$(4) \qquad R_y = \alpha S_y e^{-\beta S_y + \varepsilon_y}$$

© 2004 NRC Canada

where α is the productivity parameter, β measures the level of density dependence, and returns from brood-year y come from spawners in year y. Throughout the analysis, a Ricker spawner–recruit function was employed; however, the Beverton–Holt relationship ($R = \alpha S/(1 + \beta S)$) was also explored (see Savereide 2001).

The maximum sustainable catch (MSC) and its related exploitation rate were determined from the Ricker relationship. The equation $\alpha(1 - \beta S_m)e^{-\beta S_m} = 1$ was solved numerically for S_m, where S_m equals the optimal escapement (the escapement that produces MSC). MSC is then $R(S_m) - S_m$, and corresponding exploitation rate is MSC/$R(S_m)$ (Quinn and Deriso 1999).

In addition to the spawner–recruit relationship, we included an escapement index as auxiliary information (Table 1). From assumption *v*, the annual escapement index I_t was the proportion of the escapement observed during aerial survey counts, γ, multiplied by the total escapement:

$$(5) \qquad I_t = \gamma \sum_a S_{a,t} = \gamma S_t$$

where the absence of a subscript denotes summation over the subscript.

A single brood of retuning chinook salmon illustrates how the model works (Fig. 1). Essentially, the sum of the number at each age returning from a particular year equals the total brood-year return, whereas the catch and escapement across all ages in a particular year equals the total run for that year.

Objective function and error structure

To address the variability associated with sample estimates of catch-age data and factors that influence fish population abundance, the inclusion of an error structure into the model's objective function is required. Early approaches utilized lognormal deviations with likelihood (Fournier and Archibald 1982) and least squares (Deriso et al. 1985) formulations to describe assumed differences between observed and model catch owing to measurement error. Recent approaches have dealt with measurement and process error in a likelihood (Gudmundsson 1994; Schnute and Richards 1995) or Bayesian (McAllister et al. 1994; McAllister and Ianelli 1997) framework.

In contrast with the previous studies, our analysis utilized a least squares framework and assumed an underlying root normal distribution (Quinn 1985; Quinn et al. 1998) to accommodate measurement errors in catch and escapement. Catch observations are denoted as $C'_{a,t,g}$ and the observed escapement index is I'_t. The total brood-year return R_y is not denoted with a prime because the brood-year return comes from the SCAA model. There is a difference between brood-year return estimates from the model and those from the spawner–recruit relationship. For a particular spawning year y, the estimated total brood-year return produced by the SCAA model is equivalent to the number of recruits accumulated over years $y + 3$, $y + 4$,...,$y + 8$. The addition of a spawner–recruit relationship allowed us to estimate with some stability complete brood-year returns in years with incomplete observations.

A simple least squares objective function was the combination of catch, escapement index, and spawner–recruit residual sums of squares (RSS):

$$(6) \qquad \mathrm{RSS} = \sum_{a,t,g}\left(\sqrt{C'_{a,t,g}} - \sqrt{C_{a,t,g}}\right)^2 + \lambda_1 \sum_t \left(\sqrt{I'_t} - \sqrt{I_t}\right)^2 + \lambda_F \sum_y \left(\sqrt{R_y} - \sqrt{F(S_y)}\right)^2$$

where F represented a spawner–recruit relationship and λ_1 and λ_F were weighting terms that controlled the influence of the escapement index and spawner–recruit relationship, respectively.

Square root transformations were used for several reasons. The square root transformation is appropriate for count data distributed according to a Poisson distribution and helps to stabilize variance. While many fishery data are more clustered than in a Poisson distribution, it provides a reasonable starting point for count data such as ours. Compared with logarithmic transformations, square root transformations are more capable of handling zero values and their less aggressive nature does not overly dilute the influence that large catches may have on estimates of runs. Quinn et al. (1998) showed that an underlying root normal distribution would provide more reliable convergence of the objective function.

Population parameters estimated by the SCAA model include total brood-year returns R_y, brood-year return proportions $p_{a,y}$ for age-5 salmon, selectivities s_a for ages 3 and 4, total exploitation rates μ_t, the proportion of escapement observed through aerial sampling γ, and the α and β terms in the Ricker spawner–recruit relationship. Starting values for brood-year returns, selectivities s_a, and exploitation rates μ_t were provided by a simple run reconstruction (Appendix A); however, a variety of other values were also tested. A starting value for the proportion seen through aerial sampling was determined from personal communication with Tom Taube, an area manager for the Alaska Department of Fish and Game who conducts the aerial surveys. Finally, realistic starting values were chosen for the α and β terms in the Ricker spawner–recruit function.

Estimates of model parameters were determined by minimizing the objective function (eq. 6) using a Microsoft Excel® spreadsheet. The Excel® application Solver was set to minimize the RSS by changing the parameter vector that included all of the population parameters to be estimated. The following constraints were placed on Solver to ensure reasonable population parameter estimates: (*i*) brood-year return proportions across ages summed to 1, (*ii*) commercial exploitation rates were less than or equal to 0.70, (*iii*) total exploitation rates were less than or equal to 0.85, (*iv*) brood-year returns were greater than or equal to 10 000, and (*v*) all population parameters were positive. These constraints were determined by consultation with area biologists knowledgeable about the population and estimates of total exploitation from previous mark–recapture studies (Evenson and Wuttig 2000; Wuttig and Evenson 2001).

To ensure that the Solver application found the true minimum, the application was repeatedly set to minimize the RSS by changing portions of the parameter vector. For example, the objective function was minimized with the brood-year returns (R_y) and then the Solver application was rerun using exploitation rates (μ_t). This process continued until all

© 2004 NRC Canada

elements of the parameter vector were used to solve the objective function. At this point, the entire parameter vector was used to minimize the RSS and achieve the final result.

The only problem that we found with the Solver application was its sensitivity to the brood-year return starting values. All other population parameter starting values had no effect on Solver's ability to minimize the RSS. However, many iterations of the model were run with a multitude of different but reasonable starting values (ranging from 50 000 to 100 000) and the results presented stem from the approach that provided the lowest RSS.

The standard errors of estimated model parameters, predicted catch, total run, escapement, and forecast estimates of the total run were calculated using the bootstrap technique, described by Efron and Tibshirani (1993) and applied to catch-age data by Deriso et al. (1985).

Diagnostics and model adequacy

As with any model, the results should be insensitive to initial parameter values, and residuals from catch and auxiliary data should display no pattern in age, time, or as a function of predicted catch. Running the model with different values for the weighting terms, λ, to provide insight into the robustness of parameter estimates is recommended. In this study, all of the above diagnostic tools were utilized, as was retrospective analysis (see below).

The criteria used to judge the adequacy of the SCAA model included (*i*) a good fit to catch and escapement data, (*ii*) parameter estimates with low estimated variability, which were expressed in the form of the coefficients of variation (CVs), (*iii*) no pattern in average root residuals across ages and time, (*iv*) a reasonable fit to the chosen spawner–recruit relationship, (*v*) robust and plausible parameter estimates, and (*vi*) forecasts that are close to auxiliary estimates.

Data weighting and sensitivity analysis

Our investigation also looked at numerous weighting scenarios for each of the auxiliary data sources. To evaluate the influence of the weighting terms on the SCAA model, a sensitivity analysis is presented using the following weighting scenarios: (1) $\lambda_I = 1.0$ and $\lambda_F = 0.1$, (2) $\lambda_I = 1.0$ and $\lambda_F = 0.2$, (3) $\lambda_I = 0.5$ and $\lambda_F = 0.1$, and (4) $\lambda_I = 0.3$ and $\lambda_F = 0.2$. The weighting terms are related to the ratio of total catch variance to variance of each other data source. Therefore, values of 1.0 or less for λ_I were chosen because the uncertainty surrounding the escapement index was likely greater than the uncertainty surrounding total catch. Values of 0.2 or less for λ_F were chosen because very little is known about this population's spawner–recruit relationship. Values of zero for λ_I and λ_F were used, but brood-year return estimates in recent years were unreasonably large, greater than 250 000 (Savereide 2001).

The criteria used to choose the most appropriate weighting scenario included (*i*) the model's ability to track the trends in catch, (*ii*) the model's ability to track the trends in the aerial escapement index without taking away from the fit of the catch data, (*iii*) no pattern in average root residuals across ages and time, (*iv*) robust parameter estimates across scenarios, (*v*) a reasonable visual fit to the particular spawner–recruit relationship chosen, and (*vi*) plausible brood-year return estimates.

Retrospective analysis

Because parameter estimates can deviate greatly from true values owing to persistent autocorrelation, Parma (1993) compared retrospective estimates with corresponding reference estimates to assess the errors in brood-year return estimates. Sinclair et al. (1991) defined reference estimates as those estimates determined from the longest time series of data and retrospective estimates as those estimates obtained by running the model retrospectively to different segments of the time series database. In our analysis, the SCAA model was applied to data collected through 1994, 1995, 1996, 1997, 1998, and 1999. Retrospective data sets are referred to as reduced models and the reference data set is the full model.

Forecasting future runs

Total runs for years subsequent to this data set were projected by applying the SCAA model's proportion of a brood returning at each age to corresponding brood-year returns to estimate the number returning at each age. Yet, salmon aged 3 in 2000 were from brood-year 1997, and the SCAA model's final brood-year estimate was for 1996. Therefore, the return from brood-year 1997 was forecasted by applying the model's Ricker spawner–recruit relationship to the spawning abundance in 1997. Then, the forecast of the total run in a given year was the sum of the number at each age. Another approach to determine the 1997 brood-year return would be to simply divide the observed escapement index by γ, the estimated proportion of escapement seen during the 1997 aerial survey.

Results

SCAA model

The constant-p and time-varying approaches of the SCAA model use the same catch-age and escapement information; however, the constant-p approach assumes that brood-year return proportions $p_{a,y}$ remain constant over time and the time-varying approach allows them to vary. For comparison purposes, unweighted residual sums of squares for each data component are compared between the two approaches. Also, brood-year return estimates and CVs for estimated brood-year returns are compared. The remaining results pertain only to the time-varying approach of the SCAA model.

Brood-year return estimates from each approach (constant p and time varying) ranged from 25 000 to 115 000 chinook salmon (Fig. 3). CVs ranged from 8% to 33% (Fig. 4). It appears that the CV values are more favorable for the constant-p approach because fewer parameters are estimated. Estimates from the time-varying approach were somewhat larger than those from the constant-p approach; however, the lower RSS for all components indicates that the time-varying approach better explained the catch-age and escapement data sources (Table 2), showing that brood-year return proportions do vary over time (F test, $P < 0.001$).

One explanation for the large CVs in the earliest years is because brood-year return estimates were smaller, which is a common phenomenon for CVs (Williams and Quinn 1997).

© 2004 NRC Canada

Table 2. Total unweighted residual sums of squares from the constant-*p* approach, time-varying approach, and all weighting scenarios.

		Time varying			
	Constant *p*	Scenario 1	Scenario 2	Scenario 3	Scenario 4
Total catch at age	20 593	8 127	8 927	7 945	8 402
Escapement index	3 059	442	729	1 010	1 349
Spawner–recruit	27 396	25 465	17 905	23 371	11 698
Total	51 048	34 034	27 561	32 326	21 449

Fig. 3. Brood-year return estimates from the time-varying and pooled approaches of the SCAA model. ●, time-varying approach; ×, constant-*p* approach.

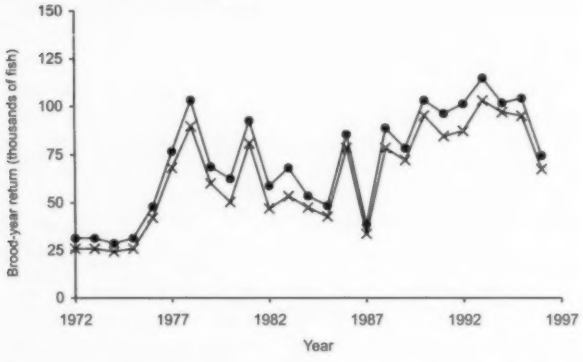

Fig. 4. CVs from the constant-*p* approach (×) and time-varying approach (●).

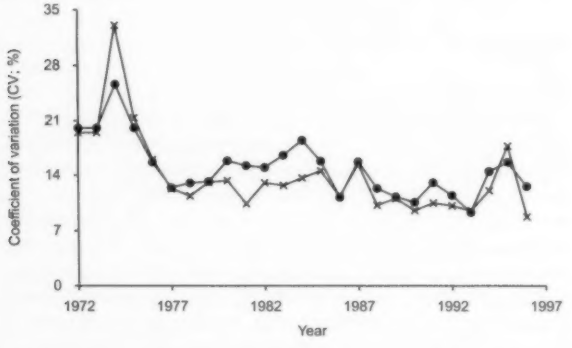

Fig. 5. Observed and estimated escapement index and CVs. Vertical bars indicate 95% confidence intervals. ×, observed aerial count; ▲, estimated aerial count; ○, CVs.

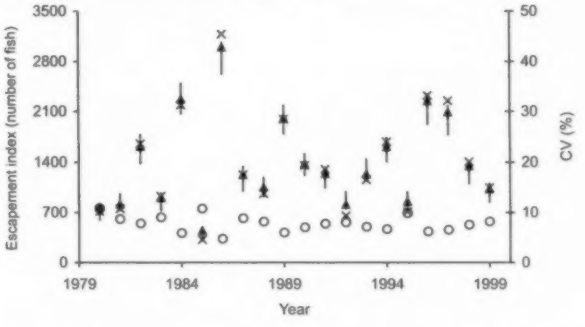

Fig. 6. Catch-age residuals; broken line without symbols, age 3; with ▲, age 4; with ●, age 5; with ■, age 6; solid line without symbols, age 7; with ●, age 8.

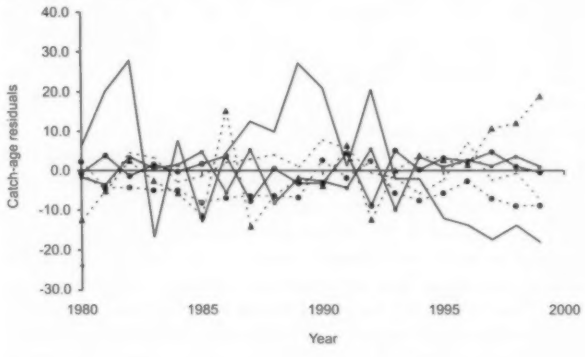

Another possibility could be the incomplete cohort information available to support these estimates.

The time-varying model fitted the escapement index data well, and CVs were generally under 10% (Fig. 5). Nearly all observed values were encompassed by the estimate's confidence intervals. The proportion of total escapement counted through aerial surveys (γ) was estimated at 0.054.

Observed trends in the catch at age were reflected in the model's estimates (Fig. 6). The fit to age-5 and age-6 salmon, which comprised 82% or more of the total observed catch, was exemplary. However, there were some slight residual patterns at the other ages due to assuming constant return proportions for those ages.

Total run estimates reflected trends in the total catch and ranged from 28 000 to 109 000 chinook salmon. Escapement estimates ranged from 8000 to 42 000 chinook salmon and large escapements were associated with large runs (Fig. 7). CVs for the run estimates were small and ranged from 8% to 18%, whereas CVs for escapement estimates were substantially higher but relatively consistent, ranging from 32% to 36%.

An analysis of the residuals revealed that the model's fit to the catch-age and escapement information produced estimates with only slight or no residual patterns (Figs. 6 and 8). In contrast, the spawner–recruit residuals displayed a positive relationship in the most recent years (Fig. 8).

Once the fit to the Ricker spawner–recruit curve was determined, biological reference points such as optimal escapement, S_m, peak spawning abundance, S_p, and the number of recruits at peak spawning abundance, R_p, were calculated,

© 2004 NRC Canada

Fig. 7. Estimates of total run (●) and escapement (▲).

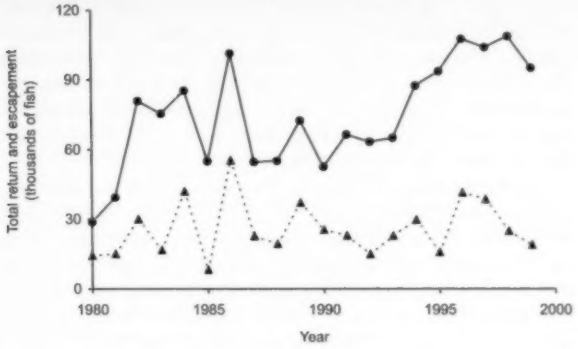

Fig. 8. Escapement index and spawner–recruit residuals.

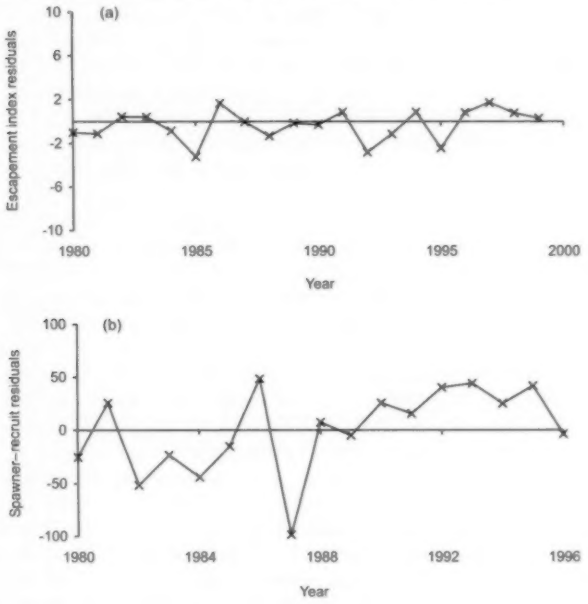

where $(R_p, S_p) = (\alpha/\beta e, 1/\beta)$ (Fig. 9). The estimate of optimal escapement was 19 711, peak spawning abundance was 25 687, the corresponding number of recruits at peak spawning abundance was 87 492, and the MSC was 65 012 chinook salmon. The total exploitation rate corresponding to MSC was 0.77.

Data weighting and sensitivity analysis

The effects of changing the weighting terms, λ_I and λ_F, on the estimated catch were negligible (Fig. 10). In contrast, changing the escapement index weight λ_I had a substantial effect on estimates of the escapement index (Fig. 10). A λ_I of 1.0 (scenarios 1 and 2) induces very little deviation around the escapement index. A λ_I of 0.5 induces the amount of variation one might expect in an escapement index. In contrast, a λ_I of 0.3 (scenario 4) results in a smoothing of extreme index values in later years and consistently overestimates the index in recent years. Although scenarios 1 and 2 relaxed the precise fit to the escapement index, the fit to the catch-age data was diminished (Table 2). We found

Fig. 9. Model fit to the Ricker spawner–recruit relationship. ●, optimal spawning and recruitment (S_m, R_m); ▲, spawner–recruit estimates; curved line, Ricker spawner–recruit relationship; straight line, replacement line where $R = S$.

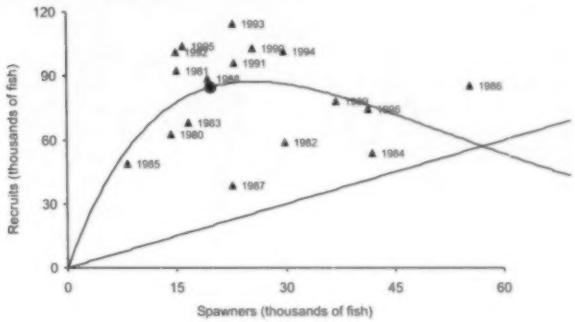

Fig. 10. Observed and estimated total catch and escapement indices from the sensitivity analysis of four different data weighting scenarios. —●—, $\lambda_I = 1.0$ and $\lambda_F = 0.1$; —▲—, $\lambda_I = 1.0$ and $\lambda_F = 0.2$; --■--, $\lambda_I = 0.5$ and $\lambda_F = 0.1$; --●--, $\lambda_I = 0.3$ and $\lambda_F = 0.2$; ×, observed total catch and escapement index.

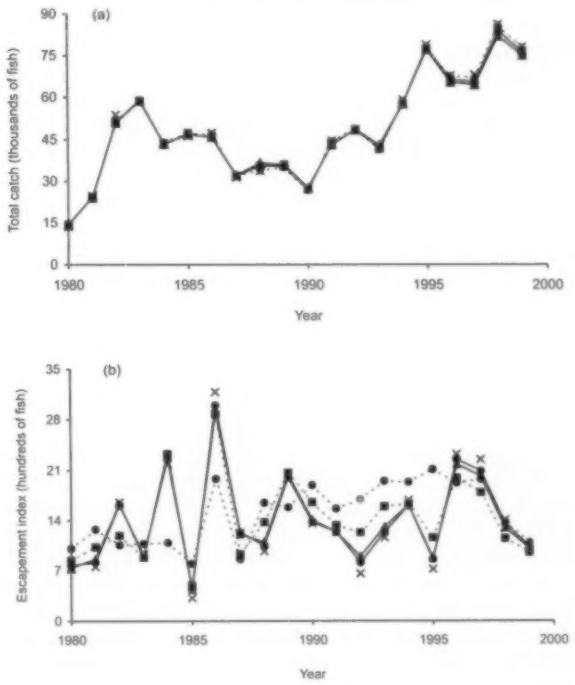

that scenario 3 with $\lambda_I = 0.5$ and $\lambda_F = 0.1$ was the best weighting scenario in terms of the criteria that we established.

A decrease in λ_I from 1.0 (scenario 1) to 0.5 (scenario 3) improved the fit to the catch data and relaxed the precise fit to the escapement index (Table 2; Fig. 10). However, a pairwise comparison test between scenarios 1 and 3 revealed no significant difference between the catch mean squared errors ($r = -0.17$, $P = 0.07$). Because the sensitivity analysis and comparison test revealed that each weighting scenario

© 2004 NRC Canada

Fig. 11. Estimates of brood-year returns from the retrospective analysis (data collected through 1994, 1995, 1996, 1997, 1998, and 1999). ▲, 1980–1999; ■, 1980–1998; ●, 1980–1997; ×, 1980–1996; ○, 1980–1995; □, 1980–1994.

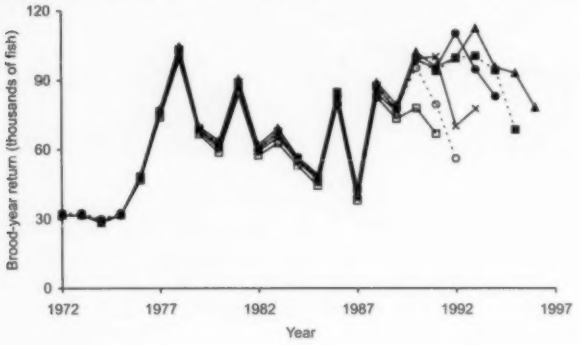

equally described the catch information, further results are given for weighting scenario 1 with $\lambda_I = 1.0$ and $\lambda_F = 0.1$.

Retrospective analysis

A retrospective analysis exposed an incongruity between the 1972 and 1973 brood-year returns and the proportion of 7- and 8-year-olds returning ($p_{a,y}$). The significant autocorrelation in the brood-year return estimates (first-order autocorrelation = 0.49 with $P = 0.02$) justified setting brood-year returns in 1972 and 1973 to the median of the returns in the following three brood years.

After the median adjustment, brood-year return estimates from early years converged to stable values, while estimates from later years tended to vary from one year to the next (Fig. 11). For example, brood-year return estimates for 1991 increased with the addition of another year of catch-age information.

Forecasting future runs

Forecasts of runs from the SCAA model were 93 087 in 1999 (catch-age data through 1998) and 94 916 in 2000 (catch-age data through 1999). The total run estimated from mark–recapture studies was 94 319 chinook salmon in 1999 (Evenson and Wuttig 2000) and 70 077 chinook salmon in 2000 (Wuttig and Evenson 2001). The confidence intervals surrounding the forecasts derived from the model encompassed the mark–recapture estimates. This implies that the model's ability to predict total runs is relatively robust. However, variability in the spawner–recruit relationship and imperfect catch-age and escapement index information will always place uncertainty on the forecasting process.

Discussion

The novel features of the SCAA model include its assimilation of data sources related to catch and escapement and the modeling of the multiyear process by which salmon return to spawn. The SCAA model differs from typical groundfish age-structured models because the estimation of brood-year return proportions eliminates the need to estimate natural mortality. Previous run reconstruction methods required estimation or projection of total escapement, whereas the SCAA model estimates total escapement internally from escapement indices. To do so accurately requires that the escapement index be proportional to total escapement over years. The specification of returning brood-year proportions is the most important aspect of the model. For applicability to multiage salmon populations in general, it appears that brood proportions must be allowed to vary over time, at least for important ages.

The foundation of the SCAA model centers on minimizing the residuals between the observed and estimated values. For Copper River chinook salmon, the SCAA model's fit to the catch-age data was good; all of the observed values fell within the bounds of their corresponding estimates and the CVs were relatively small. For the escapement index, the estimates were precise, and with few exceptions, the CVs were less than 20%.

The assumption that the index of escapement was proportional to the returning population cannot be completely validated. Studies that identify an absolute estimate of escapement or provide a more representative index of the entire escapement would help validate the SCAA model. Such estimates can easily be added into the model. Weighting the escapement index equal to 1 presumed that the uncertainty around the index was equivalent to that found in the catch-age data. Because the escapement index covered a relatively small area, and was only a sample of the true spawning abundance, we suspect that the variability and potential bias in the escapement index were larger than in the catch-age data. However, the weight chosen sufficed to decrease the patterns in the residuals and to allow the model to describe the catch-age information.

The close connection between the SCAA model formulae enabled us to estimate total runs with relatively high precision. Interestingly, CVs for estimates of total escapement were large compared with CVs for estimates of the total run each year. This was surprising because escapement was the run minus the catch, and relatively small CVs around the catch and run estimates should have provided precise estimates of escapement. The relatively poor precision of the escapement estimates may have been a consequence of the run estimates being more susceptible to estimated changes in the brood-year return proportions, which subsequently affected estimates of escapement.

Model uncertainty and residual patterns are often used to determine the value of a particular assessment model. In this analysis, the majority of estimated population parameters exhibited low bias and variability and there were no apparent patterns in the residuals. In contrast, a positive trend was seen in the spawner–recruit residuals. This result was a consequence of the weighting assigned to the spawner–recruit relationship. The Ricker relationship is internal to the model. Therefore, the amount of variation explained could have been improved by increasing the influence, λ_F, on the spawner–recruit RSS. This was not done, to a large degree, because very little is known about this population's spawner–recruit relationship. By design, the Ricker relationship was utilized mainly to provide a constraint for the SCAA model's brood-year return estimates without forcing the model to strictly follow the relationship. Without such a constraint, it was possible for the most recent brood-year returns to be extreme. Other spawner–recruit relationships (such as

© 2004 NRC Canada

Beverton–Holt, nonparametric, or semiparametric) could easily be used instead of the Ricker relationship.

Obtaining reliable measures of escapement and subsequent recruitment is arguably the most challenging problem that an assessment biologist endures. Management of many salmon stocks is based on a fixed escapement goal that provides for MSC. A combination of factors can influence a model's estimate of optimal escapement: (*i*) time series bias, (*ii*) lack of contrast in estimates of escapement, (*iii*) stock structure, and (*iv*) measurement errors in escapement (Walters and Ludwig 1981; Hilborn and Walters 1992). The extent to which these factors operate determines whether the MSC goal is reliable.

Sensitivity analysis revealed that brood-year return, catch, and escapement index estimates were robust to large changes in λs. However, the range that provided a realistic explanation of the data without patterns in the residuals was fairly small. Therefore, a weighting scenario was chosen that resulted in robust parameter estimates that followed the trends in the catch and escapement index while conveying plausible brood-year returns that exhibited a Ricker spawner–recruit relationship.

Retrospective analysis did not reveal any unusual patterns in the most recent brood-year return estimates. Parma (1993) concluded that retrospective patterns arise with the addition of updated catch-age and auxiliary information into catch-age models. One reason for this pattern may be that abundance estimates for the early years in a data series are inclined to converge to stable values, whereas estimates for the most recent years can differ considerably (Pope 1972). Another reason for this pattern stems from modeling a salmon population returning over several years. For example, data through 1999 do not contain complete information on the total return from brood-years 1992–1996. Therefore, the total brood-year returns in recent years are estimated with limited information and by relying on the model's assumptions.

Further investigation into the ratio of the variances of the catch and escapement index data sources would help decipher the most appropriate weighting scenario. Based on the results, we recommend utilizing the model to describe the various data sources and then using sensitivity analysis to ensure that each auxiliary source was weighted accordingly. This would allow managers to see how their perceptions of the auxiliary data sources influenced the model's parameter estimates. By incorporating perceptions into decision-making, beliefs in the accuracy of uncertain stock assessment information are made explicit. Merritt and Quinn (2000) showed that a perception-weighted catch-age model provided the best fit to the data, low parameter uncertainty, and low forecast risk.

The desirability of pooling or stratifying the catch-age data by gear type for Copper River chinook salmon was further explored in Savereide (2001). Estimates from the stratified, commercial, and pooled approaches (see Methods) were all able to track trends in the catch and escapement information. The commercial approach requires the unrealistic assumption that recreational and subsistence catch-age data are measured without error. The stratified approach increases the number of parameters to estimate separate gear selectivities and exploitation rates for each fishery. But small sample sizes from the recreational and subsistence fisheries resulted in an increase in the variability of the catch-age estimates. In this situation, the large proportion of the catch was from the commercial fishery, so that pooling the data maintained the signal from the commercial fishery while allowing for error in the other two data sources.

Based on these results, we think it is surprising that catch-age models are not widely used to assess and manage salmon populations when information on total run size and escapement is unavailable. Greater application of the SCAA model should lead to improvements in the management of other salmon stocks by integrating a variety of information sources into the decision-making process. The SCAA model could be easily generalized to a Bayesian setting. This model accounts for data uncertainty and provides an estimate of optimal escapement and its corresponding exploitation rate. One key to our success was the ability to increase model parsimony by assuming that some ages had constant brood-year return proportions over time. In other applications, success will also likely depend on the ability to model the time variation in the brood-year return proportions. As more ages require time dependence, then the number of parameters to be estimated increases, with the result that variance in parameter estimates goes up. Perhaps parametric representations for the proportions could be developed to maintain parsimony but still allow variation over time.

The assumption that selectivity of the gear was separable into age and time factors also reduced the number of parameters to be estimated. If time variation in selectivity is thought to occur, then it may be possible to use the nonadditivity model of Myers and Quinn (2002) to relax the separability assumption.

Acknowledgments

Financial support for this analysis was provided by the Alaska Department of Fish and Game, Sport Fish Division, through the Alaska Cooperative Fish and Wildlife Research Unit. We thank Dr. Milo Adkison, Dr. Margaret Merritt, Matt Evenson, and Don Roach for their helpful suggestions during the modeling process. We also thank Paul Starr and an anonymous referee for their reviews, which led to substantial improvement in the paper.

References

Deriso, R.B., Quinn, T.J., II, and Neal, P.R. 1985. Catch-age analysis with auxiliary information. Can. J. Fish. Aquat. Sci. **42**: 815–824.

Doubleday, W.G. 1976. A least squares approach to analyzing catch at age data. Int. Comm. Northwest Atl. Fish. Res. Bull. **12**: 69–81.

Dupont, W.D. 1983. A stochastic catch-effort method for estimating animal abundance. Biometrics, **39**: 1021–1033.

Efron, B., and Tibshirani, R.J. 1993. An introduction to the bootstrap. Chapman and Hall, Inc., New York.

Evenson, M.J., and Wuttig, K.W. 2000. In-river abundance, spawning distribution, and migratory timing of Copper River chinook salmon in 1999. Fishery Data Series No. 00-32, Alaska Department of Fish and Game, Anchorage, Alaska. (Available from Sport Fish Division, Alaska Department of Fish and Game, 333 Raspberry Road, Anchorage, AK 99515, USA.)

Fournier, D., and Archibald, C.P. 1982. A general theory for analyzing catch at age data. Can. J. Fish. Aquat. Sci. **39**: 1195–1207.

© 2004 NRC Canada

Gudmundsson, G. 1994. Time series analysis of catch-at-age observations. Appl. Stat. **43**: 117–126.

Hilborn, R., and Walters, C.J. 1992. Quantitative fisheries stock assessment: choice, dynamics, and uncertainty. Chapman and Hall, Inc., New York.

Kope, R.G. 1987. Separable virtual population analysis of Pacific salmon with application to marked chinook salmon, *Oncorhynchus tshawytscha*, from California's Central Valley. Can. J. Fish. Aquat. Sci. **44**: 1213–1220.

McAllister, M.K., and Ianelli, J.N. 1997. Bayesian stock assessment using catch-age data and the sampling-importance resampling algorithm. Can. J. Fish. Aquat. Sci. **54**: 284–300.

McAllister, M.K., Pikitch, E.K., Punt, A.E., and Hilborn, R. 1994. A bayesian approach to stock assessment and harvest decisions using the sampling/importance resampling algorithm. Can. J. Fish. Aquat. Sci. **51**: 2673–2687.

Megrey, B.A. 1989. Review and comparison of age-structured stock assessment models from theoretical and applied points of view. Am. Fish. Soc. Symp. **6**: 8–48.

Merritt, M.F., and Quinn, T.J., II. 2000. Using perceptions of data accuracy and empirical weighting of information: assessment of a recreational fish population. Can. J. Fish. Aquat. Sci. **57**: 1459–1469.

Myers, R.A., and Quinn, T.J., II. 2002. Estimating and testing non-additivity in fishing mortality: implications for detecting a fisheries collapse. Can. J. Fish. Aquat. Sci. **59**: 597–601.

Paloheimo, J.E. 1980. Estimation of mortality rates in fish populations. Trans. Am. Fish. Soc. **109**: 378–386.

Parma, A.M. 1993. Retrospective catch-at-age analysis of Pacific halibut: implications on assessment of harvesting policies. *In* Proceedings of the International Symposium on Management Strategies for Exploited Fish Populations. *Edited by* G. Kruse, D.M. Eggers, R.J. Marasco, C. Pautzke, and T.J. Quinn II. Alaska Sea Grant College Program AK-SG-93-02, Fairbanks, Alaska. pp. 247–265.

Pope, J.G. 1972. An investigation of the accuracy of virtual population analysis using cohort analysis. Int. Comm. Northwest Atl. Fish. Res. Bull. **9**: 65–74.

Pope, J.G. 1977. Estimation of fishing mortality, its precision and implication for the management of fisheries. *In* Fisheries mathematics. *Edited by* J.H. Steele. Academic Press, New York. pp. 63–76.

Quinn, T.J., II. 1985. Catch-per-unit-effort: a statistical model for Pacific halibut (*Hippoglossus stenolepis*). Can. J. Fish. Aquat. Sci. **42**: 1423–1429.

Quinn, T.J., II, and Deriso, R.B. 1999. Quantitative fish dynamics. Oxford University Press, New York.

Quinn, T.J., II, and Gates, R. 1997. Estimation of salmon escapement: models with entry, mortality, and stochasticity. Nat. Resour. Model. **10**: 217–250.

Quinn, T.J., II., Turnbull, C.T., and Fu, C. 1998. A length-based population model for hard-to-age invertebrate populations. *In* Proceedings of the International Symposium on Fishery Stock Assessment Models. *Edited by* F. Funk, T.J. Quinn II, J. Heifetz, J.N. Ianelli, J.E. Powers, J.F. Schweigert, P.J. Sullivan, and C.-I. Zhang. Alaska Sea Grant College Program AK-SG-98-01, Fairbanks, Alaska. pp. 531–556.

Saaty, T.L. 1990. Decision making for leaders. University of Pittsburg, Pittsburgh, Pa.

Savereide, J.W. 2001. An age structured model for assessment and management of Copper River chinook salmon. M.S. thesis, University of Alaska Fairbanks, Fairbanks, Alaska.

Schnute, J.T., and Richards, L.J. 1995. The influence of error on population estimates from catch-age models. Can. J. Fish. Aquat. Sci. **52**: 2063–2077.

Sinclair, A., Gascon, D., O'Boyle, D., Rivard, D., and Gavaris, S. 1991. Consistency of some northwest Atlantic groundfish stock assessments. NAFO Sci. Counc. Stud. **16**: 59–77.

Taube, T.T. 2000. Area management report for the recreational fisheries of the Upper Copper/Upper Susitna River management area, 1996–1997. Fishery Management Report No. 00-04, Alaska Department of Fish and Game, Anchorage, Alaska. (Available from Sport Fish Division, Alaska Department of Fish and Game, 333 Raspberry Road, Anchorage, AK 99515, USA.)

Templin, W.D., Collie, J.S., and Quinn, T.J., II. 1996. Run reconstruction of the wild pink salmon fishery in Prince William Sound, 1990–1991. Am. Fish. Soc. Symp. **18**: 499–508.

Walters, C.J., and Ludwig, D. 1981. Effects of measurement errors on the assessment of stock–recruitment relationships. Can. J. Fish. Aquat. Sci. **38**: 704–710.

Williams, E.H., and Quinn, T.J., II. 1997. Age-structured analysis of Pacific herring from Norton Sound, Alaska. Alaska Fish. Res. Bull. **4**: 87–109.

Wuttig, K.W., and Evenson, M.J. 2001. In-river abundance, spawning distribution, and migratory timing of Copper River chinook salmon in 2000. Fishery Data Series No. 01-22, Alaska Department of Fish and Game, Anchorage, Alaska. (Available from Sport Fish Division, Alaska Department of Fish and Game, 333 Raspberry Road, Anchorage, AK 99515, USA.)

Appendix A. Run reconstruction

A simple run reconstruction was completed under the following assumptions to obtain preliminary brood-year estimates for the salmon catch-age analysis (SCAA) model: (*i*) the estimated age composition was measured without error, (*ii*) the estimated harvest was measured without error, (*iii*) a constant commercial exploitation rate existed over all ages and years, and (*iv*) the sampled proportion at each age was the true population proportion at each age.

For each age a and year t, the total commercial catch is defined as C_t. The abundance or run by age and year equals $N_{a,t}$. The total run in year t or the sum of $N_{a,t}$ equals the Run_t. The brood-year return at each age indexed by brood-year y is defined as $R_{a,y}$. The remaining variables include the commercial exploitation rate, μ_t, and the proportion at each age in the commercial catch, $p_{a,t}$. In the run reconstruction, we assumed that the age structure in the run was the same as the age structure in the catch and substituted the catch proportions for the unknown run proportions.

The total run was estimated as the total commercial catch divided by the commercial exploitation rate:

$$\text{(A1)} \quad \text{Run}_t = \frac{C_t}{\mu_t}$$

A constant commercial fishery exploitation rate of 0.55 was used. This rate was determined from a mark–recapture experiment and the commercial catch estimate from 1999 (Evenson and Wuttig 2000).

The number of fish at each age was the total run multiplied by the proportion of the commercial catch sampled at that age:

$$\text{(A2)} \quad N_{a,t} = \text{Run}_t p_{a,t}$$

The brood-year return at each age a indexed by brood-year y was identical to the abundance at age a in year $a + y$:

© 2004 NRC Canada

(A3) $R_{a,y} = N_{a,a+y}$

For example, $R_{3,1977}$ equals the number of age-3 fish from the 1977 brood-year that returned in 1980. Finally, total brood-year returns were determined by summing the returns at each age:

(A4) $R_y = \sum_a R_{a,y}$

Reference

Evenson, M.J., and Wuttig, K.W. 2000. In-river abundance, spawning distribution, and migratory timing of Copper River chinook salmon in 1999. Fishery Data Series No. 00-32, Alaska Department of Fish and Game, Anchorage, Alaska. (Available from Sport Fish Division, Alaska Department of Fish and Game, 333 Raspberry Road, Anchorage, AK 99515, USA.)

© 2004 NRC Canada

Quantitative reconstruction of past salinity variations in African lakes: assessment of chironomid-based inference models (Insecta: Diptera) in space and time

Dirk Verschuren, Brian F. Cumming, and Kathleen R. Laird

Abstract: Faunal records of 20 common midge species (Diptera: Chironomidae) in 32 African surface waters with salinities ranging from 20 to 41 000 $\mu S \cdot cm^{-1}$ were used to develop inference models for quantitative reconstruction of past salinity variations from larval chironomid fossils preserved in lake sediments. Weighted-averaging regression and calibration models using presence–absence data (P/A) and presence–absence data with tolerance down-weighting (P/A_{tol}) produced bootstrapped coefficients of determination (r^2) of 0.78 and 0.81, respectively, and root mean squared errors (RMSE) of prediction of 0.42 and 0.39 log conductivity units. Historical conductivity data from African lakes are scarce. Therefore, model performance was tested in time by comparing chironomid-inferred conductivity estimates with the corresponding diatom-inferred estimates in sediment records of two fluctuating lakes in the Rift Valley of Kenya. A hybrid procedure in which presence–absence calibration models were applied to abundance-weighted fossil data yielded significantly higher correlation between chironomid- and diatom-inferred time series (Lake Oloidien AD 1880–1991, r^2 = 0.76–0.78; Crescent Island Crater AD 900–1993, r^2 = 0.56–0.61) than by applying the same models to presence–absence fossil data (r^2 = 0.47–0.56 and 0.26–0.42, respectively). Overall, model performance confirms that Chironomidae are valuable bioindicators for natural and man-made changes in the water balance of African lakes.

Résumé : Nous avons combiné les données de la répartition de 20 espèces de moucherons (Diptères: Chironomidae) dans 32 lacs africains aux salinités mésurant entre 20 $\mu S \cdot cm^{-1}$ et 41 000 $\mu S \cdot cm^{-1}$ avec des données chimiques de ces lacs et développé des modèles de déduction pour la reconstruction de variations de salinité à partir d'assemblages de chironomides fossiles préservés dans les sédiments lacustres. Les modèles de régression et d'étalonnage à pondération de moyenne utilisant des donneés présence–absence (P/A) ou présence–absence avec minorisation des tolérances (P/A_{tol}) produisaient des coefficients de détermination (r^2) de 0,78 et 0,81 et des erreurs quadratique moyenne bootstrap (RMSE) de 0,42 et 0,39. De mesures historiques de salinité provenant des lacs Africains étant assez rare, les testes de performance de ces modèles dans le domaine temporel ont été fait aussi par comparer les estimations de salinité passées déduites des chironomides avec celles déduites des diatomées dans les enregistrements paléolimnologiques de deux lacs fluctuants dans la Vallée du Rift au Kenya. Un procédé hybride applicant les modèles d'étalonnage présence–absence aux données fossiles d'abondances ponderées a réalisé des corrélations (Lake Oloidien AD 1880–1991, r^2 = 0,76–0,78; Crescent Island Crater AD 900–1993, r^2 = 0,56–0,61) supérieures aux celles obtenus par applicant les mêmes modèles aux données fossiles présence–absence. La performance de ces modèles confirme le potentiel des Chironomides fossiles en tant qu'indicateurs aux changements climatiques et anthropogènes de la hydrologie des lacs africains.

Introduction

Sediments accumulating on the bottom of fluctuating lakes are a major source of information on past climate change in subhumid and semiarid regions worldwide. Long-term variation in the regional balance of rainfall and evaporation (i.e., effective moisture integrated over the drainage basin) drives changes in lake level and water chemistry, which in turn influence sedimentation, oxygenation, nutrient cycling, and the osmotic stress to which aquatic biota are exposed. If limnological conditions permit undisturbed sediment accumulation over a sufficiently long period of time despite climate-driven lake-level changes (Dearing 1997; Verschuren 1999), lake-system response to climate change is incorporated in

Received 15 November 2002. Accepted 30 November 2003. Published on the NRC Research Press Web site at http://cjfas.nrc.ca on 27 July 2004.
J17186

D. Verschuren.[1] Department of Biology, Ghent University, Ledeganckstraat 35, B-9000 Ghent, Belgium.
B.F. Cumming and K.R. Laird. Paleoecological Environmental Assessment and Research Laboratory, Department of Biology, Queen's University, Kingston, ON K7L 3N6, Canada.

[1]Corresponding author (e-mail: dirk.verschuren@UGent.be).

 doi: 10.1139/F04-041 © 2004 NRC Canada

the sediment record as a datable sequence of characteristic sedimentological, geochemical, and biological signatures. This allows the sediment record to be used as a natural archive from which the history of past climate change can be reconstructed (Smol et al. 1991).

Accurate, quantitative reconstruction of climate history from lake-sediment records requires calibration of the relationships between the various sedimentary climate indicators and climate-driven changes in water balance. For biological climate indicators (e.g., diatoms, chrysophytes, ostracods, and chironomids), this most often involves the development of transfer functions (Birks et al. 1990), which mathematically describe the modern distribution of individual species across a representative collection of lakes in relation to select environmental variables that reflect a lake's hydrological status (e.g., depth or salinity). Over the past decade, these numerical methods have evolved to include robust procedures for error estimation and are now an established research tool in biological paleolimnology (Birks 1998). Nevertheless, statistical inference of past climate always carries significant uncertainty, even when the link between a particular climate indicator and climate has been validated through comparison with instrumental climate or lake-monitoring data (e.g., Laird et al. 1996). This is because linkages between aquatic community structure (more specifically, its preserved fossil counterpart) and climate-driven changes in water balance are often complex and characterized by threshold effects (Smol and Cumming 2000). Much effort is currently directed at generating multiple time series of (quasi-) independent climate-indicator data from physical, biological, and geochemical sources in the same lake-sediment record on the premise that an integrated evaluation of these multiple lines of evidence should allow a more coherent and trustworthy reconstruction of past climate.

Fossil diatoms are among the biological indicators most widely used in climate reconstruction (Stoermer and Smol 1999), and in Africa they are currently the best-studied biological indicators for climate-driven changes in lake water balance (Fritz et al. 1999). Fossil midge larvae (Diptera: Chironomidae), in contrast, had until recently been little exploited as a biomonitoring tool for past environmental change in Africa (Walker 1995), although they are well-established indicators of late Quaternary climate change in north-temperate regions (e.g., Levesque et al. 1993; Brooks et al. 1997; Brooks and Birks 2000). As in diatoms, chironomid species distribution in tropical aquatic ecosystems is strongly influenced by salinity (Pinder 1995), both directly due to variable tolerance to the osmotic stress caused by high and (or) fluctuating salinity (Bayly 1972) and indirectly due to the role of salinity in the distribution of suitable substrates and food (Williams 1984). The dominant influence of salinity on chironomid faunal composition in African lakes is amply documented by regional surveys (e.g., Tudorancea et al. 1989) and field studies of shallow lakes going through multiyear cycles of lake-level decline and recovery (McLachlan 1979; Vareschi and Vareschi 1984). Paleolimnological sensitivity studies (Verschuren et al. 1999*a*, 2000*a*) likewise demonstrated rapid restructuring of chironomid faunas in response to climate-driven changes in lake depth, salinity, or mixing regime. African Chironomidae are already being used in paleoenvironmental reconstructions (Mees et al. 1991; Verschuren et al. 1999*b*, 2002), but mainly through a qualitative, indicator-species approach. Quantitative chironomid paleoecology in Africa is hampered by inadequate knowledge of species' habitat preferences and environmental tolerances. This situation could be improved through standardized collection of linked faunal and environmental data from a suitably large number of African lakes, but political and logistic factors render rapid completion of such a reference data set unlikely.

In the context of lake-based climate reconstruction in East Africa (Verschuren et al. 2000*b*), we developed quantitative conductivity-inference models based on published presence–absence (P/A) data of 20 common species of Chironomidae in 32 African surface waters. In this paper, we assess the performance of these models in space and time by (*i*) examining associated statistical parameters; (*ii*) comparing chironomid-inferred conductivity estimates with instrumental conductivity data spanning the past 70 years; and (*iii*) comparing chironomid- and diatom-inferred conductivity estimates in the sediment records of two lakes in Kenya that cover 200 and 1100 years of environmental history. Performance assessment in time, in particular, is critical to determine the real potential and applicability of a biological inference model in paleoenvironmental reconstruction.

Methods

Chironomid calibration data set

We compiled data on the modern distribution of African Chironomidae in relation to salinity from 37 published species lists (1–13 species; mean = 3.8) from 32 African surface waters (29 lakes, two reservoirs, and one slow-flowing river), ranging from 20 to 41 000 $\mu S \cdot cm^{-1}$ (Table 1). Many of the surveyed lakes are large to very large, reflecting a historical research bias for lakes with socio-economic significance (Hare and Carter 1987). Most shallow African lakes are hydrologically closed (Livingstone and Melack 1984) or river-fed amplifier systems (Street-Perrott and Roberts 1983) characterized by significant long-term variation in depth, surface area, and water chemistry. When chemistry data from the time of collection were not available, we used the mean of historical conductivity values when variation was low (Opi, 15–25 $\mu S \cdot cm^{-1}$; Upemba, 145–255 $\mu S \cdot cm^{-1}$; George, 165–207 $\mu S \cdot cm^{-1}$; Baringo, 460–530 $\mu S \cdot cm^{-1}$; Langano, 1643–1728 $\mu S \cdot cm^{-1}$; Chitu, 40 000 – 40 810 $\mu S \cdot cm^{-1}$). In lakes with significant conductivity variation (Oloidien, 472–2900 $\mu S \cdot cm^{-1}$; Chilwa, 300–12 000 $\mu S \cdot cm^{-1}$; Nakuru, 11 000 – 160 000 $\mu S \cdot cm^{-1}$), collections without linked conductivity data were excluded, and collections from periods of distinctly different conductivity were treated separately. We also excluded faunal surveys based on light trapping of adult midges because such collections cannot be linked with certainty to a specific aquatic larval habitat.

Diatom calibration data set and conductivity-inference model

The African diatom calibration data set consists of 274 modern diatom floras and linked water-chemistry data from 164 African surface waters ranging from 40 to ~100 000 $\mu S \cdot cm^{-1}$ (Gasse et al. 1995). This data set was created by combining regional data sets from Northwest Africa,

© 2004 NRC Canada

Table 1. Geographical and conductivity data on 32 surface waters in tropical Africa with studied collections of chironomid larvae.

No.	Name	Type	Latitude	Longitude	Area (ha)	Conductivity ($\mu S \cdot cm^{-1}$)
1	Opi	Fluvial	06°45′N	07°29′E	2	20
2	Chari	River	12°03′N	15°00′E	na	60
3	Kariba	Rreservoir	17°00′S	28°00′E	525 000	75
4	Victoria	Tectonic	01°00′S	33°00′E	6 880 000	98
5	Chad South	Tectonic	12°55′N	14°15′E	950 000	108
6	George	Tectonic	00°00′N	30°13′E	25 000	186
7	Upemba	Tectonic	08°40′S	26°20′E	53 000	200
8	Koka	Reservoir	08°23′N	39°04′E	1 5 000	224
9	Naivasha	Tectonic	00°45′S	36°20′E	17 100	308
10	Ziway	Tectonic	08°00′N	38°50′E	43 400	350
11	Chilwa	Tectonic	15°20′S	35°40′E	70 000	250; 2 500[a]
12	Baringo	Tectonic	00°37′N	36°05′E	13 000	495
13	Chad North	Tectonic	13°35′N	13°40′E	950 000	525
14	Tanganyika	Tectonic	06°00′S	29°30′E	3 290 000	606
15	Oloidien	Tectonic	00°47′S	36°16′E	574	620
16	Albert	Tectonic	01°40′N	31°00′E	559 000	730
17	Abaya	Tectonic	06°20′N	37°50′E	116 200	800
18	Awasa	Tectonic	07°03′N	38°24′E	8 800	868
19	Edward	Tectonic	00°20′S	29°35′E	215 000	925
20	Chamo	Tectonic	05°50′N	37°34′E	55 100	1 078
21	Kivu	Tectonic	02°00′S	29°07′E	237 000	1 240
22	Langano	Tectonic	07°36′N	38°45′E	23 000	1 686
23	Djiboulboul	Interdunal	13°45′N	14°30′E	Fragmented	2 600
24	Sonachi	Maar crater	00°47′S	36°16′E	14	3 000
25	Aranguadi	Maar crater	00°45′N	39°00′E	54	5 100
26	Kilotes	Maar crater	00°45′N	39°00′E	77	6 300
27	Nakuru	Tectonic	00°22′S	36°05′E	4 200	11 000 – 28 000[b]
28	Abijata	Tectonic	07°36′N	38°36′E	20 500	15 120
29	Shala	Tectonic	07°28′N	38°31′E	40 900	22 470
30	Bogoria	Tectonic	00°16′N	36°09′E	3 300	35 700
31	Elementeita	Tectonic	00°27′S	36°05′E	1 800	38 000
32	Chitu	Maar crater	07°24′N	38°25′E	80	40 405

Note: Lake surface-area values are approximate, since many lakes fluctuate considerably between years. Conductivity values are those linked directly to the chironomid collections; in saline lakes, known historical ranges are often significantly larger. Primary references for the collections and linked water-chemistry data are given in Verschuren (1997). na, not applicable.

[a] $n = 2$.

[b] $n = 5$.

East Africa, and Niger and includes both live and recently buried diatom assemblages from various inland aquatic environments, including lakes, swamps, bogs, and springs. Diatom-based conductivity estimates were calculated with a weighted-averaging regression and calibration model that with inverse deshrinking, has a jackknifed coefficient of determination (r^2) of 0.81 and a root mean squared error (RMSE) of prediction of 0.39 log conductivity units.

Chironomid-based conductivity-inference models

The chironomid-based conductivity-inference models are derived from P/A data of 20 species (= taxa) at 37 different values (= sites) of surface-water conductivity. Conductivity values were log-transformed before model development to compensate for their skewed distribution towards low conductivity values. The mean and standard deviation of each species' reported conductivity range were used as estimates of its conductivity optimum and tolerance, respectively. Consequently, species with narrow tolerances in the model are either species with narrow preferences or species reported from few sites. Two species with only one confirmed occurrence each (*Psectrocladius viridescens* and *Chironomus alluaudi*) were retained for model calibration because of their high abundances in the fossil data sets available for model testing. Using the computer program WACALIB v. 3.5 (Line et al. 1994), we developed two types of models: one based on estimated conductivity optima (P/A models) and one based on estimates of both optima and tolerances (P/A_{tol} models). In the latter, *Psectrocladius viridescens* and *Chironomus alluaudi* are effectively removed from calculations because WACALIB 3.5 awards species with single occurrences in the calibration data set a default tolerance range that is several orders of magnitude larger than that of other species. In both P/A and P/A_{tol} models, an inverse

© 2004 NRC Canada

deshrinking step was used to rescale the conductivity estimates (Line et al. 1994). Conductivity inference from fossil assemblages was done (*i*) directly on fossil percent-abundance data and (*ii*) after transforming fossil percent-abundance data to P/A data. We refer to the former as hybrid model applications, because the P/A and P/A_{tol} models are calibrated using modern P/A data, but then each species in a fossil assemblage is given a weight proportional to its percent abundance. These applications should be considered as exploratory, as no sample-specific error estimates can be generated from data expressed on two different scales.

Assessment of model performance in space and time

We evaluated the capacity of our inference models to predict the modern conductivity of reference lakes from their r^2 and RMSE values and from the distribution of residuals. For this analysis, we used conductivity estimates generated through bootstrapping (Line et al. 1994) to avoid a possibly misleading inflation of the predictive ability of transfer functions that occurs when the same samples and lakes are used for model development and evaluation (Birks et al. 1990). We assessed model performance in a temporal context through comparisons of the conductivity estimates based on fossil chironomids with historical conductivity measurements and with conductivity estimates based on fossil diatoms. For these analyses, we used sediment-core data from Lake Oloidien (Verschuren et al. 1999*b*) and Crescent Island Crater (Verschuren et al. 2000*b*) and a compilation of historical water-chemistry data from these lakes (Verschuren 1996). The fossil and historical data are linked through core chronologies based on ^{210}Pb dating and anchored in a sequence of marker horizons reflecting historical events (Verschuren 1999). The fossil data from Lake Oloidien comprise 23 paired chironomid and diatom assemblages extracted at 4-cm intervals from core NO91.1-S, which covers the last ~200 years; the historical period (1883–1991) is covered by 18 paired samples. The fossil data set totals 3023.5 specimens (15–312.5 per sample, mean = 131.5), of which 99.2% is identified to species with reference to Verschuren (1997) and the primary literature mentioned therein. Twenty-seven species were found; the subset of 14 species that are represented in our calibration data set accounts for 96.9% (range 91.2%–100% per sample) of the fossil inventory. Crescent Island Crater fossil data comprise 149 paired chironomid and diatom assemblages extracted at 4-cm intervals in the upper 602 cm of core NC93.2-L, which covers the last ~1100 years; the historical period (1883–1993) is covered by 30 samples. This fossil data set totals 9264.5 specimens (4.5–188 per sample, mean = 62.2), of which 99.8% is identified to species. Twenty-five species were found; the 13 species represented in the calibration data set account for 97.5% (range 87.3%–100%) of the fossil inventory. Our comparison of conductivity-inference models used all 23 paired chironomid and diatom assemblages from Lake Oloidien and 130 paired assemblages from Crescent Island Crater. In the latter record, 20 intervals from near the surface and between 192- and 264-cm depth were combined two-by-two to obtain a chironomid fossil count of at least 20 specimens; nine samples from thick monospecific diatom mats (Verschuren et al. 2000*b*) were omitted because they likely represent short-term sedimentation events.

Results

Chironomid calibration data set

The species in the calibration data set were present at 1–15 sites (mean = 7.1). The estimated conductivity optimum of most species is below 1000 $\mu S \cdot cm^{-1}$, and tolerances typically span an order of magnitude (Fig. 1). Only three taxa, *Microchironomus deribae*, *Kiefferulus disparilis*, and *Tanytarsus minutipalpis*, have optima above 5000 $\mu S \cdot cm^{-1}$ and can be considered halobiontic. *Cladotanytarsus pseudomancus* is euryhaline, occurring throughout the freshwater range and in saline waters up to 21 000 $\mu S \cdot cm^{-1}$. Weighted-averaging inference models based on these P/A data possess high coefficients of determination (r^2_{boot} = 0.78–0.81) and fairly low RMSEs of prediction (0.39–0.42 log conductivity units; Fig. 2). However, uneven distribution of the prediction error along the conductivity gradient (i.e., systematic variation in the difference between observed and inferred values) show that both the P/A and P/A_{tol} models are rather insensitive to conductivity variation within a broad range of fresh waters. Transition from fresh to saline waters appears characterized by wholesale species replacement around 3000 $\mu S \cdot cm^{-1}$.

Lake Oloidien fossil record

We previously found good agreement between conductivity estimates inferred from fossil diatom assemblages and independent historical data (Verschuren et al. 1999*b*). Briefly, maximum inferred values of 12 700 – 13 600 $\mu S \cdot cm^{-1}$ (Figs. 3*a*–3*b*) during the mid-19th century agree with early reports from Maasai herdsmen that Lake Oloidien was not suited to water their cattle. Given the model-specific prediction error of 0.39 log conductivity units (Gasse et al. 1995), minimum inferred values of 300–350 $\mu S \cdot cm^{-1}$ during the early 20th century high stand, when Lake Oloidien was confluent with the main basin of Lake Naivasha, agree well with a measured value of 472 $\mu S \cdot cm^{-1}$ from Lake Oloidien in 1930 and values of 320–431 $\mu S \cdot cm^{-1}$ from Lake Naivasha in 1929–1931. Diatom-inferred values of 540–890 $\mu S \cdot cm^{-1}$ during recent decades also agree with measured values of 620–1040 $\mu S \cdot cm^{-1}$ for the period 1973–1984. Decreasing values of inferred conductivity to 540 $\mu S \cdot cm^{-1}$ at the sediment surface suggest that recently buried fossil assemblages do not yet reflect the renewed rise of lake-water conductivity during the late 1980s (to ~1200 $\mu S \cdot cm^{-1}$ in 1991, when the core was collected). No instrumental conductivity data are available from during or shortly after the low stand of 1946–1957, so it is uncertain whether the diatom-inferred high of 6500 $\mu S \cdot cm^{-1}$ towards the end of that low stand was in fact reached. Strong reductions in most freshwater invertebrates at that time, among the Chironomidae as well as other groups (Verschuren et al. 1999*b*), suggest that conductivity did exceed 3000 $\mu S \cdot cm^{-1}$, a common physiological limit for aquatic invertebrates (Hammer 1986).

During the past 200 years, the chironomid community of Lake Oloidien experienced several distinct shifts (Fig. 4). Assemblages from before ~1890 are characterized by the presence of halobiontic species such as *Microchironomus deribae* and *Kiefferulus disparilis* and peak abundance of the euryhaline *Cladotanytarsus pseudomancus*. A silty clay horizon at the bottom of the core, representing intermittent lake desiccation before ~1840, is dominated by the halobionts, in

© 2004 NRC Canada

Fig. 1. Range and average documented conductivity of 20 common Chironomidae in African lakes (thin lines and step, with number of records), with means and standard deviations of log-transformed values (thick lines and solid circles) as used in the inference models.

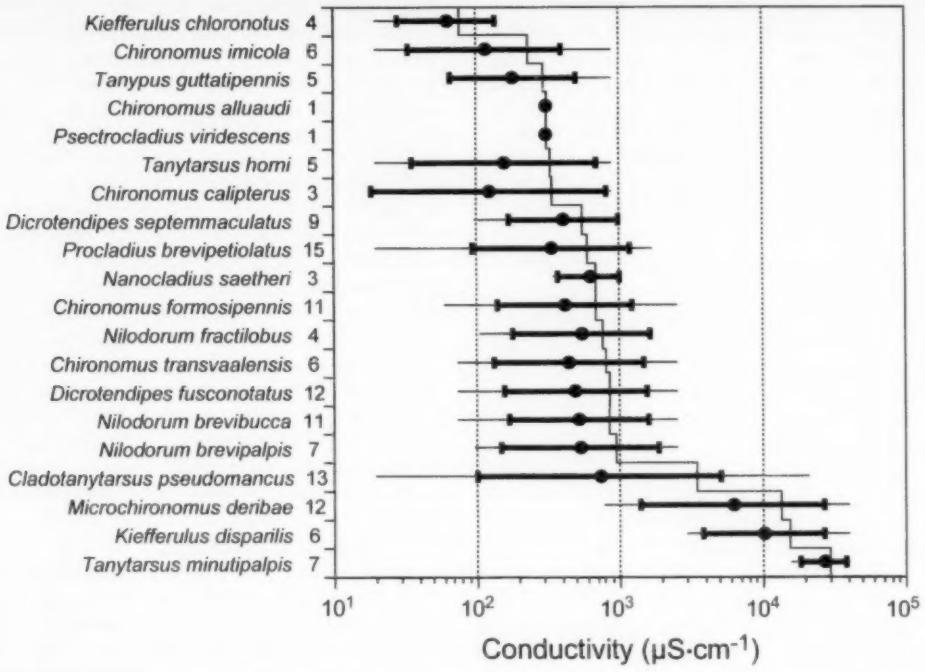

Fig. 2. Chironomid-inferred versus observed conductivity in modern African lakes (n = 37) based on presence–absence calibration models without (*a*: P/A) and with (*b*: P/A_{tol}) species down-weighing proportional to their tolerance, using inverse deshrinking and bootstrapping. Solid line, linear regression; broken line, equality between observed and predicted values.

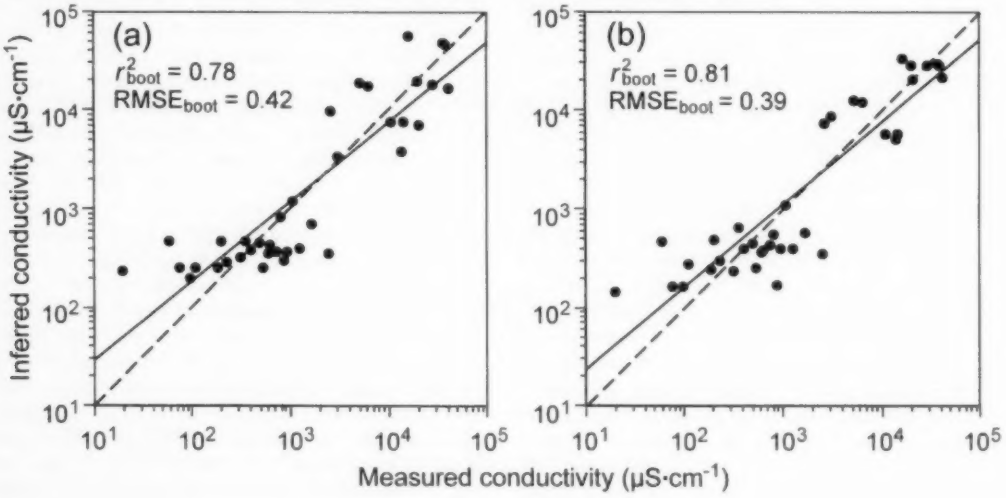

particular *Tanytarsus minutipalpis*. In contrast, assemblages dated between 1890 and 1940 are characteristic of freshwater conditions, with peak abundances of *Tanytarsus horni* and *Dicrotendipes septemmaculatus*. Between ~1940 and 1970, these are displaced again by more salt-loving and salt-tolerant species. Chironomid assemblages in the top 20 cm of the core reflect the return of freshwater conditions after ~1970.

Chironomid-inferred conductivity estimates for Lake Oloidien (Figs. 3*c*–3*f*) are within the prediction error of available instrumental data, except that surface-sediment assemblages also fail to reflect the renewed rise of lake-water conductivity during the late 1980s. Conductivity values of 475 and 345 µS·cm^{-1} inferred for ~1930 using the simple P/A and P/A_{tol} models match the measured range of 320–472 µS·cm^{-1}, and values of 400–845 µS·cm^{-1} for ~1970–

© 2004 NRC Canada

Fig. 3. Chironomid-inferred reconstructions of past conductivity variations in Lake Oloidien (Kenya) compared with diatom-inferred conductivity estimates and historical measurements. (*a*) Lake-level change over the past ~200 years (solid and stippled lines) relative to the elevation of the sill separating Lake Oloidien from Lake Naivasha (broken line; Verschuren 1999). (*b*) Diatom-inferred conductivity reconstruction using the inference model of Gasse et al. (1995), compared with historical measurements (diamonds). (*c–f*) Chironomid-inferred conductivity reconstructions using presence–absence calibration models without (*c*, *e*: P/A) and with (*d*, *f*: P/A_{tol}) tolerance down-weighing applied to fossil presence–absence data (*c*, *d*: simple P/A and P/A_{tol}) and fossil percent-abundance data (*e*, *f*: hybrid P/A and P/A_{tol}).

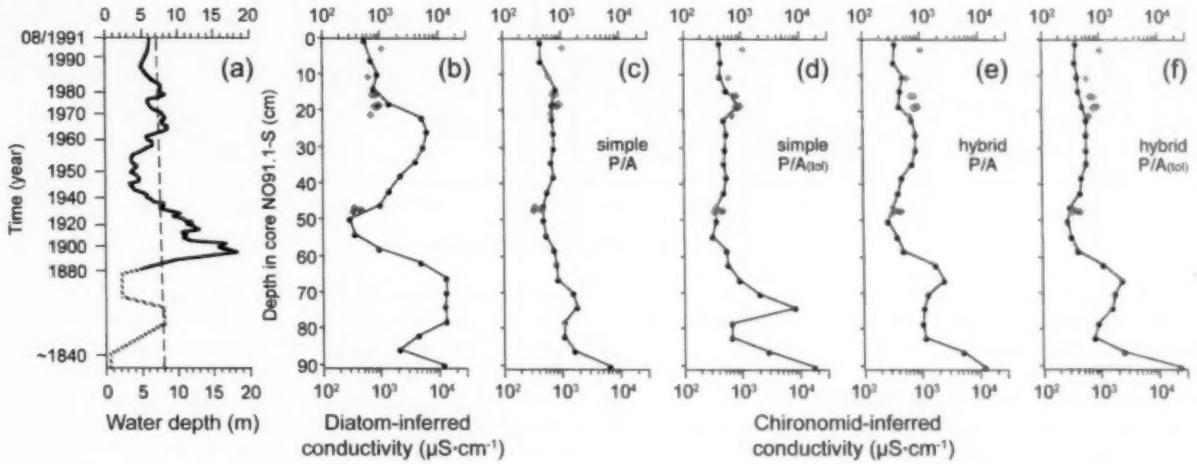

Fig. 4. Lithology of core NO91.1-S from Lake Oloidien (Kenya) and down-core distribution of fossil larval Chironomidae. Species are arranged from left to right in order of increasing salinity optima.

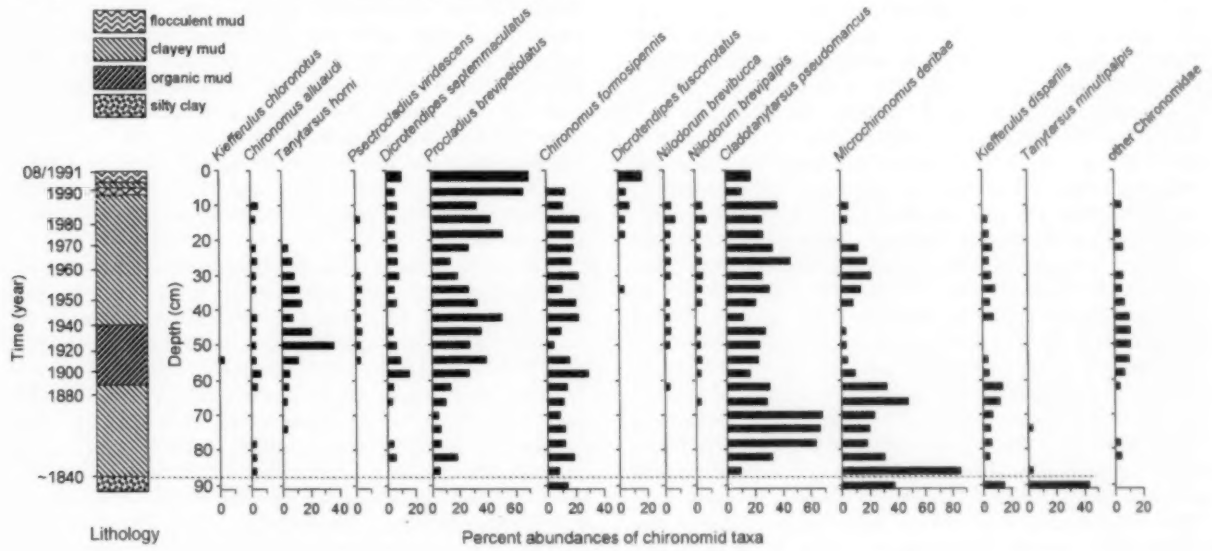

1985 overlap with the measured range of 620–1040 µS·cm^{-1}. Using the hybrid P/A and P/A_{tol} models, inferred values of 320 and 285 µS·cm^{-1} for 1930 match the measured range, but values of 380–650 µS·cm^{-1} for the period 1970–1985 fall below it. Strikingly, chironomid-inferred estimates of peak conductivity during episodes of low lake level fall consistently below the corresponding diatom-inferred estimates, no matter which model is used. They range from 515 to 780 µS·cm^{-1} for the mid-20th century lowstand, when diatom-inferred peak conductivity is 6500 µS·cm^{-1}, and from 1750 to 8200 µS·cm^{-1} during the mid-19th century, when diatom-inferred conductivity is 12 700 – 13 600 µS·cm^{-1}. An exception is the pre-1840 desiccation phase, when dominance of halobiontic species is translated into conductivity estimates ranging between 6700 and 23 500 µS·cm^{-1} compared with ~13 000 µS·cm^{-1} inferred from diatoms. Correlation between chironomid- and diatom-inferred conductivities (Figs. 5*a*–5*d*) is good for the section representing the historical period (r^2 = 0.47–0.78, n = 18, p < 0.01 in all cases), but more modest when pre-1880 samples are included (r^2 =

© 2004 NRC Canada

Fig. 5. Correlations between chironomid-inferred and diatom-inferred conductivity for the historical part of the Lake Oloidien record (1880–1991; $n = 18$) using (*a*, *b*) simple and (*c*, *d*) hybrid presence–absence models without (*a*, *c*: P/A) and with (*b*, *d*: P/A_{tol}) tolerance down-weighing. Solid line, linear regression; broken line, equality of model solutions. Inferences for the prehistorical portion of the record were added as passive data points (open circles; $n = 5$).

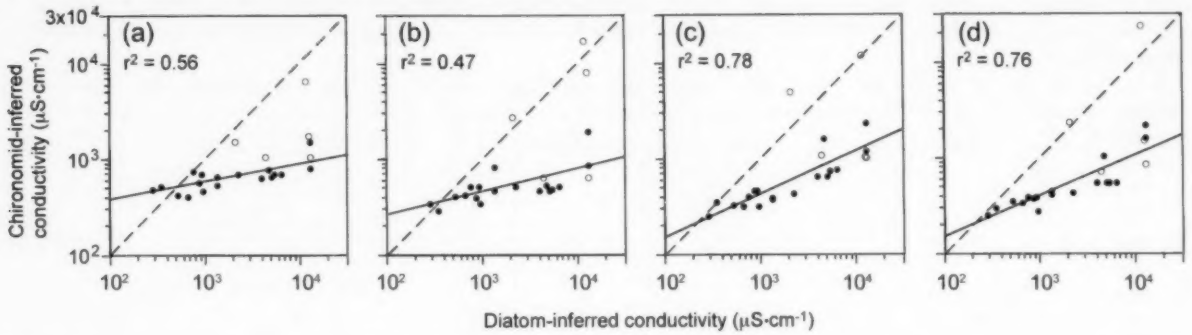

0.33–0.48, $n = 23$, $p = 0.007 - 0.035$). Samples from the ~1840–1850 phase of lake filling deviate most strongly from the general relationship.

Crescent Island Crater fossil record

Crescent Island Crater is normally confluent with the main basin of Lake Naivasha, which is hydrologically open because it loses dissolved salts to the ground water (Gaudet and Melack 1981). Consequently, Crescent Island Crater has remained fresh during historical times, and local conductivity (1929–1980: 280–491 µS·cm^{-1}, $n = 19$) has not been significantly different from that of Lake Naivasha (1929–1990: 233–499 µS·cm^{-1}, $n = 42$). Diatom-inferred conductivity estimates (Fig. 6*b*) for the upper 120 cm of core NC93.2-L are consistent with these data, ranging between 166 and 313 µS·cm^{-1} (except for an excursion to ~500 µS·cm^{-1} at 100–110 cm, dated to ~1900). However, over the past 1100 years the level of Crescent Island Crater has repeatedly dropped below the sill separating it from Lake Naivasha, namely during the Medieval Climatic Optimum (~AD 1000–1270) and on three occasions during the Little Ice Age (~AD 1380–1420, 1560–1620, and 1810–1850; Verschuren et al. 2000*b*). Diatom-based reconstruction of water-chemistry changes (Fig. 6*b*) suggests hydrologic closure of the crater and strong evaporative concentration during such arid episodes, with conductivity rising up to 20 000 µS·cm^{-1} during the Medieval Climatic Optimum. However, during the most recent severe low stand (~AD 1810–1850), Crescent Island Crater appears to have remained fresh, presumably because the preceding 150-year period of broad confluence with Lake Naivasha had removed its accumulated burden of dissolved salts.

This eventful history of Crescent Island Crater over the past 1100 years is also reflected in the evolution of its chironomid fauna. Three freshwater species (*Procladius brevipetiolatus*, *Dicrotendipes septemmaculatus*, *Chironomus formosipennis*) and the salt-tolerant species *Cladotanytarsus pseudomancus* occur throughout the core profile, but their abundances fluctuate in well-defined decade-scale patterns of ups and downs. For example, during the episode of highest inferred lake level (~AD 1650–1800; Fig. 6*a*), *Dicrotendipes septemmaculatus* expanded to 60%–70% of the fossil assemblage at the expense of the three others. During episodes of lowest inferred lake level (e.g., ~AD 1000–1270), the salt-tolerant *Cladotanytarsus pseudomancus* expanded to 70%–80%. At other times, the abundance changes were more complex, but overall the occurrence of *Dicrotendipes septemmaculatus* and *Cladotanytarsus pseudomancus* in this fossil record is consistent with their modern ecology and with a local paleolimnological study of their habitat preferences (Verschuren et al. 2000*a*). The fossil occurrence of the halobiontic species *Microchironomus deribae* and *Kiefferulus disparilis* (Fig. 7) is largely restricted to the lower third of the core, during inferred lowstand episodes when diatoms indicate lake conductivity was well above the tolerance limit of typical freshwater taxa (Figs. 6*a*–6*b*). The pulsed disappearance of these halobionts after AD 1270 mirrors the expansion of the freshwater species *Psectrocladius viridescens*, which reached 60% abundance during the early 20th century. Other freshwater species such as *Tanytarsus horni* and *Nilodorum brevibucca* occurred in Crescent Island Crater only at certain times in the past.

In Crescent Island Crater, chironomid-inferred conductivity estimates for the last 120 years agree with the available instrumental data, averaging 300–400 µS·cm^{-1} depending on the model used. Characteristically, output from simple P/A and P/A_{tol} models (Figs. 6*c*–6*d*) displays a limited number of different conductivity values, equalling the number of species combinations in the fossil record. The effect is most pronounced in P/A_{tol} model output, because *Chironomus alluaudi* and *Psectrocladius viridescens* have negligible influence on model calculations (because of their single occurrence in the calibration data set), effectively reducing species diversity and the number of possible species combinations. For example, in the simple P/A_{tol} model, a value of 330 µS·cm^{-1} is generated whenever samples only contain *Dicrotendipes septemmaculatus*, *Procladius brevipetiolatus*, *Chironomus formosipennis*, and *Cladotanytarsus pseudomancus*, besides *Chironomus alluaudi* and *Psectrocladius viridescens*. Isolated minima of 184 and 198 µS·cm^{-1} at depths of 140 and 84 cm reflect the two occurrences of *Kiefferulus chloronotus*, which in the calibration data set is limited to the most dilute lakes (<108 µS·cm^{-1}). Output from the hybrid model applications (Figs. 6*e*–6*f*) displays significantly more detail, including a discernable signal of lowest conduc-

© 2004 NRC Canada

Fig. 6. Chironomid-inferred reconstructions of past conductivity in Crescent Island Crater (Kenya) compared with diatom-inferred estimates and historical measurements. (*a*) Lake-level change over the past ~1100 years (solid and stippled line) relative to the elevation of the sill separating Crescent Island Crater from Lake Naivasha (broken line; Verschuren 2001). (*b*) Diatom-inferred conductivity reconstruction using the inference model of Gasse et al. (1995), compared with historical measurements (diamonds). (*c–f*) Chironomid-inferred conductivity reconstructions using presence–absence calibration models without (*c*, *e*: P/A) and with (*d*, *f*: P/A_{tol}) tolerance down-weighing applied to fossil presence–absence data (*a*, *b*: simple P/A and P/A_{tol}) and fossil percent–abundance data (*c*, *d*: hybrid P/A and P/A_{tol}).

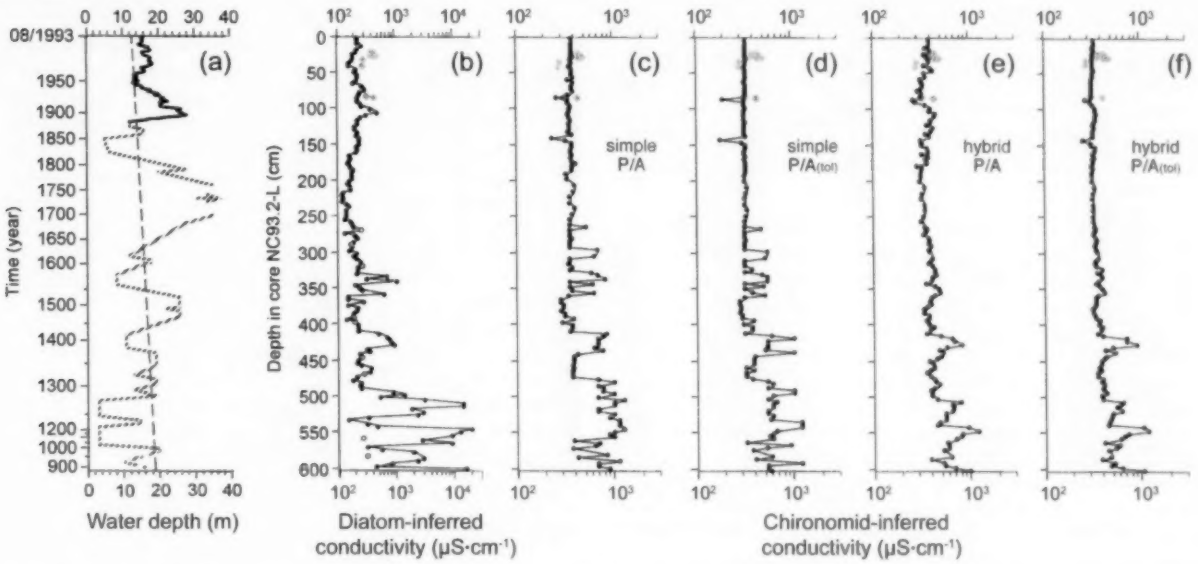

tivity values coinciding with peak lake level during AD 1650–1780 (180- to 280-cm depth). This signal is slightly more pronounced in hybrid P/A model output than in hybrid P/A_{tol}, because in the latter the influence of the highly salt-tolerant *Cladotanytarsus pseudomancus* on model calculations is muted.

Chironomid- and diatom-inferred conductivity estimates for Crescent Island Crater are significantly correlated (r^2 = 0.26–0.61, n = 130, $p < 0.01$ in all cases), with hybrid model applications yielding the best correlations (Fig. 8). As in Lake Oloidien, peak chironomid-inferred conductivity values tend to be lower than the corresponding diatom-inferred estimates. During the Medieval Climatic Optimum, chironomid-inferred conductivity remains mostly below 1500 µS·cm^{-1} (Figs. 6*c*–6*f*), whereas diatom-inferred conductivity reaches up to 20 000 µS·cm^{-1}. Similarly, during the lowstand of AD 1560–1600, diatoms infer a distinct peak of ~1000 µS·cm^{-1}, whereas chironomid-inferred conductivity barely differs from background freshwater values of 300–400 µS·cm^{-1} except in the simple P/A model (Fig. 6).

Discussion

The coefficients of determination (bootstrapped r^2 = 0.78–0.81) and RMSEs of prediction (0.39–0.42 log conductivity units) of the hybrid P/A and P/A_{tol} conductivity-inference models are comparable to those of a model based on Chironomidae from western Canada (bootstrapped r^2 = 0.72, RMSE = 0.52; Walker et al. 1995) and models based on African diatoms (jackknifed r^2 = 0.80–0.81, RMSE = 0.39–0.44; Gasse et al. 1995). Tandem application of diatom- and chironomid-based inference models on the same sediment records can greatly increase trust in the validity of reconstructed paleoenvironmental change and may help identify situations where diatom-based inferences are unreliable because of poor diatom preservation (Barker et al. 1990). Strong correlation between chironomid- and diatom-inferred conductivity estimates in both test records, when applying the hybrid P/A and P/A_{tol} models, strengthens reconstructions of lake history with regard to the timing and relative magnitude of past environmental change. Still, our analyses also revealed apparent weaknesses in the current chironomid-based models as compared with diatom-based models. These are (*i*) statistical weakness related to the use of presence–absence and hybrid models, rather than models using abundance weighting in both the calibration and fossil data sets; (*ii*) uneven distribution of residuals between inferred and observed conductivities; and (*iii*) underestimation of the inferred amplitude of past conductivity variation.

Use of presence–absence and hybrid models

The simple P/A and P/A_{tol} models, in which presence–absence data were used both in model calibration and its application to the fossil record, did reproduce historical conductivity values and some of the stronger conductivity excursions in the diatom-based reconstructions, but overall their correlation with either the lake-level or diatom-based reconstructions is unimpressive. By using presence–absence fossil data, salinity change is inferred only when the species composition of the fossil assemblage changes. These models are unresponsive to even strong fluctuations in the relative abundance of freshwater and salt-loving species; only the

© 2004 NRC Canada

Fig. 7. Lithology of core NC93.2-L from Crescent Island Crater (Kenya) and down-core distribution of fossil larval Chironomidae. Species are arranged left to right in order of increasing conductivity optima.

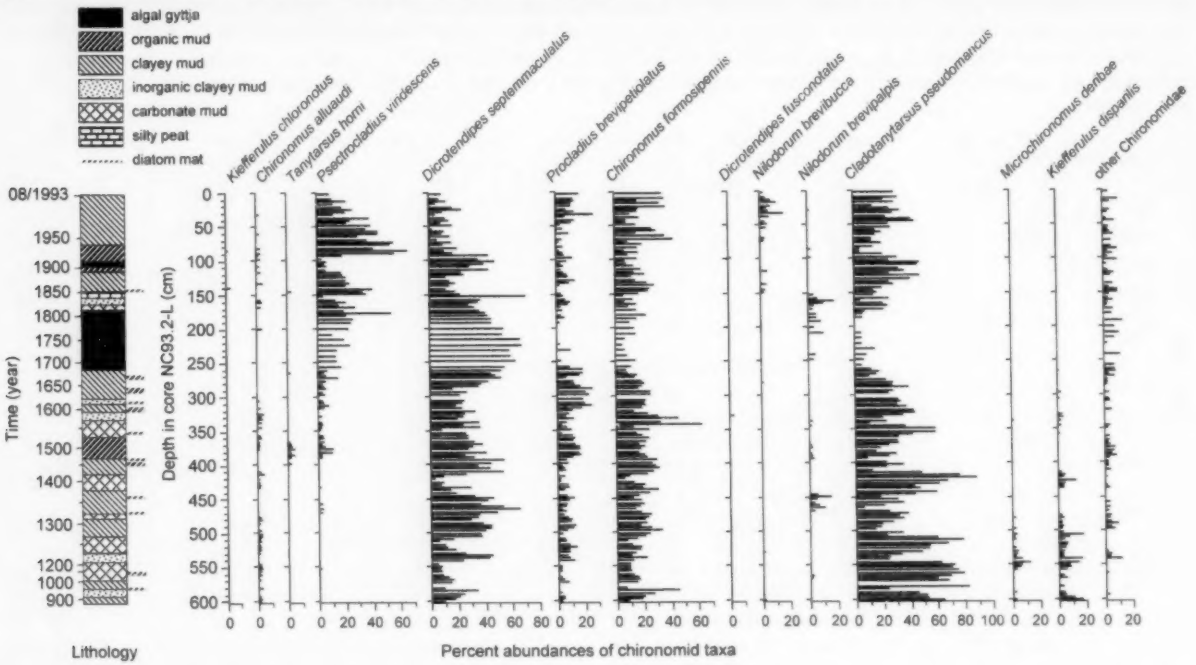

Fig. 8. Correlations between chironomid-inferred and diatom-inferred conductivity for the 1100-year Crescent Island Crater record (n = 130) using (a, b) simple and (c, d) hybrid presence–absence models without (a, c: P/A) and with (b, d: P/A_{tol}) tolerance down-weighing. Solid line: linear regression; broken line: equality of model solutions.

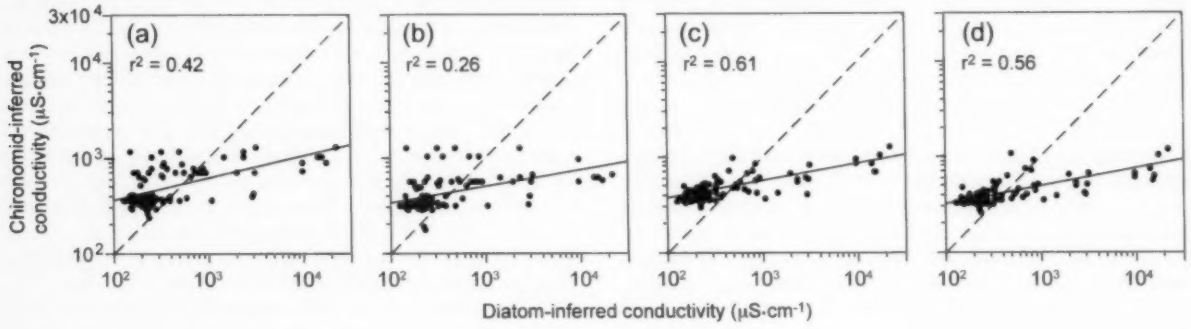

appearance or disappearance of taxa can generate signals. Consequently, the simple P/A and P/A_{tol} models yield a limited number of possible outcomes (i.e., conductivity values) equal to the number of different species combinations in the fossil record. The effect is more prominent in the Crescent Island Crater record because its fossil assemblages have low Hill's N2 species diversity (Hill 1973; mean Hill's N2 = 5.8) compared with those from Lake Oloidien (mean Hill's N2 = 8.3) and more so in model output with tolerance down-weighing (P/A_{tol}) because WACALIB 3.5 awarded a very large tolerance range to two common fossil species with single occurrences in the modern calibration data set, thus effectively reducing their influence to zero. An associated problem is the disproportionate influence that rare species with distinct optima have on the reconstruction, as for example the conductivity minima at 140 and 84 cm depth in P/A and P/A_{tol} reconstructions for Crescent Island Crater, because of isolated occurrences of *Kiefferulus chloronotus*.

Our hybrid P/A and P/A_{tol} model applications avoid some of these shortcomings by giving species a weight proportional to their importance for the reconstruction, as suggested by their percent abundance in the fossil assemblages. In their application to Crescent Island Crater data, the hybrid P/A model without tolerance down-weighing is preferable to hybrid P/A_{tol} because the former does not dilute the influence of the highly euryhaline *Cladotanytarsus pseudomancus* relative to other common species with more narrow tolerance ranges, hence producing a better signature of the conductivity minimum coinciding with peak 18th century lake level. Though the statistical robustness of these hybrid

© 2004 NRC Canada

models is uncertain, we justify their use by the observation that our presence–absence calibration model based on published species lists is not dissimilar from an abundance-weighted calibration model with additional down-weighing of rare taxa. The hybrid model applications do not, however, solve deficiencies of poor species representation in the calibration data set.

Uneven distribution of residuals

Good correlation between chironomid- and diatom-inferred conductivity estimates in the long-term history of Lake Oloidien and Crescent Island Crater suggests a very significant influence of salinity on both diatom and chironomid species composition, relative to other environmental factors known to affect algae (nutrients, turbidity, substrate) and benthic invertebrates (substrate, food quality, oxygen). The dominant control of salinity on diatom species distribution in African lakes is further demonstrated by limited variation in the prediction error of the diatom-based inference model (Gasse et al. 1995), which is a reflection of high species diversity, fairly narrow salinity tolerance ranges, and repeated species turnover along the salinity gradient (Fritz et al. 1999). This contrasts with the very substantial variation in the prediction error of our chironomid-based estimates, seemingly because of relative complacency of chironomid species composition in fresh and slightly concentrated waters (<3000 $\mu S \cdot cm^{-1}$), followed by a nearly complete replacement of salt-tolerant freshwater species with true salt-loving species once the threshold of 3000 $\mu S \cdot cm^{-1}$ is crossed. Its most notable effect is that freshwater lakes with observed conductivity values between 20 and ~3000 $\mu S \cdot cm^{-1}$ yield predicted conductivity values in a much narrower range of ~150–1000 $\mu S \cdot cm^{-1}$. Consequently, our present chironomid-based inference models can differentiate only among fresh to slightly concentrated (<3000 $\mu S \cdot cm^{-1}$), mesosaline (~3000–15 000 $\mu S \cdot cm^{-1}$), and poly- to hypersaline African waters (>15 000 $\mu S \cdot cm^{-1}$).

This apparent threshold response of African chironomid faunas to salinity and the resulting bias in model prediction error is possibly an artifact of our construction of the calibration model with presence–absence data from published species lists with an average of only 3.8 species per lake. The handful of identified species of larval Chironomidae available for most lakes suggests that these collections typically represent only those taxa that thrive in local habitat conditions and not the larger contingent of species that occur near their environmental tolerance limits or in locally restricted types of microhabitat. If this is true, then more intensive live sampling would be expected to reveal greater overlap between freshwater and salt-lake chironomid faunas, more gradual species turnover along the conductivity gradient, and less pronounced bias in the prediction error of chironomid-based salinity-inference models.

However, comprehensive surveys of aquatic invertebrate distribution in African lakes (e.g., Hammer 1986; Tudorancea et al. 1989) show the reality of an abrupt transition between fresh and soda-lake faunas near 3000 $\mu S \cdot cm^{-1}$ and of the rather poor faunal differentiation with regard to salinity in the broad range of freshwater environments below that threshold. Consequently, the overall pattern of species distribution among lakes in the available calibration data set may well reflect ecological reality. Likely, the ultimate drivers of community response in these benthic aquatic invertebrates are not the species-specific physiological tolerances to salinity stress, but large-scale restructuring of benthic habitat accompanying drastic salinity change (Williams et al. 1990), for example, the wholesale disappearance of submerged macrophytes along with the sheltered mud habitat they provide and the coarse organic detritus they produce (McLachlan 1979). In the context of paleoenvironmental reconstruction, satisfactory agreement between chironomid- and diatom-based salinity inferences requires past salinity variations that encompassed a large portion of the full salinity gradient or at least crossed the all-important threshold between freshwater and salt-lake environments.

Limited amplitude of inferred conductivity variation

Chironomid-inferred conductivity during phases of hydrologic closure is systematically lower than the corresponding diatom-inferred conductivity, more so in Crescent Island Crater than in Lake Oloidien. As a result, slopes of the relationship between chironomid- and diatom-inferred conductivities are significantly different from unity. This is partly due to limited sensitivity of the chironomid-based calibration model in the freshwater range, as discussed above. Specifically, limited model sensitivity can explain the apparent overestimation of conductivity for (diatom-inferred) values below ~500 $\mu S \cdot cm^{-1}$ and underestimation for values above ~500 up to ~2000 $\mu S \cdot cm^{-1}$, evident in the Crescent Island Crater record. However, if model insensitivity were the main cause of this collapse in chironomid-inferred conductivity values, regressions between chironomid- and diatom-inferred conductivities would display a clear signature of the sudden transition in chironomid faunas between fresh and saline environments, and the correlation between chironomid- and diatom-inferred conductivities would be significantly reduced. Instead, chironomid-inferred values continue to be much lower than, but broadly proportional to, diatom-inferred values across the full range of values reconstructed in both fossil records, up to (diatom inferred) values of >20 000 $\mu S \cdot cm^{-1}$.

In contrast to the diatom assemblages deposited during early lowstand episodes in Crescent Island Crater, which are dominated by halophilic taxa (Verschuren et al. 2000*b*), corresponding chironomid assemblages contain a mixture of freshwater and halophilic taxa in which the latter (*Microchironomus deribae*, *Kiefferulus disparilis*) account for at most 24%. This is also the case in the Lake Oloidien record, with the exception of samples from within and immediately above the pre-1840 desiccation horizon. The large majority of saline-phase samples in both studied sediment records contain mixed freshwater–halophilic chironomid assemblages that lack modern analogs. Whereas the halophilic *Microchironomus deribae* has been reported from some freshwater lakes (Verschuren 1997), *Kiefferulus disparilis* and *Tanytarsus minutipalpis* have never been found living together with any true freshwater species. The incidence of no-analog situations would be reduced if transfer functions were developed from a calibration data set based on surface-sediment chironomid assemblages rather than the life collections used here. Since surface-sediment assemblages represent an integration of biological communities over several years, lakes

© 2004 NRC Canada

which hover near the freshwater–saline transition today would likely yield mixed fossil assemblages similar to those found at depth in the Crescent Island Crater record, and introduce some degree of disharmonious species composition in the calibration data set.

Diatom floral composition and inferred conductivity (10 000 – 22 000 $\mu S \cdot cm^{-1}$) indicate that during the Medieval Climatic Optimum, Crescent Island Crater did not hover near the freshwater–saline transition but was a true salt lake for extended periods of time. Similarly, diatom-inferred conductivity (12 700 – 13 600 $\mu S \cdot cm^{-1}$; Verschuren et al. 1999*b*) and historical accounts from the mid-19th century (New 1874) indicate that Lake Oloidien was a true salt lake at that time, the type of African soda lake that today is inhabited exclusively by halobiontic chironomid species and the euryhaline *Cladotanytarsus pseudomancus*. Consequently, the mixed composition of chironomid assemblages deposited during past saline lowstands of both lakes must reflect significant postdepositional sediment mixing, with reworking of fossil assemblages deposited during earlier freshwater phases. Crescent Island Crater is highly sensitive to such mixing, because lake-level decline in the combined Lake Naivasha – Crescent Island Crater system causes resuspension of sediments recently deposited in the sector of Naivasha adjacent to the crater, which during an ensuing low stand contribute to sedimentation on the crater floor (Verschuren 1999).

The relative purity of soda-lake diatom assemblages deposited concurrently with mixed chironomid assemblages in both Lake Oloidien and Crescent Island Crater implies that chironomid larval remains must better survive cycles of resuspension and redeposition than do diatom frustules. Diatom preservation is controlled by the dissolved-silica concentration of bottom waters and the depth of sediment mixing relative to the rate of sediment accumulation (Lawson et al. 1978; Conley and Schelske 1989). In both large, stable and shallow, fluctuating lakes (Parker et al. 1977; Lent and Lyons 2001), most diatom silica is recycled to the water column before permanent burial. This process may be particularly strong in the shallow main basin of Lake Naivasha adjacent to Crescent Island Crater, considering its extensive areas of wind-induced erosion and transport relative to areas of sediment accumulation (Verschuren 1999). In contrast, preservation of chironomid remains is promoted by the chemical inertness of chitin and the resistance of sclerotized skeletal fragments to physical destruction (Frey 1988). Thus, differential preservation of diatoms and chironomids first buried in shallow sediments during fresh highstands and then redeposited during saline lowstands may result in greater contamination of those deposits with nonmatching chironomid fossils, as compared with diatoms.

Prospects

The statistical performance of the chironomid-based conductivity-inference models for African lakes, as reflected in coefficients of determination and RMSEs of prediction, is comparable to that of current diatom-based models, but threshold response of chironomid species composition to salinity change limits model sensitivity within the freshwater range. Given current limitations of the calibration data set, conductivity estimates produced by all four tested models matched historical instrumental data surprisingly well. The hybrid statistical procedure in which calibration models based on modern presence–absence data are applied to abundance-weighted fossil data rather than presence–absence data yielded the best agreement with diatom-inferred conductivity estimates, since it does not depend on complete replacement of individual species to generate variation. Weighing of species' influence inversely proportional to their estimated conductivity tolerance (the P/A_{tol} calibration model) resulted in muted signals of conductivity change in the freshwater range, in part by limiting the influence of one highly salt-tolerant species. The tendency of chironomid-inferred conductivity values for past saline phases in both test lakes to remain below corresponding diatom-inferred values is attributed to the combination of taphonomical processes in shallow fluctuating lakes with differential preservation of chironomid versus diatom fossils.

Besides diatoms and chironomids, the distribution of several other groups of aquatic biota with good fossil preservation, such as chrysophytes and cladocerans, have been investigated in relation to salinity. However, the performance of quantitative inference models based on these groups (Cumming et al. 1993; Zeeb and Smol 1995; Bos et al. 1996) is limited by the scarcity of truly halobiontic taxa. Model insensitivity at the high end of the salinity gradient also affects quantitative reconstructions based on Chironomidae of western Canada (Walker et al. 1995), where only two species tolerate conductivities above ~10 000 $\mu S \cdot cm^{-1}$. African salt lakes are inhabited by at least three chironomid species in addition to the three halobiontic species currently included in the calibration data set (D. Verschuren, unpublished data), hence chironomid-based reconstruction of past changes in lakes' water balance holds great promise. Further improvements of the performance of chironomid-based inference models is contingent upon the construction of a comprehensive calibration data set using standardized collections of surface-sediment chironomid assemblages and associated modern environmental data.

Acknowledgements

Model development was funded through US National Science Foundation EAR-9631222. We thank Christine Cocquyt, Dan Engstrom, Peter Leavitt, Neil Roberts, Koen Sabbe, and John Tibby for help in generating the multiproxy lake-history reconstructions, which we used to test the inference models described in this paper. D.V. is a postdoctoral fellow of the Fund for Scientific Research–Flanders (FWO-Vlaanderen, Belgium) and acknowledges support by the University of Minnesota for part of this work.

References

Barker, P., Gasse, F., Roberts, N., and Taieb, M. 1990. Taphonomy and diagenesis in diatom assemblages: a late Pleistocene palaeoecological study from Lake Magadi, Kenya. Hydrobiologia, **214**: 267–272.

Bayly, I.A.E. 1972. Salinity tolerance and osmotic behavior of animals in athalassic saline and marine hypersaline waters. Annu. Rev. Ecol. Syst. **3**: 233–268.

© 2004 NRC Canada

Birks, H.J.B. 1998. Numerical tools in palaeolimnology — progress, potentialities, and problems. J. Paleolimnol. **20**: 307–332.

Birks, H.J.B., Line, J.M., Juggins, S., Stevenson, A.C., and ter Braak, C.J.F. 1990. Diatoms and pH reconstruction. Phil. Trans. R. Soc. Lond. B Biol. Sci. **327**: 263–278.

Bos, D.G., Cumming, B.F., Watters, C.E., and Smol, J.P. 1996. The relationship between zooplankton, conductivity and lake-water ionic composition in 111 lakes from the Interior Plateau of British Columbia, Canada. Int. J. Salt Lake Res. **5**: 1–15.

Brooks, S.J., and Birks, H.J.B. 2000. Chironomid-inferred late-glacial and early-Holocene mean July air temperatures for Kråkenes Lake, western Norway. J. Paleolimnol. **23**: 77–89.

Brooks, S.J., Mayle, F.E., and Lowe, J.J. 1997. Chironomid-based late-glacial climatic reconstruction for southeast Scotland. J. Quat. Sci. **12**: 161–167.

Conley, D.J., and Schelske, C.L. 1989. Processes controlling the benthic regeneration and sedimentary accumulation of biogenic silica in Lake Michigan. Arch. Hydrobiol. **116**: 23–43.

Cumming, B.F., Wilson, S.E., and Smol, J.P. 1993. Paleolimnological potential of chrysophyte cysts and scales and of sponge spicules as indicators of lake salinity. Int. J. Salt Lake Res. **2**: 87–92.

Dearing, J.A. 1997. Sedimentary indicators of lake-level changes in the humid temperate zone: a critical review. J. Paleolimnol. **18**: 1–14.

Frey, D.G. 1988. Littoral and offshore communities of diatoms, cladocerans and dipterous larvae, and their interpretation in paleolimnology. J. Paleolimnol. **1**: 179–191.

Fritz, S.C., Cumming, B.F., Gasse, F., and Laird, K.R. 1999. Diatoms as indicators of hydrologic and climatic change in saline lakes. *In* The diatoms: applications to the environmental and earth sciences. *Edited by* E.F. Stoermer and J.P. Smol. Cambridge University Press, New York. pp. 41–72.

Gasse, F., Juggins, S., and Ben Khelifa, L. 1995. Diatom-based transfer functions for inferring hydrochemical characteristics of African paleolakes. Palaeogeogr. Palaeoclimatol. Palaeoecol. **117**: 31–54.

Gaudet, J.J., and Melack, J.M. 1981. Major ion chemistry in a tropical African lake basin. Freshw. Biol. **11**: 309–333.

Hammer, U.T. 1986. Saline lake ecosystems of the world. Monogr. Biol. 59. Junk, Dordrecht.

Hare, L., and Carter, J.C.H. 1987. Chironomidae (Diptera, Insecta) from the environs of a natural West African lake. Entomol. Scand. Suppl. **29**: 65–74.

Hill, M.O. 1973. Diversity and differences: a unifying notation and its consequences. Ecology, **54**: 427–432.

Laird, K.R., Fritz, S.C., Grimm, E.C., and Mueller, P.G. 1996. Century-scale paleoclimatic reconstruction from Moon Lake, a closed-basin lake in the northern Great Plains. Limnol. Oceanogr. **41**: 890–902.

Lawson, D.S., Hurd, D.C., and Pankratz, H.S. 1978. Silica dissolution rates of decomposing phytoplankton assemblages at various temperatures. Am. J. Sci. **278**: 1373–1393.

Lent, R.M., and Lyons, W.B. 2001. Biogeochemistry of silica in Devils Lake: implications for diatom preservation. J. Paleolimnol. **26**: 53–66.

Levesque, A.J., Mayle, F.E., Walker, I.R., and Cwynar, L.C. 1993. A previously unrecognized late-glacial cold event in eastern North America. Nature (Lond.), **361**: 623–626.

Line, J.M., ter Braak, C.J.F., and Birks, H.J.B. 1994. WACALIB version 3.3. A computer program to reconstruct environmental variables from fossil assemblages by weighted averaging and to derive sample-specific errors of prediction. J. Paleolimnol. **10**: 147–152.

Livingstone, D.A., and Melack, J.M. 1984. Some lakes of subsaharan Africa. *In* Lakes and reservoirs. *Edited by* F.B. Taub. Elsevier, Amsterdam. pp. 467–497.

McLachlan, A.J. 1979. Decline and recovery of the benthic invertebrate communities. Monogr. Biol. **35**: 143–160.

Mees, F., Verschuren, D., Nijs, R., and Dumont, H. 1991. Holocene evolution of the crater lake at Malha, Northwest Sudan. J. Paleolimnol. **5**: 227–253.

New, C. 1874. Life, wanderings, and labors in eastern Africa. 2nd ed. Hodder and Stoughton, London.

Parker, J.I., Conway, H.L., and Yaguchi, E.M. 1977. Dissolution of diatom frustules and recycling of amorphous silicon in Lake Michigan. J. Fish. Res. Board Can. **34**: 545–551.

Pinder, L.C.V. 1995. The habitats of chironomid larvae. *In* The Chironomidae: biology and ecology of non-biting midges. *Edited by* P.D. Armitage, P.S. Cranston, and L.C.V. Pinder. Chapman & Hall Ltd., London. pp. 107–135.

Smol, J.P., and Cumming, B.F. 2000. Tracking long-term changes in climate using algal indicators in lake sediments. J. Phycol. **36**: 986–1011.

Smol, J.P., Walker, I.R., and Leavitt, P.R. 1991. Paleolimnology and hindcasting climatic trends. Verh. Int. Ver. Theor. Angew. Limnol. **24**: 1240–1246.

Stoermer, E.F., and Smol, J.P. 1999. The diatoms: applications for the environmental and earth sciences. Cambridge Univsity Press, New York.

Street-Perrott, F.A., and Roberts, N. 1983. Fluctuations in closed-basin lakes as an indicator of past atmospheric circulation patterns. *In* Variations in the global water budget. *Edited by* A. Street-Perrott, M. Beran, and R. Ratcliffe. Reidel, Dordrecht. pp. 331–345.

Tudorancea, C., Baxter, R.M., and Fernando, C.H. 1989. A comparative limnological study of zoobenthic associations in lakes of the Ethiopian Rift Valley. Arch. Hydrobiol. Suppl. **83**: 121–174.

Vareschi, E., and Vareschi, A. 1984. The ecology of Lake Nakuru (Kenya). IV. Biomass and distribution of consumer organisms. Oecologia, **61**: 70–82.

Verschuren, D. 1996. Comparative paleolimnology in a system of four shallow tropical lake basins. *In* The limnology, climatology and paleoclimatology of the East African lakes. *Edited by* T.C. Johnson and E. Odada. Gordon & Breach, Newark, N.J. pp. 559–572.

Verschuren, D. 1997. Taxonomy and ecology of subfossil Chironomidae (Insecta: Diptera) from Rift Valley lakes in central Kenya. Arch. Hydrobiol. Beih. **107**: 467–512.

Verschuren, D. 1999. Sedimentation controls on the preservation and time resolution of sedimentary climate-proxy records from shallow fluctuating lakes. Quat. Sci. Rev. **18**: 821–837.

Verschuren, D. 2001. Reconstructing fluctuations of a shallow East African lake during the past 1800 years from sediment stratigraphy in a submerged crater basin. J. Paleolimnol. **25**: 297–311.

Verschuren, D., Cocquyt, C., Tibby, J., Roberts, N., and Leavitt, P.R. 1999*a*. Long-term dynamics of algal and invertebrate communities in a small, fluctuating tropical soda lake. Limnol. Oceanogr. **44**: 1216–1231.

Verschuren, D., Tibby, J., Leavitt, P.R., and Roberts, C.N. 1999*b*. The environmental history of a climate-sensitive lake in the former 'White Highlands' of central Kenya. Ambio, **28**: 494–501.

Verschuren, D., Tibby, J., Sabbe, K., and Roberts, N. 2000*a*. Effects of lake level, salinity and substrate on the invertebrate community of a fluctuating tropical lake. Ecology, **81**: 164–182.

© 2004 NRC Canada

Verschuren, D., Laird, K.R., and Cumming, B.F. 2000*b*. Rainfall and drought in equatorial East Africa during the past 1,100 years. Nature (Lond.), **403**: 410–414.

Verschuren, D., Johnson, T.C., Kling, H.J., Edgington, D.N., Leavitt, P.R., Brown, E.T., Talbot, M.R., and Hecky, R.E. 2002. History and timing of human impact on Lake Victoria, East Africa. Proc. R. Soc. Lond. B Biol. Sci. **269**: 289–294.

Walker, I.R. 1995. Chironomids as indicators of past environmental change. *In* The Chironomidae: biology and ecology of non-biting midges. *Edited by* P.D. Armitage, P.S. Cranston, and L.C.V. Pinder. Chapman & Hall Ltd., London. pp. 405–422.

Walker, I.R., Wilson, S., and Smol, J.P. 1995. Chironomidae (Diptera): quantitative palaeosalinity indicators for lakes of western Canada. Can. J. Fish. Aquat. Sci. **52**: 950–960.

Williams, W.D. 1984. Chemical and biological features of salt lakes on the Eyre Peninsula, South Australia, and an explanation of regional differences in the fauna of Australian salt lakes. Verh. Int. Ver. Theor. Angew. Limnol. **22**: 1208–1215.

Williams, W.D., Boulton, A.J., and Taaffe, R.G. 1990. Salinity as a determinant of salt lake fauna: a question of scale. Hydrobiologia, **197**: 257–266.

Zeeb, B.A., and Smol, J.P. 1995. A weighted-averaging regression and calibration model for inferring lakewater salinity using chrysophycean stomatocysts from western Canadian lakes. Int. J. Salt Lake Res. **4**: 1–23.

© 2004 NRC Canada

Landscape models to understand steelhead (*Oncorhynchus mykiss*) distribution and help prioritize barrier removals in the Willamette basin, Oregon, USA

E. Ashley Steel, Blake E. Feist, David W. Jensen, George R. Pess, Mindi B. Sheer, Jody B. Brauner, and Robert E. Bilby

Abstract: We use linear mixed models to predict winter steelhead (*Oncorhynchus mykiss*) redd density from geology, land use, and climate variables in the Willamette River basin, Oregon. Landscape variables included in the set of best models were alluvium, hillslope < 6%, landslide-derived geology, young (<40 years) forest, shrub vegetation, agricultural land use, and mafic volcanic geology. Our approach enables us to model the temporal correlation between annual redd counts at the same site while extracting patterns of relative redd density across sites that are consistent even among years with varying strengths of steelhead returns. We use our model to predict redd density (redds per kilometre) upstream of 111 probable migration barriers as well as the 95% confidence interval around the redd density prediction and the total number of potential redds behind each barrier. Using a metric that incorporates uncertainty, we identified high-priority barriers that might have been overlooked using only stream length or mean predicted fish benefit and we clearly differentiated between otherwise similar barriers. We show that landscape features can be used to describe and predict the distribution of winter steelhead redds and that these models can be used immediately to improve decision-making for anadromous salmonids.

Résumé : Des modèles linéaires mixtes utilisant des variables reliées à la géologie, à l'utilisation des terres et au climat nous ont servi à prédire la densité des nids de truites arc-en-ciel anadromes (*Oncorhynchus mykiss*) d'hiver dans la rivière Willamette, en Oregon. Les variables du paysage incluses dans la série des meilleurs modèles comprennent l'alluvion, les versants <6 %, la géologie reliée aux glissements de terrains, les forêts jeunes (<40 ans), la végétation arbustive, les terres agricoles et la géologie volcanique mafique. Notre méthode nous permet de modéliser la corrélation temporelle entre les inventaires annuels de nids à un même site, tout en extrayant des patterns de densité relative des nids à travers les sites qui sont cohérents même entre les années qui ont des retours de truites arc-en-ciel anadromes d'importance inégale. Notre modèle a servi à prédire la densité des nids (nids par kilomètre) en amont de 111 barrières probables à la migration, de calculer l'intervalle de confiance de 95 % autour de la prédiction de densité des nids et d'estimer le nombre total de nids potentiels derrière chaque barrière. À l'aide d'une métrique qui inclut l'incertitude, nous avons identifié des barrières de forte priorité qui ont pu passer inaperçues d'après la seule longueur du cours d'eau ou d'après le bénéfice moyen prédit pour les poissons; cela nous a permis ainsi de différencier clairement des barrières semblables par ailleurs. Nous démontrons que des caractéristiques du paysage permettent de décrire et de prédire la répartition des nids des truites arc-en-ciel d'hiver et que ces modèles peuvent servir dès à présent pour améliorer les prises de décision concernant les salmonidés anadromes.

[Traduit par la Rédaction]

Introduction

Recent advances in modeling the distribution of fish from landform and land use have taken a broad-scale approach (Thompson and Lee 2000; Pess et al. 2002; Feist et al. 2003) that differs from previous site-specific research (e.g., Bustard and Narver 1975; Geist et al. 2000). Site-specific variables such as substrate size or riparian cover clearly are important influences on salmon distribution and abundance. However, factors such as geology and land use can determine the distribution of these site-specific variables and so may have a controlling influence on the distribution of spe-

Received 28 February 2003. Accepted 23 December 2003. Published on the NRC Research Press Web site at http://cjz.nrc.ca on 27 July 2004.
J17357

E.A. Steel,[1] B.E. Feist, D.W. Jensen, G.R. Pess, M.B. Sheer, and R.E. Bilby.[2] Northwest Fisheries Science Center, NOAA Fisheries, 2725 Montlake Blvd. East, Seattle, WA 98112, USA.
J.B. Brauner. School of Aquatic and Fishery Sciences, P.O. Box 355020, University of Washington, Seattle, WA 98195, USA.

[1]Corresponding author (e-mail: Ashley.Steel@noaa.gov).
[2]Present address: Weyerhauser Company, Tacoma, WA 98477, USA.

 doi: 10.1139/F04-042 © 2004 NRC Canada

cies (Richards et al. 1996). Examining patterns of fish abundance or survival at larger scales can provide new scientific insight regarding factors determining fish distribution (Poff 1997; Poff and Huryn 1998). Because data on landscape features are often available more easily than reach-scale data describing in-stream conditions, results of these large-scale analyses may be faster to achieve and can be immediately useful in efforts to manage fish populations (Lunetta et al. 1997).

Landscape-scale analyses have yielded insights into a wide range of aquatic community and fish population metrics including aquatic community composition, salmonid spawner abundances, and juvenile salmonid distribution. Identification of patterns at these scales has been possible across dissimilar ecoregions. Catchment area and low-flow yield were used to explain fish community composition of primarily resident fishes in Michigan State (Zorn et al. 2002). Coho salmon (*Oncorhynchus kisutch*) spawner distribution in the Snohomish River basin, Washington State, can be explained as a function of wetland occurrence, local geology, stream gradient, and land use. As well, juvenile chinook salmon (*Oncorhynchus tshawytscha*) distribution in multiple drainages in Idaho State could be explained as a function of road density and precipitation while juvenile steelhead (*Oncorhynchus mykiss*) abundances in the same basins were correlated with geology (Thompson and Lee 2000). Correlations between juvenile steelhead and geology have also been identified in Oregon Coast Range streams (Hicks and Hall 2003). Landscape-scale studies have enabled comparisons between past and present land use. An analysis of patterns over whole watersheds identified links between past land-use patterns and present-day fish and invertebrate diversity in western North Carolina State (Harding et al. 1998).

We use linear mixed models to examine relationships between landscape characteristics such as geology, land use, and climate and the distribution of winter steelhead redds in four watersheds that comprise 23% of the Willamette River basin, Oregon. Steelhead exhibit a varied life history pattern that has made habitat generalizations difficult. Our statistical technique allows us to model the temporal correlation between annual fish observations at the same site while extracting patterns of relative redd density across sites that are consistent among years with varying strengths of steelhead returns. Using this technique, we are able to develop correlative models that describe landscape traits associated with areas of high steelhead spawner abundance and that can predict where in the study watersheds steelhead are most likely to spawn.

We use our model to predict steelhead redd density and abundance above barriers to passage within the four watersheds. We then estimate multiple metrics that can be used for prioritizing barriers for removal. Removal of manmade barriers to fish passage is suggested as a reasonable action during the first stages of recovery planning for listed salmonids, including winter steelhead in the Willamette River basin, because it has a high likelihood of success and a very low likelihood of negative impacts (Roni et al. 2002). However, removing or correcting passage barriers is expensive, limiting the rate at which these problems can be addressed. In the absence of detailed field data, identifying which barriers might have the greatest impact on fish abundance, and hence should be removed first, is a difficult problem. Our broad-scale analyses use existing data to support making management decisions for listed salmonids.

Materials and methods

Study area

The Calapooia, North and South Santiam, and Mollala watersheds in the Willamette River basin drain the western slopes of the Cascade Range, Oregon (Fig. 1). Annual precipitation ranges from 1000 to 5500 mm and increases with elevation. Most precipitation falls from November through March and highest river flows usually occur in December and January. Private and federal forests dominate the higher elevations of all four watersheds; agriculture is the dominant land use in the lower elevations.

Steelhead data

Steelhead populations listed under the Endangered Species Act (ESA) in the four watersheds are winter steelhead that enter fresh water in March and April and spawn soon after arrival. Spawning occurs primarily in the lower gradient reaches of the watersheds. After emergence, juvenile steelhead generally spend 2 years rearing in fresh water. Between seasons, juveniles may stay in the main channel, move upstream into smaller tributaries, or migrate downstream and then into tributaries.

We used annual steelhead redd surveys conducted by the Oregon Department of Fish and Wildlife between 1979 and 1999 at 27 index reaches distributed throughout all four watersheds (Fig. 1). Index reaches were georeferenced to US Geological Survey 1:100 000 scale digital line graph hydrographic data layers. Redd counts were normalized to the length of stream surveyed (redds per kilometre). These data provide the best available record of steelhead redd distribution in the Willamette River basin; however, sites were not randomly selected for this type of analysis. Sites were chosen to monitor specific populations of interest and therefore summarize the best steelhead spawning areas in the four watersheds rather than all available habitats.

These data may include some naturally spawning hatchery winter steelhead; however, the impact of hatchery introductions of winter steelhead on index reach redd counts in the study watersheds is limited. There is no hatchery program on the Calapooia River and hatchery winter steelhead smolts were only released into the South Santiam River during a 7-year period in the 1980s. There have been significant hatchery introductions in the Molalla since the 1960s; however, hatchery fish in the Molalla are of Big Creek origin and spawn in January and February, too early to be detected in the index reach surveys conducted in April and May (Chilcote 1998). There is a hatchery on the North Santiam River where hatchery fish made up about 17% of the run by the late 1990s. There is no estimate of what fraction of naturally spawning fish in the North Santiam River might be of hatchery origin. The redd count data do not include information about juvenile steelhead distribution or survival of eggs and fry from these sites. For this analysis, we limit our interpretation to redd distribution and do not infer that sites with consistently high numbers of redds necessarily produce large numbers of juveniles or are adjacent to prime juvenile habitat.

© 2004 NRC Canada

Fig. 1. The four study watersheds, their location in the Willamette River basin, and the Willamette's location in Oregon, USA. Black stream segments indicate Oregon Department of Fish and Wildlife index reaches used in this analysis.

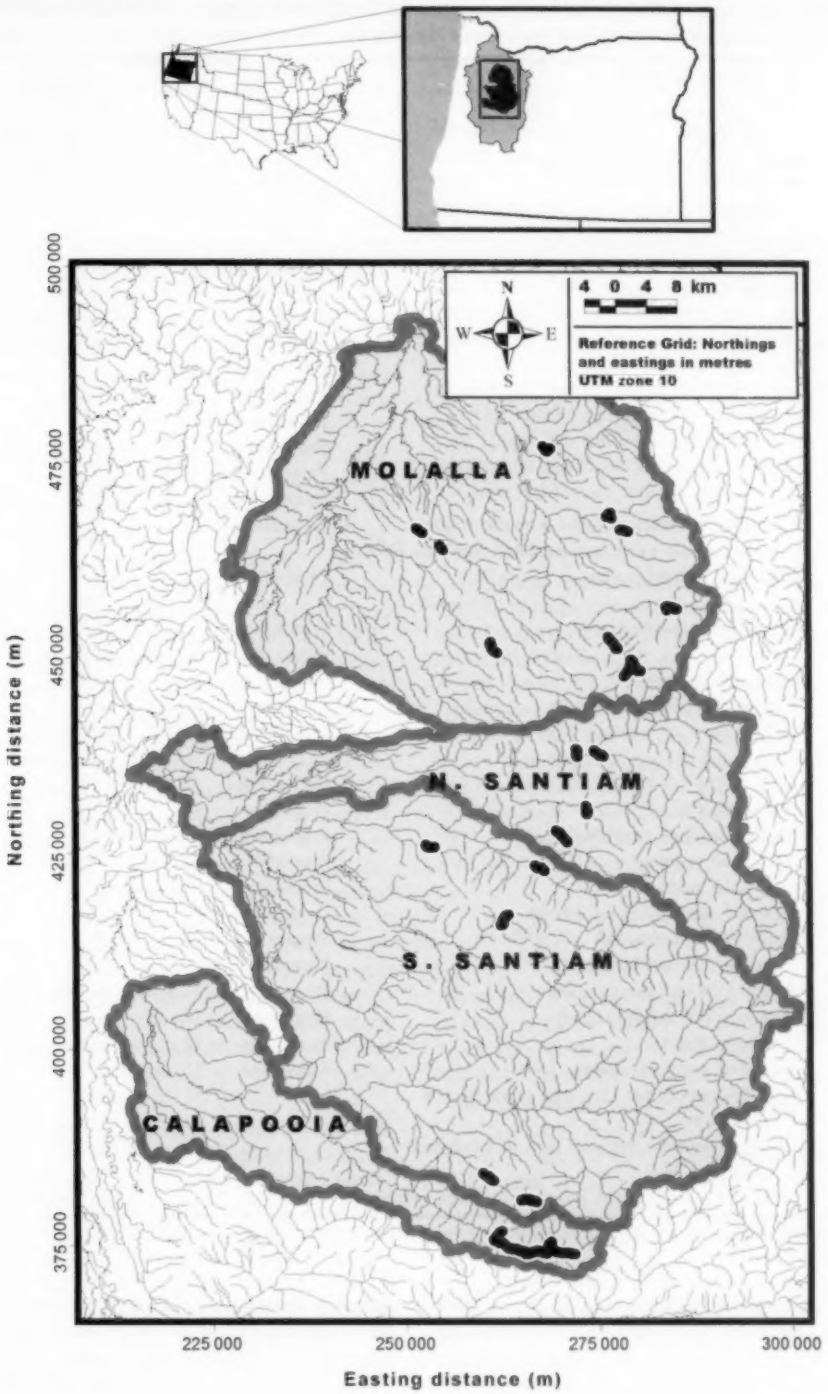

Landscape data

Our choice of landscape variables to be tested in model development was based on published relationships between site-specific habitat characteristics and steelhead distribution (Bustard and Narver 1975; Reiser and Bjornn 1979) (Table 1). We expect that substrate, water velocity, and depth

© 2004 NRC Canada

Table 1. Predictor variables used in model building, the categories used to create the predictor (if the name in the data layer is different from predictor name), whether the predictor was calculated as a proportion of the watershed draining to the index reach or as area-weighted mean (AWM) of the values within that watershed, whether the variable was entered as a continuous variable (C) or as an indicator (I) or both (although only one could remain in a model), and the data layer from which the predictor was derived (Appendix A).

Predictor	Categories/description	Calculated	Type	Data layer
Hillslope	Hillslope gradient < 6%	Proportion	C	Hillslope
Channel gradient	Range = 0.0–7.7%	AWM	C	Channel slope
Junctions	Range = 0.0–0.2 junctions·km^{-2}	AWM	C	Stream junctions
High hazard	High	Proportion	C	Debris flow hazard
Moderate hazard	Moderate	Proportion	C	
Min. temperature	Range = 2.16–5.07 °C	AWM	C	Air temperature
Max. temperature	Range = 10.98–15.68 °C	AWM	C	
Temperature range	Range = 8.61–11.55 °C	AWM	C	
Precipitation	Range = 1012–5560 mm	AWM	C	Precipitation
Alluvium		Proportion	C, I	Major lithology
Glacial drift		Proportion	C, I	
Landslide		Proportion	C, I	
Mafic intrusive		Proportion	C, I	
Mafic volcanic flow		Proportion	C, I	
Sandstone		Proportion	C, I	
Siltstone		Proportion	C, I	
Bedrock	Calc-alkaline volcanoclastic + mafic volcanic flow + mafic pyroclastic + felsic volcanic flow	Proportion	C	
Bare	Bare rock + sand + clay	Proportion	C	US Geological Survey national land cover for Oregon
Grassland	Grasslands + herbaceous	Proportion	C	
Open water	Open water	Proportion	C, I	
Shrub	Emergent herbaceous	Proportion	C	
Wetlands	Wetlands + woody wetlands	Proportion	C, I	
Agriculture		Proportion	C, I	Willamette River basin land use and land cover
Built		Proportion	C, I	
Old forest	FCC > 80 years	Proportion	C	
FCC total	All FCC classes combined	Proportion	C	
Young forest	FCC ≤ 40 years	Proportion	C	
Recent cut forest	FCC ≤ 20 years	Proportion	C	
Hardwood	Closed + semiclosed hardwood	Proportion	C	
Old hardwood	Forest closed hardwood	Proportion	C	
Young hardwood	Forest semiclosed hardwood	Proportion	C	
BLM	Bureau of Land Management	Proportion	C, I	Land ownership
ORCA	Oregon and California lands	Proportion	C	
USFS	US Forest Service	Proportion	I	
Private	Private or nongovernment	Proportion	C	
Road density	Road kilometres per unit area of catchment (length·km^{-2})		C	Roads
River density	Stream kilometres per unit area of catchment (length·km^{-2})		C	Streams
Catchment area	Total area of catchment for a given index reach		C	Catchments

Note: An indicator variable takes on a value of 1 if that feature is present in the watershed draining to the index reach or 0 if it is not present. FCC, forest cover class.

affect the distribution of steelhead spawners, as these characteristics influence spawning ability and the intragravel environment for successful incubation (Reiser and Bjornn 1979; Pauley et al. 1986). The landscape attributes that we included in our analyses have the potential to influence these finer scale habitat attributes that, in turn, influence steelhead redd density and distribution. We focused on characteristics associated with water quality (road density, land use), water quantity, depth, and velocity (precipitation, hillslope, channel gradient) and on lithology and topography, which form the template for unit-scale habitat features (Benda et al. 1992; Beechie et al. 2001). Landscape variables were calculated from existing geospatial data layers (Table 1; Appendix A). These data layers included information about geology, climate, the land surface, forest cover, land ownership, and other human impacts such as road density and

© 2004 NRC Canada

dams. To calculate values for the landscape variables associated with each index reach, we delineated the watershed draining to that particular reach. We quantified landscape variables within the delineated watersheds using area-weighted mean for continuous variables and fraction of total area for categorical variables.

Three additional landscape variables were calculated: channel gradient (percent), number of tributary junctions, and drainage density (river kilometres per square metre). We included channel gradient because it drives the distribution of habitat units such as pools and riffles as well as water depth and velocity (Bjornn and Reiser 1991; Montgomery et al. 1999). Steelhead spawning is thought to be associated with a fairly narrow range of channel gradients. We included the number of tributary junctions and drainage density for two reasons: location of tributaries within a basin may explain fish community structure (Osborne and Wiley 1992) and tributary junctions may be areas of high biological productivity (Rice et al. 2001).

We inventoried all barriers likely to be impassible to steelhead within the watersheds using a combination of data sources: culvert locations and passage information from the Oregon Department of Fish and Wildlife Fish Passage Division (C. Corrarino, Fish Screening and Passage Program, Oregon Department of Fish and Wildlife, 2501 SW First Avenue, Portland, OR 97207, USA, unpublished data), western Oregon dams and natural barriers to fish (StreamNet 2001), Bonneville Power Administration dams and possible hydroelectric development sites (Pacific Northwest Hydropower Database and Analysis System Database, NWHS Database Management Group, Bonneville Power Administration, Portland, OR 97207, USA, unpublished data), and Interior Columbia Ecosystem Management Project (ICBEMP) dams with >10 acre feet storage capacity (1 acre foot = 1233.482 m^3), originally from US Army Corps of Engineers (Quigley et al. 2001) as well as current anadromous fish distribution (StreamNet 2001), nonspatial databases, personal communications with state agencies, and published limits to fish passage by barrier height (Aaserude 1984). There is uncertainty associated with the barrier classifications because positional inaccuracy of some barriers prevented us from associating them with the stream network and because many barriers do not have complete passage information. Where passage status could not be determined, barriers were not included in our analysis.

We estimated the amount of available habitat above each barrier based on a 1 : 24 000 scale hydrographic stream network with geomorphically designated stream reaches generated from a drainage-enforced digital elevation model (DEM) (Miller 2003). Stream reaches were attributed with channel gradient, also calculated from the DEM. We calculated the total number of stream kilometres blocked by each barrier as the distance upstream from that barrier to a natural barrier. We eliminated streams with channel gradient >20% from our analysis, as these are rarely used by winter steelhead (Washington Department of Fish and Wildlife 2000). We limited redd density predictions to areas above barriers that have suitable spawning gradients and that are therefore most similar to the index reaches for which the models were built. We estimated available lengths of spawning habitat using two gradient windows. Stream segments with a channel gradient of 0.5–6% were identified as possible spawning segments. A subset of these stream segments, those with channel gradient ranging from 1% to 5%, were identified as likely spawning segments.

Model fitting and selection

Our purpose in building a model was to identify correlations between the distribution of steelhead redds and available landscape variables (Table 1) and to predict inaccessible reaches within the four watersheds that might also support large numbers of steelhead redds. Our model selection approach was designed to identify the best-fitting set of models for two specific and related purposes: (*i*) generating hypotheses about landscape factors influencing spawning suitability and (*ii*) predicting potential redd density in areas within these same watersheds for which redd count data do not exist. Our modeling approach had two distinct stages. In the first stage, we selected the model structure, including the covariance structure and random effects, and in the second, we selected the dependent predictor variables.

Model structure

We chose mixed models because they can accommodate correlated responses and heterogeneous variances. Since these spawner data were collected over time at the same sites, measurements within each site are serially autocorrelated. Using mixed linear models, we were able to model the autocorrelation and test the fit of various covariance structures (Littell et al. 1996). The Bayesian information criterion (BIC) was used to select the most appropriate covariance structure (Schwarz 1978). The BIC is essentially twice the log likelihood value plus a penalty for the number of parameters estimated; smaller values indicate a better fit. The BIC was calculated as follows:

$$\mathrm{BIC} = -2l(\theta) + (p + q)\log(N)$$

where $l(\theta)$ is the maximized log likelihood function, p is the dimension of the model (i.e., rank(X)), q is the number of covariance parameters estimated (three for these models), and N is the sample size (N = 384 in our analyses).

We also investigated whether the slope and intercept should be modeled as random effects as in the random coefficients model or hierarchical linear models (Bryk and Raudenbush 1992) used in previous, similar studies (Pess et al. 2002; Feist et al. 2003). In this scenario, the slope, intercept, or both the slope and intercept for each year are allowed to vary randomly from an average slope and intercept. A random slope would indicate that the relationship between landscape characteristics and redd density varied by year. A random intercept would suggest that average redd density varied between years. An autoregressive covariance structure was assumed, as was independence between the slope and intercept. The appropriateness of possible scenarios was assessed by testing whether the variance of the slope and (or) intercept was significantly different from zero using both Wald and likelihood ratio tests (Casella and Berger 1990).

© 2004 NRC Canada

Variable selection

Variables in the final models were selected from all possible variables (Table 1) using a modified all subsets routine. A set of candidate models was selected using BIC (Schwarz 1978). The final models from within that set were selected based on metrics describing collinearity between predictors, the stability of the model coefficient estimates, and predictive accuracy. Models with high levels of collinearity between the landscape variables were eliminated using two criteria: pairwise correlation > 0.7 or condition index > 10 (Belsey et al. 1982). Models with values of Cook's $D > 1$ for at least one site were deemed unstable and eliminated from the analysis (Cook 1977).

A cross-validation procedure was used to assess model accuracy and precision. For each model under consideration, 10% of the observations were randomly selected as a validation set and were not used in coefficient estimation. Coefficients were estimated using the remaining 90% of the data and values were predicted for each observation in the validation set. The correlation (r) between the predicted and observed values was calculated, as was the root mean squared prediction error (RMSPE). The procedure was repeated 1000 times for each model, providing estimates of the mean correlation and RMSPE (measures of accuracy) and the variance of these statistics (measures of precision). Smaller variation was taken as an indication of a more stable predictive model.

Predicting steelhead redd density and prioritizing barrier removals

For each potential barrier in the study region, we determined the watershed area draining to that point from a 10-m DEM using the same technique employed above in determining landscape characteristics for watersheds draining to index reaches. For each barrier watershed, we calculated all landscape variables included in the final models to predict redd density. Steelhead redd density within the barrier watershed was predicted to be the average of the values from the set of best models, excluding those models for which one or more of the barrier watershed landscape values fell outside the range of values used in model building. We also calculated the relative number of new redds as the predicted redd density multiplied by the length of possible or likely spawning habitat. Ninety-five percent prediction intervals were calculated for all predictions using Proc Mixed in SAS.

Results

Redd distribution

The density of steelhead redds at the index reaches fluctuated over the 20-year study period; however, the ranking of the sites was less variable (Fig. 2). We found that steelhead redds were consistently found in greater abundance in some index reaches than in others and that those sites consistently supporting the largest fraction of redds were not clustered in one watershed but were distributed throughout all four watersheds (Fig. 2). These findings support the premise that landscape variables play a contributing role in determining locations of high densities of steelhead redds. Watersheds draining to individual index reaches ranged in size from 5 to 563 km^2.

Final models

Model structure

A comparison of the BICs for each of three covariance structures — autoregressive of order 1 (correlation decreases with measurements taken farther apart in time), compound symmetry (all correlations between years equal), and independence between years — indicated that the autoregressive model gave the best fit. This structure was used for all subsequent modeling. There was little evidence that the variance of the slope was different from zero but there was convincing evidence that the intercept should be considered a random coefficient ($p < 0.01$ for all one-variable models). The final model structure included an autoregressive structure with a lag of 1 year and a random intercept across years.

Variable selection

All 37 potential explanatory variables were fit independently. After the modified all-subsets procedure, there were 19 candidate models based on BIC alone. Four models were selected as the set of final models (Fig. 3; Table 2) based on correlation, RMSPE, and variance in their correlation estimates. The correlation between observed and predicted values for the four final models ranged from 0.618 to 0.642; the RMSPEs ranged from 0.808 to 0.827 (Fig. 3). The correlation between observed and predicted steelhead redd density was higher for the averaged predictions from all four models together (0.656).

Landscape variables included in the set of best models were the proportion of the watershed in alluvium, the proportion of the watershed with a hillslope < 6%, the proportion of the watershed in ancient landslides, the proportion of the watershed in young (<40 years) forest, the proportion of the watershed with shrub vegetation, the proportion of the watershed in agriculture, and the presence of mafic volcanic lithology. None of the models were able to predict years with redd counts of zero (Fig. 3).

Barrier prioritization

We identified 168 barriers within the study area as either unlikely to be passable or completely impassable (Fig. 4). Blocked kilometres of likely spawning habitat for any one barrier ranged from 0 to 67.2; blocked kilometres of possible spawning habitat ranged from 0 to 95.7. We estimate that the study area contains 874 inaccessible stream kilometres with channel gradients in the possible spawning range (0.5–6%); of these, there are 595 inaccessible stream kilometres with channel gradients in the likely spawning range (1–5%). Total stream kilometres blocked by anthropogenic barriers accounted for 32% of the stream length in the four watersheds. The amount of possible habitat blocked by anthropogenic barriers for any one watershed ranged from 30% (South Santiam) to 39% (North Santiam). Any errors resulting from uncertainty in barrier classification or positional inaccuracy have likely resulted in underestimates of inaccessible stream kilometres.

Predicted redd density upstream of barriers ranged from 2.3 to 22.4 redds·km^{-1}. These predicted values can be interpreted as the expected average redd density across many reaches for the average returning population size between 1979 and 1999. Because returns will vary in the future, these

© 2004 NRC Canada

Fig. 2. Distribution of steelhead redds by index reach from 1979 to 1999 in the North Santiam (NS), South Santiam (SS), Calapooia (C), and Molalla (M) watersheds within the Willamette River basin. The fraction of steelhead redds was calculated as the fraction of redd density observed in a particular year within a particular reach divided by the redd density observed over all reaches surveyed in that year. The box in the boxplot represents the limits of the middle 50% of the data; the line within the box identifies the median. Whiskers identify 1.5% times the interquartile range; broken lines outside the whiskers indicate individual observations that fell outside this range.

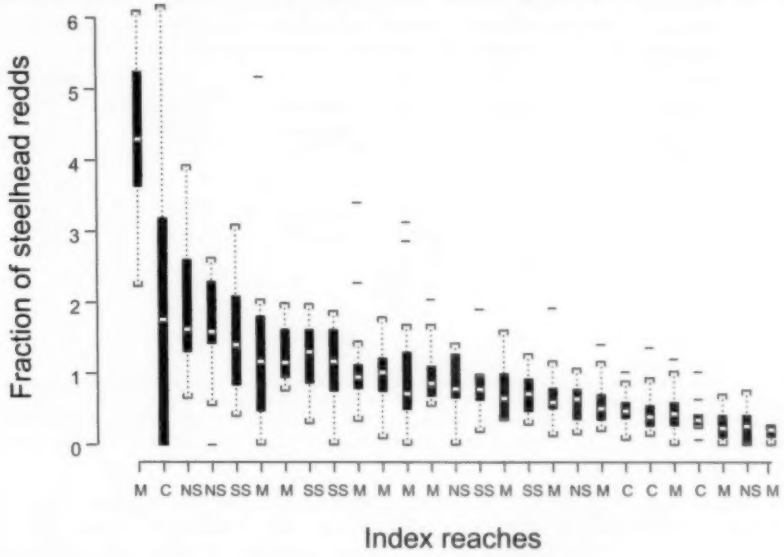

Fig. 3. Plots of predicted versus observed data in all reaches in the years 1979–1999 for the four models selected. The broken line is the 1:1 line. (*a*) $\log(\text{redds}\cdot\text{km}^{-1}) = 1.98 + 41.47 \times \text{alluvium} - 3.50 \times \text{hillslope} - 1.08 \times \text{landslide}$; (*b*) $\log(\text{redds}\cdot\text{km}^{-1}) = 1.71 + 34.98 \times \text{alluvium} - 3.43 \times \text{hillslope} + 12.41 \times \text{young forest}$; (*c*) $\log(\text{redds}\cdot\text{km}^{-1}) = 1.33 + 24.42 \times \text{alluvium} + 0.42 \times I(\text{mafic volcanic}) + 30.88 \times \text{shrub}$; (*d*) $\log(\text{redds}\cdot\text{km}^{-1}) = 1.59 + 37.79 \times \text{alluvium} + 0.47 \times I(\text{mafic volcanic}) - 8.38 \times \text{agriculture}$. $I(\cdot)$ is the indicator function: $I(\cdot) = 1$ if the feature is present, $I(\cdot) = 0$ otherwise.

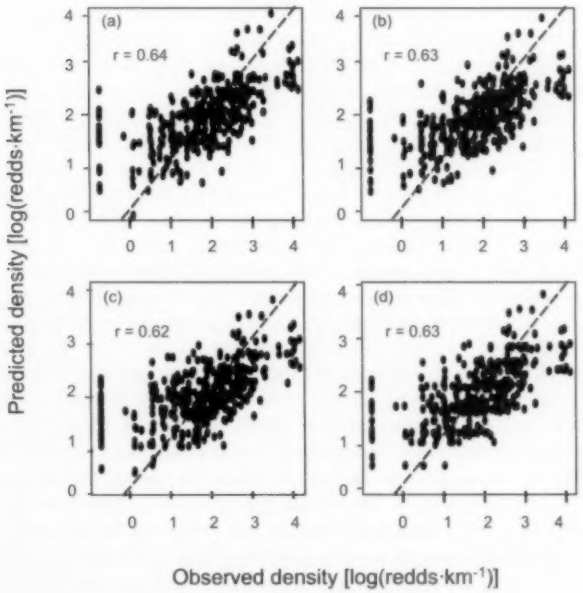

predictions are best used in a relative sense to compare the potential of one site with that of another. Predicted number of redds if only the likely gradient range was used ranged from 0 to 1363 redds. If all possible gradient ranges were used, the maximum prediction increased to 1933 redds.

The modeled predictions of redd density provided new information for solving the problem of prioritizing barriers for removal. Predicted redd density identified five barriers blocking highly suitable habitat that would have been missed if one had simply used total stream length alone to identify candidate barrier removal projects (Table 3; Fig. 4). The modeled predictions also helped to distinguish between barriers that blocked large numbers of stream miles. There was over a threefold difference in predicted redd density between the two barriers that each blocked over 200 km of stream. The lower 95% confidence interval for redd density describes the lower bound of predicted redd density, the worst-case scenario. Using this metric, we can identify those barriers with the best worst-case scenario. Managers wishing to explicitly acknowledge the uncertainty in these modeled predictions might choose such a metric. This metric identified three barriers that would have been missed in a selection process that did not include uncertainty.

Fifty-seven of the 168 barriers were excluded from the barriers analysis because one or more landscape characteristics were out of the range observed for the index reaches used in model building. In all but one case, the proportion of alluvium was >0.0432, the maximum observed for a watershed draining to an index reach used in model building. These barriers also had a larger proportion of agricultural land use than the maximum used for model building (0.1197). The excluded barriers were generally found in the

© 2004 NRC Canada

Table 2. Summary of final predictive models to predict log(redds·km^{-1}).

	Variable	Coef.	SE	Variance component	Estimate	Corr.	RMSPE
Model 1	Intercept	1.98	0.14			0.606	0.830
	Alluvium	41.47	7.77	Intercept	0.266		
	Hillslope	–3.50	1.08	Residual	0.704		
	Landslide	–1.08	0.35				
Model 2	Intercept	1.71	0.16			0.598	0.836
	Alluvium	34.98	7.38	Intercept	0.266		
	Hillslope	–3.43	1.11	Residual	0.721		
	Young forest	12.41	5.42				
Model 3	Intercept	1.33	0.18			0.585	0.850
	Alluvium	24.42	7.51	Intercept	0.238		
	I(mafic volcanic)	0.42	0.13	Residual	0.728		
	Shrub	30.88	11.93				
Model 4	Intercept	1.59	0.15			0.577	0.855
	Alluvium	37.79	7.48	Intercept	0.259		
	I(mafic volcanic)	0.47	0.13	Residual	0.711		
	Agriculture	–8.38	2.74				

Note: Coef., model coefficient; SE, standard error of the model coefficient; variance components describe the variance of the intercept and the residual variance of the model; Corr., correlation between observed and predicted redd density; RMSPE, root mean squared prediction error, describes the mean value from the cross-validation procedure.

lower parts of the drainage network and were distributed throughout all four watersheds (Fig. 4).

Discussion

Landscape factors affecting steelhead redd abundances in the Willamette basin

We found that the distribution of winter steelhead redds among sites in the Willamette River basin was fairly consistent over time. Our findings are in agreement with results from other basins and for other species (Pess et al. 2002; Feist et al. 2003) and, in combination, these results suggest that landscape features such as geology, vegetative cover, and climate should be good predictors of redd distribution in the future or in unsurveyed areas. The identification of multiple significant relationships between landscape features and steelhead redd distribution suggests that steelhead distribution is, at least in part, driven by factors operating at scales larger than those considered by traditional reach-scale models of fish habitat relationships. Consistent steelhead habitat relationships have been difficult to identify because of the flexible life history characteristics of steelhead and, perhaps, because of the emphasis on reach-scale habitat characteristics. The relationships identified here generate a series of testable hypotheses about the impacts of geology, landform, and land management on the distribution of steelhead redds.

The most important variable in our models was the proportion of the watershed composed of alluvial deposits. In each of the four best models, the proportion of alluvium was a strong positive predictor of steelhead redd abundance. Areas with high amounts of alluvial deposits are more likely to have unconstrained channels with cobble substrate, which are preferred by steelhead (Bell 1973; Reiser and Bjornn 1979). It may also be that, in the four watersheds, areas with alluvium are simply correlated with some other feature preferred by spawning winter steelhead such as downstream areas or lower gradient areas. In either case, the correlation indicates that, within the study area, percent alluvium is a good predictor of areas that could support high numbers of spawning steelhead. The contributions of the indicator variable for mafic volcanic lithology and the proportion of landslide deposits reinforce the general hypothesis that the geology of an area plays a strong role in regulating the distribution of species. In addition, landform, the proportion of the watershed with hillslope <6%, was present in two of the best models.

We would expect that vegetation and land use might also be good predictors of winter steelhead redd abundance. Surprisingly, we found that the proportion of the watershed in shrub cover and in young forest were positive predictors of steelhead redd abundance. Shrublands were sprinkled in tiny patches across all four watersheds but were more likely in the upper watersheds. Shrubland includes areas "characterized by natural or semi-natural woody vegetation with aerial stems, generally less than 6 meters tall" (US Geological Survey 1999). A visual analysis indicates that these patches are associated with logging roads, so we conclude that much of the land designated as shrubland is clearcut. Young forests tended to be clumped around particular index reaches and were not clearly correlated with other potential predictors. A positive relationship between clearcuts or new forests and fish production has been reported elsewhere for juvenile fish (Murphy and Hall 1981; Bisson and Sedell 1984; Holtby 1988). In these previous studies, short-term, positive effects result from an increase in stream productivity following an increase in available sunlight. Steelhead may be more resistant than other species to some negative impacts of timber harvest management such as increases in winter discharge; as spring spawners, steelhead eggs are not exposed to the full force of winter high flows.

Potential impacts of hatchery programs were not considered in our analysis of landscape-scale habitat features; however, hatchery management clearly impacts the distribution

© 2004 NRC Canada

Fig. 4. All barriers identified within the study area. Barriers identified with solid triangles were used in the barrier prioritization analysis. Barriers identified with open circles were excluded because one or more landscape characteristics were out of the range observed for the index reaches used in model building. Watersheds are delineated for the nine barriers selected for further investigation as identified by each of three criteria: stream length (km) (diagonal lines sloping downward to the right), predicted redd density (redds·km^{-1}) (diagonal lines sloping upward to the right), and predicted number of redds in possible spawning areas (shaded areas). Numbers correspond to barrier identification in Table 3. Note: All barriers identified by both stream length and predicted redd density (cross-hatched) were also identified using predicted number of redds and therefore have a shaded background.

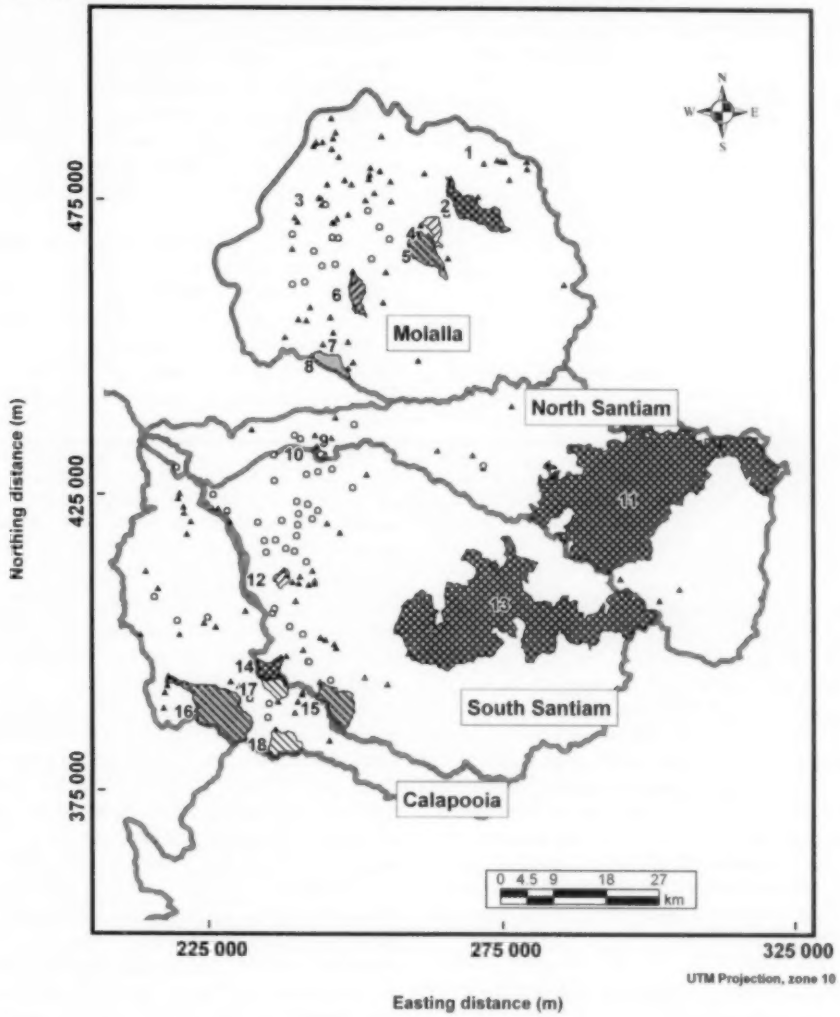

of wild spawning fish. There have been winter steelhead hatchery introductions in three of the four study watersheds and there has likely been some straying of hatchery fish into the Calapooia River (Chilcote 1998). As well, introduced summer steelhead may have a negative impact on wild winter steelhead through competition for feeding territories and spawning habitat (Chilcote 1998; Kostow et al. 2003). Detailed data on these introductions could likely explain some of the remaining variance in our models.

Advantages of the mixed-models approach

The mixed-models approach allowed us to model annual correlation explicitly, taking advantage of the information available in a 20-year time series of fish abundance data. Because mixed models allow for flexibility in the correlation matrix, we were able to calculate theoretically derived confidence intervals that can be tested or corrected using Monte Carlo simulations. Therefore, by using the mixed-models approach, we were able to develop a metric for prioritizing barrier removals that included uncertainty in model predictions. The mixed-models approach also allowed us to handle missing data. Although some sites were not surveyed every year, we were able to utilize the information that was available at those sites. While our data compared time series of redd abundances with static descriptions of landscape characteristics, the flexibility of our approach would enable analysis of a time series of landscape data if it were available. Using a time series of both fish and landscape data, our

© 2004 NRC Canada

Table 3. Prioritization information for the top nine barriers according to each of several criteria: total upstream length, predicted redd density, predicted number of redds considering either available lengths of possible or likely habitat, and the lower 95% confidence interval (CI) bound for the redd density prediction.

Barrier ID	Total upstream length (km)	Predicted redd density (redds·km^{-1})	Predicted redds (possible)	Predicted redds (likely)	Density lower 95% CI
1					5.07
2	67.05	8.52	354.22	286.10	
3		6.91			
4		7.37			5.41
5	40.48		74.14	55.41	
6		10.53	105.19	82.52	5.58
7					4.90
8			80.52	69.69	
9					4.98
10		7.22			5.32
11	265.88	22.36	1933.14	1362.65	12.56
12		6.89			
13	256.19	6.95	474.50	316.87	4.85
14	26.61	12.05	87.69		7.39
15	49.04		93.53	70.97	
16	85.57		176.26	118.08	
17	30.24				
18	30.74			45.07	

Note: Each row represents one barrier; barrier identification is used in Fig. 4. Empty cells indicate that the barrier was not in the top nine barriers according to that criterion. Predicted redd density values represent the average values from as many of the four best models as possible given that the habitat values for that barrier must fall within the range of values used to build the model. Barriers draining watersheds for which any variable was outside the range of variables used to build all four models were not included in this analysis.

modeling approach could answer questions about how fish populations respond to changes in landscape condition.

By testing a variety of model structures, we were able to learn something about the underlying relationship between landscape variables and redd distribution. The lack of evidence for a random slope despite the evidence for a random intercept implies that there is a consistent relationship between redd density and landscape characteristics that varies in magnitude from year to year as a function of population size. This model structure is consistent with our findings of relatively constant redd distribution patterns over time and our overarching hypothesis that landscape type and condition play strong roles in regulating the distribution of spawners, independent of population size.

Using model-based predictions of habitat suitability to prioritize barrier removal projects

The landscape model developed in this paper can be applied to inform decision-making for managing anadromous salmonids. Using remotely sensed data and a model of steelhead distribution built for this particular area, a series of empirically based prioritization schemes for barrier removal projects were developed. Each prioritization metric provides information that is useful for identifying high-priority barrier removal projects. The total length of stream above a barrier is clearly an important consideration and may provide information useful for other purposes such as maximizing the benefit of barrier removal for multiple species. Adding modeled redd density predictions allows a quantitative assessment of the relative value of the reopened habitat for winter steelhead. The total predicted number of redds in either likely or possible areas combines information about useable stream length and the modeled predictions into a number that can be compared across projects. For example, one could ask whether the number of new redds behind a barrier to a short stretch of river with optimal spawning habitat might be higher than the number of predicted redds behind a barrier to a long stretch of predicted low-abundance habitat. By using different classifications for predicting likely and possible spawning areas, this approach can provide managers with a range of expected numbers of new redds and an indication of the uncertainty in the estimates.

A novel aspect of our analysis to inform decisions on barrier removals was the use of a prioritization metric, the lower bound of the 95% confidence interval, which explicitly incorporates uncertainty into the ranking scheme. Such a metric selects the best barrier removals given the lowest expected redd density in the stream sections above the barrier. The use of a metric like the lower bound of a confidence interval can also remove those projects that exceed a specified risk of negative effects. Other similar metrics such as the lower bound of the 64% confidence interval or the probability of observing redd densities > 0.5 fish·km^{-1} could also be calculated and applied using our approach. In our analysis, the metric that included uncertainty selected high-priority projects that might have been missed if only stream length or predicted fish benefit were used. It also enabled a clear differentiation between the two highest-ranking projects according to either total stream length or predicted number of possible redds.

While no prioritization scheme can substitute for detailed field analysis, it can greatly reduce the time required for

© 2004 NRC Canada

such field surveys by identifying a set of projects most likely to be successful. Additional metrics such as cost, land ownership, viability of downstream populations, or recovery priorities would complement the prioritization schemes presented here. The best metric or set of metrics to use in a particular situation will depend on the exact goals of the project, the trade-offs that managers are interested in making, and the risks that they are willing to accept. Our prioritization scheme, as applied to the Willamette River basin, would be enhanced by data collection efforts in the lower parts of the drainage network where there are high proportions of both alluvium and agriculture. The current model is not suitable for these areas. A monitoring system for barrier removal programs (e.g., Pess et al. 2003) to benefit steelhead will enable refinements of potential steelhead abundance predictions.

In summary, there are two major findings from our research: landscape features can be used to describe and predict the distribution of winter steelhead redds and these models can be used immediately to improve decision-making for anadromous salmonids. The prioritization of restoration projects is a valuable application of broad-scale correlation models. Future improvements on this approach will need to consider models that incorporate simultaneous effects on multiple aquatic species. The validity of the approach can be tested after barrier removal projects are underway. In the short term, our empirical approach, based purely on remotely sensed landscape data and generally available data on redd abundance, provides a series of testable hypotheses to improve our understanding of the impacts of landscape form and condition on winter steelhead distribution and abundance as well as management tools to help prioritize potential restoration projects.

Acknowledgements

We thank Mark Wade and Wayne Hunt at the Oregon Department of Fish and Wildlife for the use of redd count data and we thank Jeff Cohen, NOAA Northwest Fisheries Science Center, for GIS programming that enabled these analyses. We also thank Kelly Burnett, US Forest Service Pacific Northwest Research Station, Tim Beechie and Martin Lierman, NOAA Northwest Fisheries Science Center, for careful reviews of the manuscript, and Karrie Hanson for assistance with manuscript preparation.

References

Aaserude, R.G. 1984. New concepts in fishway design. M.S. thesis, Department of Civil and Environmental Engineering, Washington State University, Pullman, Wash.

Anderson, J.R., Hardy, E.E., Roach, J.T., and Witmer, R.E. 1976. A land use and land cover classification system for use with remote sensor data. US Geol. Surv. Prof. Pap. 964. US Geological Survey, Reston, Va.

Beechie, T.J., Collins, B.D., and Pess, G.R. 2001. Holocene and recent geomorphic processes, land use, and salmonid habitat in two north Puget Sound river basins. *In* Geomorphic processes and riverine habitat. Water Sci. Appl. Vol. 4. *Edited by* J.B. Dorava, D.R. Montgomery, F. Fitzpatrick, and B. Palcsak. American Geophysical Union, Washington, D.C. pp. 37–54.

Bell, M.C. 1973. Fisheries handbook of engineering requirements and biological criteria. US Army Engineer Division, North Pacific Corps of Engineers, Portland, Oreg. Contract No. DACW57-68-C-0086.

Belsey, D.A., Kuh, E., and Welsch, R.E. 1982. Regression diagnostics: identifying influential data and sources of collinearity. John Wiley, New York.

Benda, L., Beechie, T.J., Wissmar, R.C., and Johnson, A. 1992. Morphology and evolution of salmonid habitats in a recently deglaciated river basin, Washington State, USA. Can. J. Fish. Aquat. Sci. **49**: 1246–1256.

Bisson, P.A., and Sedell, J.R. 1984. Salmonid populations in streams in clear-cut versus old-growth forests of western Washington. *In* Fish and wildlife relationships in old-growth forests. *Edited by* W.R. Meehan, J.T.R. Merrell, and T.A.Hanley. American Institute of Fisheries Research Biologists, Juneau, Alaska. pp. 121–129.

Bjornn, T.C., and Reiser, D.W. 1991. Habitat requirements of salmonids in steams. *In* Influences of forest and rangeland management on salmonids fishes and their habitats. *Edited by* W.R. Meehan. Am. Fish. Soc. Spec. Publ. 19. pp. 83–138.

Bryk, A.S., and Raudenbush, S.W. 1992. Hierarchical linear models. Sage Publications, Inc., Newbury Park, Calif.

Bustard, D.R., and Narver, D.W. 1975. Aspects of the winter ecology of juvenile coho salmon (*Oncorhynchus kisutch*) and steelhead trout (*Salmo gairdneri*). J. Fish. Res. Board Can. **32**: 667–680.

Casella, G., and Berger, R.L. 1990. Statistical inference. Duxbury Press, Belmont, Calif.

Chilcote, M.W. 1998. Conservation status of steelhead in Oregon. Inf. Rep. 98-3. Oregon Department of Fish and Wildlife, 2501 SW First Avenue, P.O. Box 59, Portland, Oreg.

Cook, R.D. 1977. Detection of influential observations in linear regression. Technometrics, **19**: 15–18.

Daly, C., Neilson, R.P., and Phillips, D.L. 1994. A statistical-topographic model for mapping climatological precipitation over mountainous terrain. J. Appl. Meteorol. **33**: 140–158.

Feist, B.E., Steel, E.A., Pess, G.R., and Bilby, R.E. 2003. The influence of scale on salmon habitat restoration priorities. Anim. Conserv. **6**: 271–282.

Geist, D.R., Jones, J., Murray, C.J., and Dauble, D.D. 2000. Suitability criteria analyzed at the spatial scale of redd clusters improved estimates of fall chinook salmon (*Oncorhynchus tshawytscha*) spawning habitat use in the Hanford Reach, Columbia River. Can. J. Fish. Aquat. Sci. **57**: 1636–1646.

Harding, J.S., Benfield, E.F., Bolstad, P.V., Helfman, G.S., and Jones, E.B.D., III. 1998. Stream biodiversity: the ghost of land use past. Proc. Natl. Acad. Sci. U.S.A. **95**: 14 843 – 14 847.

Hicks, B.J., and Hall, J.D. 2003. Rock type and channel gradient structure salmonid populations in the Oregon Coast Range. Trans. Am. Fish. Soc. **132**: 468–482.

Holtby, L.B. 1988. Effects of logging on stream temperatures in Carnation Creek, British Columbia, and associated impacts on the coho salmon (*Oncorhynchus kisutch*). Can. J. Fish. Aquat. Sci. **45**: 502–515.

Kostow, K.E., Marshall, A.R., and Phelps, S.R. 2003. Naturally spawning hatchery steelhead contribute to smolt production but experience low reproductive success. Trans. Am. Fish. Soc. **132**: 780–790.

Littell, R.C., Milliken, G.A., Stroup, W.W., and Wolfinger, R.D. 1996. SAS® system for mixed models. SAS Institute Inc., Cary, N.C.

Lunetta, R.S., Cosentino, B.L., Montgomery, D.R., Beamer, E.M., and Beechie, T.J. 1997. GIS-based evaluation of salmon habitat in the Pacific Northwest. Photogramm. Eng. Remote Sensing, **63**: 1219–1229.

© 2004 NRC Canada

Miller, D.J. 2003. Programs for DEM analysis. *In* Landscape dynamics and forest management. Gen. Tech. Rep. RMRS-GTR-101CD. USDA Forest Service, Rocky Mountain Research Station, Fort Collins, Co. CD-ROM.

Montgomery, D.R., Beamer, E.M., Pess, G.R., and Quinn, T.P. 1999. Channel type and salmonid spawning distribution and abundance. Can. J. Fish. Aquat. Sci. **56**: 377–387.

Murphy, M.L., and Hall, J.D. 1981. Varied effects of clear-cut logging on predators and their habitat in small streams of the Cascade Mountains, Oregon. Can. J. Fish. Aquat. Sci. **38**: 137–145.

Oregon Department of Forestry. 2000. Debris flow hazard. December 1999. Oregon Department of Forestry, Salem, Oreg. (Available at http://www.odf.state.or.us/DIVISIONS/administrative_services/ services/gis//debris.htm)

Osborne, L.L., and Wiley, M.J. 1992. Influence of tributary spatial position on the structure of warmwater fish communities. Can. J. Fish. Aquat. Sci. **49**: 671–681.

Pauley, G.B., Bortz, B.M., and Shepard, M.F. 1986. Species profiles: life histories and environmental requirements of coastal fishes and invertebrates (Pacific Northwest) — steelhead trout. Biol. Rep. 82 (11.62). US Fish and Wildlife Service, Washington, D.C.

Pess, G.R., Montgomery, D.R., Steel, E.A., Bilby, R.E., Feist, B.E., and Greenberg, H.M. 2002. Landscape characteristics, land use, and coho salmon (*Oncorhynchus kisutch*) abundance, Snohomish River, Wash., USA. Can. J. Fish. Aquat. Sci. **59**: 613–623.

Pess, G.R., Beechie, T.J., Williams, J.E., Whitall, D.R., Lange, J.I., and Klochak, J.R. 2003. Watershed assessment techniques and the success of aquatic restoration activities. *In* Strategies for restoring river ecosystems: sources of variability and uncertainty in natural and managed systems. *Edited by* R.C. Wissmar and P.A. Bisson. American Fisheries Society, Bethesda, Md. pp. 185–201.

Poff, N.L. 1997. Landscape filters and species straits: toward mechanistic understanding and prediction in stream ecology. J. North Am. Benthol. Soc. **16**: 391–409.

Poff, N.L., and Huryn, A.D. 1998. Multi-scale determinants of secondary production in Atlantic salmon (*Salmo salar*) streams. Can. J. Fish. Aquat. Sci. **55**(Suppl. 1): 201–217.

Quigley, T.M., Gravenmier, R.A., and Graham, R.T. (*Technical Editors*). 2001. Interior Columbia Basin Ecosystem Management Project: scientific assessment. (Available from US Department of Agriculture, Forest Service, Pacific Northwest Research Station, Portland, Oreg.)

Reiser, D.W., and Bjornn, T.C. 1979. Habitat requirements of anadromous salmonids. US For. Serv. Gen. Tech. Rep. USFS-GTR-PNW-96. US Forest Service, Portland, Oreg.

Rice, S.P., Greenwood, M.T., and Joyce, C.B. 2001. Tributaries, sediment sources, and the longitudinal organization of macroinvertebrate fauna along river systems. Can. J. Fish. Aquat. Sci. **58**: 824–840.

Richards, C., Johnson, L.B., and Host, G.E. 1996. Landscape-scale influences on stream habitats and biota. Can. J. Fish. Aquat. Sci. **53**: 295–311.

Robison, E.G., Mills, K.A., Paul, J., Dent, L., and Skaugset, A. 1999. Oregon Department of Forestry storm impacts and landslides of 1996: final report. For. Practices Tech. Rep. No. 4. Oregon Department of Forestry, Forest Practices Monitoring Program., Salem, Oreg.

Roni, P., Beechie, T.J., Bilby, R.E., Leonetti, F.E., Pollock, M.M., and Pess, G.R. 2002. A review of stream restoration techniques and a hierarchical strategy for prioritizing restoration in Pacific Northwest watersheds. N. Am. J. Fish. Manag. **22**: 1–20.

Schwarz, G. 1978. Estimating the dimension of a model. Ann. Stat. **6**: 461–464.

StreamNet. 2001. Current anadromous salmon distribution at a 1:100 000 scale, all species. Pacific States Marine Fisheries Commission, Gladstone, Oreg. (Available at http://www.streamnet.org/)

Thompson, W.L., and Lee, D.C. 2000. Modeling relationships between landscape-level attributes and snorkel counts of chinook salmon and steelhead parr in Idaho. Can. J. Fish. Aquat. Sci. **57**: 1834–1842.

U.S. Geological Survey. 1999. Spatial data. Oregon land cover data set, June 1999. USGS NLCD, Sioux Falls, S.D. (Available at http://edcwww.cr.usgs.gov/programs/lccp/nationallandcover.asp)

Washington Department of Fish and Wildlife. 2000. Fish passage barrier and surface water diversion screening assessment and prioritization manual. (Available from Washington Department of Fish and Wildlife Habitat Program, Environmental Restoration Division, Salmonid Screening, Habitat Enhancement, and Restoration (SSHEAR) Section, Olympia, Wash.)

Zorn, T.G., Seelbach, P.W., and Wiley, M.J. 2002. Distributions of stream fishes and their relationship to stream size and hydrology in Michigan's Lower Peninsula. Trans. Am. Fish. Soc. **131**: 70–85.

© 2004 NRC Canada

Appendix A

Table A1. Geographic information system (GIS) data layers used in habitat analysis for the Willamette River basin, Oregon, USA.

Data layer	Map scale and grid-cell size	Description
Hillslope	1:24 k 30 m	Hillslope gradient generated from US Geological Survey (USGS) 30-m digital elevation model (DEM) using ARC/INFO. Calculated the slope of every 30-m grid cell in the DEM. Hillslope is the sum all of grid cells with slope < 6%
Channel slope	1:24 k 30 m	Calculated manually using USGS 1:24 k 30-m digital elevation models (DEM). Defined as rise (upstream elevation minus downstream elevation of index reach) over run (river kilometre length of index reach) multiplied by 100
Stream junctions	1:100 k na	Used ARC/INFO to calculate the density of stream junctions for each watershed from the USGS 1:100 k stream network data layer
Debris flow hazard	1:24 k 30 m	Data layer generated by Oregon Department of Forestry (2000). Naturally occurring debris flow hazard rating generated from slope steepness, geologic units, stream channel confinement, fan-shaped geomorphology, and historical information on debris flow occurrence (Robison et al. 1999)
Air temperature	Unknown 4000 m	Gridded annual maximum and minimum air temperatures from parameter-elevation regressions on independent slopes model (PRISM) (Daly et al. 1994)
Precipitation	Unknown 500 m	Total annual precipitation for 1989, considered a "normal" year from PRISM (Daly et al. 1994)
Major lithology	1:500 k na	USGS classification of geologic map units according to major lithology
USGS National land cover data for Oregon	1:250 k 30 m	USGS classification of land cover data from LANDSAT TM satellite imagery (level 2). Generated by USGS using Anderson et al. (1976) protocols
Willamette River basin land use and land cover	1:100 k 30 m	Land use and land cover ca. 1990 (USGS 1999) derived from LANDSAT TM 30-m pixel satellite data. Developed by the Institute for a Sustainable Environment at the University of Oregon for use by the Environmental Protection Agency (EPA) Pacific Northwest Ecosystem Research Consortium
Land ownership	1:100 k na	Land ownership for Willamette River basin compiled into digital format by the Oregon State Service Center for GIS in 1992 and 1993
Roads	1:24 k na	Polyline representation of the Willamette River basin road network ca. 1997. Source material includes Oregon Department of Transportation, US Forest Service, and the Bureau of Land Management. Developed by the Institute for a Sustainable Environment at the University of Oregon for use by the EPA Pacific Northwest Ecosystem Research Consortium
Streams	1:100 k na	Polyline representation of the Willamette River basin stream network generated by USGS
Catchments	1:24 k na	Polygon representation of total area upslope of the downstream end of any given index reach. Generated from a USGS 30-m DEM

Note: All data layers were generated by other entities (such as federal, state, and academic institutions), with the exception of hillslope, channel slope, and stream junctions, which we generated ourselves. The "k" after all of the map scales is an abbreviation for "kilo" or 1000; a map scale of 1:100 k is equal to 1:100 000. Grid-cell size is the size of each individual pixel or grid cell for raster-based data layers. Grid-cell size is presented below the map scale. na, not applicable.

© 2004 NRC Canada

Effect of age and temperature on amino acid composition and the content of different protein types of juvenile Atlantic cod (*Gadus morhua*) otoliths

K. Hüssy, H. Mosegaard, and F. Jessen

Abstract: The purpose of this study was to analyse the amino acid composition of otolith matrix protein, estimate the proportion of the water-soluble protein fraction, and analyse the effect of matrix composition on otolith visual appearance. Juvenile Atlantic cod (*Gadus morhua*) were reared under constant temperature and feeding conditions and sampled at the beginning and the end of the experiment. The amino acid composition was dominated by asparagine, glutamic acid, leucine, serine, and proline. A change in amino acid composition was observed with increasing temperature and time, caused by changing proportions of the water-soluble and -insoluble protein fractions. Feeding level had no effect. The relative content of water-soluble protein was linearly related to fish dry weight and temperature. Otolith opacity, defined as the percentage of incident light absorbed by an otolith section, did not differ significantly between experimental treatments. The soluble protein fraction had a positive, albeit insignificant, correlation with opacity. Using opacity and otolith volume, deposited total otolith protein content was estimated with an R^2 of 0.91, where otolith volume alone explained 83% of the observed variation.

Résumé : L'objectif de notre étude est d'analyser la composition en acides aminés des protéines de la matrice des otolithes, d'estimer la proportion de la fraction protéinique hydro-soluble et d'analyser l'effet de la composition de la matrice sur l'apparence visuelle de l'otolithe. Nous avons élevé de jeunes morues franches (*Gadus morhua*) dans des conditions constantes de température et d'alimentation et les avons échantillonnées au début et à la fin de l'expérience. La composition en acides aminés est dominée par l'asparagine, l'acide glutamique, la leucine, la sérine et la proline. Il se produit un changement dans la composition des acides aminés en fonction de la température et du temps, qui est causé par une modification des proportions des fractions protéiniques solubles et insolubles dans l'eau. Le niveau d'alimentation est sans effet. Le contenu relatif de protéines hydrosolubles est en relation linéaire avec la masse sèche du poisson et la température. L'opacité de l'otolithe, défini comme le pourcentage de lumière incidente absorbé par une section d'otolithe, ne diffère pas selon les traitements expérimentaux. La fraction de protéines solubles est en corrélation positive, bien que non statistiquement significative, avec l'opacité. À partir de l'opacité et du volume de l'otolithe, nous avons estimé le contenu total de protéines déposées dans l'otolithe avec un R^2 de 0,91 et le volume de l'otolithe seul explique 83 % de la variation.

[Traduit par la Rédaction]

Introduction

Since Degens et al. (1969) first investigated the composition of fish otoliths, it has been known that otoliths consist of $CaCO_3$ in the aragonitic form and proteins. Calcium deposition has been studied extensively, while only relatively few authors have dealt with the protein constituent and its incorporation into the otolith (Morales-Nin 1986*a*, 1986*b*). The otolith matrix consists of both water-insoluble and at least four distinguishable water-soluble components (Baba et al. 1991; Asano and Mugiya 1993) with different properties and different biochemical compositions.

A number of studies have analysed the amino acid composition of the water-soluble (Baba et al. 1991; Asano and Mugiya 1993; Sasagawa and Mugiya 1996) and water-insoluble components (Degens et al. 1969; Davis et al. 1995) as well as the total matrix protein (Morales-Nin 1986*a*, 1986*b*). The only studies investigating matrix composition and variations in protein content with fish age are those by Morales-Nin (1986*a*, 1986*b*). By comparison of pooled sam-

Received 7 June 2002. Accepted 31 July 2003. Published on the NRC Research Press Web site at http://cjfas.nrc.ca on 27 July 2004.
J16930

K. Hüssy[1] **and H. Mosegaard.** Danish Institute for Fisheries Research, Department of Marine Fisheries, Charlottenlund Castle, DK-2920 Charlottenlund, Denmark.
F. Jessen. Danish Institute for Fisheries Research, Department of Seafood Research, DTU, Building 221, DK-2800 Lyngby, Denmark.

[1]Corresponding author (e-mail: kh@dfu.min.dk).

 doi: 10.1139/F04-037 © 2004 NRC Canada

ples of sea bass (*Dicentrarchus labrax*) otoliths of ages 4, 6, and 12 months (Morales-Nin 1986*a*) and two Cape hake (*Merluccius capensis*) otoliths of ages 1 and 11 years (Morales-Nin 1986*b*), the amino acid composition of total matrix protein was found to undergo an ontogenetic change. However, to date, no information is available on the amino acid composition and its variability in individual fish from controlled environments. One of the purposes of this study is therefore to investigate otolith matrix amino acid composition and proportion of water-soluble and -insoluble protein in relation to different experimental treatments and fish age.

In his summary of the powers of otolith microstructure analysis, Brothers (1981) highlighted the influence of otolith protein content. Already, Dannevig (1956) showed a link between otolith organic content, consisting of amino acids, and opacity. This observation has since been confirmed by Mugiya (1965), Watabe et al. (1982), Seyama et al. (1991), and others who showed that translucent structures are dominated by aragonitic calcium crystals, while protein fibres dominate opaque structures. It is also well known that both juvenile and adult fish develop opaque, high-contrast otoliths during periods of high growth and translucent, low-contrast otoliths during unfavourable growth conditions or starvation (e.g., Neilson and Geen 1985; Rice et al. 1985) and with increasing water temperature (Mosegaard and Titus 1987; Volk et al. 1990).

Thus, the terms opacity, optical density, and translucence/transparency have been used to describe otolith microstructure appearance since Reibisch (1899), but to our knowledge, these terms have never been properly defined and quantified in measurable units. The only study in which otolith transparency was applied is Gauldie et al.'s (1998) application of relative change in otolith transparency as a reaction to diffusion of different solvents. However, they did not attempt to standardize their measurements with respect to incident light level and preparation thickness. The method is therefore not universally applicable, since comparisons between individuals are impossible.

In this paper, we will propose a definition of the term otolith opacity, investigate the effect of rearing conditions and otolith composition on this parameter, and provide a method of estimating protein content in fish otoliths.

Materials and methods

Experiment description

Five hundred juvenile cod (*Gadus morhua*), the offspring of two males and two females, were obtained from the Isle of Man Marine Laboratory, University of Liverpool, at an age of 60 days and standard length of approximately 20 mm. The fish were acclimatized to the facilities of the Danish Institute for Fisheries Research for 7 days at 12 °C (the original rearing temperature), with four feedings to satiation per day. Before the experiment, a temperature mark was induced in the otoliths of the fish by alternating the water temperature between 6 and 12 °C, with three periods of 3 h of exposure to 12 °C followed by 1 h of exposure to 6 °C. After 12 h at 12 °C, this temperature cycle was repeated, resulting in a clearly visible increment pattern (Fig. 1). This method was tested on five fish prior to application in this experiment. The fish were then measured and weighed to the nearest 0.5 mm and 0.01 g, respectively, and distributed over twelve 175-L tanks (40 fish per tank). The fish were kept in 32‰ seawater at full aeration and of 16 h light – 8 h dark cycle.

Fig. 1. Otolith of an experimental fish with a temperature mark (bar = 15 μm).

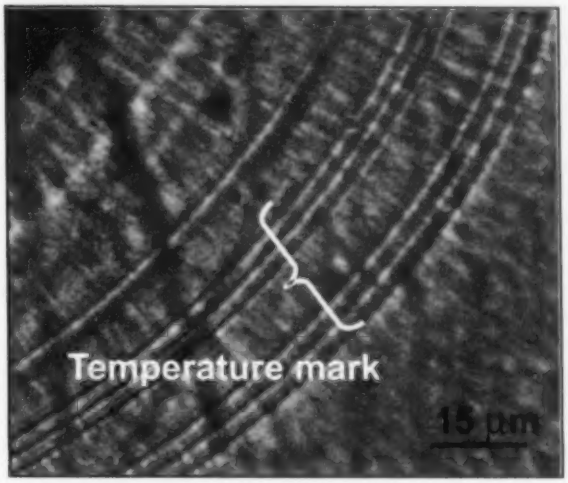

The experimental setup consisted of three temperatures (5, 10, and 15 °C) and two ration levels (ad libitum and low). The fish were fed pellets of dry food (Perla Marine, Skretting a/s Denmark) with pellet sizes increasing from 0.8 to 2 mm with increasing fish size. Within each tank, and throughout the experiment, ad libitum ration corresponded to approximately 4.0%, 5.5%, and 7.5% of fish dry weight per day for 5, 10, and 15 °C, respectively. Food was provided continually by automatic feeders throughout the daylight hours at quantities exceeding the food consumed (visual observation). Low ration was approximately 65% of the high ration for the three temperatures calculated from the difference between leftovers and food provided. No mortality occurred during the experiment.

Seventy-two fish were randomly chosen for the experiment: six fish at the beginning of the experiment and three from each tank after 40 days. They were anaesthetized with MS 222 (Sandoz), measured and weighed to the nearest 0.5 mm and 0.01 g, respectively, and sacrificed. Sagittal otoliths, henceforth called "otoliths", were extracted, rinsed in 5% NaOH and distilled water to remove adhering tissue, and stored in labelled plastic bags. Fish were dried individually at 100 °C for 24 h to obtain dry weight. The remaining fish were used in other experiments.

Analysis of amino acid composition

Both right and left otoliths were weighed to the nearest 0.001 mg. The right otolith was used for amino acid analysis and the left for microstructure and opacity measurements. The otoliths were hydrolyzed in hydrochloric acid. The amino acids were separated by elution in a column consisting of a cation-exchange resin. After separation, the amino acids were oxidized and detected by derivatization with the fluorescent reagent orthophthaldialdehyde. Total protein content was calculated as the sum of the individual amino acid con-

© 2004 NRC Canada

centrations. A detailed description of these methods is given in Barkholt and Jensen (1989). An overview of fish and otolith sizes used in this study is given in Table 1. Size distributions were relatively homogenous, with the exception of one larger fish in the 10 and 15 °C high-ration treatments.

Proportion of soluble and insoluble protein fractions

The amino acid compositions of a wide range of fish species otoliths, reported in the literature, were compared to establish the degree of species-specific differences. No significant differences were found in either the insoluble (Degens et al. 1969; Davis et al. 1995) (Wilcoxon signed rank tests, all $p > 0.5$) or the soluble fractions (Baba et al. 1991; Sasagawa and Mugiya 1996) (Wilcoxon signed-rank test, $p = 0.712$). The estimation procedure proposed here is therefore based on the assumption that there are no species-specific differences in the amino acid compositions of the matrix fractions.

To estimate the contribution of water-insoluble and -soluble components to the matrix protein of juvenile cod in this study, we used data published by Davis et al. (1995) and Sasagawa and Mugiya (1996). We transformed their compositions, reported as amino acid numbers and molar percent, respectively, to relative weight units by multiplying the occurrence of individual amino acids by their weights and dividing by total protein weight. For each fish, the proportional contribution of the two protein fractions to our observed amino acid composition was estimated by minimizing the sums of squares of the following relationship:

$$(1) \qquad AA_{observed} = aAA_{insoluble} + bAA_{soluble} + c$$

where $AA_{observed}$ is the amino acid composition observed in this study, $AA_{insoluble}$ is the composition of the insoluble fraction reported by Davis et al. (1995), $AA_{soluble}$ is the composition of the soluble fraction reported by Sasagawa and Mugiya (1996), a and b are the proportions of the insoluble and soluble fractions, respectively, and c is the unidentified fraction.

Otolith microstructure

For otolith microstructure analysis, an image analysis system (IMAGE PRO version 4) was used with a microscope coupled to a monitor screen by digital camera and frame grabber. Images were digitized and saved as TIFF files in black and white.

Whole otoliths were analysed at a magnification corresponding to 6.4 μm·pixel^{-1}. In the sagittal plane otolith area (A) and in the frontal plane area ($A_{frontal}$) and total otolith length ($L_{frontal}$) were measured (for the terminology, see Secor et al. 1992). Otolith volume was calculated as $V_{image} = AA_{frontal} \cdot L_{frontal}^{-1}$. For calibration, the actual volume of 30 randomly chosen otoliths was measured from displacement of water in a glass vial (5 mL) sealed with a small, round microscope coverslip. Volume displacement was calculated as $V = [(\text{weight}_{vial+water} + \text{weight}_{otolith}) - \text{weight}_{vial+water+otolith\ inside\ vial}] \cdot \text{density of water}^{-1}$ (density of deionized water at 20 °C = 0.998 mg·mm^{-3}). Five readings were taken per otolith and their values averaged. The image analysis derived volume was then calibrated as V_{actual} (cubic millimetres) = $0.771V_{image}$ ($n = 30$, $r^2 = 0.96$) and specific otolith density calculated as density = $W \cdot V^{-1}$ (milligrams per cubic millimetre).

Table 1. Overview of fish dry weight and otolith weight (average ± SD, $n_{start} = 6$, $n_{end} = 30$).

Sampling	Food level	Temperature (°C)	Dry weight (g)	Otolith weight (mg)
Start			0.11±0.04	0.47±0.12
End	High	5	0.36±0.09	1.58±0.44
		10	0.84±0.23	2.91±0.31
		15	1.08±0.35	3.62±0.95
	Low	5	0.28±0.11	1.36±0.49
		10	0.65±0.15	2.43±0.45
		15	1.01±0.21	3.22±0.36

Otoliths were then mounted on microscope slides with thermoplastic cement (Büehler) with the proximal side facing up. The otoliths were ground to the central plane on a rotating disc covered with lapping film (grit 1200) and polished on lapping film (3 μm) and with alumina paste (0.05 μm) (Büehler). The polished sections were turned over, carefully pressed to the surface of the microscope slide to remove air bubbles and surplus cement, and ground and polished to an approximate thickness of 80 μm.

Along the rostral axis, the following otolith lengths were measured: L_0, from the nucleus to the start of the experiment; L_1, from the nucleus to day 10 of the experiment; L_2, from the nucleus to day 20; L_3, from the nucleus to day 30; L_4, from the nucleus to day 40 (equal to L, from the nucleus to the edge of the otolith). Otolith volume and length have a functional relationship of the form $V = aL^b$, where $a = 0.542$ and $b = 2.415$. Otolith volume deposited was therefore estimated as $dV/dt = V_t - V_{t-1}$ using the increment widths to calculate L_{t-1} so that, for example, V_0 is the volume from the nucleus to the start of the experiment and V_4 is the volume between L_3 and L_4.

Otolith opacity

The otolith light absorption capability was measured using transmitted light and the "multiple area of interest" tool of IMAGE PRO, returning the distribution of grey values, increasing from 0 (black) to 255 (pure white) in absolute values, within a selected area of interest. The otolith grey value (G) was defined as the mean of the distribution of grey values within the selected area at a magnification corresponding to 2.20 μm·pixel^{-1}. The measurements were collected in sections of 10-day periods starting from the temperature mark (areas: a_0, hatching to the start of the experiment; a_1, days 1–10; a_2, days 11–20; a_3, days 21–30; a_4, days 31–40). These sections covered as large an area as possible from the rostral end along the dorsal and ventral sides of the otolith including the lobes perpendicular to the rostral axis. Cracks or otherwise damaged areas were excluded from the analysis, ensuring as uniform an opacity as possible. Since the sum of the analysed areas correlated well with total otolith area ($\Sigma(a_0{:}a_4) = 0.43A$, $r^2 = 0.97$), the five areas were scaled to total otolith area (A) (e.g., $A_1 = Aa_1 \cdot (a_0 + a_1 + a_2 + a_3 + a_4)^{-1}$).

Opacity was defined as

$$(2) \qquad O_{measured} = 100 - 100(G - L_{refracted}) \cdot L_{incident}^{-1}$$

© 2004 NRC Canada

Table 2. Amino acid (AA) composition of otoliths at the start and end of the experiment (average ± SD) as a percentage of total amino acid content weight (n_{start} = 6, n_{end} = 33).

		End		
AA	Start	5 °C	10 °C	15 °C
Ala	6.50±0.16	6.28±0.14	6.33±0.2	6.48±0.45
Arg	5.60±0.35	5.75±0.25	6.04±0.18	6.02±0.25
Asp	11.12±0.19	10.88±0.29	10.84±0.2	11.05±0.22
Glu	18.30±0.97	17.38±0.5	16.28±0.35	16.00±0.62
Gly	5.70±0.39	5.51±0.36	5.28±0.27	5.06±0.55
His	2.43±0.39	2.48±0.25	2.47±0.16	2.48±0.05
Ile	2.81±0.23	2.16±0.27	2.25±0.37	2.21±0.22
Leu	7.58±0.47	7.31±0.24	7.71±0.29	7.67±0.31
Lys	4.71±0.29	4.53±0.4	4.50±0.36	4.51±0.23
Met	2.49±0.1	2.22±0.12	2.23±0.21	2.19±0.12
Phe	4.63±0.19	4.13±0.34	4.22±0.28	3.93±0.42
Pro	5.25±0.13	7.23±0.5	7.42±0.59	7.65±0.27
Ser	7.50±0.77	7.65±0.29	7.86±0.54	8.14±0.36
Thr	4.95±0.18	5.25±0.28	4.99±0.23	4.99±0.29
Cys	1.01±0.08	1.44±0.22	1.46±0.17	1.48±0.11
Tyr	3.71±0.11	3.95±0.54	4.21±0.21	4.16±0.37
Val	5.70±0.16	5.86±0.38	5.92±0.13	5.99±0.18

where $O_{measured}$ is opacity, $L_{refracted}$ is refracted light, and $L_{incident}$ is incident light. Incident light level used was 340 (see Appendix A for calculation of $L_{refracted}$ and standardization in relation to $L_{incident}$).

Because otolith opacity is affected by preparation, thickness values have to be standardized to predetermined values of thickness. With permanent ink, four marks were set on the slide at equal distances and angles from the otolith. The thickness of the otolith was calculated from readings of the micrometre scale of the microscope: thickness = average of slide readings – reading at the otolith surface. The opacity of the different sections was then standardized to a thickness of 80 μm following the method outlined in Appendix A:

$$(3) \qquad O = a(1 - \exp(-b80))$$

where a = 100 and $b = [\ln(100) - \ln(100 - O_{measured})] \cdot \text{thickness}^{-1}$. Denomination of these opacity values corresponded to the area measurements O_0, O_1, O_2, O_3, and O_4.

Results

Amino acid composition

The otolith protein matrix from the beginning of the experiment consisted of approximately 27% acidic (asparagines (Asp) and glutamic acid (Glu)), 9% basic (arginine (Arg), histidine (His), and lysine (Lys)), and 64% neutral amino acids (Table 2). The side chains of the neutral amino acids consisted of 3% sulphur-containing (cysteine (Cys) and methionine (Met)), 9% aromatic (phenylalanine (Phe) and tyrosine (Tyr)), and 7% secondary (proline (Pro)) amino groups and 50% aliphatic side chains (alanine (Ala), glycine (Gly), valine (Val), leucine (Leu), and isoleucine (Ile)). Otoliths from the end of the experiment contained slightly less acidic and more aliphatic amino acids. On the individual level, the amino acid composition of both sampling dates was dominated by the acidic amino acids Asp and Glu followed by minor contributions of Leu, serine (Ser), and Pro.

Fig. 2. Scores of the principal components analysis of amino acid composition in juvenile Atlantic cod otoliths. Data points are representative of the four degree-day groups corresponding to the start of the experiment and the three temperature treatments at the end of the experiment. Plus signs, start of experiment; solid diamonds, 5 °C; open diamonds, 10 °C; triangles, 15 °C.

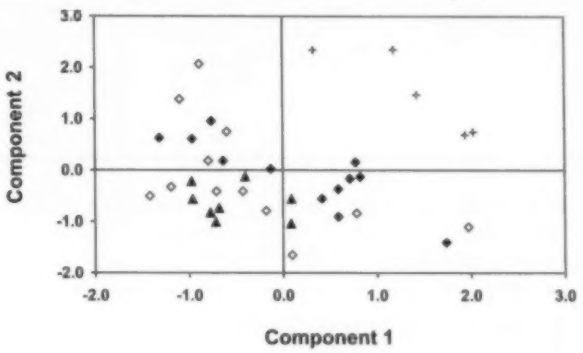

Prior to analysis, the data were tested for outliers, of which two were found: one from the beginning of the experiment and one from the 15 °C low-food treatment. These outliers were excluded from the analysis, since their composition and total protein content suggested extensive contamination of the sample.

The amino acid composition, in relative weight frequencies, was analysed using principal components analysis. The first two components (PC1 and PC2) explained 48% of the variation and only these components were used in the subsequent analyses. The amino acids with the highest eigenvector values were Pro, Asp, Cys, Arg, Glu, and Ser. For the analysis of growth and experimental treatment effects of all samples, we used fish dry weight as a proxy for growth and degree-days (equal to (Σ days × °C)/40) to separate temperature treatments and sampling dates. The effect on degree-days, ration, and growth was then analysed with PC1 and PC2 as variables in a generalized linear models approach. No interaction was found between PC1 and PC2 for degree-days, ration, and growth (all $p > 0.05$). No significant correlation was found between ration and PC1 and PC2 ($p > 0.05$), while both growth and degree-days showed a significant negative correlation (both $p < 0.001$). However, degree-days explained 62% of the variation (Fig. 2) compared with the growth effects' 42%, which indicates that experimental conditions had a higher impact on amino acid composition than on fish growth.

Otolith protein content

Total protein content was linearly related with fish dry weight (r^2 = 0.85, df = 39, $p < 0.001$) and accounted for 0.45% of otolith weight (±0.12% SD, range 0.30–0.82%). Homoscedasticity was found between relative protein content (micrograms per milligram of otolith) of all treatment groups (Bartlett, $p > 0.05$). Relative protein content was significantly affected by sampling date and temperature (ANOVA, df = 37, $p < 0.05$) but not by feeding level (ANOVA, $p > 0.05$). The highest relative protein content was observed in the smallest fish from the beginning of the ex-

© 2004 NRC Canada

Table 3. Overview of opacity, relative protein content, and relative content of water-soluble protein (WSP) (average ± SD).

Sampling	Food level	Temperature (°C)	Opacity (Σ(opacity·area)·Σarea^{-1})	Protein content (μg·mg otolith^{-1})	WSP content (μg·mg otolith^{-1})
Start			71±4	6.8±1.1	5.4±0.4
End	High	5	63±4	4.6±1.0	3.3±0.6
		10	72±5	3.8±0.9	2.4±0.2
		15	68±5	3.8±0.6	2.5±0.3
	Low	5	76±2	4.2±0.7	2.9±0.4
		10	62±5	4.6±0.6	2.8±0.4
		15	75±10	3.6±0.1	2.5±0.1

Fig. 3. Relationship between otolith density and relative protein content: density = 2.8616 – 0.172·protein content (r^2 = 0.12, df = 39, $p < 0.05$).

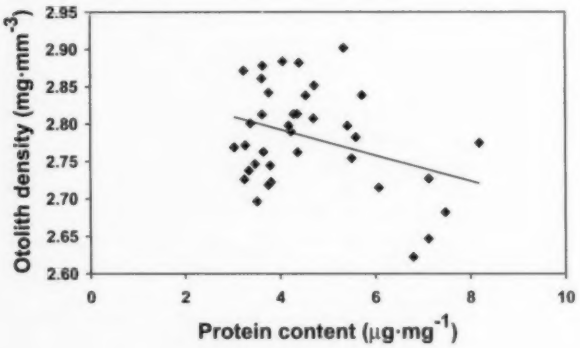

Fig. 4. Relationship between relative otolith protein content and otolith opacity ($\Sigma(O_{1-4}\,A_{1-4})\cdot A^{-1}$): protein content = 0.904 + 0.0535O (r^2 = 0.087, df = 39, p = 0.07).

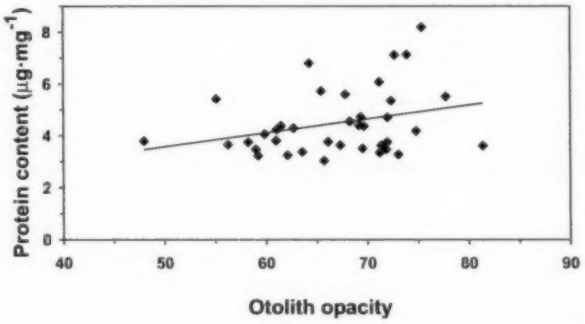

periment. Temperature was found to have a negative effect on relative protein content (see Table 3). Otolith density was found to be linearly related to relative protein content (Fig. 3). Relative protein content (micrograms per milligram of otolith) and otolith opacity ($\Sigma(O_{1-4}\,A_{1-4})\cdot A^{-1}$) were positively correlated, but the relationship was just outside the range of significance (Fig. 4).

Proportion of soluble and insoluble protein fractions

Homoscedasticity was found between proportions of soluble protein of all treatment groups (Bartlett, $p > 0.05$). The ratio of soluble to insoluble fraction (a:b) was found to be 75:19 at the beginning of the experiment and on average 68:26 at the end of the experiment, leaving an additional average fraction (c) of 6% unclassified amino acids at both sampling times. No significant differences in the unclassified fraction of the matrix amino acids (c) were found between individuals within treatments and sampling times (c = 6.1 ± 1.3 SD; nested ANOVA, all $p > 0.05$). The contribution of the water-soluble fraction decreased from 71% to 67% and 66% with increasing temperature (insoluble fraction: 23%, 27%, and 28%, respectively, see Table 3).

The soluble and insoluble fractions are inversely correlated, since the proportion of unclassified amino acids (c) did not change between treatments and sampling times. The effect of temperature, food level, and fish size on the relative content of soluble protein was analysed using generalized linear models analysis. Fish dry weight and temperature had significant effects. Data were ln transformed to increase model fit, resulting in the model

$$\ln(\mathrm{WSP}) = -1.919 - 0.316\ln(\mathrm{DW}) + 0.215\ln(T) \quad (r^2 = 0.65,\ \mathrm{df} = 33,\ \text{all } p < 0.05) \tag{4}$$

where WSP is relative soluble protein content (micrograms of protein per milligram of otolith), DW is fish dry weight (grams), and T is temperature (degrees Celsius). Adding food level or interactions between variables to the model did not result in a significant contribution.

Otolith opacity

Otolith opacity was unaffected by experimental treatments (results see Table 3). Homoscedasticity was found between all treatment groups (Bartlett, $p > 0.05$). Otolith opacity, averaged over the experimental period as $O_{\mathrm{average}} = \Sigma(O_{1-4}\,A_{1-4})\cdot A^{-1}$, was found to be unaffected by sampling time, food level, temperature, and interaction between these parameters (ANOVA, df = 37, $p > 0.05$).

The relationship between individual fish's somatic growth and opacity was analysed. For each individual, residuals were calculated as individual dry weight minus average dry weight within the tank in which the fish was reared. The larger the residuals, the faster was the individual's somatic growth rate. These residuals were regressed against otolith opacity. A significant positive relationship was found between residuals and otolith opacity, indicating that fast somatic growth is associated with high otolith opacity (Fig. 5).

© 2004 NRC Canada

Fig. 5. Relationship between residual size (individual dry weight minus average tank dry weight) and opacity: residuals = –0.5277 + 0.0072*O* (r^2 = 0.17, df = 34, $p < 0.05$).

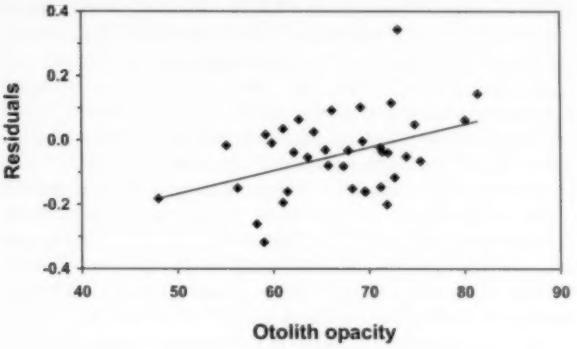

Fig. 6. Relationship between opacity and water-soluble protein content including samples from the start and end of the experiment: *O* = 59.904 + 2.211WSP (r^2 = 0.11, df = 39, p = 0.045).

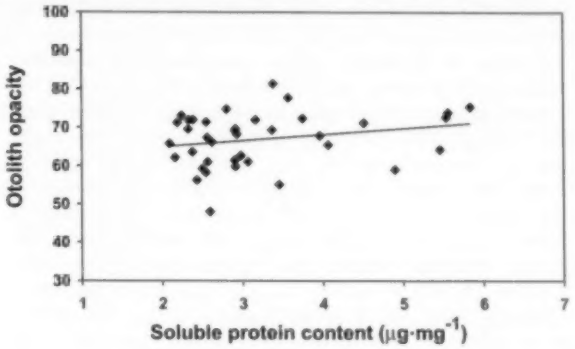

Effect of protein composition on otolith density and opacity

The effect of relative soluble protein content, fish size, temperature, and food level on otolith density and opacity was assessed using generalized linear models analysis. Content of soluble protein, fish dry weight, and the interaction between these terms had significant effects on otolith density. The ln transformation did not improve the model fit, resulting in the expression

$$\text{Density} = 3.103 - 0.763\text{WSP} - 0.493\text{DW} + 1.308\text{WSP·DW} \quad (r^2 = 0.56, \text{df} = 33, \text{all } p < 0.001) \tag{5}$$

where WSP is relative soluble protein content (micrograms of protein per milligram of otolith) and DW is fish dry weight (grams). Adding food level and (or) temperature to the model did not result in a significant contribution.

The effect of soluble protein, fish dry weight, and temperature on opacity was analysed as

$$O = 61.884 + 24.508\text{WSP} + 7.415\text{DW} - 0.366T \quad (r^2 = 0.05, \text{df} = 32, \text{all } p > 0.05) \tag{6}$$

where *O* is otolith opacity, WSP is relative soluble protein content (micrograms of protein per milligram of otolith), and DW is fish dry weight (grams). None of the parameters included in this model were significant. Adding food level or interaction terms to the model did not result in a significant contribution. However, the relationship between opacity and soluble protein was significant when samples from the start of the experiment were included (Fig. 6). No significant relationship was found between otolith opacity and density: $O = 80.65 - 5.49 \cdot \text{density}$ (df = 39, r^2 = 0.03, $p > 0.05$).

Estimation of otolith protein content

Since otolith matrix protein is distributed throughout the otolith, the parameters chosen for the estimation of total protein content were opacity and volume. The relationship between otolith volume (*V*) and otolith length (*L*) follows the function $V = 0.542L^{2.415}$. Increases in otolith volume for each 10-day interval of the experiment V_{0-4}, corresponding to volumes at L_{0-4}, were thus calculated for each individual fish as $V_n = V_{L_n} - V_{L_{n-1}}$.

Only fish from the final sampling were used. The relationship between otolith protein content and opacity can be described by the model

$$\text{Protein content (μg)} = \sum_{n=0}^{4} (a + bO_n)V_n \tag{7}$$

Model parameters were fitted with the least squares method and found to be a = 5.0625 and b = 0.0090 (r^2 = 0.91, n = 40). The residuals of this model are normally distributed around zero (Kolmogorov–Smirnov, $p > 0.05$). Of this model, otolith volume alone explained 83% of the protein content.

Discussion

The organic matrix has long been known to play a pivotal role in the biomineralization of mineralized tissues such as dentin and mollusc shells. The matrix of these tissues consists of two fractions: acidic hydrophilic proteins formed as β-pleated sheets and a hydrophobic component of collagenous proteins (Mitterer 1978; Weiner 1984). The biochemical composition of these matrix components seems to be universal for all mineralized tissues, since it is essentially identical in a wide range of phyla, such as corals, foraminifers, echinoderms, and molluscs (Mitterer 1978; Weiner 1984). The insoluble protein, which is spatially removed from the mineral phase, forms a structural fundament for crystal growth, while the soluble proteins, which are associated with the mineral phase, direct crystal growth (Weiner 1984; Wheeler et al. 1988; Nakahara 1991). The growth regulatory capabilities of the soluble protein is linked to their calcium-binding properties: the water-soluble proteins isolated from organisms forming either calcite or aragonite promote the same crystal type in vitro (Watabe and Wilbur 1960; Falini et al. 1996). Which of the two protein types actually causes crystal nucleation is not known, but cooperation seems to be the most likely mechanism (Wheeler et al. 1981, 1988).

Comparatively few authors have studied the organic matrix composition of fish otoliths and its role in otolith formation.

© 2004 NRC Canada

Davis et al. (1995) identified the DNA sequence encoding an inner ear specific collagenous protein, the water-insoluble fraction of the otolith matrix of bluegill (*Lepomis macrochirus*). This protein contains in addition to Pro, Leu, and Glu relatively high concentrations of Gly. The water-soluble component of the otolith organic matrix consists of polysaccharides, lipoproteins, and glycoproteins (Baba et al. 1991; Murayama et al. 2000). Sasagawa and Mugiya (1996) found that in tilapia (*Oreochromis niloticus*) otoliths, these proteins are dominated by Glu, Asp, Ser, and Gly, a result confirmed by Asano and Mugiya (1993). Some of the glycoprotein subunits have been shown to have calcium-binding properties, just like some of the soluble matrix proteins of molluscs (Wright 1991; Asano and Mugiya 1993). These results show that the organic matrix composition of otoliths is very similar to that found in dentin and mollusc shells, and the formation mechanisms may therefore be the same. The ratio between soluble and insoluble proteins may therefore explain otolith growth and the resulting microstructure.

Records of the two protein types' contribution to total matrix protein are sparse. In pooled samples, but of different species, Baba et al. (1991) found an 85%:15% insoluble to soluble ratio, whereas Asano and Mugiya (1993) found a 47%:45% ratio with an urea-soluble fraction of 8%. We made an attempt to estimate the contribution of the water-insoluble and -soluble components to the matrix protein of juvenile cod using the data published by Davis et al. (1995) and Sasagawa and Mugiya (1996). The methods used by these authors were considered to give the best estimates of the actual matrix amino acid composition: screening of the saccular cDNA library encoding the water-insoluble protein as Davis et al. (1995) did yields information of high precision on the amino acid sequence of this protein. Before analysing the composition of the water-soluble proteins, Sasagawa and Mugiya cleaned their otoliths in 5% NaOH to remove adhering tissue and minimize contamination, a procedure that was also carried out in the present study but was neglected by all other authors.

Our analysis of factors influencing the proportion of water-soluble matrix protein showed a negative fish size and a positive temperature effect, while food level did not have any effect. These results are supported by our principal components analysis, where a separation between sampling dates and temperature treatments was caused by the amino acids typical for the two protein types. However, relative protein content was negatively correlated with both fish size and temperature.

The negative effect of fish size on deposition rates of both relative protein content and the two types of protein is indicative of an ontogenetic development, where the total protein incorporation decreases with fish size, while the insoluble fraction becomes more dominant. An ontogenetic decrease in protein incorporation has been observed before (Morales-Nin 1986*a*; Hoff and Fuiman 1993), but only Morales-Nin (1986*a*) made an attempt to investigate ontogenetic changes in amino acid composition. She found a decrease in Leu and an increase in Asp, Glu, and Pro with age, which does not allow any conclusion with respect to changes in the ratio of the two protein types. What causes this development is still unknown.

Otolith matrix composition is also affected by environmental temperature, in that juvenile cod reared at higher temperatures incorporated progressively less protein but with an increasing proportion of soluble protein. Several mechanisms may be the cause for the decrease in total protein incorporation: a direct effect of temperature on the protein-synthesizing tissue, a relatively faster increase in $CaCO_3$ accretion, or an interaction of both. The ratio between the two protein fractions changes with temperature, indicative of a direct effect on protein synthesis, where the tissue synthesizing the insoluble fraction is affected to a higher degree. Since $CaCO_3$ accretion is known to be highly temperature dependent (Mosegaard and Titus 1987), it seems likely that our observations are the result of an interaction between $CaCO_3$ accretion and a direct effect on the protein-synthesizing tissues.

One objective of this study was to examine the effect of protein content on otolith density and light absorption. In the otoliths examined in this study, density was negatively correlated with relative protein content. This is different from Hoff and Fuiman (1993), who found that the organic content of otoliths decreased to a stable level with fish size but that density continued to increase. Part of the discrepancy in results could originate from the relative small size range analysed in this study. However, our analysis of factors regulating otolith density found a negative fish size effect but a negative correlation with the proportion of the water-soluble fraction. The phenomenon described by Hoff and Fuiman (1993) may thus be the result of a change in protein composition toward a higher content of the insoluble component.

The otolith light absorption capacity was defined as opacity. This study failed to show a significant relationship between opacity and both relative protein content and density. The most likely explanation for this is the relatively small variation in otolith opacity and protein content in the samples. For both parameters, the smallest value is about 80% of the largest. Protein synthesis is directly related to consumption, and synthesis rates in different tissues are correlated (Houlihan et al. 1989). Therefore, ration level could be expected to have a significant effect on otolith protein content, density, and opacity. However, conversion efficiency decreases at high rations (Cui et al. 1996), and the low ration levels provided in this experiment may not have been low enough to induce a significant effect. One major flaw in this study is that individual feeding rates are not available. However, individual growth rates, visualized as the difference between individual and average tank size, were significantly correlated with opacity, supporting the assumption of a relationship between consumption, protein synthesis, and opacity. The positive, albeit only weakly, significant relationship between the proportion of soluble protein and opacity indicates that particularly the ratio between the soluble and insoluble fractions is of importance. Opacity has also been shown to decrease significantly during starvation, with a significant temperature effect on the slope of opacity on time of starvation (ANCOVA, df = 412, $p < 0.01$) (Hüssy and Mosegaard 2004). The estimation procedure for protein content in fish otoliths has a positive intercept, indicating that a certain amount of protein has to be incorporated into the otolith before an effect can be measured on opacity. This phenomenon

© 2004 NRC Canada

may therefore bias the estimation of protein content if concentrations are low.

Environmental conditions affecting fish growth have long been known to be recorded in the microstructure with respect to both increment width and opacity (Brothers 1981; Rice et al. 1985). Traditionally, growth has been estimated from analyses of increment widths only (Campana and Jones 1992), while the information stored in otolith opacity has been greatly neglected. The organic matrix seems to be the driving force behind otolith formation. Knowledge of its structure, incorporation mechanisms, and optic characteristics seems to be the key to understanding otolith growth with respect to increment formation, density, and visual appearance. This study is an attempt to establish a link between the otolith's light absorption and the matrix's two major protein types. Understanding the mechanisms of otolith growth and microstructure will eventually lead to an improvement in understanding the link between otolith and fish somatic growth.

Acknowledgements

Financial support of the Danish Institute for Fisheries Research, the University of Copenhagen, and the Danish Research Academy is gratefully acknowledged. Anne Blicher, Department of Biochemistry and Nutrition, Technical University of Denmark, is thanked for performing the amino acid analysis. Finally, we would like to thank three anonymous reviewers for their helpful comments on a previous version of the manuscript.

References

Asano, M., and Mugiya, Y. 1993. Biochemical and calcium-binding properties of water-soluble proteins isolated from otoliths of the tilapia *Oreochromis niloticus*. Comp. Biochem. Physiol. B Comp. Biochem. **104**: 201–205.

Baba, K., Shimizu, M., Mugiya, Y., and Yamada, J. 1991. Otolith matrix proteins of walley pollock: biochemical properties and immunohistochemical localization in the saccular tissue. *In* Mechanisms and phylogeny of mineralization in biological systems. *Edited by* S. Suga and H. Nakahara. Springer Verlag, Tokyo. pp. 57–61.

Barkholt, V., and Jensen, A.L. 1989. Amino acid analysis: determination of cysteine plus half-cystine in proteins after hydrochloric acid hydrolysis with a disulfide compound as additive. Anal. Biochem. **177**: 318–322.

Brothers, E.B. 1981. What can otolith microstructure tell us about daily and subdaily events in the early life history of fish? Rapp. P.-V. Réun. Cons. Int. Explor. Mer, **178**: 393–394.

Campana, S.E., and Jones, C.M. 1992. Analysis of otolith microstructure data. *In* Otolith microstructure examination and analysis. *Edited by* D.K. Stevenson and S.E. Campana. Can. Spec. Publ. Fish. Aquat. Sci. No. 117. pp. 73–100.

Cui, Y., Hung, S.S.O., and Zhu, X. 1996. Effect of ration and body size on the energy budget of juvenile white sturgeon. J. Fish Biol. **49**: 863–876.

Dannevig, E.H. 1956. Chemical composition of the zones in cod otoliths. J. Cons. Int. Explor. Mer. **21**: 156–159.

Davis, J.G., Oberholtzer, J.C., Burns, F.R., and Greene, M.I. 1995. Molecular cloning and characterization of an inner ear-specific structural protein. Science (Wash., D.C.), **267**: 1031–1034.

Degens, E.T., Deuser, W.G., and Haedrich, R.L. 1969. Molecular structure and composition of fish otoliths. Mar. Biol. **2**: 105–113.

Falini, G., Albeck, S., Weiner, S., and Addadi, L. 1996. Control of aragonite or calcite polymorphism by mollusc shell macromolecules. Science (Wash., D.C.), **271**: 67–69.

Gauldie, R.W., Thacker, C.E., West, I.F., and Wang, L. 1998. Movement of water in fish otoliths. Comp. Biochem. Physiol. A Comp. Physiol. **120**: 551–556.

Hoff, G.R., and Fuiman, L.A. 1993. Morphometry and composition of red drum otoliths: changes associated with temperature, somatic growth rate, and age. Comp. Biochem. Physiol. A Comp. Physiol. **106**: 209–219.

Houlihan, D.F., Hall, S.J., and Gray, C. 1989. Effects of ration on protein turnover in cod. Aquaculture, **79**: 103–110.

Hüssy, K., and Mosegaard, H. 2004. Atlantic cod (*Gadus morhua*) growth and otolith accretion characteristics modelled in a bioenergetics context. Can. J. Fish. Aquat. Sci. **61**. This issue.

Mitterer, R.M. 1978. Amino acid composition and metal binding capability of the skeletal protein of corals. Bull. Mar. Sci. **28**: 173–180.

Morales-Nin, B. 1986*a*. Structure and composition of otoliths of Cape hake *Merluccius capensis*. S. Afr. J. Mar. Sci. **4**: 3–10.

Morales-Nin, B. 1986*b*. Chemical composition of the otoliths of the sea bass (*Dicentrarchus labrax* Linnaeus, 1758) (Pisces, Serranidae). Cybium, **10**: 115–120.

Mosegaard, H., and Titus, R. 1987. Daily growth rates of otoliths in yolk sac fry of two salmonid species at five different temperatures. *In* Proceedings of the V Congress of European Ichthyology, Stockholm. *Edited by* S.O. Kallander and B. Farnholm. Swedish Museum of Natural History, Stockholm, Sweden. pp. 221–227.

Mugiya, Y. 1965. Calcification in fish and shell-fish. IV. The differences in nitrogen content between the translucent and opaque zones of otolith in some fish. Bull. Jpn. Soc. Sci. Fish. **31**: 896–901.

Murayama, E., Okuno, A., Ohira, T., Takagi, Y., and Nagasawa, H. 2000. Molecular cloning and expression of an otolith matrix protein cDNA from the rainbow trout, *Oncorhynchus mykiss*. Comp. Biochem. Physiol. B Comp. Biochem. **126**: 511–520.

Nakahara, H. 1991. Nacre formation in bivalve and gastropod molluscs. *In* Mechanisms and phylogeny of mineralization in biological systems. *Edited by* S. Suga and H. Nakahara. Springer Verlag, Tokyo. pp. 343–350.

Neilson, J.D., and Geen, G.H. 1985. Effects of feeding regimes and diel temperature cycles on otolith increment formation in juvenile chinook salmon, *Oncorhynchus tshawytscha*. Fish. Bull. **83**: 91–101.

Reibisch, J. 1899. Eizahl bei *Pleuronectes platessa* und die Altersbestimmung dieser Form aus den Otolithen. Wiss. Meeresunters. **4**: 232–248.

Rice, J.A., Crowder, L.B., and Binkowski, F.P. 1985. Evaluating otolith analysis for bloater *Coregonus hoyi*: do otoliths ring true? Trans. Am. Fish. Soc. **114**: 532–539.

Sasagawa, T., and Mugiya, Y. 1996. Biochemical properties of water-soluble otolith proteins and the immunobiochemical detection of the proteins in serum and various tissues in the tilapia *Oreochromis niloticus*. Fish. Sci. **62**: 970–976.

Secor, D.H., Dean, J.M., and Laban, E.H. 1992. Otolith removal and preparation for microstructure examination. *In* Otolith microstructure examination and analysis. *Edited by* D.K. Stevenson and S.E. Campana. Can. Spec. Publ. Fish. Aquat. Sci. No. 117. pp. 19–57.

Seyama, H., Edmonds, J.S., Moran, M.J., Shibata, Y., Soma, M., and Morita, M. 1991. Periodicity in fish otolith Sr, Na, and K corresponds with visual banding. Experientia, **47**: 1193–1196.

© 2004 NRC Canada

Volk, E.C., Schroder, S.L., and Fresh, K.L. 1990. Inducement of unique otolith banding patterns as a practical means to mass-mark juvenile Pacific salmon. Am. Fish. Soc. Symp. **7**: 203–215.

Watabe, N., and Wilbur, K.M. 1960. Influence of the organic matrix on crystal type in molluscs. Nature (Lond.), **188**: 334.

Watabe, N., Tanaka, K., Yamada, J., and Dean, J.M. 1982. Scanning electron microscope observations of the organic matrix in the otolith of the teleost fish *Fundulus heteroclitus* (Linnaeus) and *Tilapia nilotica* (Linnaeus). J. Exp. Mar. Biol. Ecol. **58**: 127–134.

Weiner, S. 1984. Organization of organic matrix components in mineralized tissues. Am. Zool. **24**: 945–951.

Wheeler, A.P., George, J.W., and Evans, C.A. 1981. Control of calcium carbonate nucleation and crystal growth by soluble matrix of oyster shell. Science (Wash., D.C.), **212**: 1397–1398.

Wheeler, A.P., Rusenko, K.W., Swift, D.M., and Sikes, C.S. 1988. Regulation of in vitro and in vivo $CaCO_3$ crystallization by fractions of oyster shell organic matrix. Mar. Biol. **98**: 71–80.

Wright, P.J. 1991. Calcium binding by soluble matrix of the otoliths of Atlantic salmon (*Salmo salar* L.). J. Fish Biol. **38**: 625–627.

Appendix A

Incident light

For standardization, incident light ($L_{incident}$) was measured through the microscope slide only. Because the incident light levels used exceeded the upper limit of 255 set by the image analysis system, a filter was used to dim the incident light before measurements were taken. Within the range of $L_{incident} < 255$, incident light levels with and without filter were correlated:

$$\text{(A1)} \quad L_{\text{incident}_{\text{without filter}}} = 2.294 \cdot L_{\text{incident}_{\text{with filter}}}^{-1}$$

$$(n = 20, r^2 = 0.999)$$

This relationship was also assumed to apply to higher light levels, where incident light levels were measured with filter and then transformed to actual levels.

Refracted light

Because of refraction of light within the microscope and the otolith, a grey level of 0 will never be obtained. To estimate the amount of this refraction, light was prevented from penetrating through the otolith by covering the backside of the slide, underneath the otolith, with black plastic. Refraction ($L_{refracted}$) was then measured over the covered otolith at $L_{incident}$ values ranging from 270 to 405. $L_{refracted}$ was found to relate to $L_{incident}$ by the linear function

$$\text{(A2)} \quad L_{\text{refracted}} = 25.919 + 0.0173 L_{\text{incident}}$$

$$(r^2 = 0.69, n = 20)$$

Definition of otolith opacity

Opacity (O) was then defined as the percentage of $L_{incident}$ absorbed by the otolith, corrected for $L_{refracted}$:

$$\text{(A3)} \quad O_{\text{measured}} = 100 - 100(G - L_{\text{refracted}}) \cdot L_{\text{incident}}^{-1}$$

where G is defined as the mean of the distribution of grey values within a selected area of interest.

Standardization of opacity measurements

The effect of microscope magnification, otolith thickness, and incident light intensity was assessed by measuring the grey value of 10 randomly selected otoliths at three predetermined magnification levels (640×, 320×, and 160× corresponding to 8.80, 4.40, and 2.20 μm·pixel^{-1}), four light intensities (270, 315, 360, and 405), and five thickness levels (range 50–160 μm). Grey value measurements (G) were taken covering as large an area of the otolith as possible and at the same position for every light and thickness level.

The one-way ANOVA of the 10 randomly selected otoliths showed that otolith opacity was not significantly affected by microscope magnification (ANOVA, $p > 0.05$). The relationship between otolith opacity and incident light and sample thickness can be described as $O = 69.28 - 0.04 L_{incident} + 0.22 \times$ thickness ($r^2 = 0.45$, $n = 160$). Opacity was found to be linearly related to incident light level ($O = 82.513 - 0.0241 L_{incident}$, $n = 160$), and opacity measured at different incident light levels can thus be standardized by converting measurements corresponding to an $L_{incident}$ of 340:

$$\text{(A4)} \quad O_{L_{\text{incident}=340}} = O_{\text{measured}} - 0.0241(L_{\text{measured}} - 340)$$

The functional relationship between opacities standardized to $L_{incident} = 340$ and otolith preparation thickness is described by the model

$$\text{(A5)} \quad O = a[1 - \exp(-b \cdot \text{thickness}_{\text{standard}})]$$

where $a = 100$ and $b = 0.0136$ ($r^2 = 0.42$, $n = 160$). Otolith opacity of individual samples can thus be standardized to an otolith preparation thickness by solving this equation for each sample ($b_{sample} = (\ln(a) - \ln(a - O)) \cdot \text{thickness}^{-1}$) and inserting b_{sample} in eq. A5 with the desired standard preparation thickness.

© 2004 NRC Canada

Atlantic cod (*Gadus morhua*) growth and otolith accretion characteristics modelled in a bioenergetics context

K. Hüssy and H. Mosegaard

Abstract: The purpose of this work is to present a conceptual model for fish otolith growth in which somatic growth is related to otolith growth and opacity. The model is based on known mechanisms of $CaCO_3$ and protein incorporation into the otolith. Model parameters were derived from laboratory experiments and from the literature. A sensitivity analysis showed that the model was robust to measurement errors in most input parameters. The most sensitive parameters were the exponents of the otolith length–weight and otolith protein – whole-body protein synthesis relationships and the proportionality constant between metabolism and otolith growth rate. Application to experimental data resulted in good agreement between back-calculated and observed fish sizes. In the growth experiment, the average back-calculated weights were slightly lower than the average observed weights, but the correlation was highly significant. In the starvation experiment, the back-calculated weights were also highly correlated with observed weights, with slightly declining residuals with fish size. Unlike previous back-calculation methods, this model has the ability to detect periods of starvation and estimate growth histories in both growing and starving fish.

Résumé : Le but de notre étude est la mise au point d'un modèle conceptuel de la croissance des otolithes de poissons dans lequel la croissance somatique est reliée à la croissance et à l'opacité de l'otolithe. Le modèle se base sur les mécanismes connus d'incorporation du $CaCO_3$ et des protéines dans l'otolithe. Les variables du modèle sont tirées d'expériences de laboratoire et de la littérature. Une analyse de sensibilité montre la robustesse du modèle aux erreurs de mesure pour la plupart des variables d'entrée. Les variables les plus sensibles sont les exposants des relations entre la masse et la longueur des otolithes et entre la concentration de protéines de l'otolithe et la synthèse des protéines du corps entier, ainsi que la constante de proportionnalité entre le métabolisme et le taux de croissance de l'otolithe. L'utilisation du modèle avec des données expérimentales donne une bonne correspondance entre les tailles de poissons observées et celles obtenues par rétrocalcul. Dans l'expérience de croissance, les masses moyennes obtenues par rétrocalcul sont légèrement plus faibles que celles observées, mais la corrélation est fortement significative. Dans l'expérience de jeûne, les masses obtenues par rétrocalcul sont aussi en forte corrélation avec les masses observées et les résidus décroissent légèrement en fonction de la taille du poisson. Contrairement aux méthodes antérieures de rétrocalcul, notre modèle peut détecter les périodes de jeûne et estimer l'évolution de la croissance tant chez les poissons en croissance que chez les poissons privés de nourriture.

[Traduit par la Rédaction]

Introduction

The discovery of daily growth increments in fish otoliths (Pannella 1971) opened a potential for studying individual growth trajectories. Different techniques for back-calculating fish size from otolith size have been developed and applied over the years (e.g., Francis 1990). These techniques have been based on three assumptions: (*i*) that the formation of periodically formed features is daily, (*ii*) that deposited material is not reabsorbed, and (*iii*) that the distance between these features is proportional to fish growth. All of these back-calculation procedures involve fish and otolith sizes at capture, otolith size at previous times, and different assumptions of the fish size – otolith size relationship (e.g., Francis 1990).

The permanence and daily periodicity of microincrement formation have been verified for many species (see review by Campana and Neilson 1985). Otolith and somatic growth are proportional within the range of environmental conditions allowing positive somatic growth (Campana and Neilson 1985; Neilson and Geen 1985). However, a decoupling between the two parameters can be caused by several factors such as starvation (Campana 1983), low growth rate (Secor and Dean 1989), ontogenetic development (Otterlei et al. 2000), and supraoptimal temperatures (Mosegaard et al. 1988). These results led to the hypothesis that otolith growth is governed by metabolism rather than by growth (Mosegaard et al. 1988). Inclusion of parameters such as age, fish size, and temperature in more sophisticated quadratic response and multiple regression methods can improve growth estimates in some situations (Mosegaard et al.

Received 7 June 2002. Accepted 26 January 2004. Published on the NRC Research Press Web site at http://cjfas.nrc.ca on 27 July 2004.
J16931

K. Hüssy[1] and H. Mosegaard. Danish Institute for Fisheries Research, Department of Marine Fisheries, Charlottenlund Castle, DK-2920 Charlottenlund, Denmark.

[1]Corresponding author (e-mail: kh@dfu.min.dk).

 doi: 10.1139/F04-038 © 2004 NRC Canada

1988; Secor and Dean 1992). However, so far the link between metabolism and otolith growth mechanisms has seldom been included in growth models (e.g., Schirripa and Goodyear 1997), nor has any growth model been able to detect zero or negative fish growth.

Fish otoliths consist of $CaCO_3$ in the aragonitic form embedded in a protein matrix accounting for 0.45–2.3% of otolith weight (Asano and Mugiya 1993; Hüssy et al. 2004). Several studies have shown a close relationship between otolith growth and standard metabolic rate, even though the two appear not to be directly proportional (Wright 1991*a*; Yamamoto et al. 1998; Wright et al. 2001). Another study indicated that otolith accretion is regulated by total metabolism and particularly by feeding-induced thermogenesis (Huuskonen and Karjalainen 1998). Matrix protein is synthesized by the subcupular meshwork and the squamous epithelium surrounding the otolith (Takagi and Takahashi 1999). The amount of protein secreted into the endolymphatic sac should be correlated with whole-body protein synthesis, since the synthesis rates of different tissues in a fish's body are proportional to each other (Houlihan et al. 1988; Foster et al. 1992). The effect of matrix protein on otolith growth and microstructure has not yet been analysed in detail. But protein plays an important role in the formation and growth of mineralized tissues (Nakahara 1991) and influences the visual appearance of the otolith (Hüssy et al. 2004).

The objective of this study is to develop a conceptual growth model that links measures of otolith growth and microstructure to metabolic processes in juvenile Atlantic cod (*Gadus morhua*) based on the hypotheses that $CaCO_3$ accretion is regulated by fish metabolism and that the amount of protein incorporated into the otolith is proportional to whole-body protein synthesis.

Materials and methods

Model components

The objective of this model is to estimate whole-fish protein synthesis based on measures of otolith growth and protein content. The model builds on the assumptions that (*i*) $CaCO_3$ accretion is dependent on fish metabolism and thereby indirectly by factors affecting metabolism, particularly temperature, (*ii*) protein accretion is determined by whole-fish protein synthesis, and (*iii*) there is no functional relationship between the two fractions transport across the endolymphatic membrane, so the transport mechanisms are considered independent of each other. This does not apply to the accretion process, where protein is assumed to affect the speed and density of crystal growth but not the total amount of $CaCO_3$ deposited. The variables presented here were chosen based on existing knowledge of otolith growth and mechanisms of protein synthesis. In the following, the conceptual presentation of the accretion processes is followed by a description of the experimental work behind the estimation of model parameters and the parameter estimation itself. All variables used are listed in Appendix A together with their abbreviations and units.

$CaCO_3$ incorporation

A coupling between metabolic rate and otolith growth has been observed (Wright 1991*a*; Yamamoto et al. 1998; Wright et al. 2001). Because the body tissue in small juvenile cod almost exclusively consists of protein, the rate of dry weight loss in starved fish is caused by degradation of proteins (Black and Love 1986) and assumed to be representative of routine metabolism (Beck and Gropp 1995). Therefore, routine metabolic rate at a given time (M_i, g dry weight·g^{-1}·$time^{-1}$) was modelled as a function of change in otolith weight per time (W, g·g^{-1}·$time^{-1}$):

$$(1) \qquad M_i = a\Delta W \cdot W^{-1} \cdot \Delta t_i^{-1}$$

Protein incorporation

Protein synthesis and degradation are usually expressed as fractional rates defined as the percentage of tissue protein mass synthesized/degraded per day. Because the otolith is completely enclosed by the saccular epithelium, we assumed that the rate of matrix incorporation depends on this protein synthesis rate in the saccular epithelium. The mass (μg) of matrix protein incorporated into the otolith can be estimated from otolith opacity (O) and volume (V) (Hüssy et al. 2004) (see Table 1) :

$$\text{Protein content} = \sum_{n=0}^{4} (b + cO_n)V_n$$

and the mass of matrix protein incorporated within a given time interval is

$$(2) \qquad \text{Protein deposited (g)} = (b + cO)\Delta V/\Delta t \cdot 10^{-6}$$

The fractional rate of matrix synthesis (P, g·g^{-1}·$time^{-1}$) can thus be calculated from the protein deposited divided by the protein mass of the saccular epithelium (E) (see Table 1):

$$(3) \qquad P = (b + cO)\Delta V/\Delta t \cdot 10^{-6} \cdot E^{-1}$$

Whole-body protein turnover

Protein turnover is the result of protein synthesis and degradation where the magnitude of the two processes determines the rate of net protein accretion or loss. At maintenance synthesis and degradation balance each other. The masses and fractional synthesis rates of a wide range of tissues such as liver, gills, intestine, spleen, ventricle, stomach, gonads, and white muscle are related by the function $Y = aX^b$ (Houlihan et al. 1986, 1988; Foster et al. 1992). We therefore assumed that the same applies for the whole fish – matrix relationship so that the fractional rates of whole-body protein synthesis (S) can be modelled as a function of otolith matrix synthesis (P):

$$(4) \qquad S = dP^e$$

Degradation rates (D) are usually calculated from the difference between synthesis and net protein accretion (G): $D = S - G$ (Houlihan et al. 1986, 1988, 1995). The fractional rates of protein synthesis (S) and protein degradation (defined as actual degradation plus cost of synthesis) in growing fish are linear functions of fish growth: $S = Y + b_sG$ and $D = Z + b_dG$, where growth is in % body wet weight·day^{-1}, Y is maintenance synthesis, and Z is maintenance degrada-

© 2004 NRC Canada

Table 1. Overview of parameters and their values used to implement an energetic model for juvenile Atlantic cod.

Process	Equation	Parameter value
Otolith measurements	$W = iL^j$	$i = 1.500^a$
	$\Delta W \cdot W^{-1} \cdot \Delta t^{-1} = i(L_t^j - L_{t-1}^j)/L_t^j$	$j = 2.420^a$
	$A = kL^l$	$k = 1.860^a$
	$\Delta A/\Delta t = k(L_t^l - L_{t-1}^l)$	$l = 1.696^a$
	$V = mL^n$	$m = 0.542^a$
	$\Delta V/\Delta t = m(L_t^n - L_{t-1}^n)$	$n = 2.415^a$
Routine metabolism	$M_{routine} = a\Delta W \cdot W^{-1} \cdot \Delta t^{-1}$	$a = 1.016^b$
Otolith protein content	Protein $= (b + cO) \cdot 10^{-6} \cdot \Delta V/\Delta t$	$b = 5.063^c$
		$c = 0.009^c$
Protein synthesis	$S = dP^e$	$d = 4.150^d$
		$e = 0.637^d$
Maintenance synthesis	$Y = Z = gD^h$	$g = 0.0368^e$
		$h = -0.200^e$
Protein degradation	$D = Y + f(S - Y)$	$f = 0.404^f$
Dry weight change	$\Delta D \cdot D^{-1} \cdot \Delta t_{growth}^{-1} = (S - D)/p$	If $S \geq Y$
	$\Delta D \cdot D^{-1} \cdot \Delta t_{starvation}^{-1} = -M_{routine}$	If $S < Y$
Weight conversion	$D = oC^q$	$o = 0.201^a$
		$q = 1.117^a$
Protein content	Protein weight $= pD$	$p = 0.750^g$
Saccular epithelium mass	$E = rAtsop$	$r = 4.5^h$
		$t = 0.01^h$
		$s = 0.001^h$

Note: Variable names and abbreviations are referred to in the text and listed in Appendix A. All units are in grams and millimetres.

[a]Data from this study.

[b]Data from this study. Estimated from the relationship between $\Delta D \cdot D^{-1} \cdot \Delta t^{-1}$ and $\Delta W \cdot W^{-1} \cdot \Delta t^{-1}$ of fish from the starvation experiment.

[c]From Hüssy et al. (2004).

[d]Estimated from average daily protein deposition and whole-body protein synthesis from this study.

[e]Their fractional rate of total body protein maintenance synthesis of 0.0142 (in wet weight) for a 300-g cod results in a synthesis–weight expression of $0.0142 = 0.0444 \times 300^{-0.2}$, which corresponds to $0.0142 = 0.0368\, D_{(\text{corresponding to } 300\text{ g})}^{-0.2}$ in grams dry weight.

[f]In growing cod, Houlihan et al. (1988) found the slopes of synthesis and degradation on growth rate to be 0.0138 and 0.00678, respectively, and the intercept to be 0.0142. Rearranging the two equations yields a slope of degradation on growth rate of $f = 0.00678/0.0138 = 0.404$.

[g]From Holdway and Beamish (1984).

[h]Epithelium to otolith area ratio (r) from Saitoh and Yamada (1989), epithelium thickness (t) from Takagi and Takahashi (1999), epithelium density (s) assumed to be 0.001 g·mm^{-3}.

tion (Houlihan et al. 1988). Rearranging these equations, degradation can be expressed as a function of synthesis:

$$D = Z + f(S - Y) \quad (5)$$

In juvenile cod, the weight exponents of protein synthesis and degradation are similar (Houlihan et al. 1995) so that b_d/b_s from the relationship between the two parameters (equal to f in Table 1) is constant over fish size. The intercept of this expression corresponds to the fractional rates of synthesis (Y) and degradation (Z) at zero growth (i.e., maintenance). Houlihan et al. (1988) showed this rate to be 1.42% for a 300-g cod. Since protein synthesis and degradation rates are size dependent, these values have to be corrected for fish weight ($Y = Z = gD^h$) (see Table 1).

If $S > Y$, meaning that fish are growing, growth is calculated as the difference between synthesis and degradation multiplied by the protein content to dry weight ratio. The complete expression for fish somatic growth can be written as

$$\Delta D \cdot D^{-1} \cdot \Delta t_{growth}^{-1} = \left\{ \left\lfloor d((b + cO)\Delta V/\Delta t \cdot 10^{-6} \cdot E^{-1})^e \right\rfloor - \left[gD^h + f(d((b + c\,O)\Delta V/\Delta t \cdot 10^{-6} \cdot E^{-1})^e - gD^h) \right] \right\} /p \quad (6)$$

If $S < Y$, the fish were considered to be starving and their weight loss estimated from routine metabolic rates, calculated from otolith weight change, as suggested by Beck and Gropp (1995):

© 2004 NRC Canada

(7) $$\Delta D \cdot D^{-1} \cdot \Delta t_{starvation}^{-1} = -a\Delta W \cdot W^{-1} \cdot \Delta t^{-1}$$

All relationships between variables and parameter values referred to here are summarized in Table 1.

Experiments

Growth experiment

For the parameter estimation and validation of the model, juvenile cod were reared at densities of 40 fish per tank under constant temperature conditions at 5, 10, and 15 °C at two ration levels, ad libitum and 65% thereof, as described in Hüssy et al. (2004). Before the start of the experiment, a mark was introduced into the otoliths by a series of temperature changes (Hüssy et al. 2004).

At days 0, 10, 20, 30, and 40, all fish were anaesthetized with MS 222, measured, and weighed and a random subsample of 10 fish from each treatment were killed, except for day 40 of the 15 °C low-food treatment in which only five fish remained. Sagittal otoliths, henceforth called "otoliths", were extracted, rinsed in water, and stored in labelled plastic bags. Fish were dried individually at 60 °C for 48 h.

Starvation experiment

At a size of approximately 2.5 g wet weight (on days 20, 30, and 40 for the 5, 10, and 15 °C treatments, respectively), 28 fish were randomly chosen from each of the high-food treatments and transferred to small plastic containers inside the experimental tanks with six fish in each container. Sizes differed just enough for fish to be individually recognizable. Every day at 0800, the containers were transferred to 5 °C colder water for 1 h, except for the 5 °C containers, which were transferred to 10 °C, leaving a visible check in the otoliths. On days 0, 5, and 10, all fish were anaesthetized, measured and weighed (C), and a subsample of four fish from each temperature sacrificed. After 15 days, the remaining 48 fish were sacrificed and dried at 100 °C for 24 h (D).

0.9 and 20 °C temperature change experiment

To establish the response of otolith growth over the whole of the juvenile cod temperature range, fish were also exposed to the two extremes 0.9 and 20 °C. Because fish hardly grow in these temperatures, we decided to use fish from the end of the growth experiment for this treatment.

On day 40, four fish from each treatment were measured, weighed, and transferred to individual containers within two different tanks. Over the next 24 h, temperatures were gradually increased to 20 °C in one tank and decreased to 0.9 °C in the other. Only one fish from the 20 °C treatment accepted minimal amounts of food. We assumed that the fish rejected food to avoid the extra metabolic load of consumption and decided therefore not to feed any of these fish. Fish from the 0.9 °C treatment were fed to satiation once a day. Fish were sacrificed after 5 and 50 days, respectively, and dried.

Otolith measurements

Otolith volume and length

The right otoliths were weighed to the nearest 0.001 mg (W). From digitized TIFF images (IMAGE PRO version 4), measurements of otolith area in the sagittal (A) and frontal planes ($A_{frontal}$) and otolith length from anterior to posterior edge in the frontal plane ($L_{frontal}$) were taken at a magnification corresponding to 6.4 µm·pixel^{-1} (see Secor et al. (1992) for terminology). From these measurements, otolith volume (V) was calculated following the method described in Hüssy et al. (2004).

The otoliths were then ground to an approximate thickness of 80 mm (see Hüssy et al. 2004). Because of overpolishing and breaking, two otoliths per treatment were discarded. Only in the 10 and 15 °C with low-food treatment were all otoliths useable.

Otolith length measurements were taken along the longest distance from the nucleus to the tip of the rostrum from digitized TIFF images in black and white at a magnification corresponding to 2.2 µm·pixel^{-1}. Total length from the nucleus to the edge (L) and increment widths from the temperature mark to the edge (I_1–I_{40}) as well as the daily increments of the starvation period (I_1–I_{15}) were measured.

Increment widths were analysed along a profile of grey values (from 0 = black to 255 = pure white, band width = 50 µm) with the "caliper" tool of IMAGE PRO. The start of an increment was defined as a rising point of inflection based on the residuals of individual pixels' grey value from the running average. Measurements taken at a slightly different angle were scaled to L. From L and I_1–I_{40}, the following otolith lengths were calculated: L_0, L_{10}, L_{20}, and L_{30} corresponding to the otolith length from the nucleus days 0, 10, 20, and 30.

Otolith opacity

The otolith thickness and average of the distribution of grey values within five areas of interest, A_0 = hatching to the start of the experiment, A_1 = days 1–10, A_2 = days 11–20, A_3 = days 21–30, and A_4 = days 31–40, were measured following the method described in Hüssy et al. (2004). In fish from the starvation experiment, the values within each increment, measured along a profile of grey values using a profile width of 100 µm, were averaged. The individual area and increment opacity was then calculated as

(8) $$O_{measured} = 100 - 100(\text{grey value} - L_{incident}) \cdot L_{refracted}^{-1}$$

where $L_{incident}$ is the incident light from the microscope light source = 340 and $L_{refracted}$ is the light refracted within the microscope = 32 and standardized to an otolith thickness of 80 µm (see Hüssy et al. 2004). In the growth experiment, the standardized opacities of areas A_0–A_4 were called O_0, O_1, O_2, O_3, and O_4 and in the starvation experiment O_{0-5}, O_{5-10}, and O_{10-15} for the three 5-day intervals, respectively.

Parameter estimation

Otolith weight and volume increase

Otolith weight/volume and length have a functional relationship of the form $W/V = aL^b$. Otolith weight and volume increase between time periods was estimated as $\Delta W/\Delta t = W_t - W_{t-1}$ and $\Delta V/\Delta t = V_t - V_{t-1}$ using the increment widths to calculate L_{t-1}. Relative rates of otolith weight change were calculated as $\Delta W \cdot W^{-1} \cdot \Delta t^{-1} = \Delta W/\Delta t \cdot W_t^{-1}$. In the present context, t may be 1 or 10 days, depending on the experiment type. In the following, V_0 will refer to the volume from the nucleus to the start of the experiment and V_4 to the vol-

© 2004 NRC Canada

ume between L_3 and L_4. The same denomination will be used for otolith weight unless reported otherwise. Otolith volume and weight changes corresponding to days 0–5, 5–10, and 10–15 of the starvation period were calculated using the observed otolith length–weight and volume relationships.

Mass of the saccular epithelium

The mass of the saccular epithelium (E) was estimated as E = epithelium area × thickness × density, where epithelium area = rA and r = 2 × epithelium – otolith area ratio (ratio = 2.25; from Saitoh and Yamada 1989). The epithelium thickness (t) averages 0.01 mm (Takagi and Takahashi 1999) and the specific density of the epithelium (s) was assumed to be 0.001 g·mm^{-3}. The protein content of the saccular epithelium has apparently not been investigated and no information on the epithelium composition could be found in the literature. Therefore, the protein mass of the saccular epithelium (E) was calculated by converting epithelium mass to grams protein using the same dry weight – wet weight and protein content – dry weight conversion coefficients as for whole fish.

Routine metabolism

Since the body tissue in small juvenile cod almost exclusively consists of protein, the rate of dry weight loss is caused by degradation of proteins (Black and Love 1986) and assumed to be representative of routine metabolism (M) (Beck and Gropp 1995). The expected dry weights of fish at days 0, 5, and 10 of the experiment were calculated using the corresponding dry–wet weight ratios of the subsamples. Otolith weight changes corresponding to days 0–5, 5–10, and 10–15 of the starvation period were calculated using the observed otolith length–weight relationship. The scaling constant in the $\Delta D{\cdot}D^{-1}{\cdot}\Delta t^{-1}$ (grams per gram per day) = $a\Delta W{\cdot}W^{-1}{\cdot}\Delta t^{-1}$ (grams per gram per day) equation was estimated with the least squares method.

Q_{10} of otolith growth

The temperature response of standard oxygen consumption is often described by a quotient, $Q_{10} = (R_1/R_2)^{10/(T_1-T_2)}$, where R_1 and R_2 are oxygen consumptions at temperatures T_1 and T_2, respectively. To validate the assumption of a direct coupling of otolith growth and standard metabolism, we used fish sampled on day 40 of the high-food experiment from all three temperatures as well as fish from the 0.9 and 20 °C treatments. From the average otolith weight changes (grams per gram per day) of these treatments, we calculated a hypothetical $Q_{10} = (\Delta W{\cdot}W^{-1}{\cdot}\Delta t^{-1})_{T_1}/(\Delta W{\cdot}W^{-1}{\cdot}\Delta t^{-1})_{T_2}^{10/(T_1-T_2)}$, where T is temperature.

Protein synthesis

For the estimation of parameters in the whole-body protein – otolith matrix synthesis relationship, specific growth rates of the final sample were calculated as G = ((D – intercept)/40)/((D + intercept)/2), where "intercept" is the intercept of the dry weight – day of experiment regression from the individual treatments and 40 is days of experiment duration. Protein synthesis was then calculated as $S = Y + b_sG$, where Y = 0.0142, b_s = 0.0116, and G is the specific growth rate and scaled to observed fish size following the procedure described by Houlihan et al. (1988) (also see above). Otolith matrix synthesis rate was calculated from otolith protein deposited over the whole experimental period and the average saccular epithelium weight: P = (protein deposited/40)/(($E_{t=40}$ + $E_{t=0}$)/2), where E is the mass of saccular epithelium and t = 0 and t = 40 are the start and end of the experiment. The constants of the $S = dP^e$ relationship were estimated with the least squares method.

Sensitivity analysis

A sensitivity analysis was done for each parameter of the model following the method presented by Kitchell and Stewart (1977). The estimated change in fish dry weight from day 1 to day 40 of the experiment was used as the output parameter. Each of the input parameters was separately varied ±10% from the standard values before the simulation was rerun. This procedure was done for all fish individually. The resulting changes in the output parameter were then compared with values from the standard simulation.

The sensitivity of the output parameter (change in fish dry weight) to changes in individual input parameters was calculated as

$$S(z) = z\Delta x/x\Delta z \quad (9)$$

where $S(z)$ is the sensitivity of the output parameter to changes in input parameter z, z is the nominal value of the input parameter from the standard simulation, Δz is the deviation of input parameter z, x is the nominal value of output parameter x from the standard simulation, and Δx is the deviation of output parameter x caused by a deviation in input parameter z.

Sensitivities were calculated for each parameter and fish. Values were averaged across individuals to result in one single sensitivity value per parameter.

Results

Estimation of model parameters

An overview of all parameters and their estimates is given in Table 1. Note that the equations represent relative rates of protein synthesis, degradation, metabolism, and growth and that all measurements are in grams and millimetres. Size distributions were relatively homogenous, with the exception of one larger fish in the 10 and 15 °C high-ration treatments. It was therefore assumed that all fish were feeding at approximately the same rate.

Otolith weight and volume increase

In the present material, otolith weight and area are quite well explained by otolith length (r^2 = 0.95 and 0.95, respectively) (Table 1), with residuals normally distributed around zero. Otolith protein content, which influences otolith density, may affect these relationships, but because of the good correlations between weight/volume and length, density was not included in the estimation. No significant effects of food level, temperature, and interactions between these variables were found on the intercept and slope of the otolith length–weight/volume relationship (both relationships: generalized linear model, ln-transformed data, df = 270, all $p > 0.05$).

Q_{10} of otolith growth

The relationship between the average otolith weight changes within the different treatments and temperature was found to be curvilinear (Fig. 1). The temperature response of otolith

© 2004 NRC Canada

Fig. 1. Relationship between otolith weight change and temperature for juvenile Atlantic cod reared at constant temperature (average ± SD). Otolith growth at 20 °C was measured in starving fish.

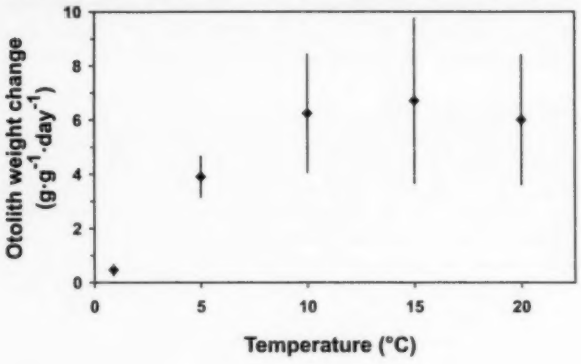

Fig. 2. Dry weight to wet weight ratio with time of starvation in juvenile Atlantic cod (average ± SD). Solid diamonds, 5 °C; solid triangles, 10 °C; open diamonds, 15 °C. On the *x* axis, 0.5 was subtracted from the values for the 5 °C group and added to the values for the 15 °C group to improve the appearance of the plot.

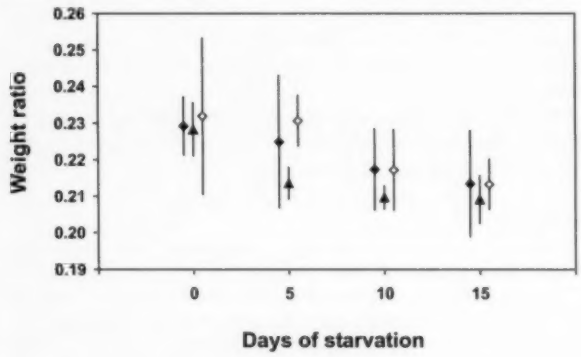

growth was evaluated using a temperature coefficient Q_{10} and these average otolith weight changes. This resulted in a Q_{10} of 71.3, 2.6, 1.2, and 0.8 for the temperature ranges 0.9–5, 5–10, 10–15, and 15–20 °C, respectively, and a Q_{10} of 1.7 between 5 and 15 °C.

Dry weight – wet weight relationship

The effect of temperature on the dry weight – wet weight relationship was analysed. Temperature and food had no significant effect (ANCOVA, $p > 0.05$), and dry weight is therefore best described by the model $D = oC^q$, where $o = 0.201$ and $q = 1.117$ ($r^2 = 0.82$, $p < 0.01$). This conversion was therefore used in all analyses. A decrease in the dry weight/wet weight ratio with length of starvation period was observed from the subsamples (Fig. 2), in accordance with observations by other authors (e.g., Black and Love 1986).

Routine metabolism

A decrease in metabolic rate with time of starvation is reflected in the changing dry–wet weight ratio and the decreasing rates of dry weight loss and otolith growth with time of starvation (Figs. 3 and 4). The relationship between

Fig. 3. Change in increment width with time of starvation in juvenile Atlantic cod of 2–3 g wet weight (average ± SD). Solid diamonds, 5 °C; solid triangles, 10 °C; open diamonds, 15 °C. On the *x* axis, 0.1 was subtracted from the values for the 5 °C group and added to the values for the 15 °C group to improve the appearance of the plot.

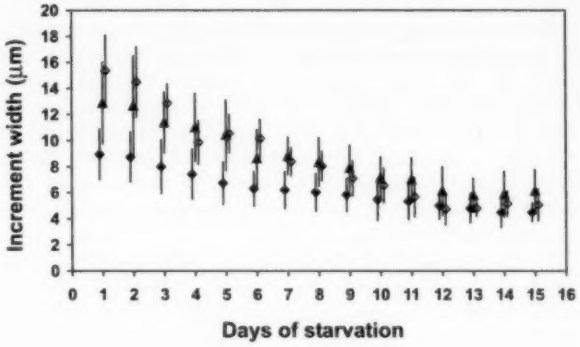

Fig. 4. Dry weight with time of starvation in juvenile Atlantic cod (average ± SD). Solid diamonds, 5 °C; solid triangles, 10 °C; open diamonds, 15 °C. On the *x* axis, 0.5 was subtracted from the values for the 5 °C group and added to the values for the 15 °C group to improve the appearance of the plot.

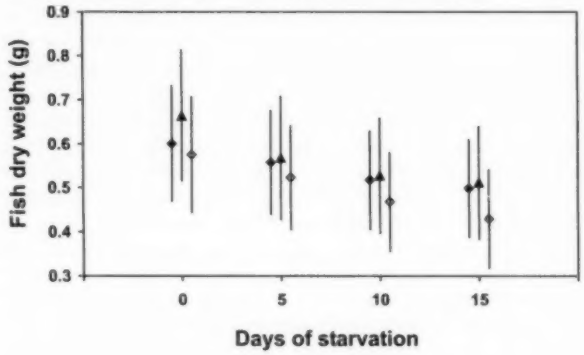

dry weight changes over the three 5-day intervals (corresponding to *M*) and the corresponding change in otolith $CaCO_3$ accretion for fish of similar size were found to be linear (Fig. 5). Because the residuals from the regression of fish weight change on otolith weight change were evenly scattered around zero, the scaling constant in the $\Delta D{\cdot}D^{-1}{\cdot}\Delta t^{-1} = a\Delta W{\cdot}W^{-1}{\cdot}\Delta t^{-1}$ equation was estimated to be $a = 1.016$ with the least squares method ($n = 106$, $r^2 = 0.46$), where $\Delta D{\cdot}D^{-1}{\cdot}\Delta t^{-1}$ is equal to *M*.

Otolith opacity and density during starvation

Otolith density is determined by the otolith protein content (see Hüssy et al. 2004). The effect of starvation was therefore analysed using otolith density as an expression of matrix accretion. Otolith density change with starvation, including the subsamples of 5 and 10 days of starvation, was analysed in a multiple regression design for each individual temperature regime as density = ln(*B*) + ln(*D*). Starvation led to a negative standard length (*B*) and positive dry weight (*D*) effect. These effects were only significant in the 15 °C

© 2004 NRC Canada

Fig. 5. Relationship between change in otolith weight and juvenile Atlantic cod dry weight owing to starvation: dry weight loss = 1.016 × otolith weight change, $r^2 = 0.39$. Solid diamonds, 0–5 days of starvation; open diamonds, 5–10 days of starvation; solid triangles, 10–15 days of starvation.

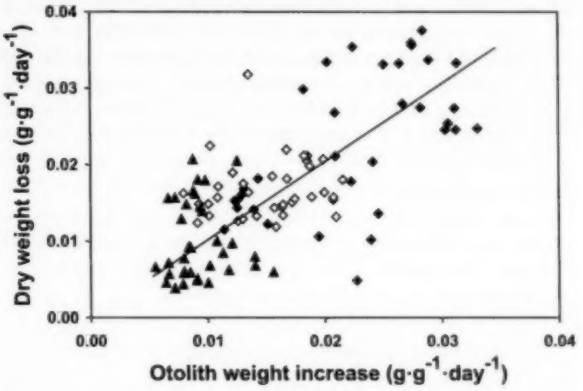

Fig. 6. Otolith opacity with time of starvation in juvenile Atlantic cod (average ± SD). Solid diamonds, 5 °C; solid triangles, 10 °C; open diamonds, 15 °C. On the *x* axis, 0.1 was subtracted from the values for the 5 °C group and added to the values for the 15 °C group to improve the appearance of the plot.

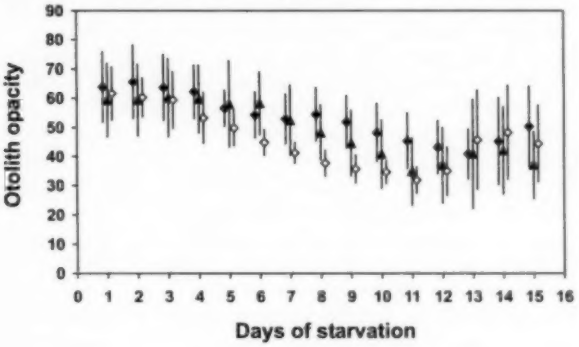

treatment. The intercepts were found to increase with temperature (see Table 2).

The decrease in protein synthesis during starvation is reflected in the otolith opacity (see Fig. 6). A significant effect of temperature on the slope of opacity on time of starvation was found for the first 12 days of the experiment (ANCOVA, df = 412, $p < 0.01$).

Protein synthesis

For all individuals of the experimental samples, the otolith protein content, epithelial mass, and body protein content were calculated. From these values, the constants of the $S = dP^e$ relationship were estimated as $d = 4.55$ and $e = 0.637$ ($n = 55$, $r^2 = 0.43$).

Sensitivity analysis

Since the sensitivities calculated are self-normalizing, a value of $S(z) = \pm 1$ indicates that a 10% change (or error) in the input parameter causes a 10% change in calculated growth. Absolute values of $S(z) < 1$ indicate a general robustness of the model, while the higher the absolute value of $S(z)$, the greater the effect of a potential error. This type of analysis may be used in the assessment of the importance of individual parameters for the model (see Table 3). The results show that the model generally is robust to parameter changes. All sensitivities fell within the range of ±1, except for *e*, which lay just above 1. Absolute sensitivities for the parameters *i*, *k*, *m*, *n*, *g*, *h*, *b*, *c*, *p*, and *f* are all below 0.5. A measurement error of 10% results in much less than 10% change in the output variable and these parameters are therefore assumed to be reliable estimators of otolith volume, protein synthesis and degradation, the fish protein content parameter *p* as well as the relationship between otolith opacity and protein content. Slightly greater sensitivity is involved in the estimation of the routine metabolism parameter *a*, where particularly a lower estimate leads to a

Table 2. Relationship between juvenile Atlantic cod otolith density, fish dry weight (*D*), and standard length (*B*) during starvation (generalized linear model, ln-transformed data, df = 30).

Temperature (°C)	Parameter	Estimate	*t*	*p*
5	Intercept	3.063	1.108	0.277
	ln(*D*)	–0.057	–0.090	0.929
	ln(*B*)	0.037	0.189	0.851
10	Intercept	3.487	3.489	0.0015
	ln(*D*)	–0.170	–0.739	0.466
	ln(*B*)	0.036	0.470	0.642
15	Intercept	4.794	6.99	$9.12 \cdot 10^{-8}$
	ln(*D*)	–0.457	–2.908	0.007
	ln(*B*)	0.181	3.084	0.004

Table 3. Sensitivities of accumulated growth estimates of juvenile Atlantic cod reared over a 40-day period to errors in measurement of input variables.

		Parameter input error	
Parameter		+10%	–10%
Otolith measurements	*i*	–0.00	–0.00
	j	–0.05	+0.54
	k	–0.05	+0.04
	l	–0.05	+0.51
	m	–0.04	+0.41
	n	–0.02	+0.25
Routine metabolism	*a*	–0.10	+1.00
Protein synthesis, fish	*g*	+0.01	–0.09
	h	+0.02	–0.14
Protein degradation	*f*	+0.04	–0.34
Protein content	*p*	+0.039	–0.40
Saccular epithelium	*r*	+0.04	–0.40
	s	+0.04	–0.40
	t	+0.04	–0.40
Protein synthesis, otolith	*d*	–0.06	+0.65
	e	+0.12	–1.18
Opacity, otolith protein	*b*	–0.04	+0.38
	c	–0.003	+0.03

Note: Variable names and abbreviations are referred to in the text and listed in Appendix A.

© 2004 NRC Canada

substantial deviation in weight change. Not surprisingly, the model is relatively sensitive to errors in measurement of the exponents of the otolith length–area (j) or weight–area (l) relationships. Great care must therefore be taken in estimation and validation of these parameter values.

Discussion

The main effort of back-calculation studies has so far been directed at solving the relationship between fish and otolith growth in terms of otolith size only. Estimation of otolith protein content and its relationship to fish growth has been neglected. The presentation of this conceptual model is therefore an attempt to promote interest in this topic and to propose an alternative way of back-calculating juvenile fish size.

$CaCO_3$ incorporation

The most correct way of evaluating the relationship between $CaCO_3$ accretion and metabolism would be to estimate the amount of $CaCO_3$ deposited as $\Delta W_{Ca}/\Delta t_i$ = density × $\Delta V/\Delta t_i$ – protein deposited$_i/\Delta t_i$ using model 2 to calculate the amount of protein deposited and the protein content – otolith density relationship published in Hüssy et al. (2004). However, otolith weight increase is probably a more reliable proxy for $CaCO_3$ accretion, since the protein content – otolith density relationship is relatively poor (r^2 = 0.12. df = 39, $p < 0.05$) and protein accounts for less than 0.45% of otolith weight Hüssy et al. (2004).

In cod of 80–500 g, values of Q_{10}, the temperature response of oxygen consumption, decrease from 2.6 to 1.9 in the temperature ranges 5–10 and 10–15 °C (Q_{10} for 5–15 °C = 2.2) (Schurmann and Steffensen 1997). Our otolith growth derived Q_{10} values were similar, supporting a link between otolith growth and metabolism. The Q_{10} between 15 and 20 °C was probably underestimated, since fish held at 20 °C were not fed and otolith growth was therefore possibly reduced.

In a similar approach, Mosegaard et al. (1988) obtained Q_{10} values of 2.0–2.3 for Arctic char (*Salvelinus alpinus*) fry, with a leveling out of otolith growth at the highest temperatures. Correspondingly, Wright et al. (2001) found a more conservative temperature response of standard oxygen consumption than the Q_{10} of otolith growth. This phenomenon may not necessarily represent a decrease in $CaCO_3$ accretion. In our study, otolith density increased with temperature, and calculation of otolith weight change from length measurements may thus lead to an underestimation of actual $CaCO_3$ accretion.

The standard metabolic rate of juvenile cod has been shown to decrease significantly over 23 days of starvation (O'Connor et al. 2000). In our study, this decrease in metabolism was reflected in the co-occurring decreasing rates of dry weight loss and otolith growth beyond the first 3 days of starvation. This also supports the hypothesis of a link between otolith growth and fish metabolism.

From our results, it is not possible to infer which component of fish metabolism regulates otolith growth. Studies dealing with this topic have shown a close correlation between otolith growth and specific rates of standard oxygen consumption (Wright 1991*b*; Yamamoto et al. 1998) and both total metabolism and particularly feeding-induced thermogenesis (specific dynamic action (SDA), calculated as the difference between total and standard metabolic rates) (Huuskonen and Karjalainen 1998). However, the latter's results are probably biased, since standard rates were measured within 8 h of a meal, when the effect of SDA has not yet ceased (e.g., Johnston and Battram 1993). Other studies seem also to reject a coupling of otolith growth to SDA and total metabolism, since increment widths were unaffected by ration within a short period of time (e.g., Neilson and Geen 1985) and in fish fed at irregular intervals (Campana 1983).

Protein synthesis

In our model, we assume that the incorporation of matrix protein into the otolith is correlated with whole-body protein synthesis. No studies have yet addressed this relationship, but inferences to support our assumptions can be drawn from the protein turnover in other fish tissues.

Consumption is the factor with the highest regulatory impact on protein synthesis, since protein synthesis is directly correlated with protein consumption (Houlihan et al. 1988). Hüssy et al. (2004) found no significant effect of consumption on matrix incorporation, most likely because of inadequate experimental design. In the myotomal muscles, the largest protein store of fish, the synthesis rate decreases with time of starvation (Loughna and Goldspink 1984; Lowery and Somero 1990), which may be the explanation for the concurrent decrease in metabolic rate. This decrease in synthesis is reflected in the otolith opacity and density, supporting the correlation between protein synthesis in the whole body and the saccular epithelium. The increase in opacity during the last 3 days of the starvation experiment is caused by refraction of light at the interface between the otolith and thermoplastic glue, a general problem in otolith microstructure analysis (Klink and Eckmann 1992).

Protein synthesis rates decline exponentially with increasing body weight (e.g., Houlihan et al. 1986), and so does the incorporation of matrix into the otolith (Hüssy et al. 2004). The value of the weight exponent differs between tissue types but is similar to the exponent of oxygen consumption (Houlihan et al. 1986). In otoliths, matrix accretion also decreases with fish size (Hüssy et al. 2004). A concurrent decrease in otolith opacity with fish size has been observed by Victor and Brothers (1982) but not by Hüssy et al. (2004).

A positive relationship between protein synthesis rate and temperature has been observed by a number of authors (e.g., McCarthy et al. 1999), while others have found no temperature effect (e.g., Foster et al. 1992). These apparently conflicting results may be explained with differences in the experimental design, where a temperature effect is related to ad libitum feeding. This implies that the observed positive correlation could in fact be biased, reflecting a consumption rather than a temperature effect (Foster et al. 1992). Otolith matrix incorporation is inversely related to temperature, a phenomenon that may be explained by the interaction with the temperature-dependent accretion of $CaCO_3$ (Hüssy et al. 2004).

Protein degradation

In growing fish, degradation increases linearly with positive fish growth rate, but the response to starvation is not

© 2004 NRC Canada

fully understood. Degradation rates of white muscle seem to increase for a few days, with a subsequent return to just above prestarvation levels (Loughna and Goldspink 1984; Lowery and Somero 1990). However, these degradation rates were estimated as the difference between synthesis and specific wet weight growth rates without considering the decreasing protein content with time of starvation. The resulting rates may therefore be underestimated. The result is a decoupling between synthesis and degradation rates during starvation, and estimation of protein degradation from synthesis rates is therefore impossible. As a consequence, we estimated dry weight loss from estimates of routine metabolism derived from otolith growth.

Evaluation of the conceptual growth model

$CaCO_3$ incorporation

In this study, otolith weight increase was used as a proxy for $CaCO_3$ accretion. The sensitivity of the relationship between otolith weight accretion and metabolism was moderately high. Whether this is the result of high individual variability in the metabolic regulation of $CaCO_3$ accretion or of an inappropriate approximation method is not evident from this study. A relatively high sensitivity to measurement errors for the exponent of the otolith length–weight relationship indicates that the method used may be critical. However, the exponent from our data seems to be applicable to different cod stocks, since Böttcher and Oeberst (1996) reported a similar value for juvenile Baltic cod. To improve confidence in this relationship, data for a wider size range and for different species need to be assessed.

Protein incorporation and whole-body protein turnover

The method of estimating otolith protein content from opacity is based on a relatively weak correlation (Hüssy et al. 2004). Since sensitivities to the parameters in question (b and c) were low, confidence in the method applied is justifiable.

Possibly the weakest point of this model, because of the lack of available data, is the assumed relationship between fish somatic and otolith protein synthesis, even though sensitivities of these parameters (d and e) are moderate. For the application of this model in back-calculation of fish size, experiments specifically targeting this subject are needed.

Protein degradation and somatic protein content of cod are well investigated and sensitivities of these models are moderate. The parameters used for the estimation of the saccular epithelium mass also show moderate sensitivities, but since they are pure approximations, a thorough examination of the relationship between otolith and epithelium size as well as the epithelium composition is needed.

The shortcoming of traditional growth models is that they fail to predict fish size at previous age during starvation and temperature-dependent decoupling of otolith and somatic growth. A method dealing with this problem would therefore be of great value for fisheries research. We believe that the key to improving traditional growth models is to include structural details of the otolith that have so far been neglected. With the presentation of this model, we would like to show that this new approach has the potential to deal with the unsolved problems of otolith and fish growth and may be worth investigating. However, this study has also shown that this model is not yet suitable as a back-calculation method. To allow the application of this model in back-calculation studies, specifically targeted experiments linking the dynamics of fish otolith protein synthesis and opacity should be key topics for future research.

Acknowledgements

Financial support of the Danish Institute for Fisheries Research, the University of Copenhagen, and the Danish Research Academy is gratefully acknowledged. We thank Skretting a/s Denmark for providing food pellets for the experimental part of this work. Finally, we would like to thank two anonymous reviewers for their helpful comments on a previous version of the manuscript.

References

Asano, M., and Mugiya, Y. 1993. Biochemical and calcium-binding properties of water-soluble proteins isolated from otoliths of the tilapia, *Orechromis niloticus*. Comp. Biochem. Physiol. B Comp. Biochem. **104**: 201–205.

Beck, F., and Gropp, J. 1995. Estimation of the starvation losses of nitrogen and energy in the raibow trout (*Oncorhynchus mykiss*) with special regard to protein and energy maintenance requirements. J. Appl. Ichthyol. **11**: 263–275.

Black, D., and Love, R.M. 1986. The sequential mobilization and restoration of energy reserves in tissues of Atlantic cod during starvation and refeeding. J. Comp. Physiol. B Comp. Biochem. **156**: 469–479.

Böttcher, U., and Oeberst, R. 1996. Investigations to the otolith-microstructure of juvenile Baltic cod in the phase of the settling. ICES CM 1996/J:9.

Campana, S.E. 1983. Feeding periodicity and the production of daily growth increments in otoliths of steelhead trout (*Salmo gairdneri*) and starry flounder (*Platichthys stellatus*). Can. J. Zool. **61**: 1591–1597.

Campana, S.E., and Neilson, J.D. 1985. Microstructure of fish otoliths. Can. J. Fish. Aquat. Sci. **42**: 1014–1032.

Foster, A.R., Houlihan, D.F., Hall, S.J., and Burren, L.J. 1992. The effects of temperature acclimation on protein synthesis rates and nucleic acid content of juvenile cod (*Gadus morhua*). Can. J. Zool. **70**: 2095–2102.

Francis, R.I.C.C. 1990. Back-calculation of fish length: a critical review. J. Fish Biol. **36**: 883–902.

Holdway, D.A., and Beamish, F.W.H. 1984. Specific growth rate and proximate body composition of Atlantic cod (*Gadus morhua* L.). J. Exp. Mar. Biol. Ecol. **81**: 147–170.

Houlihan, D.F., McMillan, D.N., and Laurent, P. 1986. Growth rates, protein synthesis, and protein degradation rates in rainbow trout: effects of body size. Physiol. Zool. **59**: 482–493.

Houlihan, D.F., Hall, S.J., Gray, C., and Noble, B.S. 1988. Growth rates and protein turnover in Atlantic cod, *Gadus morhua*. Can. J. Fish. Aquat. Sci. **45**: 951–964.

Houlihan, D.F., Carter, C.G., and McCarthy, I.D. 1995. Protein synthesis in fish. *In* Biochemistry and molecular biology of fishes. *Edited by* P. Hochachka and B. Mommsen. Elsevier Science, B.V., Amsterdam, the Netherlands. pp. 191–220.

Hüssy, K., Mosegaard, H., and Jessen, F. 2004. Effect of age and temperature on amino acid composition and the content of different protein types of juvenile cod (*Gadus morhua*) otoliths. Can. J. Fish. Aquat. Sci. **61**: 1012–1020. This issue.

Huuskonen, H., and Karjalainen, J. 1998. A preliminary study on the relationships between otolith increment width, metabolic rate and

© 2004 NRC Canada

growth in juvenile whitefish (*Coregonus lavaretus* L.). Arch. Hydrobiol. **142**: 371–383.

Johnston, I.A., and Battram, J. 1993. Feeding energetics and metabolism in demersal fish species from Antarctic, temperate and tropical environments. Mar. Biol. **115**: 7–14.

Kitchell, J.F., and Stewart, D.J. 1977. Applications of a bioenergetics model to yellow perch (*Perca flavescens*) and walleye (*Stizostedion vitreum vitreum*). J. Fish. Res. Board Can. **34**: 1922–1935.

Klink, A., and Eckmann, R. 1992. Limits for the detection of daily otolith increments in whitefish (*Coregonus lavaretus* L.) larvae. Hydrobiologia, **231**: 99–105.

Loughna, P.T., and Goldspink, G. 1984. The effect of starvation upon protein turnover in red and white myotomal muscle of rainbow trout, *Salmo gairdneri* Richardson. J. Fish Biol. **25**: 223–230.

Lowery, M.S., and Somero, G.N. 1990. Starvation effects on protein synthesis in red and white muscle of the barred sand bass, *Paralabrax nebulifer*. Physiol. Zool. **63**: 630–648.

McCarthy, I.D., Moksness, E., Pavlov, D.A., and Houlihan, D.F. 1999. Effects of water temperature on protein synthesis and protein growth in juvenile Atlantic wolffish (*Anarhichas lupus*). Can. J. Fish. Aquat. Sci. **56**: 231–241.

Mosegaard, H., Svedäng, H., and Taberman, K. 1988. Uncoupling of somatic and otolith growth rates in Arctic char (*Salvelinus alpinus*) as an effect of differences in temperature response. Can. J. Fish. Aquat. Sci. **45**: 1514–1524.

Nakahara, H. 1991. Nacre formation in bivalve and gastropod molluscs. *In* Mechanisms and phylogeny of mineralization in biological systems. *Edited by* S. Suga and H. Nakahara. Springer Verlag, Tokyo. pp. 343–350.

Neilson, J.D., and Geen, G.H. 1985. Effects of feeding regimes and diel temperature cycles on otolith increment formation in juvenile chinook salmon, *Oncorhynchus tshawytscha*. Fish. Bull. **83**: 91–101.

O'Connor, K.I., Taylor, A.C., and Metcalfe, N.B. 2000. The stability of standard metabolic rate during a period of food deprivation in juvenile Atlantic salmon. J. Fish Biol. **57**: 41–51.

Otterlei, E., Folkvord, A., and Nyhammer, G. 2000. Temperature dependent otolith growth of larval and early juvenile Atlantic cod (*Gadus morhua*). Ph.D. thesis, University of Bergen, Bergen, Norway.

Pannella, G. 1971. Fish otoliths: daily growth layers and periodical patterns. Science (Wash., D.C.), **173**: 1124–1127.

Saitoh, S., and Yamada, J. 1989. Ultrastructure of the saccular epithelium and the otolithic membrane in relation to otolith growth in tilapia, *Oreochromis niloticus* (Teleostei: Cichlidae). Trans. Am. Microsc. Soc. **108**: 112–127.

Schirripa, M.J., and Goodyear, C.P. 1997. Simulation of alternative assumptions of fish otolith–somatic growth with a bioenergetics model. Ecol. Model. **102**: 209–223.

Schurmann, H., and Steffensen, J.F. 1997. Effects of temperature, hypoxia and activity on the metabolism of juvenile Atlantic cod. J. Fish Biol. **50**: 1166–1180.

Secor, D.H., and Dean, J.M. 1989. Somatic growth effects on the otolith – fish size relationship in young pond-reared striped bass, *Morone saxatilis*. Can. J. Fish. Aquat. Sci. **46**: 113–121.

Secor, D.H., and Dean, J.M. 1992. Comparison of otolith based back-calculation methods to determine individual growth histories of larval striped bass, *Morone saxatilis*. Can. J. Fish. Aquat. Sci. **49**: 1439–1454.

Secor, D.H., Dean, J.M., and Laban, E.H. 1992. Otolith removal and preparation for microstructural examination. *In* Otolith microstruture examination and analysis. *Edited by* D.K. Stevenson and S.E. Campana. Can. Spec. Publ. Fish. Aquat. Sci. No. 117. pp. 19–57.

Takagi, Y., and Takahashi, A. 1999. Characterisation of otolith soluble-matrix producing cells in the saccular epithelium of rainbow trout (*Oncorhynchus mykiss*) inner ear. Anat. Rec. **254**: 322–329.

Victor, B.C., and Brothers, E.B. 1982. Age and growth of the fallfish *Semotilus corporalis* with daily otolith increments as a method of annulus verification. Can. J. Zool. **60**: 2543–2550.

Wright, P.J. 1991*a*. The influence of metabolic rate on otolith increment width in Atlantic salmon parr, *Salmo salar* L. J. Fish Biol. **38**: 929–933.

Wright, P.J. 1991*b*. Calcium binding by soluble matrix of the otoliths of Atlantic salmon (*Salmo salar* L.). J. Fish Biol. **38**: 625–627.

Wright, P.J. Fallon-Cousins, P., and Armstrong, J.D. 2001. The relationship between otolith accretion and resting metabolic rate in juvenile Atlantic salmon during a change in temperature. J. Fish Biol. **59**: 657–666.

Yamamoto, T., Ueda, H., and Higashi, S. 1998. Correlation among dominance status, metabolic rate and otolith size in masu salmon. J. Fish Biol. **52**: 281–290.

© 2004 NRC Canada

Appendix A

Table A1. Variable names, units, and abbreviations used in the text.

Process	Variable	Units	Abbreviation
Fish measurements	Wet weight	g	C
	Dry weight	g	D
	Standard length	mm	B
	Specific growth rate	$g \cdot g^{-1} \cdot time^{-1}$	G
Otolith measurements	Length, sagittal	mm	L_n
	Length, frontal	mm	$L_{frontal}$
	Weight	g	W
	Area, sagittal	mm^2	A
	Area, frontal	mm^2	$A_{frontal}$
	Volume	mm^3	V
	Increment width	mm	I
	Opacity		O
Metabolism	Routine metabolism	$g \cdot g^{-1} \cdot time^{-1}$	M
Saccular epithelium	Epithelium mass	g	E
Protein synthesis	Otolith matrix	$g \cdot g^{-1} \cdot time^{-1}$	P
	Whole fish	$g \cdot g^{-1} \cdot time^{-1}$	S
	Maintenance	$g \cdot g^{-1} \cdot time^{-1}$	Y
Protein degradation	Whole-fish degradation	$g \cdot g^{-1} \cdot time^{-1}$	D
	Maintenance degradation	$g \cdot g^{-1} \cdot time^{-1}$	Z
Light measurements	Incident light		$L_{incident}$
	Refracted light		$L_{refracted}$

© 2004 NRC Canada

A Bayesian hierarchical analysis of stock–recruit data: quantifying structural and parameter uncertainties

Catherine G.J. Michielsens and Murdoch K. McAllister

Abstract: Stock–recruit functions are important in fisheries stock assessment, but there is often uncertainty surrounding the appropriate stock–recruit model and its parameter values. Combining different stock–recruit data sets of related species through Bayesian hierarchical analysis can decrease these uncertainties and help to characterize appropriate stock–recruit forms and ranges of plausible parameter values. Two different stock–recruit functions (Beverton–Holt and Ricker) have been parameterized in terms of the steepness, which is a parameter that is comparable between populations. In the hierarchical analysis, the prior probability distribution of parameters for the cross-population variation in steepness is determined through a concise model structure. By calculating the Bayes' posteriors for alternative model forms, model uncertainty is accounted for. This methodology has been applied to Atlantic salmon (*Salmo salar*) stock–recruit data to provide predictions for the steepness of the stock–recruit function for Baltic salmon for which no stock–recruit data exist.

Résumé : Les fonctions stock–recrutement sont de grande importance pour l'évaluation des stocks des pêches commerciales, mais il y a souvent de l'incertitude au sujet du choix d'un modèle approprié et des valeurs de ses paramètres. La combinaison de plusieurs séries de données de stock–recrutement d'espèces apparentées dans une analyse hiérarchique bayésienne peut réduire ces incertitudes, aider à identifier les relations stock–recrutement appropriées et déterminer les étendues plausibles des valeurs des paramètres. Nous avons caractérisé les paramètres de deux fonctions stock–recrutement (Beverton–Holt et Ricker) en ce qui concerne l'inclinaison de la pente, qui est un paramètre comparable entre les populations. Dans l'analyse hiérarchique, la distribution de probabilité a priori des paramètres en ce qui a trait à la variation de l'inclinaison d'une population à une autre est déterminée par une structure de modèle concis. Le calcul des distributions bayésiennes a posteriori pour les différentes formes de modèles permet de tenir compte de l'incertitude. Nous avons appliqué cette méthodologie à des données de stock–recrutement du saumon de l'Atlantique (*Salmo salar*) afin de pouvoir prédire l'inclinaison de la fonction stock–recrutement du saumon de la Baltique pour lequel il n'existe pas de données sur la relation stock–recrutement.

[Traduit par la Rédaction]

Introduction

The parameters and the functional form of the stock–recruit function are among the most important model specifications in fisheries stock assessments. This is because the parameter values and functional forms determine the predicted impacts of changes in the fish stock on future fish recruitment. Quantitative–empirical knowledge of the stock–recruit function for a fish stock can thus improve the ability of managers to make appropriate policy decisions. However, stock–recruit data sets are often short and noisy (Myers et al. 1995), which increases the uncertainty about the underlying stock–recruit relationships. Combining different stock–recruit data sets of related species within an hierarchical model can decrease that uncertainty (Myers 2001). Several such hierarchical analyses have been undertaken for stock–recruit data (Liermann and Hilborn 1997; Myers et al. 1999; Dorn 2002).

This paper provides a general framework for the analysis of stock–recruit data through a Bayesian hierarchical analysis whereby both model form and parameter uncertainties are taken into account. The paper reformulates a set of methodologies to be used for the construction and validation of Bayesian hierarchical models (Gelman et al. 1995). It presents an Atlantic salmon (*Salmo salar*) case study to which the methodology is applied and the stock–recruit data used in the analysis. The models are run using these data to obtain the posterior probability density functions for the steepness of the different stock–recruit functions and to predict the steepness of the stock–recruit function of Baltic salmon

Received 6 February 2003. Accepted 30 January 2004. Published on the NRC Research Press Web site at http://cjfas.nrc.ca on 30 July 2004.
J17324

C.G.J. Michielsens[1,2] and M.K. McAllister. Renewable Resources Assessment Group, Department of Environmental Science and Technology, Imperial College, Prince Consort Road, London SW7 2BP, UK.

[1]Corresponding author (e-mail: catherine.michielsens@rktl.fi).
[2]Present address: Finnish Game and Fisheries Research Institute, Pukinmaenaukio 4, P.O. Box 6, FIN-00721 Helsinki, Finland.

 doi: 10.1139/F04-048 © 2004 NRC Canada

for which no stock–recruit data have been available. The credibility of the stock–recruit functions is examined by computing the marginal posterior probabilities of the different models.

Methodology

This paper advocates the use of hierarchical models for the analysis of a group of related stock–recruit data sets. Hierarchical modelling is a statistical technique that allows the modelling of the dependence among parameters that are related or connected through the use of a hierarchical model structure (Gelman et al. 1995). Hierarchical models can be used to combine data from several independent sources (Liermann and Hilborn 1997). In contrast with non-hierarchical models, hierarchical models can estimate parameters simultaneously at the population level and at the metapopulation level. In doing so, hierarchical models also allow the prediction of parameters of a population for which no data are observed, based on the estimates for the metapopulation and the similarities between individual stocks. Furthermore, by structuring some dependence among parameters, we can avoid the problem of overfitting the data, i.e., producing models that fit the data very well but provide inferior predictions for new data (Su et al. 2001).

To allow different stock–recruit data to be used together in the same meta-analysis, stock–recruit functions can be parameterized in terms of steepness (Mace and Doonan 1988; Punt and Hilborn 1997). The steepness of a stock–recruit function is the proportion of the long-term unfished recruitment obtained when the stock abundance is reduced to 20% of the virgin level. The advantage of this parameterization is that the steepness parameter is transportable or comparable between stocks (Hilborn and Liermann 1998). Because of this advantage, this parameterization is a common feature of hierarchical analyses of stock–recruit data (Liermann and Hilborn 1997; Myers et al. 1999; Dorn 2002). The parameterization in terms of steepness was originally derived for the Beverton–Holt stock–recruit function (Beverton and Holt 1957), but a similar parameterization in terms of steepness can be derived for other stock–recruit functions such as the Ricker stock–recruit function (Ricker 1954).

The steepness parameterization permits comparison of estimates of the same parameter between fits of different stock–recruit functions to the same data. If different steepness estimates are found between different models, this may require an evaluation of the goodness-of-fit of the different models to the data to facilitate model selection. However, comparing the fit of the different stock–recruit functions to the data is, by itself, insufficient. Instead, the model uncertainty should be assessed probabilistically to allow it to be incorporated in stock assessments and decision analysis (McAllister and Kirchner 2002).

A Bayesian hierarchical analysis (Gelman et al. 1995) offers a natural way to incorporate both model and parameter uncertainty regarding stock–recruit relationships. The prior probability density function (pdf) of the steepness values for the different stocks used in the hierarchical analysis is determined through the model structure. This is achieved through the use of a mean steepness for the combined set of populations and a cross-population variance in the steepness, which is made to depend on the mean. By calculating the Bayes' posteriors for each stock–recruit model, the model uncertainty can be formally incorporated in fisheries stock assessments and decision analyses. This paper, however, is restricted to the stock–recruit analysis.

The Bayesian hierarchical analysis within this paper has been implemented using a Gibbs sampler to sample from the posterior distribution. Such a method can be executed using WinBUGS (Bayesian inference Using Gibbs Sampling) software (available from http://mrc-bsu.cam.ac.uk/bugs) (Meyer and Millar 1999). As with any Markov Chain Monte Carlo simulation, the Gibbs sampler requires an evaluation to determine if it is reasonable to believe that the samples are representative of the underlying stationary distribution, i.e., if the Markov Chain has converged. To examine convergence, a convergence diagnosis and output analysis software for Gibbs sampling output (CODA) is used (Best et al. 1995). All of the modelling results described in this paper have undergone tests to remove the "burn-in" and to assess convergence and it is assumed that the reported distributions obtained through Gibbs sampling are representative of the underlying stationary distributions.

The hierarchical analysis developed for this paper has been thoroughly tested using a variety of different model forms and data distributional assumptions. The posterior probability distribution for model parameters is determined by the product of the prior pdf of the parameters and a likelihood function of the data given these parameters. Bayesian methodology has been criticized because of the subjective choices of the prior pdf and the likelihood function. Therefore, it is important to assess the sensitivity of the posterior probability distribution to reasonable changes in the choices for the prior probabilities and likelihood functions (Clarke and Gustafson 1998).

To assess the fit of the stock–recruit models to the data, the data can be compared with the posterior predictive distribution of the model, i.e., the distribution of data simulated from the model (Gelman et al. 1995). This will allow us to assess whether the observed data look plausible under the posterior predictive distribution. Systematic differences between the simulations and the data indicate potential failings of the model. We define R^{rep} as the replicated data point on recruitment that could have been observed as the data if we were to replicate the recruitment data using the model and the observed stock abundance data. Simulation of potential data given the observed data and the joint posterior for θ is easily obtained using WinBUGS. The distribution of R^{rep} is called the posterior predictive distribution:

$$(1) \qquad p(R^{\text{rep}}|\underline{R}^{\text{obs}}) = \int p(R^{\text{rep}}|\theta)p(\theta|\underline{R}^{\text{obs}})\mathrm{d}\theta$$

The underlined symbols represent vectors of either data or parameters. For example $\underline{R}^{\text{obs}}$ represents the vector of observed recruitment data. We can thereafter compare the observed data with the posterior predictive distribution. The results of this comparison can be expressed in terms of a Bayesian p-value (Meng 1994; Gelman et al. 1995, 1996). Bayesian p-values can be defined as the probability that the replicated data could be as extreme or more extreme than the observed data (Meng 1994):

$$(2) \qquad \text{Bayesian } p\text{-value} = p(R^{\text{rep}}|\theta) \geq R^{\text{obs}}$$

© 2004 NRC Canada

We can also measure the discrepancy between the model and the data using test quantities or discrepancy measures, $T(R,\theta)$. A discrepancy measure is a scaler summary of parameters and data that is used as a standard when comparing data with predictive simulations. One test quantity useful for routine checks of goodness-of-fit is the χ^2 discrepancy measure (Gelman et al. 1995):

$$(3) \qquad \chi^2 \text{ discrepancy: } T(R,\theta) = \sum_i \frac{(R_i - E(R_i|\theta))^2}{\text{var}(R_i|\theta)}$$

It is therefore possible to compare the realized discrepancy $T(R,\theta)$ with the discrepancy under the posterior predictive distribution $T(R^{rep},\theta)$. To do this, we take a random sample from the posterior distribution for the full set of parameters in the model, θ. For each set of parameter values θ_j, we can simulate a new recruitment data set, R^{rep}, and we can then plot $T(R^{rep},\theta_j)$ against $T(R,\theta_j)$. The estimated Bayesian p-value is the proportion of times that $T(R^{rep},\theta_j)$ is greater than $T(R,\theta_j)$ (Brooks et al. 2002). It is recommended that both the graphical summary and Bayesian p-value be used, since it is possible for the distributions of $T(R^{rep},\theta_j)$ and $T(R,\theta_j)$ to differ even though a p-value of 0.5 is obtained (Brooks et al. 2000).

Apart from the models themselves, the data used in these hierarchical models need to be tested on certain assumptions. For a hierarchical analysis, the different data sets need to be exchangeable, i.e., the differences among the data sets should not have predictable effects on the results of the analysis (Gelman et al. 1995). To examine the exchangeability of the data sets, the hierarchical analysis can be run excluding one data set each time. The marginal probability distributions for the steepness parameter of the stock–recruit function obtained from the remaining data sets can be compared to assess the exchangeability of the data sets. If the different data sets are exchangeable in terms of the steepness parameter, the exclusion of one data set should not substantially alter the marginal posterior predictive distribution for the steepness. These different tests on model and data assumptions will be applied within this paper.

Bayesian analyses also allow us to compare the probability of the different models given the stock–recruit data. The posterior probability distribution of model i given the observed data is given by the equation

$$(4) \qquad P(M_i|\,\text{data}) = \frac{P(\text{data}|\,M_i)P(M_i)}{P(\text{data})}$$

or

$$(5) \qquad P(M_i|\,\text{data}) \propto P(M_i)\int_{\theta_i} P(\text{data}|\,\theta_i, M_i)P(\theta_i|\,M_i)\text{d}\theta_i$$

Kass and Raftery (1995) have proposed a method to approximate the Bayes' posterior using the harmonic mean of the likelihood function

$$(6) \qquad P(\text{data}|M_i) \approx \frac{m}{\sum_{k=1}^{m} \frac{1}{P(\text{data}|\theta_i^k, M_i)}}$$

where θ^k is the kth set of draws from the different model parameters and m is the number of Markov Chain Monte Carlo iterations. The harmonic mean of the likelihood values converges to the correct value as the number of samples m approaches infinity (Newton and Raftery 1994). However, the harmonic mean of the likelihood value does not satisfy the Gaussian central limit theorem. The occasional occurrence of a value of θ^k with a small likelihood, resulting in large values for the harmonic mean, makes the harmonic mean unstable (Kass and Raftery 1995). The harmonic mean cannot be obtained directly from WinBUGS. Instead, WinBUGS will calculate the deviance ($-2 \times$ log likelihood). Using these output values, the harmonic mean and the Bayes' posterior can be derived.

Case study: Atlantic salmon

The proposed methodology can be applied to any species, and in this paper, Atlantic salmon stocks are taken as an example. Stock–recruit data exist for some Atlantic salmon stocks and not for others. For example, in the Baltic Sea area, no stock–recruit data have been compiled and no information exists about the stock–recruit function of Baltic salmon stocks. Potentially, we could assume that nothing is known about the stock–recruit function and its parameters in the Baltic Sea area, but this would be ignoring all of the Atlantic salmon stock–recruit data from outside this area (Myers et al. 1999; Barrowman and Myers 2000; Prévost et al. 2001). Because each Baltic salmon stock could be considered as one of the many different Atlantic salmon stocks, the stock–recruit functions obtained by analysing stock–recruit data of Atlantic salmon index rivers can be extrapolated to salmon stocks in the Baltic Sea area. Three components are involved in the extrapolation: a functional form, a scale component, and a population dynamics component (Prévost et al. 2001). Although functional forms could vary among stocks, it is generally accepted that owing to similarities in biology, life history, and ecology among populations of the same species, the functional form is the same. The scale component, irrespective of the functional form, is related to the concept of carrying capacity and can be obtained through an evaluation of habitat quality and (or) availability (Uusitalo 2001). The third component is the population dynamics component, i.e., the steepness parameter, which is comparable between stocks and which can be obtained through a hierarchical analysis of stock–recruit data. The concept of steepness also holds across different functional forms. Bayesian hierarchical analyses therefore allow an extrapolation of the stock–recruit functions of sampled Atlantic salmon stocks to unsampled salmon stocks such as those in the Baltic Sea area (Prévost et al. 2001).

Stock–recruit data

The stock–recruit data of Atlantic salmon used in the hierarchical analysis are obtained through a search of both published and grey literature. The number of stock–recruit data sets is small and limited compared with the number of Atlantic salmon stocks present. Therefore, it is crucial to make sure that the data set is representative for the entire Atlantic salmon population and that no bias is introduced when selecting the data sets (Myers and Mertz 1998; Prévost et al.

© 2004 NRC Canada

Table 1. Description of the different Atlantic salmon stock–recruit data sets found in the literature according to the river and country of occurrence, data format, number of data points collected, form and language in which they have been published, and the publication reference.

River	Country	Data format	Data points	Publication	Language	Reference(s)
Little Codroy River	Canada	Eggs–smolts	7	Journal	English	Chadwick 1982
Margaree River	Canada	Eggs–adults	36	Research document	English	Chaput and Jones 1992
Pollett River	Canada	Eggs–smolts	8	Journal	English	Elson 1975; Myers et al. 1995
Trinite River	Canada	Eggs–smolts	8	Research document	French	Caron 1992; Myers et al. 1995
Western Arm Brook	Canada	Eggs–smolts	15	Research document	English	Chaput et al. 1992
River Bush	United Kingdom	Eggs–smolts	17	Journal	English	Crozier and Kennedy 1995
River Ellidaar	Iceland	Eggs–adults	37	Journal	English	Mundy et al. 1978
River Oir	France	Eggs–smolts	10	Journal	French	Prévost et al. 1996
River Bec-Scie	Canada	Eggs–smolts	5	Research document	French	Caron 1992

2001). The selected stock–recruit data sets needed to be transformed to express the relationship between eggs and smolts. Eggs–adults data were transformed by applying an approximation of the survival rate from smolts to adults (10%). This transformation does not account for any uncertainty in the value for the survival rate from smolts to adults. The assumed survival rate from smolts to adults will affect the estimated steepness parameters of the stocks in question, but sensitivity analyses demonstrate that the impact of the assumed survival rate on the predicted steepness parameter for the Baltic salmon stocks is relatively small owing to the large amount of uncertainty surrounding these estimates. Eggs–parr data, on the other hand, were not transformed and used because of the possible density-dependent relationship between the parr and smolt stage.

In total, nine different stock–recruit data sets (consisting of 143 data points in total) were found covering both sides of the Atlantic Ocean (Table 1). The data sets were found in journal articles and research documents and were all independent of each other. Although searched for, no publications of stock–recruit data were encountered in languages other than English or French.

Description of stock–recruit functions and their parameterization

In order for a stock–recruit model to be useful, it should adequately represent the biological processes of the stock, fit well to the stock–recruit data and behave sensibly in probabilistic projections (Needle 2002). For Salmonids, the most commonly used stock–recruit functions are the Ricker and the Beverton–Holt stock–recruit functions (Hilborn and Walters 1992). These stock–recruit functions are governed by the following equations (eq. 7, Beverton and Holt 1957; eq. 8, Ricker 1954):

$$(7) \qquad R = \frac{S}{\alpha + \beta S}$$

$$(8) \qquad R = aSe^{-bS}$$

where S is a measure of the spawning stock size and R is the number of recruits. These two functions can be parameterized in terms of river specific parameters: steepness (z), recruitment at equilibrium (R_0), and spawner biomass per recruit ($\tilde{S}$). The definition for steepness is illustrated for the Beverton–Holt curve through the following equation (Liermann and Hilborn 1997):

$$(9) \qquad z R_0 = \frac{0.2 S_0}{\alpha + 0.2\beta S_0}$$

The following equations convert steepness (z), recruitment at equilibrium (R_0), and spawner biomass per recruit ($\tilde{S}$) into the alpha and beta parameters of the Beverton–Holt stock–recruit function:

$$(10) \qquad \alpha = \frac{(1-z)}{4z} \cdot \frac{S_0}{R_0} = \frac{(1-z)}{4z} \cdot \tilde{S}$$

$$\beta = \frac{5z-1}{4zR_0}$$

Similarly, the a and b parameter of the Ricker stock–recruit function can be expressed in terms of steepness (z), recruitment at equilibrium (R_0), and spawner biomass per recruit ($\tilde{S}$):

$$(11) \qquad a = \frac{(5z)^{5/4}}{\tilde{S}}$$

$$b = \frac{5}{R_0 \tilde{S}} \cdot \log(5z)$$

The similar parameterization of the Beverton–Holt and the Ricker models allows us to estimate the steepness of the different stock–recruit models within similar overall model structures.

Description of the prior pdfs

According to Liermann and Hilborn (1997), the most difficult part of using hierarchical models is the construction of prior probability distributions. Some prior information about the model parameters will be present based on their definitions and the structural limitations of the models in which they are placed. By definition, the steepness parameter for the Beverton–Holt stock–recruit function can only have values between 0.2 and 1. Therefore, the mean steepness (μ_z) across salmon stocks will lie between those boundaries. A flat distribution for the mean steepness would be inappropriate, since a mean steepness of 0.2 or 1 would imply zero variation around the mean, i.e., all stocks would have a

© 2004 NRC Canada

Fig. 1. Prior probability density functions of (*a* and *b*) mean steepness across Atlantic salmon stocks, (*c* and *d*) maximum standard deviation around the mean steepness, (*e* and *f*) cross-population standard deviation in steepness, and (*g* and *h*) steepness for each of the different Atlantic salmon stocks assuming a Beverton–Holt (B–H) or Ricker stock–recruit function.

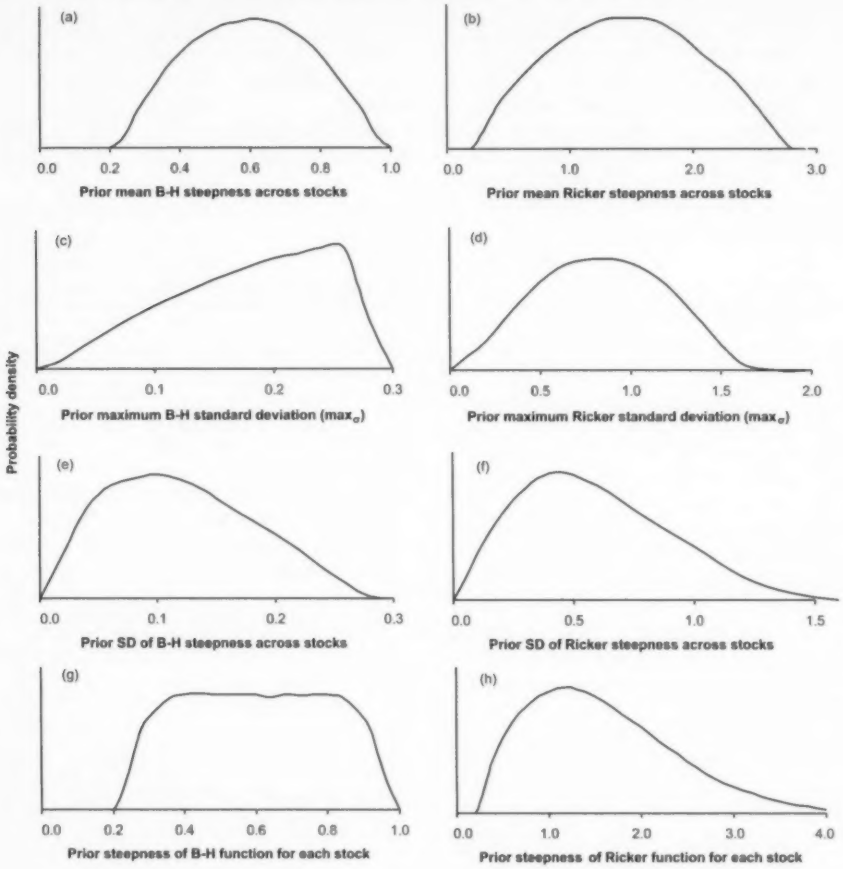
(a)
0.0 0.2 0.4 0.6 0.8 1.0
Prior mean B-H steepness across stocks
(b)
0.0 1.0 2.0 3.0
Prior mean Ricker steepness across stocks
(c)
0.0 0.1 0.2 0.3
Prior maximum B-H standard deviation (max$_\sigma$)
(d)
0.0 0.5 1.0 1.5 2.0
Prior maximum Ricker standard deviation (max$_\sigma$)
Probability density
(e)
0.0 0.1 0.2 0.3
Prior SD of B-H steepness across stocks
(f)
0.0 0.5 1.0 1.5
Prior SD of Ricker steepness across stocks
(g)
0.0 0.2 0.4 0.6 0.8 1.0
Prior steepness of B-H function for each stock
(h)
0.0 1.0 2.0 3.0 4.0
Prior steepness of Ricker function for each stock

steepness of exactly 0.2 or 1, which is a highly unlikely event considering previous steepness estimates (Myers et al. 1999). The pdf of the mean steepness is therefore assumed to follow a beta distribution Beta(2,2) rescaled to lie between 0.2 and 1 and with unlikely outer values. The prior pdf for the mean steepness is shown in Fig. 1*a*.

Apart from a cross-population mean steepness, we also need to define a cross-population variance in steepness. The maximum possible variance $\max(\sigma_z^2)$ given a particular value for mean steepness, a symmetrical uniform distribution for z under the maximum possible variance, and the 0.2–1 boundaries can be calculated using equation (Evans et al. 2000)

$$(12) \qquad \max(\sigma_z^2) = [\max(z) - \min(z)]^2/12$$

where $\max(\sigma_z^2)$ is the maximum possible variance in steepness z, $\max(z)$ is the upper limit of the range of steepness z, and $\min(z)$ is the lower limit of the range of steepness z. Practically speaking, if, for example, one particular draw from the prior distribution for the mean steepness is 0.8, then the upper limit of the range for steepness would be 1 and the minimum would be 0.6. The corresponding maximum possible standard deviation in steepness in this example is therefore 0.12. The prior pdf for the maximum standard deviation in steepness $\max(\sigma_z)$ is also shown in Fig. 1*c*. It is assumed that the maximum standard deviation is the most likely value for the cross-stock standard deviation with a linear relationship expressing the reduction in probability

Table 2. Median and 95% probability interval of the prior probability distributions for the spawner biomass (eggs) per recruit (smolts) (SBPR) parameter of the different Atlantic salmon stocks.

River	Median SBPR	95% probability interval
Little Codroy River	308	81–613
Margaree River	367	95–762
Pollett River	368	95–759
Trinite River	360	93–749
Western Arm Brook	294	73–593
River Bush	210	54–410
River Ellidaar	282	73–555
River Oir	388	101–806
River Bec-Scie	409	106–859
Baltic salmon rivers	500	127–1000

© 2004 NRC Canada

Table 3. Summary of model parameters and their description and WinBUGS representation.

Model parameter	Description	WinBUGS representation
$\underline{z}$	Steepness of the Beverton–Holt stock–recruit function for stock j	z[j]
$\underline{zt}$	Steepness of the Beverton–Holt stock–recruit function for stock j scaled to lie between 0 and 1	zt[j]
α_{zt}	First shape parameter of the beta distribution for scaled steepness	alpha_zt
β_{zt}	Second shape parameter of the beta distribution for scaled steepness	beta_zt
μ_{zt}	Mean of the steepness across stocks scaled to lie between 0 and 1	mu_zt
μ_z	Mean steepness across stocks	mu_z
σ_{zt}	Cross-stock standard deviation in the scaled steepness	sd_zt
σ_{ztt}	Cross-stock relative standard deviation in the scaled steepness	sd_ztt
$\max(\sigma_{zt})$	Maximum cross-stock standard deviation in the scaled steepness	max_sd_zt
$\underline{\tilde{S}}$	River-specific spawner biomass per recruit	SBPR[j]
$\underline{R}$	River-specific recruitment potential	R[j]
μ_R	Mean recruitment potential across stocks	mu_R
τ_R	Cross-stock precision of recruitment potential	tau_R
$\underline{\alpha}$	Alpha parameter of the Beverton–Holt stock–recruit function for stock j, where $1/\alpha$ is the maximum recruitment per spawner as spawner abundance approaches 0	alpha[j]
$\underline{\beta}$	Beta parameter of the Beverton–Holt stock–recruit function for stock j, where $1/\beta$ is the maximum number of recruits	beta[j]
$\underline{\theta}$	Vector of parameters that are treated as random variables	exp_Smolts[i]
$\underline{\text{Eggs}}$	Observed number of eggs counted in sample i	Eggs[i]
$\underline{\text{smolts}}^{\text{obs}}$	Observed number of smolts resulting from eggs of sample i	obs_Smolts[i]
$\underline{\text{smolts}}^{\text{exp}}$	Mean number of smolts expected from eggs of sample i	exp_Smolts[i]
$\underline{\text{smolts}}^{\text{rep}}$	Replicated number of smolts that could have been observed using the model	rep_Smolts[i]
τ_{smolts}	Precision of the number of smolts expected	tau_Smolts

as the cross-stock standard deviation approaches 0 (Beta(2, 1)). The resulting prior for the cross-stock standard deviation (σ_z) is also shown (Fig. 1*e*). The prior pdf of the mean steepness of the meta-population, μ_z, and of the standard deviation of steepness of the meta-population, σ_z, are used to define the marginal prior pdf of the steepness for each population or stock ($\underline{z}$) (Fig. 1*g*).

For the Ricker stock–recruit function, the steepness parameter cannot be smaller than 0.2 but it can be larger than 1. Applying the same prior probability distribution for the steepness parameter as for the Beverton–Holt stock–recruit model would result in an underestimation of the steepness of the Ricker curve. Instead, a new prior needs to be constructed for the steepness parameter of the Ricker model. The main problem when constructing such a prior is to define the upper limit for the prior mean steepness across populations. This prior knowledge has been based on the results of Myers et al. (1999) who have estimated the slope at the origin for many different stocks. Based on their results obtained for Salmonidae (transformed into steepness values for the Ricker model using eq. 11), it is unlikely that the mean steepness across stocks will be larger than 2.8. This prior knowledge can be translated into a prior probability distribution for the mean steepness across stocks defined by a beta distribution Beta(2, 2) rescaled between 0.2 and 2.8 (Fig. 1*b*).

Using the same rules as for the steepness-related priors of the Beverton–Holt function, it is possible to derive the corresponding prior probability distributions for the maximum standard deviation around the mean steepness, the cross-standard deviation in steepness, and the steepness of the Ricker stock–recruit function for each stock (Figs. 1*d*, 1*f*, and 1*h*). Compared with the prior for the Beverton–Holt function, the maximum standard deviation around the mean steepness only has a lower boundary but no upper boundary when assuming a symmetrical distribution for σ_z.

The prior probability distributions for the smolt production capacity are assumed to be lognormally distributed. The log-transformed mean smolt production capacity across Atlantic salmon stocks is given an uninformative normal distribution $N(0, 1000^2)$. The cross-stock deviance around that mean capacity is defined in terms of precision (precision = 1/variance) and given an uninformative gamma distribution $G(0.001, 0.001)$.

The spawner biomass per recruit parameter is given stock-specific informative priors. The spawner biomass per recruit can be calculated through the following equation:

$$\tilde{S} = HF \sum_{k=1\text{SW}}^{3\text{SW}} p_k s_k W_k \quad (13)$$

where H is the smolt to grilse survival rate from natural mortality (expressed as a proportion), p is the relative proportion given natural mortality and homing rates of one-sea-winter (1SW), 2SW, or 3SW salmon, s is the proportion of females, W is the weight of the fish, and F is the relative fecundity of female salmon (eggs per kilogram). Different Atlantic salmon stocks may have a different productivity depending on the relative proportion of female salmon in different age groups. River-specific estimates for the relative proportion of 1SW, 2SW, and 3SW salmon and the propor-

© 2004 NRC Canada

Fig. 2. Prior and marginal posterior predictive probability distribution of the steepness for (*a*, *c*, *e*, and *g*) Beverton–Holt and (*b*, *d*, *f*, and *h*) Ricker stock–recruit functions for Baltic salmon when using different prior probability distributions for the mean steepness across Atlantic salmon stocks: (*a* and *b*) Beta(2, 2); (*c* and *d*) *U*(0,1); (*e* and *f*) Beta(1, 2); (*g* and *h*) Beta(2, 1).

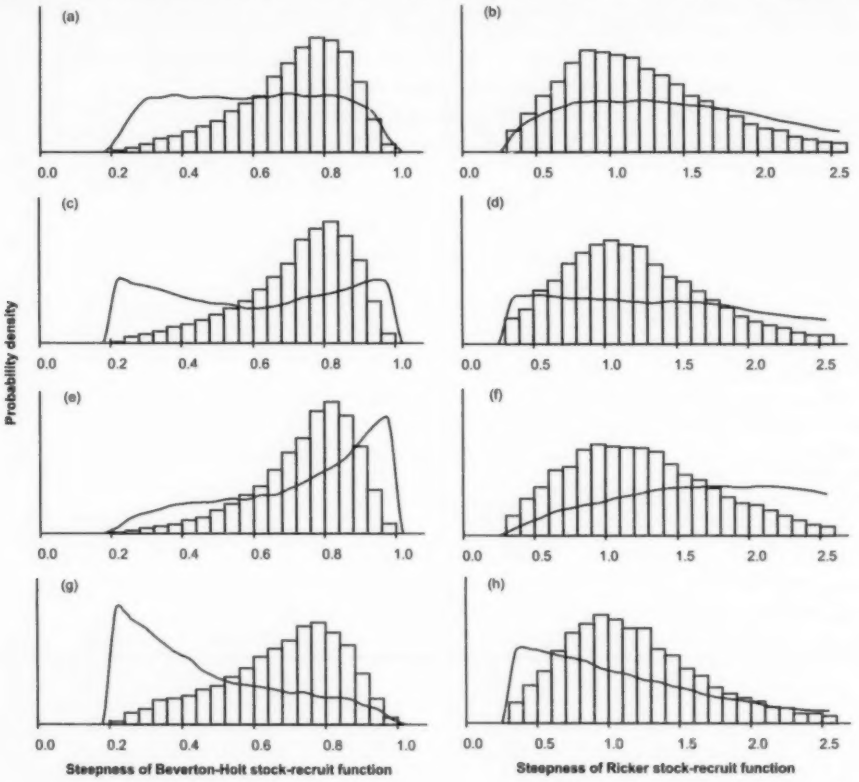

tion of females have been obtained from Hutchings and Jones (1998) and the International Council for the Exploration of the Sea (2003). Where river specific estimates were missing, as for example for the Rivers Pollet and Bec-Scie, region-specific estimates have been chosen (Hutchings and Jones 1998). Hutchings and Jones (1998) also provided estimates for the smolt to grilse survival (1.3–17.4%). This has been translated into a probability distribution for H in eq. 13 ($N(0.1, 0.05^2)|(0.013, 0.17)$, meaning that the normal distribution has been truncated at 0.013 and 0.17). The weight of a grilse is assumed to be between 1.5 and 3 kg ($N(2.25, 0.38^2)|(1.5, 3)$), while the weight of a 2SW and 3SW salmon is assumed to vary between 3 and 7 kg ($N(5, 1.2^2)|(3,7)$) and between 6 and 14 kg ($N(10, 2.24^2)|(6, 14)$), respectively. The relative fecundity is given a uniform distribution between 1600 and 1800 eggs per kilogram female salmon ($U(1600, 1800)$) (Bardonnet and Bagliniere 2000). The resulting statistics for the prior probability distributions of the spawner biomass per recruit parameter for the different rivers are presented in Table 2.

Description of the hierarchical model

The joint posterior density function of the hierarchical model parameters is given by the equation

$$(14)\quad p(\theta|\underline{\text{smolts}}^{\text{obs}}) = p(\mu_z)p(\sigma_z)p(\mu_R)p(\tau_R)p(\tau_{\text{smolts}}) \times p(\underline{\tilde{S}})p(\underline{z}|\mu_z,\sigma_z)p(\underline{R}|\mu_R,\tau_R)p(\underline{\text{smolts}}^{\text{obs}}|\underline{z},\underline{\tilde{S}},\underline{R})$$

where θ represents all parameters treated as random variables in the model, namely

$$(15)\quad \theta = \underline{z}, \mu_z, \sigma_z, \underline{\tilde{S}}, \underline{R}, \mu_R, \tau_R, \tau_{\text{smolts}}$$

We give an overview of all the model parameters and their description in Table 3. We also present part of the WinBUGS code for the hierarchical model for the Beverton–Holt stock–recruit function of different Atlantic salmon stocks (Appendix A). The model assumes a lognormal likelihood function. The WinBUGS code for the Ricker model is similar to this code except for the stock–recruit function. In the model, the river-specific values of $\tilde{S}$ are to be obtained from eq. 13.

In this model, we are mainly interested in the marginal posterior distribution of the steepness for some unsampled stock, which is determined by the mean and standard deviation in steepness across stocks. The joint posterior distribution for the mean and standard deviation in steepness is governed by the equation

© 2004 NRC Canada

Fig. 3. Prior and marginal posterior predictive probability distribution of the steepness for (*a*, *c*, and *e*) Beverton–Holt and (*b*, *d*, and *f*) Ricker stock–recruit functions for Baltic salmon when using different prior probability distributions for the precision of the likelihood function: (*a* and *b*) $G(0.001, 0.001)$; (*c* and *d*) $G(0.1, 0.001)$; (*e* and *f*) $G(10, 10)$.

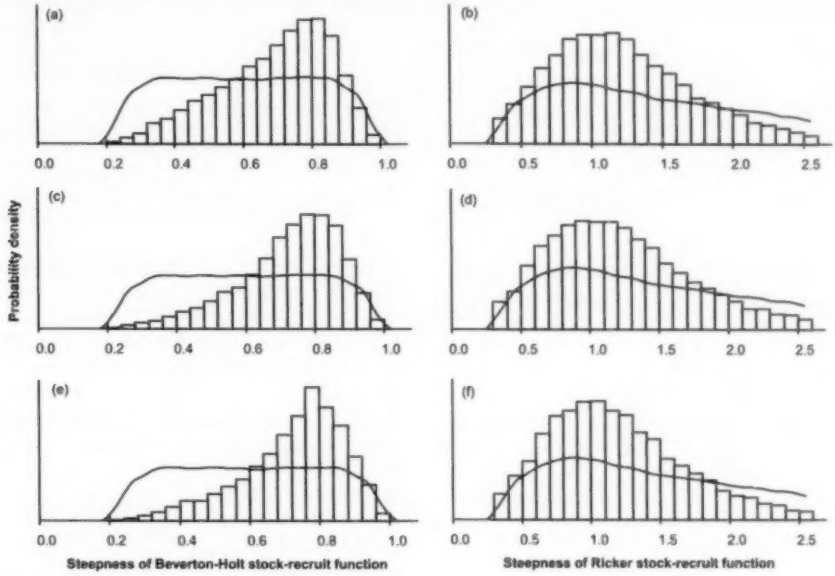

Fig. 4. Discrepancy plots between the data and the models using (*a*) Beverton–Holt and (*b*) Ricker stock–recruit functions. The corresponding Bayesian *p*-values, computed as the proportion of points above the line, are 0.78 and 0.8, respectively. Values close to 0.5 represent a good fit to the data.

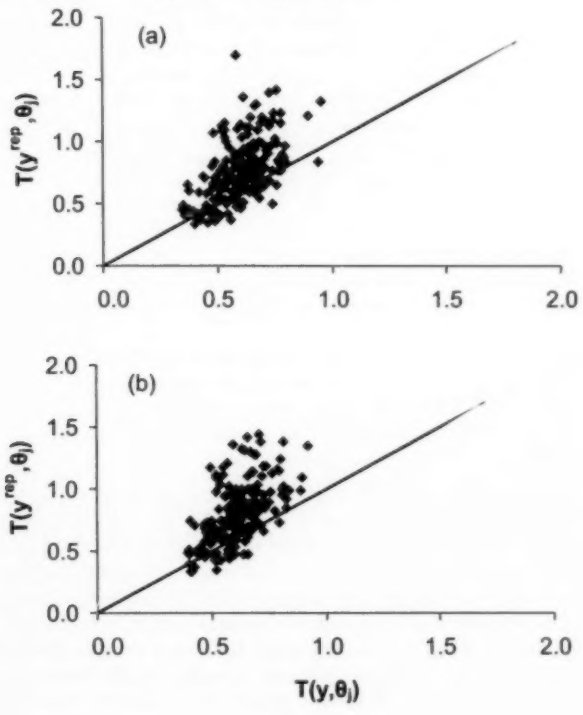

$$(16)\quad p(\mu_z, \sigma_z | \underline{\text{smolts}}^{\text{obs}}) = \int\int\int\int\int\int p(\theta | \underline{\text{smolts}}^{\text{obs}})\, d\mu_R\, d\tau_R\, d\tau_{\text{smolts}}\, d\underline{z}\, d\underline{\tilde{S}}\, d\underline{R}$$

The marginal predictive posterior distribution function of the steepness for some unsampled stock, z_j, is given by the equation

$$(17)\quad p(z_j | \underline{\text{smolts}}^{\text{obs}}) = \int\int p(z_j | \mu_z, \sigma_z)\, p(\mu_z, \sigma_z | \underline{\text{smolts}}^{\text{obs}})\, d\mu_z\, d\tau_z$$

Results

Tests concerning model structure and data assumptions

Evaluations of the sensitivity of results to prior pdf specifications for all of the major model parameters have been conducted. However, since the probability distribution for the steepness parameter is of most interest for the current analysis, we present mostly results for changes in the prior for the steepness parameter. We have replaced the dome-shaped prior probability distribution (Beta(2, 2) rescaled to lie between 0.2 and 1 or between 0.2 and 2.8 depending on the stock–recruit function) with distinctly different prior distributions ($U(0, 1)$, Beta(1, 2), and Beta(2, 1) all rescaled, e.g., to lie between 0.2 and 1) to assess the impacts on the marginal posterior distribution of the steepness parameter for Baltic salmon. The graphs (Fig. 2) show limited differences between the posterior density functions when using different prior density functions. Similar sensitivity analyses have been done for the distribution of the precision parameter of the likelihood function. The graphs show no substantial differences in the marginal posterior probability distribution for

© 2004 NRC Canada

Fig. 5. For each data set, the observed smolt abundance at the lowest stock level is compared with the predictive probability distribution. The observed number of smolts (vertical line) is compared with the posterior predictive distribution of the number of smolts using a Beverton–Holt (broken line) or Ricker (solid line) stock–recruit function. The posterior predictive *p*-value is defined as the probability that the replicated data are more extreme than the observed data.

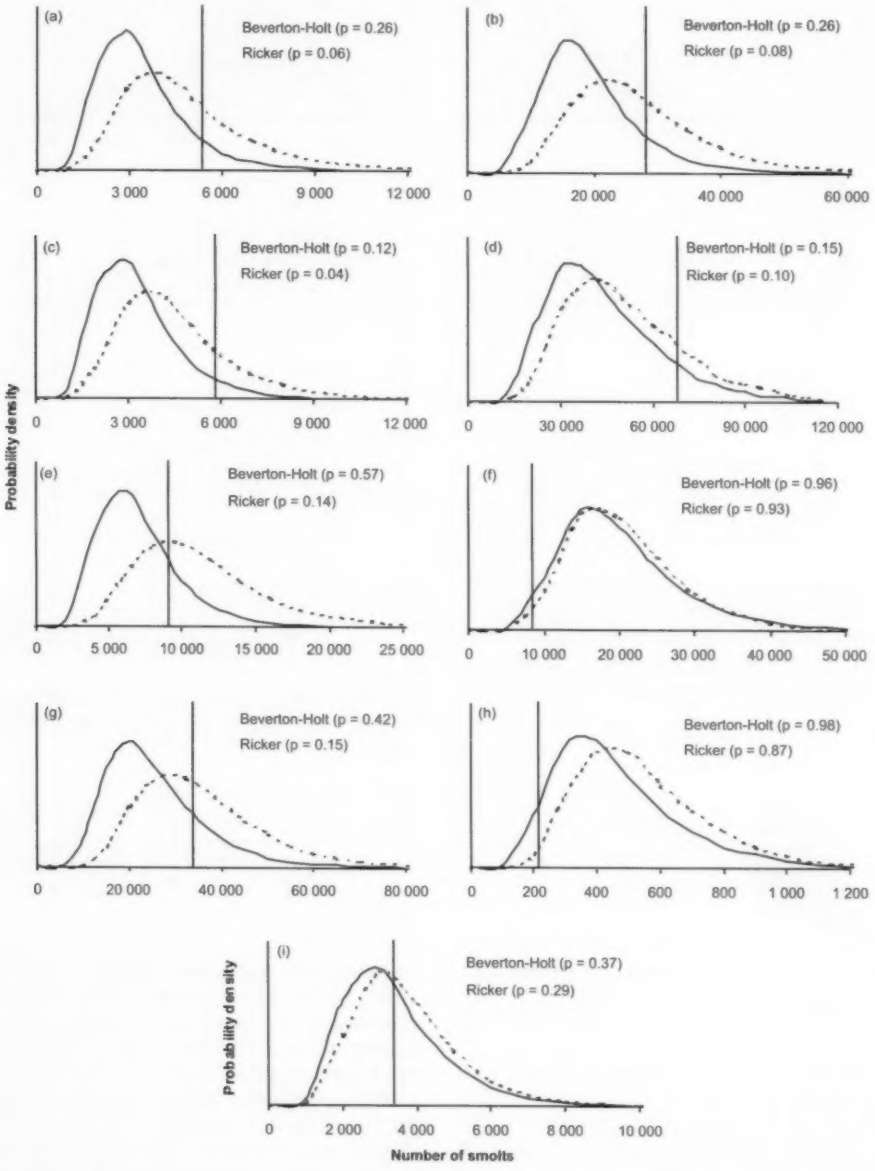

the steepness of the different stock–recruit functions for Baltic salmon (Fig. 3).

The observed data have been compared with the posterior predictive distributions of the data. When looking at the resulting Bayesian *p*-values for all of the data points, 4.9% of the data points fell outside the 95% probability intervals of the predictive probability distribution when using a Beverton–Holt stock–recruit function compared to 2.1% of the data points when assuming a Ricker stock–recruit function. The discrepancy plots indicate that the models fit the data relatively well and that the Beverton–Holt stock–recruit model is performing slightly better than the Ricker stock–recruit model (Fig. 4). Because of the concern of Barrowman and Myers (2000) that at low stock or egg abundance, the Ricker and the Beverton–Holt functions tend to lie above the observed data points, we have selected from each data set the point at the lowest stock level and compared this point with the predictive probability distribution of the data (Fig. 5). We have done this graphical comparison for the two different stock–recruit functions. When comparing the

© 2004 NRC Canada

observed value against the predictive probability distribution for each data point at the lowest stock level, there does not seem to be consistent overprediction of smolt recruitment.

To examine the exchangeability of the data sets, the two different stock–recruit models are each run nine times, excluding one data set each time. The graphs (Fig. 6) indicate that none of the data sets substantially alter the outcome of the hierarchical analysis. Therefore, it is concluded that the requirement of exchangeability between data sets has been met.

Fig. 6. Marginal predictive probability distributions of the steepness parameter for two different stock–recruit functions excluding one data set from the analysis at a time.

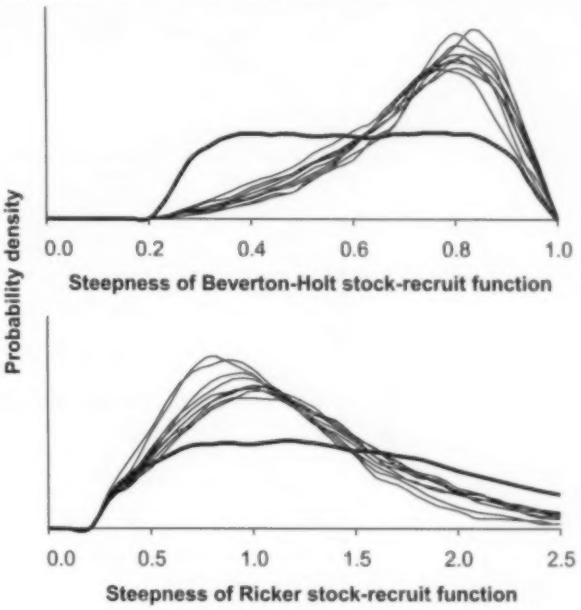

Estimating and predicting the steepness of different stock–recruit functions

After having tested the different model and data assumptions, the models have been used to estimate the steepness parameter of the different stocks and to predict the steepness parameter of an unsampled stock such as the salmon stock in the Baltic Sea. The results of the hierarchical analysis for the two stock–recruit functions are presented in Figs. 7 and 8 and Table 4. The posterior probability distributions of steepness are markedly more informative than the prior probability distributions but still reflect considerable uncertainty. The lower percentiles of the posterior probability distributions for the steepness of the Ricker stock–recruit function overlap with the posterior pdfs for the Beverton–Holt function. There does not seem to be a relationship between the origin of the stock–recruit data (Europe or Canada) and the estimated values for steepness. The marginal probability distribution of the steepness parameter for the Beverton–Holt stock–recruit function is much more informative than the marginal pdf for the steepness of the Ricker stock–recruit function. The medians of the marginal probability distributions for steepness of the Beverton–Holt and Ricker stock–recruit functions for Baltic salmon are 0.72 and 1.15, respectively. The probability distributions for steepness can be compared with the steepness calculated by Myers et al. (1999). By using a standard linear mixed model and a Ricker stock–recruit function, Myers et al. (1999) obtained a median steepness of 0.54 for Atlantic salmon with a 60% probability interval between 0.46 and 0.62. The results for the steepness of Atlantic salmon by Myers et al. (1999) are lower and the confidence interval is narrower than the probability intervals obtained in the current study. The reasons for the differences in results will be discussed in the Discussion section.

From the graphs of the fitted stock–recruit functions (Fig. 7), it becomes clear that the Beverton–Holt model consistently estimated a higher slope at the origin than the Ricker model, resulting in a higher predictive value for the slope at the origin for the Baltic salmon population (Table 5). Significant autocorrelation in the stock–recruit data has only been detected for one data set and there was no strong correlation between the steepness parameter and the smolt production capacity.

Calculating Bayes' posteriors for the different models

The previous section illustrated that depending on the stock–recruit model, the marginal predictive posterior density function for the steepness is very different. It is common to assess the fit of the individual models with the data, continue with the model that fits best, and discard the other models. In WinBUGS, the statistic used for this is the deviance information criterion (DIC), which is a Bayesian measure of model complexity and fit that can be used to compare models of arbitrary structure (Spiegelhalter et al. 2002). It is the sum of the posterior mean of the deviance (defined as –2 times the log likelihood from the Markov chain) and the effective number of parameters (defined as the posterior mean of the deviance minus the deviance of the posterior means). In this case, the DIC for the model with the Beverton–Holt function is 311, while the DIC for the Ricker model is 336. Discarding the Ricker stock–recruit function, however, would be ignoring model uncertainty.

Using the harmonic mean of the likelihood function, it is possible to calculate the Bayes' posterior model probability. The Beverton–Holt model obtains 99.9% probability, while the Ricker model obtains 0.1%, given the current stock–recruit data. This result was obtained consistently from several different chains with different starting values and is therefore reliable. The Beverton–Holt is favoured over the Ricker stock–recruit function, largely because it fits the data better. In addition, the Bayes' posterior, based on the harmonic means, tends to favour models containing less uncertainty whereby the variance of the deviances is smaller and this variance was less for the Beverton–Holt model (Fig. 9). The statistical models using the Beverton–Holt and Ricker stock–recruit functions are practically identical except for the prior for the steepness parameter. This steepness prior pdf is much more informative for the Beverton–Holt stock–recruit function than for the Ricker stock–recruit function owing to the strict boundaries for this parameter when using the Beverton–Holt function. This results in a smaller variance in

© 2004 NRC Canada

Fig. 7. Median values of the marginal posterior probability distributions for the Beverton–Holt (broken line) and Ricker (solid line) stock–recruit functions for (*a*) Little Codroy River, (*b*) Margaree River, (*c*) Pollett River, (*d*) Trinite River, (*e*) Western Arm Brook, (*f*) River Bush, (*g*) River Ellidaar, (*h*) River Oir, and (*i*) River Bec-Scie.

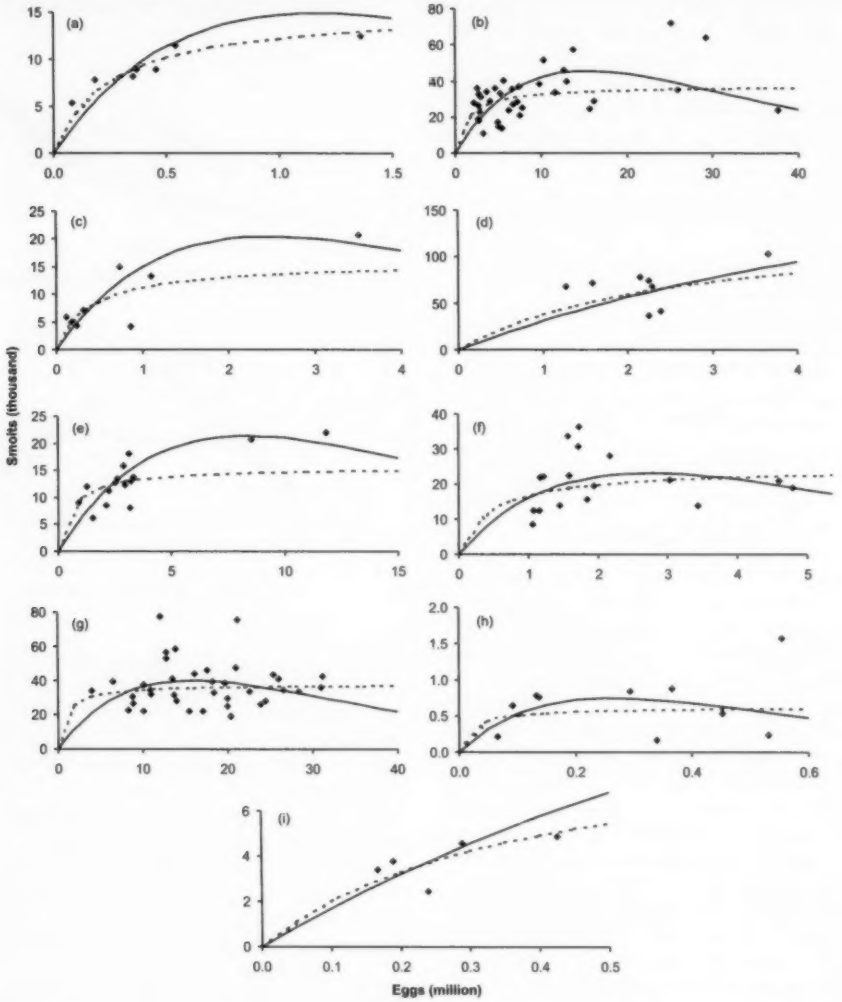

deviances in the Beverton–Holt model output than in that for the Ricker model and contributes further to the higher weighting for the Beverton–Holt model. This issue is treated in further detail below.

Discussion

Hierarchical analyses have become standard methods to obtain stock–recruit functions for fisheries stock assessment (Liermann and Hilborn 1997; Myers and Mertz 1998). The Beverton–Holt stock–recruit function is commonly parameterized in terms of the steepness parameter, which is transportable from stock to stock, making it ideal for hierarchical analyses of stock–recruit data. This paper advocates a similar parameterization for other possible stock–recruit functions such as the Ricker function, allowing estimation of the parameters of the stock–recruit function and estimation of the probability of the different stock–recruit functions given the stock–recruit data through the use of Bayes' posterior probabilities.

However, several dangers are connected to the use of a hierarchical analysis of stock–recruit data, which can make the results invalid: publication and selection bias, the use of studies of poor academic quality, and the mixing of dissimilar studies (Arnqvist and Wooster 1995). Furthermore, the different studies used in the hierarchical analysis should be exchangeable (Gelman et al. 1995). Most authors conclude that it is more important to be unbiased than to include every existing study (Englund et al. 1999).

As mentioned before, a steepness parameter is transportable from stock to stock. However, the value of the steepness parameter is not independent of the functional form of the stock–recruit function (e.g., steepness values above 1 can only occur for a Ricker stock–recruit function and not for

© 2004 NRC Canada

Fig. 8. Prior (thick broken line) and posterior probability distributions for stock–recruit data sets from Europe (thin solid line) and Canada (thin broken lines) and the corresponding marginal predictive probability distributions for Baltic salmon (thick solid lines) of the steepness parameter for different stock–recruit functions.

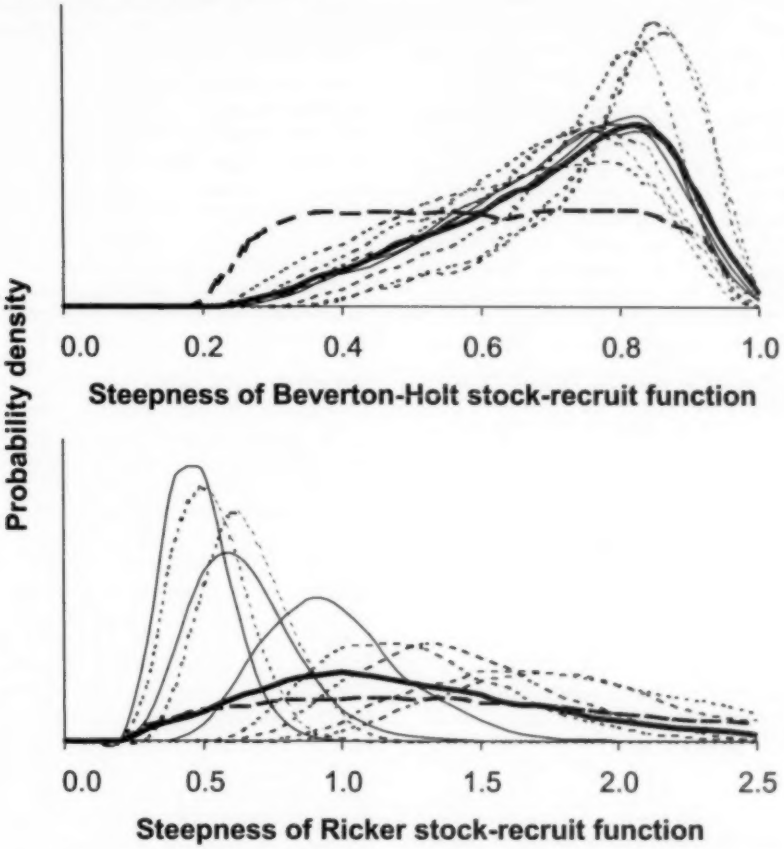

Table 4. Estimated mean and CV for the posterior probability distribution of the steepness for the Beverton–Holt and Ricker stock–recruit functions.

	Beverton–Holt		Ricker	
Parameter	Mean	CV	Mean	CV
Little Codroy River	0.78	0.15	1.75	0.29
Margaree River	0.65	0.22	0.61	0.25
Pollett River	0.72	0.17	1.40	0.27
Trinite River	0.78	0.16	1.91	0.29
Western Arm Brook	0.63	0.26	0.48	0.27
River Bush	0.69	0.22	0.93	0.27
River Ellidaar	0.70	0.22	0.44	0.27
River Oir	0.69	0.22	0.60	0.32
River Bec-Scie	0.67	0.22	1.25	0.31
Baltic rivers	0.70	0.23	1.24	0.48

the Beverton–Holt function). Myers et al. (1999) have used a Ricker stock–recruit function within an hierarchical model to estimate the slope at the origin. From these results, they have estimated a steepness value for the Beverton–Holt function based on the assumption that the slope at the origin is the same for the Ricker and Beverton–Holt stock–recruit functions. According to our results (Table 5), the estimates for the slope at the origin can be distinctly different between the two different functions given the same stock–recruit data. By assuming the slopes to be the same and transforming the slope at the origin of a Ricker stock–recruit function to a steepness value for the Beverton–Holt function, Myers et al. (1999) have underestimated the steepness parameter for the Beverton–Holt function. This explains their lower steepness estimates compared with the current analysis.

Within this paper, a different approach has been advocated by implementing the same definition of steepness to both the Beverton–Holt and Ricker stock–recruit functions (i.e., the corresponding proportion of virgin recruitment when reducing the stock biomass to 20% of its virgin level). Using this parameterization, posterior distributions can be obtained for the steepness parameter for each stock–recruit function whereby the steepness parameters are dependent on the functional form of the stock–recruit function. This parameterization has produced plausible results for both the Beverton–Holt and Ricker stock–recruit functions. Potentially, this parameterization could also be expanded to other stock–recruit formulations. For some stock–recruit functions, however, there may be no reduction in recruitment when reducing the stock biomass to 20% of its virgin level. This, for

© 2004 NRC Canada

Table 5. Estimated mean and 95% probability interval for the posterior probability distribution of the slope at the origin for the Beverton–Holt and Ricker stock–recruit functions.

	Beverton–Holt		Ricker	
Parameter	Mean	95% probability interval	Mean	95% probability interval
Little Codroy River	0.060	0.031–0.207	0.035	0.022–0.053
Margaree River	0.025	0.013–0.082	0.008	0.006–0.010
Pollett River	0.038	0.022–0.094	0.022	0.015–0.032
Trinite River	0.052	0.028–0.235	0.034	0.023–0.052
Western Arm Brook	0.026	0.009–0.138	0.007	0.005–0.010
River Bush	0.051	0.022–0.227	0.023	0.015–0.034
River Ellidaar	0.040	0.015–0.204	0.007	0.005–0.010
River Oir	0.027	0.010–0.146	0.008	0.004–0.012
River Bec-Scie	0.025	0.013–0.106	0.018	0.011–0.030
Baltic rivers	0.026	0.009–0.153	0.017	0.004–0.039

Fig. 9. Probability density function of the log-likelihood values for samples of the posterior distributions when fitting the Beverton–Holt (solid line) and Ricker (broken line) stock–recruit functions to Atlantic salmon stock–recruit data.

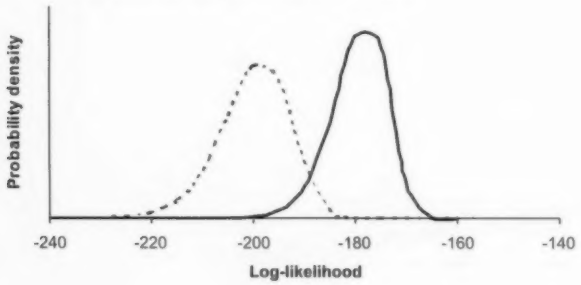

example, is the case for the hockey stick model, a simple segmented regression line that starts at the origin at a certain slope and whereby the recruitment becomes constant above some level of spawner abundance (Barrowman and Myers 2000). Unless the steepness parameter is actually 1 or the slope parameter is very low and gives a high value for the spawning stock inflection point relative to the carrying capacity, and there are some data available near the origin, this parameterization will not contain the necessary information to estimate the slope at the origin for the hockey stick model.

Within this paper, two different stock–recruit functions have been fitted to stock–recruit data within a Bayesian framework. This requires the selection of appropriate prior probability distributions for the model parameters. The prior for the steepness parameter has traditionally been given distributions between 0.2 and 1 because of the shape of the Beverton–Holt stock–recruit function. When expanding the concept of steepness to other stock–recruit functions, this prior needs to be revised. For the Ricker stock–recruit function, it is, for example, possible to obtain a value for the steepness parameter larger than 1. Therefore, the prior distribution for steepness should be dependent on the functional form of the stock–recruit function. The prior for steepness proposed within this paper is formed by the structure of the model. The mean steepness and standard deviation, which is dependent on the mean, shape the probability distribution of the steepness through a concise model structure.

The steepness parameter is commonly used in population assessments. By parameterizing more than one stock–recruit function in terms of steepness, the uncertainty in the stock–recruit function can be incorporated in the population assessments by running the same assessment models using different stock–recruit functions. The DIC has been developed to compare the fit of hierarchical models to the data (Spiegelhalter et al. 2002). This criterion, however, does not provide a mechanism to compare the overall plausibility of the different model structures given the data.

Within this paper, the computation of marginal Bayes' posterior probabilities for alternative models is advocated because this allows the estimation of the probability (or credibility) of each stock–recruit function given the available stock–recruit data (McAllister and Kirchner 2002). The Bayes' posterior probabilities have been calculated using the harmonic mean of the likelihood (Kass and Raftery 1995). This harmonic mean, however, may be unstable owing to the occasional occurrence of a set of parameters with a very small likelihood. Furthermore, the harmonic mean can be biased towards models with lower prior uncertainty in the parameter values owing to smaller prior variances. Gelman et al. (1995) identified this biasing effect as a potential distraction and suggested an alternative approach to accounting for model uncertainty that instead uses a continuous family of models. If the alternative model structures only differ in the use of the stock–recruit function and are limited to a Beverton–Holt or Ricker stock–recruit function, then the two discrete models could be replaced with a continuous family of models by using a three-parameter model for which the Ricker and Beverton–Holt stock–recruit functions are special cases.

The use of alternative discrete models, however, still has some advantages (McAllister and Kirchner 2002). It is more flexible when it is of interest to explore the probability of a wide variety of different model structures. The use of two two-parameter models as opposed to a single generalized three-parameter model may offer improved statistical performance in parameter estimation, particularly for stock–recruit data that are typically relatively uninformative even for two-parameter models. Instability problems from using the har-

© 2004 NRC Canada

monic mean likelihood can be overcome by using other computational methods such as reversible jump or importance sampling (Kass and Raftery 1995; Patterson 1999; McAllister and Kirchner 2002). Moreover, in our calculations, instability was not a problem because Markov chains with different starting points gave the same results. Also, when the harmonic means for the two alternative stock–recruit models were recalculated using deviances with the original mean deviance but constrained to have the same variance in deviances, practically the same results were obtained.

The proposed methodology enables prediction of the steepness of the stock–recruit function for unsampled salmon stocks such as the salmon in the Baltic Sea even though no stock–recruit data have been collected in the region. The means of the marginal probability distributions for steepness of the Beverton–Holt and Ricker stock–recruit functions for Baltic salmon are 0.70 (CV 23%) and 1.24 (CV 48%), respectively. Although by definition, the steepness of the different stock–recruit functions has the same meaning, the estimated value for steepness is dependent on the functional form of the stock–recruit function, thus explaining the different results obtained for the different stock–recruit functions. According to the Bayes' model posteriors, the Beverton–Holt stock–recruit function is more likely than the Ricker stock–recruit function given the current stock–recruit data, although the Ricker model cannot be ruled out. This model uncertainty should be carried along into fisheries stock assessments and decision analyses. To identify plausible stock–recruit functions for a given stock where no stock–recruit data exist, the posterior predictive distribution for steepness obtained through hierarchical modelling can be used in combination with estimates for the carrying capacity of salmon in the Baltic Sea area (Geiger and Koenings 1991; Adkison and Peterman 1996). For example, estimates for the smolt carrying capacity of salmon in the Baltic Sea have been obtained through an evaluation of habitat availability and quality (Uusitalo 2001). When incorporating the stock–recruit functions in fisheries stock assessments, the steepness parameter still needs to be adjusted for region-specific mortality effects. In the Baltic Sea, for example, this should include the juvenile mortality resulting from the M74 syndrome (Karlsson and Karlström 1994). This syndrome occurs only in the Baltic Sea and not in the areas where the stock–recruit data have been collected and should lower the steepness for salmon stocks in this region.

Acknowledgements

The authors are especially grateful to Robin Wyatt for his in-depth comments on the model and suggestion for the revised steepness parameterisation of the Ricker stock–recruit model. His many insightful comments have substantially improved this paper and its presentation. We thank Clare Marshall and Nicky Best for helpful comments on developing the hierarchical modelling method and Samu Mäntyniemi and Geoff Kirkwood for their constructive comments on the manuscript. This paper has been partly funded by EU project No. 99/064 "Probabilistic modelling of Baltic salmon stocks" and the Wildlife Conservation Society.

References

Adkison, M.D., and Peterman, R.M. 1996. Results of Bayesian methods depend on details of implementation: an example of estimating salmon escapement goals. Fish. Res. **25**: 155–170.

Arnqvist, G., and Wooster, D. 1995. Meta-analysis — synthesizing research findings in ecology and evolution. Trends Ecol. Evol. **10**: 236–240.

Bardonnet, A., and Bagliniere, J.L. 2000. Freshwater habitat of Atlantic salmon (*Salmo salar*). Can. J. Fish. Aquat. Sci. **57**: 497–506.

Barrowman, N.J., and Myers, R.A. 2000. Still more spawner–recruitment curves: the hockey stick and its generalizations. Can. J. Fish. Aquat. Sci. **57**: 665–676.

Best, N., Cowles, M.K., and Vines, K. 1995. CODA manual version 0.30. MRC Biostatistics Unit, Cambridge, UK.

Beverton, R.J.H., and Holt, S.J. 1957. On the dynamics of exploited fish populations. Chapman and Hall, London, UK.

Brooks, S.P., Catchpole, E.A., and Morgan, B.J.T. 2000. Bayesian animal survival estimation. Stat. Sci. **15**: 357–376.

Brooks, S.P., Catchpole, E.A., Morgan, B.J.T., and Harris, M.P. 2002. Bayesian methods for analysing ringing data. J. Appl. Stat. **29**(1–4): 187–206.

Caron, F. 1992. Relation enter le nomber d'oefs déposés et la production de saumonneaux Rivières de la Trinité et Bec-Scie. CAFSAC Res. Doc. No. 92/125.

Chadwick, E.M.P. 1982. Stock–recruitment relationship for Atlantic salmon (*Salmo salar*) in Newfoundland rivers. Can. J. Fish. Aquat. Sci. **39**: 1496–1501.

Chaput, G., and Jones, R. 1992. Stock–recruit relationship for multi-sea-winter salmon from the Margaree River, N.S. CAFSAC Res. Doc. No. 92/124:17.

Chaput, G., Mullins, C., and Chadwick, E.M.P. 1992. Stock–recruit relationship for Atlantic salmon from Western Arm Brook, Newfoundland. CAFSA Res. Doc. No. 92/123.

Clarke, B., and Gustafson, P. 1998. On the overall sensitivity of the posterior distribution to its inputs. J. Stat. Plan. Inference, **71**: 137–150.

Crozier, W.W., and Kennedy, G.J.A. 1995. The relationship between a summer fry (0+) abundance index derived from semi-quantitative electrofishing, and egg deposition of Atlantic salmon, in the River Bush, Northern Ireland. J. Fish Biol. **47**: 1055–1062.

Dorn, M.W. 2002. Advice on West Coast rockfish harvest rates from Bayesian meta-analysis of stock–recruit relationships. N. Am. J. Fish. Manag. **22**: 280–300.

Elson, P.F. 1975. Atlantic salmon rivers smolt production and optimal spawning. An overview of natural production. Int. Atl. Salmon Found. Spec. Publ. Ser. **6**: 96–119.

Englund, G., Sarnelle, O., and Cooper, S.D. 1999. The importance of data-selection criteria: meta-analyses of stream predation experiments. Ecology, **80**: 1132–1141.

Evans, M., Hastings, N., and Peacock, B. 2000. Statistical distributions. 3rd ed. Wiley, New York.

Geiger, H.J., and Koenings, J.P. 1991. Escapement goals for sockeye salmon with informative prior probabilities based on habitat considerations. Fish. Res. **11**: 239–256.

Gelman, A., Carlin, J.B., Stern, H.S., and Rubin, R.B. 1995. Bayesian data analysis. Chapman and Hall, London, UK.

Gelman, A., Meng, X., and Stern, H. 1996. Posterior predictive assessment of model fitness via realised discrepancies. Stat. Sinica, **6**: 733–807.

Hilborn, R., and Liermann, M. 1998. Standing on the shoulders of giants: learning from experience in fisheries. Rev. Fish Biol. Fish. **8**: 273–283.

© 2004 NRC Canada

Hilborn, R., and Walters, C.J. 1992. Quantitative fisheries stock assessment. Choice, dynamics and uncertainty. Chapman and Hall, London, UK.

Hutchings, J.A., and Jones, M.E.B. 1998. Life history variation and growth rate thresholds for maturity in Atlantic salmon, *Salmo salar*. Can. J. Fish. Aquat. Sci. **55**(Suppl. 1): 22–47.

International Council for the Exploration of the Sea. 2003. Report of the Baltic salmon and trout assessment working group. International Council for the Exploration of the Sea, Copenhagen, Denmark.

Karlsson, L., and Karlström, Ö. 1994. The Baltic salmon (*Salmo salar* L.): its history, present situation and future. Dana, **10**: 61–85.

Kass, R.E., and Raftery, A.E. 1995. Bayes factors. J. Am. Stat. Assoc. **90**: 773–795.

Liermann, M., and Hilborn, R. 1997. Depensation in fish stocks: a hierarchical Bayesian meta-analysis. Can. J. Fish. Aquat. Sci. **54**: 1976–1984.

Mace, P.M., and Doonan, I.J. 1988. A generalized bioeconomic simulation model for fish population dynamics. N.Z. Fish. Assess. Res. Doc. No. 88/4.

McAllister, M.K., and Kirchner, C.H. 2002. Accounting for structural uncertainty to facilitate precautionary fishery management: illustration with Namibian orange roughy. Bull. Mar. Sci. **70**: 499–540.

Meng, X. 1994. Posterior predictive *p*-values. Ann. Stat. **22**: 1142–1160.

Meyer, R., and Millar, R.B. 1999. BUGS in Bayesian stock assessments. Can. J. Fish. Aquat. Sci. **56**: 1078–1086.

Mundy, P.R., Alexandersdottir, M., and Eiriksdottir, G. 1978. Spawner–recruit relationship in Ellidaar. J. Agric. Res. Icel. **10**: 47–56.

Myers, R.A. 2001. Stock and recruitment: generalizations about maximum reproductive rate, density dependence and variability using meta-analytic approaches. ICES J. Mar. Sci. **58**: 937–951.

Myers, R.A., and Mertz, G. 1998. Reducing uncertainty in the biological basis of fisheries management by meta-analysis of data from many populations: a synthesis. Fish. Res. **37**: 51–60.

Myers, R.A., Bridson, J., and Barrowman, N.J. 1995. Summary of worldwide spawner and recruitment data. Can. Tech. Rep. Fish. Aquat. Sci. No. 2024.

Myers, R.A., Bowen, K.G., and Barrowman, N.J. 1999. Maximum reproductive rate of fish at low population sizes. Can. J. Fish. Aquat. Sci. **56**: 2404–2419.

Needle, C.L. 2002. Recruitment models: diagnosis and prognosis. Rev. Fish Biol. Fish. **11**: 95–111.

Newton, M.A., and Raftery, A.E. 1994. Approximate Bayesian inference with the weighted likelihood bootstrap. J. R. Stat. Soc. Ser. B (Methodol.), **56**(3): 3–48.

Patterson, K.R. 1999. Evaluating uncertainty in harvest control law catches using Bayesian Markov Chain Monte Carlo virtual population analysis with adaptive rejection sampling and including structural uncertainty. Can. J. Fish. Aquat. Sci. **56**: 208–221.

Prévost, É., Bagliniére, J., Maisse, G., and Nihouarn, A. 1996. Premiers éléments d'une relation stock/recrutment chez le saumon atlantique (*Salmo salar*) en France. Cybium, **20**(Suppl. 3): 7–26.

Prévost, É., Chaput, G., and Chadwick, E.M.P. 2001. Transport of stock–recruitment reference points for Atlantic salmon. *In* Stock, recruitment and reference points. *Edited by* É. Prévost and G. Chaput. Assessment and management of Atlantic salmon. INRA, Paris. pp. 95–135.

Punt, A.E., and Hilborn, R. 1997. Fisheries stock assessment and decision analysis: the Bayesian approach. Rev. Fish Biol. Fish. **7**: 35–63.

Ricker, W. 1954. Stock and recruitment. J. Fish. Res. Board Can. **11**: 559–623.

Spiegelhalter, D.J., Best, N.G., Carlin, B.P., and van der Linde, A. 2002. Bayesian measures of model complexity and fit. J. R. Stat. Soc. Ser. B (Methodol.), **64**(3): 583–639.

Su, Z.M., Adkison, M.D., and Van Alen, B.W. 2001. A hierarchical Bayesian model for estimating historical salmon escapement and escapement timing. Can. J. Fish. Aquat. Sci. **58**: 1648–1662.

Uusitalo, L. 2001. Expert knowledge based Bayesian Belief Network for estimation of salmon smolt carrying capacity in the Gulf of Bothnia wild salmon rivers. M.Sc. thesis, University of Helsinki, Helsinki, Finland.

Appendix A. WinBUGS code for a Bayesian hierarchical model of the Beverton–Holt stock–recruit function

```
model {
for(j in 1:n) { # for the n samples
  obs_Smolts[j] ~ dlnorm(X[j], tau_Smolts) # Likelihood function
  X[j] <- log(exp_Smolts[j])
  exp_Smolts[j] <- Eggs[j] / (alpha[river[j]] + (beta[river[j]] * Eggs[j])) # B-H function
}
for(j in 1:m) { # for the m Atlantic salmon stocks
  alpha[j] <- ((1 – z[j]) / (4 * z[j])) * SBPR[j] # definition of alpha in terms of steepness
  beta[j] <- ((5 * z[j]) – 1) / (4 * z[j] * R[j]) # definition of beta in terms of steepness
  z[j] <- (0.8 * zt[j]) + 0.2 # transformation to beta distribution between 0.2 and 1
  zt[j] ~ dbeta(alpha_zt, beta_zt) # prior for the transformed steepness
  R[j] ~ dlnorm(mu_R, tau_R)I(0.001, ) # prior for recruitment potential
  SBPR[j] # river specific prior for spawner biomass per recruit
  # the detailed code for the calculation of the river specific SBPR is not shown to avoid cluttering the presentation
}
tau_Smolts <- 1/pow(sigma, 2) # derived prior for precision of predicted smolts
sigma ~ dgamma(0.001, 0.001) # prior for the standard deviation of predicted smolts
mu_R ~ dnorm(0.0, 1.0E-6)I(1.01, 25) # hyperprior for mean of recruitment potential
```

© 2004 NRC Canada

```
tau_R ~ dgamma(0.001, 0.001) # hyperprior of precision of recruitment potential
alpha_zt <- (pow(mean_zt, 2) - pow(mean_zt, 3) - (mean_zt * pow(sd_zt, 2))) / pow(sd_zt, 2)
beta_zt <- ((1 - mean_zt) / pow(sd_zt, 2)) * ((mean_zt * (1 - mean_zt)) - pow(sd_zt, 2))
# reparameterisation from mean and variance to alpha and beta parameters
sd_zt <- sd_ztt * max_sd_zt # defining the distribution of the transformed variance zt
sd_ztt ~ dbeta(2, 1)
mean_zt ~ dbeta(2, 2)
mean_z <- (0.8 * mean_zt) + 0.2 # transformation to beta dist. between 0.2 and 1
k <- step(mean_zt - 0.5) # if mean_zt - 0.5 > 0 then k = 1 else k = 0
   min <- (1 - ((1 - mean_zt) * 2)) * k
   max <- ((1 - (mean_zt * 2)) * k) + (mean_zt * 2)
max_sd_zt <- sqrt(pow((max - min), 2) / 12)} # maximum variance given a mean
```

© 2004 NRC Canada

A Bayesian hierarchical formulation of the De Lury stock assessment model for abundance estimation of Falkland Islands' squid (*Loligo gahi*)

Murdoch K. McAllister, Simeon L. Hill, David J. Agnew, Geoffrey P. Kirkwood, and John R. Beddington

Abstract: In stock assessments of short-lived species, De Lury depletion models are commonly applied in which commercial catches and changing catch rates are used to estimate resource abundance. These methods are applied within fishing seasons to decide when to close the fishery and can be reliable if the data show a distinct decline in response to the catch removals. However, this is not always the case, particularly when sampling error variation masks trends in abundance. This paper presents a Bayesian hierarchical formulation of the De Lury model in which data from previous years are combined hierarchically in the same stock assessment model to improve parameter estimation for future stock assessments. The improved precision in parameter estimates is demonstrated using data for the Falkland Islands' *Loligo gahi* squid fishery.

Résumé : Les modèles d'épuisement de De Lury sont couramment appliqués aux prises commerciales et aux taux de capture changeants pour estimer l'abondance de la ressource dans l'évaluation des stocks des espèces à vie brève. Ces méthodes sont utilisées au cours de la saison de pêche pour décider quand mettre fin à la pêche et elles sont fiables lorsque les données montrent un net déclin en réaction aux retraits dus à la pêche. Cependant, cela n'est pas toujours le cas, surtout lorsque la variation de l'erreur d'échantillonnage masque les tendances dans l'abondance. Nous présentons une formulation hiérarchique bayésienne du modèle de De Lury dans laquelle les données des années antérieures sont combinées de façon hiérarchique dans un même modèle d'évaluation du stock afin d'améliorer l'estimation des paramètres pour les évaluations futures. Des données provenant de la pêche commerciale du calmar *Loligo gahi* des îles Falklands nous servent à démontrer l'amélioration obtenue dans l'estimation des paramètres.

[Traduit par la Rédaction]

Introduction

Leslie–De Lury depletion models (hereafter referred to as De Lury models) for estimating population size rely on the fact that removing individuals from a population often has a noticeable effect on some observable index of abundance. In a fisheries context, such methods can be used when commercial catch rates show a distinct decline in response to catch removals (see overview in Hilborn and Walters 1992). For example, these methods have been successfully used in the assessment of squid stocks around the Falkland Islands (also referred to hereafter as the Falklands) (Rosenberg et al. 1990; Basson et al. 1996; Agnew et al. 1998). In this case, catch per unit effort (CPUE) is assumed to be directly proportional to abundance. The scaling factor, known as catchability, represents the proportion of the population that will be caught per unit effort. A maximum likelihood method is used to fit a model to the declining period in the CPUE data and estimate parameters representing initial abundance and catchability (Rosenberg et al. 1990). With these parameters, the data can also be used to estimate abundance up to the last recorded catch removal and to predict the abundance in future weeks. Prediction of the total removals that would leave the stock at or above an agreed biological reference point can facilitate in-season management of the fishery.

De Lury models are useful provided that (*i*) the catch rate data show a distinct decline in response to catch removals, (*ii*) there is relatively little emigration and immigration during the depletion, (*iii*) a linear relationship holds between catch rate and abundance, and (*iv*) the natural mortality rate and catchability remain constant over the period in the data. However, these conditions seldom hold all at once, which can produce biased results.

For years in which the first condition does not hold, for example, because sampling error in CPUE data masks declines in abundance, and the other three conditions hold, ad hoc methods have been proposed in which the value for the catchability coefficient (q) is fixed at some previously esti-

Received 12 August 2003. Accepted 13 April 2004. Published on the NRC Research Press Web site at http://cjfas.nrc.ca on 30 July 2004.
J17700

M.K. McAllister,[1] **D.J. Agnew, G.P. Kirkwood, and J.R. Beddington.** Department of Environment Science and Technology, Imperial College, RSM Building, Prince Consort Road, London, SW7 2BP UK.
S.L. Hill. British Antarctic Survey, High Cross, Madingley Road, Cambridge, CB3 0ET, UK.

[1]Corresponding author (e-mail: m.mcallister@imperial.ac.uk).

 doi: 10.1139/F04-084 © 2004 NRC Canada

mated value (Agnew et al. 1998). Whereas this sensibly makes use of historical data to confine parameter estimates, it does not formally account for the interannual variability in values for the parameter and the effect of this on estimation uncertainty in the present year.

In contrast, methods since the early 1990s have been developed to probabilistically share information among populations and improve the estimation properties of stock assessments (e.g., Collie and Walters 1991; McAllister et al. 1994; Rivot and Prévost 2002). Among these, Bayesian hierarchical modeling (BHM) methods have been devised to model the cross-population variability in parameters that underlie different sets of historical data and to develop posterior predictive probability density functions (pdfs) of the parameters in unsampled populations (Gelman et al. 1995; Adkison and Su 2001; Harley and Myers 2001). Posterior predictive pdfs obtained from BHM can serve as prior pdfs of the parameters in analyses of data sets for newly sampled populations to help improve precision in parameter estimation (Michielsens 2003). The resulting posterior pdfs of model parameters can then help to reduce uncertainty when evaluating the potential consequences of alternative fishery management actions that can be taken.

The squid species *Illex argentinus* and *Loligo gahi* are the main commercial stocks exploited in the Falkland Islands' conservation zones and have been major contributors to the economy of the Islands since the Falkland Islands government began the active management of fishery resources in 1987. Both squid are short lived, with life spans of about 1 year. They are both migratory species and the fisheries operate in adult feeding areas where the squid populations are resident for several months. There are two fishing seasons for *L. gahi* each year, exploiting two main pulses of recruitment resulting from spawning events in spring and autumn. De Lury estimation methods are applied to the fisheries data to provide in-season management advice (Rosenberg et al. 1990; Agnew et al. 1998). Because they are annual species, all historical data are excluded in each new assessment. Whereas informative depletions in catch rates occur in most years, there are others where the De Lury estimations fail to provide sensible results because the data are not well behaved (Agnew et al. 1998).

In this paper, we develop a Bayesian hierarchical formulation of the De Lury depletion model, which incorporates historical CPUE series to improve estimation of the catchability coefficient and preseason abundance. The application of the approach is illustrated using data for the Falkland Islands' *L. gahi* squid fishery.

Bayesian methodology

There are eight steps in the Bayesian hierarchical estimation of De Lury model parameters. These are summarized below and explained in detail afterwards. It is necessary to use some technical terms in the summary. These are defined in the detailed explanation. (1) Specify the De Lury model of interest and identify the key parameters to be estimated. (2) Construct a likelihood function of the catch rate data. (3) Construct a hierarchical probability model for the De Lury model parameters that incorporates historical data. (4) Identify the hyper-parameters and marginal posterior predictive distributions of interest (i.e., marginal posterior probability distributions for parameters (e.g., catchability) that could be used as priors for a new analysis and that summarize all that is known about the parameter). (5) Apply a method to integrate the joint posterior pdf of the hierarchical De Lury model parameters to produce marginal posterior pdfs of the parameters of interest. (6) Simulation test the estimation procedure using fixed known parameter values to simulate data series and then evaluate the precision and bias in hierarchical model parameters. Consider readjusting hierarchical model parameterization if poor estimation performance is detected. (7) Compute and evaluate convergence diagnostics for the Bayesian integration method used. (8) Evaluate the characteristics of the marginal and joint posterior probability distributions obtained from the hierarchical modeling of the De Lury model, e.g., the interannual variation in key model parameters and the precision in the predictive distribution. Each of these steps is outlined in further detail below.

(1) Specifying the De Lury model of interest and identifying the parameters to be estimated

We apply the De Lury model formulation in Rosenberg et al. (1990) that is applied in the stock assessment of Falkland Islands' squid stocks. The predicted CPUE in a given week w for year y is obtained by

$$(1)\quad \widehat{\mathrm{CPUE}}_{y,w} = q_y N_{0,y} \exp[-(w+0.5)M] - q_y \sum_{k=0}^{w-1} C_{y,k} \exp[-(w-k)M]$$

where q_y is the catchability coefficient, $N_{0,y}$ is the abundance at the beginning of the season in week 0, M is the weekly rate of natural mortality, and $C_{y,k}$ is the catch in numbers taken in week k. The estimable parameters are $N_{0,y}$ and q_y. M is typically not known with certainty; however, for the sake of simplifying the illustration, M will be fixed at 0.06, as is typically done for the Falklands' *L. gahi* (Agnew et al. 1998). This need not be the case and an informative prior pdf of M could be applied in future applications to take into account uncertainty in this parameter.

(2) Constructing a likelihood function of the catch rate data

It is assumed that the deviations between predicted and observed catch rates are lognormally distributed (Rosenberg et al. 1990). The likelihood function of the CPUE data in year y is as follows:

$$(2)\quad L(\underline{\mathrm{CPUE}}_y \mid q_y, N_{0,y}, \tau_L) = \prod_{w=1}^{nwk(y)} \frac{1}{\mathrm{CPUE}_{y,w}\sqrt{2\pi\tau_L^{-1}}} \exp\{-0.5\tau_L[\ln(\mathrm{CPUE}_{y,w}) - \ln(\widehat{\mathrm{CPUE}}_{y,w})]^2\}$$

© 2004 NRC Canada

where $\underline{\text{CPUE}}_y$ represents a vector containing several weeks of CPUE data for year y, τ_L is the precision ($1/\sigma^2$ and σ is the standard deviation (SD)) in the natural logarithm of the deviations between observed and predicted CPUE, $nwk(y)$ is the number of weeks in year y, and $\text{CPUE}_{y,w}$ is the observed catch rate in week w. τ_L is also an estimated parameter and is assumed to be constant across years. In the example below, we had tried to model τ_L using a hierarchical structure in which a value for $\tau_{L,y}$ for each year was estimated as well as the mean and variance in $\tau_{L,y}$ across years. However, because of the relatively limited time series (e.g., <20 weeks) and hence insufficient information in the data about $\tau_{L,y}$ for several of the years (Table 1), this hierarchical model was overparameterized. For example, the posterior correlations among the parameters q_y, $N_{0,y}$, and $\tau_{L,y}$ became very high and Monte Carlo integration became intractable. In contrast, the high posterior correlations vanished and it became feasible to reliably estimate the parameters q_y and $N_{0,y}$ when a single value for τ_L was estimated across all years.

(3) Constructing a hierarchical probability model for the De Lury model parameters from historical data

Here we develop a Bayesian hierarchical probability model for q_y and $N_{0,y}$ (Gelman et al. 1995; Rivot and Prévost 2002). This assumes that there is a population of q_y and $N_{0,y}$ across years and that a value in any one year comes from some particular parametric pdf. We illustrate the hierarchical approach using normal and lognormal density functions and keep the example simple for illustrative purposes. A lognormal probability density function is applied to model the variation in values for q_y over years with a median q_y of μ_q and precision in the natural logarithm of q_y of τ_q. $N_{0,y}$ are lognormally distributed over years with a median $N_{0,y}$ of μ_{N_0} and precision of τ_{N_0}. It is also assumed that q_y and $N_{0,y}$ are uncorrelated. Thus,

$$(3) \quad q_y|\mu_q, \tau_q \sim \log\text{Norm}(\mu_q, \tau_q)$$
$$N_{0,y}|\mu_{N_0}, \tau_{N_0} \sim \log\text{Norm}(\mu_{N_0}, \tau_{N_0})$$

In BHM, the parameters describing cross-population distributions, such as the parameters μ_q, τ_q, μ_{N_0}, and τ_{N_0}, are typically called hyper-parameters (Gelman et al. 1995). In empirical Bayes' methods, which preceded BHM, hyper-parameters were estimated from data for related populations but then treated as fixed and known in subsequent estimation. In contrast, one of the goals of BHM is to estimate posterior pdfs of the hyper-parameters from historical data, and BHM requires that prior pdfs, i.e., hyper-priors, are specified for the hyper-parameters. Thus, we need to specify hyper-priors for μ_q, τ_q, μ_{N_0}, and τ_{N_0}. These hyper-priors are denoted by $P(\mu_q)$, $P(\tau_q)$, $P(\mu_{N_0})$, and $P(\tau_{N_0})$, respectively. Another estimated parameter is τ_L in the lognormal likelihood function of the data (eq. 2), and a prior pdf was assigned to τ_L, denoted as $P(\tau_L)$.

The set of parameters to be estimated in hierarchical analysis is then $\underline{q}_y$, $\underline{N}_{0,y}$, μ_q, τ_q, μ_{N_0}, τ_{N_0}, and τ_L, where the underlined parameters indicate the vector over the years of historical data. The joint posterior density for this vector of parameters, i.e., the hierarchical probability model for the De Lury model parameters, is given by

$$(4) \quad P(\underline{q}_y, \underline{N}_{0,y}, \mu_q, \tau_q, \mu_{N_0}, \tau_{N_0}, \tau_L|\underline{\text{CPUE}}) =$$
$$P(\mu_q)P(\tau_q)P(\mu_{N_0})P(\tau_{N_0})P(\tau_L)\prod_{y=1}^{nyr}\left(P(q_y|\mu_q,\tau_q)P(N_{0,y}|\mu_{N_0},\tau_{N_0})\prod_{w=1}^{nwk(y)}P(\text{CPUE}_{y,w}|q_y,N_{0,y},\tau_L)\right)$$

where nyr is the number of years of historical data, and $P(\text{CPUE}_{y,w}|q_y, N_{0,y}, \tau_L)$ is the likelihood function of the CPUE data in year y and week w. In practice, it is common to assign relatively uninformative priors to the hyper-parameters (Gelman et al. 1995). The prior and hyper-prior pdfs applied in the hierarchical model (eq. 4) were assumed to be normally distributed with a very large prior coefficient of variation (CV) (CV = (prior SD)/(prior mean) = 100) (Table 2). The posterior pdfs where thus determined almost entirely by the data. The prior and posterior CVs provide standardized measures of spread in the pdfs and enable comparisons of uncertainty between quantities with different units or different means. The prior mean for the initial abundances was chosen to be a few orders of magnitude as large as the observed weekly catches, and the prior mean value for q_y was chosen to be a few orders of magnitude less than the observed CPUE divided by the mean observed weekly catch.

(4) Identify the hyper-parameters and posterior predictive distributions of interest

As noted above, for assessments in new years, the use of an informative prior pdf of q_y and $N_{0,y}$ based on the analysis of historical data could help to improve precision in these values particularly in the first few weeks of the fishing season. For the purpose of constructing a prior pdf of these parameters for use in future assessments, this work focuses on the development of a hierarchical probability model for $N_{0,y}$ and q_y, so only the estimates for quantities associated with these parameters will be evaluated. For example, the posterior CV in the range of historical estimates for these parameters will be computed, since this will show how well historical estimates can help to inform us about the potential range of future estimates. Posterior distributions for μ_q, τ_q, μ_{N_0}, and τ_{N_0} will also inform us about the central tendency and spread of historical estimates for q_y and $N_{0,y}$.

One output of BHM is a predictive marginal posterior (PMP) pdf of each key parameter. The PMP pdf summarizes what can be inferred about the value of a parameter for some unsampled population given the estimated mean and variance in the parameter across sampled populations and the uncertainty in the mean and variance. PMP pdfs can serve as prior pdfs of key parameters in sequential Bayesian data analysis (McAllister and Kirkwood 1999; Michielsens 2003). PMP pdfs were obtained for q_y and $N_{0,y}$ in the De Lury stock assessment model. The PMP pdf for q_y was obtained first by integrating the joint pdf with respect to all parameters except μ_q and τ_q:

© 2004 NRC Canada

Table 1. The total catch (in tonnes (t)) and catch per unit effort (CPUE) (in tonnes per hour towed, for medium-sized Spanish- and Falkland-registered trawlers) data for Falkland Islands' *Loligo gahi* from 1987 until 2000.

Year	Week	CPUE ($t \cdot h^{-1}$)	Catch (t)	Mass (g)[a]	Year	Week	CPUE ($t \cdot h^{-1}$)	Catch (t)	Mass (g)[a]
1987	11	5.43	8755	43	1993	15	2.76	3636	53
1987	12	4.52	7581	44	1993	16	2.16	2750	55
1987	13	4.20	4476	43	1993	17	1.60	2546	56
1987	14	1.91	3116	46	1993	18	1.46	1664	58
1987	15	1.48	3365	47	1994	7	2.30	3001	32
1987	16	1.57	3261	49	1994	8	2.34	2829	32
1987	17	0.73	1291	57	1994	9	1.42	2291	32
1987	18	0.56	956	58	1994	10	1.36	2010	32
1988	6	2.90	3914	37	1994	11	1.19	1536	32
1988	7	2.25	4965	38	1994	12	0.99	1417	32
1988	8	1.63	4382	40	1994	13	1.49	2038	32
1988	9	1.68	4686	41	1995	11	14.98	4243	53
1988	10	1.65	3872	42	1995	12	9.72	4885	54
1988	11	1.45	3771	43	1995	13	6.91	3579	54
1988	12	1.29	3454	44	1995	14	6.06	4663	55
1988	13	0.69	1548	43	1995	15	5.19	4281	56
1988	14	1.07	2034	46	1995	16	4.80	3197	57
1988	15	0.72	1503	47	1995	17	4.47	3620	57
1988	16	0.68	1684	49	1995	18	3.59	2983	58
1988	17	0.65	1358	57	1995	19	3.23	2796	59
1989	10	10.60	6540	42	1996	7	1.59	2041	43
1989	11	8.54	7992	43	1996	8	2.16	2362	46
1989	12	4.46	7856	44	1996	9	1.49	1860	48
1989	13	4.55	7412	43	1996	10	0.34	453	50
1989	14	4.24	7170	46	1996	11	0.32	378	53
1989	15	4.21	7020	47	1996	12	0.48	690	55
1989	16	3.15	6743	49	1997	10	1.40	1306	43
1989	17	2.91	5277	57	1997	11	1.33	1416	44
1989	18	2.31	4773	55	1997	12	1.10	1160	44
1989	19	1.95	3076	57	1997	13	0.87	837	44
1989	20	1.44	4010	59	1997	14	0.73	662	45
1990	7	7.75	7472	38	1997	15	0.76	756	45
1990	8	7.31	6708	40	1998	9	3.25	3271	43
1990	9	5.00	5173	41	1998	10	2.73	2566	44
1990	10	3.01	4738	42	1998	11	2.31	2812	46
1990	11	5.85	6914	43	1998	12	2.94	2987	47
1990	12	4.04	4774	44	1998	13	3.02	2411	48
1990	13	3.55	3113	43	1998	14	1.20	1202	50
1990	14	2.20	3818	46	1999	6	2.01	2569	39
1990	15	2.50	4515	47	1999	7	1.20	1576	40
1991	6	6.47	3686	37	1999	8	1.09	1518	41
1991	7	6.35	3142	38	1999	9	1.15	1561	42
1991	8	3.42	2577	40	1999	10	1.30	1618	43
1991	9	4.18	2808	41	1999	11	1.01	1214	44
1991	10	2.73	2608	42	1999	12	0.79	1062	45
1991	11	2.88	2243	43	1999	13	0.96	1091	45
1991	12	1.93	1522	44	1999	14	0.76	1186	46
1992	8	5.14	4055	30	1999	15	0.55	892	47
1992	9	2.75	3166	31	1999	16	0.54	934	48
1992	10	4.89	4583	31	2000	5	1.76	1883	27
1992	11	3.05	3734	32	2000	6	1.86	2953	29
1992	12	1.44	1264	33	2000	7	1.70	3102	30
1992	13	1.58	1693	33	2000	9	1.25	1921	34
1992	14	2.20	2170	34	2000	11	1.80	2465	37
1992	15	1.97	1894	34	2000	12	1.62	1909	38
1992	16	2.15	1778	35	2000	13	1.39	1299	40
1993	14	2.54	2799	51	2000	14	1.41	1658	42

[a]Smoothed mean mass of squid. Mean mass data for 1987–1991 are illustrative.

© 2004 NRC Canada

$$(5)\quad P(\mu_q, \tau_q|\underline{\text{CPUE}}) = \int\int\int\int\int P(\mu_q)P(\tau_q)P(\mu_{N_0})P(\tau_{N_0})P(\sigma_L)\prod_{y=1}^{nyr}\left[P(q_y|\mu_q, \tau_q)P(N_{0,y}|\mu_{N_0}, \tau_{N_0})\prod_{w=1}^{nwk(y)}P(\text{CPUE}_{y,w}|q_y, N_{0,y}, \tau_y)\right]\mathrm{d}\underline{N}_{0,y}\,\mathrm{d}\underline{q}_y\,\mathrm{d}\tau_L\,\mathrm{d}\mu_{N_0}\,\mathrm{d}\tau_{N_0}$$

The marginal predictive posterior pdf of q_y is then given by integrating the following joint pdf:

$$(6)\quad P(q_y|\underline{\text{CPUE}} = \int\int P(q|\mu_q, \tau_q)P(\mu_q, \tau_q|\underline{\text{CPUE}})\mathrm{d}\mu_q\mathrm{d}\tau_q$$

The marginal predictive posterior pdf of N_0 is obtained similarly.

$$(7)\quad P(N_{0,y}|\underline{\text{CPUE}}) = \int\int P(N_0|\mu_{n_0}, \tau_{N_0})P(\mu_{N_0}, \tau_{N_0}|\underline{\text{CPUE}})\mathrm{d}\mu_{N_0}\,\mathrm{d}\tau_{N_0}$$

The conditional density functions $P(q_y|\mu_q,\tau_q)$ and $P(N_{0,y}|\mu_{N_0}\tau_{N_0})$, were taken to be lognormal. The prespecified values for the median and precision in these density functions, where required, are given in Table 2.

Additionally, the sensitivity of the central tendency and spread of these historical estimates to relatively low sample size (in terms of number of historical data sets) is also of interest and was also evaluated. This was done by repeating the hierarchical analysis, each time eliminating one of the historical data sets from the hierarchical model. The sensitivity of estimates of the properties for the meta-population to low sample size was evaluated by comparing the degree of similarity between the resulting posterior predictive distributions for N_0 and q.

(5) Integrating the hierarchical probability model to produce marginal posterior pdfs

The integrations required in eqs. 5–7 were approximated using importance sampling (Rubin 1988; McAllister et al. 1994; McAllister and Ianelli 1997). The importance functions used were multivariate log-t pdfs based on the posterior mode, which was obtained from nonlinear minimization and the estimate of the posterior covariance matrix at the mode using the Hessian matrix. Further details on the minimizer used, how the Hessian matrix was calculated, and the steps applied in the importance sampling procedure applied can be found in McAllister and Ianelli (1997).

The rate at which the pdf from importance sampling approaches the estimated posterior pdf and the stability of the results obtained from importance sampling are determined by the closeness of approximation of the importance function to the posterior pdf (Geweke 1989). Inefficiency and instability can occur if the importance function is considerably more diffuse than the posterior pdf and a large proportion of the sampling is from regions of parameter space with negligible posterior density. Instability will also result if the tails of the importance function taper off faster than the tails of the posterior pdf. Instability will be manifested by occasional large changes in the computed posterior expected values even after hundreds of thousands of draws from the importance function. If this occurs, sampling should be stopped, the run discarded, and the importance function adjusted (Geweke 1989; McAllister and Ianelli 1997).

Convergence of the approximated pdf to a stable result was evaluated using diagnostics developed in previous works (Geweke 1989; McAllister and Ianelli 1997). One diagnostic is the percentage of the maximum importance weight from the set of draws relative to the sum of the importance weights, where the importance weight, $W(\theta_k)$, for draw k is the product of the prior pdf and likelihood, $P(\theta_k)L(\text{data}|\theta_k)$, divided by the density of the importance function, $h(\theta_k)$, all evaluated at the parameter values θ_k in draw k (i.e., $W(\theta_k) = P(\theta_k)L(\text{data}|\theta_k)/h(\theta_k)$). If draws were to be obtained from the posterior pdf as the importance function, this percentage should be equal to $100\%/m$, where m is the number of importance samples. This is because $W(\theta_k)$ would be constant across draws if the importance function was the posterior pdf. Thus, the percent maximum weight should drop to a low value within several hundred thousand draws from a well-chosen importance function. In this application, importance sampling was stopped after this percentage dropped below 3% and this occurred after several hundred thousand draws. Also, the CV in the importance weights (CV(W)) was computed and compared with the CV in the product of the prior and likelihood function (CV($P{\cdot}L$)). If draws of parameter values were to be taken from the posterior pdf, the CV(W) should be 0. If the importance function is to give reliable results, then CV(W) can be expected to be not much larger than the CV($P{\cdot}L$). We have found from numerical experiments that when CV(W) is approximately five or more times larger than the CV($P{\cdot}L$), the marginal posterior estimates can be strongly biased or numerically unstable, and an importance function that is either more similar in central tendency and spread to the posterior pdf or has less sharp tails is required.

Hierarchical modeling of catch rate data from the Falklands' *L. gahi* trawl fishery

Implementation of BHM

The hierarchical model described above was applied using a subset of the Falkland Islands' *L. gahi* squid fishery weekly catch and CPUE data (Table 1). These data relate to February to April when the fishery exploits the first of the two annual and unrelated recruitment pulses (the first cohort). Weeks listed in Table 1 are sequential 7-day periods, with week 1 beginning 1 January, week 2 beginning 8 January, and so on. These are the time units commonly used in assessments of this stock. Data for years 1987–2000 were used. Total removals by week and CPUE in tonnes per hour fished by week were compiled from data provided by the industry as part of the license requirements. The trawl vessels in this fishery are assigned to a number of fleets on the basis of flag nation and vessel size, and a separate catchability coefficient is calculated for each fleet in routine assessments. For simplicity, the current study considers a single-fleet implementation, so CPUE data were used only for the most common

© 2004 NRC Canada

Table 2. Specifications of the priors and hyper-priors used in the De Lury stock assessment of Falkland Islands' fisheries for *Loligo gahi*.

Hyper-parameters	Symbol	Value assigned
Prior median for μ_q	$\mu(\mu_q)$	0.00005
Prior CV for μ_q	$CV(\mu_q)$	100
Prior median for τ_q	$\mu(\tau_q)$	5
Prior CV for τ_q	$CV(\tau_q)$	100
Prior median for μ_{N_0}	$\mu(\mu_{N_0})$	5000 million
Prior CV for μ_{N_0}	$CV(\mu_{N_0})$	100
Prior median for τ_{N_0}	$\mu(\tau_{N_0})$	5
Prior CV for τ_{N_0}	$CV(\tau_{N_0})$	100
Prior median for τ_L	$\mu(\tau_L)$	25
Prior CV for τ_L	$CV(\tau_L)$	100

Note: CV, coefficient of variation; q_y, catchability of squid in year y; μ_q, median q_y; τ_q, precision in q_y; $N_{0,y}$, the initial abundance of squid in year y; μ_{N_0}, median $N_{0,y}$; τ_{N_0}, precision in $N_{0,y}$; τ_L, the precision of the lognormal likelihood function; and τ, precision ($1/\sigma^2$, where σ is standard deviation).

fleet (Spanish- and Falklands-registered vessels with a gross registered tonnage of 1000–2000 t). The mean mass per animal at week was calculated from data collected by shipboard observers. A smoothed growth function was obtained by fitting a linear model to these data. Total catch and CPUE data were expressed in numbers of squid by dividing by the smoothed mass at week (Table 1). Estimations were implemented only on the set of weeks in which a decline in catch rates was observed in a given fishing season (Table 1).

The hierarchical modeling procedure was first tested using simulated data to evaluate whether it could be effectively implemented and was reasonably unbiased. Because of the enormous volume of results produced, only the key findings will be reported. Reasonably unbiased results were obtained using importance sampling after reparameterizing the variances in the normal and lognormal density functions as precision τ, where $\tau = 1/\sigma^2$ and σ is the standard deviation. For example, when a diffuse lognormal or normal prior was placed on σ_q, and the true simulated value for σ_q was set at 0.2 or more, the posterior modal estimate for σ_q obtained with simulated catch and catch rate data was often 0. This is because $1/\sigma$ is part of the normal and lognormal density functions, and tiny values for σ when data are relatively uninformative can maximize the density function. With the prior placed instead on $\tau_q = 1/\sigma_q^2$ (Table 2), the joint posterior modal estimate for σ_q was in all trials larger than 0 and approximately equal to the true simulated value. To facilitate the numerical integration of eqs. 5–7, the normal and lognormal density functions were reparameterized to use τ_q instead of σ_q, and priors were placed on $\tau_q = 1/\sigma_q^2$ rather than on σ_q (Table 2). The same was also done in the normal and lognormal density functions for $N_{0,y}$. This same reparameterization of σ in the normal and lognormal density functions has been used in other Bayesian estimation problems (e.g., Meyer and Millar 1999).

The Bayesian hierarchical model for q_y and $N_{0,y}$ was fitted to the *L. gahi* fishery data from 1987 to 2000. Diffuse hyper-priors with normal pdfs were assigned to τ_L, μ_q, τ_q, μ_{N_0}, and τ_{N_0} (Table 2). Importance sampling was applied to produce a marginal predictive posterior distributions for q_y and $N_{0,y}$ based on the data from 1987 to 2000 (eqs. 5–7). The analysis was then repeated, each time leaving out one of the years from 1987 to 2000 to evaluate the sensitivity of the results to the relatively low number of years included in the analysis.

To illustrate the features of BHM, a Bayesian nonhierarchical estimation was conducted for comparison. In the nonhierarchical model, the parameters $N_{0,y}$ and q_y were independently estimated for each individual year, i.e., the parameters for the cross-year median value and variance for these parameters were not included in the nonhierarchical model. The same De Lury model and likelihood function (eqs. 1 and 2) were applied. The estimation for all years, however, was conducted in the same statistical model assuming that the precision parameter in the likelihood function was the same across years.

In Bayesian estimation, the most commonly used value for central tendency is the posterior mean value, and we have reported these in the Results section. However, to facilitate comparisons of results with those from the Bayesian nonhierarchical estimators, we report posterior modes when making these comparisons.

Results

BHM produces marginal posterior pdfs of the key parameters of each individual population included, taking into account cross-population variance in these parameters. Marginal posteriors are shown for the parameters q_y and $N_{0,y}$ for the years 1987–2000 (Fig. 1). For comparison, the diffuse prior pdfs applied for each of these quantities are also plotted. The central tendencies of the marginal posterior pdfs of $N_{0,y}$ vary considerably from year to year and are far more precise than the flat prior density. The posterior mean values for $N_{0,y}$ range from 0.3 to 4.4 billion animals (Table 3). The posterior CVs range from 0.02 to 0.36, and many of the distributions have extremely low overlap with others. This indicates that some of the data are highly informative. However, not all of the data are informative. The large range of posterior CVs for the marginal distributions for $N_{0,y}$ indicates that the information value in the data varies considerably across years. The central tendencies for q_y vary considerably less (i.e., from 0.3×10^{-4} to 1.8×10^{-4}) (Table 3). The posterior CV in the estimates of q_y varies less, from 0.12 to 0.42.

Hierarchical modeling also quantifies how a parameter varies across different members of a population. In this case, the population is the set of years in which De Lury assessments have been applied. It is assumed that a parametric distribution can be used to describe how the values of the parameter vary across members of the population. In this analysis, it is assumed that the population of true values for $N_{0,y}$ across years is normally distributed. The same is assumed about the distribution for q_y. The median and precision of these lognormal distributions were estimated for $N_{0,y}$ and q_y (i.e., μ_q, τ_q, μ_{N_0}, and τ_{N_0}, respectively). The posterior mean estimates for μ_q and μ_{N_0} were 9.3×10^{-5} and 2.1×10^9 squid, respectively (Fig. 2, Table 4). μ_q and μ_{N_0} are precisely estimated with posterior CVs of 0.16 and 0.15, re-

© 2004 NRC Canada

Fig. 1. Marginal posterior probability density functions (pdfs) for (*a*) the initial abundance of squid in year *y* ($N_{0,y}$) and (*b*) catchability coefficient of squid in year *y* (q_y) from the Bayesian hierarchical De Lury model for years 1987–2000. The diffuse priors are shown as bold broken lines. The predictive posterior pdfs are shown are the bold lines.

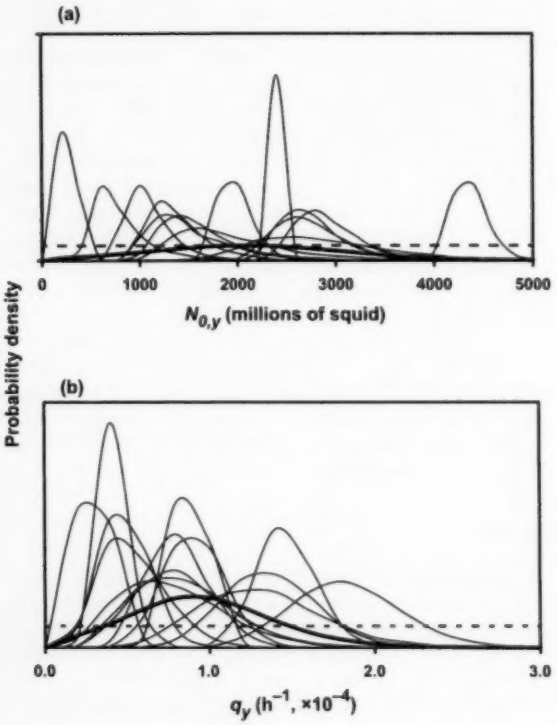

spectively. The estimates of variance in values across years are also of interest because they indicate the spread of the distribution of historical estimates and the potential distribution of future values. The posterior mean values for the CVs in N_0 and q_y are intermediate and are 0.49 and 0.47, respectively. Whereas the prior CVs for τ for N_0 and q_y and τ_L were very large, i.e., 100, the posterior CVs for the corresponding quantities CV($N_{0,y}$), CV(q_y), and σ_L were much smaller, i.e., 0.22, 0.24, and 0.08, respectively (Table 4). This indicates that the data, not the priors, largely determined the posterior pdfs for these quantities.

The Bayesian nonhierarchical De Lury model provided plausible parameter estimates for all years except for 1998 and 2000. In these years, the catch rate series did not show a distinct decline and were quite variable over the time series (Table 1). The posterior modal estimates for $N_{0,y}$ (analogous to maximum likelihood estimates currently applied in the stock assessment) were implausibly large (millions of times larger than other values), and the estimates for q were millions of times less than the estimates in the other years. The individual posterior modal estimates of q_y and $N_{0,y}$ for the years that worked under nonhierarchical modeling were more variable than the values obtained from hierarchical modeling, but overall the two groups of estimates were largely similar (Table 5). For q_y, the most extreme estimates were

Table 3. Posterior mean estimates and posterior coefficients of variation (CVs) of hierarchical model quantities for years 1987–2000.

Year	$N_{0,y}$	CV	q_y	CV
1987	2398	0.02	1.50×10^{-4}	0.12
1988	1974	0.09	4.10×10^{-5}	0.17
1989	4360	0.04	8.80×10^{-5}	0.13
1990	2918	0.12	9.10×10^{-5}	0.20
1991	1385	0.23	1.30×10^{-4}	0.28
1992	2747	0.14	8.10×10^{-5}	0.23
1993	1502	0.28	8.40×10^{-5}	0.36
1994	1932	0.30	5.40×10^{-5}	0.37
1995	2743	0.12	1.40×10^{-4}	0.21
1996	293	0.06	1.80×10^{-4}	0.18
1997	796	0.36	7.80×10^{-5}	0.42
1998	1627	0.27	8.50×10^{-5}	0.35
1999	1100	0.22	4.90×10^{-5}	0.29
2000	2844	0.24	3.10×10^{-5}	0.31

Note: Abundance is in millions of animals. $N_{0,y}$ is the initial abundance of squid in year *y*, and q_y is the catchability of squid in year *y*.

pulled toward the central tendency in the hierarchical modeling. However, this was not apparent for $N_{0,y}$ because for all years where both were estimated, the estimates of $N_{0,y}$ were similar between the hierarchical and nonhierarchical methods. The cross-year CVs (excluding 1998 and 2000) in the posterior modal estimates for $N_{0,y}$ were 0.59 and 0.61 for the hierarchical and nonhierarchical methods, respectively (Table 5). The corresponding CVs in the posterior modal estimates for q_y were 0.45 and 0.61 for the hierarchical and nonhierarchical methods, respectively. The estimated posterior CVs for each annual value were similar between the two estimation approaches and similarly variable between years.

The hierarchical estimates of $N_{0,y}$ for years that did not work under nonhierarchical modeling (1998 and 2000) were within the range of estimates for other years (Table 5). However, the hierarchical estimates for q were slightly lower than the lowest nonhierarchical estimates obtained. This is not surprising given the very low decline in the CPUE data. The estimates of the posterior CVs for these parameters in these years were intermediate relative to the estimates in other years (Table 5). Therefore, the use of hierarchical information (e.g., among year variances in q_y and $N_{0,y}$) obtained by hierarchical modeling combined with the available catch rate and catch data for 1998 and 2000 to produce plausible estimates of q_y and $N_{0,y}$.

One of the key assumptions of hierarchical modeling is that the modeled populations are exchangeable (Gelman et al. 1995). This is reasonable if there are no reasons to suspect a priori that some populations are different from others. In this application, the main exchangeability assumption is that there is no temporal autocorrelation in the parameter values. Given experience in other fisheries, the existence of autocorrelation in recruitment and catchability could be reasonable assumptions. If $N_{0,y}$ was found to be related to some environmental variable (Agnew et al. 2000; Chang 2001), then this variable could be included as an explanatory variable, and the hierarchical application could become even more powerful at prediction (Myers et al. 2001). However,

© 2004 NRC Canada

Fig. 2. Marginal posterior probability density functions (pdfs) for the median in the lognormal distribution of (*a*) the initial abundance of squid in year *y* ($N_{0,y}$) and (*b*) catchability coefficient of squid in year *y* (q_y) across the years 1987–2000. The broken line is the prior pdf and the solid line is the posterior pdf.

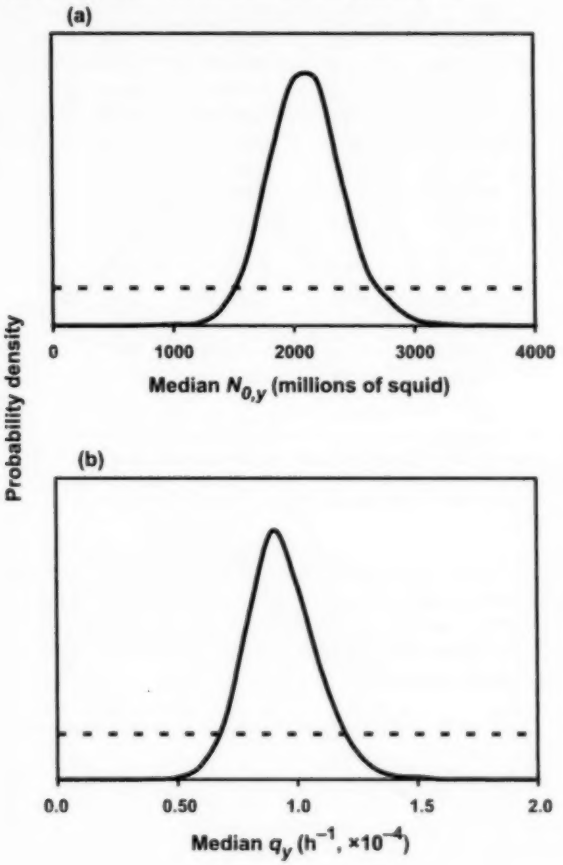

the hierarchical model would become more complex if the assumption of autocorrelation or an environmental covariate was adopted in the model structure. Thus, for the purpose of illustration, autocorrelation and environmental covariates were not modeled. However, autocorrelations were negligible and nonsignificant in the annual hierarchical posterior estimates of $N_{0,y}$ (e.g., for lag = 1 year, $\rho = 0.13$, p value = 0.60) and q_y (for lag = 1 year, $\rho = 0.06$, p value = 0.80) (Table 5).

It is also of interest to evaluate whether the estimates for μ_q, and μ_{N_0} are correlated. If they were, this would suggest that this correlation should be incorporated in the development of a prior pdf of q_y and $N_{0,y}$ for assessments in future years. The joint posterior distribution for μ_q and μ_{N_0} shows no appreciable correlation (corr = –0.09) (Fig. 3). This indicates that it is reasonable to assume no posterior correlation between μ_q and μ_{N_0}.

As mentioned above, the precision of parameter estimates in future assessments could be increased if historical data were used to develop informative priors, and hierarchical probability modeling does so by developing posterior predictive distributions for key parameters. Here we developed posterior predictive distributions for q_y and $N_{0,y}$, assuming that values for these are independent. Importance sampling was applied to do the required integrations in eqs. 5–7. The posterior mean of this distribution was similar to the posterior mean estimate of the μ_{N_0} at 1900 million individuals (Fig. 4). The posterior predictive distribution for $N_{0,y}$ was much wider than the posterior distribution for μ_{N_0} with a posterior CV of 0.45 (Table 4). The posterior predictive mean value for q_y was also similar to the posterior mean estimate of μ_q at 9.7×10^{-5}. The CV for the posterior predictive distribution for q_y was 0.45 (Fig. 4).

Table 4. Posterior mean estimates and posterior coefficients of variation (CVs) of the hierarchical De Lury model quantities.

Parameter	Mean	CV
Median q_y	9.40×10^{-5}	0.16
Median $N_{0,y}$	2100	0.15
CV(q_y)	0.47	0.24
CV($N_{0,y}$)	0.49	0.22
Predictive q_y	9.70×10^{-5}	0.45
Predictive $N_{0,y}$	2177	0.45
σ_L	0.22	0.08

Note: The medians q_y and $N_{0,y}$ refer to the median values for q_y and $N_{0,y}$, respectively, in the lognormal density function describing the distribution of q_y and $N_{0,y}$ across years. The CV(q_y) and CV($N_{0,y}$) refer to the CVs for q_y and $N_{0,y}$, respectively, in the lognormal density function describing the distribution of q_y and $N_{0,y}$ across years. Abundance is in millions of animals.

The posterior predictive distributions for key parameters can be sensitive when the number of populations for which data exist are relatively few. In this case, 14 different years of data are available. The sensitivity of the posterior predictive distributions for q_y and $N_{0,y}$ to few years being included was evaluated by redoing the analysis, each time leaving out a single year from the analysis. The resulting set of 14 predictive distributions for q_y and $N_{0,y}$ were very similar (Fig. 5). The years making the most difference were not the same for q_y and $N_{0,y}$, i.e., 1996 and 1989, respectively. The 1989 catch rate data had one of the lowest gradients, so when these data were removed, the predictive distribution for $N_{0,y}$ shifted to the left. The marginal posterior estimate of q_y for 1996 was the highest, and when 1996 was left out, the marginal predictive posterior for q_y shifted to the left.

Discussion

The development of a Bayesian hierarchical approach to the estimation of De Lury model parameters offers to provide more reliable estimates of population abundance than nonhierarchical methods. This is demonstrated, for instance, by the successful versus unsuccessful results from 1998 and 2000 with the hierarchical and nonhierarchical models, respectively. We have previously encountered this problem with the 1998 and 2000 populations, which resisted attempts to apply either simple or multifleet De Lury likelihood models (Rosenberg et al. 1990). In the past, we have developed a

© 2004 NRC Canada

Table 5. Posterior modal estimates and posterior coefficients of variation (CVs) for catchability coefficient of squid in year y (q_y) and the initial abundance of squid in year y ($N_{0,y}$) from hierarchical and nonhierarchical De Lury models.

	Hierarchical		Nonhierarchical		Hierarchical		Nonhierarchical	
Year	$N_{0,y}$	CV	$N_{0,y}$	CV	q_y	CV	q_y	CV
1987	2385	0.02	2371	0.01	0.00015	0.11	0.00016	0.11
1988	1932	0.08	1962	0.09	0.00004	0.17	0.00004	0.17
1989	4334	0.04	4417	0.04	0.00009	0.12	0.00008	0.13
1990	2829	0.11	2958	0.14	0.00009	0.20	0.00009	0.24
1991	1232	0.19	973	0.13	0.00014	0.27	0.00021	0.23
1992	2643	0.13	2873	0.20	0.00008	0.24	0.00007	0.32
1993	1290	0.24	1225	0.27	0.00009	0.36	0.00010	0.43
1994	1751	0.31	2128	0.49	0.00005	0.42	0.00004	0.62
1995	2621	0.11	2434	0.10	0.00014	0.20	0.00017	0.21
1996	286	0.06	268	0.04	0.00019	0.17	0.00025	0.15
1997	644	0.28	623	0.33	0.00009	0.41	0.00009	0.49
1998	1427	0.24	NA	NA	0.00009	0.37	NA	NA
1999	1006	0.18	1035	0.19	0.00005	0.28	0.00005	0.28
2000	2781	0.24	NA	NA	0.00003	0.31	NA	NA
CV_{est}	0.59	0.66	0.61	0.83	0.45	0.49	0.61	0.56
Mean	1913	0.14	1939	0.17	0.00010	0.30	0.00011	0.28

Note: The posterior CVs were obtained from the Hessian matrix evaluated at the mode of the posterior. NA, not obtainable; CV, the posterior CV in the estimate; CV_{est}, the CV in the set of point estimates in the column above (standard deviation of estimates/mean of estimates). Abundance is in millions of animals.

Fig. 3. Contour plot of the joint posterior estimate of the median values for the initial abundance of squid in year y ($N_{0,y}$) and catchability coefficient of squid in year y (q_y). Darker shades indicate higher joint posterior probability density.

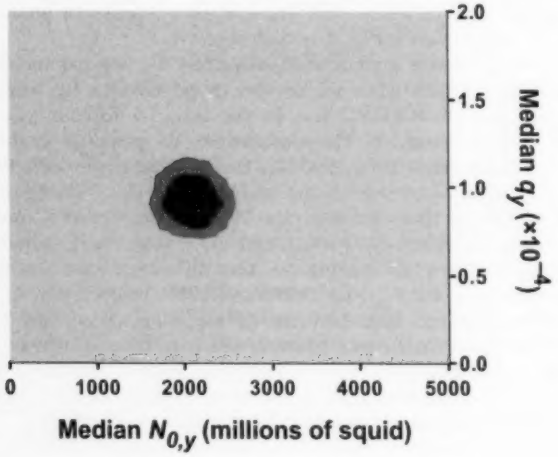

Fig. 4. Plot of the marginal posterior predictive probability density functions (pdfs) for (*a*) the initial abundance of squid in year y ($N_{0,y}$) and (*b*) catchability coefficient of squid in year y (q_y). The broken line is the prior pdf and the solid line is the posterior pdf.

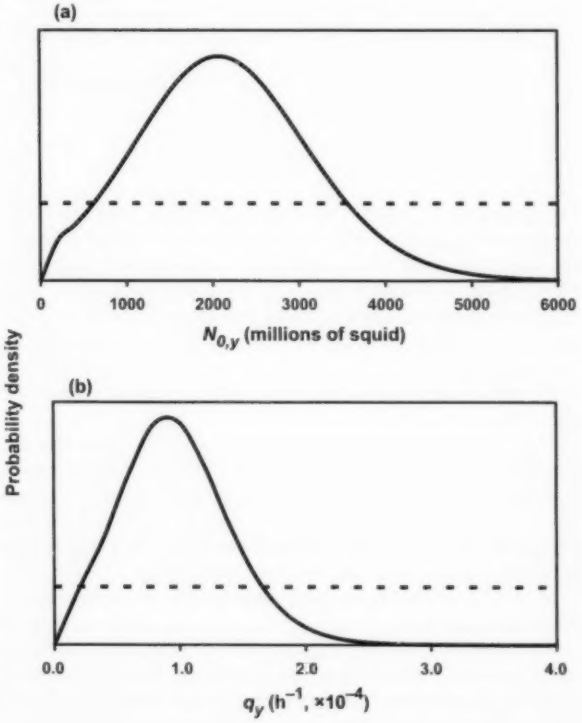

pragmatic response to the problem of nonconvergence of a multifleet De Lury model (Agnew et al. 1998), which applies prior knowledge of the catchabilities of each fleet to CPUE and derives from this an estimate of stock size. This pragmatic solution is similar to the method used in the Bayesian hierarchical approach, in that the latter uses prior information about the properties of catchabilities across all years. The Bayesian hierarchical approach developed in the present paper is a formalized and much more robust realization of that philosophy and appears to perform well.

© 2004 NRC Canada

Fig. 5. Plot of the marginal posterior predictive probability density functions (pdfs) for (*a*) the initial abundance of squid in year y ($N_{0,y}$) and (*b*) catchability coefficient of squid in year y (q_y) with a missing year of data. For $N_{0,y}$, the most influential year is 1989. The dotted line illustrates the result when data for 1989 are left out. For q_y, the most influential year is 1996. The broken line illustrates the result when data for 1996 are left out. The bold line illustrates the result when all data are included.

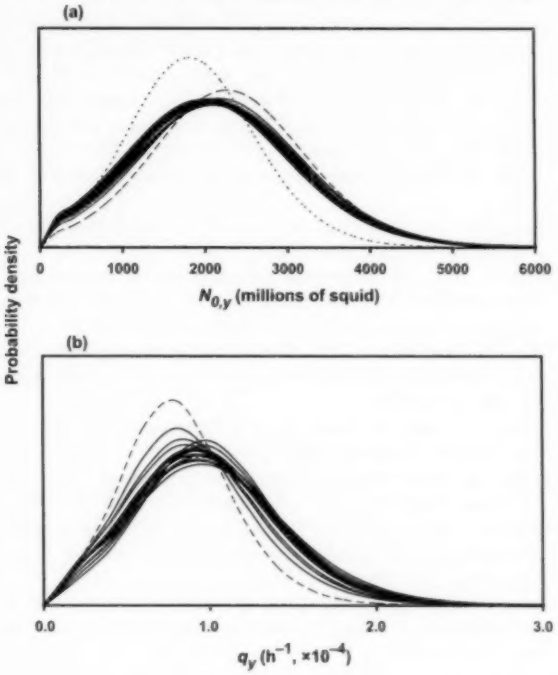

The use of BHM (Gelman et al. 1995; Rivot and Prévost 2002) to construct prior distributions for q_y and $N_{0,y}$ from historical data is one of the main strengths of the approach. BHM is particularly useful when the De Lury model is applied for in-season management controls. For example, BHM is helpful near the beginning of the fishing season when only a few weeks of catch rate data are available and estimates from the conventional estimation method for the De Lury model can be highly imprecise. BHM is useful for years when the catch rate data are not well behaved. For example, they show a decline for only a very short part of the weekly time series, relatively little decline, or excessive decline.

There are at least two options for applying a BHM in stock assessment. A stock assessment could employ the hierarchical model of all previous years and the current year's data. If the hierarchical model were very quick and simple to operate, this would be a viable and straightforward option. However, because the Bayesian Monte Carlo integration in the analysis of historical data can be time consuming owing to slow convergence, an in-season De Lury stock assessment application that included the data for the current year and all historical years would be cumbersome. The full historical data analysis would have to be rerun with each new addition of weekly data. It would instead be more efficient to first analyze all of the historical data to produce a predictive posterior pdf of the De Lury stock assessment model parameters given the historical data. In Bayesian analysis, the posterior pdf contains all of the information in the data about the model parameters. This posterior pdf could then serve as a prior pdf for the current year's assessment. It would be much easier with each new week's data to rerun the stock assessment model that incorporated a prior pdf based on the hierarchical analysis of the historical data and was fitted only to the current year's data. Thereby, the historical data analysis is conducted only once at the beginning of the season rather than repeatedly with the reapplication of the De Lury model in each new week of the season. This type of estimation in which the posterior from one data analysis becomes the prior for a new data analysis is one form of sequential Bayesian analysis (Berger 1985; McAllister and Kirkwood 1999; Michielsens 2003).

Markov Chain Monte Carlo (MCMC) methods have recently been taken to be synonymous with Bayesian estimation (e.g., Meyer and Millar 1999; Harley and Myers 2001; Rivot and Prévost 2002). However, other reliable non-MCMC methods of Bayesian integration also exist (Rubin 1988; Walters and Ludwig 1994; Rivot et al. 2001), and the choice of method is a matter of personal preference. Thus, in this paper, importance sampling (Rubin 1987, 1988; McAllister and Ianelli 1997) was used rather than a MCMC method. Whichever integration method is applied, it is important to apply diagnostics to evaluate whether convergence has been achieved. If possible, it is even better to apply both approaches to check for consistency in results after diagnostics of each suggest convergence (McAllister and Ianelli 1997).

There are a few hazards when applying the suggested methodology to develop prior pdfs in future stock assessments. The first occurs if the range of hierarchical estimates from the historical years does not reflect that in future years. This is conceivable if the properties of the fishery changed systematically. For example, the efficiency of the fleet often increases systematically over time. Priors that assume constant catchability could then bias the parameter estimates. This could be overcome by conducting Bayesian De Lury assessments with both informative and uninformative priors and (or) by weighting the posterior predictive distributions towards the most recent years. The second occurs if the catch rate data do not follow a distinctive declining pattern over a series of several weeks into the fishing season. This may not necessarily imply that abundance is extremely high or catchability very low for that season. It could be that other processes are occurring. For example, this could reflect a lagged migration of some part of the population. In reality, all data sets subjected to De Lury assessment, either by traditional or Bayesian methods, must be selected carefully to ensure that only the declining phases of the fishery are included. The initial recruitment to the fishing grounds and spawning emigration at the end of the fishing season are excluded from the analysis. It might also be advisable to construct some alternative structural models that account for a limited set of alternative processes to those considered in the De Lury depletion model and fit these also to the data. Auxiliary data such as maturity and mean length data could be helpful for distinguishing among them. Model-checking methods such as those suggested in Chapter 6 of Gelman et al. (1995) could be applied to evaluate whether the model choice is appropriate.

© 2004 NRC Canada

In this particular application, the catch rate data from only one of the fleets was used. Catch rate data from other fleets exist and are used in routine assessments of Falkand Islands' *L. gahi* and *I. argentinus*. Because of the information in these additional data, the next step in the hierarchical modeling would be to extend the model structure to model CPUE data from the different fleets to help to estimate posterior predictive distributions for q_y for each fleet and $N_{0,y}$.

The posterior predictive distributions obtained for q_y and $N_{0,y}$ appear to be sufficiently precise but not too precise for use as prior pdfs in future stock assessments (McAllister and Kirkwood 1998). For example, it has been found that informative prior pdfs of key parameters in stock assessment, e.g., constants of proportionality for relative abundance indices, should have prior CVs of no more than about 0.7 to be useful as informative priors (McAllister et al. 1994; McAllister and Ianelli 1997; McAllister and Kirchner 2002). However, prior CVs should be no less than about 0.5 to avoid potential bias in posterior estimates because of being "precisely wrong" in the prior distributions used (McAllister and Kirkwood 1998). With this in mind, it would also be of interest to evaluate how the prior estimates of $N_{0,y}$ and q_y are updated as new catch and CPUE data are gathered in each week. In particular, it would be of interest to identify whether priors for both $N_{0,y}$ and q_y or only one or the other of these parameters should be incorporated in new estimations, taking into account the potential effects of bias and precision of these alternative estimation approaches.

As more years go by, the number of years in the hierarchical probability model for De Lury model parameters could be increased to improve estimates of the hierarchical model's parameters, but weighted towards the most recent years. In sequential Bayesian estimation, it is common for priors to narrow as more data are incorporated (McAllister and Kirkwood 1999). In the present situation, it is unlikely that the posterior predictive distributions will narrow considerably. This is because one of the key parameters in determining the predictive distributions is the cross-year variance in q_y and $N_{0,y}$, and it is expected that the CVs of the resulting posterior predictive distributions for these parameters should not decrease progressively and should instead stabilize at values reflecting the actual long-run interannual variances in these parameters. However, as more years of data become available, the presence of autocorrelation should be tested for and incorporated if found to be substantial.

Acknowledgements

The work was funded by the Government of the Falkland Islands and a grant awarded to Dr. McAllister from the Nuffield Foundation (Nuffield Awards to Newly Appointed Lecturers, NUF–NAL). The authors are most grateful to John Barton, Director of Fisheries of the Falkland Islands' government, for allowing access to the fisheries data; David Middleton for comments on an earlier draft; and to Louise Choo for her assistance in helping with simulations to evaluate earlier versions of the hierarchical De Lury model. Two anonymous reviewers are thanked for their comments on an earlier version of the manuscript.

References

Adkison, M.D., and Su, Z. 2001. A comparison of salmon escapement estimates using a hierarchical Bayesian approach versus separate maximum likelihood estimation of each year's return. Can. J. Fish. Aquat. Sci. **58**: 1663–1671.

Agnew, D.J., Baranowski, R., Beddington, J.R., des Clers, S., and Nolan, C.P. 1998. Approaches to assessing stocks of *Loligo gahi* around the Falkland Islands. Fish. Res. **35**: 155–169.

Agnew, D.J., Hill, S., and Beddington, J.R. 2000. Predicting the recruitment strength of an annual squid stock: *Loligo gahi* around the Falkland Islands. Can. J. Fish. Aquat. Sci. **57**: 2479–2487.

Basson, M., Beddington, J.R., Crombie, J.A., Holden, S.J., Purchase, L.V., and Tingley, G.A. 1996. Assessment and management techniques for migratory squid stocks: the *Illex argentinus* fishery in the Southwest Atlantic as an example. Fish. Res. **28**: 3–27.

Berger, J.O. 1985. Statistical decision theory and Bayesian analysis. 2nd ed. Springer-Verlag New York Inc., New York.

Chang, C. 2001. Environmental influences on the recruitment of *Illex argentinus* in the Southwest Atlantic. Ph.D. thesis, Imperial College of Science, Technology and Medicine, London.

Collie, J.S., and Walters, C.J. 1991. Adaptive management of spatially replicated groundfish populations. Can. J. Fish. Aquat. Sci. **48**: 1273–1284.

Gelman, A., Carlin, J., Stern, H., and Rubin, D. 1995. Bayesian data analysis. Chapman & Hall Ltd., London.

Geweke, J.F. 1989. Bayesian inference in econometric models using Monte Carlo integration. Econometrica, **57**: 1317–1340.

Harley, S.J., and Myers, R.A. 2001. Hierarchical Bayesian models of length-specific catchability of research trawl surveys. Can. J. Fish. Aquat. Sci. **58**: 1569–1584.

Hilborn, R., and Walters, C.J. 1992. Quantitative fisheries stock assessment: choice, dynamics and uncertainty. Chapman & Hall Inc., New York.

McAllister, M.K., and Ianelli, J.N. 1997. Bayesian stock assessment using catch-age data and the sampling – importance resampling algorithm. Can. J. Fish. Aquat. Sci. **54**: 284–300.

McAllister, M.K., and Kirchner, C.H. 2002. Accounting for structural uncertainty to facilitate precautionary fishery management: illustration with Namibian orange roughy. Bull. Mar. Sci. **70**(2): 499–540.

McAllister, M.K., and Kirkwood, G.P. 1998. Using Bayesian decision analysis to help achieve a precautionary approach for managing developing fisheries. Can. J. Fish. Aquat. Sci. **55**: 2642–2661.

McAllister, M.K., and Kirkwood, G.P. 1999. Applying multivariate conjugate priors in fishery-management system evaluation: how much quicker is it and how does it bias the ranking of management options? ICES J. Mar. Sci. **56**: 884–889.

McAllister, M.K., Pikitch, E.K., Punt, A.E., and Hilborn, R. 1994. A Bayesian approach to stock assessment and harvest decisions using the sampling/importance resampling algorithm. Can. J. Fish. Aquat. Sci. **51**: 2673–2687.

Meyer, R., and Millar, R.B. 1999. BUGS in Bayesian stock assessments. Can. J. Fish. Aquat. Sci. **56**: 1078–1086.

Michielsens, C.G.J. 2003. Bayesian decision theory for fisheries management of migratory species with multiple life histories. Imperial College, London.

Myers, R.A., MacKenzie, B.R., Bowen, K., and Barrowman, N.J. 2001. What is the carrying capacity of fish in the ocean? A meta-analysis of population dynamics of North Atlantic cod. Can. J. Fish. Aquat. Sci. **58**: 1464–1476.

© 2004 NRC Canada

Rivot, E., and Prévost, E. 2002. Hierarchical Bayesian analysis of capture–mark–recapture data. Can. J. Fish. Aquat. Sci. **59**: 1768–1784.

Rivot, E., Prévost, E., and Parent, E. 2001. How robust are Bayesian posterior inferences based on a Ricker model with regards to measurement errors and prior assumptions about parameters? Can. J. Fish. Aquat. Sci. **58**: 2284–2297.

Rosenberg, A.A., Kirkwood, G.P., Crombie, J.A., and Beddington, J.R. 1990. The assessment of stocks of annual squid species. Fish. Res. **8**: 335–350.

Rubin, D.B. 1987. Comment on 'The calculation of posterior distributions by data augmentation'. J. Am. Stat. Assoc. **82**: 543–546.

Rubin, D.B. 1988. Using the SIR algorithm to simulate posterior distributions. *In* Bayesian Statistics 3: Proceedings of the Third Valencia International Meeting, 1–5 June 1987, Valencia, Spain. *Edited by* J.M. Bernardo, M.H. Degroot, D.V. Lindley, and A.M. Smith. Clarendon Press, Oxford. pp. 385–402.

Walters, C.J., and Ludwig, D. 1994. Calculation of Bayes' posterior probability distributions for key population parameters: a simplified approach. Can. J. Fish. Aquat. Sci. **51**: 713–722.

© 2004 NRC Canada

Fisheries and Aquatic Sciences
Sciences halieutiques et aquatiques

Photographic Atlas of Fish Otoliths of the Northwest Atlantic Ocean
By / Par Stephen E. Campana

$54.95 CAN. Other countries $54.95 US
54,95 $CAN. À l'étranger 54,95 $US
Softcover / Édition brochée
(*Can. Spec. Publ. Fish. Aquat. Sci. / Publ. spéc. can. sci. halieut. aquat. 133*)
284 pages ISBN 0-660-19108-3 ISSN 0706-6481 NRC / CNRC 46328

Salmonine Introductions to the Laurentian Great Lakes:
An Historical Review and Evaluation of Ecological Effects
By / Par Stephen S. Crawford

$42.95 CAN. Other countries $42.95 US
42,95 $CAN. À l'étranger 42,95 $US
Softcover / Édition brochée
(*Can. Spec. Publ. Fish. Aquat. Sci. / Publ. spéc. can. sci. halieut. aquat. 132*)
215 pages ISBN 0-660-17639-4 ISSN 0706-6481 NRC / CNRC 42734

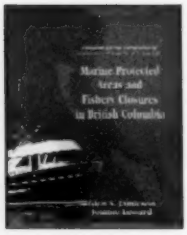

Marine Protected Areas and Fisheries Closures in British Columbia
By Glen S. Jamieson and Joanne Lessard

$69.95 CAN. Other countries $69.95 US
69,95 $CAN. À l'étranger 69,95 $US
Softcover / Édition brochée
(Can. Spec. Publ. Fish. Aquat. Sci. / Publ. spéc. can. sci. halieut. aquat. 131)
414 pages ISBN 0-660-17788-9 ISSN 0706-6481 NRC / CNRC 42846

Workshop on Rebuilding Abalone Stocks in British Columbia
By / Par Alan Campbell

$42.95 CAN. Other countries $42.95 US
42,95 $CAN. À l'étranger 42,95 $US
Softcover / Édition brochée
(*Can. Spec. Publ. Fish. Aquat. Sci. / Publ. spéc. can. sci. halieut. aquat. 130*)
158 pages ISBN 0-660-18292-0 ISSN 0706-6481 NRC / CNRC 42841

To order any of the above titles / Commandez n'importe quel titre ci-dessus à :

Telephone / Téléphone : (613) 990-2254
Fax / Télécopieur : (613) 952-7656
E-mail / Courriel : pubs@nrc-cnrc.gc.ca
Web site / Site web : http://pubs.nrc-cnrc.gc.ca

Order Office / Bureau des commandes
NRC Research Press / Presses scientifique du CNRC
National Research Council / Conseil national de recherches
Ottawa, ON K1A 0R6, Canada

Canadian customers add GST (7%). Prepayment required unless order is accompanied by a purchase order number. Cheques or money orders should be made payable to : "Receiver General for Canada, Credit NRC". For all orders outside Canada, rates are in U.S. Dollars. All sales are final.
Clients du Canada, ajoutez la TPS (7 %). Les commandes doivent être payées d'avance à moins qu'elles ne soient accompagnées d'un numéro de bon de commande. Les chèques ou mandats doivent être libellés au « Receveur général du Canada, crédit du CNRC ». Pour les commandes hors-Canada, les tarifs sont en dollars américains. Toutes les ventes sont finales.

George J. Klein: The Great Inventor

Richard I. Bourgeois-Doyle

NRC Press Biography Series No. 2 / Collection de biographies des Presses du CNRC No 2

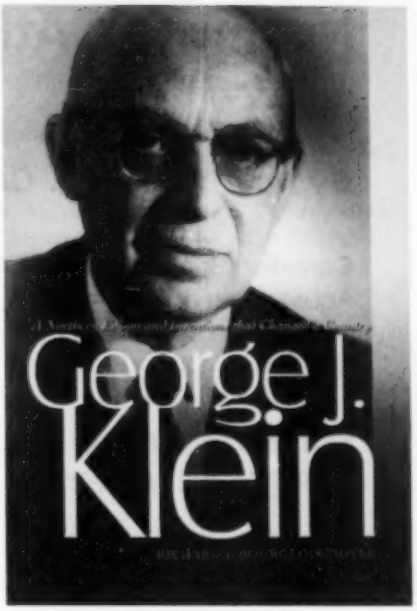

$49.95 CAN. Other countries $49.95 US
49,95 $CAN. À l'étranger 49,95 $US

Canadian customers add GST (7%) / Clients du Canada, ajoutez la TPS (7 %)

Hardcover / Édition reliée
ISBN 0-660-19322-1
ISSN 1701-1833
NRC No. / Nº du CNRC 46323

Orders may be submitted by mail or fax to:
Les commandes peuvent être soumises par courrier ou par télécopieur à :

Order Office / Bureau des commandes

NRC Research Press / Presses scientifique du CNRC
National Research Council / Conseil national de recherches
Ottawa, ON K1A 0R6, Canada
Telephone / Téléphone : (613) 990-2254
Fax / Télécopieur : (613) 952-7656
E-mail / Courriel : pubs@nrc-cnrc.gc.ca
Website / Site web : http://pubs.nrc-cnrc.gc.ca

PLEASE PRINT/LETTRES MOULÉES

☐ Payment enclosed / Paiement inclus ☐ Charge to/ Imputer à ☐ Visa ☐ MasterCard

Account no./Nº de compte | Expiry date/Date d'expiration

Name/Nom

Signature

Address/Adresse

City/Ville | Province

Postal code/Code postal | Country/Pays

Telephone/Téléphone | Fax/Télécopieur

E-mail/Courriel

Prepayment required unless order is accompanied by a purchase order number. Cheques or money orders should be made payable to: "Receiver General for Canada, Credit NRC". All sales are final.
Les commandes doivent être payées d'avance à moins qu'elles ne soient accompagnées d'un numéro de bon de commande. Les chèques ou mandats doivent être libellés au « Receveur générale du Canada, crédit du CNRC ». Toutes les ventes sont finales.

Photographic Atlas of Fish Otoliths of the Northwest Atlantic Ocean

By / par Steven E. Campana

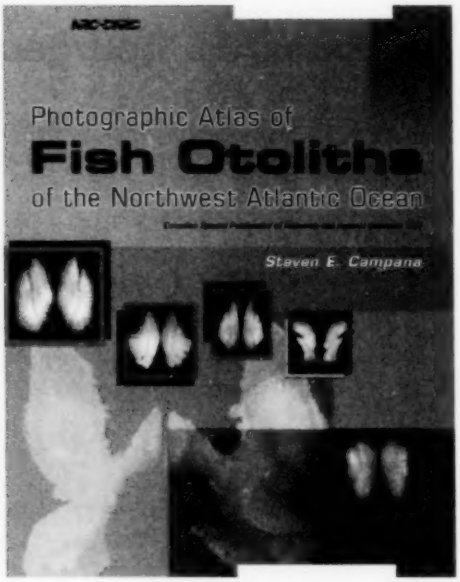

Canadian Special Publications of Fisheries and Aquatic Sciences / Publication spéciale canadienne des sciences halieutiques et aquatiques 133

$54.95 CAN. Other countries $54.95 US
54,95 $CAN. À l'étranger 54,95 $US

Canadian customers add GST (7%) / Clients du Canada, ajoutez la TPS (7 %)

284 Pages 2004
Softcover / Édition brochée
ISBN 0-660-19108-3
ISSN 0706-6481
NRC No. / Nº du CNRC 46328

Orders may be submitted by mail or fax to:
Les commandes peuvent être soumises par courrier ou par télécopieur à :

Order Office / Bureau des commandes

NRC Research Press / Presses scientifiques du CNRC
National Research Council / Conseil national de recherches
Ottawa, ON K1A 0R6, Canada
Telephone / Téléphone : (613) 990-2254
Fax / Télécopieur : (613) 952-7656
E-mail / Courriel : research.press@nrc-cnrc.gc.ca
Website / Site web : http://pubs.nrc-cnrc.gc.ca

PLEASE PRINT/LETTRES MOULÉES

☐ Payment enclosed / Paiement inclus Visa ☐ Mastercard ☐

Account no./Nº de compte Expiry date/Date d'expiration

Name/Nom

Signature

Address/Adresse

City/Ville Province

Postal code/Code postal Country/Pays

Telephone/Téléphone Fax/Télécopieur

E-mail/Courriel

Prepayment required unless order is accompanied by a purchase order number. Cheques or money orders should be made payable to: "Receiver General for Canada, Credit NRC". All sales are final.
Les commandes doivent être payées d'avance à moins qu'elles ne soient accompagnées d'un numéro de bon de commande. Les chèques ou mandats doivent être libellés au « Receveur général du Canada, crédit du CNRC ». Toutes les ventes sont finales.

Contents (concluded) / Table des matières (suite et fin)

K. Hüssy, H. Mosegaard, and F. Jessen	**1012–1020**	Effect of age and temperature on amino acid composition and the content of different protein types of juvenile Atlantic cod (*Gadus morhua*) otoliths
K. Hüssy and H. Mosegaard	**1021–1031**	Atlantic cod (*Gadus morhua*) growth and otolith accretion characteristics modelled in a bioenergetics context
Catherine G.J. Michielsens and Murdoch K. McAllister	**1032–1047**	A Bayesian hierarchical analysis of stock–recruit data: quantifying structural and parameter uncertainties
Murdoch K. McAllister, Simeon L. Hill, David J. Agnew, Geoffrey P. Kirkwood, and John R. Beddington	**1048–1059**	A Bayesian hierarchical formulation of the De Lury stock assessment model for abundance estimation of Falkland Islands' squid (*Loligo gahi*)

NRC Research Press 75th Anniversary

Since the publication of the first issue of the *Canadian Journal of Research* in 1929, the National Research Council has provided scientists and engineers in Canada and elsewhere with a means to communicate with their peers in the international research community through the production of high-quality journals. NRC Research Press is proud to celebrate 75 years of science and technology publishing in Canada.

Le 75e anniversaire des Presses scientifiques du CNRC

Depuis la parution du premier numéro du *Canadian Journal of Research* en 1929, le Conseil national de recherches du Canada publient des revues savantes de qualité grâce auxquelles les chercheurs et ingénieurs du Canada et d'ailleurs peuvent partager les résultats de leurs recherches avec leurs pairs de la collectivité scientifique internationale. Les Presses scientifiques du CNRC sont fières de célébrer 75 ans d'édition scientifique et technique au Canada.

National Research Council Canada
Ottawa, Canada K1A 0R6

Conseil national de recherches Canada
Ottawa, Canada K1A 0R6

Postage paid at Ottawa
Publications mail
Registration No. 40062591

Port payé à Ottawa
Poste-publication
Enregistrement n° 40062591

USPS periodical postage paid at Champlain, N.Y.

Canadian Journal of Fisheries and Aquatic Sciences

Volume 61, Number 6, June 2004

Journal canadien des sciences halieutiques et aquatiques

Volume 61, numéro 6, juin 2004

	ARTICLES	ARTICLES
Brett Albanese, Paul L. Angermeier, and Sundar Dorai-Raj	**857–869**	Ecological correlates of fish movement in a network of Virginia streams
Hans J. Skaug, Nils Øien, Tore Schweder, and Gjermund Bøthun	**870–886**	Abundance of minke whales (*Balaenoptera acutorostrata*) in the Northeast Atlantic: variability in time and space
Stephen B. Heard and Corinne K. Buchanan	**887–897**	Grazer–collector facilitation hypothesis supported by laboratory but not field experiments
Heather M. Patterson, Michael J. Kingsford, and Malcolm T. McCulloch	**898–904**	The influence of oceanic and lagoonal plume waters on otolith chemistry
Emily M. Standen, Scott G. Hinch, and Peter S. Rand	**905–912**	Influence of river speed on path selection by migrating adult sockeye salmon (*Oncorhynchus nerka*)
Sherri L. Johnson	**913–923**	Factors influencing stream temperatures in small streams: substrate effects and a shading experiment
David L. Strayer, Kathryn A. Hattala, and Andrew W. Kahnle	**924–941**	Effects of an invasive bivalve (*Dreissena polymorpha*) on fish in the Hudson River estuary
S. Niyogi, P. Couture, G. Pyle, D.G. McDonald, and C.M. Wood	**942–953**	Acute cadmium biotic ligand model characteristics of laboratory-reared and wild yellow perch (*Perca flavescens*) relative to rainbow trout (*Oncorhynchus mykiss*)
Steven S. Wall, Charles R. Berry, Jr., Carmen M. Blausey, Jonathan A. Jenks, and Chad J. Kopplin	**954–973**	Fish-habitat modeling for gap analysis to conserve the endangered Topeka shiner (*Notropis topeka*)
James W. Savereide and Terrance J. Quinn II	**974–985**	An age-structured assessment model for chinook salmon (*Oncorhynchus tshawytscha*)
Dirk Verschuren, Brian F. Cumming, and Kathleen R. Laird	**986–998**	Quantitative reconstruction of past salinity variations in African lakes: assessment of chironomid-based inference models (Insecta: Diptera) in space and time
E. Ashley Steel, Blake E. Feist, David W. Jensen, George R. Pess, Mindi B. Sheer, Jody B. Brauner, and Robert E. Bilby	**999–1011**	Landscape models to understand steelhead (*Oncorhynchus mykiss*) distribution and help prioritize barrier removals in the Willamette basin, Oregon, USA

Continued on inside back cover / Suite au verso

Printed in Canada by / Imprimé au Canada par
NRC Reprographic Services / Service de reprographie CNRC
Page production by / Mise en page par
NRC Research Press / Presses scientifiques du CNRC

0706-652X(200406)61:6;1-3